Edited by
Avraam I. Isayev

Encyclopedia of
Polymer Blends

Related Titles

Elias, H.-G.

Macromolecules

Volume 4: Applications of Polymers

2008

ISBN: 978-3-527-31175-0

Elias, H.-G.

Macromolecules

Volume 3: Physical Structures and Properties

2007

ISBN: 978-3-527-31174-3

Matyjaszewski, K., Gnanou, Y., Leibler, L. (eds.)

Macromolecular Engineering

Precise Synthesis, Materials Properties, Applications

2007

ISBN: 978-3-527-31446-1

Elias, H.-G.

Macromolecules

Volume 2: Industrial Polymers and Syntheses

2007

ISBN: 978-3-527-31173-6

Elias, H.-G.

Macromolecules

Volume 1: Chemical Structures and Syntheses

2005

ISBN: 978-3-527-31172-9

Kemmere, M. F., Meyer, T. (eds.)

Supercritical Carbon Dioxide

in Polymer Reaction Engineering

2005

ISBN: 978-3-527-31092-0

Meyer, T., Keurentjes, J. (eds.)

Handbook of Polymer Reaction Engineering

2005

ISBN: 978-3-527-31014-2

Xanthos, M. (ed.)

Functional Fillers for Plastics

Second Edition

2010

ISBN: 978-3-527-32361-6

Advincula, R. C., Brittain, W. J., Caster, K. C., Rühe, J. (eds.)

Polymer Brushes

Synthesis, Characterization, Applications

2004

ISBN: 978-3-527-31033-3

Elias, H.-G.

An Introduction to Plastics

2003

ISBN: 978-3-527-29602-6

Edited by
Avraam I. Isayev

Encyclopedia of Polymer Blends

Volume 2: Processing

WILEY-VCH Verlag GmbH & Co. KGaA

The Editor

Prof. Avraam I. Isayev
The University of Akron
Department of Polymer Engineering
250 South Forge Street
Akron, OH 444325-0301
USA

All books published by **Wiley-VCH** are carefully produced. Nevertheless, authors, editors, and publisher do not warrant the information contained in these books, including this book, to be free of errors. Readers are advised to keep in mind that statements, data, illustrations, procedural details or other items may inadvertently be inaccurate.

Library of Congress Card No.: applied for

British Library Cataloguing-in-Publication Data
A catalogue record for this book is available from the British Library.

Bibliographic information published by the Deutsche Nationalbibliothek
The Deutsche Nationalbibliothek lists this publication in the Deutsche Nationalbibliografie; detailed bibliographic data are available on the Internet at http://dnb.d-nb.de.

© 2011 Wiley-VCH Verlag & Co. KGaA, Boschstr. 12, 69469 Weinheim, Germany

All rights reserved (including those of translation into other languages). No part of this book may be reproduced in any form – by photoprinting, microfilm, or any other means – nor transmitted or translated into a machine language without written permission from the publishers. Registered names, trademarks, etc. used in this book, even when not specifically marked as such, are not to be considered unprotected by law.

Cover Design Adam Design, Weinheim
Typesetting Thomson Digital, Noida, India
Printing and Bookbinding betz-druck GmbH, Darmstadt

Printed in the Federal Republic of Germany
Printed on acid-free paper

ISBN: 978-3-527-31930-5

Contents

Preface *XIII*
List of Contributors *XVII*

1 Polymer Blend Compounding and Processing *1*
James L. White and Sug Hun Bumm
1.1 Introduction and Early Studies of Blending *1*
1.2 Methods of Compounding *2*
1.2.1 Batch Mixers *2*
1.2.1.1 Introductory *2*
1.2.1.2 Non-intermeshing Rotor Mixers *3*
1.2.1.3 Intermeshing Rotor Mixers *5*
1.2.1.4 Post-World War II Development *7*
1.2.2 Continuous Mixers *10*
1.2.2.1 Early Activities *10*
1.2.2.2 Single-Screw Extrusion *11*
1.2.2.3 Co-rotating Twin-Screw Extrusion *11*
1.2.2.4 Tangential Counter-Rotating Twin-Screw Extrusion *15*
1.2.2.5 Modular Intermeshing Counter-Rotating Twin-Screw Mixer *16*
1.2.2.6 Modular Buss Kokneter *16*
1.2.3 Comparisons *16*
1.3 Processing Polymer Blends *18*
1.3.1 Early Synthetic Polymer Blends *18*
1.3.2 General Ideas and Stability of Blend Phase Morphology *18*
1.3.3 Phase Morphology Variations in Processing Operations *21*
1.3.3.1 Melt Spinning *21*
1.3.3.2 Die Extrusion *21*
1.3.3.3 Injection Molding *22*
References *23*

2 Rheology of Polymer Blends *27*
Leszek A. Utracki
2.1 Introduction *27*
2.1.1 Rheological Models for Miscible Blends *28*

2.1.1.1 Solutions *28*
2.1.1.2 Homologous Polymer Blends *31*
2.1.2 Model Systems for Immiscible Blends *31*
2.1.2.1 Interphase and Percolation *31*
2.1.2.2 Suspensions *34*
2.1.2.3 Emulsion Rheology *39*
2.1.2.4 Melt Flow of Block Copolymers *45*
2.2 Theoretical Treatment of Polymer Blends *45*
2.3 Rheology of Miscible Blends *47*
2.3.1 General *47*
2.3.2 Phase Separation and Flow *52*
2.3.2.1 Influence of Thermodynamics on Rheology *52*
2.3.2.2 Influence of Rheology on Thermodynamics *54*
2.4 Rheology of Immiscible Blends *57*
2.4.1 Rheological Equations of State *57*
2.4.2 Morphology of Immiscible Blends *60*
2.4.3 Microrheology of Polymer Blends *61*
2.4.3.1 Deformation and Breakup of Viscoelastic Drops *61*
2.4.3.2 Coalescence of Viscoelastic Drops *63*
2.4.4 Flow Imposed Morphology *65*
2.4.5 Shear Flows *66*
2.4.5.1 Concentration Dependence of Viscosity *66*
2.4.5.2 Dynamic Flow *68*
2.4.5.3 Steady-State versus Dynamic Viscosity *69*
2.4.5.4 Blend Elasticity *70*
2.4.6 Elongational Flows *72*
2.5 Rheology of Blends with Nanoparticles *76*
2.5.1 General *76*
2.5.2 Rheology of Blends with Spherical SiO_2 Particles *78*
2.5.3 Rheology of Blends with Nanoparticles Near Binodal *80*
2.5.4 Rheology of Immiscible Blends with Organoclay *81*
2.6 Conclusions *83*
References *89*

3 Compounding and Processing of Plastic/Rubber Blends *109*
Raman P. Patel and Jinwoong Shin
3.1 Plastic/Rubber Blends *109*
3.1.1 Introduction *109*
3.1.2 Classification of Polymer Blends *110*
3.1.3 Types of Plastic/Rubber Blends *111*
3.2 Methods of Blend Preparation *112*
3.3 Equipment for Blend Preparation by Melt Mixing of Polymers *113*
3.3.1 Batch Mixers *113*
3.3.1.1 Roll Mill *113*

3.3.1.2 Banbury or Kneader Mixer *114*
3.3.2 Continuous Mixers *117*
3.3.2.1 Twin-Screw Mixer *117*
3.3.2.2 Buss Continuous Kneader *123*
3.4 Preparation of Physical Blends of Plastics and Rubbers *125*
3.4.1 Laboratory Preparation of the Blends *125*
3.4.2 Production of Blends by a Batch Process *127*
3.4.3 Production of Blends by a Continuous Process in a Twin-Screw Mixer *128*
3.5 Crosslinking Agents and Crosslinking Processes *131*
3.6 Preparation of the Blends of Plastics and Crosslinked Rubbers *137*
3.6.1 Preparation of Plastic and Crosslinked Rubber Blends (TPVs) by a Batch Process *140*
3.6.1.1 Preparation of TPVs in a Brabender *140*
3.6.1.2 Production of TPVs in a Banbury or Similar Batch Processing Equipment *141*
3.6.1.3 Production of TPVs by a Continuous Process in a Twin-Screw Mixer *143*
3.7 Blends of Plastics and Crosslinked Rubbers by Dynamic Vulcanization *144*
3.8 Compatibilization and Compatibilized Blends *146*
3.8.1 Preparation of a Compatibilizer *148*
3.8.2 Production of Compatibilized Blends *149*
3.8.3 Compatibilized Blends *149*
3.9 Processing of Plastic/Rubber Blends *151*
3.9.1 General *151*
3.9.2 Injection Molding *152*
3.9.3 Extrusion *155*
3.10 Conclusions and Outlook *158*
References *160*

4 Compounding and Processing of Rubber/Rubber Blends *163*
Brendan Rodgers and Adel Halasa
4.1 Introduction *163*
4.1.1 Fundamentals of Applied Polymer Chemistry *164*
4.1.2 Multiple T_g Elastomer Compositions *169*
4.2 Elastomers and Tire Compounding *170*
4.2.1 Tire Component Parts *171*
4.2.2 Tire Elastomers *172*
4.3 Blending Elastomers *174*
4.4 Solubility Parameters *178*
4.4.1 Definition of Solubility Parameters *178*
4.4.2 Estimation of Solubility Parameters *180*
4.5 Processing of Elastomer Blends *181*
4.5.1 General Remarks *181*

4.5.2 Natural Rubber/Bromobutyl Rubber Blends *183*
4.5.3 Bromobutyl/Butyl Rubber Blends *186*
4.5.4 Bromobutyl/Chlorobutyl Rubber Blends *186*
4.5.5 Bromobutyl/Styrene Butadiene Rubber Blends *186*
4.5.6 Bromobutyl/GPR/EPDM Rubber Triblends *187*
4.5.7 Distribution of Compounding Ingredients: Insoluble Chemicals *187*
4.5.8 Distribution of Compounding Ingredients: Soluble Chemicals *189*
4.5.9 Effect of Blending on Compound Physical Properties *192*
4.6 Secondary Polymer Blends Systems *193*
4.6.1 Resins Systems *193*
4.6.2 Tackifying Resins *194*
4.6.3 Reinforcing Resins *194*
4.6.4 Curing Resins *196*
4.6.5 Polymeric Green Strength Promoters *198*
4.7 Elastomer Blends and Tire Performance *199*
4.8 Tire Tread Compound Formulary *201*
4.9 Summary *203*
References *204*

5 Extrusion Technology for Manufacturing Polymer Blends *207*
Kun Sup Hyun, Costas G. Gogos, and Myung-Ho Kim
5.1 Introduction *207*
5.1.1 Hierarchy of Equipment in Manufacturing Polymer Blends *210*
5.1.2 Brief Historical Facts and Needs for Manufacturing of Polymer Blends *212*
5.2 Multiple-Screw Extruders *212*
5.2.1 Twin-Screw Extrusion Technology *212*
5.2.1.1 Coperion Werner & Pfleiderer: ZSK MEGAcompounder *217*
5.2.1.2 Effect of D_o/D_i and Screw Speed on Average Shear Rate *217*
5.2.1.3 Leistritz: HSEI (High Speed Energy Input) Twin-Screw Extruder *218*
5.2.1.4 KraussMaffei Berstorff Twin-Screw Extrusion System *222*
5.2.1.5 Japan Steel Works TEX Twin-Screw Extrusion Systems *223*
5.2.1.6 High Efficiency Twin-Screw Extruder *226*
5.2.1.7 Intelligent Extruder for Polymer Compounding *227*
5.2.2 Single-Screw Extrusion Technology *229*
5.2.2.1 High-Performance Screws *231*
5.2.2.2 Secondary Mixing Processes and Devices *237*
5.2.2.3 Helibar® Transfer Mixing Screw in Groove Barrel *240*
5.2.2.4 Dynamic Mixers *241*
5.3 Most Critical Step in the Production of Polymer Blends – Melting/Mixing *243*
5.3.1 Extrusion Process Simulator Version II (EPSIM II) *243*

5.3.2 Twin-Screw Melt Mixing Evaluator (TSMEE) *244*
5.3.3 Melting of Virgin Polymers *245*
5.3.3.1 Melting and Remelting *246*
5.3.4 Classification and Discussion of Melting Mechanisms Important to Polymers *247*
5.3.5 Characterization of Mixing Elements *251*
5.3.6 Melting of Solid Mixtures of Polymer Blend Components *253*
5.3.6.1 Melting Behavior of Single Components and the Blend *254*
5.4 Monitoring of Morphology and Compositions of Polymer Blends *257*
5.5 Future Development in Polymer Blends Compounding *257*
5.5.1 Mass Customization *257*
5.5.2 Single-, Twin-, or Multiple-Screw Extruders *259*
References *259*

6 Manufacturing of Polymer Blends Using Polymeric and Low Molecular Weight Reactive Compatibilizers *263*
Eung Kyu Kim and James L. White
6.1 Introduction *263*
6.2 Reactive Blending and Compatibilization *264*
6.3 Mixing Mechanism and Morphology Development *265*
6.3.1 Distributive Mixing *266*
6.3.2 Dispersive Mixing *270*
6.3.2.1 Interfacial Tension *270*
6.3.2.2 Shear Viscosity of Polymer Blends *272*
6.3.3 Morphology Development *273*
6.3.3.1 Initial Breakup of Polymer Melt Phases *273*
6.3.3.2 Breakup of Liquid Filaments in a Liquid Matrix *275*
6.3.3.3 Deformation of Droplets *276*
6.3.3.4 Observations on Mechanically Mixed Polymer Blends *280*
6.3.3.5 Coalescence *281*
6.4 Intermeshing Co-rotating Twin-Screw Extruder *282*
6.4.1 Geometry and Flow Mechanisms *282*
6.4.1.1 Right-Handed Screw Elements *285*
6.4.1.2 Left-Handed Screw Elements *288*
6.4.1.3 Kneading Disc Blocks *288*
6.4.1.4 Special Distributive Mixing Elements *290*
6.4.2 Residence Time Distributions *292*
6.4.3 Morphology Development for Reactive Blends *295*
6.4.4 Process Simulation of Intermeshing Co-rotating Twin-Screw Extruders *297*
6.5 Manufacturing Process Design for Polymer Blending Process *300*
6.6 Concluding Remarks *305*
References *309*

7 Polymer Blend Compatibilization by Copolymers and Functional Polymers *315*
Jose A. Covas, Luiz Antonio Pessan, Ana V. Machado, and Nelson M. Larocca
7.1 Introduction *315*
7.1.1 Polymer Blends and the Need for Compatibilization *315*
7.1.2 Compatibilization Routes *316*
7.1.3 Reactive Extrusion/Processing *317*
7.2 Compatibilization by Copolymers *317*
7.3 *In Situ* Compatibilization or Reactive Blending *320*
7.3.1 Kinetics of Melt Coupling Reactions at Interfaces *321*
7.3.2 Effect of Interfacial Reactions on the Interface Morphology *323*
7.3.3 Effect of the Interfacial Copolymer Structure *324*
7.3.4 Effect of the Reactive Precursor Molecular Weight *325*
7.3.5 Effect of the Flow *326*
7.3.6 Role of the Reaction Rate on the Dispersed Phase Morphology *328*
7.3.7 Examples of Applications of Reactive Blending in Polyesters and Polyamides Blends *332*
7.3.7.1 Polybutadiene Terephthalate Blends *332*
7.3.7.2 Polyamide-6 Blends *336*
7.4 Application to Manufacturing of Polymer Blends *337*
7.4.1 Equipment *337*
7.4.1.1 Introduction *337*
7.4.1.2 Main Operational Features of Co-rotating Twin-Screw Extruders *340*
7.4.2 Evolution Along the Extruder *343*
7.4.3 Modeling and Optimization *345*
7.5 Conclusions *350*
References *351*

8 Chemical and Engineering Aspects of Morphology Development and Processing of Multiphase Polymer Blend Nanocomposites *357*
I. Sedat Gunes and Sadhan C. Jana
8.1 Introduction: The Promise and Challenge of Polymer Blending *357*
8.2 Inorganic Particles in Small Molecule Liquid Emulsion: A Model System for Filled Polymer Blends? *358*
8.3 Chemical Aspects of Morphology Development and Processing of Multiphase Polymer Blend Nanocomposites *360*
8.3.1 Conventional Fillers in Polymer Blends *360*
8.3.2 Nanofillers in Polymer Blends *364*
8.4 Engineering Aspects of Morphology Development and Processing of Multiphase Polymer Blend Nanocomposites *369*
8.4.1 Miscibility, Homogeneity, and Interfaces of Polymer Blends *369*
8.4.2 Definition of Mixing and Intermaterial Area Generation *370*

8.4.3 Mixing Flow and Kinematics of Mixing *372*
8.4.3.1 Intermaterial Area Generation in Miscible Fluids *374*
8.4.3.2 Relevance of Intermaterial Area Generation to Dispersive Mixing *381*
8.4.4 Demixing of Filler Particles and Droplets Induced by Non-uniform Shear Flows Encountered During Usual Processing Operations *381*
8.5 Conclusions *382*
References *385*

Index *395*

Preface

The *Encyclopedia of Polymer Blends* will include scientific publications in various areas of blends. Polymer blends are mixtures of two or more polymers and/or copolymers. Polymer blending is used to develop new materials with synergistic properties that are not achievable with individual components without having to synthesize and scale up new macromolecules. Along with a classical description of polymer blends, chapters in the encyclopedia will describe recently proposed theories and concepts that may not be accepted yet but reflect future development. Each chapter provides current points of view on the subject matter. These up-to-date reviews are very helpful for understanding the present status of science and technology related to polymer blends.

The encyclopedia will be the source of existing knowledge related to polymer blends and will consist of five volumes. Volume 1 describes the fundamentals, including the basic principles of polymer blending, thermodynamics, miscible, immiscible, and compatible blends, kinetics, and composition and temperature dependence of phase separation. Volume 2 provides the principles, equipment and machinery for polymer blend processing. Volume 3 deals with the structure of blended materials that governs their properties. Volume 4 describes various properties of polymer blends. Volume 5 discusses the blended materials and their industrial, automotive, aerospace, and other high technology applications. Individual chapters in the encyclopedia describe the topics with historical perspective, state-of-the-art science and technology and the future.

This encyclopedia is intended for use by academicians, scientists, engineers, researchers and graduate students working on polymers and their blends.

Volume 2 is devoted to the principles, equipment and machineries for polymer blend processing and it consists of eight chapters. These chapters cover compounding and processing with a major emphasis on extrusion technology for manufacturing plastic/rubber and rubber/rubber blends and blend nanocomposites. Existing routes for compatibilization by copolymers, functional polymers and low molecular weight compatibilizers are discussed extensively. The importance of flow, rheology of components, and rheological aspects of blends is emphasized. These aspects are detailed below and build on each other.

Chapter 1, starting with a historical perspective of blending and blends, describes various methods and machines for compounding. It includes rotor designs in batch

mixers and screw designs in single- and twin-screw compounding extruders and Buss Kokneter with comparative analysis of these machines. Finally, this chapter discusses the phase morphology development in blends and their stability during processing, including melt spinning, extrusion, and injection molding.

Chapter 2 provides an extensive description of the rheology and microrheology of polymer blends and their nanocomposites, including the theoretical and experimental aspects. Rheological models for miscible and immiscible systems are discussed, including solutions, suspensions and emulsion, and filled polymer rheology. The rheology of block copolymers and the influence of thermodynamics on rheology and the influence of rheology on thermodynamics of blends are also elucidated. Newtonian and non-Newtonian behaviors of blends in steady state and oscillatory shear and elongational flow are also discussed. The deformation and breakup behavior of viscoelastic drops and flow imposed morphology are described. Emphasis is made on rheology of blends with nanoparticles.

Chapter 3 is devoted to compounding and processing of plastic/rubber blends. Starting with the classification of polymer blends, this chapter discusses physical blends of plastics and rubbers and blends of plastics with partially or highly crosslinked rubbers with and without use of compatibilizers. Compounding methods using batch and continuous mixers are also considered, including roll mills, Banbury or kneader mixers, twin-screw extruders, and Buss continuous kneader. Various aspects of making blends and products in the laboratory and manufacturing line are considered, including arrangements for feeding of various ingredients in the process. Basic mechanisms of crosslinking and interface reactions occurring during compounding are also elucidated.

Chapter 4 is devoted to compounding and processing of rubber/rubber blends. It discusses fundamentals of applied polymer chemistry and science relevant to the miscible, semi-miscible, immiscible, and compatible rubber blends. Solubility aspects of elastomers are described with an emphasis on solubility parameters and their estimation. Principles of elastomer compounding for tire manufacturing, including discussions of various elastomers used in tire component parts, are described. Blending of elastomers through the latex, solution and their combination, and mechanical and mechanochemical methods is considered. An emphasis is given to specific blends and various ingredients used in tire manufacture to achieve the target performance characteristics. This chapter concludes by presenting the tire formulary and opportunities for further research.

Chapter 5 provides an extensive description of the extrusion technology for manufacturing polymer blends. A brief history of manufacturing polymer blends and classification of extrusion equipment for their preparation is given. A detailed description of multiple- and single-screw extruders is provided and peculiar features of polymer blend melting and mixing mechanisms are given. Extrusion process simulator and twin-screw melt mixing evaluator are described, including the means for monitoring morphology and compositions of polymer blends. The future development of polymer blend compounding is discussed.

Chapter 6 describes manufacturing of polymer blends using polymeric and low molecular weight reactive compatibilizers. In particular, this chapter considers

mixing mechanisms and morphology development through distributive and dispersive mixing. The importance of the interfacial tension and viscosity ratio of the components in the development of blend morphologies is stressed. The early stages of breakup of polymer melt phases, liquid filament breakup in a liquid matrix, and deformation and coalescence of droplets during flow are discussed along with some morphological observations in mixed blends. The geometry, residence time distribution, flow mechanisms, and simulation of flow in intermeshing co-rotating twin-screw extruders are described, including their effects on the morphology development in reactive blends and manufacturing process design.

Chapter 7 is devoted to polymer blend compatibilization by copolymers and functional polymers. This chapter includes the compatibilization by various copolymers, reaction kinetics and reactive blending between two functional polymeric components, melt coupling reactions at interfaces, and the mechanism of interfacial reactions along with their effects on the interface morphology. The effects of the molecular weight of reactive precursors, reaction rate, and flow on the morphology of blends are also reported. Various examples of the applications of reactive blending to specific polymer blends are presented along with equipment used for their manufacturing. Modeling and optimization of processes are also considered.

Chapter 8 reviews morphology development and processing of multiphase polymer blend nanocomposites. A brief summary of allied fields, such as polymer blend composites, is also given. Examples are presented to highlight the influence of filler–matrix interactions, thermodynamic effects, interfacial tension, and rheology on morphology development. A review of the effects of kinetic conditions, such as mixing protocol and flow field, is also presented. Finally, some engineering aspects of the processing of blend nanocomposites are discussed, such as migration and demixing of dispersed droplets and filler particles during common processing flows.

There are many people who contributed to the completion of this volume. I wish to express my profound appreciation to the contributors of the various chapters for being patient with my requests for revisions and corrections. I am thankful to Wiley-VCH Publishers for undertaking this project and for their patience, understanding, and cooperation with the authors at all stages of preparation. Finally, the support and patience of my family and the families of all the chapter authors contributed to the completion of this volume.

Akron, Ohio, USA
January 2011

Avraam I. Isayev

List of Contributors

Sug Hun Bumm
The University of Akron
Department of Polymer Engineering
250 South Forge Street
Akron, OH 44325-0301
USA

Jose A. Covas
University of Minho
Institute of Polymers and
Composites/I3N
Department of Polymer Engineering
4800 058 Guimarães
Portugal

Costas G. Gogos
New Jersey Institute of Technology
Otto H York Department of Chemical,
Biological & Pharmaceutical
Engineering
Polymer Processing Institute
GITC Bldg Suite 3901
University Heights
Newark, NJ 07102-1982
USA

I. Sedat Gunes
The University of Akron
Department of Polymer Engineering
360 South Forge Street
Akron, OH 44325-0301
USA

Adel Halasa
The University of Akron
Department of Polymer Science
170 University Avenue
Akron, OH 44325-3909
USA

Kun Sup Hyun
New Jersey Institute of Technology
Otto H York Department of Chemical,
Biological & Pharmaceutical
Engineering
Polymer Processing Institute
GITC Bldg Suite 3901
University Heights
Newark, NJ 07102-1982
USA

Sadhan C. Jana
The University of Akron
Department of Polymer Engineering
250 South Forge Street
Akron, OH 44325-0301
USA

Eung Kyu Kim
The Dow Chemical Company
Materials Transformation Group
433 Building
Midland, MI 48667
USA

Myung-Ho Kim
Hannam University
MIC/MIRI
305-811 Daejeon
Korea

Nelson M. Larocca
Federal University of São Carlos
Department of Materials Engineering
Rodovia Washington Luís
km 235 - SP 310
São Carlos, SP 13565-905
Brazil

Ana V. Machado
University of Minho
Institute of Polymers and
Composites/I3N
Department of Polymer Engineering
4800 058 Guimarães
Portugal

Raman P. Patel
Teknor Apex Company
505 Central Avenue
Pawtucket, RI 02861
USA

Luiz Antonio Pessan
Federal University of São Carlos
Department of Materials Engineering
Rodovia Washington Luís
km 235 - SP 310
São Carlos, SP 13565-905
Brazil

Brendan Rodgers
ExxonMobil Chemical Company
Global Specialty Polymers
5200 Bayway Drive
Baytown, TX 77501-2101
USA

Jinwoong Shin
41 Magnolia Road
Sharon, MA 02067
USA

Leszek A. Utracki
National Research Council Canada
Industrial Materials Institute
75 de Mortagne
Boucherville, QC J4B 6Y4
Canada

James L. White[†]
The University of Akron
Department of Polymer Engineering
250 South Forge Street
Akron, OH 44325-0301
USA

1
Polymer Blend Compounding and Processing

James L. White and Sug Hun Bumm

1.1
Introduction and Early Studies of Blending

Humankind has been mixing together different materials since the dawn of written history to produce products with improved engineering properties. The term "Bronze Age" (which began around 3000 BC) indicated the blending of tin into copper to improve its mechanical performance. Concrete was also introduced by the ancients with similar purposes in mind.

The polymer industry as we know it dates only from the first part of the nineteenth century, where the major industrial polymers aside from wood were natural rubber (*cis*-1,4-polyisoprene) from Brazil, gutta-percha (*trans*-1,4-polyisoprene) from Singapore and Malaya from the 1840s, and natural fibers, including cellulose (cotton, linen) and protein (wool) fibers and leather. Many of the earliest patents involved coating fabrics and leather with natural rubber [1–6]. There was a gradual realization in this period of the usefulness, in terms of improving the properties or rubber, of introducing solid particulates [7–10] or chemicals such as sulfur and its compounds [10–13], which caused vulcanization/crosslinking.

It was only with the commercial appearance of gutta-percha in about 1845 [14–17] that there were investigations of polymer blends (gutta-percha with natural rubber). These were reported in patents of C. Hancock [17, 18], A. Parkes [13] and W. Brockedon and T. Hancock [19] in 1846. All of these inventors knew each other, Two were brothers (C. Hancock and T. Hancock) and two others (Brockedon and Parkes) were at the time business colleagues of the above T. Hancock. The patents cited above generally cite one or more of the others. This all took place in or near London, England.

The mixing processes are usually not critically discussed in these early patents. Brockedon and Hancock [19] indicate they used the single rotor masticating machine discussed in T. Hancock's earlier patents [6, 7]. One can conclude by reading their patents that C. Hancock and Parkes used the same or similar machines. Parkes [13] mentioned using rollers, perhaps similar to the machine of Chaffee's patent [5]. In addition, significant amounts of solvents derived from coal tar were used.

Encyclopedia of Polymer Blends: Volume 2: Processing, First Edition. Edited by Avraam I. Isayev.
© 2011 Wiley-VCH Verlag GmbH & Co. KGaA. Published 2011 by Wiley-VCH Verlag GmbH & Co. KGaA.

Blending technology developed slowly. The third processable polymer of the nineteenth century was cellulose nitrate, developed by Schonbein [20] as an explosive. An 1855 patent by Parkes [21] describes the blending of natural rubber and gutta-percha with a solution of cellulose nitrate, and fabricating the resultant sheets for various applications.

Cellulose nitrate was a particularly difficult material to work with because it could only be shaped when in solution. We find Parkes [22, 23] a decade later dissolving cellulose nitrate into organic oils, introducing his sulfur dichloride invention into the mix for crosslinking. He also used vegetable oils [22] and blended in camphor [23]. Further efforts to produce cellulose nitrate–camphor compounds were made in 1869–1872 patents of Spill [24, 25] and the Hyatt Brothers [26, 27]. Camphor was useful because it was not volatile and did not evaporate like vegetable oils, leading to residual stresses in products.

Blends involving synthetic polymers were not developed until the twentieth century. The first synthetic high molecular weight polymers were developed by Farbenfabriken Bayer in the first two decades of the twentieth century. These were the first synthetic elastomers. Poly(dimethyl butadiene), widely used in Germany, was used in World War I (Section 1.3.1).

1.2 Methods of Compounding

1.2.1 Batch Mixers

1.2.1.1 Introductory

The earliest blends developed that we discussed in Section 1.1 were prepared in batch mixers, notably T. Hancock's (1820–1838) masticator (or "Pickle" [6, 28]) or Chaffee's (1836) two roll mill [5]. The two roll mill was widely manufactured by machinery companies in the USA and Europe. It became the primary method of preparing compounds in the (natural) rubber industry well into the second decade of the twentieth century [29, 30].

Single-screw extruders seem to have been introduced in the 1870s, but were primarily used for wire coating and profiles.

These were not the only mixing machines developed in the nineteenth century. The food industry, especially the baking industry, had needs for such machines. This led Paul Pfleiderer and Hermann Werner to undertake the manufacture of batch mixers for this purpose in Stuttgart in Germany about 1880 [31–33]. Werner & Pfleiderer GmbH was organized and developed and manufactured a batch mixer based upon a twin rotor design due to Paul Pfleiderer [34]. This was marketed as a "Universal Misch und Knet Maschine." This is shown in Figure 1.1 and is essentially a double rotor mixer open to the environment. Werner & Pfleiderer subsequently became an international company. They set up Werner & Pfleiderer, Ltd. in London and merged in 1893 with A. M. Perkins and Son of London (whose principal had

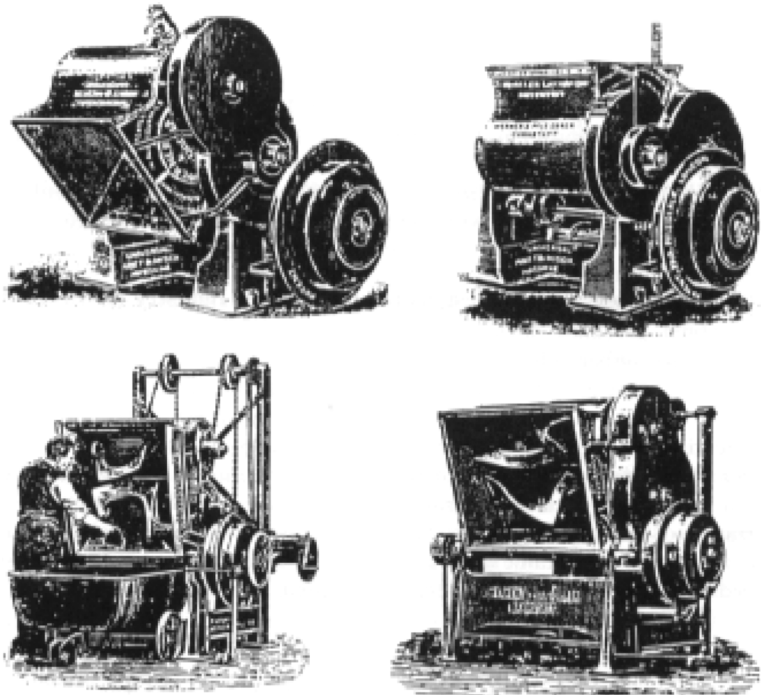

Figure 1.1 Werner & Pfleiderer 1895 Universal Misch und Knet Maschine.

recently died) to form Werner, Pfleiderer and Perkins [31, 33]. They then had manufacturing facilities in England and could trade within the British Empire.

This seems to have been masterminded by Paul Pfleiderer, who had already moved to England and would manage the company. Hermann Werner remained in Stuttgart. The Perkins family largely withdrew from this company.

In 1897, Werner & Pfleiderer GmbH, presumably together with Werner, Pfleiderer and Perkins, established a manufacturing facility in the United States in Saginaw, Michigan. They, however, lost both their English and American facilities in World War I.

1.2.1.2 **Non-intermeshing Rotor Mixers**

Werner & Pfleiderer sought to broaden their mixing activities beyond baking dough to industrial materials in general. The internal combustion engine based automobile had its origins in Stuttgart with Gottfried Daimler. The automobile would need tires, which would be largely made out of vulcanized rubber–small particulate compounds. Soon, rubber product manufacturers around the world were trying to produce tires for automobile manufacturers. Most of the mixing at first used large two roll mills [29, 30]. Werner & Pfleiderer GmbH then sought to develop an internal mixer for rubber compounding. It required sturdier rotors than those of Figure 1.1. Such an internal mixer was developed by Kempter [35, 36]. Figure 1.2 shows a 1910 Werner & Pfleiderer Universal Gummi Kneter [32].

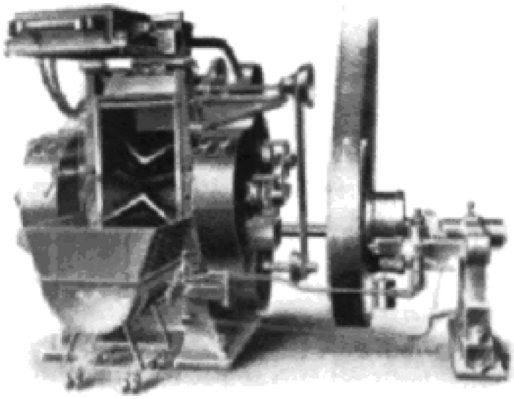

Figure 1.2 Werner & Pfleiderer 1910 Universal Gummi Kneter.

As Paul Pfleiderer had become ill in the late 1890s, he along with Hermann Werner decided that he would be replaced at Werner, Pfleiderer and Perkins by F. C. Ihlee. Pfleiderer's son Kurt also worked at the firm. Paul Pfleiderer died in 1903.

Werner, Pfleiderer and Perkins was also concerned with the new tire industry and its needs for mixing machines. D.H. Killheffer [30] describes Banbury's various meetings with Kurt Pfleiderer and of being convinced by him to join Werner & Pfleiderer in Saginaw, Michigan. Banbury was sent to Werner, Pfleiderer and Perkins' facility in Peterborugh, England, where he met with F.C. Ihlee and the chief engineer, J. H. Pointon. This was in late 1913. Banbury later stated that he designed a new set of rotors and these gave improved mixing performance [30]. The rotors were then patented by Pointon in his own name [37], to Banbury's dismay [30].

Banbury now returned to the USA and was soon visiting Werner & Pfleiderer customers. He found there were various problems, including the mixer being open to the atmosphere and the design of the rotors. The mixer's large opening not only lowered the ability of the rotors to mix the compound but allowed various chemicals in the compound, notably amine accelerators, to escape into the atmosphere and poison workers. Banbury saw that the introduction of a ram into the mixer's opening to push the rubber into the rotors would substantially improve the mixing and improve the safety of the workers. In the fall of 1915, he wrote a patent application on an internal mixer with a ram. However, the management of the Saginaw based Werner & Pfleiderer refused to file the application. Banbury then resigned from the firm.

Banbury filed his patent [38] in January 1916 in the United States and sought a new machinery manufacturer to support his efforts [30]. He found this support from the Wanning family and their Birmingham Iron Foundry of Ansonia, CT, to whom he assigned his patent. Banbury was able to negotiate that his name would be associated with the mixer as a trademark. The Banbury® Mixer was born. Banbury's patent drawing showing a mixing chamber with a ram is given in Figure 1.3 [38].

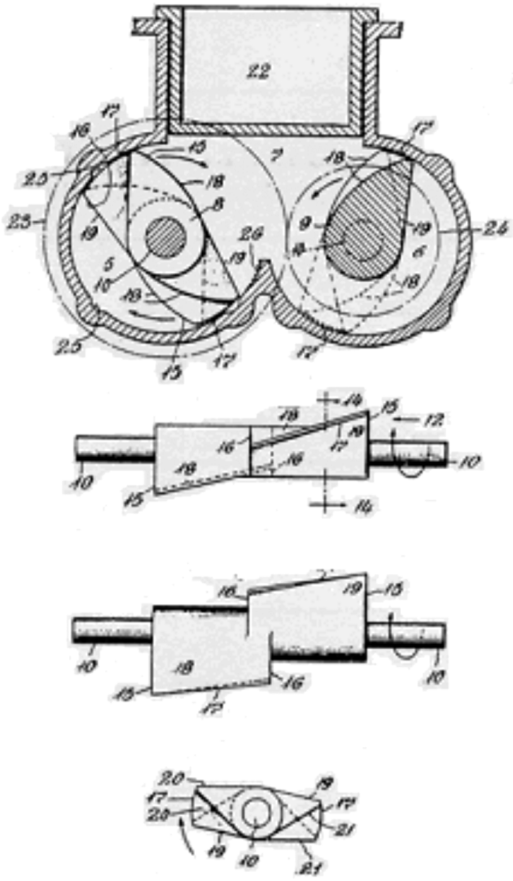

Figure 1.3 Banbury's 1915 US patent drawing showing a ram and mixing chamber. From Reference [38].

Banbury now worked out a more detailed design of his internal mixer, including the ram system, a mixing chamber with a bottom door and cooling channels, a feeding system, and take-off equipment for compounding rubber. These are described in several patent applications that were filed beginning in late 1916 [39–42]. Figures 1.4 and 1.5 show more comprehensive descriptions of Banbury's internal mixer design.

The Banbury mixer prospered through the 1920s, but not the Wanning family that owned the Birmingham Iron Foundry. In 1927, it was merged with Farrel Foundry and Machine to form Farrel Birmingham (later Farrel Inc.). They continued to manufacture the Banbury mixer [30].

1.2.1.3 **Intermeshing Rotor Mixers**

In the 1930s, there was a major innovation in the rubber industry with the invention of intermeshing rotor internal mixers. A June 1934 British patent

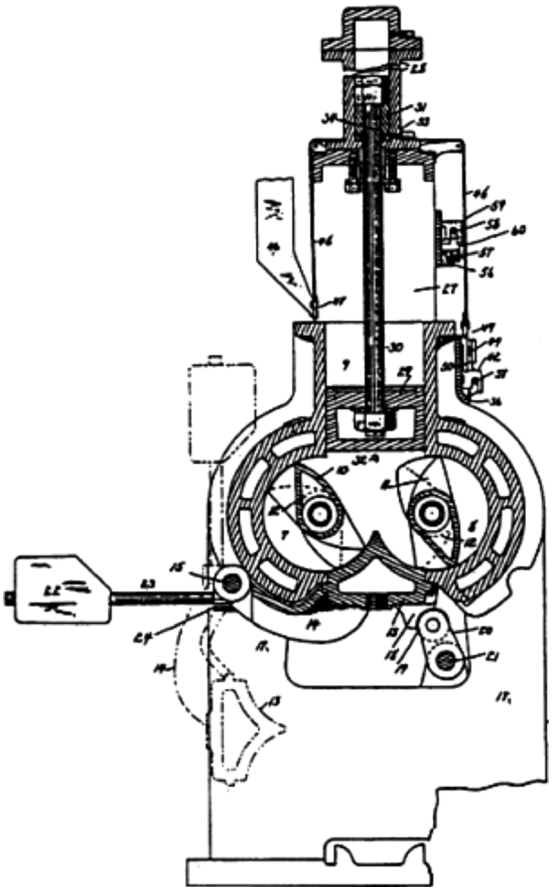

Figure 1.4 Banbury's November 18, 1916 US patent application drawing showing internal mixer ram system and mixing chamber with door. From Reference [39].

application by R.T. Cooke [43] described such a machine (Figure 1.6). High shear stresses were applied to the compounds between the rotors as well as between the rotor and the mixing chamber wall. The design of the remainder of the machine, which also has a ram, followed the ideas contained in Banbury's earlier patents [39–42]. An October 1934 German patent application of A. Lasch and E. Stromer [44] of Werner & Pfleiderer GmbH also has intermeshing rotors. The design of this machine has no ram. Cooke's intermeshing internal mixer was soon commercialized by Francis Shaw and Company as Shaw Intermix. In the years that followed, the Shaw Intermix and a similar intermeshing machine developed by Werner & Pfleiderer GmbH [45] obtained a major position in the rubber mechanical goods industry, especially in Europe, for products such seals, gaskets, and timing belts. The machines were not successful in the tire industry, where the lower mixing chamber volumes compared to Banbury's design were viewed unfavorably.

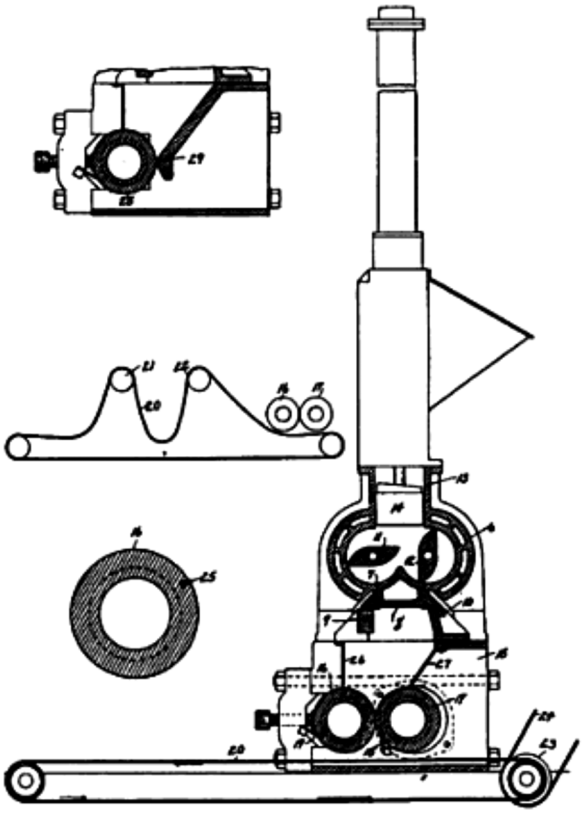

Figure 1.5 Banbury's January 31, 1921 US patent application drawing showing internal mixer with keep section, sheeting rolls, and continuous apron following discharge. From Reference [42].

1.2.1.4 **Post-World War II Development**

A new direction in the design of the separated rotor internal mixers came with the doubling of the number of flights on the rotors from two to four. This was first done by Lasch and Frei of Werner & Pfleiderer in an October 1939 patent application [46] (Figure 1.7a). A second four-flighted rotor design was contained in a January 1964 patent application of Tyson and Comper [47] of Goodyear (Figure 1.7b). This patent seems to have been licensed to Farrel-Birmingham/Farrel Inc. who then manufactured machines of this design. In the post-war period, Farrel Inc. set up new licensees in Asia and Europe. Kobe Steel of Kobe, Japan became a licensee in Asia and Pomini of Castellanza, Italy became a licensee in Europe. Both began manufacturing internal mixers of Farrel design. Kobe Steel and its largest customer, the Bridgestone Tire Company of Tokyo, concluded that the two-flighted and four-flighted Banbury mixer rotors were not of optimal design. In the 1970s, they carried out a joint research program that included flow visualization of a polymer solution with polystyrene beads in a transparent glassy poly(methyl methacrylate) internal mixer. The flight lengths and angles of the rotors were varied. This was described in a patent

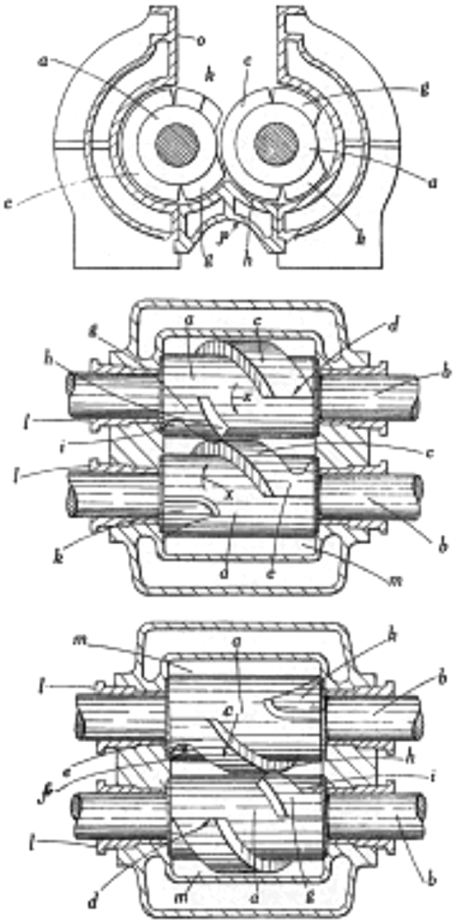

Figure 1.6 Cook's June 14 1934 British patent application drawing for an internal mixer with intermeshing rotor. From Reference [43].

application by N. Sato *et al.*, representing both Bridgestone and Kobe Steel, in a June 1979 US patent application [48] and by Kobe Steel's, Asai *et al.* in a subsequent presentation [49] at the International Rubber Conference in Paris in 1983 (Figure 1.7c). They concluded that the best results are obtained when the ratio of the lengths of the short to long flight are 0.15–0.3. However, ratios of greater than 0.4 are not recommended because longer flights are too dominant. Too much thrust load is created on the rotors in the chamber and this also leads to overheating. A second Sato *et al.* US patent application [50] is similar to the first one.

Other Kobe Steel patents followed. In a February 1981 US patent application, Inoue *et al.* [51] described a pair of juxtaposed double flighted rotors. In an August 1986, patent application Asai and Hagiwara [52] described a new double flighted rotor design. The intention was to increase the rotor tip flight clearance to values greater

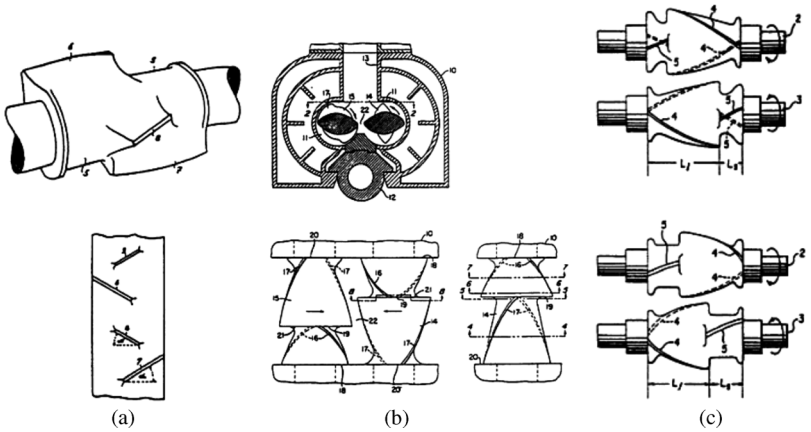

Figure 1.7 Four flighted non-intermeshing rotors: (a) Lasch and Frei 1938 design; (b) Tyson and Comper 1964 design; (c) Sato *et al.* 1979 design.

than those used for conventional mixing. They sought to increase rotor speed and machine productivity. In 1988, Kobe Steel acquired the Stewart Bolling Company (based in Cleveland, Ohio), a small manufacturer of internal mixers. They established a new manufacturing site in Hudson, Ohio (near Akron, Ohio) near Goodyear plus Bridgestone-Firestone, the American subsidiary of Bridgestone. The licensing relationship with Farrel had ended in 1985.

There have also been new designs of internal mixer rotors, notably by Millauer [53] of Werner & Pfleiderer (Figure 1.8a) and Johnson *et al.* [54] of Francis Shaw (Figure 1.8b). Passoni [55] of Pomini has described a completely new design of intermeshing rotor internal mixer in which the rotor inter-axial distances may be

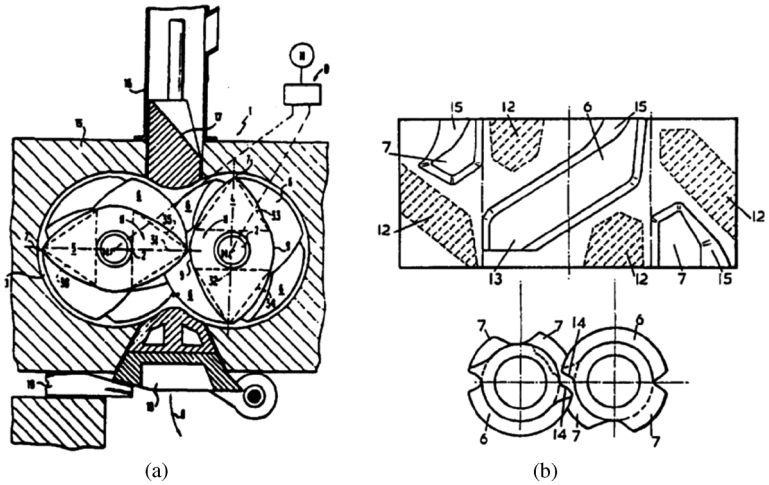

Figure 1.8 Post-Cooke intermeshing internal mixer rotors: (a) Millauer [53]; (b) Johnson *et al.* [54].

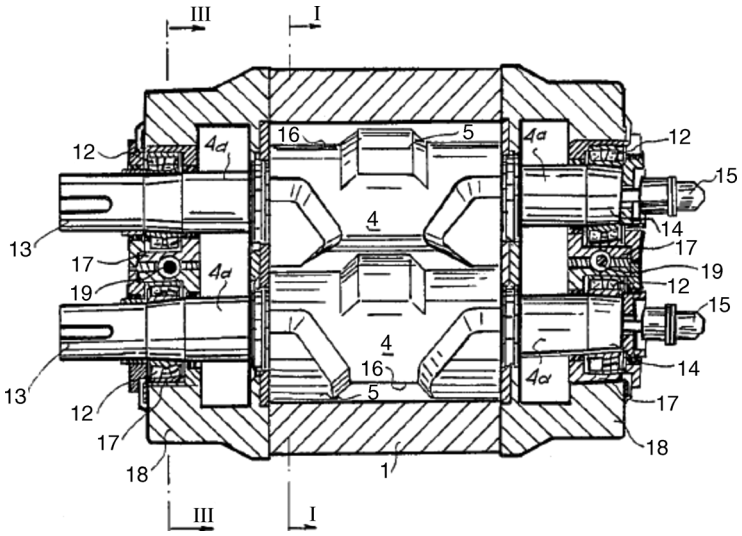

Figure 1.9 Passoni's [55] variable clearance intermeshing internal mixer.

varied for the preparation of different compounds or during the mixing cycle itself for different compounds (Figure 1.9). Again the licensing relationship with Farrel had ended in 1985.

1.2.2 Continuous Mixers

1.2.2.1 Early Activities

The earliest description of a continuous mixer appeared in an 1882 patent of Paul Pfleiderer (Figure 1.10) [56]. It was certainly intended for dough in a large bakery. It contains two non-intermeshing counter-rotating shafts with sigma blade and screw sections.

Single-screw extruders dominated continuous blending and compounding in the first part of the twentieth century and, indeed, through the 1960s. More sophisticated

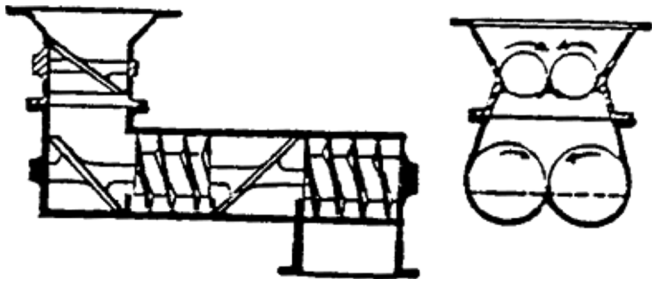

Figure 1.10 Pfleiderer's [56] continuous mixer.

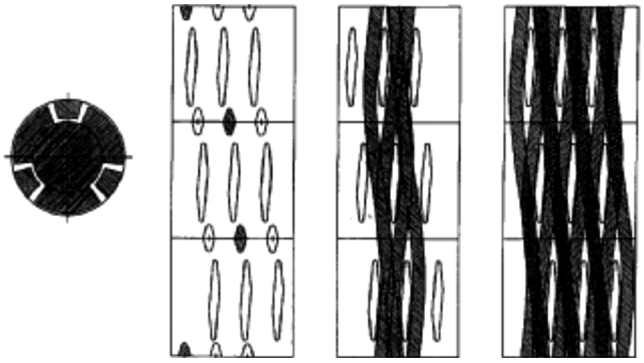

Figure 1.11 Buss Kokneter.

machine devices for mastication, compounding, and blending occur in the patent literature in the 1930s and 1940s [57–71]. Some are single screw devices such as List's Buss Kokneter. These include the intermeshing counter-rotating kneading pumps of the IG Farbenindustrie [58–62] and Maschinenfabrik Paul Leistritz [63–65], the "Knetwolf" of Krupp [66–68], and the modular tangential counter-rotating twin-screw extruder of Welding Engineers [71]. These machines have been reviewed in the books of Herrmann [67] and White [68]. Of these early machines only the Buss Kokneter (Figure 1.11) [69, 70] and the Welding Engineers modular tangential counter-rotating screw extruder (Figure 1.12) [71] survived and were successful.

1.2.2.2 **Single-Screw Extrusion**

Many modified screw designs for improved mixing have appeared in the patent literature [72–76]. Some of these designs are shown in Figure 1.13. In the last 30 years of the twentieth century it was realized that twin screw machines were better continuous mixers.

1.2.2.3 **Co-rotating Twin-Screw Extrusion**

The concept of a self-wiping co-rotating twin-screw extruder dates to the beginning of the twentieth century (Figure 1.14) [77, 78]. However, an intermeshing co-rotating twin-screw extruder was not commercialized until 1939. This was initiated by Roberto Colombo [79] and Lavorazione Materie Plastische (LMP) in Turin, Italy.

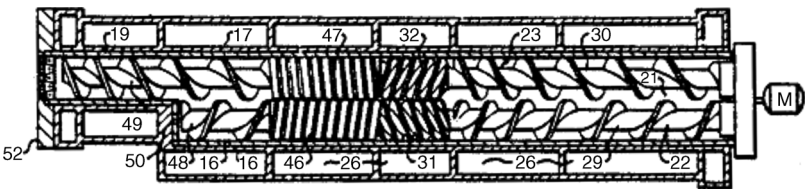

Figure 1.12 Fuller Welding Engineering modular tangential counter-rotating twin-screw extruder [71].

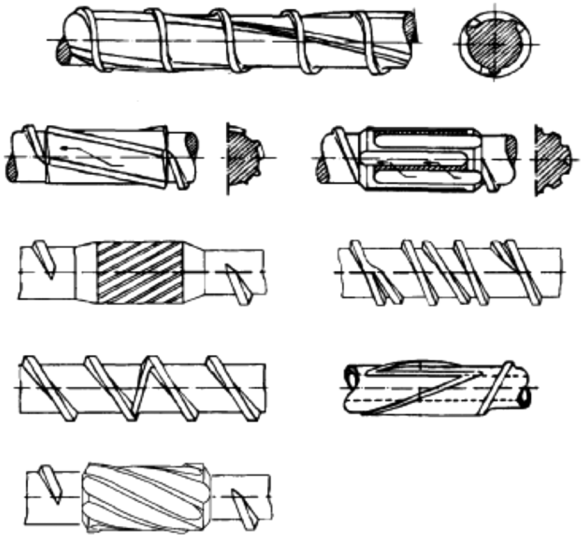

Figure 1.13 Mixing screw sections for single-screw extruders [77].

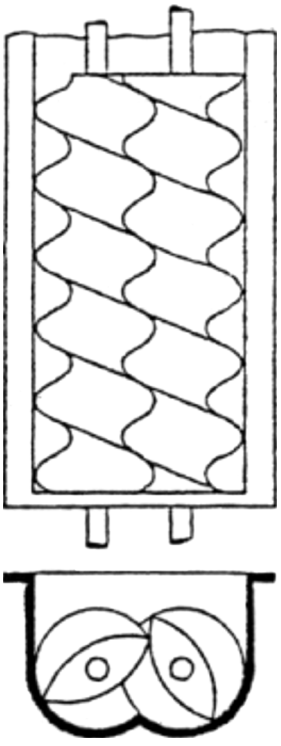

Figure 1.14 Wunsche 1901 self-wiping co-rotating twin-screw extruder.

Several of these machines were purchased by the IG Farbenindustrie and applied to reactive extrusion [80], dewatering [81], and kneading [82]. The most enthusiastic supporters of this machine in IG Farbenindustrie were Walter Meskat, Rudolf Erdmenger, and A. Geberg at the Wolfen Works on the Elbe River [81, 82]. They believed it would be much better if the screws were self-wiping and Geberg devised mathematical formulae for the necessary screw cross-section, a problem previously developed by Wunsche [77].

Following World War II, Meskat and Erdmenger were able to escape to the British zone and obtain positions in the re-invented Farbenfabriken Bayer, working for their former Wolfen Works manager, Kurt Riess. Meskat based in Dormagen and Erdmenger in Leverkusen set out with their new coworkers to develop a new generation of intermeshing co-rotating machines. As soon as the German patent office was back in operation in July 1949, Meskat and Erdmenger began submitting patent applications [83–86]. The second of these patents by Erdmenger was for a continuous twin rotor kneading disc block mixing machine [84] and the third for a twin screw devolatilizer [85]. Meskat and Pawlowski [86] on December 10, 1950 filed a patent for a modular co-rotating twin-screw extruder (Figure 1.15). In August 1958 Erdmenger filed for a German patent on a machine with screw and kneading disc blocks and in August 1959 for an American patent. The German patent application was rejected and the US patent application accepted [87]. Figure 1.16 shows the Erdmenger machine.

Notably, these were not the only co-rotating twin screw extrusion patents. Colombo and LMP filed for patents in France, Switzerland [88], and Germany [89] in the early 1940s and after the WWII in England [90], USA [91], and Canada [92]. These expanded on his 1939 Italian patent [79]. They had various screw designs and machine designs including six- and eight-screw machines. The machines seemed to be intended by the inventor to be profile extruders. W. Ellermann [93, 94] now based in Dusseldorf, who had invented the Krupp "Knetwolf" [66–68], filed patent applications on intermeshing counter-rotating and co-rotating machined shaft continuous mixers.

The Bayer co-rotating twin screw technology was licensed in the mid-1950s to Werner & Pfleiderer GmbH (now Coperion) of Stuttgart (Figure 1.17) [95].

At about the same the time, the Ellermann machine was licensed to Krauss-Maffei of Munich (Figure 1.18) [96] and later to the Japan Steel Works. When the Bayer AGs patent system expired in the early 1970s, other machinery manufacturers began to

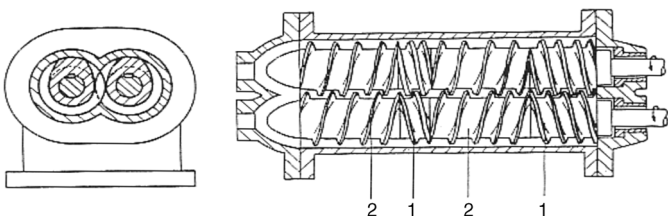

Figure 1.15 Meskat–Pawlowski modular co-rotating twin-screw extruder [86].

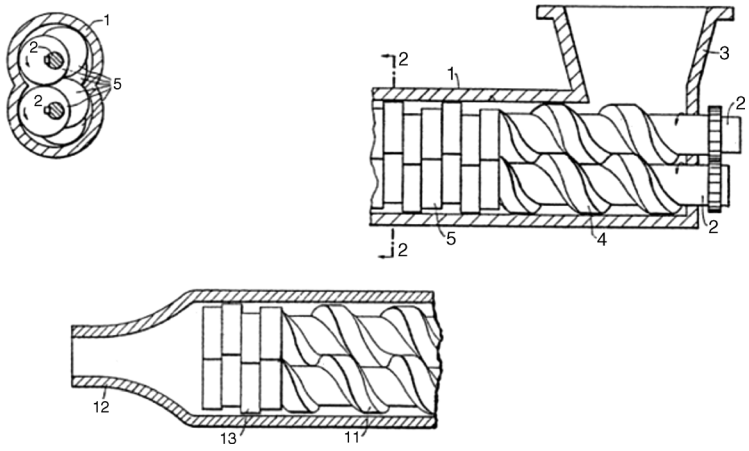

Figure 1.16 Erdmenger 1958 modular co-rotating twin-screw extruder [87].

produce modular co-rotating twin-screw extruders. These included Berstorff of Hannover, Germany; Leistritz AG of Nuremberg, Germany; Farrel Inc. of Ansonia; CT, USA; Japan Steel Works, Kobe Steel, and Toshiba Machine of Japan; in total more than 50 concerns around the world.

New mixing elements have been devised more recently, including (i) "Banbury Mixer" similar rotors by Kobe Steel and Farrel Inc. [97, 98] to be used in place of kneading disc blocks and (ii) special milder mixing in elements by Berstorff and Werner & Pfleiderer [99–101] to be used in place of kneading disc blocks for specific applications such as brittle glass fibers. Baker Perkins was in this period a major stockholder in Werner & Pfleiderer. They began to manufacture these machines on their own in the 1960s [102].

There have been many efforts directed towards modeling flow, both in individual modules [103–105] and in composite modular machines [103, 106–109]. The latter models can predict fill factor and pressure and temperature profiles along the screws.

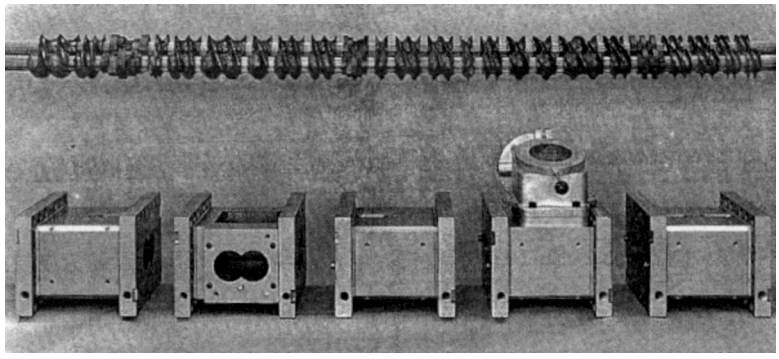

Figure 1.17 Werner & Pfleiderer ZSK modular co-rotating twin-screw extruder.

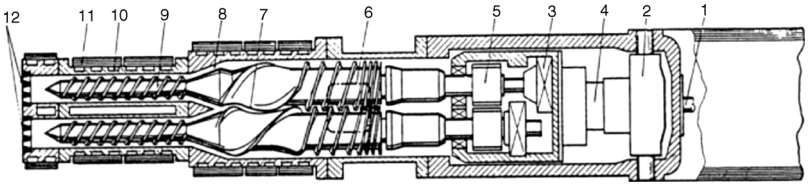

Figure 1.18 Ellermann machine licensed to Krauss-Maffei.

1.2.2.4 **Tangential Counter-Rotating Twin-Screw Extrusion**

Tangential counter-rotating twin-screw extruders begin with the patents of Fuller [71] and later Street [110] in the 1940s and 1950s. This machine is shown in Figure 1.18. The tangential counter-rotating twin-screw extruder was widely discussed and used from about 1950. From the 1960s it has received more attention from the chemical processing industry [111, 112] as opposed to it being used for polymer blending. Many efforts have been made to simulate the flow in individual modules of the machine [113–115] as well as composite models of the mixing and metering section near the machine exit [115].

A second non-intermeshing counter-rotating twin-screw extruder is the Farrel Continuous Mixer™ (Figure 1.19) [116, 117]. It has rotors consisting of screws leading to Banbury-like rotors. It was originally intended to be a continuous Banbury Mixer for the tire industry but met with greater success in the compounding and polymerization industries.

These machines were also produced by Kobe Steel and Pomini. Various calculations have been made to analyze the flow in their mixing, including fill factors and pressure profiles [118, 119].

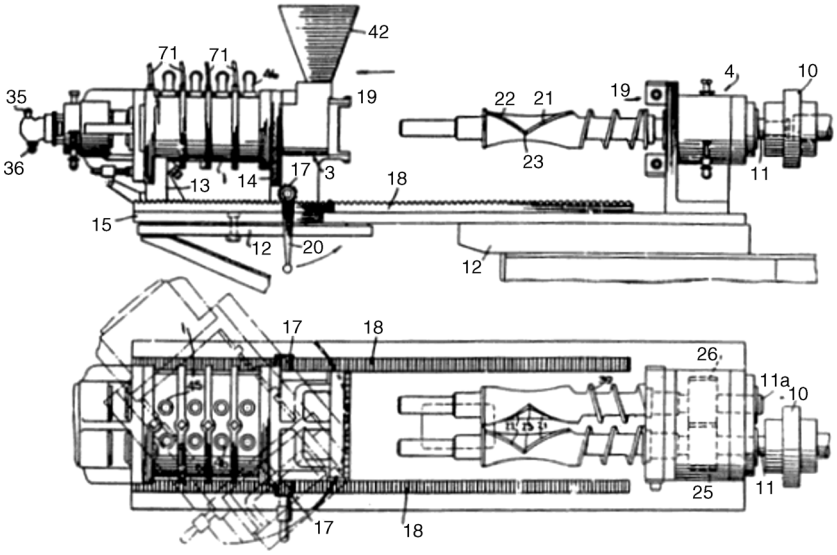

Figure 1.19 Farrel Continuous Mixer [116].

1.2.2.5 Modular Intermeshing Counter-Rotating Twin-Screw Mixer

Early intermeshing counter-rotating twin-screw mixers including the Krupp Knetwolf [66, 68] and Ellermann's post-World War II 1951 Eck Mixtruder [88], did not prove successful. The Leistritz modular intermeshing counter rotating twin-screw extruder (Figure 1.20) of Tenner [120] and Thiele [121–123] (GG and Counterflight models) have proven more successful [124]. These machines were developed from the 1960s through to the 1990s.

1.2.2.6 Modular Buss Kokneter

The modular Buss Kokneter [125–128] is an excellent distributive mixer that is widely used in the food and polymer industries (Figure 1.21). It consists of a single screw with slices in its flights in a barrel containing pins or clogs. The screw both rotates and reciprocates in such a manner as to be self-wiping. The individual modules are designed for melt pumping, mixing, and melting. This machine has been analyzed for flow both in individual elements and global behavior [129, 130].

1.2.3 Comparisons

There are very few comparisons of different types of mixers. It is worth summarizing what we do know. We begin with batch mixers. Obviously, the Banbury design internal mixers were found to be superior to the Werner & Pfleiderer Gummikneter. In comparing two-flight and four-flight rotors in Banbury design internal mixers,

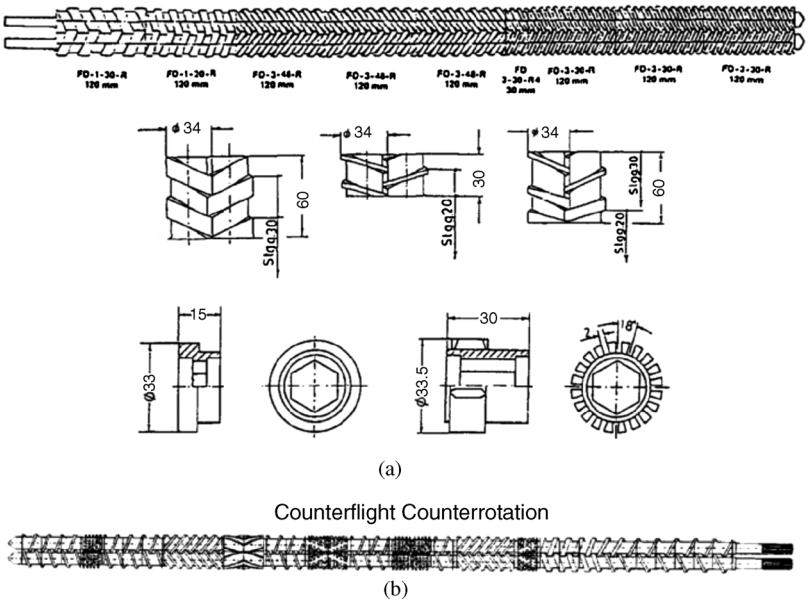

Figure 1.20 Leistritz modular intermeshing counter-rotating twin-screw extruders [120–124]: (a) Tenner GG machine; (b) Thiele counter flight machine.

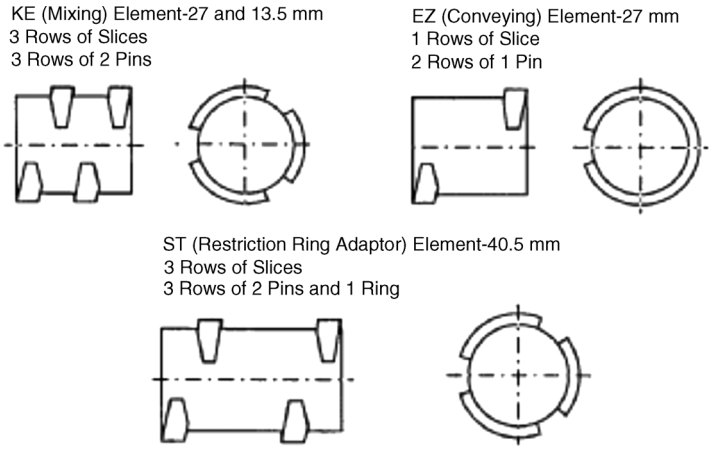

Figure 1.21 Modular Buss Kokneter Elements.

various patents describe four-flighted rotors as providing both better mixing and greater heat buildup. A clear comparison of two- and four-flighted rotors was given by Cho *et al.* [131] in a 1997 paper showing the superior mixing ability of the four-flighted rotors.

Turning now to intermeshing rotor machines versus Banbury-type separate rotor machines, we find the various manufacturers defending their designs. P. S. Kim and J. L. White [132] have published experimental studies showing that intermeshing rotor internal mixers are much superior to separated rotor machines in dispersive mixing. Machine manufacturers (e.g., Techint Pomini) claim they have better heat transfer because of the lower operating temperatures than FH Banbury design machine because they have much more machine surface area. Mixing of rubber mechanical goods in Europe and East Asia is carried out in intermeshing rotor machines and tire compounds in separated rotor machines. The separated rotor machines are preferred by the tire industry because of their larger mixing chamber volumes.

We now turn to continuous mixers. Again, we must be concerned about the claims of machinery manufacturers. In recent years, Shon *et al.* have made comparative studies of the mixing of glass fibers [133] and small particulates [134] into polymer melt matrices as well as dispersive mixing of blends [135]. They seek to compare machine characteristics with regard to dispersive mixing and glass fiber breakage. They found the severity (breakage of glass fibers, fineness of dispersion) of the mixing machines to order as Leistritz GG Intermeshing counter-rotating > Intermeshing co-rotating > Buss Kokneter.

However, the results depend on the arrangement of the modular elements. The modular co-rotating machine is much milder in the absence of kneading disc blocks.

Generally, continuous mixers are superior to batch mixers. The compounds are more uniform have superior mechanical properties and much shorter residence times [135, 136]. The major continuous mixers used commercially in 2009 for compounding and blending are modular co-rotating self-wiping twin-screw extruders.

1.3
Processing Polymer Blends

1.3.1
Early Synthetic Polymer Blends

As described in Section 1.1, the first commercial polymers, which were naturally occurring, were polyisoprenes (natural rubber and gutta-percha) and subsequently cellulose derivatives. From the early twentieth century, various totally synthetic polymers were introduced. Farbenfabriken Bayer introduced bulk polymerized totally synthetic elastomers in 1910. Poly(dimethyl butadiene) synthetic rubber was produced commercially by Bayer in Leverkusen during World War I. The 1920s saw the commercial development of polystyrene (PS) and poly(vinyl chloride) (PVC). In 1934, the IG Farbenindustrie (a combine of Bayer, BASF, Hoechst, and other firms) began to commercially manufacture butadiene–acrylonitrile copolymer (NBR) as an oil resistant rubber and in 1937 butadiene–styrene copolymer (SBR) intended for pneumatic tires.

Blends of the natural rubber and the new synthetic elastomers must have been studied by the I.G. Farbenindustrie and various German rubber fabricators such as Continental Gummi-Werke in the 1930s. Perhaps the first widely used synthetic polymer blend was the NBR–poly(vinyl chloride) system. NBR was widely used in under the hood applications in automobiles. It aged badly because of ozone attack in these applications. Introducing PVC into NBR improved its aging at some expense in stiffening. The IG Farbenindustrie would seem to have marketed NBR grades that were blends [137]. NBR is miscible with PVC so it would seem that this was a feasible solution at the time. In the 1940s, the United States went into large-scale production of butadiene styrene and acrylonitrile elastomers (SBR and NBR). Polystyrene (PS) and styrene–acrylonitrile copolymer (SAN) also became major commercial polymers. Both were brittle and tougher rubber modified blends were developed. Notably, high-impact polystyrene (HIPS) and ABS resins were devised by introducing polybutadiene or its copolymers (SBR and NBR). These new blends were in time optimized by producing them by polymerizing monomer solutions of the elastomers. Research activities on improving the properties of polymers by blending have continued since that time.

From the 1960s onwards there have been extensive investigations of polymers blends in both industrial and academic laboratories around the world.

1.3.2
General Ideas and Stability of Blend Phase Morphology

Polymer melt blends may be miscible or immiscible. Miscible blends form solutions and there is no phase morphology to be of concern. Immiscible blends are characterized by two or more phases that are separated by interfaces. Most polymer blend systems are immiscible because of the low entropies of mixing associated with mixing chain-like molecules to produce homogeneous solution.

The interface between two phases in a liquid system is characterized by an interfacial tension (κ), which seeks to control the interface shape and coalesce with other dispersed phase. The interfacial tension is generally resisted by the melt viscosity, which slows the changes the interfacial tension seeks to achieve.

Notably, interfacial tension in two-phase low viscosity systems has been recognized and studied since the nineteenth century. Indeed Clerk Maxwell [138] discussed it in an 1879 *Encyclopedia Britannica* review. Various researchers developed methods and made measurements of the interfacial tension in the nineteenth century and early twentieth century. Measurements for combinations of polymer melts, however, date back only to the 1960s [139–142] and generally accepted values were available by the 1990s [143–146]. We summarize data for various binary systems in Table 1.1.

When the interfacial tension goes to zero, the blend becomes miscible. Large interfacial tensions lead to unstable interfaces, especially when the viscosity is low. This leads to coalescence phenomena, which are best known in "salad dressing" but also occur in polymer melt blends.

It is possible to modify the interfaces between liquids with specific additives. This was discovered by ancient and medieval investigators and applied in the form of soaps, and later in food technology and in the application of dyes. The mechanisms of these additives only came to be realized in about 1900. Such additives are generally molecules with hydrophobic and hydrophilic sections that align along interfaces between the two liquid phases. They reduce interfacial tension and stabilize phase morphology to smaller dispersed phase sites. This phenomenon was realized by IG Farbenindustrie chemists who applied it in the late 1920s in emulsion polymerization that they used to produce synthetic rubber.

As described in Section 1.3.1, many polymer blends were developed in the years following World War I. By the 1960s, there was interest in understanding the interfaces between the individual polymers in the blends. It came to be realized that in some of the successful blend systems such as HIPS and ABS resins there were substantial amounts of graft copolymer products at the interface between the polymer phases.

Table 1.1 Interfacial tension (κ) between polymer melts based upon the breaking thread method (Yoon and White [146]).

Polymer 1	Polymer 2	Temperature (°C)	κ (dyne cm^{-1})
Polyethylene	Polystyrene	290	5.0
Polyethylene	Polysulfone	290	6.5
Polyethylene	Poly(*p*-phenylene sulfide)	290	7.2
Polyethylene	Poly(ethylene terephthalate)	290	9.2
Polyethylene	Poly(bisphenol A carbonate)	290	13.0
Polyethylene	Polyamide 6	290	13.2
Poly(*p*-phenylene sulfide)	Polysulfone	290	1.6
Poly(*p*-phenylene sulfide)	Polycarbonate	290	3.5
Poly(*p*-phenylene sulfide)	Polyamide 6	290	9.9

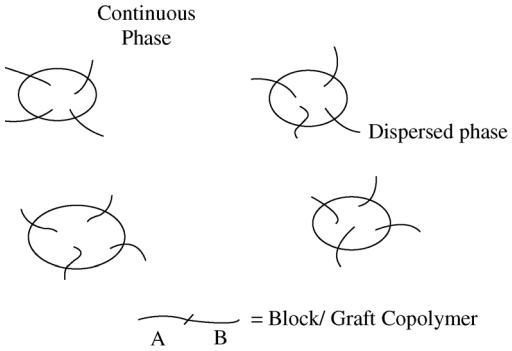

Figure 1.22 Compatibilized dispersed polymer blend phase showing compatibilizing agents.

This led to extensive investigations of polymeric interfacial agents, increasingly known as "compatibilizing agents," in polymer blends [145, 147–152]. These produced a reduction in dispersed phase size, enhanced phase stability, and increased mechanical properties (Figure 1.22). These were invariably block and graft copolymers. The property enhancement is due to their occupying the blend interface and having long chains in each phase. Subsequently, various investigators [145, 153] measured the interfacial tensions in these compatibilized blends and found that they were significantly reduced when appropriate compatibilizing agent were introduced. Typical results are shown in Table 1.2, where great reductions interfacial tension of polyethylene/poly(ethylene terephthalate) (PET) produced by the introduction of compatibilizing agents can be seen. Note the effectiveness of the maleated polymers, which react with the PET chain ends to produce block copolymers.

Generally, phase morphologies produced in blending involve disperse phases sizes that vary with interfacial tension, κ, or with the dimensionless group $\kappa/\eta v$ or $\kappa/\sigma_{12}d$, where η is viscosity, v is velocity, and σ_{12} a shear stress [154, 155]. This dimensionless group represents a ratio of interfacial to viscous forces.

Table 1.2 Interfacial tension (κ) between polymer melts in compatibilized blend systems [153].

Polymer 1	Polymer 2	Additive (5pt)	Temperature (°C)	κ (dyne cm^{-1})
Polyethylene	Poly(ethylene terephthalate) (PET)	—	270	9.7
Polyethylene	PET	PBT-*b*-PE copolymer	270	1.7
Polyethylene	PET	Maleated HDPE (high density polyethylene)	270	1.9
Polyethylene	PET	SEBS (styrene–ethylene/ butylene–styrene)	270	7.5
Polyethylene	PET	Maleated SEBS	270	1.8

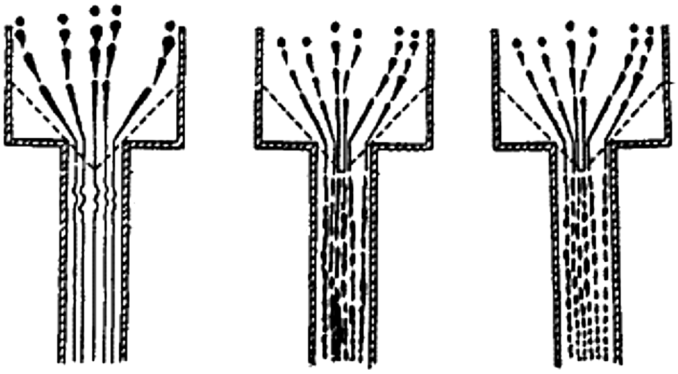

Figure 1.23 Formation of mini-fibers in melt spinning.

1.3.3 Phase Morphology Variations in Processing Operations

1.3.3.1 Melt Spinning

The phase morphology of polymer blends shows significant variations in polymer melt processing. One of the most striking observations is the formation of mini-fibers in melt spun blends (Figure 1.23), where the blend experiences uniaxial elongational flow. If the major phase can be dissolved away, these mini-fibers can be isolated [156, 157]. Experiments of this type have notably been carried out by Japanese fiber companies since 1970 in trying to produces small diameter fibers for luxury clothing. One published study of this type involves the formation of polyethylene mini-fibers (0.2 μm) from polyethylene/polystyrene blends by Min *et al.* (Figure 1.24) [158].

Mini-fibers have also been observed by Liang *et al.* [159] on melt spinning polypropylene/polyamide blends. The diameters of the dispersed polyamide 6 phase mini-fibers are tens of microns and more. This is clearly due to the large interfacial tension in this system (polypropylene/polyamide 6) as compared to polyethylene/polystyrene blends of Min *et al.* (Table 1.1).

1.3.3.2 Die Extrusion

Another geometry that has received some study is extrusion through dies. In flow through a die, there is Poiseuille flow with high shear stress near the die wall and low shear stresses at the center-line or center-plane. The situation here is more complex than in melt spinning because of the distributions across the die radius. Generally, dispersed phase droplets at high radii in a cylindrical die where shear stresses and shear rates are large are stretched out into long filaments. However, at the center-line, where deformation rates and shear stresses are small and near zero, the dispersed phase is not stretched out and remains as nearly isotropic droplets [160].

Figure 1.24 Polyethylene mini-fibers produced from polyethylene/polystyrene blends.

1.3.3.3 Injection Molding

Injection molded parts also exhibit blend morphology variations associated with melt processing. These tend to be more complex than those described earlier. As a hot blend melt moves through a cold mold, the dispersed phase in regions near the mold

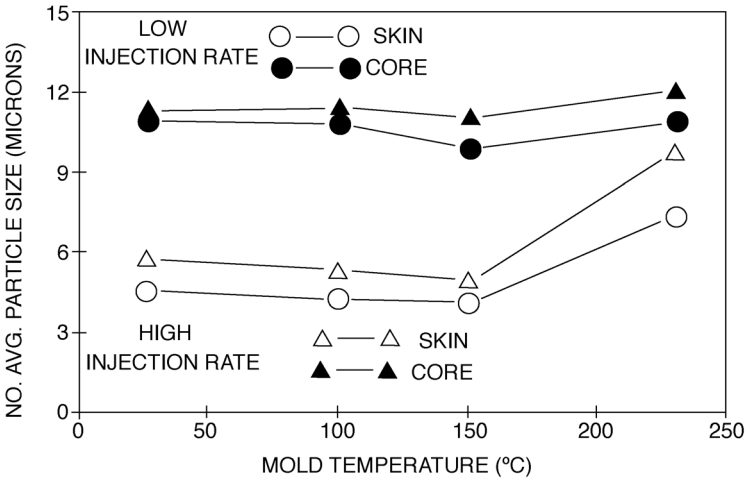

Figure 1.25 Dispersed number average phase size as a function of injection rate and mold temperature for an 80/20 polyamide 6/HDPE injection molded blend.

wall tends to be drawn out more than in the low deformation rate core region. However, the moving melt front has a fountain like flow that deposits isotropic core melt blend on the mold walls. The result is that the greatest blend anisotropy is not in the skin layer but at intermediate positions between the core and the mold wall.

Ghiam and White [161] have studied this behavior in the injection molding of blends of polyethylene and polyamide 6, which as we have already seen has a high interfacial tension. Figure 1.25 shows that the smallest dispersed phase is in the high stress region near the mold wall and a much coarser morphology exists in the core [161]. If the mold temperature is maintained above the melting temperatures, coalescence proceeds. It has been observed that the greatest coalescence occurs not in the layer near the wall rather than in the core.

References

1 Macintosh, C. (1823) English Patent 4804.
2 Fleetwood, C.B. (1824) English Patent 4915.
3 Hancock, T. (1825) English Patent 5120.
4 Hancock, T. (1830) English Patent 5970.
5 Chaffee, E.M. (1836) US Patent 16.
6 Hancock, T. (1837) English Patent 7344.
7 Hancock, T. (1838) English Patent 7549.
8 Fansanwe, J.A. (1841) English Patent 9189.
9 Hancock, W. (1843) English Patent 9935.
10 Hancock, T. (1843) English Patent 9952.
11 Hayward, N. (1839) US Patent 1090.
12 Goodyear, C. (1844) US Patent 3633.
13 Parkes, A. (1846) English Patent 11,147.
14 Brooman, R.A. (1845) English Patent 10,582.
15 Nickels, C. (1845) English Patent 10,673.
16 Bewley, H. (1845) English Patent 10,825.
17 Hancock, C. (1846) English Patent 11,032.
18 Hancock, C. (1846) English Patent 11,208.
19 Brockedon, W. and Hancock, T. (1846) English Patent 11,455.
20 Schonbein, C.F. (1876) US Patent 4,874.
21 Parkes, A. (1855) English Patent 2359.
22 Parkes, A. (1864) English Patent 2675.
23 Parkes, A. (1865) English Patent 1313.
24 Spill, D. (1869) US Patent 91,377.
25 Spill, D. (1869) US Patent 97,454.
26 Hyatt, J.W. and Hyatt, I.S. (1870) US Patent 105,222.
27 Hyatt, I.S. and Hyatt, J.W. (1872) US Patent 133,229.
28 Hancock, T. (1857) *Personal Narrative of the Origin and Progress of the Caoutehous or India Rubber Manufacture in England*, Longmans, London.
29 Springfield, R.B. (1925) *Chem. Met. Eng.*, **32**, 51.
30 Killheffer, D.H. (1962) *Banbury the Master Mixer*, Palmerton, New York.
31 Muir, A. (1968) *The History of Baker Perkins*, W. Heffer & Sons, Cambridge.
32 Herrmann, H. (1985) in *Kunststoffe ein Werkstoffe Macht Karrier* (ed. W. Glenz) Carl Hanser, Munich.
33 White, J.L. (1992) *Rubber Chem. Technol.*, **65**, 527.
34 Pfleiderer, P. (1880) German Patent (filed April 4, 1879) 10,164.
35 Kempter, F. (1914) German Patent (filed Nov. 16, 1913) 279,649.
36 Kempter, F. (1916) German Patent (filed July 7, 1914) 295,431.
37 Pointon, J.H. (1915) US Patent (filed Jan 21, 1914) 1,138,410.
38 Banbury, F.H. (1916) US Patent (filed Jan 15, 1916) 1,200,070.
39 Banbury, F.H. (1917) US Patent (filed Nov 18, 1916) 1,227,522.
40 Banbury, F.H. (1918) US Patent (filed April 20, 1917) 1,279,220.
41 Banbury, F.H. (1921) US Patent (filed Sept 4, 1920) 1,370,398.
42 Banbury, F.H. (1923) US Patent 1,449,930 (filed Jan 31, 1921).
43 Cooke, R.T. (1935) British Patent (filed June 14, 1934) 431, 012.

44 Lasch, A. and Stromer, E. (1937) German Patent (filed Oct 16, 1934) 641,685.

45 Millauer, C. (1974) German Offenlegung schrift (filed April 30, 1973) 2,321,854.

46 Lasch, A. and Frei, K. (1943) German Patent (filed Oct 10, 1939) 738,787.

47 Tyson, D.Z. and Comper, L.F. (1966) US Patent (filed Jan 25, 1964) 3 230, 581.

48 Sato, N., Miyaoka, M., Yamasaki, S., Inoue, K., Kuriyama, M., Fukui, T., Asai, T., Nakagawa, K., and Masaki, T. (1981) US Patent (filed June 22, 1979) 4284,358.

49 Asai, T., Fukui, T., Inoue, K., and Kuriyama, A. (1983) Proceedings International Rubber Conference, Papers III-4 Paris.

50 Sato, N., Miyaoka, M., Yamasaki, S., Inoue, K., and Kuriyama, A. (1981) US Patent (filed June 22, 1979) 4,300,838.

51 Inoue, K., Fukui, T., Asai, T., Nakagima, K., and Kuriyama, A. (1984) US Patent (filed Feb 17, 1981) 4456,381.

52 Asai, T. and Hagiwara, K. (1988) US Patent (filed Aug 15, 1986) 4718,771.

53 Millauer, C. (1977) German Offenlegungschrift (filed April 30, 1973) 4,058,297.

54 Johnson, F., Hormann, H., Rother, H., and Weckerle, G. (1990) European Patent (filed June 26, 1985) 0170,397.

55 Passoni, G.C. (1988) US Patent (filed Jan 16, 1987) 4775,240.

56 Pfleiderer, P. (1882) German Patent (filed June 10, 1881) 18,797.

57 Ahnhudt, H. (1924) German Patent (filed May 29, 1923) 397,961.

58 Kiesskalt, S., Tampke, H., Winnacker, K., and Weingaertner, E. (1937) German Patent (filed July 26, 1935) 652,990.

59 Kiesskalt, S. (1939) US Patent (filed July 23, 1937) 2148,205.

60 Farbenindustrie, I.G. (1939) A.G. Italian Patent (filed April 9, 1938) 373,183.

61 Kiesskalt, S. and Borgwardt, E. (1943) German Patent (filed July 10, 1938) 739,278.

62 Kiesskalt, S. (1942) *Vol Zeitschrift*, **86**, 752.

63 Leistritz, P. and Burghauser, F. (1939) German Patent (filed Dec 1, 1935) 682,787.

64 Leistritz, P. and Burghauser, F. (1940) German Patent (filed July 31, 1936) 699,757.

65 Burghauser, F. and Erb, K. (1941) US Patent (filed Feb 1, 1939) 2231,357.

66 Anonymous (W. Ellermann), German Patent (filed Jan 31, 1941) 750,509 (1945)

67 Herrmann, H. (1972) *Schneckenmaschinen in der Verfahrenstechnik*, Springer, Berlin.

68 White, J.L. (1990) *Twin Screw Extrusion: Technology and Principles*, Carl Hanser, Munich.

69 List, H. (1957) Swiss Patent (filed Aug 20, 1945) 247,704.

70 List, H. (1950) *Kunststoffe*, **40**, 185.

71 Fuller, L.J. (1952) US Patent (filed May 15, 1945) 2615,199.

72 Stich, E. (1929) German Patent 476, 748.

73 Anderson, F.B. (1929) US Patent 1848,236.

74 Royce, V. (1933) US Patent 1904,884; Royce, V. (1940) US Patent 2200,997.

75 Henning, G.F. (1950) US Patent 2496,625.

76 Dulmage, F.E. (1952) US Patent 2607,077; Dulmage, F.E. (1956) US Patent 2753,595.

77 Wunsche, A. (1902) German Patent (filed Sept 12, 1901) 131,392.

78 Easton, R.W. (1917) British Patent (filed Sept 25, 1916) 109,663.

79 Colombo, R. (1939) Italian Patent (filed Feb 6, 1939) 370,578.

80 Anonymous (1953) German Patent (filed July 24, 1943) 895,058.

81 Meskat, W. (1952) German Patent (filed Oct 17, 1943) 852,203.

82 Meskat, W. and Erdmenger, R. (1953) German Patent 862,668 (filed July 7, 1944).

83 Erdmenger, R. (1951) German Patent (filed Sept 24, 1949) 815,641.

84 Erdmenger, R. (1951) German Patent (filed Sept 29, 1949) 813,154.

85 Winkelmuller, W., Erdmenger, R., Neidhardt, S., Hirschberg, E., and Fortuna, B. (1951) German Patent (filed Dec 30, 1951) 813,154.

86 Meskat, W. and Pawlowski, J. (1956) German Patent (filed Dec 10, 1950) 949,162.

87 Erdmenger, R. (1964) US Patent (filed Aug 17, 1959) 3,122,356.

88 Liguna, SA. (1942) Swiss Patent (filed Jan 3, 1941) 220,550.

89 Colombo, R. (1956) German Patent (filed July 20, 1944) 883,338.

90 Lavoriazone Materie Plastiche (1949) British Patent (filed May 2, 1946) 629,109.

91 Colombo, R. (1951) US Patent (filed Aug 7,1947) 2,563,396.

92 Colombo, R. (1955) Canadian Patent (filed Dec 27, 1949) 517,911.

93 Ellermann, W. (1953) German Patent (filed July 4, 1951) 879,164.

94 Ellermann, W. (1954) US Patent (filed Oct 12, 1953) 2,693,348.

95 Fritsch, R. and Fahr, G. (1959) *Kunststoffe*, **43**, 543.

96 Proksch, W. (1964) *Kunststoffe Gummi*, **3**, 426.

97 Inoue, K. Internal mixers, in *Mixing and Compounding of Polymers: Theory and Practice*, 2nd edn (ed. I. Manas-Zloczower), ch. 23, pp. 831–852, Carl Hanser, Munich.

98 Valsamis, L.C. and Canedo, E. (1994) *Int. Polym. Process*, **9**, 226.

99 Burbank, F., Brauer, F., and Anderson, P. (1991) *SPE Antec. Tech. Paper*, **37**, 149.

100 Grillo, J., Anderson, P., and Papazoglou, E. (1992) *SPE Antec. Tech. Papers*, **38**, 20.

101 Wobbe, H. and Uhland, E. (1994) US Patent (filed Oct 15, 1992) 5,318,358.

102 Loomans, B.A. and Brennan, A.K. (1965) US Patent (filed March 21,1962) 3,195, 868.

103 Wang, Y., White, J.L., and Szydlowski, W. (1979) *Int. Polym. Proc.*, **4**, 262.

104 Lai-Fook, R.A., Li, Y., and Smith, A.C. (1991) *Polym. Eng. Sci.*, **31**, 1157.

105 Goffart, D., Van der Wal, D.J., Klomp, E.M., Hoogstraten, H.W., Janssen, L.P.B.M., Breysse, L., and Trolez, Y. (1996) *Polym. Eng. Sci.*, **36**, 901, Goffart, D., Van der Wal, D.J., Klomp, E.M., Hoogstraten, H.W., Janssen, L.P.B.M., Breysse, L., and Trolez, Y. (1996) *Polym. Eng. Sci.*, **36**, 912.

106 Chen, Z. and White, J.L. (1994) *Int. Polym. Process*, **9**, 310.

107 Bawiskar, S. and White, J.L. (1997) *Int. Polym. Process*, **12**, 331.

108 Vergnes, B., Deil Nalle, G., and Delamere, L. (1998) *Polym. Eng. Sci.*, **38**, 1781.

109 Potente, H., Bastian, M., and Flecke, J. (1997) *Adv. Polym. Technol.*, **18**, 147.

110 Street, L.F. (1956) US Patent (filed Aug 16, 1952) 2733,051; Street, L.F. (1962) US Patent (filed Feb 23, 1954) 3,068,514.

111 Skidmore, R.H. (1963) US Patent (filed Dec 28, 1959) 3082,816.

112 Skidmore, R.H. (1973) US Patent (filed April 8, 1970) 3742,093.

113 Kaplan, A. and Tadmor, Z. (1974) *Polym. Eng. Sci.*, **14**, 58.

114 Nguyen, K. and Lindt, J.L. (1989) *Polym. Eng. Sci.*, **29**, 709.

115 Bang, D. and White, J.L. (1997) *Int. Polym. Process*, **12**, 278.

116 Ahlefeld, E.H., Baldwin, A.J., Hold, P., Rapetzki, W.A., and Scharer, H.R. (1964) US Patent (filed May 15, 1962) 3,154,808.

117 Hold, P. (1984) *Adv. Polym. Technol.*, **4**, 281.

118 Bang, D. and White, J.L. (1997) *Polym. Eng. Sci.*, **37**, 1210.

119 Canedo, E.L. and Valsamis, L.N. (2009) Continuous mixers, in *Mixing and Compounding of Polymers: Theory and Practice*, 2nd edn (ed. I. Manas-Zloczower), ch. 28, pp. 1081–1138, Carl Hanser, Munich.

120 Tenner, H. (1976) *Kunststoff Berater*, **6**, 3.

121 Thiele, W. (1983) *SPE Antec. Tech. Papers*, **29**, 127.

122 Thiele, W. (1998) *Plastics Compounding* (ed. D.B. Todd), Carl Hanser, Munich.

123 Thiele, W. (2003) *Pharmaceutical Extrusion Technology* (eds I. Ghebre Sellassie and C. Martin) Marcel Dekker, New York.

124 Lim, S.H. and White, J.L. (1994) *Int. Polym. Process*, **9**, 33.

125 Gubler, E. (1965) US Patent (filed Dec 6, 1961) 3,189324.

126 Sutter, F. (1965) US Patent (filed Sept 19, 1963) 3219,320.

127 Gresch, W. (1968) US Patent (filed Jan 26, 1966) 3367,635.

128 Lyu, M.Y. and White, J.L. (1995) *Int. Polym. Process*, **10**, 305.

129 Lyu, M.Y. and White, J.L. (1996) *Int. Polym. Process*, **11**, 208.

130 Elemans, P.H.M. (2009) Continuous equipment simulations – co-kneader, in *Mixing and Compounding of Polymers:*

Theory and Practice, 2nd edn (ed. I. Manas-Zloczower), ch. 13, pp. 419–450, Carl Hanser, Munich.
131 Cho, J.W., Kim, P.S., White, J.L., and Pomini, L. (1997) *Kautsch Gummi, Kunsts*, **50**, 496.
132 Kim, P.S. and White, J.L. (1994) *Rubber Chem. Technol.*, **67**, 871; Kim, P.S. and White, J.L. (1996) *Kautsch Gummi Kunsts*, **49**, 10.
133 Shon, K. and White, J.L. (1999) *Polym. Eng. Sci.*, **39**, 1757.
134 Shon, K., Liu, D., and White, J.L. (2005) *Int. Polym. Process*, **20**, 322.
135 Shon, K., Bumm, S.H., and White, J.L. (2008) *Polym. Eng. Sci.*, **48**, 756.
136 White, J.L., Liu, D., and Bumm, S.H. (2006) *J. Appl. Polym. Sci.*, **102**, 3940.
137 Hofmann, W. (1963) *Rubber Chem. Technol.*, **37** (2), 52.
138 Maxwell, J.C. (1879) *Encyclopedia Britannica* 9th edn, Encyclopedia Britannica, London.
139 Chappelear, D.C. (1964) *ACS Polym. Papers*, **5**, 363.
140 Roe, R.J. (1969) *J. Colloid Interface Sci.*, **31**, 228.
141 Wu, S. (1970) *J. Phys. Chem.*, **74**, 632.
142 Peterson, H.T., Hu, K.H., and Grindstaff, T.H. (1971) *J. Polym. Sci.*, **34**, 31.
143 Carriere, C.J., Cohen, A., and Arends, C.B. (1989) *J. Rheol.*, **33**, 681.
144 Elemans, P.H.M., Janssen, J.M.H., and Meijer, H.E.H. (1990) *J. Rheol.*, **34**, 1311.
145 Chen, C.C. and White, J.L. (1993) *Polym. Eng. Sci.*, **33**, 923.
146 Yoon, P.J. and White, J.L. (1994) *J. Appl. Polym. Sci.*, **51**, 1515.
147 Barentsen, W. and Heikens, D. (1973) *Polymer*, **14**, 579.
148 Barentsen, W., Heikens, D., and Piet, P. (1974) *Polymer*, **15**, 119.
149 Ide, F. and Hasegawa, A. (1974) *J. Appl. Polym. Sci.*, **18**, 963.
150 Heikens, D., Hoen, N., Barentsen, W., Piet, P., and Linden, H. (1978) *J. Polym. Sci. Symp.*, **62**, 309.
151 Endo, S., Min, K., White, J.L., and Kyu, T. (1986) *Polym. Eng. Sci.*, **26**, 45.
152 Jiang, R., Quirk, R.P., White, J.L., and Min, K. (1991) *Polym. Eng. Sci.*, **31**, 1545.
153 Ihm, D. and White, J.L. (1996) *J. Appl. Polym. Sci.*, **60**, 1.
154 Min, K., White, J.L., and Fellers, J.F. (1984) *Polym. Eng. Sci.*, **24**, 1327.
155 White, J.L. and Min, K. (1984) *Adv. Polym. Technol.*, **24**, 1327.
156 Miller, W.A. and Merriam, C.N. (1961) US Patent 3097,991.
157 Shimizu, J., Okui, N., Yamamoto, T., Isai, M., and Takaka, A. (1982) *Sen'i Gakkaishi*, **38**, T–1.
158 Min, K., White, J.L., and Fellers, J.F. (1984) *J. Appl. Polym. Sci.*, **29**, 2117.
159 Liang, B.R., White, J.L., Spruiell, J.E., and White, J.L. (1983) *J. Appl. Polym. Sci.*, **28**, 2011.
160 Yang, J., White, J.L., and Jiang, Q.B. (2010) *Polym. Eng. Sci.*, **50**, 1969.
161 Ghiam, F. and White, J.L. (1991) *Polym. Eng. Sci.*, **31**, 76.

2
Rheology of Polymer Blends

Leszek A. Utracki

2.1
Introduction

The first polymer blend was patented in 1846 and since then blends have became ubiquitous. Blending may provide a full set of material properties, improving processability and/or specific properties. With the advancement of technology there is the notorious growth of complexity – while in the beginning blending involved two polymers, initially without a compatibilizer, more recent commercial alloys have up to five polymers, three compatibilizers, and frequently are reinforced with macro- or nanoparticles [1].

Blends are classified as either thermodynamically miscible or immiscible, with the latter dominating. However, imposition of a flow affects the thermodynamic equilibrium and it may enhance the miscibility of immiscible blends or vice-versa – there is an interrelation between rheology and thermodynamics. Similarly, flow affects the degree of deformation of the dispersed phase, thus in immiscible blends there are other interrelations between rheology and morphology, which affect the blend performance. To the complexity of polymer alloys and blends (PAB) behavior one must add the incorporation of solids, either in the form of filler and nanofiller particles or by simple fact of blending two components with widely different transition temperatures.

Since the flow of PAB is complex, it is useful to revert to simple models, for example, for miscible blends to solutions or mixtures of polymer fractions, for immiscible blends to emulsions or suspensions, and for compatibilized blends to block copolymers (Table 2.1). It is also advisable to study flow behavior of multiphase systems at constant stress (not at constant deformation rate) [2, 3].

For miscible blends, the free volume theory predicts a positive deviation from the log-additivity rule (PDB, positively deviating blend). However, depending on the system and method of preparation, these blends may show a positive deviation, negative deviation, or additivity [4]. Upon mixing, the presence of specific interactions may change the free volume and degree of entanglement, which in turn affect the flow behavior [5, 6]. For immiscible blends the flow is similarly affected, but in addition there are at least three contributing phases: of the polymeric matrix, of the

Encyclopedia of Polymer Blends: Volume 2: Processing, First Edition. Edited by Avraam I. Isayev.
© 2011 Wiley-VCH Verlag GmbH & Co. KGaA. Published 2011 by Wiley-VCH Verlag GmbH & Co. KGaA.

Table 2.1 Rheological models for miscible and immiscible blends.

1. Miscible blends	2. Immiscible blends
1.1 Solutions	2.1 Suspensions
1.2 Homologous polymer blends	2.2 Emulsions
	2.3 Block copolymers

polymeric dispersed phase, and of the interphase. Flow of emulsion provides a good model for blends with a low viscosity ratio of the dispersed-to-matrix phase ($\lambda \equiv \eta_2/\eta_1 \cong 1$), while for blends with $\lambda > 4$ the suspensions model might be more appropriate (NB, subscripts 1 and 2 (or m and d) refer to the matrix and dispersed phase, respectively).

The basic assumption of classical rheological theories is that the liquid structure is either stable (Newtonian behavior) or its changes are well defined (non-Newtonian behavior). This is rarely the case for flow of multiphase systems. For example, orientation of sheared layers may be responsible for either dilatant or pseudoplastic behavior, while strong interparticle interactions may lead to yield stress or transient properties. Liquids with yield stress show a plug flow. As a result, these liquids have drastically reduced extrudate swell, $B_e \equiv d/d_o$ (d is extrudate diameter, d_o that of the die) [7]. Since there is no deformation within the plug volume, the molecular theories of elasticity are not applicable.

For most blends, the morphology changes with the imposed strain. Thus, it is expected that the dynamic low strain data will not follow the pattern observed for the steady-state flow. One may formulate it more strongly: in polymer blends the material morphology and the flow behavior depend on the deformation field, thus under different flow conditions different materials are being tested. Consequently, for immiscible blends the steady state relation may be quite different from the dynamic one in shear or elongation.

Rheological measurements of PAB most often apply the three types of flow: steady state shearing, dynamic shearing, and elongation. The three can be classified according to the strain, (γ), vorticity (ω_v), as well as uniformity of stress (σ), and γ within the rheometer test cavity. The characteristics listed in Table 2.2 indicate that the steady-state flows, elongation, and shear strongly affect the morphology, whereas the dynamic shear effect is less significant. The elongational flows are characterized by uniform deformation and lack of vorticity and, thus, they are the most effective in changing the morphology and orientation of PAB.

2.1.1 Rheological Models for Miscible Blends

2.1.1.1 Solutions

The flow of miscible blends may be compared to that of solutions, or to the flow of mixtures of polymeric fractions. Both models are far from perfect, but they illustrate

Table 2.2 Characteristics of flow fields.

No.	Type	γ	ω_v	Uniformity of σ	γ	Comments
1	Steady-state shear					
1.1.	Sliding plate, and rotational cone-&-plate	Large	Yes	Homogeneous	Homogeneous	For small gap, or for cone angle $<4°$
1.2.	Poiseuille (capillary or slit), Couette, and rotational parallel plates	Large	Yes	Functions of spatial coordinates	Functions of spatial coordinates	For laminar flows small measuring thickness is required
2.	Dynamic shear					
2.1.	Cone-&-plate	Small	Yes	Homogeneous	Homogeneous	For cone angle $<4°$
2.2.	Parallel plates	Small	Yes	Linear	Linear	Gap 0.8–2.0 mm
2.3.	Couette	Small	Yes	Variable	Variable	Gap 0.2–0.5 mm
3.	Elongational flows					
3.1.	Uniaxial	Mid	No	Homogeneous	Homogeneous	
3.2.	Biaxial	Mid	No	Homogeneous	Homogeneous	

the basic behavior of miscible systems. In the first case one can learn about the effects of the thermodynamic interactions between chemically different components on flow. In the second case it is the effect of molecular weight and molecular weight distribution that can be assessed.

The simplest expression for the zero-shear solution viscosity of liquid mixtures was proposed by Arrhenius in 1887 [8]:

$$\ln \eta_o = \sum_i (x_i \ln \eta_{oi}) + \ln \eta^e \tag{2.1}$$

with x_i and $\ln \eta^e$ being the mole fraction and the excess viscosity term, respectively. The Eyring theory of rate processes offers a similar expression with the term $\ln \eta^e$ directly related to the excess Gibbs free energy of mixing, ΔG_m, [9, 10]:

$$\ln(V \eta_o) = \sum_i x_i (\ln V_i \eta_{oi}) - \Delta G_m / 2.45\, RT \tag{2.2}$$

where V is the specific volume. For miscible blends, $\Delta G_m < 0$ and Eq. (2.2) suggests a positive deviation from the log-additivity rule.

There are several other blending rules for solution viscosity; for example, see References [10–12]. The simple additivity rule expressed by Eq. (2.1) or (2.2) might be applicable to mixtures of liquids with dispersive-type interactions but, as shown in Figure 2.1, not to strongly interacting polar, associating ones. The third-order McAllister equation has four interaction parameters for a mixture of liquid 1 with liquid 2, that is, 11, 22, 12, and 21, and thus it can describe more complex viscosity dependencies.

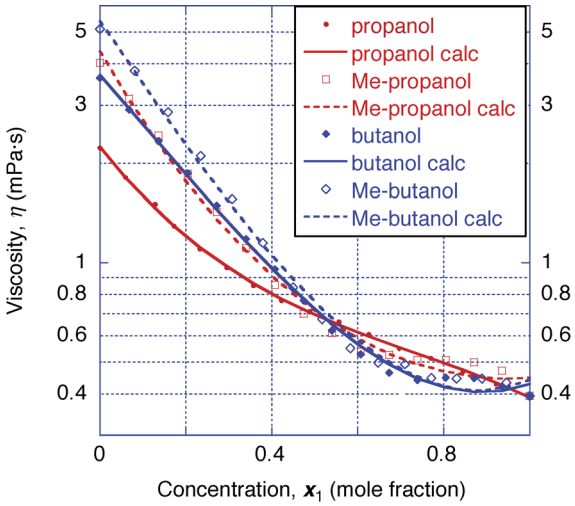

Figure 2.1 Viscosity at 293.15 K of 2-propanone with four alcohols: propanol, methylpropanol, butanol, and methylbutanol. Points: experimental data from Reference [13]; lines: calculated from the McAllister equation [11].

2.1.1.2 Homologous Polymer Blends

Homologous polymer blends (HPBs) are mixtures of fractions of the same polymer having the same chemical constituting units (mers); hence, any polydispersed polymer is a HPB. In accord with the old alchemist maxim *similia similibus solvuntur*, blending the narrow molecular weight distribution (MWD) fractions leads to a miscible system, which offers information on the key properties of commercial materials. For example, since the zero-shear viscosity for narrow molecular weight distribution samples follows the power-law: $\eta_o = KM_w^{\alpha}$ (where K and $\alpha = 1$ or 3.4 are parameters), while $M_w = \sum_i w_i M_i$ (w_i is weight faction of component i), then [14]:

$$\eta_o = \left[\sum_i w_i \eta_{o,i}^{1/\alpha}\right]^{\alpha} \tag{2.3}$$

Since Eq. (2.3) is valid for fractions of the same polymer that are thermodynamically miscible, it is expected that the dependence might be valid also for "ideal" (zero enthalpy of mixing) blends of chemically different polymers. However, the relation applied to binary mixtures predicts PDB behavior, which is not universal. For macromolecular systems with low configurational entropy, miscibility depends on specific interactions, which affect the free volume and, thus, the rheological behavior [15]. The double reptation model applied to homologous mixtures of polybutadiene (PBD) offers a good description of smoothly varying PDB viscosities of binary mixtures, but it is not adequate for predicting the behavior of strongly interacting binary mixtures [16, 17].

During the last 30 years hundreds of articles have been written on the correlation between MWD and rheological functions; for example, see References [18–24]. Particularly successful is the use of the dynamic or relaxation moduli to compute these functions from MWD, or vice versa. Good agreement has been obtained between MWD derived from rheological measurements and those measured by size exclusion chromatography (SEC). The agreement was reported for the linear and branched systems as well as for those with a single and multiple distributions.

2.1.2 Model Systems for Immiscible Blends

2.1.2.1 Interphase and Percolation

The simplest immiscible polymer blend has three phases: matrix polymer #1, dispersed polymer #2, and an interphase between them. The thickness of the interphase ranges from 2 nm (immiscible blends) to 60 nm (reactively compatibilized blends) and it may constitute the key-phase for the rheological behavior [3].

The first theoretical modeling of polymer blends was carried out by Helfand and his colleagues [25–27]. Their lattice theory approximated the polymer #1–polymer #2 interactions via the Huggins–Flory binary parameter, χ_{12}. The derivation provided expressions for the concentration gradient across the interface, as well as for the interfacial tension coefficient, ν_{12}, and the interphase thickness, Δl:

$$\left.\begin{aligned} \nu_{12} &= (k_B T/a)(m\chi_{12})^{1/2} \\ \Delta l &= 2(m/\chi_{12})^{1/2} \end{aligned}\right\} \Rightarrow \quad \Delta l \nu_{12} = 2\, m k_B T/a \tag{2.4}$$

where k_B is Boltzmann constant and a and m are the lattice parameters. Thus, since $\nu_{12}\Delta l$ is independent of χ_{12}, the theory predicts a universal reciprocity between the interfacial tension coefficient and the thickness of the interphase. While the prediction is correct for binary systems, it breaks down upon compatibilization (especially reactive compatibilization). The theory also implies that:

- The interface energy depends on χ_{12}, and thus on molecular weight: $\nu_{12} = \nu_\infty - a_o M_n^{-2/3}$.
- The polymer chain-ends, oligomers, and other low molecular weight components migrate to the interphase. Thus, in solid state the immiscible blends are brittle, requiring compatibilization.

These implications are important for understanding the flow behavior of immiscible blends.

The principal goal of compatibilization is modification of the interphase – reduction of the interfacial energy and thus an increase in its thickness [29, 30]. Tang and Huang proposed a semiempirical equation [31]:

$$(\gamma - \gamma_{CMC})/(\gamma_o - \gamma_{CMC}) = \exp\{-K\phi_c\}; \quad \gamma \in d_2, \nu_{12} \tag{2.5}$$

where

d_2 is the drop diameter (polymer # 2),
K is an equation constant,
ϕ_c is the compatibilizer volume fraction,
the γ-subscripts "o" and "CMC" refer to the absence of compatibilizer and its critical micelle concentration (CMC), respectively.

The consequences of Eq. (2.5) are displayed in Figure 2.2. Independently of the compatibilizer efficiency, the postulated parallel concentration dependence of d_2 and ν_{12} is observed. The rheological outcome of compatibilization is related to the increased volume fraction of the dispersed phase and enhanced interactions between particles, which often lead to the appearance of yield stress in a compatibilized blend (usually yield stress is absent in non-compatibilized blends).

Equation (2.5) and the discussed change of drop diameter imply that the concentration of dispersed phase is below the percolation threshold, $\phi < \phi_{perc} \approx 0.19 \pm 0.09$. Above this limit the dispersed phase forms continuous clusters, which progressively increase the degree of co-continuity from zero to 100% where the distinction between the dispersed and the matrix polymeric phase vanishes – this limit is known as the phase inversion volume fraction, ϕ_I, [32, 33]. An assumption that at the inversion concentration the *relative* viscosity of both phases is equal leads to [34, 35]:

$$\lambda \equiv \eta_2/\eta_1 = [(\phi_m - \phi_{2I})/(\phi_m - \phi_{1I})]^{[\eta]\phi_m}; \quad \text{where} \quad \phi_m = 1 - \phi_{perc} \tag{2.6}$$

As shown in Figure 2.3, for most blends the parameters: $[\eta] \cong 1.9$; $\phi_m \cong 1 - \phi_{perc} = 0.84$ provide good approximation [33, 36]. Expanding Eq. (2.6) into a Maclaurin

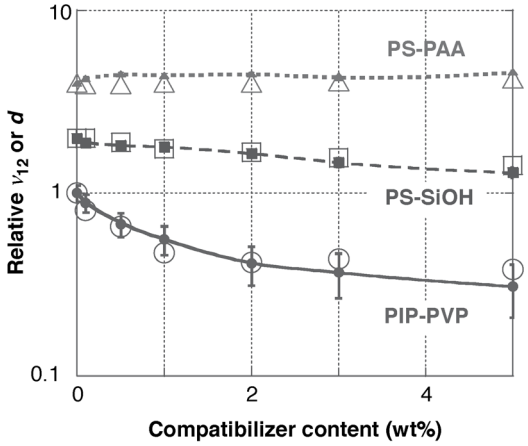

Figure 2.2 Relative interfacial tension coefficient (filled symbols) and drop diameter (open symbols) of the linear low density polyethylene (LLDPE) blend with poly(vinyl chloride) (PVC), LLDPE/PVC = 3:1, compatibilized by addition of three compatibilizers. The two upper sets of data are displaced by a factor of two and four, respectively. Data from Reference [28].

series, then truncating after the second term, gives a simplified version that is valid within the range $-1 < \phi_{1i}/\phi_m < 1$:

$$\phi_{12} = \{1-(\ln\lambda)/[\eta]\}/2 \tag{2.6a}$$

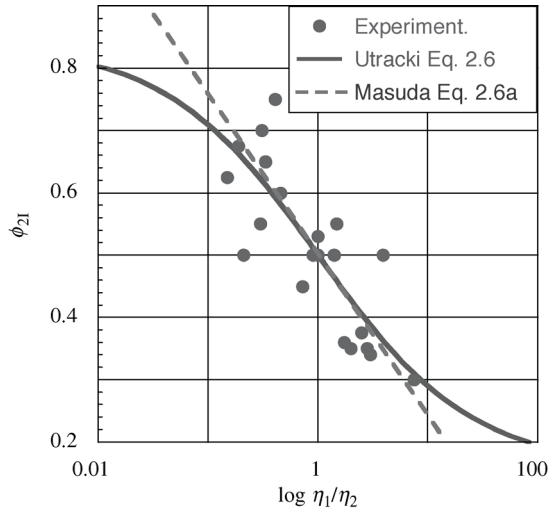

Figure 2.3 Experimental ϕ_{2i} versus log λ for thermoplastic blends. For $[\eta] = 1.9$ and $\phi_m = 0.84$ the solid and broken lines represent Eqs. (2.6) and (2.6a), respectively.

In 1992, after LAU lecture on "Polymer Alloys and Blends" at the *4th Society of Polymer Science Japan International Polymer Conference*, Yokohama, 1992, Prof. T. Masuda mentioned using an empirical, unpublished semi-logarithmic expression, similar to Eq. (2.6a).

Most polymer blends are immiscible. Their flow is complex not only due to the presence of several phases having different rheological properties (as will be demonstrated later, even in blends of two polymers the interphase must be taken into account), but also due to strain sensitivity of blends' morphology. Such a complexity might be best put in perspective by comparing the flow of blends with that of better understood systems, for example, suspensions, emulsions, and block copolymers.

2.1.2.2 Suspensions

Zero-Shear Viscosity The flow of dilute suspensions ($\phi < 0.05$) of rigid spheres in Newtonian liquid was described by Einstein in an article of 1906 on "a new method for estimation of molecular dimension" [37], and then corrected in 1911 [38]:

$$\begin{aligned} &\langle \sigma_{ij} \rangle = -p\delta_{ij} + 2\eta_o[1 + (5/2)\phi]\dot{\gamma}_{ij} \\ &\text{or} \quad \eta_r \equiv \eta/\eta_o = 1 + (5/2)\phi \end{aligned} \tag{2.7}$$

where η_o and η_r is the suspending liquid viscosity (solvent viscosity) and relative viscosity of the suspension, respectively. Einstein's basic assumptions were: (i) the size of a rigid particle is large in comparison to the suspending medium molecules, but small compared to the smallest characteristic diameter of the flow channel so the continuum theories are applicable; (ii) the flow is steady state, without inertia or sedimentation; and (iii) the suspending medium perfectly adheres to the particles. Extensive discussion on the Einstein theory can be found in Simha's dissertation [39]. An excellent review of the earlier works on suspension viscosity has been published by Brenner [40]. Numerical simulation of suspension rheology has been carried out since 1985 [41, 42].

The largest contribution to energy loss (viscosity) comes from the hydrodynamic interactions of particles with different velocities, which increases with ϕ and the degree of aggregation. The maximum packing volume fraction, ϕ_m, corresponds to a percolation-like threshold for agglomerate formation that causes the viscosity to increase to infinity (∞). Microstructural theories are well suited to treating the time-dependent flows, thixotropy, and rheopexy [2, 43, 44].

One of the most interesting derivations of the η versus ϕ dependence was published by Simha in 1952 [45]. He considered the effects of concentration on the hydrodynamic interactions between rigid spheres, taking into account the shielding effects of final size particles. The shielding effect is characterized by scaled length, L/R_{12}, where R_{12} is an average interparticle distance. Thus the shielding importance vanishes at particles volume fraction $\phi = 0$, increasing with ϕ up to its maximum packing value, $\phi = \phi_m$. Starting with such a cage model, Simha placed solid, spherical particle of radius a inside a spherical enclosure of radius b, defining the concentration-dependent parameter $\gamma(\phi) \equiv a/b$, with b being proportional to $(a - R_{12})$. These assumptions lead to a modified Einstein [37, 38] relation:

$$\eta_r \equiv \eta/\eta_o = 1 + \phi[\eta]\lambda(\gamma); \quad \lambda(\gamma) = \frac{4\left(1-\gamma^7\right)}{4(1+\gamma^{10})-25\gamma^3(1+\gamma^4)+42\gamma^5}$$
$$\gamma = \left[\left(f/\phi^{\frac{1}{3}}\right)-1\right]^{-1} = \left[\left(2/\tilde{\phi}^{\frac{1}{3}}\right)-1\right]^{-1}; \quad \tilde{\phi} \equiv \phi/\phi_m \tag{2.8}$$

where $\lambda(\gamma)$ is the shielding (or interaction) function and $1.3 \leq f_s \leq 1.9$ is a packing factor; for example, for hexagonal and cubic packing $f_s = 1.81$ and 1.61, respectively. In suspension rheology it is more convenient to use the maximum packing volume fraction, $\phi_m \cong f_s^3/8$. Thus, the magnitude of the shielding function $\lambda(\gamma)$ depends on the reduced volume fraction, $\tilde{\phi} = \phi/\phi_m$.

At low concentration the relative viscosity of hard sphere suspension is usually approximated by a polynomial:

$$\eta_r = 1 + \tfrac{5}{2}\phi + K\phi^2 + O\left(\phi^3\right) \tag{2.9}$$

Expansion of Eq. (2.9) gives the initial slope $[\eta] = 5/2$ while the second term is given as $K = 15.625/f_s^3$, to be compared with the experimental values of $K = 5.2$–7.6; thus experimentally $f_s = 1.3$–1.4, that is, larger than monodispersed, regularly packed spheres. The high concentration limit of Eq. (2.8) is: $\lambda(\gamma), \eta_r \to \infty$.

There are numerous semiempirical and empirical relations proposed for describing the concentration dependence of suspension viscosity. For example, the first category of relations has the algebraic form [44]:

$$\eta_r = (1 + \alpha\phi)^\beta \tag{2.10}$$

where the equation parameters, α and β, are treated as constants, for example, respectively 2.5 and 1, or -2.5 and -1, or -1.73 and -2.0, and so on. However, in the Krieger–Dougherty [46] relation, these two parameters depend on the system: $\alpha = -1/\phi_m$, and $\beta = -[\eta]\phi_m$.

Thomas [47] compiled the relative viscosity data from 16 laboratories at $\phi \leq 0.6$, for different types of spherical particles in suspensions such as pollen in water, steel balls in oil, and so on. The data were corrected for immobilized adsorbed layer of the suspending liquid. The results followed the empirical dependence:

$$\eta_r = 1 + (5/2)\phi + 10.05\phi^2 + 0.00273\exp\{16.6\phi\} \tag{2.11}$$

(expanding the exponent gives $K = 10.43$ and, thus, $f = 1.14$). Detailed analysis of Thomas' data was published by Utracki and Fisa [48].

Figure 2.4 displays η_r versus ϕ experimental dependence as given by Thomas' empirical equation (Eq. (2.11)) along with fits to the Krieger–Dougherty and Simha equations. In each case the fitting parameters are $[\eta]$ and ϕ_m. Their values are respectively: $(1.91 \pm 0.01;\ 0.725 \pm 0.008)$ and $(2.49 \pm 0.01;\ 0.784 \pm 0.006)$. The correlation coefficient squared, $r^2 = 0.9983$ and 0.9998, respectively (the Krieger–Dougherty equation deviates within the mid-concentration range). The theoretical Eq. (2.8) is shown as a broken line for $[\eta] = 2.5$ and $\phi_m = 0.74$, that is, theoretical dependence for monodispersed hard spheres. The deviation from Thomas' relation indicates polydispersity of sizes in the measured suspensions.

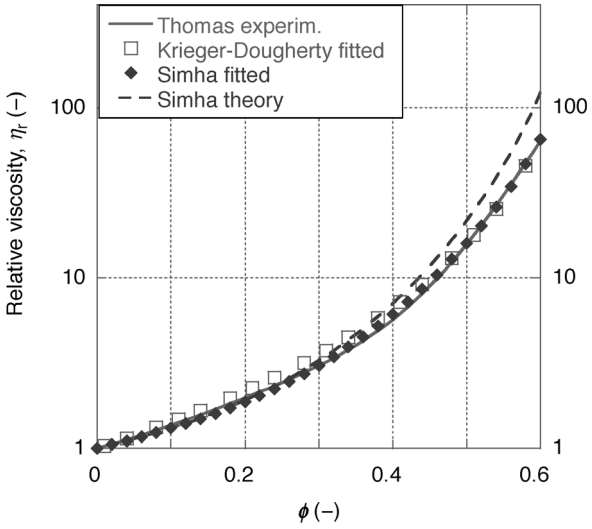

Figure 2.4 Relative viscosity of a hard-sphere suspension in Newtonian fluid as a function of volume fraction. The Thomas solid line is for analyzed and corrected experimental data from 16 laboratories. The Krieger–Dougherty and Simha equations were fitted to the Thomas equation by selecting optimum values of $[\eta]$ and ϕ_m (see text). The broken line represents Simha's theoretical prediction for monodispersed hard sphere suspensions with $[\eta] = 2.5$ and $\phi_m = 0.74$.

The polydispersity of particle size increases ϕ_m, for example, of randomly packed uniform spheres from 0.62 to about 0.9. Thus, while for small and large monodispersed spheres $\phi_m = 0.62$, for the mixtures, depending on composition and size ratio, $\phi_m \rightarrow 1.0$. For polydispersed spheres of diameter d_i and average diameter $\bar{d}$, Pishvaei *et al.* [49] used the model of Ouchiyama and Tanaka [50–55] to calculate the maximum packing volume fraction, ϕ_m, and the average number of spherical particles, $\bar{n}$:

$$\phi_m = \frac{\sum_{i=1}^{u} d_i^3 f_i}{\sum_{i=1}^{u} \left(d_i \approx \bar{d}\right)^3 f_i + \frac{1}{\bar{n}} \sum_{i=1}^{u} \left\{ \left(d_i + \bar{d}\right)^3 - \left(d_i \approx \bar{d}\right)^3 \right\} f_i}$$

$$\bar{n} - 1 = \left(\frac{4\bar{d}}{13}\right)\left(8\phi_m^o - 1\right) \frac{\sum_{i=1}^{u} \left(d_i + \bar{d}\right)^2 f_i \left[1 - \frac{3\bar{d}}{8\left(d_i + \bar{d}\right)}\right]}{\sum_{i=1}^{u} \left\{ d_i^3 - \left(d_i \approx \bar{d}\right)^3 \right\} f_i} \tag{2.12}$$

In Eq. (2.12) $f(d)$ is the number-frequency size distribution, $\left(d \approx \bar{d}\right)$ is defined as:

$$\left(d \approx \bar{d}\right) = \begin{cases} 0 & \text{for} \quad d \leq \bar{d} \\ d - \bar{d} & \text{for} \quad d > \bar{d} \end{cases}$$

Good prediction was obtained for the zero-shear viscosity of latexes and plastisols [56] computed from the Krieger–Dougherty equation, Eq. (2.10), with ϕ_m obtained from Eq. (2.12).

An ICI recipe for ϕ_m maximization requires four generations of nearly spherical particles with the diameter ratios 1 : 3 : 9 : 17, blending at the volume ratios 4 : 1 : 1 : 4. These suspensions have the maximum packing volume fraction of $\phi_m = 0.78$, are non-sedimenting, and the dry solids have uniform porosity [57, 58]. Packing optimization of filler particles of different shapes (e.g., $CaCO_3$ + glass fibers) has also been developed [59–63]. These considerations also apply to polymer blends at $\phi > \phi_{perc}$, where the morphology is complex, consisting of spheres, fibers, and lamellas.

According to Eq. (2.8) or (2.10) the concentration dependence of η_r has two parameters, $[\eta]$ and ϕ_m. Both are measures of a specific physical quantity (respectively, shape and packing) and may be independently determined, for example, $[\eta]$ from viscosity of diluted suspensions and ϕ_m from *dry packing* of solid particles. For anisometric particles, the magnitude of these parameters may also be theoretically predicted; see the rheological summary in a quite recent monograph [64]. Once $[\eta]$ and ϕ_m are known, Eq. (2.8) will correctly describe the η_r versus ϕ dependence for complex industrial systems, for example, PVC (poly(vinyl chloride)) emulsions and plastisols, mica-reinforced polyolefins, and sealant formulations [44, 65]. However, in some suspensions and blends, $[\eta]$ and ϕ_m may vary with composition [66].

Flow and Aggregation Effects The discussion on suspension viscosity would not be complete without at least mentioning the effects of orientation and aggregation. Under steady state shear flow the vorticity component of the stress tensor is responsible for rotation of particles, whereas in the irrotational elongational field the particles remain oriented in the stress direction. The anisometric particles with aspect ratio p rotate in shear within the encompassed volume, which leads to a stronger concentration dependence, $\eta_r \propto \phi^3$ [67]. In uniaxial flow the particles align with the main axis in the flow direction and the relative elongational viscosity strongly depends on p [68, 69]. Particle behavior during flow is treated by microrheology [70, 71]. The essential aspects of microrheology are discussed in Section 2.1.2 and 2.4.3.

There is a reciprocal relation between the liquid structure and its rheological response: orientation, deformation, and aggregation are the principal factors. In shear, aggregation starts within the dilute region with transitory rotating doublets, goes through a stage of dynamic fractal structures, and ends with a pseudo-solid-like behavior of flocculated suspensions with yield stress. Initially, aggregation is a means for the reduction of interfacial tension complemented at higher ϕ by geometric crowding.

The pseudoplastic flow relation for molten polymer follows the Carreau–Yasuda equation [44, 72, 73]:

$$(\eta - \eta_\infty)/(\eta_o - \eta_\infty) = [1 + (\tau\dot{\gamma})^{m_1}]^{-m_2} \tag{2.13}$$

where

η_o and η_∞ are upper and lower values of Newtonian viscosity, respectively [74–76],

τ is the relaxation time,
m_1 and m_2 are polydispersity parameters.

In viscoelastic systems the lower Newtonian viscosity is several orders of magnitude smaller than the upper one, $\eta_\infty \ll \eta_o$, and is frequently neglected. At high deformation rates Eq. (2.13) reverts to the power-law dependence:

$$\sigma_{12} = K\dot{\gamma}^n; \quad n = 1 - m_1 m_2 \tag{2.14}$$

These dependencies describe the pseudoplastic flow behavior without time-effects or the yield stress (σ_y).

Several direct and indirect methods for determining σ_y are described in the *Polymer Blends Handbook* [1]. According to von Mises, the yield stress in elongation flow should be larger than that in shear by the factor of $\sqrt{3}$. However, for highly concentrated suspensions of anisometric particles, this criterion might not be applicable.

It is appropriate to consider the multiphase systems as composed of a matrix and concentration-dependent dynamic clusters or aggregates characterized by specific strength, σ_y^∞, the aggregate relaxation time, τ_y, and the cluster size polydispersity index, $u \approx 0.2 - 1.0$ [44]. Thus the apparent shear stress may be expressed as:

$$\sigma_{app}(\dot{\gamma}) = \sigma_{12}(\dot{\gamma}) + \sigma_y(\dot{\gamma}); \quad \sigma_y(\dot{\gamma}) = \sigma_y^\infty \left[1 - \exp\{-\tau_y \dot{\gamma}\}\right]^u \tag{2.15}$$

The dependence holds in steady-state as well as dynamic flow in shear or elongation, it is easy to use, and the extracted parameters calculated from equation fitting to experimental data agree with the directly measured values. The magnitude of σ_y increases with aspect ratio, p, their rigidity, and concentration. Some consequences of σ_y are the plug flow [77, 78], reduction of the extrudate swell, B_e [7, 79], and increase of the entrance–exit pressure drop, P_e [80, 81]. In multiphase systems both B_e and P_e depend mainly on the inter-domain interactions and morphology.

Suspensions and emulsions, even in a Newtonian matrix, display time effects, thixotropy, or (less common) rheopexy (e.g., see Figure 2.5 below); thixotropy is characterized by a decrease of apparent viscosity under steady-state deformation, while rheopexy relates to an apparent increase. Thixotropy in systems with a polymeric matrix is frequently neglected or combined with the rate-dependent pseudoplastic behavior. In fine dispersions even weak interactions may produce thixotropic effects, following the single-exponential relation:

$$\left(\eta - \eta_\infty^t\right) / \left(\eta_o^t - \eta_\infty^t\right) = \exp\{-t/\tau^*\} \tag{2.16}$$

where

t is the shearing time,
η_o^t and η_∞^t are values of shear viscosity at $t = 0$ and ∞, respectively,
τ^* is the relaxation time of the system.

Filled and Reinforced Molten Polymers These suspensions in non-Newtonian liquids have been frequently reviewed [82–94]. The non-Newtonian behavior of filled

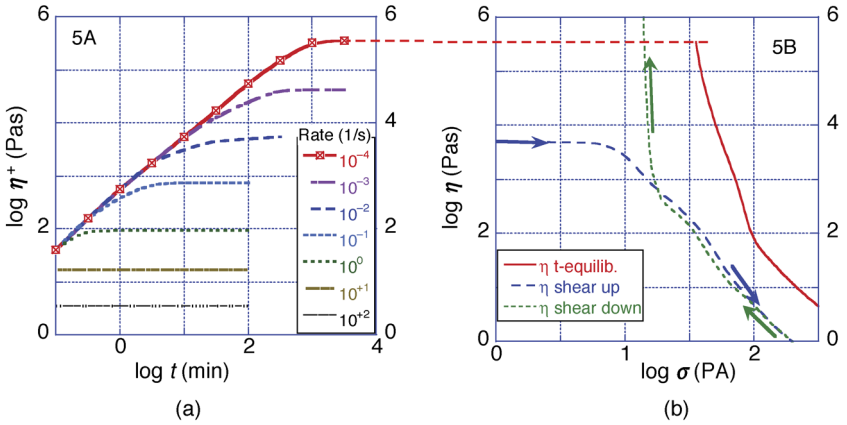

Figure 2.5 Viscosity of highly concentrated emulsion. (5A) Rheopectic character at $\dot{\gamma} = 10^{-4}$–$10^{2}\,s^{-1}$; (5B) summary of the stress-dependence of shear viscosity: the solid line represents the equilibrium values from (5A), the dashed and dotted lines represent emulsion sheared increasing and decreasing stress, respectively. See text for details. Data from Masalova and Malkin [116].

polymer melts may originate from the non-Newtonian matrix or from the effect of filler particles, namely, interparticle interactions or orientation [95–98]. Since the yield stress aspect was briefly treated above, only the orientation effects will be mentioned here. Elongational flow fields are the most efficient for controlling orientation of anisometric particles or crystallizable polymers [65, 84, 89, 99]. Orientation during processing profoundly affects the product performance by generating fibrillar or layered structures, creating weld and/or splice lines, swirls, surface blemishes, and so on.

2.1.2.3 **Emulsion Rheology**

Liquid-in-liquid systems can be divided into three categories: those in which both liquids are Newtonian, those in which both phases are viscoelastic, and systems consisting of one Newtonian and one viscoelastic liquid. The first of these categories are emulsions, E, the second polymer blends, B, and the third undefined class of system is usually used as a model, M, for gaining insight into the effects of elasticity on flow and morphology. Some polymer blends may also be type M.

Several reviews on the emulsion rheology have been published [65, 89, 100–109]. Emulsions containing a high volume fraction of the dispersed phase, $\phi > 0.74$, have been reviewed by Cameron and Sherrington [110]. Emulsions as models for flow of polymer blends and alloys have been discussed by Utracki [1, 4].

A number of factors affect the rheology of emulsions: composition, the viscosity ratio of the dispersed-to-matrix phase ($\lambda \equiv \eta_2/\eta_1$), the droplet size and its distribution, rheology of the interphase, and so on. Often, well-stabilized emulsions follow the viscosity–concentration relationships developed for hard sphere suspensions, including the yield phenomena. In contrast, emulsions with deformable dispersed

phase show elastic responses above a critical deformation rate. The systems are viscoelastic, as observed in the frequency-dependent storage and loss moduli or the time-dependent creep modulus, even if the neat liquids of the two phases are Newtonian.

Newtonian Flow Einstein's treatment of suspensions was extended to emulsions by Oldroyd [111, 112], who incorporated the effects of interphase:

$$\begin{aligned} &[\eta]_e = (5/2)[\Lambda + 2/5]/[\Lambda + 1] \text{ where :} \\ &\Lambda \equiv (\eta_d + \eta_i/5d)/\eta_m; \quad \eta_i = 2\eta_{Si} + 3\eta_{Ei} \end{aligned} \tag{2.17}$$

where the interphase is characterized by two viscosity components: shear (subscript S*i*) and elongation (subscript E*i*). Thus, in emulsions, the intrinsic viscosity is in the range $1 \leq [\eta]_e \leq 5/2$, with the lower limit expected for $\Lambda \to 0$ and the upper for $\Lambda > 100$, where the dispersed drops behave like hard spheres.

Starting with cell model of creeping flow, Choi and Schowalter [113] derived a constitutive equation for an emulsion of deformable Newtonian drops in a Newtonian matrix. The authors characterized the interphase with an ill-defined interfacial tension coefficient, ν_{12}, affecting the capillarity number, $\kappa = \sigma_{12} d/\nu_{12}$. The analysis indicated that depending on magnitude of $\kappa\dot{\gamma}$ the emulsion may be elastic, characterized by two relaxation times. For the steady-state shearing, the authors expressed the relative viscosity of emulsions and the first normal stress difference as:

$$\begin{aligned} \eta_{r,e} &= 1 + \phi \frac{5\lambda + 2}{2(\lambda + 1)} \left[1 + \phi \frac{5}{4} \frac{(5\lambda + 2)}{(\lambda + 1)} + O\left(\phi^{\frac{5}{3}}\right) \right] \\ N_{1,e} &= \phi \frac{2\kappa\eta_m\dot{\gamma}}{5(1 + Z^2)} \left[\frac{(19\lambda + 16)}{4(\lambda + 1)} \left(1 + \phi \frac{5(5\lambda + 2)}{4(\lambda + 1)} \right) + O\left(\phi^{\frac{5}{3}}\right) \right]^2 \\ Z &= \frac{\kappa(19\lambda + 16)(2\lambda + 3)}{40(\lambda + 1)} \left(1 + \phi \frac{5(19\lambda + 16)}{4(\lambda + 1)(2\lambda + 3)} + O\left(\phi^{\frac{5}{3}}\right) \right) \end{aligned} \tag{2.18}$$

The two relaxation times are given as:

$$\begin{aligned} \tau_1 &= \tau_m \left[1 + \frac{5\phi(19\lambda + 16)}{4(\lambda + 1)(2\lambda + 3)} \right] \\ \tau_2 &= \tau_m \left[1 + \frac{3\phi(19\lambda + 16)}{4(\lambda + 1)(2\lambda + 3)} \right] \\ \text{where} \quad \tau_m &= (\dot{\gamma}\kappa/2) \frac{(19\lambda + 16)(2\lambda + 3)}{40(\lambda + 1)} \end{aligned} \tag{2.18a}$$

In Eqs. (2.18) and (2.18a) the subscript m indicates the matrix. For diluted emulsions, the predicted relative viscosity depends on the viscosity ratio and

concentration, but not on the deformation rate. By contrast, $N_{1,e}$ (and the second normal stress difference, $-N_{2,e}$, not shown in this chapter) are proportional to shear stress, $\sigma_{12} = \eta_m \dot{\gamma}$. Since both liquids are Newtonian and the origin of the normal force is drop deformability, the derived relations are equally valid for diluted emulsions of liquid 2 dispersed in liquid 1 or liquid 1 in liquid 2 (the modeled droplet deformation must not be complicated by crowding; hence $\phi \to 0$).

Industrial emulsions are usually prepared as concentrated systems, containing $\phi_m \leq 0.96$ with a wide range of drop sizes with mean of $\bar{d} \cong 15 \pm 5\,\mu$m. Owing to interface interactions and deformability of droplets, at low $\dot{\gamma}$ these systems resemble elastic, soft solids without wall slip, with high normal stresses (N_1 and $-N_2$) and an unexpected shape of the rheological functions. Thus, initially, the $N_{1,e}$ plateau may exceed by several decades that of shear stresses, and then at increasing $\dot{\gamma}$ it could fall to a value below it. Between the highly concentrated and dilute regions, there is a wide zone of structural change reflected in a spectrum of non-Newtonian behavior [114–116].

Drop deformability in dilute emulsion was treated by Taylor [117, 118], who introduced three dimensionless, microrheological parameters: the viscosity ratio, the capillarity number, and the reduced time, namely:

$$\lambda \equiv \eta_2/\eta_1; \quad \kappa \equiv \sigma_{ij} d/\nu_{12}; \quad \text{and} \quad t^* = \gamma/\kappa \tag{2.19}$$

where

η_1 and η_2 are viscosities of the matrix and the dispersed phase,
σ_{ij} is the stress (either in shear, $ij = 12$, or elongation, $ij = 11$),
d is the initial drop diameter,
γ is the strain,
ν_{12} is the interfacial tension coefficient between two phases.

Starting from Taylor's theory, Luciani *et al.* [119, 120] derived an expression for the retraction of slightly deformed drops (about 15% deformation) toward an equilibrium spherical form:

$$\begin{aligned} D(t) &= D_0 \exp\{-t/\tau_{rest}\} \\ \tau_{rest} &= (d\eta_2/80\nu_{12})[(2\lambda+3)(19\lambda+16)/(\lambda+1)] \end{aligned} \tag{2.20}$$

where t is the retraction time and τ_{rest} is the relaxation time. Equation (2.20) has been used to compute the interfacial tension coefficient of polymer blends from slightly deformed drops in shear or elongation.

Taylor derived the equilibrium drop deformability in shear and in elongation as:

$$D \equiv \frac{a_1 - a_2}{a_1 + a_2} = \begin{cases} (\kappa/2)[(19\lambda+16)/(16\lambda+16)]; & \alpha = \pi/4 \\ [\exp\{3\varepsilon/2\} - 1]/[\exp\{3\varepsilon/2\} + 1]; & \alpha = 0 \end{cases}$$

$$\alpha = \pi/4 - \kappa(19\lambda+16)(2\lambda+3)/[80(2\lambda+1)] \tag{2.21}$$

where the initially spherical drop becomes deformed into a prolate ellipsoid with the long axis, a_1, and two orthogonal short axes, a_2, ε is the uniaxial elongational strain (Hencky strain), the orientation angle is α, and $D \cong 0.55\,\kappa$ to $5\,\kappa/8$. The Choi and Schowalter model [113] leads to the following expressions for drop deformability and long axis of the elongated in shear flow ellipsoid:

$$D = \left(\frac{\kappa}{16}\right)\frac{(19\lambda+16)}{\left[(\lambda+1)(1+Z^2)^{1/2}\right]}\left[1+\phi\frac{5(5\lambda+2)}{4(\lambda+1)}+O\left(\phi^{\frac{5}{3}}\right)\right] \qquad (2.21a)$$
$$\alpha = \pi/4 - \tfrac{1}{2}\tan^{-1}(Z)$$

where the Z-parameter is defined in Eq. (2.18).

Since the critical value of drop deformability (D_{cr}) is 0.5, Eqs. (2.21) and (2.21a) predict that drops break at different critical values of the capillarity number, $\kappa_{crit} = \kappa_{crit}(\lambda)$. There are four regions of the reduced capillarity numbers, $\tilde{\kappa} = \kappa/\kappa_{crit}$, in shear and elongation:

$0.1 > \tilde{\kappa}$, droplets do not deform,
$0.1 < \tilde{\kappa} < 1$, droplets deform but they do not break,
$1 < \tilde{\kappa} < 2$, droplets deform then split into two primary droplets,
$\tilde{\kappa} > 2$, droplets deform into stable filaments.

The critical time for drop breakup also varies with λ: $\tilde{t}_b = t_b^*/t_{b,cr}^* = \tilde{t}_b(\lambda)$. Furthermore, when $\tilde{\kappa}$ and $\tilde{t}_b$ are within the drop breakup regions, according to Goldsmith and Mason [70] four mechanisms of drop breakup in shear lead to different blend morphologies:

$0.1 \gg \lambda$, small droplets are shed from sigmoid drops – "tip spinning,"
$0.1 < \lambda < 1$, drop breaks into two principal and an odd number of satellite droplets,
$1 < \lambda < 3.8$, drop deforms into a fiber that then disintegrates into small droplets,
$\lambda > 3.8$ drop may deform but does not break.

However, the morphology of an emulsion or blend depends not only on the discussed above dispersive processes, but also on coalescence observed at low dispersed-phase polymer volume fraction, $\phi_o \approx 0.005$ [121]. Analysis of the steady-state shear coagulation of PVC lattices leads to the critical time [122]:

$$t_{coag} = \left[a_o E^+ d^3\right] / \left[\varrho_d \phi_d^{8/3} \dot{\gamma}^2 (1 + N^+/N^o)\right] \qquad (2.22)$$

where

a_o is a numerical parameter;
E^+ is the threshold energy of coagulation;
N^o and N^+ are the number of coagulating drops, initially at $t = t_o$ and after shearing (coalescence) time, $t = t_c$, respectively;

ϱ_d is the drop density;
ϕ_d the drop volume fraction.

Consequently, Eq. (2.22) predicts that $t_c \propto \dot{\gamma}^{-2}$ and $dt_c/d\phi_d < 0$ – both confirmed by experiments. The coalescence involves collision between two drops, which flattens them, entrapping the matrix. Drainage of the entrapped liquid depends on λ and κ [123]. The film might break when the separation between drops is smaller than the critical separation distance, $h_c \cong 5$ nm [124, 125].

Non-Newtonian Flows Newtonian behavior has been reported for dilute emulsions or emulsions subjected to slow deformation. As the concentration and deformation rate increases, the flow becomes more complex. One, frequently neglected, complication is the time effect – at lower concentration the emulsions may show thixotropy, while in highly concentrated emulsions, $\phi \approx 0.9$, rheopexy dominates. Once the time effects are subtracted, the emulsion usually shows a pseudoplastic character, often with the yield stress. Evidently, the rheological response is a reflection of the inner structure of the emulsion; hence a change of its morphology is inherent to flow.

A linear viscoelastic constitutive model of dilute emulsion viscoelastic properties was proposed by Oldroyd [111, 112]. The model considered low deformation of monodispersed drops of one Newtonian liquid in another, with an interphase. Choi and Schowalter [113] extended their cell model to dilute emulsions with Newtonian matrix and viscoelastic drops under infinitesimally small oscillatory deformation. Oldroyd's model was modified by Palierne [126, 127] for dilute viscoelastic liquids emulsions with polydispersed spherical drops (thus, subject to small deformations) with constant interfacial tension coefficient, ν_{12}, at concentrations below that where the drop–drop interactions start complicating the flow field, that is, $\phi < 0.1$:

$$G^*(\omega) = G^*_m(\omega)\frac{\left[1+3\sum_{i=1}^{n}\phi_i H_i\right]}{\left[1-2\sum_{i=1}^{n}\phi_i H_i\right]} \qquad (2.23)$$

$$H_i = \frac{(4/R'_{di})(5G^*_d+2G^*_m)+(G^*_d-G^*_m)(19G^*_d+16G^*_m)}{(40/R'_{di})(G^*_d+G^*_m)+(2G^*_d+3G^*_m)(19G^*_d+16G^*_m)}$$

$$G^*_i = G^*_i(\omega)\,; \quad R'_{di} = R_{di}/\nu_{12}\,; \quad \text{thus}: \quad H_i = H_i(\omega; R'_d)$$

where

$R_d = d/2$ is the drop radius,
$G^*_i(\omega)$ is the complex modulus,
subscripts m and d indicate matrix and disperse phase, respectively.

The theory is applicable to strain regions without yield stress [128, 129].

Pal [130] modified Eq. (2.23) by introducing an effective volume fraction (ϕ_{eff}), with the following properties: $\phi_{eff} \to 1$ at $\phi = \phi_m$, $\phi_{eff} \to 0$ at $\phi = 0$, and $d(\phi_{eff})/d\phi = 1$ at

$\phi = 0$. These boundary conditions lead to:

$$\phi_{\text{eff}} = 1 - \exp\left\{\frac{-1}{\phi^{-1} - \phi_{\text{m}}^{-1}}\right\} \tag{2.24}$$

Thus, Pal's modification requires that ϕ in Eq. (2.23) is replaced by its effective quantity, ϕ_{eff}, defined in Eq. (2.24), which extends the applicability of Eq. (2.23) up to $\phi \leq 0.449$ in systems with an experimental $\phi_{\text{m}} = 0.57$. Good agreement was demonstrated for G' and G'' at $\omega = 0.001 \rightarrow 8.0$ (rad s^{-1}). Evidently, Eqs. (2.23) and (2.24) are applicable to linear viscoelastic emulsions at $\phi \leq \phi_{\text{m}}$.

The nonlinear flow behavior of concentrated oil-in-water emulsions was studied by Bower *et al.* [131]. Vlahovska *et al.* [132] developed a nonlinear theory of dilute emulsions for surfactant-covered spherical drops with $\kappa \ll 1$. The authors considered Marangoni relaxation, drop rotation, and oscillations in flow. The behavior was described by a nonlinear matrix equation for conditions where the surfactant distribution is slightly perturbed, The interplay between the three dimensionless time-scale parameters leads to a complex rheological behavior, observed in phase-separating polymer blends (or block copolymer gels) at low frequency oscillatory flow as well as in micellar solutions upon start-up of shear flow. Owing to the industrial importance of concentrated emulsions in lubrication, household uses, cosmetics, explosives, and petroleum recovery, there has been significant progress in understanding emulsion behavior at $\phi > \phi_{\text{m}}$ [115, 116, 130, 133–139].

Figure 2.5 shows an example of the rheological behavior of these complex systems. In these emulsions $\phi > \phi_{\text{m}}$ and the droplet diameter ranged from 8 to 21 μm. Figure 2.5a schematically illustrates the creep behavior of W/O emulsion [116]. The water (W) phase was a concentrated NH_4NO_3 solution (density, $\varrho = 1.45$ g ml^{-1}), the oil (O) phase was an emulsified solution of hydrocarbon oil ($\varrho = 0.8$–0.9 g ml^{-1}). Figure 2.5b displays the shear viscosity versus shear stress dependencies. The solid line was constructed from the equilibrium η^+ values in Figure 2.5a, that is, after eliminating the time effect that transformed the zero-shear structure into several ones, each corresponding to the specific stress and deformation. The two other curves show the variation of viscosity with shear rate, $\dot{\gamma}$, first increasing it (broken line) and then decreasing (dotted line). The initial shearing up or down $\dot{\gamma}$ conserves the initial structures and only in the vicinity of $\sigma \approx 10$ Pa do the flow curves suggest formation of a new structure. The loss modulus was nearly constant at frequency $\omega = 0.01$ to 20 rad s^{-1}, showing a solid-like behavior.

The effects of wall slip, interfacial properties, drop size distribution, and drop deformability in emulsions have been discussed in References [134, 140–143]. The performance of bio-emulsions was considered by Stokes *et al.* [144] and Danker *et al.* [145].

Owing to the surface energy, single droplets rarely exist. At low concentration they form doublets, chain structures, and then fractal-type aggregates [134, 146]. The morphological changes may occur during flow as an effect of particle–particle interactions, drop deformation and coalescence (e.g., fibrillation, formation of lamellae), wall and inserts effects, flow segregation (e.g., skin–core structures

developed during flows through long tubes), and so on. Knowledge of the emulsion structures and their changes is essential for understanding the rheology. Despite the discussed complexity of emulsion rheology, these systems may be more precisely designed than polymer blends and thus may be successfully used as their models [30].

2.1.2.4 Melt Flow of Block Copolymers

Styrene–butadiene block copolymers, BCs, were first commercialized by Phillips in 1962. Three years later Shell entered the market with anionic BCs: the diblock, AB, triblock, ABA, and multi-block, $A(BA)_n$. These thermoplastic elastomers are composed of two types of macromolecules, one having rigid and the other elastomeric segments. Depending on the composition and molecular weight of the segments various structures may be produced, namely, lamellar, gyroid, hexagonal, body-centered-cubic (BCC), and, evidently, disordered. The low stress (especially dynamic) flow of a BC accelerates structure ordering, while the high stress leads to its destruction. Heating a BC above the microphase separation temperature (MST) also leads to disordered structures [147]. Leibler [148] has shown that phase separation takes place at $(\chi_{AB}N) \geq 10.5$, where χ_{AB} is the binary interaction parameter and N is the degree of polymerization [149]. Depending on the domain size, domain shape, and the interfacial thickness, BCs exhibits a wide variety of rheological responses [150–154]. Theoretically, the thickness of interphase, Δl, increases with the magnitude of $(N\chi_{AB})^{1/2}$ [155–158]. Experimentally, BC with the interphase thickness, $\Delta l = 2$–6 nm, is unaffected by the addition of homopolymers.

Because of the well-defined molecular configuration that leads to specific morphologies and transitions between them, BCs provide excellent models for the behavior of immiscible PAB. Early work on styrene–butadiene–styrene (SBS) identified two regions of flow: at low deformation rates the "domain" flow might be characterized by yield stress while at high rates the flow is pseudoplastic [159]. More recently, the simultaneous measurements of flow behavior and the structures (by small-angle neutron and X-ray scattering, SANS and SAXS, respectively) has demonstrated close relationships between the two [160–162]. At the same time, simulation has traced the dynamics of structural transformations in the absence or presence of stress [163–167]. Owing to the tendency for formation of regular structures governed by molecular design, BCs are good models for compatibilized, two-phase polymer alloys. These systems show similar rheological behavior to that of BCs, but since their morphology is more difficult to control the interpretation of data is often complicated.

2.2
Theoretical Treatment of Polymer Blends

The theoretical treatment of two-phase flow has been reviewed by several authors [168–170]. As indicated before, dispersions of one Newtonian liquid in another result in systems that are characterized by elasticity and relaxation times, for example, see Eq. (2.18).

In 1990, Honerkamp and Weese published a seminal paper on the use of Tikhonov's regularization for the determination of material functions [171]. The developed method of data treatment was found to be particularly useful for computation of the relaxation and retardation spectra [172, 173]. It has also been used to compute the sphere-size distribution of the dispersed phase in binary blends [174], as well as the ratio of the dispersed drop diameter divided by the interfacial tension coefficient, d/ν_{12} [175]. Friedrich *et al.* [176] modified Eq. (2.23) to read:

$$G^*(\omega) = G^*_{\mathrm{M}}(\omega)\frac{1+3\int_{-\infty}^{\infty} H(\omega, R')u(R')R'\mathrm{d}\ln R'}{1-2\int_{-\infty}^{\infty} H(\omega, R')u(R')R'\mathrm{d}\ln R'} \tag{2.25}$$

where $R' \equiv R/\nu_{12}$, and the new size distribution of sphere sizes $u(R') = \nu_{12}v(R)$ is scaled, derived from-the original distribution. Using Tikhonov's regularization method the distribution function, $u(R')$, may be computed. Experimental data (storage and loss shear moduli, G' and G'', respectively, within six decades of frequency) were determined and transmission electron microscopy (TEM) images obtained for 2, 5, 10, and 20 wt% of PS (polystyrene) in PMMA (poly(methyl methacrylate)). From the dynamic viscoelastic data of neat blend components the monomodal distribution of the $u(R')$ function versus log (R/ν_{12}) was computed and compared with data obtained from the TEM. The agreement found for blends containing 2 and 5 wt% PS was excellent, for 10 wt% it was fair, and for 20 wt% PS, poor. In the latter case, TEM shows a bimodal distribution (possibly resulting from coalescence) whereas from the rheological data a monomodal distribution was obtained. The interfacial tension coefficient computed from these results varied from $\nu_{12} = 2.08$ to $3.10\,\mathrm{mN\,m^{-1}}$. The average value, $\nu_{12} = 2.5\,\mathrm{mN\,m^{-1}}$ at 190 °C, is comparable with the average literature values of: $\nu_{12} = 0.8$ to $1.8\,\mathrm{mN\,m^{-1}}$ at 200 °C [119].

For infinitely diluted viscoelastic emulsions the shear dependence of inherent viscosity was derived as [177]:

$$\eta_{\mathrm{inh}} \equiv \frac{\eta_{\mathrm{r,e}}-1}{\phi} = \frac{1+(5\lambda/2)}{\lambda+1} - f(\lambda)(\sigma_{12}/E_{\mathrm{int}})^2 + O(\sigma_{12}^3) \tag{2.26}$$

where $f(\lambda) > 0$ is a rational function of λ. The relation predicts that, in dilute emulsions subjected to small deformations, η_{inh} should decrease with the square of the shear stress. The effect of stress is moderated by interphase elasticity expressed as E_{int}. The theory was verified experimentally.

Semi-concentrated emulsions were examined theoretically and experimentally only within the linear viscoelastic region [178–181]. Recognizing that the interphase has a final thickness (sometimes the total volume of interphase exceeds that of the dispersed phase) the authors postulated that it might have two interfacial coefficients, ν' and ν'', facing the two principal polymer domains. Next, two models of the interphase were evaluated: (i) a two-dimensional viscoelastic film and (ii) the interphase of final thickness. Both led to at least two relaxation times [181]:

$$\tau_1 = O\left\{\eta(R+\Delta L)\left(1+\frac{R}{\Delta L}\right)^2\left(\frac{1}{\nu'}+\frac{1}{\nu''}\right)\right\}$$
$$\tau_2 = O\left\{\frac{\eta(R+\Delta L)}{(\nu'\nu'')}\right\} \tag{2.27}$$

where $\nu_{12} = \nu' + \nu''$.

The dynamic test data in the kHz region of ionic emulsions could be described using either model. The emulsion elasticity originates in the interphase deformation. For non-ionic emulsions, only one relaxation time was observed. The data were interpreted in terms of the second Oldroyd model in which the interfacial tension is more important than the viscoelasticity of the interphase. The steady state viscosities of both ionic and non-ionic systems at the volume fraction $\phi \leq 0.2$ were found to follow Simha's equation (Eq. (2.8)).

For concentrated emulsions and foams, Princen [182, 183] proposed a stress–-strain theory based on a two-dimensional cell model. Consider a steady state shearing of such a system. Initially, at small values of strain, the stress increases linearly as in elastic body. As the strain increases, the stress reaches a yield point, and then at higher deformation it catastrophically drops to negative values. The reason for the latter behavior is the creation of unstable cell structure that relaxes by recoil. For "real" emulsions the shear modulus and yield stress are expected to follow the expressions:

$$G \equiv \frac{\sigma}{\gamma} \propto \frac{\nu_{12}\phi^{\frac{1}{3}}}{d}; \qquad \sigma_y \propto \; G\tilde{F}_{\max}(\phi) \tag{2.28}$$

where the function $\tilde{F}_{\max}(\phi)$ is the concentration-dependent, dimensionless contribution to stress per single drop. The theory was evaluated using a concentrated oil-in-water system. Reinelt [184] extended Princen's work to sheared, three-dimensional, concentrated foams and emulsions. Initially, the structure was an assembly of interlocked tetrakaidecahedra (with six square surfaces and eight hexagonal ones). An explicit relation for stress tensor up to the elastic limit was derived.

2.3
Rheology of Miscible Blends

2.3.1
General

Miscibility of polymer blends is relatively rare, and is usually limited to a narrow range of independent variables, such as composition of a copolymer, molecular weight, temperature, pressure, and so on [185]. The miscible blends are mainly of academic interest – the information obtained is useful for designing compatibilizers. Exceptions are blends of poly(vinylidene fluoride) (PVDF) with acrylic or polyimide (e.g., PMMA), which are characterized by outstanding UV stability and are used for

outdoor architectural applications. Miscibility of two polymers does not make their rheology simple. For example, in miscible blends of two polymers having glass transition temperatures, T_gs, about 60 °C apart, the molecular dynamics change little from that in the neat state, but the time–temperature superposition fails [186].

Determination of the miscibility of two polymers is not simple. For a semi-crystalline system the depression of melting point provides a measure of the inter-molecular interaction function, χ_{12} [187]. Small-angle neutron or X-ray scattering may also be used for determining χ_{12}. However, since this "parameter" is a complex function of virtually all independent variables, spatially resolved NMR spin diffusion seems to be a more discriminating method, as it provides information of structural and dynamic heterogeneity on the scale from 1 to 200 nm, rendering it capable of resolving even the interphasial thickness [188]. The method identified blends of amorphous PVC (a-PVC) with PMMA, PS with poly(vinyl methyl ether) (PVME), poly(*n*-butyl methacrylate) (PnBMA) with PS and poly(styrene-*co*-acrylonitrile) (SAN) with PMMA as homogenous at 20 nm, but heterogeneous at 2 nm. Only blends of amorphous polyethylene terephthalate (a-PET) with polycarbonate (PC) of bis-phenol-A, of a-PVDF with PMMA, and of amorphous polycaprolactam (a-PCL) with PVC were found homogenous at 2 nm. In PS/PPE (PPE, poly(phenylene ether)) only about 30% of blend components participate in intimate interactions on the scale of <2 nm [1].

The Simha and Somcynsky [189] (S-S) statistical thermodynamic theory offers a way of computing the cohesive energy density (CED) or the solubility parameter as a function of temperature and pressure, $\delta = \delta(T, P)$:

$$\delta \equiv \sqrt{\mathrm{CED}} = \sqrt{\frac{\tilde{U}P^*}{\tilde{V}}}; \quad \tilde{U} = -\frac{\gamma}{2} \cdot \left[\frac{2.409}{\left(\gamma\tilde{V}\right)^2} - \frac{1.011}{\left(\gamma\tilde{V}\right)^4}\right] \tag{2.29}$$

where

U is the internal energy,
V is the specific volume,
P^* is the characteristic reducing pressure,
$\gamma = 1\text{-}h$ is the occupied volume fraction of the hole-cell lattice model.

Symbols with a tilde are scaled [189]. Note that δ depends on the reduced independent variables, $\tilde{P}$ and $\tilde{T}$. Minimization of the entropic contribution to the Huggins–Flory binary interaction parameter leads to Hildebrand's dependence:

$$\chi_h = \frac{\Delta U_m}{V\phi_1\phi_2} \cong (\delta_1 - \delta_2)^2 \Rightarrow 0; \quad \delta_1 \Rightarrow \delta_2 \tag{2.30}$$

Furthermore, since the entropic contribution is usually negative, Eq. (2.30) suggests that minimization of the enthalpic term might provide the necessary condition for miscibility [190]. The required characteristic scaling parameters, P^*, T^*, and V^*, are readily extracted from the *PVT*, data. For polymers δ has been determined in a series of solvent solutions. Since solvents have a much higher free volume fraction than polymer melts, the use of solution data is only acceptable for predicting miscibility in the presence of solvent (e.g., in the paint industry), but not in

its absence. A theoretical derivation based on Eq. (2.29) indicated that solvent may increase the macromolecular mobility equivalent to that found at a temperature about 300 °C higher than the glass transition temperature, that is, at $T_g + 300$ [190].

Rheology may also be used for detecting blend miscibility in the molten state. First, one assumes miscibility of two polymers, from a mixing rule predicts rheological properties of their blends, and then checks if the prediction agrees with the experiment. This approach has been used by Utracki and Schlund [87, 88] for detecting the miscibility of polyethylene blends, LLDPE/LLDPE or LDPE/LLDPE (LLDPE, linear low density polyethylene). Substituting Eq. (2.13) into Gross' frequency relaxation spectrum, H_G, leads to:

$$\tilde{H}_G \equiv H_G/\eta_o = (2/\pi)r^{-m_2}\sin(m_2\theta); \qquad \int_{-\infty}^{\infty} \tilde{H}_G \, d\ln\omega = 1 \tag{2.31}$$

where the two equation parameters r and θ are defined in terms of those in Eq. (2.13). Since the integral over the reduced Gross frequency spectrum equals unity, the coordinates of the maximum $(\omega_{max};\ \tilde{H}_{G,max})$ are related to molecular weight and its polydispersity, respectively. In miscible blends the general relation between the relaxation spectrum of a mixture and its composition follows the third-order blending rule:

$$H_G(\tau) = \sum w_{ijk} H_{Gijk}(t/\tau_{ijk}) \quad \Rightarrow \quad H_G(\omega) = \sum w_i H_{Gi}(\omega) \tag{2.32}$$

The second dependence in Eq. (2.32) is valid when all fractions are either entangled or not. In consequence, the relaxation spectrum of a miscible polymer blend is a linear combination of the component relaxation spectra and their weight fractions, w_i. A strong deviation from linearity in plots of log H_G versus M_w/M_n and log w_{max} versus log η_o indicates immiscibility [87, 88]. The principle that in miscible blends polydispersity can be calculated and used to test for system miscibility was extended to other rheological functions sensitive to polydispersity, namely, the power-law exponent (n), the cross-point coordinates (G_x, ω_x), the free volume gradient of viscosity, the initial slope of stress growth function, and so on [3].

The Doi and Edwards [67] reptation model provides simple mixing rules for miscible systems without the thermodynamic interactions. For athermal systems Tsenoglou [16, 191] proposed the "double reptation model:"

$$G_N^o = \left[\sum_{i=1}^{2} \phi_i (G_{Ni}^o)^{\frac{1}{2}}\right]^2; \qquad \eta_o = \int_0^{\infty} \left[\sum_{i=1} \phi_i G_i^{\frac{1}{2}}(t)\right]^2 dt$$

$$\eta_o = \eta_{o1}\phi_1^2 + \eta_{o2}\phi_2^2 + \frac{4(G_{N1}^o G_{N2}^o)^{\frac{1}{2}}\phi_1\phi_2}{\left[(G_{N1}^o/\eta_{o1}) + (G_{N2}^o/\eta_{o2})\right]}$$

$$J_e^o\eta_o^2 = J_{e1}^o\eta_{o1}^2\phi_1^2 + J_{e2}^o\eta_{o2}^2\phi_2^2 + \frac{8\phi_1\phi_2}{\dfrac{(G_{N1}^o/G_{N2}^o)^{\frac{1}{4}}}{(J_{e1}^o\eta_{o1}^2)^{\frac{1}{2}}} + \dfrac{(G_{N2}^o/G_{N1}^o)^{\frac{1}{4}}}{(J_{e2}^o\eta_{o2}^2)^{\frac{1}{2}}}} \tag{2.33}$$

where

G_N^o is the plateau modulus,
η_o is the zero-shear viscosity,
J_e^o is the recoverable shear compliance.

The dependence was found to be valid for entangled, narrow molecular weight distribution blends of poly(ethylene-*alt*-propylene) with head-to-head PP (polypropylene) [192], and for blends of linear and branched PE (polyethylene) with similar molecular weights and rheological properties [193].

While Eq. (2.33) is valid for monodispersed athermal polymers, in reality polymers are polydispersed and do interact with each other. Consequently, application of the model to a real system requires that the influence of individual molecular weight fractions on the rheological functions is taken into account. For example, in the simplest case of the zero-shear viscosity-composition dependence for entangled systems [194, 195] the prediction is:

$$\eta = 2\sum_i \sum_j \phi_i \phi_j \sqrt{G_{N,i}^0 G_{N,j}^0} \int_{M_e}^{\infty} \int_{M_e}^{\infty} \frac{W_i(M_k) W_j(M_l)}{\frac{M_e^{3.4}(\phi)}{\tau_{e,i}(\phi) M_k^{3.4}} + \frac{M_e^{3.4}(\phi)}{\tau_{e,j}(\phi) M_l^{3.4}}} \mathrm{d}M_k \mathrm{d}M_l \tag{2.34}$$

$$\eta = \phi_a^2 G_{N,a}^0 \tau_{1,a}(\phi) + \phi_b^2 G_{N,b}^0 \tau_{1,b}(\phi) + \frac{4\phi_a \phi_b \tau_{1,a}(\phi) \sqrt{G_{N,a}^0 G_{N,b}^0}}{1 + \tau_{1,a}(\phi)/\tau_{1,b}(\phi)}$$

where

$W(M)$ describes the molecular weight distribution,
M_e is the entanglement molecular weight,
G_N^0 is the plateau modulus,
τ_e is the relaxation time of the entangled segment.

The temperature dependence of the latter function was assumed to follow the Willams-Landel-Ferry (WLF) relation. Eq. (2.34) is fully determined by the component properties. The model prediction was confronted with the experimental data in plots of log η versus ϕ. Agreement was observed for the PMMA/SAN blend. For mixtures of 1,4-polyisoprene (PI) with poly(vinyl ethylene) (PVE) (i.e., PI/PVE), the experimental data followed Eq. (2.34) only when PI and PVE had similar molecular weights. In addition, poor agreement was reported for PMMA with PVDF or with poly(ethylene glycol) (PEG). Booij and Palmen [196] reported that the latter blends are rheologically complex, not following the time–temperature (t–T) superposition. The authors postulated that the deviation originates in the temperature and composition dependent relaxation times of individual macromolecules. Haley and Lodge [195] improved the model accuracy by taking into account tube dilation for predicting the terminal relaxation time of the slower component. In principle, this modification should provide answer whether Booij and Palmen postulate was correct.

Kapnistos *et al.* [197] showed good fit of data to the semiempirical log-additivity equation proposed by Mertsch and Wolf [198]:

$$\ln \eta_o = \phi_1 \ln \eta_{o,1} + \phi_2 \ln \eta_{o,2}^{fit} + \left(\ln \frac{\eta_{o,2}^{fit}}{\eta_{o,1}} \right) \left(\frac{\gamma_{fit} \phi_1 \phi_2}{1 + \gamma_{fit} \phi_2} \right) \tag{2.35}$$

where subscripts 1 and 2 refer to PVME and PS, respectively, while $\eta_{o,2}^{fit}$ and γ_{fit} are fitting parameters of the equation. The γ_{fit} parameter has been introduced to convert the volume into surface fraction of the second component, thus correcting for different shapes of the two statistical segments. As it would be expected from the Arrhenius Eq. (2.1), within the miscible region Eq. (2.35) offered excellent description – the dynamic frequency sweep produced the expected dependencies: $G' \sim \omega^2$ and $G'' \sim \omega$. However, the regular rheological behavior broke down near binodal. Apparently, the phase separation leads to more elastic blends; thus variation of the independent variables affected G' more than G''.

Low molecular weight PS was mixed with poly(methyl phenyl siloxane), PMPS, to form an immiscible blend with an upper critical solution temperature (UCST) [199]. The viscoelastic properties were studied by dynamic and steady-state shearing; the neat polymers showed Newtonian behavior. Within the miscible region the blend viscosity followed the Mertsch and Wolf equation, Eq. (2.35), but with the parameter $\gamma_{fit} = -0.5$ calculated from Bondi's tables. The phase separation created a rheologically complex behavior.

As quoted by different authors, blends of SAN with styrene–maleic anhydride (SMA) are miscible. The glass transition temperatures of the neat polymers are $T_g^{SAN} = 106$ °C and $T_g^{SMA} = 153$ °C, while the blends show the dependence $T_g = 106.3 + 0.161w + 0.00299w^2$, with $r = 0.999$. Notwithstanding the difference in molecular dynamics, the blends obeyed the time–temperature superposition principle [200].

Despite the customary identification of PPE/PS blends as miscible, their miscibility is limited to about 30% of directly interacting segment – the rest forms nanometer-size dispersed domains in this matrix [1]. As shown in Figure 2.6, the data of the plateau modulus and the zero-shear viscosity at a constant distance from the glass transition, $T = T_g + 15$, nearly follow the log-additivity rule proposed for liquid mixtures, Eq. (2.1) or (2.2).

Blends of PS with PVME have a lower critical solution temperature (LCST) of 90–180 °C, thus their flow behavior may be studied within the miscible, immiscible, and phase separating regions. In the miscible region, addition of PVME plasticizes PS [202–204]. Near T_g the time–temperature superposition principle (t–T) is not valid [205], but it is obeyed for deutereous PS below LCST(PS) + 40 °C [202]. However, at higher temperatures their relaxation times deviate with a magnitude dependent on the molecular weight ratio [206–210]. Kim and Son [211] plotted log G' versus log G'' for different compositions and temperatures; at 10 wt% PS the data formed a linear dependence independent of T, stretching from below to above LCST. As PS content increased to 30 or 50 wt% the superposition was limited to the miscible region at $T <$ LCST. A plot of isothermal log η_o versus composition showed negative deviation from the log-additivity rule – stronger within the metastable region of phase separation than within the immiscible one.

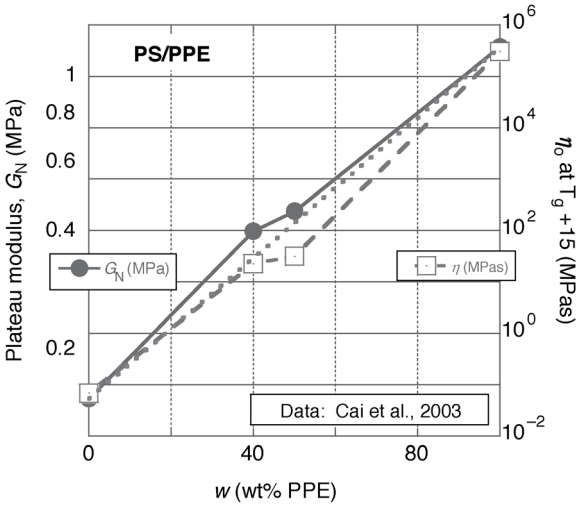

Figure 2.6 Plateau modulus and zero-shear viscosity of PPE/PS blends as functions of composition. Points are experimental; the lines are to guide the eye. Error bars are within the symbols. The dotted line represents the log-additivity dependence. Data from Cai *et al.* [201].

2.3.2 Phase Separation and Flow

Most polymer blends phase-separate with LCST; thus the miscibility region stretches from the melting point or T_g up to the binodal while the phase-separated region exists above the spinodal temperature, T_s [1, 212]. Within the region between binodal and spinodal the system is metastable, characterized by strong interrelation between the rheology and thermodynamics [211, 213–215].

2.3.2.1 Influence of Thermodynamics on Rheology

Rapid change of temperature to T_s causes phase separation by the mechanism known as spinodal decomposition (SD), which is characterized by the presence of two interpenetrating continuous phases that coarsen with time. Thus, the morphology within the metastable region is time dependent and in consequence so is the rheological response. Theoretically, instantaneous SD formation of interpenetrated structures causes the linear viscoelastic functions to go to infinity [216, 217]:

$$G'(\omega) \propto \frac{\omega^2}{\left[(\chi N)-(\chi N)_s\right]^{\frac{5}{2}}}; \qquad G''(\omega) \propto \frac{\omega}{\left[(\chi N)-(\chi N)_s\right]^{\frac{3}{2}}}$$

$$\therefore \quad \lim_{T \to T_s} G'(\omega) = \lim_{T \to T_s} G''(\omega) = \infty \tag{2.36}$$

where $|(\chi N)_s - (\chi N)|$ is a thermodynamic distance from the spinodal. The theory indicates that approaching phase separation the rheological functions should

increase. However, in practical systems the rate and the magnitude of the increase vary from one system to another.

For steady-state shear flow of a spinodal blend, Onuki [218–220] postulated that the shear stress is the same in two phase-separating liquids, which leads to the effective viscosity and the first normal stress difference as:

$$\text{at SD}: \qquad \frac{1}{\eta_{\text{eff}}} = \frac{\phi_1}{\eta_1} + \frac{\phi_2}{\eta_2} \approx \frac{2\phi_1}{\eta_1}; \qquad N_1 \propto \dot{\gamma}\frac{\phi_1\eta_2}{\phi_2} \approx \dot{\gamma}\frac{\phi_1\eta_1}{\phi_1} \approx \sigma_{12} \tag{2.37}$$

The dependence implies that at SD or phase inversion the viscosity ratio equals the volume fraction ratio of the separated phases: $\lambda \equiv \eta_2/\eta_1 = \phi_2/\phi_1$ – this assumption also was used in deriving Eq. (2.6).

Sharma and Clarke [221] suggested the use of an isochronal ($\omega = 1\,\text{rad}\,\text{s}^{-1}$) dynamic temperature scan for detecting the critical temperature of miscibility. A plot of either log G' or log(tanδ) versus T for deuterated-PS (PSD)/PPE blend had a slope that changed at LCST = 104 °C. The method also provided information on the range of the metastable zone of temperatures. A similar conclusion was draw from the dynamic data at $\omega = 0.1\,\text{rad}\,\text{s}^{-1}$ [197].

As PS/PVME blends have a LCST at a convenient temperature of about 110 °C they have been studied since the early 1970s [222]. Dynamic scattering indicates that depending on the temperature and composition the phase separation follows either the nucleation and growth (NG) or spinodal decomposition (SD) mechanism – the former occurs within the metastable region between binodal and spinodal and the latter within the spinodal region. Following NG or SD the morphology coarsens with time, following several mechanisms. Since blend morphology and kinetics of phase separation are expected to affect the rheological functions, great care is needed in collecting rheological data and interpreting them [223, 224]. The two polymers have widely different glass transitions, T_g(PS) = 373–378 and T_g(PVME) = 227–247 K. The T_g of their blends shows a negative deviation from additivity, that is, PVME acts as a macromolecular solvent/plasticizer of PS, especially when the ratio of molecular weights, M_w(PS)/M_w(PVME), is large [202–209]. When the ratio is about 2, a passage through the phase separation region affects G' but not G'', while for the ratio <1 the moduli increase upon entering the phase separation region.

LCST-type blends of PMMA (containing 12 wt% of ethyl acrylate) with 10–60 wt% of SMA were studied in terms of dynamic shear flow, turbidity, and light scattering [225]. The binodal and spinodal temperatures (T_b and T_s, respectively) were extracted from the linear viscoelastic moduli. The former was determined by plotting log G' versus T (temperature sweep data) – departure from a straight line was taken as T_b. Determination of the spinodal T_s involved linear extrapolation to zero of the increasing ratio: $[G''(\omega)]^2/[TG'(\omega)]^{2/3}$ plotted against $1/T$. The rheological results corresponded qualitatively to results from the scattering data.

Mani *et al.* [210, 226] have measured the fluorescence intensity during a temperature scan (at $1\,\text{K}\,\text{min}^{-1}$) of PS/PVME blends while shearing in a cone-and-plate

geometry, thus mapping the phase separation region and recording σ_{12} and N_1 at shear rates of $\dot{\gamma} = 0$, 1, 2, and 8 s^{-1}. The shear and normal stresses showed a similar dependence; crossing the binodal introduced little if any change, but crossing the spinodal disturbed the plot. The *t–T* superposition principle was found valid only within the miscible region. The phase separation temperature increased with $\dot{\gamma}$.

A series of rheological and thermodynamic data for polymer blends was published by Bousmina and his colleagues. For example, El-Mabrouk and Bousmina [227] studied phase separation of PS/PVME under quiescent and shear flow conditions, using an on-line optical microscope and rheo-optics on the constant strain in ARES-LS. As $\dot{\gamma}$ increased from zero, T_b decreased to the composition-independent minimum value, inversely proportional to the Rouse relaxation time, τ. A weak and a strong shear regime exist below and above the $\dot{\gamma}\tau = 1$ condition, respectively. The former induces shear de-mixing (SID) and the latter shear mixing (SIM). At low $\dot{\gamma}$ flow enhanced concentration fluctuation and phase segregation, while at high $\dot{\gamma}$ flow preserved the apparent miscibility. Empirically, the reduced $\tilde{T}_b \equiv [T_b(\dot{\gamma}) - T_b(0)]/T_b(0) \propto \dot{\gamma}^{\frac{2}{3}}$ agreed with the theoretical predictions. The *t–T* superposition was observed only at $T < T_b$. In blends of PVME ($M_w = 90.7$ kg mol^{-1}) with PS ($M_w = 34.5$, 62, 104, and 345 kg mol^{-1}), T_b decreased with increasing M_w of PS [228, 229]. Next, PS/PVME films, 15–300 nm thick, were prepared by spin casting, followed by annealing at 150 °C, that is, at $T > T_s$. The slowly heated films (0.2 °C min^{-1}) were observed by small-angle laser light scattering (SALLS), atomic force microscopy (AFM), optical microscope, and X-ray photoelectron spectroscopy (XPS). SD was found only in thick films, while in the thin ones rapid phase separation proceeded by NG. The difference might be related to the surface energy effect on the molecular mobility [230, 231].

2.3.2.2 Influence of Rheology on Thermodynamics

Miscible blends that separate with LCST at $T \leq T_b$, are characterized by slow fluctuation with the characteristic lifetime of τ_γ. The shear flow may suppress these fluctuations [232], but if the Deborah number (*De*) is large then shearing may lead to phase separation [220]:

$$De \equiv \dot{\gamma}\tau_\gamma > 1 \tag{2.38}$$

In other words, LCST blends sheared slightly below binodal may phase separate in a manner similar to shear coagulation or crystallization. The situation is different within the metastable region at $T_b \leq T \leq T_s$. For $De < 1$ the blends may phase separate by a slow NG process, while for $De > 1$ shearing may result in finer dispersion down to drops with commeasurable size to the radius of gyration. The process would suppress turbidity and delay detection of the phase separation, giving the impression that $T_b(0) \leq T_b(\dot{\gamma})$. Homogenization of LCST blends by shearing has been related to the reduction of drop diameter [233–236].

The strain compatibilization of LCST blends was found to be similar [4] to that reported by Lyngaae-Jørgensen [237] for the styrene–butadiene–styrene (SBS) block copolymer that separates with the upper critical solution temperature, UCST. Thus, low, steady state shearing shifted the spinodal temperature: $T_s(\gamma) - T_s(0) \leq 29$ °C.

The data followed a semiempirical relation:

$$\sigma_{12,\mathrm{cr}}^2 \cong a_\mathrm{o} T(T_\mathrm{s} - T) \tag{2.39}$$

where a_o is a material parameter. The relation was found valid for PS/polybutadiene/di-octyl phthalate (the critical point shifted as $\Delta T_\mathrm{c}(\dot{\gamma}) \approx a_\mathrm{o} T_\mathrm{c} \dot{\gamma}^{\frac{1}{2}}$ [223]) as well as for other systems [4].

Horst and Wolf [238, 239] postulated that, for flowing blends, the free energy of mixing, ΔG_m, is reduced by the flow-induced stored energy, ΔE_s, related to the average compliance, $\langle J_\mathrm{e}^0 \rangle$, and average zero-shear viscosity, $\langle \eta_\mathrm{o} \rangle$:

$$\Delta G_{\dot{\gamma}} = \Delta G_\mathrm{m} - \Delta E_\mathrm{s} = \left(\sum x_i V_i\right) \langle J_\mathrm{e}^0 \rangle [\langle \eta_\mathrm{o} \rangle \dot{\gamma}]^{2n}$$

$$\text{where : } \langle J_\mathrm{e}^0 \rangle = \left(\sum w_i J_{\mathrm{e},i}^0 \eta_i^{4.4/3.4}\right) \Big/ \left(\sum w_i \eta_i^{1/3.4}\right)^{4.4}$$

$$\langle \eta_\mathrm{o} \rangle = \left(\sum w_i \eta_i^{1/3.4}\right)^{3.4} \tag{2.40}$$

The relation predicts that, initially, as $\dot{\gamma}$ increases the system undergoes homogenization, then phase separation, followed by another homogenization and demixing. These predictions were confirmed by experiments on blends of ethylene-*co*-vinyl acetate (EVAc) with chlorinated polyethylene, CPE, and PS/PVME [240–244]. The shear-induced mixing was also observed in PS blends with polyisobutylene, PIB [245].

The planar elongational flow of PS/PVME at $\dot{\varepsilon} = 0.012 - 26\,\mathrm{s}^{-1}$ increased T_s by $\Delta T_\mathrm{s} = 2\text{–}6\,^\circ\mathrm{C}$ [241]. The homogenization was controlled by the elongational strain. Its critical value for miscibility was found to be $\varepsilon_\mathrm{c} = \dot{\varepsilon} t_\mathrm{c} = 44 \pm 14$ (t_c is the time for achieving miscibility). This observation suggests that the mechanism of flow induced miscibility is related to deformation; after cessation of flow, the deformation dissipates and the homogenized blend phase separates within 20–70 s. However, at high planar stresses, $\sigma_{11} \geq 30\,\mathrm{MPa}$, the PS/PVME blend undergoes phase separation, possibly caused by a difference in the rheological behavior of the blend components.

The relation between rheology and morphology during late stages of SD was investigated by means of several techniques [247, 248]. The results were interpreted using the Doi–Ohta theory [249]. Shearing the two-phase blend reduced the scattering dimensions, which decreased turbidity. Matsuzaka *et al.* [250] sheared polyisoprene/polybutadiene (PI/PB) blends at $\omega = 0.63$ and $6.3\,\mathrm{rad\,s}^{-1}$ and a high strain of $\gamma_\mathrm{o} = 0.8$. The spinodal decomposition after a temperature jump was observed *in situ* only at the lower frequency, while at the higher frequency a modified SD pattern emerged only after ending of oscillation. The same blends were also studied by Jeon *et al.* [246].

Figure 2.7 displays a η_o versus ϕ of PI plot at 130 °C, that is, at variable distance from the binodal – only the limiting data points were measured near the cloud-point curve, the rest within the metastable or spinodal region. Despite the phase separation, η_o shows additivity for $\phi \leq 0.3$ and negative deviation above. Remarkably, the dynamic moduli of the blend with $\phi = 0.4$, measured at 30–130 °C, obeyed the t–T superposition principle with the terminal slope of loss modulus,

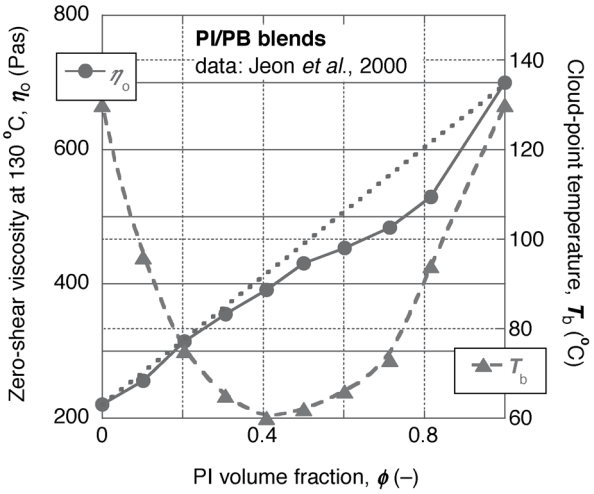

Figure 2.7 Zero-shear viscosity of polyisoprene/polybutadiene (PI/PB) blends at $T = 130\,^{\circ}\mathrm{C}$ as a function of composition. Points are experimental; the solid line is to guide the eye, the dotted line indicates additivity. Error bars are within the symbols. The dashed line represents the binodal temperature at rest. Data from Jeon *et al.* [246].

$\partial \ln G''/\partial \ln(\omega a_T) = 1$. The terminal region for G' was more complex, as the predicted slope of 2 decreased to a final $^1/_2$. This deviation was interpreted as caused by the presence of elastic membranes with the ϕ-dependent interfacial tension coefficient calculated from Palierne [126] or Gramespacher and Meissner [251] models. The authors observed different responses when tested (i) at constant strain amplitude of $\gamma_o = 0.08$ and (ii) at constant stress, $\sigma = 5\ \mathrm{kN\ m^{-2}}$. Thus, in the terminal zone the blends with $\phi = 0.4$ measured at constant strain showed high G' values, whereas at constant stress the theoretical slope of $\partial \ln G'/\partial \ln(\omega a_T) = 2$ was obtained – the difference was assigned to the different domain deformation.

The final set of papers examined here is not connected with the relationships between flow and phase separation, but rather with that between flow and morphology. The blends of narrow molecular weight distribution ($M_w/M_n \leq 1.1$) poly(ethyl ethylene) (PEE) with poly(dimethylsiloxane) (PDMS) were compatibilized with their diblock copolymer: PEE/PDMS/PEE-PDMS; the polymer molecular weight of the was: 1.71, 2.13, and 10.4 ($\phi_{PEE} = 0.52$) kg mol^{-1}, respectively [252, 253]. The dynamic and steady shearing tests were carried out at $T = 15$–$30\,^{\circ}\mathrm{C}$ – the t–T superposition principle was not obeyed. *In situ* neutron and light scattering as well as optical microscopy showed four ranges of $\dot{\gamma}$, corresponding to flow-induced domain structures. At low $\dot{\gamma} \leq 0.1\ \mathrm{s^{-1}}$ the Newtonian $\eta = \eta_o$ plateau was observed, whereas at $0.1 \leq \dot{\gamma} \leq 1.3$ the shear thinning resulted from anisotropy of morphology. Increasing $\dot{\gamma}$ to $20\ \mathrm{s^{-1}}$ caused an abrupt breakdown of the bi-continuous structure, resulting in flow-induced phase separation where σ_{12} was almost independent of $\dot{\gamma}$. Within the highest shear range, $20 \leq \dot{\gamma} \leq 300$, the sample resembled a highly elongated, immiscible binary blend. These experimental results were qualitatively reproduced by

computer simulation using Brownian dynamics of non-interacting bead-spring macromolecules, postulating that polymer chain conformations and their flow deformations affect the phase, structural, and rheological behavior [254]. A similar sequence of rheological responses and domain deformations might be expected when shearing binary blends in their late stage of spinodal decomposition.

2.4 Rheology of Immiscible Blends

2.4.1 Rheological Equations of State

In immiscible PAB the rheology and morphology are interrelated through the evolution of interphase with its own rheological properties. Thus, the most promising route to a comprehensive theory of blend flow may start with the Helfand and Fredrickson [255] lattice theory. However, over the years the theoretical treatment of emulsions and blends has been based on a microrheological model for drop deformation and breakup [117, 118], which is applicable to highly diluted mixtures of Newtonian liquids. These droplet-based theories predict droplet deformation and breakup by capillary waves during the steady state and dynamic flow – once the morphology is correctly predicted, the rheology follows. The limiting volume fraction of the dispersed phase of this model is about $\phi \leq 0.01$ – extension to higher concentrations, $\phi \leq 0.2$, involve incorporation of flow-induced coalescence [121, 124, 256–258].

Doi and Ohta [249], and then Doi and Onuki [259], considered a simplified model of two immiscible liquids at $\phi_1 = \phi_2 = {}^1/_2$, having the same viscosity and density, focusing primarily on the interface and the flow-induced evolution of the interfacial area and orientation. Instead of the interphase the authors assumed an interface without thickness – consequently, postulating that the interface does not perturb the flow field (the passively advected interface). Thus, a semi-phenomenological kinetic equation describes the time evolution in a given flow field of the interfacial area per unit volume, Q, and its anisotropy, tensor q_{ij}:

$$\begin{aligned} Q &= \frac{1}{V}\int \mathrm{d}s; \quad \mathrm{d}Q/\mathrm{d}t = -d_{ij}q_{ij} \\ q_{ij} &= \frac{1}{V}\int \left[n_i n_j - \frac{\delta_{ij}}{3}\right]\mathrm{d}s \\ \mathrm{d}q_{ij}/\mathrm{d}t &= -q_{ik}d_{kj} - q_{jk}d_{ik} + \tfrac{2}{3}\, d_{ij}d_{lm}q_{lm} - \frac{Q}{3}(d_{ij}+d_{ji}) + \frac{q_{lm}d_{lm}}{Qq_{ij}} \end{aligned} \tag{2.41}$$

where

n_i is the unit vector normal to interface,
V is the system volume,

ds is an interface element,
$d_{ij} \equiv du_i/dx_j$ is the macroscopic velocity gradient tensor.

The stress tensor for the model system was expressed as:

$$\sigma_{ij} = \eta_m(d_{ij} + d_{ji}) - \nu_{12} q_{ij} - P d_{ij} \tag{2.42}$$

where η_m is the matrix viscosity and ν_{12} is the interfacial tension coefficient. The relation predicts a scaling behavior for the stress and the velocity gradient tensors, σ and κ:

$$\begin{aligned} &\sigma(t, [\tilde{\kappa}(t)]) = c\sigma(ct, [\kappa(t)]) \quad \text{and} \qquad \tilde{\kappa}(t) = c\kappa(ct) \\ &\sigma(c\dot{\gamma}) = c\sigma(\dot{\gamma}); \quad \sigma_{12} \propto \dot{\gamma} \quad \text{and} \qquad (\sigma_{11} - \sigma_{22}) \propto \dot{\gamma} \end{aligned} \tag{2.43}$$

where c is a number. The model has been applied mainly to blends with a low concentration of the dispersed phase. As might have been expected, it failed describing the rheology of a simple Newtonian liquid emulsion [260] or poly(ethylene terephthalate)/polyamide-66 (PET/PA-66) blends [261] – only the scaling relationships were found valid. However, it correctly predicted an extra stress arising from the interfacial tension and the transients (in η and N_1) at startup. In the steady shear flow the agreement was poor, the recovery overshoot and shear thinning and the experimental transient stress curves after step-change of shear rate were not predicted. Better agreement for the transient effects at the startup of steady state shearing was reported for PIB/PDMS [262]. The scaling laws in Eq. (2.43) were also obeyed.

Lee and Park [263] derived a more general constitutive equation for immiscible blends, which compared well with the dynamic shear data of PS/LLDPE blends over a full range of frequency and composition. Their model included the dissipative time evolution of Q and q_{ij}, written as functions of (i) the degree of total relaxation, (ii) the size relaxation strongly dependent on concentration, viz. $\propto \phi^2$, and (iii) the break-up and shape relaxation, assumed dependent on $(1-\phi)$. The parameters contain adjustable constants and depend on concentration as well as on the deformation mode. The interfacial tension coefficient was assumed to be constant, independent of ϕ. As before [249, 264], the constitutive equation was written in form of three functions: $\partial q_{ij}/\partial t$, $\partial Q/\partial t$ and σ_{ij}. The model predicts well the dynamic moduli of PS/LLDPE blends, but not the shear thinning.

Lacroix *et al.* [265–267] studied evolution of the morphology in immiscible polymer blends in shear and extensional flows. The authors used Lee and Park's relaxation term but replaced the stress expression with the one derived by Grmela and Aït-Kadi [264], and introduced a conformation tensor, $\mathbf{C}$: $(\partial C_{ij}/\partial t) + C_{kj}\kappa_{ki} + C_{ki}\kappa_{kj} = 0$, which characterizes a surface element. In the absence of flow, the relaxation terms of the Doi–Ohta model eventually drive the interfacial area to zero. This correctly represents the long-term equilibrium state of complete phase segregation. For PP/EVAc/EMA blends the theory qualitatively described the morphology evolution as well as the morphological changes after stress relaxation. However, for PS/PE blends the comparison between theory and experiments was less satisfactory.

For several decades Grmela and his colleagues developed a general framework for rheological functions, based on thermodynamics. The work eventually led to the so-called "general equation for the non-equilibrium reversible-irreversible coupling" (GENERIC) [268–270]. Thus, for isothermal and incompressible fluids, GENERIC expresses the time evolution of a state variable, x, combining the thermodynamics and mechanics, viz.:

$$\dot{x} = \boldsymbol{L}\boldsymbol{\Phi}_x - \partial\Xi/\partial\boldsymbol{\Phi}_x \tag{2.44}$$

where

$\dot{x}$ is a time derivative,
$\boldsymbol{L}$ is a Poisson bivector,
$\boldsymbol{\Phi}_x$ is the x-derivative of the total free energy, $\boldsymbol{\Phi}$,
Ξ is the dissipation potential.

Thus, the first term on the right-hand side of Eq. (2.44) expresses compatibility with mechanics, and the second term that with thermodynamics. The Poisson bivector transforms a potential gradient into a vector, that is, kinematics of the state variable x. The GENERIC formalism was applied to the flow of polymer blends [271].

The morphology is considered using the Doi–Ohta type interfacial conformational tensor as well as the droplet deformation approach. Assuming isothermal conditions, the authors formulated time evolution of several state variables, viz. the extra stress tensor, the conformation tensor, local morphology, global morphology, and the number of droplets. Depending on the assumed form of the Helmholtz free energy, the time evolution equation takes on different forms, for example, that derived by Doi and Ohta [249] or that of Maffettone and Minale [272]. The obtained expressions were compared with detailed dependencies of the interface morphology and rheology. Another publication examined the theoretical and experimental dependencies for the ellipsoidal droplet-type morphology of two Newtonian liquids, PDMS and PIB [273]. The authors first compared the prediction of the theory with deformation of PDMS drops in PIB during slow steady-state shearing at $\dot{\gamma} \leq 1\ s^{-1}$, and then relaxing [274]. Excellent agreement with the model behavior was obtained for η and N_1 [275, 276]. This work demonstrated that it is possible to extract morphology from the rheological data and vice versa, to predict rheological functions from morphology in transient or steady state flow.

Recently, Gu and Grmela [277] published a clear, concise review of the use of the GENERIC for describing flow behavior of immiscible blends. The authors also converted the Doi–Ohta model from the passive into active advection by filling the thermodynamic framework of the GENERIC with the mesoscopic formulation of Stokes problem. The perturbation of flow caused by the presence of the interface and the "rheological inhomogeneity" of the two polymers was incorporated by introduction of a tensor $\boldsymbol{w}$ that is a conjugate of the perturbed velocity gradient. The modified Doi–Ohta model was compared with published experimental data [266, 276, 278, 279]. Good agreement was obtained for the nonlinear rheological responses to imposed shear flows – significantly better than that of the original Doi–Ohta model

and its modifications. However, the agreement for the time evolution of η at the startup was less satisfactory – the predicted magnitude of the overshoot was correct, but the time needed for reaching the steady-state value was much longer than computed.

2.4.2 Morphology of Immiscible Blends

The properties of immiscible blends depend on the component polymers and their concentration, the interphase and the morphology. The latter is controlled by the thermodynamics, the flow during compounding and forming, as well as by the post-processing treatments. At low volume fraction of the dispersed phase, droplets are expected, while in the middle concentration range phase co-continuity is anticipated [32, 33, 280, 281]. Under stationary conditions the spherical drop dispersion region stretches up to the percolation volume fraction, $\phi_{perc} \approx 0.16$. Thus, at equilibrium the phase co-continuity exists within the concentration range $\phi_{perc} \leq \phi \leq (1 - \phi_{perc})$, with the phase inversion at ϕ_I, calculable from Eq. (2.6) [34, 35]. However, as discussed above, strain causes drop deformation and imposes orientation controlled by the three microrheological dimensionless parameters of Eq. (2.19). For example, owing to fibrillation, the phase co-continuity was observed by Lyngaae-Jørgensen and Utracki at $\phi \leq 0.001$ [36].

In most cases, the change of morphology by thermodynamics (e.g., SD versus NG phase separation) or flow (namely, shear versus irrotational flow field) evidences the non-equilibrium conditions. However, when such a transient structure is preserved by rapid solidification, the blend performance might be strongly influenced. Su *et al.* [282] reported that the morphology of a high-density polyethylene (HDPE) blend with polyoxymethylene (POM) was affected by stresses during the dynamic injection molding in three ways: (i) by improving dispersion of the minor phase, (ii) by elongating the dispersed drops, and (iii) by changing the macromolecular conformation; the latter effect was deduced from comparison with homopolymer performance.

Highly interesting is the region near the phase separation where, depending on the processing conditions, one may engender either a dispersed or co-continuous morphology by falling into NG or SD region, respectively. The latter possibility is particularly interesting when toughening a rigid polymer by incorporating an elastomer, which if done correctly may lead to co-continuous morphology. The size of the SD structure depends on the kinetics and flow – extensive coarsening changes SD morphology to droplet dispersion (similar to that obtained in the NG phase separation) and eventual full phase segregation. Thus, the coarsening needs to be controlled by adjusting the quenching rate, addition of a stabilizing or interfacial agent, addition of a third polymer (immiscible with the two main blend components), and so on. The final size of the fibrillated minor phase ranges from about 10 to 105 nm. Recently, the Fourier-transform rheological method was used to characterize a diluted ($\phi = 0.1$) blend's morphology [283]. The extracted volume-average drop diameter was consistent with that computed from dynamic data using Eq. (2.23).

2.4.3 Microrheology of Polymer Blends

The microrheology discussed in Section 2.1.2.3 describes the breakup of isolated drops in a Newtonian system. The mechanisms leading to deformation and breakup take into account the three principal variables: the viscosity ratio (λ), critical capillary number (κ_{crit}), and the reduced time (t^*), defined in Eq. (2.19). For application of microrheology to polymer blends the theories developed for Newtonian emulsions need to be extended to viscoelastic systems in the full range of composition, that is, they must take into account coalescence. Since the microrheology evolution up to about the year 2000 has been summarized by Utracki and Kamal [3] the following text will focus on more recent developments.

2.4.3.1 Deformation and Breakup of Viscoelastic Drops

Emulsion microrheology predicts that in a Newtonian system a drop will break when the deformability exceeds $D > {}^1/_2$, that is, when the reduced capillarity number $1 < \tilde{\kappa} = \kappa/\kappa_{cr} < 2$ (Eq. (2.21)). Most experimental data for viscoelastic systems indicate that the drop elasticity has a stabilizing effect thus, that κ_{cr} and the minimum drop diameter for drop break increase with drop elasticity [284–286]. When conditions are identical for Newtonian and viscoelastic drops, the latter fibrillate easier and upon cessation of flow the filament breakup and formation of satellite drops are retarded by elasticity [287].

Vinckier *et al.* [262, 278, 279, 288] have studied the relationship between flow and morphology in a model system of PIB/PDMS using one grade of viscoelastic PDMS and two grades of Newtonian PIB. First, the blends were pre-sheared in steady state then probed in dynamic mode. As predicted by Eq. (2.23) the presence of the interface significantly enhanced the storage modulus, G'. The volume-average drop diameter, d_v, was nearly proportional to inversed shear rate: $d_v \propto 1/\dot{\gamma}$. However, the magnitude of the G' enhancement in the secondary plateau was the largest for the slowest pre-shearing, that is, for blends with the largest and the easiest deforming drops. The steady state behavior of the blend was compared with the Doi–Ohta model (Section 2.4.1). The authors extracted from the theory the dependence for the "surface-to-volume" drop diameter:

$$\bar{d}_{sv} = \frac{6\phi}{Q} \cong \left(\frac{12\mu}{\mu+1}\right)\left(\frac{\phi\nu_{12}}{N_{1,excess}}\right) \tag{2.45}$$

where

Q is the interfacial area per unit volume,
ν_{12} is the interfacial tension coefficient,
$N_{1,\ excess}$ is the excess normal force due to the interface,
$\mu = \mu(\phi)$ is a concentration-dependent parameter (displayed in Figure 2.8).

In a subsequent publication the authors concentrated on the transient rheology/morphology response to flow [262]. For affine deformation at $\kappa > 2\kappa_{crit}$ the authors

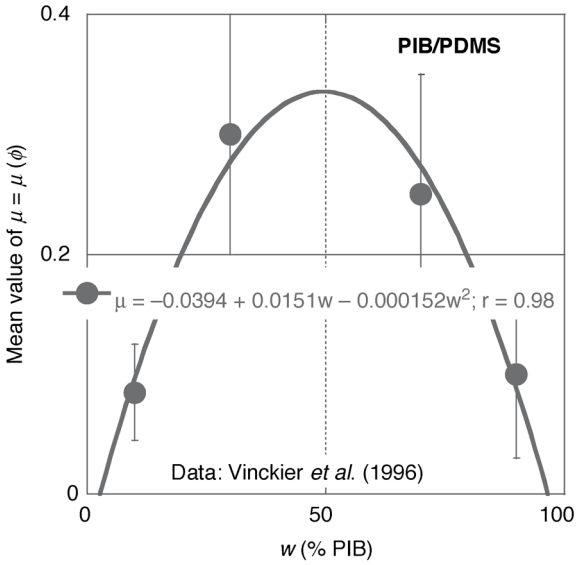

Figure 2.8 Mean-average phenomenological parameter: $\bar{\mu} = \bar{\mu}(\phi)$ at $\dot{\gamma} = 0.3{-}6.0(1/s)$ for PIB/PDMS blends as a function of PIB content. The error bars indicate the observed spread of values. Data from Vinckier *et al.* [288].

derived simple relations for the steady-state shear and normal stresses as functions of the rate of shear, $\dot{\gamma}$, strain, γ, and the initial drop diameter, d_o:

$$\sigma_{12}(\gamma, \dot{\gamma}, d_o) = \dot{\gamma} \sum \phi_i \eta_i + \tilde{\Upsilon}$$
$$N_1(\gamma, \dot{\gamma}, d_o) = \sum \phi_i N_{1,i} + \tilde{\Upsilon}\dot{\gamma}$$

where :

$$\tilde{\Upsilon} \equiv \frac{2\nu_{12}\phi\left(1 + \frac{\gamma^2}{2} + \frac{\gamma}{2}\sqrt{\gamma^2+4}\right)^{1/4}}{d_o\sqrt{\gamma^2+4}} = \Upsilon(\gamma)\left(\frac{\nu_{12}\phi}{d_o}\right) \cong \left(\frac{2}{\gamma^{1/2}}\right)\left(\frac{\nu_{12}\phi}{d_o}\right) \tag{2.46}$$

The relations well described the experimental stress growth data for slightly viscoelastic PIB/PDMS blends containing 10% of either component. Since the scaling relationships in Eq. (2.43) have been preserved, the authors recommended that Eq. (2.46) be used for the affine polymer blends as a substitute for the original Doi–Ohta expressions. Furthermore, recent numerical analysis of the $\Upsilon(\gamma)$ function for $\gamma = 10$–500 is well approximated by $\Upsilon(\gamma) \cong 2/\gamma^{\frac{1}{2}}$.

In the next paper, Vinckier *et al.* [279] fitted the viscosity and the first normal stress difference of the model PIB/PDMS emulsions to Eq. (2.18). A reasonable description of the rheological behavior was obtained for the diluted and semi-diluted concentrations with the viscosity ratios $\lambda = 1.5$–4. The experiments were carefully conducted within the range of the capillarity numbers ($\kappa < \kappa_{cr}$) and:

$$\kappa \equiv \eta_m \dot{\gamma}/\nu_{12} \leq \left(4h_{cr}/\sqrt{3}R\lambda\right)^{2/3} \tag{2.47}$$

where the shearing caused neither drops breakup nor coalescence. In Eq. (2.47) h_{cr} is a critical thickness at which the fluid layer between coalescing drops ruptures and R is the drop diameter above which drop coalescence is unlikely to occur. Thus, the experiments were conducted within the range of capillary numbers where drop size determined under the preceding dispersion process remained relatively unchanged.

While the Choi and Schowalter [113] theory is fundamental in understanding the rheological behavior of Newtonian emulsions under steady-state flow, the Palierne equation [126], Eq. (2.23), and its numerous modifications is the preferred model for the dynamic behavior of viscoelastic liquids under small oscillatory deformation. Thus, the linear viscoelastic behavior of such blends as PS with PMMA, PDMS with PEG, and PS with PEMA (poly(ethyl methacrylate))at $\phi \leq 0.15$ followed Palierne's equation [129]. From the single model parameter, $R' = R/\nu_{12}$, the extracted interfacial tension coefficient was in good agreement with the value measured directly. However, the theory (developed for dilute emulsions) fails at concentrations above the percolation limit, $\phi \geq \phi_{perc} \approx 0.19 \pm 0.09$.

Starting with Kerner's model Bousmina [289] derived a simplified expression for the complex shear modulus of emulsions containing two viscoelastic liquids within the linear region:

$$G^* = G_m^* \left[\frac{2(G_d^* + 1/R') + 3G_m^* + 3\phi(G_d^* - G_m^* + 1/R')}{2(G_d^* + 1/R') + 3G_m^* - 2\phi(G_d^* - G_m^* + 1/R')}\right]; \quad R' \equiv R/\nu_{12} \tag{2.48}$$

The experimental data for G' and G'' of PS/PE = 85/15 were well predicted by this expression with a single parameter $1/R' = 500$ Pa. The prediction seems to be closer to the experimental data than that given by the original Eq. (2.23) using the same value of R'.

The rheological behavior of more concentrated polymer blends must take into account coupling between flow and morphology, that is, drop deformation, breakup, and coalescence. Starting with Grmela's Poisson bracket formalism Bousmina *et al.* [290] derived a set of equations that describe blend performance in the shear and elongational flow field. The theory was compared with experimental data for PDMS/PB and PP/PS blends. While the theory well described two-component systems, it failed for the compatibilized blends, which contain a third component. Hopefully, the thermodynamic framework of the GENERIC formalism will accommodate the interphase modifying influences of a compatibilizer [277].

2.4.3.2 **Coalescence of Viscoelastic Drops**

Coalescence occurs in quiescent as well as in sheared systems. In the former it starts by molecular diffusion from smaller to larger diameter drops, caused by the difference in surface energy. This mechanism, known since 1896 as "Ostwald ripening," was originally proposed for rain drop formation. Small drops may also coalesce by Brownian motion, dynamics of concentration fluctuation, and so on. Shearing enhances the coalescence [291]:

$$(d/d_o)^{n(\dot{\gamma})} = 1 + a_o t; \qquad n(\dot{\gamma}) = 3 \searrow 3/2 \tag{2.49}$$

where d_o is the drop diameter at the moment of imposition of stress and a_o is a constant. The shear-dependent exponent n decreases with increasing shear rate from the Ostwald value of $n = 3$ to 3/2.

By contrast with the flow-induced dispersion, the flow-induced coalescence is not as well described. For example, there is a critical capillarity number for breakup, but not for coalescence. Three approaches have been used, based on: (i) the minimization of energy [129], (ii) the frequency of collisions assumed proportional to the shear energy, $\dot{\gamma}\sigma_{12}$ [292], and (iii) the instability of the liquid layer trapped between two drops with an immobile or mobile interface [125, 293–297]:

$$\begin{aligned} &\text{immobile}: \quad -(\mathrm{d}h/\mathrm{d}t)_{\mathrm{ii}} \approx \frac{8\pi\nu_{12}^2 h^3}{3\eta_m R_d^2 F_c}; \qquad t_{\mathrm{ii,drain}} \cong \frac{3\eta_m R_d^2 F_c}{16\pi\nu_{12}^2}\left(\frac{1}{h_{crit}^2} - \frac{1}{h_o^2}\right) \\ &\text{mobile}: \qquad -(\mathrm{d}h/\mathrm{d}t)_{\mathrm{mi}} \approx \frac{2\nu_{12} h}{3\eta_m R_d}; \qquad t_{\mathrm{mi,drain}} \cong \frac{3\eta_m R_d}{2\nu_{12}}\ln\left(\frac{h_o}{h_{crit}}\right) \end{aligned} \tag{2.50}$$

where

ν_{12} is the interfacial tension coefficient,
η_m is the matrix viscosity,
R_d is the drop radius,
F_c is the contact force,
h_o and h_{crit}, are the initial and critical (for coalescence) liquid film thickness, respectively.

Equation (2.50) expresses the rate of interphase thinning, $-(\mathrm{d}h/\mathrm{d}t)$, and the time required for draining the matrix liquid from between the drop, t_{drain}. The latter was obtained by integrating the rate expression for reduction of h from h_0 to h_{crit}.

Most theories consider both effects – breakup and coalescence, which leads to the equilibrium drop diameter, d_{eq}. For example, starting with the theory of latex stability Huneault *et al.* [257] equated the rate of drop dispersion with that of collision, arriving at:

$$d_{eq} = d_T + \sqrt{6C\kappa_{cr} t_b^* \phi^{8/3}} \tag{2.51}$$

where d_T is the Taylor value for infinite dilution and C is an experimental coalescence constant. Fortelný *et al.* [298, 299], following Tokita's model, derived the expression:

$$d_{eq} = d_T + 2R_d p_r \phi\dot{\gamma}/\kappa f(\kappa) \tag{2.52}$$

where $f(\kappa)$ is a function of the capillarity number and p_r is the probability of drop collision that results in coalescence.

Vinckier *et al.* [278] used the third coalescence model for the analysis of experimental coalescence data in the PIB/PDMS system without drop breakup. The point of departure was that the probability function for coalescence was assumed

proportional to the ratio of the time for breaking the film to that while drops are in contact [300]:

$$p_r \propto \exp\{-t_{break}/t_{contact}\} \tag{2.53}$$

The authors demonstrated that the time-dependent drop diameter can be scaled with strain, $\gamma = \dot{\gamma}t$, and the ratio of the shear rates:

$$d(t)/d_o = f[\gamma, (\dot{\gamma}/\dot{\gamma}_o)] \tag{2.54}$$

The steady-state drop diameter during coalescence follows the dependence:

$$d_{ss} = c/\left(m\dot{\gamma}^{\frac{3}{5}}\right); \quad m = 0.385(\lambda/h_c)^{\frac{2}{5}}(\eta_m/\nu_{12})^{\frac{3}{5}} \tag{2.55}$$

where c is a concentration-dependent parameter and h_c is the critical distance for coalescence.

Chen *et al.* [301] used a surface forces apparatus (SFA) to measure the force between two hard, solid-like polybutadiene (PB; $M_w = 10^6$ Da) layers, about 110 nm thick, immersed in liquid PDMS. The measured force was found to be independent of the approach velocity in the range $V = 0.01$–$50\ \text{nm s}^{-1}$. Four stages were identified: (i) an initial smooth approach, (ii) a jump when the two layers were about 250 nm apart, (iii) an approximately 4-nm thick layer of PDMS was trapped between the two PBD surfaces (1 or 2 molecular layers), and (iv) coalescence. Large normal and lateral deformations were consistent with the calculated van der Waals forces. The results imply that liquid droplets (or biological cells) can sense each other at relatively large distances.

2.4.4
Flow Imposed Morphology

The morphology of immiscible blends is defined as the spatial arrangement of phases forming disperse, stratified (e.g., lamellar), or co-continuous structures. Flow changes the blend morphology, which in reciprocity affects the flow. The great morphological diversity is augmented by the effect of flow on miscibility. Evidently, at higher concentrations of dispersed phase the flow engenders diversity of domain shapes and sizes. The diversity is particularly great in complex shear/elongational flows in mixing, compounding, and forming processes, as reported for blends of thermoplastics with low-temperature glass [302, 303]. At high deformation the stresses may induce such chemical modifications as chain scission, grafting or crosslinking, dehydrochlorination, and so on.

Generation of morphology depends on the viscosity and elasticity ratio of the polymeric blend components (at corresponding stress). Both ratios vary with the type and intensity of the flow field. While the viscosity ratio controls the ease of dispersing the minor component, and thus the degree of dispersion, the elasticity ratio contributes to shaping the phases – the resulting type of the flow-induced morphology. The additional parameters are the concentration and the level of interfacial interactions. To modify the interfacial energy, blends are usually compatibilized

either by addition of a compatibilizer or by reactive blending. Once formed, the morphology needs to be stabilized against a possible destruction during the formation steps (achieved by controlling the interphase thickness).

As discussed above, the rheological properties of immiscible blends depend on the rheological behavior of neat components as well as on morphology. The micro-rheological approach to the rheology/morphology problems considers the reciprocal effects of flow and morphology on the local level of the degree and type of dispersion, that is, drop deformation, breakup and coalescence. During compounding and processing polymer blends, the melt flowing through a processing equipment and dies is exposed to different types of stresses and their gradients, which may lead to a concentration gradient that results in different morphology at different locations of the formed parts, namely, skin–core structures, weld lines, blush lines, and so on.

As a result, the flow imposed morphologies may be classified as (i) dispersion (mechanical compatibilization), (ii) fibrillation, (iii) lamellae formation, (iv) coalescence, (v) interlayer slip, (vi) encapsulation, and others [3].

2.4.5 Shear Flows

Because of the complex flow behavior of viscoelastic polymer blends its interpretation becomes easier when compared with the simpler, model systems discussed in Sections 2.1.1 and 2.1.2. For the dominant immiscible blends the emulsions of one liquid dispersed in another provide the best model. While compatibilizers are used for stabilization of blends, in emulsion a diversity of surfactants has been employed. As in blends, a progressive increase of concentration of the emulsion minor phase invariably leads to the co-continuity of phases and phase inversion. However, while emulsion phase inversion is controlled mainly by the emulsifier, in blends the inversion mainly depends on the viscosity ratio, $\lambda \equiv \eta_2/\eta_1$ (Figure 2.3) [4].

2.4.5.1 Concentration Dependence of Viscosity

In multiphase polymeric systems the zero-shear Newtonian coefficient of shear viscosity, η_o, is difficult to determine, but the constant stress viscosity, η_σ, provides an acceptable alternative. The equivalence is easy to note considering superposition of flow curves – if the flow curves superpose at any stress then they also superpose within the Newtonian plateau.

Plots of $\ln \eta_o$ or $\ln \eta_\sigma$ versus composition yields five different families of dependencies:

1) positively deviating blend (PDB),
2) negatively deviating blend (NDB),
3) log-additivity: $\ln \eta = \sum w_i \ln \eta_i$,
4) positively-negatively deviating blend (PNDB),
5) negatively-positively deviating blend (NPDB) [34].

Since for miscibility the free energy of mixing must be negative, $\Delta G_m < 0$, a loss of free volume and PDB behavior have been expected and observed [15]. Similarly, a

positive deviation is predicted by the emulsion and suspension models as well as that of phase separation. Evidently, there must be other mechanisms that cause the negative deviation.

Interlayer slip in immiscible blends has long been known and has been elegantly demonstrated by Lyngaae-Jørgensen and his colleagues [280, 304]. Thus, shear viscosity was measured of sandwiches containing 40–160 alternating films of PS and PMMA, each 0.2–0.3 mm thick. Assuming that the viscosity of such a three-materials construct (PS, PMMA, and the interphase) follows the fluidity equation, and knowing that the thickness of the interphase is about 10 nm, its shear viscosity was calculated as $\eta_o = 0.15 \pm 0.06$ kPa s, which is to be compared with corresponding values for neat PS and PMMA of 3.4 and 15.5 kPa s, respectively. More recently, Bousmina *et al.* [305] derived an expression for the effective viscosity of binary polymer blends:

$$\frac{1}{\eta_{\text{eff}}} = \frac{\phi_A}{\eta_A} + \frac{\phi_B}{\eta_B} + k\sqrt{\phi_A \phi_B}; \quad k \propto 1/(\Delta l \cdot \eta_I) \tag{2.56}$$

The slip factor, k, depends on the interphase property, expressed as a product of the interphase thickness, Δl, and its viscosity, η_I. Thus, Eq. (2.56) indicates that the effective viscosity, η_{eff}, decreases with the reduction of the interphase thickness and viscosity. While it is expected that reduction of η_I will augment the interlayer slip the effect of Δl is best discussed in terms of the Helfand *et al.* model [25–27], which suggests high concentration of low molecular weight components in decreasing interphase thickness, which increases the slip.

Considering Eq. (2.56) as the basic dependence for blends with $k \geq 0$, the emulsion-like viscosity enhancement may be written as [34]:

$$\Delta\eta_{\text{ex}} = \eta_{\max}\left\{1 - \left[\frac{(\phi_A - \phi_{IA})^2}{(\phi_A \phi_{IB}^2 + \phi_B \phi_{IA}^2)}\right]\right\} \tag{2.57}$$

where $\phi_{IA} = 1 - \phi_{IB}$ is the phase inversion coefficient of phase A. Combining Eqs. (2.56) and (2.57) provides a reasonable description of the five types of $\ln \eta$ versus ϕ dependencies, schematically shown in Figure 2.9. These dependencies well represented the observed blend behavior for nine different binary polymer systems [34].

Shi *et al.* [306] studied the melt rheology of polypropylene/polyamide-6 (PP/PA-6) blends with and without a compatibilizer (maleated-PP or PP-MA). The concentration dependence of the capillary viscosity was calculated as a difference, δ, between truncated Eqs. (2.56) and (2.57), assuming that k and $\Delta\eta_{\text{ex}}$ are zero. In non-compatibilized blends the experimental values were smaller than predicted, thus $\delta < 0$. The value of δ increased with the dispersed-phase content and the degree of its dispersion, indicating a growing contribution of the neglected slip factor, k. In the compatibilized blends the experimental values were larger than predicted – the δ values increased with the degree of dispersion and decreased with increasing shear stress. Evidently, in this case the neglected contribution of $\Delta\eta_{\text{ex}}$ was responsible for the difference between the experiment and prediction.

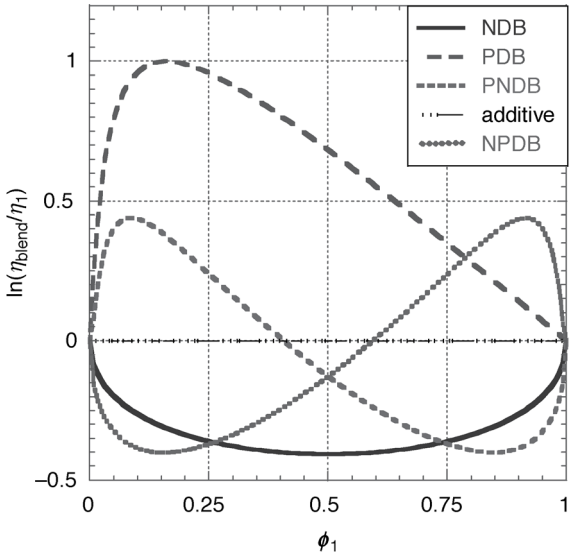

Figure 2.9 Five types of the relation between shear viscosity and concentration for immiscible polymer blends: NDB, PDB, PNDB, log-additivity, and NPDB.

2.4.5.2 **Dynamic Flow**

For characterization of polymer blends, low strain dynamic rheological measurements are preferred over steady-state shearing (e.g., in a capillary viscometer). Since the morphology depends on the type of flow and its intensity, serious differences between results from the steady-state shear, oscillatory shear, and extensional deformations are to be expected.

The dynamic tests at small amplitude in parallel plates or cone-and-plate geometry are simple and reproducible. From the experimental values of storage and loss shear moduli, G' and G'', respectively, first the yield stress ought to be extracted and then the characteristic four material parameters in Eq. (2.13), η_o, τ, m_1, and m_2, might be calculated. Next, knowing these parameters one may calculate the Gross frequency relaxation spectrum (see Eqs. (2.31) and (2.32)) and then other linear viscoelastic functions.

The dynamic behavior of polymer blends under low strain has been theoretically treated from the perspective of microrheology. Table 2.3 lists a summary of this approach. These models well describe the experimental data within the range of stresses and concentrations where neither drop-breakup nor coalescence takes place. The two latter models yield similar predictions as that of Palierne. The last entry in the Table 2.3 is an empirical modification of Palierne's model by replacement of the volume fraction of dispersed phase by its effective quantity (Eq. (2.24)), which extends the applicability of the relation up to $\phi \leq 0.449$. However, at these high concentrations the drop–drop interactions absent in the Palierne model must complicate the flow and coalescence is expected. The practical solution to the latter problem is compatibilization, but the presence of the third component in blends has not been treated theoretically.

Table 2.3 Summary of low-strain expressions for dynamic moduli of emulsions and blends.

Author	Concentration	Liquids	Drops	Results
Taylor [117]	Dilute	Newtonian	Non-deformable	$\eta = \eta(\lambda, \phi)$
Oldroyd [111]	Dilute	Newtonian	Deformable	G', G'', $\eta = f(\omega, \lambda, \phi, \nu_{12})$
Palierne [126, 127]	Moderately concentrated	Viscoelastic	Deformable, polydispersed	$G_b^*(\omega, H); H = H\left(G_m^*, G_d^*, R/\nu_{12}, \phi\right)$
Bousmina [289]	Moderately concentrated	Viscoelastic	Deformable, polydispersed	$G_b^* = G_b^*\left(\omega, G_m^*, G_d^*, R/\nu_{12}, \phi\right)$
Yu *et al.* [273, 307]	Moderately concentrated	Viscoelastic	Deformable, polydispersed	$G_b', G_b'' = f(\omega, \lambda, \eta_m, R/\nu_{12}, \phi)$
Pal [130]	Concentrated	Viscoelastic	Deformable, polydispersed	$G_b^*(\omega, H); H = H\left(G_m^*, G_d^*, R/\nu_{12}, \phi_{eff}\right)$

As discussed in Section 2.1.2, compatibilization offers a control of the interfacial tension and thickness of the interphase. Upon reduction of the drop size the volume fraction of the interphase increases, often exceeding that of the dispersed phase. Compatibilization by addition of a compatibilizer or by reactive blending may lead to hydrogen bonding that greatly increases the effective molecular weight and/or generates an additional phase composed of compatibilizer micelles or polar aggregates [308–310]. Evidently, all these aspects are not yet incorporated into constitutive equations.

The rheological behavior of these complex systems cannot be predicted from the developed rheological models, but the observations can be interpreted on the basis of simple model systems. For example, the emulsion model indicates that making the interface more rigid causes the viscosity to increase; increasing the volume of the dispersed phase increases viscosity; increasing interactions between the phases not only may increase viscosity, but also leads to the apparent yield stress; by contrast in the absence of interaction between phases the interlayer slip should be expected. In short, the model systems often help in understanding the rheological behavior of concentrated and/or compatibilized polymer blends. Numerous examples can be found in the literature [174, 175, 308, 311–320].

2.4.5.3 Steady-State versus Dynamic Viscosity

There is a reciprocal cause and effect between polymer rheology and morphology. In particular, morphology is strongly affected by the total strain (especially in irrotational stress field). Since the steady-state shearing engenders larger strains than the dynamic one, one should not expect that the rheological data from different strain fields will be the same. Since performance of polymer blends depend on morphology, the different flow fields creating different morphologies in effect generate different materials. Even if the low strain dynamic data obey the *t*–*T* principle, those determined in steady state shear or elongation will follow a different pattern.

There are two types of disparities between the steady-state and dynamic flow behavior, one related to the interlayer slip (Eq. (2.56)) and the second to the flow engendered migration of the low viscosity component to the high stress location. Blends of liquid crystal polymer (LCP) with polycarbonate (PC) or poly(ethylene-terephthalate) (PET) may serve as an example of the first type [321, 322], whereas those of EPDM (ethylene-propylene-diene terpolymer) with poly(vinylidene-*co*-hexafluoropropylene), Viton™, exemplify the second [323–325]. In both cases the steady-state shearing was performed in a capillary viscometer – the viscosity ratio of the dynamic to the steady-state data for these two blends was about two and six, respectively.

2.4.5.4 **Blend Elasticity**

Emulsion elasticity expressed by Eq. (2.18) as the first normal stress difference, N_1, originates from the deformability of the interphase; thus it is present even in Newtonian liquid blends [113]. The relation predicts that N_1 increases with ν_{12} without bound. Since drops do not deform at high viscosity ratio, $\lambda > 4$, as well as when the interfacial tension coefficient is high, the elasticity should decrease as the dispersed liquid viscosity or the interfacial tension coefficient became large. Similarly, G' in Eq. (2.23) and its homologues depends on the R/ν_{12} ratio [126], but here the prediction for both limiting values of ν_{12} is the same. As in the case of viscosity, these two direct measures of elasticity are expected to differ due to different strains imposed in the steady-state and dynamic flow fields.

The elasticity of molten polymer may also be assessed by indirectly measuring the entrance–exit pressure drop (Bagley correction), P_e [326, 327], or the extrudate swell (B_e) [328]. However, the capillary flow of polymer blends under the usually applied high deformation rates may cause a morphological change, starting with flow segregation (low-viscosity component migrates toward the wall) followed by deformation of the dispersed phase, its coalescence and break. When the highly deformed phase exits from the die, it undergoes the form recovery, which leads to unduly large extrudate swell, related to strain recovery, $\gamma_R \leq 6.5$. These complex structures are quite different from those engendered in dynamic flow (or the steady-state shearing) and as a consequence the indirect measures of blend elasticity should not be calculated from the expressions developed for homogeneous melts.

In miscible blends the *t*–*T* superposition, $G^*(\omega, T) = b_T G^*(a_T\omega, T_o)$, has been observed [200, 210]. The temperature dependence of the horizontal shift factor, a_T, is expressed in Figure 2.10 as a temperature gradient of the loss tangent, $\tan\delta$, versus w. Despite the excellent superposition of the dynamic data, the nonlinear variation of the gradient indicates concentration-dependent binary interactions. Next, the linear viscoelastic complex shear modulus of SAN/PMMA and polyisoprene/poly(vinyl ethylene) (PI/PVE) miscible blends was analyzed [329, 330]. Following the "double reptation" model the authors computed the behavior of blends from the neat component data without adjustable parameters. The computed frequency dependence of the complex PI/PVE modulus agreed well with the experimental data, despite the thermo-rheological complexity of the system. Turati *et al.* [331] also studied miscible and compatibilized blends, noting that in the case of miscibility the dynamic data plotted as log G' versus log G'' followed a single straight line.

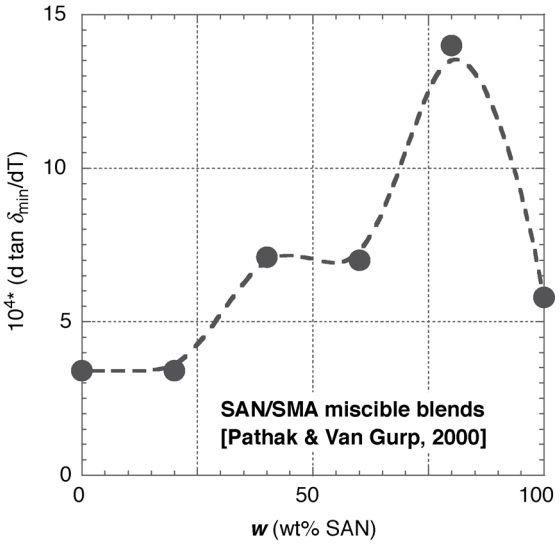

Figure 2.10 Temperature gradient of the loss tangent minimum for the miscible SAN/SMA blends versus composition. Data from Pathak and van Gurp [200].

Several studies have focused on the changes of the rheological behavior of miscible blends caused by the phase separation [197, 211, 221, 332]. The preferred object of these studies was the PS/PVME blend having LCST $\approx$ 90–110 °C, dependent on the components molecular weight. The difference in dynamic flow behavior was presented by using the *t*–*T* superposition principle, or by plotting the data as log G' versus log G''. Measuring the shear moduli versus angular frequency (ω) of a single composition over a wide range of temperatures (e.g., $T = 70$–130 °C) generated good superposition of data at $T <$ LCST and lack of superposition at $T >$ LCST.

Evidently, deep within the spinodal region the immiscible polymer blends will behave similarly as the above discussed compositions. Isothermal plots of G' versus ω for the increasing concentration of the dispersed phase show a progressive increase of G' in the terminal zone [333–335]. In some cases the increase becomes significant for concentrations just above the percolation threshold.

Owing to experimental difficulties, steady-state shear measurements of N_1 and σ_{12} are relatively rare. Their rate of shear gradients, $N_1/\dot{\gamma}, \eta = \sigma_{12}/\dot{\gamma}$ usually show a similar dependence [322]. The value of the complex viscosity is $\eta^* > \eta$. In the steady shear flow of a two-phase system, the stress is continuous across the interphase, but the rate of deformation is not. Thus, for polymer blends, plots of the rheological functions versus stress are more appropriate than those versus rate, that is, a $N_1 = N_1(\sigma_{12})$ plot is similar to $G' = G'(G'')$.

Gramespacher and Meissner [251] measured the recovered creep compliance for PMMA/PS blends. Interestingly, the composition PMMA/PS = 16/84 behaved regularly, similar to what has been observed for the neat polymers. However, when the composition was reversed, 8, 12, 16, or 20 wt% PS in PMMA, the recovery creep compliance showed a maximum at which the recovery direction was reversed.

The height of the maximum increased with PS loading from negligible at 8 wt% to large at 20 wt%. The authors attributed the dissymmetry of behavior to the action of the interphase and different retardation times of the blend components.

2.4.6 Elongational Flows

As the elongational viscosity of molten polymers is difficult to measure, several "simplifying" procedures have been proposed. For example, Laun and Schuch [336] calculated η_E indirectly, from the entrance pressure drop in a capillary and the shear stress at the capillary wall: $\eta_E/\eta \propto (P_e/\sigma_{12})^2$. The dependence offers a reasonable estimate of η_E for homopolymers (e.g., PP or PA-6), but for their blends the calculated values were one decade larger than those measured directly [3]. Thus, the data discussed below will be limited to those measured directly, that is, determining the stress growth function, η_E^+, versus time, t, at constant Hencky deformation rate, $\dot{\varepsilon}$, and analyzing the data.

Since these tests are carried out by stretching unconfined melt, the difficulties are related on the one hand to the preparation of homogeneous sample and on the other hand to the correct determination of strain during the test. Since polymers and their mixtures rarely deform homogenously, the evolution of strain during deformation must be measured. As in shear, also in elongational flows the morphology depends on the test procedure and in turn it affects the rheological response.

As shown in Figure 2.11, the stress growth function in elongation has three zones:

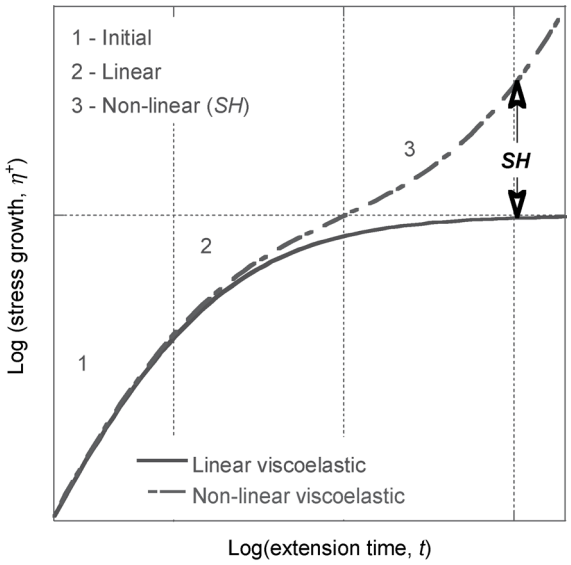

Figure 2.11 Stress growth function in elongation at constant Hencky strain rate, $\dot{\varepsilon}$, for linear and nonlinear viscoelastic melt – the latter shows the strain hardening (*SH*); see text.

1) Initial, with the slope $S_i = \mathrm{d}\ln\eta_E^+/\mathrm{d}\ln t$, related to polydispersity of molecular weights, M_z/M_n, where M_z and M_n are the z- and number-average molecular weight, respectively [337].
2) Linear viscoelastic zone.
3) Strain hardening, $SH \equiv \log\left[\eta_{obs}^+/\eta_{lin\ vis}^+\right]_{\dot\varepsilon} = SH(\varepsilon)$, zone.

Three sources of the SH have been identified: (i) the intermolecular interactions or macromolecular entanglements evident in long-chain branched polymers; (ii) the bi-modality of the molecular weight distribution (MWD) observed, for example, in metallocene polyolefins; and (iii) high polydispersity, for example, for $M_w/M_n > 20$ as in some linear low density polyethylenes, LLDPE. It has been observed that for neat polymers the plot of SH as function of Hencky strain, $\varepsilon = \dot\varepsilon t$, yields superposition of data. An example is displayed in Figure 2.12 for a rheologically simple, branched polycarbonate of bis-phenol-A (PC, grade PK-2870). At a given temperature, the slope of strain hardening: $SSH \equiv \mathrm{d}SH/\mathrm{d}\varepsilon$, is a material constant, characterizing the effective entanglement within the system. The values of SSH range from 0 to about 0.25 – the latter determined for long-chain branched macromolecules such as low density polyethylene (LDPE).

The presence of SH facilitates processing, for example, film blowing, wire coating, or foaming. In wire-coating, blends with SH and low viscosity resulted in a superior surface finish and uniformity of the deposited layer [89]. However, too high a SH may make processing difficult, as observed for film blowing of some grades of LDPE. Blending has been used for SH optimization.

Studies of the elongational flow of blends initially concentrated on polyolefin resins, namely, a diversity of polyethylenes (PEs), polypropylenes (PPs), and their copolymers (EPR, ethylene–propylene rubber) [337–339]. It was noted that in these

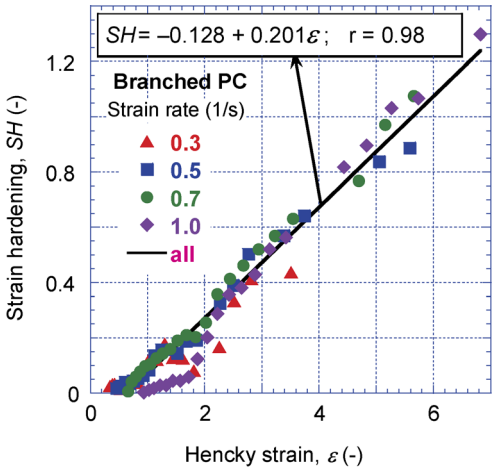

Figure 2.12 Strain hardening (SH) versus Hencky strain for branched polycarbonate of bis-phenol-A (PC, grade PK-2870) at $T = 270\,^\circ\mathrm{C}$ and $\dot\varepsilon = 0.3$–$1\,\mathrm{s}^{-1}$. The slope of the dependence, $SSH = 0.201$, is a characteristic material parameter at the test temperature.

systems the rheological behavior of blends were determined by the neat polymers and their miscibility – when the two polymers were linear viscoelastic, their blend rarely showed *SH*, but if one or both polymers showed *SH* then that behavior was also present in their blends. Furthermore, while about 20 wt% of LLDPE with low *SH* was needed to introduce *SH* to another LLDPE, only 5 wt% of LDPE was required to engender the same effect – evidently the *SH* of the latter polymer was significantly larger than that of LLDPE [337]. Thus, *SH* control is simple, provided that within the desired range of concentration the modifying polymer with *SH* is miscible with the one that needs modification. In the case of immiscibility the phase co-continuity offers an elegant solution. This has been noted for some LDPE/LLDPE blends [88].

The flow behavior of highly immiscible PS/LDPE blends was also studied [309]. Both polymers show *SH* – evidently, PS significantly less so than LDPE. However, their blends showed enhanced *SH* by virtue of the morphology and presence of an interphase. Figure 2.13 shows the *SH* behavior for binary blend of LDPE/PS = 85/15 wt%, measured in a Meissner elongational rheometer, RME (Rheometrics elongational rheometer for melt), at $\dot{\varepsilon} = 0.001–1.0\ s^{-1}$ [309]. There is no superposition of data, observed in Figure 2.12 for a single-phase melt. At low deformation rates the *SH* is large, decreasing with $\dot{\varepsilon}$. This behavior is similar to that observed for solid-reinforced polymer melts, such as polymer composites (e.g., glass-fiber filled PP [96]) or nanocomposites (Figure 2.14).

An attempt was made to compatibilize the blend by addition of 5 wt% (styrene–ethylene/butene–styrene, SEBS), which reduced the *SH* as well as the mechanical properties in the solid state. The effects have been related to the formation of phase-separated SEBS clusters, which changed the flow lines, introducing local stress concentration in molten and solid phase.

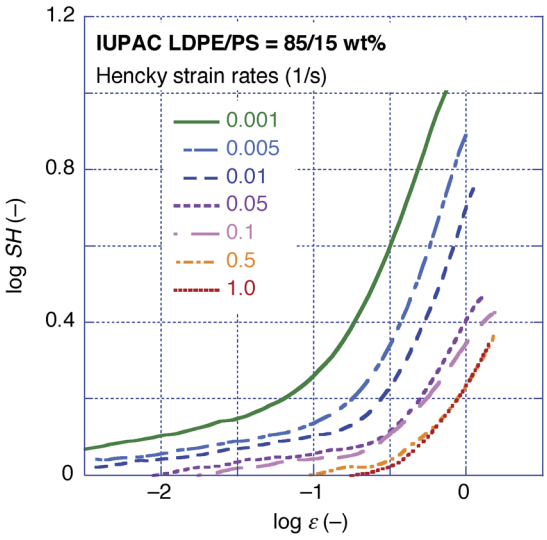

Figure 2.13 Stress growth functions for LDPE blended with 15 wt% PS. Data from Figure 4 in Reference [309].

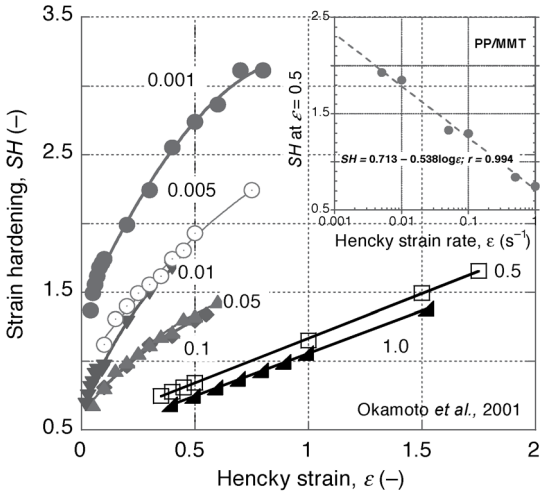

Figure 2.14 Strain hardening in extensional flow of lightly-maleated PP with 4 wt% MMT-ODA at 150 °C and Hencky strain rates $\dot{\varepsilon} = 0.001$ to $1.0\,s^{-1}$. Inset: *SH* at $\varepsilon = 0.5$ is plotted against $\dot{\varepsilon}$ (see broken vertical line in the main graph). Data from Okamoto *et al.* [386].

Delaby *et al.* [340–343] studied the low-strain drop deformation as a function of viscosity ratio at $\dot{\gamma} = 0.0173\,s^{-1}$, $D_E = D_E(\lambda)$. The authors prepared a series of binary blends from PE, PS, and PMMA in various proportions. The blends had a wide range of λ_E:

$$0.005 \leq \lambda_E \equiv \eta(\text{drop})/\eta(\text{matrix})|_{\dot{\gamma}=\text{const}} \leq 13 \tag{2.58}$$

Starting with Palierne model the authors derived an expression between elongational viscosity ratio and strains:

$$\frac{\gamma_d - 1}{\gamma_m - 1} = \frac{5}{2\lambda + 3} \tag{2.59}$$

where γ_d and γ_m are, respectively, strain of the drop (defined as a ratio of the long axis of prolate ellipsoid to the original drop diameter) and the matrix. For $\lambda = 1$ and $\gamma_d = \gamma_m$, the drop co-deforms with the matrix, as expected. The experiments showed good agreement with the predicted behavior over the full range of λ. Note that in Eq. (2.59) the limiting value of drop deformability at $\lambda \to 0$ is 5/3. This is relatively close to the value of 2 computed using the 2D boundary element method [344, 345].

The ever-popular PS/PMMA blends have been studied in extensional field by several groups [346–350]. The blends were subjected to uniaxial elongation, and then the stress relaxation was measured. Mechbal and Bousmina have shown that droplet deformation and the decay of the extra extensional stress are inter-related through the theory of Yu *et al.* [273]. The studies indicated that in polymer blends there are two mechanisms of relaxation, a fast and a slow one, with the former related to molecular dynamics and the later to the interphase.

Compatibilization, especially the reactive-type, affects the properties of the interphase and, thus, the relaxation dynamics [351]. The effect of copolymer addition on stress growth function and recovery was studied as well [318, 319]. The matrix polymer was PA-6 blended with either EPR or SAN, and compatibilized with maleated-EPR (EPR-MA) or maleated-SAN (SNA-MA), respectively. Thus, in both systems the compatibilization was based on the reaction between PA-6 amine groups and maleic anhydride (MA) [318].

All compositions of the PA-6/EPR/EPR-MA blends showed strong SH for the Hencky strain $\varepsilon > 1$. The largest effect was obtained by replacing 25% of EPR with EPR-MA – the smallest SH was for the blend of PA-6 with EPR-MA, suggesting hardening of the interphase. However, independently of the hardening, the rheological data in oscillatory shear, uniaxial extension, and stress relaxation in shear showed two relaxations of the blends, one molecular and another directly related to the amount of EPR-MA content and, thus, to the interphase. After elongation of non-compatibilized blends the drops were spherical, whereas those of the compatibilized blends were elongated, indicating a reduction of the interfacial slip and hardening of the interphase.

The second system, PA-6/SAN with w(SMA-MA) = 0–4.8, was examined at low Hencky strains, $\varepsilon < 0.6$. As before, SH systematically increased with the compatibilizer content. However, the increase was significantly larger in blends PA-6/SAN = 30/70 than in the 70/30 one. Sailer [319] emphasized the asymmetrical properties of the interphase deduced from significant differences between the rheological properties of 30/70 than 70/30 main component blends. Furthermore, SH was found to be related to stretch recovery.

2.5 Rheology of Blends with Nanoparticles

2.5.1 General

Compatibilization of polymer blends aims to improve the interaction between phases, ascertaining the appropriate, stable morphology and improved performance. Blends have been compatibilized mainly by addition of a compatibilizer, a co-solvent, or in a reactive process, where the compatibilizing molecules are formed within the interphase [1, 73, 302]. About 20 years ago a note in a USSR technological journal reported that the addition of a small amount of PMMA to a PE/PS blend reduced the PS drop diameter by a factor of ten. The effect was later explained by a balance of the three interfacial tension coefficients in the blends, inter-related by Neuman's triangle equation [1, 352, 353]. In simple terms, the PMMA, immiscible in PE and PS, formed a layer around PS drops, preventing coalescence. In a sense, addition of nanoparticles to polymer blends acts similarly.

Polymer blends have been used as matrices of polymeric nanocomposites (PNCs) or more precisely clay-containing polymeric nanocomposites (CPNCs) since the early 1990s [64]. The clay platelets migrate to the interphase, strengthen and rigidify it,

reduce the molecular mobility within, and eventually develop bridging monolayers between drops, which hinder the drop–drop drainage, stabilizing the dispersion. Incorporation of a modified organoclay into a multiphase polymeric system has led to finer dispersion, for example, in PS/PEMA [354, 355], PS/PMMA [356, 357], or in PS/PP [358].

Clay has also been dispersed in polymer blends for other reasons, namely, enhancement of mechanical, thermal, barrier or other property, improvement of processability, good balance of performance, and so on. In these cases it is important that the clay be placed in a specific phase. For example, incorporation of montmorillonite (MMT) intercalated with 12-aminododecanoic acid (ADA) with free acidic groups will preferentially enter into polyamide (PA), polyester (PEST), polyurethane (PU) or other polar polymer phases, away from non-polar ones (e.g., a polyolefin, PO = PE or PP) [356, 359–366]. Evidently, in blends with such acidified compatibilizer, such as SAN-MA or EPR-MA, clay will preferably migrate to its locality, being an interphase or polar aggregates within the PO phase.

Before discussing the flow behavior it would be beneficial to consider the governing thermodynamic principles of these materials. A theoretical analysis of the phase behavior of nanoparticle filled binary blends was published by He *et al.* [367]. The authors' aim was to determine the best conditions for thermodynamically stable, non-aggregating, non-phase separating systems in the form of a mean-field based equation for the free energy of mixing. The model was composed of homopolymers, A and B, with the degrees of polymerization $N_A = N_B$. Their volume fractions were ϕ and $(1 - \phi)$, respectively. The blend contained the volume fraction ψ of spherical nanoparticles (P) having radius R_P. The binary interaction parameters were χ_{ij}, where ij = A, B, or P, with χ_{AP}, $\chi_{BP} \geq 0$, thus assuming that nanoparticle have unfavorable interactions with either homopolymer. The theory takes into account such variables as: interactions between different species, polymer molecular weights, composition, concentration of nanoparticles and their diameter. The particles may have negative enthalpic interactions with each of the polymeric components that affect the phase diagram. There is a minimum concentration of nanoparticles, ψ, required for stabilization of the system. The computed maps of the system stability show that owing to entropic effects smaller particles better stabilize the system. Furthermore, for a given set of interaction parameters χ_{ij}, there is an optimal value of ψ that offers the largest stability region. In short, the theory presented for spherical nanoparticles might be used as a guide for developing new classes of nanocomposites, in particular those of the functional type.

Fenouillot *et al.* [368] reviewed polymer blends with solid nanoparticles. The authors briefly discussed oil/water emulsions with solid colloidal particles, considering their wettability and location. Next, polymer blends with nanoparticles were discussed, starting with systems near the phase separation, and then within the immiscibility region. Some similarities and differences between the low- and high-viscosity emulsions were highlighted. The particular reason for preparing the review seems to be the authors search for factors that may affect nanoparticle localization at the thermodynamic equilibrium. Diverse polymer blends with pseudo-spherical

particles (namely, carbon black, SiO_2, TiO_2, Fe_2O_3) and with organoclay were discussed. The authors' findings may be summarized as follows:

1) Nanoparticles are surface active, adsorbing macromolecules and reducing their mobility.
2) For minimization of the system's free energy the thermodynamics adjusts the interphase compositions as a function of interactions.
3) The calculations are difficult due to the lack of information on the temperature and concentration effects on the interaction energies. These difficulties notwithstanding, optimization of blends' performance using nanoparticles may be guided by the results of theoretical analyses.
4) Most often incorporation of nanoparticles results in finer and more stable drop dispersion with improved performance. This effect is related to migration of particles to the interphase, which might lead to additional benefits, for example, reduction of the percolation threshold for blends' conductivity.
5) Incorporation of nanoparticles into a polymeric phase enhances its mechanical performance. Thus, it is desirable to place nanoparticles in the stiffer polymer, preserving the toughening effects of the dispersed elastomeric domains.
6) Owing to matrix viscosity and low mobility of solid particles, the time required for dispersion equilibration is long (purely thermal randomization without stirring takes hours). As a result, most filled blends are quenched before the equilibrium particle dispersion can be achieved.
7) The kinetics of solid particles dispersion depend on the local concentration and possible overlapping with the adsorbed polymeric layers with low molecular mobility. Rheologically, flow of such aggregates must take into account the local yield stress.
8) Addition of organoclay to polymer blends may lead to improvement of "miscibility," for example, such as observed for PC blends with PMMA or SAN. Several mechanisms may contribute to this effect, such as reduction of the interfacial energy, coalescence inhibition, increase of viscosity, drop immobilization, steric hindrance, and so on.

The following three subsections summarize the reported rheological effects of the addition of nanoparticles to polymer blends. First, the effects of incorporating spherical particles into immiscible blends are discussed, then the effect of nanoparticles of any shape to a blend near phase separation is considered, and finally the effects of addition of organoclay to immiscible blends are presented. Because of space limitations, interested readers should also consult Reference [369] and the cited literature therein.

2.5.2
Rheology of Blends with Spherical SiO_2 Particles

Because of the flow-induced segregation of phases with different shear viscosity, the preferred method of testing multiphase polymeric systems is dynamic, in cone-and-plate geometry (alternatively, between parallel plates). An exception is a study of the

fumed hydrophilic silica effect on flow and morphology of PP blended with 20 wt% LCP using a capillary viscometer at $\dot{\gamma} = 50-5000\,s^{-1}$ [370]. After addition of 5 wt% SiO_2 (primary particle size = 12 nm) to PP the shear viscosity of the PP at low-$\dot{\gamma}$ increased and became more shear thinning, suggesting formation of nanoparticle 3D aggregates. With the addition of 20 wt% LCP to PP the viscosity was reduced by about 25%, becoming proportional to the mean value. The $\eta = \eta(\dot{\gamma})$ dependence was nearly the same for a blend without SiO_2 as for that containing 5 wt% silica added to PP. Since LCP is about fivefold less viscous than PP, it should diffuse to the high-stress wall region, lubricating the flow; hence the same viscosity with and without SiO_2 may suggest that the nanoparticles were locked in the PP-phase. However, there are two reasons why this explanation is incorrect: (i) since silica is hydrophilic it should migrate to the LCP phase and (ii) the LCP drop size was greatly reduced after addition of nanoparticles, in agreement with the capillarity parameter in Eq. (2.19). Thus, silica did migrate to the LCP phase, increased its viscosity, but (as evident by reduction of the drop size) it probably also reduced the thickness of the lubricating layer on the capillary wall, thereby lowering the viscosity to original level.

Elias *et al.* [371] investigated the effects of SiO_2 addition on the morphology and rheology of PP/PS polymer blends with hydrophilic or hydrophobic pyrogenic SiO_2 (specific surface area $A_{sp} = 200$ and $150\,m^2\,g^{-1}$, respectively; primary particle size $d = 12$ nm). PS or PP with 3, 6, and 10 wt% hydrophilic silica showed linear viscoelastic behavior only at the lowest concentration; low yield stress behavior was present at an angular frequency (ω) $< 0.1\,rad\,s^{-1}$ for either polymer with 6 wt% and was very strong at 10 wt% SiO_2 loading. The PP/PS = 70/30 blend with 0 and 3 wt% hydrophilic or hydrophobic silica was prepared by compounding the filler to one polymer then adding the other, or adding to both simultaneously. The compounding procedure affected the distribution of silica, reduction of PS domain size, and the dynamic flow behavior.

An addition of 3 wt% of either type of SiO_2 to PP/PS = 70/30 blend reduced the PS drop size from about 3.25 to 1 μm, with hydrophilic silica being slightly more effective. Next, the dynamic flow data of blends with silica were compared with the predictions by the Palierne model, Eq. (2.23). The model was applied to two molten phases, each containing SiO_2 (their rheological characteristic was measured). The success of the prediction for blends depended on the assumed partition of SiO_2 between the two polymer phases. Scanning electron microscopy and TEM micrographs showed that hydrophilic SiO_2 migrated towards PS drops (aggregates) and to the interface, whereas the hydrophobic one formed a ca. 100-nm thick interphase, PP/silica/PS, and preferentially entered the PP phase. Accordingly, good fit of data to Eq. (2.23) was obtained assuming that the hydrophilic silica particles were located in the PS phase, which reduced the interfacial tension from $\nu_{12} = 2.15$ to 0.085 mN m^{-1}. For the blend with hydrophobic silica, two SiO_2 locations were postulated: in the PP matrix and uniformly in both phases. Comparison of experimental and computed results indicated that the former assumption is a better one, even without adjustment of the interfacial tension. The authors concluded that two different mechanisms are responsible for the PS drop-size reduction: (i) hydrophilic silica

affects the interfacial tension and (ii) hydrophobic silica rigidifies the interphase, preventing coalescence of PS drops.

The difficulties encountered while analyzing the PP/PS/hydrophobic silica system once more show the limitation of a two-phase model application to three-phase materials. In a subsequent paper Elias *et al.* [372] improved the theoretical analysis by assuming that the global, complex modulus has two contributions:

$$G^*\left(\nu_{12}, G_m^*, G_d^*\right) = G_{composition}^*\left(0, G_m^*, G_d^*\right) + G_{drop}^*\left(\nu_{12}, \eta_m, \eta_d\right) \tag{2.60}$$

Here $G_{composition}^*$ represents complex shear modulus of the blend without interfacial effects while G_{drop}^* is the interface contribution, which comprises the extra elasticity originating in drop deformability. The former contribution was computed from the Kerner model [equivalent to Eq. (2.23) with $\nu_{12} = 0$], while the second was calculated from the Palierne model. The computed dependencies for PP with ethylene–vinyl acetate (EVAc) copolymer and SiO_2, hydrophilic or hydrophobic, well represented the frequency dependencies of G', G'', and η''. Also, the addition of 3 wt% silica reduced EVAc droplet size from 2.2 to about 0.5 μm. The hydrophilic silica migrated to EVAc, while hydrophobic silica migrated to the PP phase.

Thareja and Velankar [373] added 0.2 wt% of hydrophobic silica (particle diameter: $d = 2.7\,\mu$m) to blends of PIB with 5, 10, and 20 wt% of PEG. While addition of this quantity of SiO_2 to neat PEG or PIB hardly changed the flow behavior, the effect on the blends' flow was pronounced. The SiO_2 particles migrated to the hydrophilic surface of a single PEG drop, stiffening the interphase, or bridged two PEG drops to form non-coalescing clusters. Shearing promoted bridging and clustering, which in turn resulted in a gel-like behavior, as evidenced by a G'-plateau at low frequencies. Thus, these large hydrophobic SiO_2 particles promoted the coalescence instead of hindering it, as is the case for nanoparticles.

2.5.3
Rheology of Blends with Nanoparticles Near Binodal

The phase behavior of PS/PVME blends treated with nanoparticles was studied in the dynamic flow field [228, 229, 374]. El-Mabrouk *et al.* used 1 and 5 wt% of commercial organoclays while Gharachorlou and Goharpey employed 4 wt% of fumed SiO_2 (diameter: $d = 7$ nm; $A_{sp} = 300\,m^2\,g^{-1}$). The effect of these two families of nanoparticles on the binodal was similar – the LCST $\geq 100\,^\circ$C increased by about 4 and 13 °C, respectively. The organoclays were immiscible with either polymer, and the flow curves for the blend with 5 wt% organoclay, below and above binodal, showed an apparent yield stress – larger in the steady-state than in the dynamic shear flow. This suggests the existence of 3D structures in a miscible and immiscible blend, on both sides of LCST – in the second case the effect was larger.

Furthermore, Gharachorlou and Goharpey [374], following Ajji and Choplin [209] theory, derived a simple relation between the dynamic moduli at the thermodynamic distance from spinodal, $(\chi_s - \chi)$:

$$\frac{G'(\omega)}{[G''(\omega)]^2} = \frac{30\pi}{Tk_B}\left\{\frac{b_1^2}{36\phi} + \frac{b_2^2}{36(1-\phi)}\right\}^{\frac{3}{2}} \frac{1}{(\chi_s - \chi)^{\frac{3}{2}}}; \quad \chi \approx A + B/T \tag{2.61}$$

where b_i is the statistical segment length of species i, and χ_s is the binary interaction parameter at the spinodal. Accordingly, plotting $[(G'')^2/(G'T)]^{2/3}$ versus $1/T$ should yield a straight line extrapolating to $1/T_s$. The dynamic data for blends with and without nanoparticles yielded values of $T_s \pm 3\,^\circ$C, which were confirmed by DSC and turbidity measurements. Incorporation of 4 wt% nanosilica particles increased the cloud-point curve by about 12 °C.

2.5.4
Rheology of Immiscible Blends with Organoclay

Organoclays have been added to a great variety of polymer blends, replacing the single-component matrix with a multiphase one, either for compatibilization or reinforcement of blend. The most popular blends are PA-6/PP types, usually compatibilized with PP-MA [1, 73, 302]. Since the maleic ring opens up with two acidic groups, after processing the amount of insoluble crosslinked material increases to 20%, making recycling difficult [375]. Thus, the possibility of replacing PP-MA with a small quantity of organoclay is an attractive proposition.

In PA-6/PO blends there is a natural tendency for clay or organoclay to migrate to the polar PA-6 phase or (especially in the presence of a paraffinic compatibilizer and/or intercalant) to the interphase, forming a 100–200 nm thick, rigid membrane [376]. The presence of such an interphase reduces drop fibrillation and coalescence; thus it increases the low frequency G' plateau as well as the complex viscosity.

Gahleitner *et al*. [366] compounded various combinations of PA-6, PP, two compatibilizers, two organoclays based on MMT, and sodium-montmorillonite (Na-MMT). The clay loading to polymers or their blends was high, namely, 5.5–13 wt% organoclay or 6 wt% Na-MMT. In blends PA-6 constituted the minor phase (12–19 wt%), and since MMT prefers the polar phase the addition of PA-6 to PP-based PNC caused coarsening of morphology. The dynamic shear data plotted as either complex viscosity, η^*, or storage moduli, G', versus frequency indicated that addition of clay results in the formation of 3D structures – at low frequency η^* showed an apparent yield stress and G' an initial plateau. The tensile modulus of these reinforced blends was slightly higher than that of neat polymers, while the impact strength was reduced. Similar observations were reported for the HDPE/PA-6 = 75/25 blend, to which 5 wt% of Cloisite®-15A (MMT-2M2HTA) organoclay was added [377]. The authors reported that Eq. (2.23) well-described G' of the binary blend matrix, but no attempt was made to fit it to blends with organoclay. Compared with the matrix performance, at low frequency the values of G' and G'' were larger by about two and one decade, respectively.

Owing to the large aspect ratio of individual clay platelets, the performance of nanocomposites is sensitive to the degree of dispersion and, thus, to the preparation method. For example, better performance has been reported for PP-based PNC prepared by the master batch (MB) method than by a single pass (SP) [378]. A similar

observation was reported for blends of PA-6 with organoclay (MMT-ODA) (ODA, octadecyl-ammonium intercalant) and EPDM-*g*-MA – the material prepared in MB by pre-blending PA-6 with MMT-ODA then compounded with EPDM-g-MA showed better flexural modulus and notched Izod impact strength than the material prepared in SP [77]. At low loading (about 1 wt%) MMT-ODA acted as a compatibilizer for PA6/EPDM-g-MA blends, but at 4 wt% the presence of clay weakened the interactions between the polymeric components. Addition of 1 phr of glycidyl methacrylate compatibilizer required in the SP product was not needed in the MB one. As with other PA-6/PO/clay systems, the intensity of the dynamic moduli low-frequency plateau increased with the degree of compatibilization.

During the last few years the preparation of PNC with polymer blends as the matrix has expanded for two reasons: (i) improved dispersion of the minor polymer phase and (ii) improvement of the blend performance. Several publications include experimental data on the flow properties in dynamic shear. As already discussed, the only fundamental approach involved the use of Palierne model, and thus has been limited to low clay content [371, 372, 377]. Table 2.4 lists the publications that detail the dynamic shear behavior of these systems.

In discussing the elongational flow behavior of polymer blends, the difference between single-phase (homopolymer or miscible blend) and multiphase (antagonistically immiscible PE/PS blend) was demonstrated in Figures 2.12 and 2.13,

Table 2.4 Summary of the rheological behavior of polymer blends with organoclay.

Blend	Organoclay[b)]	Concentration	Observation	Reference
PEG/PMMA = 50/50	C-25A?	0, 2, 5 wt%	Elasticity	[379]
PS/PMMA = 30/70	C-6A	0, 10	Smaller drops, interphase clay	[380]
PC/SAN = 70/30	C-20A	0,1, 3, 5, 10	Smaller drops, interphase clay	[380]
PVC/PS = 50/50	C-6A	0, 10	Smaller drops, interphase clay	[380]
PMMA/EVAc = 50/50	C-6A	0, 10	Smaller drops, interphase clay	[380]
PMMA/PS/EVAc = 33.3/33.3/33.3	C-6A	0, 10	Smaller drops, interphase clay	[380]
PA-6/PPE = 95/5	MMT	0, 0.5	Reactive; small PPE drops	[381]
PC/PMMA = 30/70	C-20A	0, 3, 6	Small drops, translucent	[382]
PP/PBSA[a)] = 80/20	C-20A	0, 5	Small drops, high performance	[383]
PP/PS = 25/75; 75/25	C-10A	0, 3	Smaller drops, sonication	[384]
PPS/PBT = 60/40	C-30B	0, 1, 2, 3, 4, 6	Severe morphological changes	[385]

a) PBSA = poly[(butylene succinate)-*co*-adipate]; b) MMT is sodium montmorillonite, organoclay abbreviation starting with "C" (for Cloisite) is MMT pre-intercalated with di-methyl di-hydrogenated tallow ammonium chloride (C-6A and C20-A), with di-methyl benzyl hydrogenated tallow ammonium chloride (C-10A), with di-methyl hydrogenated tallow 2-ethylhexyl ammonium methyl sulfate (C-25A), and with methyl tallow di-ethoxy ammonium chloride (C-30B).

respectively. To the author's knowledge, the extensional flow behavior of CPNC based on a blend has not been published. However, Okamoto *et al.* [386] reported on the house-of-cards formation in a lightly-maleated PP (0.2 wt% maleic anhydride, MA; $M_w = 195$ kDa, $T_m = 141\,^{\circ}C$) with 4 wt% of organoclay (MMT-ODA). The house-of-cards formation is well known in aqueous clay suspension – evidenced by gelation after dispersing about 5 wt% of clay in water. The mechanism involves the edge–plate interaction that crosslinks the nano-suspension.

Okamoto *et al.* measured the elongational flow behavior of the CPNC using a Meissner-designed rheometer (RME) at 150 °C. As is customary, the authors compared the stress growth functions (measured at $\dot{\varepsilon} = 0.001$–$1.0\,s^{-1}$) with its analog in shear at $\dot{\gamma} = 0.001$. The latter curve, instead of showing similar behavior to that in elongation (at least for the short time data), was about ten-times lower. The data indicated strong *SH,* related by the authors to the house-of-card clay structure. Their recalculated data are displayed in Figure 2.14.

The *SH* behavior in Figure 2.14 is far removed from that recorded for the rheologically simple polymer melts (e.g., see Figure 2.12), but it closely resembles the data obtained for the immiscible LDPE + 15 wt% PS blend displayed in Figure 2.13, or to that reported for composites, for example, short glass fiber-filled PP [96, 387]. The mechanism responsible for the lack of superposition shown in Figure 2.12 is the presence of a stress-sensitive 3D structure that engenders an apparent yield stress. Such a structure in PE/PS blend is created by interacting PS drops, in the PP/MMT-ODA system the clay platelets or their short-stacks interact, forming the reported house-of-cards structures, while in short-glass fiber filled PP the glass interactions at 10–40 wt% loading was evidenced by the apparent yield stress. In consequence, it is to be expected that the CPNC based on polymer blends will also display the 3D-type behavior.

2.6 Conclusions

This chapter summarizes more recent publications on the theoretical and experimental rheological behavior of polymer blends and their nanocomposites. The problem is not trivial as in these multiphase systems the rheology is strongly coupled with thermodynamics, morphology, and their evolutions during testing. For this reason, it is beneficial to analyze the complex system behavior from the perspective of simpler ones, namely, emulsions and suspensions. Emulsions show that owing to the third phase in a binary Newtonian system, the interphase, these systems are elastic. Suspensions offer good model for blends with "rigid" drops formed of a viscous dispersed phase or having a rigid interphase. Both these multiphase systems are characterized by the presence of an apparent yield stresses – the presence of non-zero stress at vanishingly small deformation rate, which may result in non-Newtonian flow curve or frequency-independent values of the dynamic moduli in the "terminal zone." The magnitude of these effects depends on the viscoelastic character of polymers, volume fraction of the dispersed phase, interparticle interactions and morphology – the stronger are the interactions, the stiffer is the 3D structure and the

stronger the rheological response. Nonlinear viscoelastic effects are also evident in elongational tests as an enhancement of strain hardening, most prominent at low Hencky strain rates.

During the last decade there has been a significant progress in understanding the various aspects of polymer blends rheology. For example, the shape of the constant-stress viscosity versus composition provides information on the thickness and viscosity of interphases [289]. The dynamic behavior of blends with spherical drops is characterized by a single parameter, $R' \equiv R_d/\nu_{12}$, which is given by the ratio of volume-averaged drop radius divided by the interfacial tension coefficient. The relation, originally derived for diluted systems [126], has been empirically modified, offering respectable agreement between theory and experiments up to a volume fraction of $\phi \leq 0.449$ [130]. There has also been a concerted effort to provide constitutive equations directly binding rheology and morphology in the full range of concentrations. Several approaches have been published, starting with morphology-dependent blends at $\phi = 0.5$ [249, 260]. A highly promising approach to a full description of the complex system rheology starts with equilibrium thermodynamics principles [268]. However, so far these theories deal with binary systems, treating the interphase in a classical manner as a mathematical plane without thickness. As a result, they are non-applicable to ternary systems, such as reactively compatibilized or nanoparticle filled blends or blends with nanoparticles. It is worth recalling that the properties of the interphase were taken into account in the early classical derivations by Oldroyd [111, 112] or by the group from Twente University [178–181].

Incorporation of nanoparticles affects blend rheology through the morphology modification and/or viscoelasticity of the phases. Most tests have been carried out in dynamic shearing. Owing to the lack of theoretical analysis of tertiary systems only the experimental data have been presented.

Abbreviations:

AFM	atomic force microscopy
BC	block copolymer
BCC	body-centered-cubic
CED	cohesive energy density
CPE	chlorinated polyethylene
CPNC	clay-containing polymeric nanocomposite
EMA	poly(ethylene-*co*-maleic anhydride)
EPDM	ethylene-propylene-diene terpolymer
EPR	ethylene-propylene rubber
EVAc	ethylene-vinyl acetate copolymer
HDPE	high density polyethylene
LCP	liquid crystal polymer
LCST	lower critical solution temperature
LDPE	low density polyethylene

LLDPE	linear low density polyethylene
MA	maleic anhydride
MMT	montmorillonite
MST	microphase separation temperature
NG	nucleation and growth
ODA	octadecyl-ammonium intercalant
PA	polyamide
PAA	polyacrylic acid
PB	polybutadiene
PC	polycarbonate
PCL	polycaprolactone
PDMS	poly(dimethylsiloxane)
PE	polyethylene
PEE	poly(ethyl ethylene)
PEG	polyethyleneglycol
PEMA	poly(ethylmethacrylate)
PET	poly(ethylene terephthalate)
PI	polyisoprene
PIB	polyisobutylene
PMMA	polymethylmethacrylate
PMPS	poly(methyl phenyl siloxane)
PNC	polymeric nanocomposite
PO	polyolefin (e.g., PE, PP, . . .)
POM	polyoxymethylene (polyacetal)
PP	polypropylene
PPE	polyphenyleneether
PS	polystyrene
PSD	deuterated-PS
PVC	polyvinyl chloride
PVE	poly(vinyl ethylene)
PVME	polyvinylmethylether
RME	Rheometrics elongational rheometer for melts
RMS	Rheometrics Mechanical Spectrometer
SALLS	small-angle laser light scattering
SAN	poly(styrene-*co*-acrylonitrile)
SANS	small-angle neutron scattering
SAXS	small-angle X-ray scattering
SBR	styrene-butadiene rubber
SBS	styrene-butadiene-styrene three block copolymer
SD	spinodal decomposition
SEBS	styrene-ethylene/butene-styrene three block copolymer
SEC	size exclusion chromatography
SFA	surface forces apparatus
SMA	poly(styrene–*co*–maleic anhydride)
TEM	transmission electron microscopy

UCST	upper critical solution temperature
UV	ultraviolet radiation
XPS	X-ray photoelectron spectroscopy

Symbols

Symbols that are used in this chapter and also others that are commonly employed in the field of polymer blends are given below:

A_{sp}	specific surface area of (nano) particles
$a, b, k, K, n, u,$	equation constants
a_v	interfacial area density
B_{AB}	reduced binary thermodynamic interaction parameter ($B_{AB} = \chi_{AB}RT/V$)
B	droplet width
B_e	extrudate swell
b_i	segment length
c_i	Lee and Park relaxation parameters
$\boldsymbol{D}$	deformation
De	Deborah number
d	droplet diameter
d^*	equilibrium droplet diameter
d_o	diameter of the die
d_T	Taylor value for infinite dilution
E^+	threshold energy of coagulation
E_{DK}	macroscopic bulk breaking energy
E_{int}	interphase elasticity
F	intrinsic thermodynamic function
F_c	contact force
f_s	packing fraction, or shielding function in Eq. (2.8)
$f(d)$	number-frequency size distribution
G^*, G', G''	complex, storage, and loss shear modulus, respectively
G_N^o	plateau modulus
$H(\tau)$	relaxation time spectrum
$\tilde{H}(\omega)$	reduced frequency relaxation spectrum
$\tilde{H}_G(\omega)$	Gross' frequency relaxation spectrum
H_{max}	maximum of the relaxation spectrum
h_c	critical separation distance between coalescing drops
h_o and h_{crit}	initial and critical (for coalescence) liquid film thickness, respectively
k	interlayer slip factor
G_N^o	plateau modulus
J_e^o	recoverable shear compliance
k_B	Boltzmann constant
$\boldsymbol{L}$	Poisson bivector

L	droplet length
M	Onsager-type mobility factor
M_e	entanglement molecular weight
M_n, M_w, M_z	number, weight, and z-average molecular weight, respectively
MWD	molecular weight distribution
m_1 and m_2	polydispersity parameters
N_1	$\sigma_{11} - \sigma_{22}$, the first normal stress difference
N_o,N_N	initial and final number of particles, respectively
N^o, N^+	number of coagulating drops, initially and at $t = t_c$, respectively
N_T	total number of collisions per unit time
n	number of particles
n_i	number of moles unit volume
P	pressure
P^*	characteristic reducing pressure
Pe	Péclet number
Pe	entrance–exit pressure drop (Bagley correction)
p_r	probability that two particles that have collided result in coalescence
Q	interfacial area per unit volume
$\boldsymbol{q}$	wave vector, or sinusoidal distortion
R	ideal gas constant
R_d	drop radius
$R(q)$	fluctuation function
$\bar{r}$	reduced drop radius
$\langle r_\Theta^2 \rangle^{1/2}$	-unperturbed, average radius of gyration
rad	radian
r_N	radius of the critical nucleus
SH; SSH	strain hardening; slope of strain hardening
$S(q)$, S_0	virtual structure function
S_o, S	interfacial area per unit volume of spherical particles before and after coalescence
s	spinodal
T	absolute temperature
T_g	glass transition temperature
T_b, T_s	binodal, spinodal temperature
t	time
t_b	necessary time for breakup of droplets
t_b^*	dimensionless breakup time
t_c	coalescence time, which may eventually leads to coagulation
U	internal energy
V	volume
V_x/V	volume fraction of emulsion undergoing uniform shear
w_i	weight fraction of component i
x_i	mole fraction of component i.
γ =1-h	occupied volume fraction in the S-S lattice theory.
z	reduced frequency

Greek Symbols

α, β	equation constants
α	orientation angle
α_o	the distortion at $t = 0$
γ, $\dot{\gamma}$	shear strain and rate of shearing, respectively
γ_d and γ_m	strain of the drop (defined as a ratio of the long axis of prolate ellipsoid to the original drop diameter) and the matrix, respectively
δ_{ij}	unit tensor from Eq. (2.7)
Δ	thermodynamic distance from the spinodal; $\Delta \equiv 2[(\chi_{AB}N)_s - (\chi_{AB}N)]$
ΔE	activation energy, for example, of flow: ΔE_η
ΔG_m	Gibbs free energy of mixing
ΔH_m, ΔS_m	enthalpy and entropy of mixing, respectively
Δl	interphase thickness
$\delta = \delta(T, P)$	solubility parameter as a function of temperature and pressure, Eq. (2.29)
ε,$\dot{\varepsilon}$	Hencky strain and Hencky strain rate in extension, respectively
η	viscosity
$[\eta]$	intrinsic viscosity
η^e	excess viscosity
η^E	elongational viscosity
η_{inh}	inherent viscosity
η_m; η_d	matrix and dispersed polymer viscosity,
η_o	zero-shear viscosity
η_r	relative viscosity
η_∞	lower Newtonian viscosity
η'	dynamic viscosity
η^*	complex viscosity
η^+	stress growth function
η_1, η_2	viscosity of dispersed and matrix phase, respectively
$\kappa = \sigma_{\iota\varphi} d/\nu_{12}$	capillarity number
κ_{crit}	critical capillary number
Λ	distortion wavelength
$\lambda \equiv \eta_2/\eta_1$	dispersed phase-to-matrix viscosity ratio
λ_s	wavelength
ν_{12}^o	interfacial tension in a quiescent blends
ν_{12}; ν_∞	interfacial tension coefficient between phase 1 and 2; and that for infinite molecular weight
Ξ	dissipation potential
ϱ	density
ϱ_d	droplet density
σ	stress
σ_{11}	elongational stress

$\sigma_{11} - \sigma_{22}$	N_1, first normal stress difference
σ_{12}	shear stress
σ_{m}	stress in the matrix phase
σ_{y}	yield stress
$\sigma_{\mathrm{y}}^{\mathrm{o}}$	permanent yield stress
τ	relaxation time
τ^*	mean relaxation time
τ_{e}	relaxation time of the entangled segment
ϕ_1, ϕ_2	volume fraction of dispersed and matrix phase, respectively
ϕ_{c}	volume fraction of the crosslinked monomer units, or compatibilizer content in Eq. (2.5)
ϕ_I	volume fraction of phase i at phase inversion
ϕ_{m}	maximum packing volume fraction
ϕ_{perc}	percolation threshold
χ_{AB}, χ_{12}	binary thermodynamic interaction parameter between polymers A and B or phase 1 and 2
ψ_1, ψ_2	first and second normal stress difference coefficient, respectively
$\Omega(\Lambda, \lambda)$	tabulated function for capillary instability
ω	angular frequency during dynamic shearing, in (rad/s)
$\omega_{\max}$	frequency at which $\tilde{H}(\omega)$ is maximum
ω_{v}	vorticity
ω_x	crossover frequency

References

1 Utracki, L.A. (ed.) (2002) *Polymer Blends Handbook*, Kluwer Academic Press, Dordrecht.

2 Utracki, L.A. (1995) The rheology of multiphase systems, in *Rheological Fundamentals of Polymer Processing* (eds J.A. Covas, J.F. Agassant, A.C. Diogo, J. Vlachopoulos, and K. Walters), Kluwer Academic Publishers, Dordrecht, 113-137.

3 Utracki, L.A. and Kamal, M.R. (2002) The rheology of polymer alloys and blends *Polymer Blends Handbook* (ed. L.A. Utracki), Kluwer Academic Press, Dordrecht, 449-546.

4 Utracki, L.A. (1989) *Polymer Alloys and Blends*, Hanser Publishers, Munich.

5 Steller, R. and Żuchowska, D. (1990) Free volume theory for rheological properties of polymer blends. *J. Appl. Polym. Sci.*, **41** (7–8), 1595–1607.

6 Couchman, P.R. (1996) The viscosity of miscible blends. *J. Appl. Polym. Sci.*, **60** (7), 1057–1060.

7 Utracki, L.A., Kamal, M.R., and Al-Bastaki, N.M. (1984) Elongational flow of polyethylenes and polyethylene blends. *SPE-Techn. Papers.*, **30**, 417–420.

8 Arrhenius, S. (1887) Über die innere Reibung verdünnter wässeriger Lösungen (On the dissociation of substances dissolved in water). *Z. Phys. Chem. (Leipzig)*, **1**, 285-298; 631-648.

9 Powell, R.E., Roseveare, W.E., and Eyring, H. (1941) Diffusion, thermal conductivity, and viscous flow of liquids. *Ind. Eng. Chem.*, **33** (4), 430–435.

10 Glasstone, S., Laidler, K.L., and Eyring, H. (1941) *Theory of Rate Processes*, McGraw-Hill, New York.

11 McAllister, R.A. (1960) The viscosity of liquid mixtures. *AIChE J.*, **6**, 427–431.

12 Bondi, A. (1967) Viscosity and molecular structure, in *Rheology Theory and Applications*, vol. 4 (ed. F.R. Eirich), Academic Press, New York, 1–83.

13 Lomte, S.B., Bawa, M.J., Lande, M.K., and Arbad, B.R. (2009) Densities and viscosities of binary liquid mixtures of 2-butanone with branched alcohols at 293.15 to 313.15K. *J. Chem. Eng. Data*, **54** (1), 127–130.

14 Friedman, E.M. and Porter, R.S. (1975) Polymer viscosity-molecular weight distribution correlations via blending: for high molecular weight poly(dimethy1 siloxanes) and for polystyrenes. *Trans. Soc. Rheol.*, **19** (4), 493–508.

15 Utracki, L.A. (1986) Correlation between P–V–T behavior and the zero-shear viscosity of liquid mixtures, in proceeding of the Symposium on Applications of Equations of State in Rheology, B. Hartmann (Ed.). *J. Rheol.*, **30** (4), 829–841.

16 Tsenoglou, C. (1991) Molecular weight polydispersity effects on the viscoelasticity of entangled linear polymers. *Macromolecules*, **24** (8), 1762–1767.

17 Graessley, W.W. (2008) *Polymeric Liquids and Networks: Dynamics and Rheology*, Garland Science, London.

18 Bersted, B.H. and Slee, J.D. (1977) A relationship between steady-state shear melt viscosity and molecular weight distribution in polystyrene. *J. Appl. Polym. Sci.*, **21** (10), 2631–2644.

19 Gusmán, J.D., Schieber, J.D., and Pollard, R. (2005) A regularization-free method for the calculation of molecular weight distributions from dynamic moduli data. *Rheol. Acta*, **44** (4), 342–351.

20 Llorens, J., Rude, E., and Marcos, R.M. (2005) Prediction of polymer molecular weight distribution from rheology: polydimethylsiloxane blends. *Mater. Sci. Forum*, **480–481**, 281–286.

21 Borg, T. and Pääkkönen, E.J. (2009) Linear viscoelastic models: Part I. Relaxation modulus and melt calibration. *J. Non-Newtonian Fluid Mech.*, **156** (1–2), 121–128.

22 Borg, T. and Pääkkönen, E.J. (2009) Linear viscoelastic models: Part II. Recovery of the molecular weight distribution using viscosity data. *J. Non-Newtonian Fluid Mech.*, **156** (1–2), 129–138.

23 Borg, T. and Pääkkönen, E.J. (2009) Linear viscoelastic models: Part III. Start-up and transient flow effects from the molecular weight distribution. *J. Non-Newtonian Fluid Mech.*, **159** (1–3), 17–25.

24 Borg, T. and Pääkkönen, E.J. (2010) Linear viscoelastic models: Part IV. From molecular dynamics to temperature and viscoelastic relations using control theory. *J. Non-Newtonian Fluid Mech.*, **165** (1–2), 24–31.

25 Helfand, E. and Tagami, Y. (1971) Theory of the interface between immiscible polymers. *J. Polym. Sci., Polym. Lett.*, **9** (10), 741–746.

26 Helfand, E. and Tagami, Y. (1972) Theory of the interface between immiscible polymers. II. *J. Chem. Phys.*, **56** (7), 3592–3601.

27 Helfand, E. and Sapse, A.M. (1975) Theory of unsymmetric polymer–polymer interfaces. *J. Chem. Phys.*, **62** (4), 1327–1331.

28 Liang, H., Favis, B.D., Yu, Y.S., and Eisenberg, A. (1999) Correlation between the interfacial tension and dispersed phase morphology in interfacially modified blends of LLDPE and PVC. *Macromolecules*, **32** (5), 1637–1642.

29 Noolandi, J. (1984) Recent advances in the theory of polymeric alloys. *Polym. Eng. Sci.*, **24** (1), 70–78.

30 Bélanger, C., Cielo, P., Patterson, W. I., Favis, B. D., and Utracki, L. A. (1992) Morphological Characterization of Simulated Polymer Blends by Light Scattering, *Polym. Eng. Sci.*, **32** (24), 1886 – 1895.

31 Tang, T. and Huang, B. (1994) Interfacial behavior of compatibilizers in polymer blends. *Polymer*, **35** (2), 281–285.

32 Lyngaae-Jørgensen, J. and Utracki, L.A. (1991) Melt rheology and dual phase continuity in polymer blends. *Makromol. Chem., Macromol. Symp.*, **48/49**, 189–209.

33 Lyngaae-Jørgensen, J., Lunde Rasmussen, K., Chtcherbakova, E.A., and Utracki, L.A. (1999) Flow induced formation of dual-phase continuity in polymer blends and alloys, Part I. *Polym. Eng. Sci.*, **39** (6), 1060–1971.

34 Utracki, L.A. (1991) On the viscosity–concentration dependence of

immiscible polymer blends. *J. Rheol.*, **35** (8), 1615–1637.

35 Utracki, L.A. (volume and series ed.) (1991) *Two-Phase Polymer Systems, Progress in Polymer Processing*, vol. 2, Carl Hanser, Munich.

36 Lyngaae-Jørgensen, J. and Utracki, L.A. (2003) Structuring polymer blends with bicontinuous phase morphology. Part II. Tailoring blends with ultralow critical volume fraction. *Polymer*, **44** (5), 1661–1669.

37 Einstein, A. (1906) Eine neue Bestimmung der Moleküldimensionen. *Ann. Phys.*, **324** (2), 289–306.

38 Einstein, A. (1911) Berichtigung zu meiner Arbeit: "Eine neue Bestimmung der Moleküldimensionen." *Ann. Physik.*, **339** (3), 591–592.

39 Simha, R.(18 February 1935) Beiträge zur Hydrodynamik der Kolloide, PhD Dissertation, Vienna University.

40 Brenner, H. (1974) Rheology of a dilute suspension of axisymmetric Brownian particles. *Int. J. Multiphase Flow.*, **1**, 195–341.

41 Denisov, I.E., Krasheninnikov, A.I., and Chervin, V.G. (1985) Modeling rheological properties of a suspension by the molecular dynamics method. *Kolloid. Zh.*, **47**, 790.

42 Brady, J.F. and Bossis, G. (1985) The rheology of concentrated suspensions of spheres in simple shear flow by numerical simulations. *J. Fluid Mech.*, **155**, 105–129.

43 Russel, W.B. (1983) Effects of interactions between particles and rheology of dispersions, in *Theory of Dispersed Multiphase Flow* (ed. R.E. Meyer), Academic Press, New York, 1-34.

44 Utracki, L.A. (1989) Melt flow of polyethylene blends, in *Multiphase Polymers: Blends and Ionomers*, (eds L.A. Utracki and R.A. Weiss), ACS Symposium Series, vol. 395, American Chemical Society, Washington, D.C., series ed. M. Joan Comstock, 153–210.

45 Simha, R. (1952) A treatment of the viscosity of concentrated suspensions. *J. Appl. Phys.*, **23** (9), 1020–1024.

46 Krieger, I.M. and Dougherty, T.J. (1959) A mechanism for non-Newtonian flow in suspensions of rigid spheres. *Trans. Soc. Rheol.*, **3** (1), 137–152.

47 Thomas, D.G. (1965) Transport properties of suspension: VII. A note on the viscosity of Newtonian suspensions of uniform spherical particles. *J. Colloid Sci.*, **20** (3), 267–273.

48 Utracki, L.A. and Fisa, B. (1982) Rheology of fiber or flake filled plastics. *Polym. Comp.*, **3** (4), 193–211.

49 Pishvaei, M., Graillat, C., Cassagnau, P., and McKenna, T.F. (2006) Modeling the zero shear viscosity of bimodal high solid content latex: Calculation of the maximum packing fraction. *Chem. Eng. Sci.*, **61**, 5768–5780.

50 Ouchiyama, N. and Tanaka, T. (1975) The probability of coalescence in granulation kinetics. *Ind. Eng. Chem. Process Des. Dev.*, **14** (3), 286–289.

51 Ouchiyama, N. and Tanaka, T. (1980) Estimation of the average number of contacts between randomly mixed solid particles. *Ind. Eng. Chem. Fundam.*, **19** (4), 338–340.

52 Ouchiyama, N. and Tanaka, T. (1981) Porosity of a mass of solid particles having a range of sizes. *Ind. Eng. Chem. Fundam.*, **20** (1), 66–71.

53 Ouchiyama, N. and Tanaka, T. (1984) Porosity estimation for random packing of spherical particles. *Ind. Eng. Chem. Fundam.*, **23** (4), 490–493.

54 Ouchiyama, N. and Tanaka, T. (1986) Porosity estimation from particle size distribution. *Ind. Eng. Chem. Fundam.*, **25** (1), 125–129.

55 Ouchiyama, N. and Tanaka, T. (1989) Predicting the densest packing of ternary and quaternary mixtures of solid particles. *Ind. Eng. Chem. Res.*, **28** (10), 1530–1536.

56 Lainé, C. and Cassagnau, P. (2006) Prediction of zero-shear viscosity of poly (vinyl chloride) plastisols. *Appl. Rheol.*, **16** (2), 136–144.

57 Ritter, J. (1971) Sphere-filled plastic composites. *Appl. Polym. Symp.*, **15**, 239.

58 Lord, F.W. (1971) UK Pat. Appl. 51,292.

59 Więckowski, A. and Stręg, F. (1966) Porowatość mieszenin ciał sypkich. Mieszaniny dwuskładnikowe (Porosity of mixtures of granular

materials. Two-component mixtures). Chemia Stosowana, B 3 (1), 96–128.
60 Milewski, J.V. (1973) A study of the packing of fibers and spheres, PhD. Thesis, Rutgers University, New Brunswick, NJ.
61 Milewski, J.V. (1977) Science and potentials of micro packing, *ACS. Div. Org. Coat. Plast. Chem. Prepr.*, **38**, 127.
62 Milewski, J.V. (1978) The combined packing of rods and spheres in reinforcing plastics. *Ind. Eng. Chem. Prod. Res. Dev.*, **17**, 363–366.
63 Milewski, J.V. and Katz, H.S. (1987) *Handbook of Reinforcements for Plastics*, Van Nostrand Reinhold Co., New York.
64 Utracki, L.A. (2004) *Clay-Containing Polymeric Nanocomposites*, Rapra Technology Ltd., Shawbury, UK.
65 Utracki, L.A. (1988) Viscoelastic behavior of polymer blends. *Polym. Eng. Sci.*, **28** (21), 1401–1404.
66 Chang, C. and Powell, R.L. (1994) Effect of particle size distribution on the rheology of concentrated bimodal suspensions. *J. Rheol.*, **38** (1), 85–98.
67 Doi, M. and Edwards, S.F. (1978) Dynamics of rod-like macromolecules in concentrated solution. Part 1. *J. Chem. Soc., Faraday Trans. 2*, **74**, 560–570; Doi, M. and Edwards, S.F. (1978) Dynamics of rod-like macromolecules in concentrated solution. Part 2 *J. Chem. Soc., Faraday Trans. 2*, **74**, 918–932.
68 Batchelor, G.K. (1970) Slender-body theory for particles of arbitrary cross-section in Stokes flow. *J. Fluid Mech.*, **44**, 419–440.
69 Batchelor, G.K. (1971) The stress generated in a non-dilute suspension of elongated particles by pure straining motion. *J. Fluid Mech.*, **46**, 813–829.
70 Goldsmith, H.L. and Mason, S.G. (1967) The microrheology of dispersions, in *Rheology*, vol. **4** (ed. F.R. Eirich), Academic Press, New York, 85-250.
71 van de Ven, T.G.M. (1989) *Colloidal Hydrodynamics*, Academic Press, New York.
72 Carreau, P.J. (1972) Rheological equation from molecular network theories. *Trans. Soc. Rheol.*, **16** (1), 99–127.
73 Utracki, L.A. (ed.) (1994) *Encyclopaedic Dictionary of Commercial Polymer Blends*, ChemTec Publishing, Toronto.
74 Cross, M.M. (1965) Rheology of non-Newtonian fluids: A new flow equation for pseudoplastic systems. *J. Colloid Sci.*, **20** (5), 417–437.
75 Cross, M.M. (1970) Kinetic interpretation of non-Newtonian flow. *J. Colloid Sci.*, **33** (1), 30–35.
76 Cross, M.M. (1973) Rheology of synthetic latices: influence of shear rate and temperature. *J. Colloid Sci.*, **44** (1), 175–176.
77 Zhang, L., Wan, C., and Zhang, Y. (2008) Polyamide 6/maleated ethylene–propylene–diene rubber/organoclay composites with or without glycidyl methacrylate as a compatibilizer. *J. Appl. Polym. Sci.*, **110** (3), 1870–1879.
78 Zhuang, H., Ren, P., Zong, Y., and Dai, G.C. (2008) Relationship between fiber degradation and residence time distribution in the processing of long fiber reinforced thermoplastics. *Express Polym. Lett.*, **2** (8), 560–568.
79 Crowson, R.J. and Folkes, M.J. (1980) Rheology of short glass fiber-reinforced thermoplastics and its application to injection molding. II. The effect of material parameters. *Polym. Eng. Sci.*, **20** (14), 934–940.
80 Sobhanie, M., Isayev, A.I., and Fan, Y. (1997) Viscoelastic plastic rheological model for particle filled polymer melts. *Rheol. Acta*, **36** (1), 66–81.
81 Sobhanie, M. and Isayev, A.I. (1999) Modeling and experimental investigation of shear flow of filled polymer. *J. Non Newtonian Fluid Mech.*, **85** (1–2), 189–212.
82 White, J.L. (1982) Rheological behavior of molten polymer blends and particle filled melts, in *Polymer Compatibility and Incompatibility: Principles and Practice*, (volume and series ed. K. Šolc), MMI Press Symposium Series, vol. 2, Harwood Academic Publishers, New York, 413–441.
83 Chaffey, C.E. (1983) Reinforced thermoplastics: through flow to use. *Annu. Rev. Mater. Sci.*, **13**, 43–65.
84 Goettler, L.A. (1984) Mechanical property enhancement in short-fiber composites

through the control of fiber orientation during fabrication. *Polym. Composites*, **5** (1), 60–71.

85 Metzner, A.B. (1985) Rheology of suspensions in polymeric liquids. *J. Rheol.*, **29** (6), 739–775.

86 Utracki, L.A. (1987) Rheology and processing of multiphase systems, in *Current Topics in Polymer Science*, vol. 2 (eds R.M. Ottenbrite, L.A. Utracki, and S. Inoue), Hanser Publishers, Munich, 7–59.

87 Schlund, B. and Utracki, L.A. (1987) Linear low density polyethylenes and their blends. Part 2: shear flow of LLDPEs. *Polym. Eng. Sci.*, **27** (5), 367–379.

88 Utracki, L.A. and Schlund, B. (1987) Linear low density polyethylenes and their blends. Part 4, shear flow of LLDPE blends. *Polym. Eng. Sci.*, **27** (20), 1512–1522.

89 Utracki, L.A. (1988) The rheology of two-phase flows in *Rheological Measurements* (eds A.A. Collyer and D.W. Clegg), Elsevier Applied Science, London, 479–594

90 Utracki, L.A. and Vu-Khanh, T. (1992) Filled polymers in *Multicomponent Polymer Systems* (eds I.S. Miles and S. Rostami), Longman Scientific & Technical, Harlow, 207–268.

91 Shenoy, A.V. (1999) *Rheology of Filled Polymer Systems*, Kluwer Academic Publishers, Dordrecht.

92 Solomon, M.J. and Lu, Q. (2001) Rheology and dynamics of particles in viscoelastic media. *Curr. Opin. Colloid Interface Sci.*, **6** (5–6), 430–437.

93 Leblanc, J.L. (2002) Rubber-filler interactions and rheological properties in filled compounds. *Progr. Polym. Sci.*, **27** (4), 627–687.

94 Hausnerova, B., Honkova, N., Lengalova, A., Kitano, T., and Saha, P. (2008) Rheological behavior of fiber-filled polymer melts at low shear rate. Part I. *Polimery*, **53** (7–8), 507–512;Hausnerova, B., Honkova, N., Lengalova, A., Kitano, T. and Saha, P. (2008) Rheological behavior of fiber-filled polymer melts at low shear rate. Part II, *Polimery*, **53** (7–8), 649–656.

95 Leonov, A.I. (1990) The effect of surface tension on stretching of very thin highly elastic filaments. *J. Rheol.*, **34** (2), 155–167.

96 Mutel, A.T. and Kamal, M.R. (1991) Rheological properties of fiber-reinforced polymer melts, in *Two-Phase Polymer Systems* (volume and series ed. L.A. Utracki), Progress in Polymer Processing, vol. 2, Carl Hanser, Munich, 305–331.

97 Vincent, M. and Agassant, J.F. (1986) Experimental study and calculations of short glass fiber orientation in a center gated molded disc, *Polym. Compos.*, **7** (2), 76–83; Vincent, M. and Agassant, J.F. (1991) Prediction fiber orientation in injection molding, in Two-Phase Polymer Systems, Progress in Polymer Processing, vol. 2 (volume and series ed. L.A. Utracki), Carl Hanser, Munich, 227–303.

98 Shikata, T. and Pearson, D.S. (1994) Viscoelastic behavior of concentrated spherical suspensions. *J. Rheol.*, **38** (3), 601–616.

99 Goettler, L.A. and Shen, K.S. (1983) Rheological and dynamic properties of unvulcanized natural rubber and regenerated cellulose compositions. *Rubber Chem. Technol.*, **56**, 619–633.

100 Sherman, P. (1963) in *Rheology of emulsions in Emulsion Science*, (ed. P. Sherman) Pergamon Press, Oxford, 217–351.

101 Sherman, P. (1968) General properties of emulsions and their constituents, in *Emulsion Science* (ed. P. Sherman), Academic Press, London, 131–216.

102 Barry, B.W. (1977) Viscoelastic properties of concentrated emulsions. *Adv. Colloid Interface Sci.*, **5** (1), 37–75.

103 Nielsen, L.E. (1977) *Polymer Rheology*, Marcel Dekker, New York.

104 Tadros, Th.F. (1994) Fundamental principles of emulsion rheology and their applications. *Colloids Surf. A: Physicochem. Eng. Aspects*, **91**, 39–55.

105 Barnes, H.A. (1994) Rheology of emulsions – a review. *Colloids Surf. A*, **91**, 89–95.

106 Pal, R. (1994) Metering of two-phase liquid-liquid emulsions: A state of the art review. *Ind. Eng. Chem. Res.*, **33** (6), 1413–1435.

107 Pal, R. (1994) Techniques for measuring the composition (oil and water content) of emulsions – a state of the art review, *Colloids Surf. A, Physicochem. Eng. Aspects*, **84** (2–3), 141–193.

108 Pal, R. (1996) Rheology of emulsions containing polymeric liquids, in *Encyclopedia of Emulsion Technology* (ed. P. Becher), Marcel Dekker, New York, 93–263.

109 Lequeux, F. (1998) Emulsion rheology. *Curr. Opin. Colloid Interface Sci.*, **3** (4), 408–411.

110 Cameron, N.R. and Sherrington, D.C. (1996) High internal phase emulsions (HIPEs) – structure, properties and use in polymer preparation. *Adv. Polym. Sci.*, **126**, 163–214.

111 Oldroyd, J.C. (1953) The elastic and viscous properties of emulsions and suspensions. *Proc. Roy. Soc., A*, **218**, 122–132.

112 Oldroyd, J.C. (1955) The effect of interfacial stabilizing films on the elastic and viscous properties of emulsions. *Proc. R. Soc. London, Ser. A*, **232**, 567–577.

113 Choi, S.J. and Schowalter, W.R. (1975) Rheological properties of nondilute suspensions of deformable particles. *Phys. Fluids*, **18**, 420–427.

114 Malkin, A.Ya. and Isayev, A.I. (2006) *Rheology: Concepts, Methods and Applications*, ChemTec Publishing, Toronto.

115 Malkin, A.Ya. and Masalova, I. (2007) Shear and normal stresses in flow of highly concentrated emulsions. *J. Non-Newtonian Fluid Mech.*, **147** (1–2), 65–68.

116 Masalova, I. and Malkin, A.Ya. (2007) Peculiarities of rheological properties and flow of highly concentrated emulsions: the role of concentration and droplet size. *Colloid J.* (Russian Academy of Sciences), **69** (2), 185–202.

117 Taylor, G.I. (1932) The viscosity of a fluid containing small drops of another fluid. *Proc. Roy. Soc. London, Ser. A*, **138**, 41–48.

118 Taylor, G.I. (1934) The formation of emulsions in definable fields of flow. *Proc. Roy. Soc. London, Ser. A*, **146**, 501–523.

119 Luciani, A., Champagne, M.F., and Utracki, L.A. (1996) Interfacial tension in polymer blends. Part 1: Theory. *Polym. Networks Blends*, **6** (1), 41–50; Luciani, A., Champagne, M.F. and Utracki, L.A. (1996) Interfacial tension in polymer blends. Part 2: Measurements. *Polym. Networks Blends*, **6** (2), 51–62.

120 Luciani, A., Champagne, M.F., and Utracki, L.A. (1997) Interfacial tension determination by retraction of an ellipsoid. *J. Polym. Sci. B, Polym. Phys. Ed.*, **35** (9), 1393–1403.

121 Utracki, L.A. and Shi, Z.-H. (1992) Development of polymer blend morphology during compounding in a twin screw extruder – part 1: droplet dispersion and coalescence – a review. *Polym. Eng. Sci.*, **32** (24), 1824–1833.

122 Utracki, L.A. (1973) The mechanical stability of polymer latex's. *J. Colloid Interface Sci.*, **42** (1), 185–197.

123 Ha, J.W., Yoon, Y., and Leal, L.G. (2003) The effect of compatibilizer on the coalescence of two drops in flow. *Phys. Fluids*, **15**, 849–867.

124 Elmendorp, J.J. (1986) A study of polymer blending microrheology, PhD Thesis, Delft University of Technology, The Netherlands;Elmendorp, J.J. (1986) Study on polymer blending microrheology. *Polym. Eng. Sci.*, **26** (6), 418–426.

125 Chesters, A.K. (1991) The modeling of coalescence process in fluid-liquid dispersions – a review of current understanding. *Trans. Ind. Chem. Eng., A*, **69**, 352–361.

126 Palierne, J.F. (1990) Linear rheology of viscoelastic emulsions with interfacial tension. *Rheol. Acta*, **29** (3), 204–214.

127 Palierne, J.F. (1991) Linear rheology of viscoelastic emulsions with interfacial tension. Erratum, *Rheol. Acta*, **30** (5), 497.

128 Graebling, D. and Muller, R. (1991) Determination of interfacial tension of polymer melts by dynamic shear measurements. *Colloids Surf.*, **55**, 89–103.

129 Graebling, D., Muller, R., and Palierne, J.F. (1993) Linear viscoelastic behavior of some incompatible polymer blends in the melt interpretation of data with a model of emulsion of viscoelastic liquids. *Macromolecules*, **26** (2), 320–329.

130 Pal, R. (2008) A new linear viscoelastic model for emulsions and suspensions. *Polym. Eng. Sci.*, **48** (7), 1250–1253.

131 Bower, C., Gallegos, C., Mackley, M.R., and Madiedo, J.M. (1999) The rheological and microstructural characterisation of the non-linear flow behaviour of concentrated oil-in-water emulsions. *Rheol. Acta*, **38** (2), 145–159.

132 Vlahovska, P., Bławzdziewicz, J., and Loewenberg, M. (2002) Nonlinear rheology of a dilute emulsion of surfactant-covered spherical drops in time-dependent flows. *J. Fluid Mech.*, **463**, 1–24.

133 Pal, R. (1999) Yield stress and viscoelastic properties of high internal phase ratio emulsions. *Colloid Polym. Sci.*, **277** (6), 583–588.

134 Pal, R. (1999) Rheology of blends of suspensions and emulsions. *Ind. Eng. Chem. Res.*, **38** (12), 5005–5010.

135 Pal, R. (2000) Viscosity-concentration equation for emulsions of nearly spherical droplets. *J. Colloid Interface Sci.*, **231** (1), 168–175.

136 Pal, R. (2000) Slippage during the flow of emulsions in rheometers. *Colloid Surf. A: Physicochem. Eng. Aspects*, **162** (1–3), 55–66.

137 Pal, R. (2001) Evaluation of theoretical viscosity models for concentrated emulsions at low capillary numbers. *Chem. Eng. J.*, **81** (1–3), 15–21.

138 Malkin, A.Ya., Masalova, I., and Slatter, P. and Wilson, K. (2004) Effect of droplet size on the rheological properties of highly-concentrated w/o emulsions. *Rheol. Acta*, **43** (6), 584–591.

139 Quintero, C.G., Noïk, C., Dalmazzone, C., and Grossiord, J.-L. (2008) Modeling and characterization of diluted and concentrated water-in-crude oil emulsions: comparison with classical behavior. *Rheol. Acta*, **47** (4), 417–424.

140 Tolstoguzov, V.B., Mzhel'sky, A.I., and Gulov, V.Ya. (1974) Deformation of emulsion droplets in flow. *Colloid Polym. Sci.*, **252**, 124–132.

141 Sánchez, M.C., Valencia, C., Franco, J.M., and Gallegos, C. (2001) Wall slip phenomena in oil-in-water emulsions: Effect of some structural parameters. *J. Colloid Interface Sci.*, **241** (1), 226–232.

142 Peker, S., Bora, K., and Över, Y. (2001) Effect of interfacial properties on the drop size distribution of high internal phase ratio emulsions. *Colloids Surf. A: Physicochem. Eng. Aspects*, **182** (1–3), 43–56.

143 Saiki, Y., Prestidge, C.A., and Horn, R.G. (2007) Effects of droplet deformability on emulsion rheology. *Colloids Surf. A: Physicochem. Eng. Aspects*, **299** (1–3), 65–72.

144 Stokes, J.R., Wolf, B., and Frith, W.J. (2001) Phase-separated biopolymer mixture rheology: prediction using a viscoelastic emulsion model. *J. Rheol.*, **45** (5), 1173–1191.

145 Danker, G., Verdier, C., and Misbah, C. (2008) Rheology and dynamics of vesicle suspension in comparison with droplet emulsion. *J. Non-Newtonian Fluid Mech.*, **152** (1–3), 156–167.

146 Lee, H.M., Lee, J.W., and Park, O.O. (1997) Rheology and dynamics of water-in-oil emulsions under steady and dynamic shear flow. *J. Colloid Interface Sci.*, **185**, 297–305.

147 Lyngaae-Jørgensen, J. (1989) Phase transitions in simple flow fields in *Multiphase Polymers: Blends and Ionomers* (eds L.A. Utracki and R.A. Weiss), ACS Symposium Series, vol. **395**, M. Joan Comstock, series ed., American Chemical Society, Washington, D.C., 128–152.

148 Leibler, L. (1980) Theory of microphase separation in block copolymers. *Macromolecules*, **13** (6), 1602–1617.

149 Folkes, M.J. (eds) (1985) *Processing, Structure and Properties of Block Copolymers*, Elsevier Applied Science, London.

150 Inoue, T., Soen, T., Hashimoto, T., and Kawai, H. (1969) Thermodynamic interpretation of domain structure in solvent-cast films of A-B type block copolymers of styrene and isoprene. *J. Polym. Sci., Part A-2*, **7** (8), 1283–1301.

151 Meier, D.J. (1969) Theory of block copolymers. I. Domain formation in A-B block copolymers. *J. Polym. Sci., Part C, Polym. Symp.*, **26**, 81–98.

152 Hashimoto, T., Nagatoshi, K., Todo, A., and Kawai, H. (1974) Domain-boundary structure of styrene-isoprene block

copolymer films cast from toluene solutions. *Macromolecules,* **7** (3), 364–373.

153 Hashimoto, T., Shibayama, M., and Kawai, H. (1980) Domain-boundary structure of styrene-isoprene block copolymer films cast from solution. 4. Molecular-weight dependence of lamellar microdomains. *Macromolecules,* **13** (5), 1237–1247.

154 Hashimoto, T., Fujimura, M., and Kawai, H. (1980) Domain-boundary structure of styrene-isoprene block copolymer films cast from solutions. 5. Molecular-weight dependence of spherical microdomains. *Macromolecules,* **13** (6), 1660–1669.

155 Helfand, E. and Wasserman, Z.R. (1976) Block copolymer theory. 4. Narrow interphase approximation. *Macromolecules,* **9** (6), 879–888.

156 Helfand, E. and Wasserman, Z.R. (1978) Block copolymer theory. 5. Spherical domains. *Macromolecules,* **11** (5), 960–966.

157 Helfand, E. and Wasserman, Z.R. (1980) Block copolymer theory. 6. Cylindrical domains. *Macromolecules,* **13** (4), 994–998.

158 Spontak, R.J. and Zielinski, J.M. (1993) Dependence of the interphase thickness on chain length in block copolymers: revisited. *Macromolecules,* **26** (2), 396–397.

159 Arnold, K.R. and Meier, D.J. (1970) A rheological characterization of SBS block copolymers. *J. Appl. Polym. Sci.,* **14** (2), 427–440.

160 Hamley, I.W., Pople, J.A., Gleeson, A.J., Komanschek, B.U., and Towns-Andrews, E. (1998) Simultaneous rheology and small-angle scattering experiments on block copolymer gels and melts in cubic phases. *J. Appl. Crystallogr.,* **31**, 881–889.

161 Vigild, M.E., Almdal, K., Mortensen, K., Hamley, I.W., Fairclough, J.P.A., and Ryan, A.J. (1998) Transformations to and from the gyroid phase in a diblock copolymer. *Macromolecules,* **31** (17), 5702–5716.

162 Sebastian, J.M., Lai, C., Grassley, W.W., and Register, R.A. (2002) Steady-shear rheology of block copolymer melts and concentrated solutions: disordering stress in body-centered-cubic systems. *Macromolecules,* **35** (7), 2707–2713.

163 Yamada, K., Nonomura, M., and Ohta, T. (2004) Kinetics of morphological transitions in microphase-separated diblock copolymers. *Macromolecules,* **37** (15), 5762–5777.

164 Yamada, K., Nonomura, M., Saeki, A., and Ohta, T. (2005) Metastable and unstable structures in microphase separated diblock copolymers. *J. Phys.: Condens. Matter,* **17**, 4877–4887.

165 Yamada, K., Nonomura, M., and Ohta, T. (2006) Fddd structure in AB-type diblock copolymers. *J. Phys.: Condens. Matter,* **18**, L421–L427.

166 Pinna, M., Zvelindovsky, A.V., Todd, S., and Goldbeck-Wood, G. (2006) Cubic phases of block copolymers under shear and electric fields by cell dynamics simulation. *J. Chem. Phys.,* **125** (15), 154905.

167 Tamate, R., Yamada, K., Viñals, J., and Ohta, T. (2008) Structural rheology of microphase separated diblock copolymers. *J. Phys. Soc. Jpn.,* **77** (3), 034802.

168 Cox, R.G. and Mason, S.G. (1971) Suspended particles in fluid flow through tubes. *Annu. Rev. Fluid Mech.,* **3**, 291–316.

169 Leal, L.G. (1980) Particle motion in a viscous fluid. *Annu. Rev. Fluid Mech.,* **12**, 435–476.

170 Barthès-Biesel, D. (1988) Mathematical modeling of two-phase flows in *Rheological Measurements* (eds A.A. Collyer and D.W. Clegg), Elsevier Applied Science, London, 595-634.

171 Honerkamp, J. and Weese, J. (1990) Tikhonov's regularization method for ill-posed problems: a comparison of different methods for the determination of the regularization parameter. *Continuum Mech. Thermodyn.,* **2**, 17–30.

172 Elster, C., Honerkamp, J., and Weese, J. (1991) Using regularization methods for the determination of relaxation and retardation spectra. *Rheol. Acta,* **30** (2), 161–174.

173 Honerkamp, J. and Weese, J. (1993) A note on estimating mastercurves. *Rheol. Acta,* **32** (1), 57–64; Honerkamp, J. and Weese, J.

(1993) A nonlinear regularization method for the calculation of relaxation spectra *Rheol. Acta*, **32** (1), 65–73.

174 Gleisner, W., Maier, D., Schneider, M., Weese, J., Friedrich, Chr., and Honerkamp, J. (1994) Estimation of sphere size distributions in two-phase polymeric materials from transmission electron microscopy data. *J. Appl. Polym. Sci.*, **53** (1), 39–50.

175 Gleisner, W., Braun, H., Friedrich, Chr., and Cantow, H.-J. (1994) Correlation between rheology and morphology of compatibilized immiscible blends. *Polymer*, **35** (2), 128–135.

176 Friedrich, Chr., Honerkamp, J., and Weese, J. (1996) New ill-posed problems in rheology. *Rheol. Acta*, **35** (2), 186–193.

177 Barthès-Biesel, D. and Acrivos, A. (1973) Deformation and burst of a liquid droplet freely suspended in a linear shear field. *J. Fluid Mech.*, **61** (1), 1–21.

178 Oosterbroek, M. and Mellema, J. (1981) Linear viscoelasticity of emulsions. I. The effect of an interfacial film on the dynamic viscosity of nondilute emulsions. *J. Colloid Interface Sci.*, **84**, 14–26.

179 Oosterbroek, M., Lopulissa, J.S., and Mellema, J. (1980) An experimental study of the dynamic viscosity of emulsions with small droplets in the kHz region, in *Rheology*, vol. 2 (eds G. Astarita, G. Marrucci, and L. Nicolais), Plenum Press, New York, 601–606.

180 Oosterbroek, M., Mellema, J., and Lopulissa, J.S. (1981) Linear viscoelasticity of emulsions. II. Measurements of the linear viscoelastic behavior of emulsions in the kilohertz range. *J. Colloid Interface Sci.*, **84**, 27–35.

181 Eshuis, A. and Mellema, J. (1984) Viscoelasticity and microstructure of non-ionic microemulsions. *Colloid Polym. Sci.*, **262**, 159–170.

182 Princen, H.M. (1983) Rheology of foams and highly concentrated emulsions: I. Elastic properties and yield stress of a cylindrical model system. *J. Colloid Interface Sci.*, **91**, 160–175.

183 Princen, H.M. (1985) Rheology of foams and highly concentrated emulsions. II. Experimental study of the yield stress and wall effects for concentrated oil-in-water emulsions. *J. Colloid Interface Sci.*, **105**, 150–171.

184 Reinelt, D.A. (1993) Simple shearing flow of tree-dimensional foams and highly concentrated emulsions with planar films. *J. Rheol.*, **37** (6), 1117–1139.

185 Krause, S. and Goh, S.H. (2003) Miscible Polymer Blends Appendix II, in *Polymer Blends Handbook* (ed. L.A. Utracki), Kluwer Academic Publishers, Dordrecht, 1215–1322.

186 Kannan, R.M. and Kornfield, J. (1994) Stress-optical manifestations of molecular and microstructural dynamics in complex polymer melts. *J. Rheol.*, **38** (4), 1127–1150.

187 Goh, S.H. and Siow, K.S. (1988) Interactions in poly(vinylidene fluoride)/poly(methyl methacrylate-*co*-ethyl methacrylate) blends. *Polym. Bull.*, **20** (4), 393–398.

188 Weigand, F., Demco, D.E., Blümich, B., and Spiess, H.W. (1996) Spatially resolved NMR spin diffusion in solid polymers. *J. Magn. Reson.*, **120**, 190–200.

189 Simha, R. and Somcynsky, T. (1969) On the statistical thermodynamics of spherical and chain molecule fluids. *Macromolecules*, **2** (4), 342–350.

190 Utracki, L.A. (2004) Statistical thermodynamics evaluation of solubility parameters and polymer miscibility. *J. Polym. Sci. Part B: Polym. Phys.*, **42** (15), 2909–2915.

191 Tsenoglou, C. (1988) Network architecture and modulus of miscible heteropolymer blends. *J. Polym. Sci.: Polym. Phys. Ed.*, **26** (11), 2329–2339.

192 Gell, C.B., Krishnamoorti, R., Kim, E., Graessley, W.W., and Fetters, L.J. (1997) Viscoelasticity and diffusion in miscible blends of saturated hydrocarbon polymers. *Rheol. Acta*, **36** (3), 217–228.

193 Groves, D.J., McLeish, T.C.B., Chohan, R.K., and Coates, P.D. (1996) Predicting the rheology of linear with branched polyethylene blends. *Rheol. Acta*, **35** (5), 481–491.

194 Haley, J.C. and Lodge, T.P. (2004) A framework for predicting the viscosity of miscible polymer blends. *J. Rheol.*, **48** (2), 463–486.

195 Haley, J.C. and Lodge, T.P. (2005) Viscosity predictions for model miscible polymer blends: including self-concentration, double reptation, and tube dilation. *J. Rheol.*, **49** (6), 1277–1302.

196 Booij, H.C. and Palmen, J.H.M. (1992) Linear viscoelastic properties of melts of miscible blends of poly (methylmethacrylate) with poly (ethylene oxide), in *Theoretical and Applied Rheology: Proceedings of the XIth International Congress on Rheology, Brussels, Belgium, 17–21 August 1992* (eds P. Moldenaers and R. Keunings), Elsevier Science Ltd, 321–323.

197 Kapnistos, M., Hinrichs, A., Vlassopoulos, D., Anastasiadis, S.H., Stammer, A., and Wolf, B.A. (1996) Rheology of a lower critical solution temperature binary polymer blend in the homogeneous, phase-separated, and transitional regimes. *Macromolecules*, **29** (22), 7155–7163.

198 Mertsch, R. and Wolf, B.A. (1994) On the significance of molecular surfaces and thermodynamic interactions for the excess viscosities of liquid mixtures. *Ber. Bunsenges. Phys. Chem.*, **98**, 1275–1280.

199 Vlassopoulos, D., Koumoutsakos, A., Anastasiadis, S.H., Hatzikiriakos, S.G., and Englezos, P. (1997) Rheology and phase separation in a model upper critical solution temperature polymer blend. *J. Rheol.*, **41** (3), 739–755.

200 Pathak, J.A. and van Gurp, M. (2000) Rheology of a miscible blend of SAN and SMA. *J. Appl. Polym. Sci.*, **78** (6), 1245–1249.

201 Cai, H., Aït-Kadi, A., and Brisson, J. (2003) Dynamic rheological analysis of a miscible blend showing strong interaction. *Polymer*, **44** (5), 1481–1489.

202 Schneider, H.A. and Brekner, M.J. (1985) Thermodynamic aspects of the glass-transition in the compatible blend poly(styrene)-poly(vinylmethyl ether). *Polym. Bull.*, **14** (2), 173–178.

203 Brekner, M.J., Cantow, H.J., and Schneider, H.A. (1985) Interactions in compatible polymer systems – 1. Viscoelasticity and glass transition of polystyrene-poly(vinylmethylether) blends. *Polym. Bull.*, **14** (1), 17–24.

204 Yang, H., Shibayama, H., Stein, R.S., Shimuzu, N., and Hashimoto, T. (1986) Deuteration effects on the miscibility and phase separation kinetics of polymer blends. *Macromolecules*, **19** (6), 1667–1674.

205 Cavaille, J.Y., Perez, J., Jourdan, C., and Johari, G.P. (1987) Dynamic mechanical behavior of poly(vinyl-methyl ether)-poly (styrene) blends. *J. Polym. Sci. B: Polym. Phys.*, **25** (9), 1847–1858.

206 Stadler, R., de Lucca Freitas, L.L., Krieger, V., and Klotz, S. (1988) Influence of the phase separation on the linear viscoelastic properties of a polystyrene-poly(vinyl methyl ether) blend. *Polymer*, **29** (9), 1643–1647.

207 Ajji, A., Choplin, L., and Prud'homme, R.E. (1988) Rheology and phase separation in polystyrene/poly (vinyl methyl ether) blends. *J. Polym. Sci., Part B, Polym. Phys.*, **26** (11), 2279–2289.

208 Ajji, A., Choplin, L., and Prud'homme, R.E. (1991) Rheology of polystyrene/poly(vinyl methyl ether) blends near the phase transition. *J. Polym. Sci. B: Polym. Phys.*, **29** (13), 1573–1578.

209 Ajji, A. and Choplin, L. (1991) Rheology and dynamics near phase separation in a polymer blend: model and scaling analysis. *Macromolecules*, **24** (18), 5221–5223.

210 Mani, S., Malone, M.F., and Winter, H.H. (1992) Influence of phase separation on the linear viscoelastic behavior of a miscible polymer blend. *J. Rheol.*, **36** (8), 1625–1649.

211 Kim, J.K. and Son, H.W. (1999) The rheological properties of polystyrene/poly(vinylmethyether) blend near the critical region and in the homogenous region. *Polymer*, **40** (24), 6789–6801.

212 Koningsveld, R., Stockmayer, W.H., and Nies, E. (2001) *Polymer Phase Diagrams – A Textbook*, Oxford University Press, Oxford.

213 Rangel-Nafaile, C., Metzner, A.B., and Wissbrun, K.F. (1984) Analysis of stress-induced phase separations in polymer solutions. *Macromolecules*, **17** (6), 1187–1195.

214 Larson, R.G. (1992) Instabilities in viscoelastic flows. *Rheol. Acta*, **31** (3),

213–263; Larson, R.G. (1992) Flow-induced mixing, demixing, and phase transitions in polymeric fluids. *Rheol. Acta*, **31** (6), 497–520.

215 Kammer, H.W., Kressler, J., and Kummerloewe, R. (1993) Phase behavior of polymer blends – effects of thermodynamics and rheology – Review. *Adv. Polym. Sci.*, **106**, 31–85.

216 Fredrickson, G.H. and Larson, R.G. (1987) Viscoelasticity of homogeneous polymer melts near critical point. *J. Chem. Phys.*, **86** (3), 1553–1560.

217 Larson, R.G. and Fredrickson, G.H. (1987) Viscometric properties of block polymers near a critical point. *Macromolecules*, **20** (8), 1897–1900.

218 Onuki, A. (1994) Domain growth and rheology in phase-separating binary mixtures with viscosity difference. *Europhys. Lett.*, **28** (3), 175–179.

219 Onuki, A. (1986) Shear flow problems in critical binary mixtures. *Physica A*, **140** (1–2), 204–209.

220 Onuki, A. (1997) Phase transitions of fluids in shear flow (review). *J. Phys.: Condens. Matter*, **9**, 6119–6157.

221 Sharma, J. and Clarke, N. (2004) Miscibility determination of a lower critical solution temperature polymer blend by rheology. *J. Phys. Chem.*, **108** (35), 13220–13230.

222 Nishi, T., Wang, T.T., and Kwei, T.K. (1975) Thermally induced phase separation behavior of compatible polymer mixtures. *Macromolecules*, **8** (2), 227–234.

223 Hashimoto, T., Takebe, T., and Fujioka, K. (1990) Phase transition and self-assembling structures of polymer mixtures under shear flow in *Dynamics and Patterns in Complex Fluids* (eds A. Onuki and K. Kawasaki), Springer-Verlag, Berlin, 86–99.

224 Hashimoto, T. and Jinnai, H. (1997) Control of morphology in polymer alloys, in *Macromolecular Design of Polymeric Materials* (eds K. Hatada, T. Kitayama, and O. Vogl), ch. 42, Marcel Dekker, New York, 747–759 .

225 Vlassopoulos, D. (1996) Rheology of critical LCST polymer blends: poly (styrene-*co*-maleic anhydrite)/poly (methyl methacrylate). *Rheol. Acta*, **35** (6), 556–566.

226 Mani, S., Malone, M.F., Winter, H.H., Halary, J.L., and Monnerie, L. (1991) Effects of shear on miscible polymer blends: in situ fluorescence studies. *Macromolecules*, **24** (19), 5451–5458.

227 El-Mabrouk, K. and Bousmina, M. (2005) Effect of hydrodynamics on dynamics of phase separation in polystyrene/poly (vinyl methyl ether) blend. *Polymer*, **46** (21), 9005–9014.

228 El-Mabrouk, K. and Bousmina, M. (2006) Assessment of morphology in transient and steady state regimes resulting from phase separation in polystyrene/poly (vinyl methyl ether) blend. *Rheol. Acta*, **45** (6), 877–889.

229 El-Mabrouk, K. and Bousmina, M. (2006) Effect of molecular weight and shear on phase diagram of PS/PVME blend. *Rheol. Acta*, **45** (6), 959–969.

230 El-Mabrouk, K., Belaiche, M., and Bousmina, M. (2006) Phase separation of polystyrene/poly(vinylmethyl ether)/ organoclay nanocomposites. *J. Nanosci. Nanotechnol.*, **6**, 472–482.

231 El-Mabrouk, K. and Bousmina, M. (2007) Phase separation in PS/PVME thin and thick films. *J. Colloid Interface Sci.*, **306**, 354–367.

232 Nakatani, A.I., Kim, H., Takahashi, Y., Matsushita, Y., Takano, A., Bauer, B.J., and Han, C.C. (1990) Shear stabilization of critical fluctuations in bulk polymer blends studied by SANS. *J. Chem. Phys.*, **93** (1), 795–810.

233 Silberberg, A. and Kuhn, W. (1952) Miscibility of liquids influenced by rate of shear. *Nature*, **170** (4324), 450–451.

234 Silberberg, A. and Kuhn, W. (1954) Size and shape of droplets of demixing polymer solutions in a field of flow. *J. Polym. Sci.*, **13** (1), 21–42.

235 Wolf, B.A. (1980) Theoretical description of the phase separation in flowing polymer solutions. *Makromol. Chem. Rapid Commun.*, **189**, 1613.

236 Wolf, B.A. (1984) Thermodynamic theory of flowing polymer solutions and its application to phase separation. *Macromolecules*, **17** (2), 615–618.

237 Lyngaae-Jørgensen, J. (1985) Melt flow properties of block copolymers, Ch. 3 in *Processing, Structure and Properties of Block Copolymers* (ed. M.J. Folkes), Elsevier Applied Science, London, 75–123.

238 Horst, R. and Wolf, B.A. (1991) Calculation of shear influences on the phase separation behavior of polymer solutions in the region of their lower critical solution temperature. Creation of closed miscibility gaps. *Macromolecules*, **24** (9), 2236–2239.

239 Horst, R. and Wolf, B.A. (1992) Calculation of the phase separation behavior of sheared polymer blends. *Macromolecules*, **25** (20), 5291–5296; Horst, R. and Wolf, B.A. (1993) Refined calculation of the phase separation behavior of sheared polymer blends: closed miscibility gaps within two ranges of shear rates. *Macromolecules*, **26** (21), 5676–5680.

240 Mazich, K.A. and Carr, S.T. (1983) The effect of flow on the miscibility of a polymer blend. *J. Appl. Phys.*, **54** (10), 5511–5514.

241 Katsaros, J.D., Malone, M.F., and Winter, H.H. (1986) Extensional flow induced miscibility in a polymer blend. *Polym. Bull.*, **16** (1), 83–88.

242 Hindawi, I.A., Higgins, J.S., and Weiss, R.A. (1992) Flow-induced mixing and demixing in polymer blends. *Polymer*, **33** (12), 2522–2529.

243 Fernandez, M.L., Higgins, J.S., and Richardson, S.M. (1993) When rheology interacts with thermodynamics in polymer blends. (Symposium on distillation, Institute of Chemical Engineers). *Trans IChemE*, **71**, 239.

244 Fernandez, M.L., Higgins, J.S., Horst, R., and Wolf, B.A. (1995) Complex miscibility behavior for polymer blends in flow. *Polymer*, **36** (1), 149–154.

245 Wu, R., Shaw, M.T., and Weiss, R.A. (1992) Rheo-optical studies of stress-induced phase changes in blends exhibiting UCST: polystyrene and polyisobutylene. *J. Rheol.*, **36** (8), 1605–1623.

246 Jeon, H.S., Nakatani, A.I., Han, C.C., and Colby, R.H. (2000) Melt rheology of lower critical solution temperature polybutadiene/polyisoprene blends. *Macromolecules*, **33** (26), 9732–9739.

247 Ohta, T. and Jasnow, D. (1997) Interface dynamics for layered structures. *Phys. Rev. E*, **56** (5), 5648–5658.

248 Polios, I.S., Soliman, M., Lee, C., Gido, S.P., Schmidt-Rohr, K., and Winter, H.H. (1997) Late stages of phase separation in a binary polymer blend studied by rheology, optical and electron microscopy, and solid state NMR. *Macromolecules*, **30** (15), 4470–4480.

249 Doi, M. and Ohta, T. (1991) Dynamics and rheology of complex interfaces. I. *J. Chem. Phys.*, **95** (2), 1242–1248.

250 Matsuzaka, K., Jinnai, H., Koga, T., and Hashimoto, T. (1997) Effect of oscillatory shear deformation on demixing processes of polymer blends. *Macromolecules*, **30** (4), 1146–1152.

251 Gramespacher, H. and Meissner, J. (1995) Reversal of recovery direction during creep recovery of polymer blends. *J. Rheol.*, **39** (1), 151–160.

252 Krishnan, K., Almdal, K., Burghardt, W.R., Lodge, T.P., and Bates, F.S. (2001) Shear-induced nano-macro structural transition in a polymeric bicontinuous microemulsion. *Phys. Rev. Lett.*, **87** (9), 098301-1–098301-4.

253 Krishnan, K., Chapman, B., Bates, F.S., Lodge, T.P., Almdal, K., and Burghardt, W.R. (2002) Effects of shear flow on a polymeric bicontinuous microemulsion: equilibrium and steady state behaviour. *J. Rheol.*, **46** (2), 529–554.

254 Narayanan, B., Pryamitsyn, V., and Ganesan, V. (2006) Shear-induced phase transition in ternary polymer blends. *Phys. Rev. Lett.*, **96** (2), 028302-1–028302-4.

255 Helfand, E. and Fredrickson, G.H. (1989) Large fluctuations in polymer solutions under shear. *Phys. Rev. Lett.*, **62** (21), 2468–2471.

256 Elemans, P.H.M. (1989) Modeling of the processing of incompatible polymer blends, PhD Thesis, Eindhoven University of Technology.

257 Huneault, M.A., Shi, Z.H., and Utracki, L.A. (1995) Development of polymer blend morphology during compounding in a twin screw extruder. Part IV: a new computational model with

coalescence. *Polym. Eng. Sci.*, **35** (1), 115–127.

258 Huneault, M.A., Champagne, M.F., Luciani, A., Hetu, J.-F., and Utracki, L.A. (1995) Generation of polymer blends' morphology. Presented at the European Meeting of the Polymer Processing Society, Stuttgart, Germany, 26–28 September, 1995.

259 Doi, M. and Onuki, A. (1992) Dynamic coupling between stress and composition in polymer solutions and blends. *J. Phys. (Paris)*, **2**, 1631–1656.

260 Takahashi, Y., Kurashima, N., Noda, I., and Doi, M. (1994) Experimental tests of the scaling relation for textured materials in mixtures of two immiscible fluids. *J. Rheol.*, **38** (3), 699–712.

261 Guenther, G.K. and Baird, D.G. (1996) An evaluation of the Doi–Ohta theory for an immiscible polymer blend. *J. Rheol.*, **40** (1), 1–20.

262 Vinckier, I., Moldenaers, P., and Mewis, J. (1997) Transient rheological response and morphology evolution of immiscible polymer blends. *J. Rheol.*, **41** (3), 705–718.

263 Lee, H.M. and Park, O.O. (1994) Rheology and dynamics of immiscible polymer blends. *J. Rheol.*, **38** (5), 1405–1425.

264 Grmela, M. and Aït-Kadi, A. (1994) Comments on the Doi–Ohta theory of blends. *J. Non-Newtonian Fluid Mech.*, **55** (2), 191–195.

265 Lacroix, C., Aressy, M., and Carreau, P.J. (1997) Linear viscoelastic behavior of molten polymer blends: a comparative study of the Palierne and the Lee and Park models. *Rheol. Acta*, **36** (4), 416–428.

266 Lacroix, C., Grmela, M., and Carreau, P.J. (1998) Relationships between rheology and morphology for immiscible molten blends of polypropylene and ethylene copolymers under shear flow. *J. Rheol.*, **42** (1), 41–62.

267 Lacroix, C., Grmela, M., and Carreau, P.J. (1999) Morphological evolution of immiscible polymer blends in simple shear and elongational flows. *J. Non-Newtonian Fluid Mech.*, **86** (1–2), 37–59.

268 Grmela, M. and Öttinger, H.C. (1997) Dynamics and thermodynamics of complex fluids. I. Development of generic formalism. *Phys. Rev. E*, **56** (6), 6620–6626.

269 Öttinger, H.C. and Grmela, M. (1997) Dynamics and thermodynamics of complex fluids. II. Illustration of the GENERIC formalism. *Phys. Rev. E*, **56** (6), 6633–6655.

270 Öttinger, H.C. (2005) *Beyond Equilibrium Thermodynamics*, John Wiley & Sons, Inc., Hoboken.

271 Grmela, M., Bousmina, M., and Palierne, J.F. (2001) On the rheology of immiscible blends. *Rheol. Acta*, **40** (6), 560–569.

272 Maffettone, P.L. and Minale, M. (1998) Equation of change for ellipsoidal drops in viscous flow. *J. Non-Newtonian Fluid Mech.*, **78** (2–3), 227–241.

273 Yu, W., Bousmina, M., Grmela, M., and Zhou, C. (2002) Modeling of oscillatory shear flow of emulsions under small and large deformation fields. *J. Rheol.*, **46** (6), 1401–1418.

274 Guido, S. and Greco, F. (2001) Drop shape under slow steady shear flow and during relaxation. Experimental results and comparison with theory. *Rheol. Acta*, **40** (2), 176–184.

275 El-Mesri, Z. (2002) Rhéo-optique des mélanges des polymères immiscible Master's Thesis, Laval University, Ste.-Foy, QC, Canada.

276 Grizzuti, N., Buonocore, G., and Iorio, G. (2000) Viscous behavior and mixing rules for an immiscible model blend. *J. Rheol.*, **44** (1), 149–164.

277 Gu, J.F. and Grmela, M. (2008) Flow properties of immiscible blends: Doi–Ohta model with active advection. *Phys. Rev. E*, **78** (5), 056302.

278 Vinckier, I., Moldenaers, P., Terracciano, A.M., and Grizzuti, N. (1998) Droplet size evolution during coalescence in semiconcentrated model blends. *AIChE J.*, **44** (4), 951–958.

279 Vinckier, I., Minale, M., Mewis, J., and Moldenaers, P. (1999) Rheology of semi-dilute emulsions: viscoelastic effects caused by the interfacial tension. *Colloids Surf.*, **150**, 217–228.

280 Lyngaae-Jorgensen, J., Thomsen, L.D., Rasmussen, K., Søondergaard, K., and Andersen, F.E. (1988) On the influence of interfacial slip on melt flow properties of polymer blends. *Intern. Polym. Process*, **2** (3/4), 123–130.

281 Lyngaae-Jørgensen, J., Sondergaard, K., Utracki, L.A., and Valenza, A. (1993) Formation of ellipsoidal drops in simple shear flow: transient behavior. *Polym. Networks Blends*, **3** (4) 167–181.

282 Su, R., Su, J., Wang, K., Yang, C., Zhang, Q., and Fu, Q. (2009) Shear-induced change of phase morphology and tensile property in injection-molded bars of high-density polyethylene/polyoxymethylene blends. *Eur. Polym. J.*, **45**, 747–756.

283 Carotenuto, C., Grosso, M., and Maffettone, P.L. (2008) Fourier transform rheology of dilute immiscible polymer blends: a novel procedure to probe blend morphology. *Macromolecules*, **41** (12), 4492–4500.

284 Gauthier, F., Goldsmith, H.L., and Mason, S.G. (1971) Particle motions in non-Newtonian media I: Couette flow. *Rheol. Acta*, **10** (3), 344–364.

285 Flumerfelt, R.W. (1972) Drop breakup in simple shear fields of viscoelastic fluids. *Ind. Eng. Chem. Fundam.*, **11** (3), 312–318.

286 De Bruijn, R.A. (1989) Deformation and breakup of drops in simple shear flows, PhD Thesis, Eindhoven University of Technology.

287 Bousfield, D.W., Keunings, R., Marucci, G., and Denn, M.M. (1986) Nonlinear analysis of the surface-tension driven breakup of viscoelastic fluid filaments. *J. Non-Newton Fluid Mech.*, **21**, 79–97.

288 Vinckier, I., Moldenaers, P., and Mewis, J. (1996) Relationship between rheology and morphology of model blends in steady shear flow. *J. Rheol.*, **40** (4), 613–631.

289 Bousmina, M. (1999) Rheology of polymer blends: linear model for viscoelastic emulsions. *Rheol Acta*, **38** (1), 73–83.

290 Bousmina, M., Aouina, M., Chaudry, B., Guénette, R., and Bretas, R.E.S. (2001) Rheology of polymer blends: non-linear model for viscoelastic emulsions undergoing high deformation flows. *Rheol. Acta*, **40** (6), 538–551.

291 Ratke, L. and Thieringer, F W.K. (1985) The influence of particle motion on Ostwald ripening in liquids. *Acta Metall.*, **33**, 1793–1802.

292 Tokita, N. (1977) Analysis of morphology formation in elastomer blends. *Rubber Chem. Tech.*, **50** (2), 292–300.

293 MacKay, G.D.M. and Mason, S.G. (1963) The gravity approach and coalescence of fluid drops at liquid interfaces. *Can. J. Chem. Eng.*, **41**, 203–212.

294 MacKay, G.D.M. and Mason, S.G. (1963) Some effects of interfacial diffusion on the gravity coalescence of liquid drops. *J. Colloid Sci.*, **18** (7), 674–683.

295 MacKay, G.D.M. and Mason, S.G. (1964) Particle motions in sheared suspensions – XV. Effects of diffusion on collision doublets of fluid drops. *Kolloid-Z. & Z. Polym.*, **195** (2), 138–148.

296 Chesters, A.K. (1975) The applicability of dynamic-similarity criteria to isothermal, liquid–gas, two-phase flows without mass transfer. *Int. J. Multiphase Flow*, **2**, 191–212.

297 Chesters, A.K. (1988) Drainage of partially mobile films between colliding drops: a first-order model, in *Proc. Euromech*, Toulouse, France, p. 234 Paper presented at Euromech 234, International Conference on Turbulent Flow of Two-Phase Systems, Toulouse France, May 9–13, 1988.

298 Fortelný, I., Kamenická, D., and Kovář, J. (1988) Effect of the viscosity of components on the phase structure and impact strength of polypropylene/ethylene-propylene elastomer blends. *Angew. Makromol. Chem.*, **164**, 125–141.

299 Fortelný, I., Michálková, D., Kopliková, J., Navrátilová, E., and Kovář, J. (1990) The effect of conditions of mixing of polypropylene/ethylene-propylene elastomer blends on their morphological structure and impact strength. *Angew. Makromol. Chem.*, **179**, 185–201.

300 Ross, S.I., Verhoff, F.H., and Curl, R.I. (1978) Droplet breakage and coalescence processes in an agitated dispersion. 2. Measurement and interpretation of mixing experiments. *Ind. Eng. Chem. Fundam.*, **17**, 101–108.

301 Chen, N., Kuhl, T., Tadmor, R., Lin, Q., and Israelachvili, J. (2004) Large

deformations during the coalescence of fluid interfaces. *Phys. Rev. Lett.*, **92** (2), 245011–245014.

302 Utracki, L.A. (1998) *Commercial Polymer Blends,* Chapman & Hall, London.

303 Frayer, P.D., Monahan, R.J., and Pierson, M.D.(15 August (2000)) Glass/polymer melt blends, US Pat. 6,103,810 to Corning Inc.

304 Valenza, A., Lyngaae-Jorgensen, J., Utracki, L.A., and Sammut, P. (1991) Rheological characterization of polystyrene/polymethylmethacrylate blends. Part 2. Shear flow. *Polym. Networks Blends,* **1** (2), 79–92.

305 Bousmina, M., Palierne, J.F., and Utracki, L.A. (1999) Modeling of polymer blends' behavior during capillary flow. *Polym. Eng. Sci.*, **39** (6), 1049–1059.

306 Shi, D., Jiang, F., Ke, Z., Yin, J., and Li, R.K.-Y. (2006) Melt rheological properties of polypropylene–polyamide 6 blends compatibilized with maleic anhydride-grafted polypropylene. *Polym. Int.*, **55** (6), 701–707.

307 Yu, W., Bousmina, M., Zhou, C., and Tucker, C.L. III (2004) Theory for drop deformation in viscoelastic systems. *J. Rheol.*, **48** (2), 417–438.

308 Utracki, L.A. and Sammut, P. (1988) Rheological evaluation of polystyrene/polyethylene blends. *Polym. Eng. Sci.*, **28** (21), 1405–1415.

309 Utracki, L.A. and Sammut, P. (1990) On the uniaxial extensional flow of polystyrene/polyethylene blends. *Polym. Eng. Sci.*, **30** (17), 1019–1026.

310 Brahimi, B., Aït-Kadi, A., Ajji, A., and Fayt, R. (1991) Rheological properties of copolymer modified polyethylene/polystyrene blends. *J. Rheol.*, **35** (6), 1069–1091.

311 Scholz, P., Froelich, D., and Muller, R. (1989) Viscoelastic properties and morphology of two-phase polypropylene/polyamide 6 blends in the melt. Interpretation of results with an emulsion model. *J. Rheol.*, **33** (3), 481–499.

312 Aït-Kadi, A., Ajji, A., and Brahimi, B. (1992) Linear rheology of copolymer modified blends: Experiments and predictions of emulsion models in *Theoretical and Applied Rheology, Proceedings of the 11 International Congress on Rheology vol. 1, Brussels* (volume and series editors P. Moldenaers and R. Keunings), Elsevier Science Publishers, New York, 315–317

313 Nishio, T(aichi)., Suzuki, Y., Kojima, K., and Kakugo, M. (1990) Twin extruder developed for analysis of reactive process and its application for analysis of reactive processing of maleic anhydride grafted polypropylene/polyamide-6. *Kobunshi Ronbunshu,* **47** (4), 331–337

314 Utracki, L.A. and Sammut, P. (1992) Rheological response of polyamide/polypropylene blends. Part 2: extensional flow. *Polym. Networks Blends,* **2** (2), 85–93.

315 Pascault, J.P., Frèrejean, V., and Taha, M. (1994), paper presented at the Polymer Process. Society European Meeting, Strasbourg, 29–31 August 1994, pp. 31.

316 Germain, Y., Ernst, B., Genelot, O., and Dhamani, L. (1994) Rheological and morphological analysis of compatibilized polypropylene/polyamide blends. *J. Rheol.*, **38** (3), 681–697.

317 Silva, J.M., Machado, A.V., and Maia, J.M. (2006) Transient rheological behavior of PA6/EPM/EPM-g-MA blends. *Adv. Mater Forum III,* **514–516**, 853–857.

318 Silva, J., Machado, A.V., and Maia, J. (2007) Rheological behavior of compatibilized and non-compatibilized PA6/EPM blends. *Rheol. Acta,* **46** (8), 1091–1097.

319 Sailer, C.F. (2008) Blends of polyamide-6 and styrenic polymers: Influence of reactive compatibilization on melt rheology and morphology, PhD thesis, Die Eidgenössische Technische Hochschule Zürich (ETH – Zürich).

320 Abbassi-Sourki, F., Huneault, M.A., and Bousmina, M. (2009) Effect of compatibilization on the deformation and breakup of drops in step-wise increasing shear flow. *Polymer,* **50** (2), 645–653.

321 Hsieh, T.-T., Tiu, C., Simon, G.P., and Wu, R.Y. (1999) Rheology and miscibility of thermotropic liquid crystalline polymer blends. *J. Non-Newtonian Fluid Mech.*, **86** (1–2), 15–35.

322 Hashmi, S.A.R. and Kitano, T. (2007) Shear rate dependence of viscosity and first normal stress difference of LCP/PET blends at solid and molten states of LCP. *J. Appl. Polym. Sci.*, **104** (4), 2212–2218.

323 Shih, C.K. (1976) Rheological properties of incompatible blends of two elastomers. *Polym. Eng. Sci.*, **16** (11), 742–746.

324 Shih, C.K. (1979) Capillary extrusion and mold flow characteristics of an incompatible blend of two elastomers, in *Science and Technology of Polymer Processing* (eds Nam P. Suh and N.-H. Sung), MIT Press, Cambridge, Massachusetts, 528.

325 Kanu, R.C. and Shaw, M.T. (1982) Rheology of polymer blends: simultaneous slippage and entrance pressure loss in the EPDM/Viton system. *Polym. Eng. Sci.*, **22** (8), 507–511.

326 Philippoff, W. and Gaskins, F.H. (1958) The capillary experiment in rheology. *Trans. Soc. Rheol.*, **2** (1), 263–284.

327 Tuna, N.Y. and Finlayson, B.A. (1984) Exit pressure calculations from numerical extrudate swell results. *J. Rheol.*, **28** (2), 79–93.

328 Tanner, R.I. (1970) A theory of die-swell. *J. Polym. Sci., A-2: Polym. Phys.*, **8** (12), 2067–2078.

329 Pathak, J.A., Colby, R.H., Kamath, S.Y., Kumar, S.K., and Stadler, R. (1998) Rheology of miscible blends: SAN and PMMA. *Macromolecules*, **31** (25), 8988–8997.

330 Pathak, J.A., Kumar, S.K., and Colby, R.H. (2004) Miscible polymer blend dynamics: double reptation predictions of linear viscoelasticity in model blends of polyisoprene and poly (vinyl ethylene). *Macromolecules*, **37** (18), 6994–7000.

331 Turati, E., Vitale, A., Gallazzi, M., Seves, A., and Testa, G. (1998) Melt rheology of miscible or compatibilized polymer blends obtained from polyamidic and polyolefinic polymers. *Adv. Polym. Technol.*, **17** (4), 317–327.

332 Bousmina, M., Lavoie, A., and Riedl, B. (2002) Phase segregation in SAN/PMMA blends probed by rheology, microscopy and inverse gas chromatography techniques. *Macromolecules*, **35** (16), 6274–6283.

333 Bousmina, M. and Muller, R. (1996) Rheology/morphology/flow conditions relationships for polymethylmethacrylate/rubber blend. *Rheol. Acta*, **35** (4), 369–381.

334 Lee, J.H., Fetters, L.J., Archer, L.A., and Halasa, A.F. (2005) Tube dynamics in binary polymer blends. *Macromolecules*, **38** (9), 3917–3932.

335 Carrot, C., Mbarek, S., Jaziri, M., Chalamet, Y., Raveyre, C., and Prochazka, F. (2007) Immiscible blends of PC and PET, current knowledge and new results: rheological properties. *Macromol. Mater. Eng.*, **292**, 693–706.

336 Laun, H.M. and Schuch, H. (1989) Transient elongational viscosities and drawability of polymer melts. *J. Rheol.*, **33** (1), 119–175.

337 Schlund, B. and Utracki, L.A. (1987) Linear low density polyethylenes and their blends: Part 5, Extensional flow of LLDPE blends. *Polym. Eng. Sci.*, **27** (20), 1523–1529.

338 Dumoulin, M.M., Utracki, L.A., and Farha, C. (1984) Rheological and mechanical properties of LLDPE/PP/EP – block polymer blends. *Polym. Eng. Sci.*, **24** (17), 1319–1326.

339 Dumoulin, M.M., Utracki, L.A., and Lara, J. (1984) Rheological and mechanical behavior of the UHMWPE/MDPE mixtures. *Polym. Eng. Sci.*, **24** (2), 117–126.

340 Delaby, I., Ernst, B., Germain, Y., and Muller, R. (1994) Droplet deformation in polymer blends during uniaxial elongational flow - influence of viscosity ratio for large capillary numbers. *J. Rheol.*, **38** (6), 1705–1720.

341 Delaby, I., Ernst, B., and Muller, R. (1995) Drop deformation during elongational flow in blends of viscoelastic fluids. Small deformation theory and comparison with experimental results. *Rheol. Acta*, **34** (6), 525–533.

342 Delaby, I., Ernst, B., and Muller, R. (1996) Drop deformation in polymer blends during elongational flow. *J. Macromol. Sci. Phys.*, **B35** (4), 547–561.

343 Delaby, I., Ernst, B., Froelich, D., and Muller, R. (1996) Droplet deformation in immiscible polymer blends during transient uniaxial elongational flow. *Polym. Eng. Sci.*, **36** (12), 1627–1635.

344 Khayat, R.E., Luciani, A., and Utracki, L.A. (1996) Influence of shear and elongation on drop deformation in confined flow, in *Boundary Element VIII* (eds M. Tanaka and C.A. Brebbia, series eds C.A. Brebbia, J.B. Martins, M.H. Alibadi, and N. Haie), Springer-Verlag, Berlin: pp. 515–525.

345 Stradins, L. and Osswald, T.A. (1996) Predicting the effect of viscosity ratios on the mixing of polymer blends using the boundary element method. *Polym. Eng. Sci.*, **36** (7), 979–984.

346 Gramespacher, H. and Meissner, J. (1997) Melt elongation and recovery of polymer blends, morphology, and influence of interfacial tension. *J. Rheol.*, **41** (1), 27–44.

347 Mechbal, N. and Bousmina, M. (2004) Uniaxial deformation and relaxation of polymer blends: relationship between flow and morphology development. *Rheol. Acta*, **43** (2), 119–126.

348 Handge, U.A. and Potschke, P. (2004) Interplay of rheology and morphology in melt elongation and subsequent recovery of polystyrene/poly(methyl methacrylate) blends. *J. Rheol.*, **48** (5), 1103–1122.

349 Oosterlinck, F., Mours, M., Laun, H.M., and Moldenaers, P. (2005) Morphology development of a polystyrene/polymethylmethacrylate blend during start-up of uniaxial elongational flow. *J. Rheol.*, **49** (4), 897–918.

350 Starý, Z. and Münstedt, H. (2008) Morphology development in PS/LLDPE blend during and after elongational deformation. *J. Polym. Sci., Part B: Polym. Phys.*, **46** (1), 16–27.

351 Van Hemelrijck, E., Van Puyvelde, P., Velankar, S., Macosko, C.W., and Moldenaers, P. (2004) Interfacial elasticity and coalescence suppression in compatibilized polymer blends. *J. Rheol.*, **48** (1), 143–158.

352 Hobbs, S.Y., Dekkers, M.E.J., and Watkins, V.H. (1988) Effect of interfacial forces on polymer blend morphologies. *Polymer*, **29** (9), 1598–1602.

353 Inoue, T. (2002) Morphology of polymer blends, in *Polymer Blends Handbook* (ed. L.A. Utracki), ch. 8, Kluwer Academic Publishers, Dordrecht, 547–576.

354 Ferreiro, V., Douglas, J.F., Amis, E.J., and Karim, A. (2001) Phase ordering in blend films of semi-crystalline and amorphous polymers. *Macromol. Symp.*, **167**, 73–88.

355 Voulgaris, D. and Petridis, D. (2002) Emulsifying effect of dimethyldioctylammonium-hectorite in polystyrene/poly(ethyl methacrylate) blends. *Polymer*, **43** (8), 2213–2218.

356 Wang, H., Zeng, C.-C., Elkovitch, M., Lee, L.J., and Koelling, K.W. (2001) Processing and properties of polymeric nano-composites. *Polym. Eng. Sci.*, **41** (11), 2036–2046.

357 Gelfer, M.Y., Song, H.H., Liu, L., Hsiao, B.S., Chu, B., Rafailovich, M., Si, M., and Zaitsev, V.J. (2003) Effects of organoclays on morphology and thermal and rheological properties of polystyrene and poly(methyl methacrylate) blends. *Polym. Sci. Part B: Polym. Phys.*, **41** (1), 44–54.

358 Sinha Ray, S., Pouliot, S., Bousmina, M., and Utracki, L.A. (2004) Role of organically modified layered silicate as a compatibilizer for immiscible polystyrene/polypropylene blends. *Polymer*, **45** (25), 8403–8413.

359 Fukui, O., Tsutsui, K., Akagawa, T., Sakai, I., Nomura, T., Nishio, T., Yokoi, T., and Kawamura, N.,Thermoplastic resin composition US Pat. 5,091,462 to Ube Industries Ltd., 25.02.1992.

360 Chen, T.-K., Tien, Y.-I., and Wei, K.H. (1999) Synthesis and characterization of novel segmented polyurethane/clay nanocomposite via poly(ε-caprolactone)/clay. *J. Polym. Sci. A: Polym. Chem.*, **37** (13), 2225–2233.

361 Tabtiang, A., Lumlong, S., and Venables, R.A. (2000) Effects of shear and thermal history on the microstructure of solution polymerized poly(methyl methacrylate)-clay composites. *Polym. Plast. Technol. Eng.*, **39**, 293–303.

362 Hasegawa, N., Okamoto, H., Kawasumi, M., Usuki, A., and Okada, A. (1998) Resin composite, US Pat. 6,117,932 2000.09.12, Appl.

1998.09.17, to Kabushiki Kaisha Toyota Chuo Kenkyusho.

363 Wang, Y., Zhang, Q., and Fu, Q. (2003) Compatibilization of immiscible poly (propylene)/polystyrene blends using clay. *Macromol. Rapid Commun.*, **24** (3), 231–235.

364 Wang, S., Hu, Y., Song, L., Liu, J., Chen, Z., and Fan, W. (2004) Study on the dynamic self-organization of montmorillonite in two phases. *J. Appl. Polym. Sci.*, **91** (3), 1457–1462.

365 Sinha Ray, S. and Bousmina, M. (2005) Compatibilization efficiency of organoclay in an immiscible polycarbonate/poly(methyl methacrylate) blend. *Macromol. Rapid Commun.*, **26** (6), 450–455.

366 Gahleitner, M., Kretzschmar, B., Van Vliet, G., Devaux, J., Pospiech, D., Bernreitner, K., and Ingolic, E. (2006) Rheology/morphology interactions in polypropylene/polyamide-6 nanocomposites. *Rheol. Acta*, **45** (4), 322–330.

367 He, G., Ginzburg, V.V., and Balazs, A.C. (2006) Determining the phase behavior of nanoparticle-filled binary blends. *J. Polym. Sci. Part B: Polym. Phys.*, **44** (17), 2389–2403.

368 Fenouillot, F., Cassagnau, P., and Majeste, J.-C. (2009) Uneven distribution of nanoparticles in immiscible fluids: morphology development in polymer blends. *Polymer*, **50** (6), 1333–1350.

369 Utracki, L.A., Sepehr, M., and Carreau, P.J. (2010) Rheology of polymers with nano-fillers, in *Polymer Physics: From Suspensions to Nanocomposites and Beyond* (eds L.A. Utracki and A.M. Jamieson), ch. 16, John Wiley & Sons, Inc., Hoboken, 639–708.

370 Zhang, L., Tam, K.C., Gan, L.H., Yue, C.Y., Lam, Y.C., and Hu, X. (2003) Effect of nano-silica filler on the rheological and morphological properties of polypropylene/liquid- crystalline polymer blends. *J. Appl. Polym. Sci.*, **87** (9), 1484–1492.

371 Elias, L., Fenouillot, F., Majeste, J.C., and Cassagnau, Ph. (2007) Morphology and rheology of immiscible polymer blends filled with silica nanoparticles. *Polymer*, **48** (20), 6029–6040.

372 Elias, L., Fenouillot, F., Majeste, J.C., Alcouffe, P., and Cassagnau, Ph. (2008) Immiscible polymer blends stabilized with nano-silica particles; rheology and effective interfacial tension. *Polymer*, **49** (20), 4378–4385.

373 Thareja, P. and Velankar, S. (2008) Rheology of immiscible blends with particle-induced drop clusters. *Rheol. Acta*, **47** (2), 189–200.

374 Gharachorlou, A. and Goharpey, F. (2008) Rheologically determined phase behavior of LCST blends in the presence of spherical nanoparticles. *Macromolecules*, **41** (9), 3276–3283.

375 Utracki, L.A. and Sammut, P. (1982) Rheological response of polyamide/polypropylene blends. Part 1: shear flow. *Polym. Networks Blends*, **2** (1), 23–39.

376 Feng, M., Gong, F., Zhao, C., Chen, G., Zhang, S., and Yang, M. (2004) Effect of clay on the morphology of blends of poly (propylene) and polyamide 6/clay nanocomposites. *Polym. Int.*, **53** (10), 1529–1537.

377 Filippone, G., Dintcheva, N.Tz., Acierno, D., and La Mantia, F.P. (2008) The role of organoclay in promoting co-continuous morphology in high-density poly(ethylene)/poly(amide) 6 blends. *Polymer*, **49** (5), 1312–1322.

378 Li, J., Ton-That, M.-T., Leelapornpisit, W., and Utracki, L.A. (2007) Melt compounding of polypropylene-based clay nanocomposites. *Polym. Eng. Sci.*, **47** (9), 1447–1458.

379 Kim, H.B., Choi, J.S., Lee, C.H., Lim, S.T., Jhon, M.S., and Choi, H.J. (2005) Polymer blend/organoclay nanocomposite with poly(ethylene oxide) and poly(methyl methacrylate). *Eur. Polym. J.*, **41**, 679–685.

380 Si, M., Araki, T., Ade, H., Kilcoyne, A.L.D., Fisher, R., Sokolov, J.C., and Rafailovich, M.H. (2006) Compatibilizing bulk polymer blends by using organoclays. *Macromolecules*, **39** (14), 4793–4801.

381 Liu, A., Xie, T., and Yang, G. (2006) Effect of Na + -MMT platelets on monomer casting polyamide 6/polyphenylene oxide

blends. *Macromol. Chem. Phys.*, **207**, 2180–2187.

382 Sinha Ray, S., Bousmina, M., and Maazouz, A. (2006) Morphology and properties of organoclay modified polycarbonate/poly(methyl methacrylate) blend. *Polym. Eng. Sci.*, **46** (8), 1121–1129.

383 Sinha Ray, S., Bandyopadhyay, J., and Bousmina, M. (2007) Effect of organoclay on the morphology and properties of poly (propylene)/poly[(butylene succinate)-*co*-adipate] blends. *Macromol. Mater. Eng.*, **292**, 729–747.

384 Kim, K.Y., Ju, D.U., Nam, G.J., and Lee, J.W. (2007) Ultrasonic effects on PP/PS/clay nanocomposites during continuous melt compounding process. *Macromol. Symp.*, **249–250**, 283–288.

385 Wu, D., Wu, L., Zhang, M., Zhou, W., and Zhang, Y. (2008) Morphology evolution of nanocomposites based on poly (phenylene sulfide)/poly(butylene terephthalate) blend. *J. Polym. Sci. Part B: Polym. Phys.*, **46** (12), 1265–1279.

386 Okamoto, M., Nam, P.H., Maiti, P., Kotaka, T., Hasegawa, N., and Usuki, A. (2001) A house of cards structure in polypropylene/clay nanocomposites under elongational flow. *Nano Lett.*, **1**, 295–298.

387 Kamal, M.R., Mutel, A.T., and Utracki, L.A. (1984) Elongational behavior of short glass fiber reinforced polypropylene melts. *Polym. Compos.*, **5** (4), 289–298.

3
Compounding and Processing of Plastic/Rubber Blends

Raman P. Patel and Jinwoong Shin

3.1
Plastic/Rubber Blends

3.1.1
Introduction

Polymers are rarely used alone without compounding. Compounding, as used here, refers to melt mixing the blend components and preparing a finished compound from all the components of the blend. The compounding ingredients are of different types, each with a different function to enhance the polymer performance. Table 3.1 shows some of them.

In addition to the above-mentioned ingredients, a vast number of polymers are used as blends with other polymers.

Historically, the first patent covering a polymer blend was issued to Badum [1] in 1942 and it was for nitrile rubber and poly(vinyl chloride) blend compositions.

Commercially, in the polymer sector of materials, polymer blends play a very important role. These blends represent a very significant amount of polymer usage and are one of the higher growth sectors in the polymer field. This is evident from the patent literature, where numerous patents relating to polymer blends are issued each year. The technical literature on polymer blends related topics, which include composition of matter, preparation, processing, properties, applications, morphology, theoretical aspects, and so on, is expanding at an even faster pace. The blending of existing polymers offers the possibility of creating a compound that has desired properties of the individual polymer components [2].

It is very time consuming and very expensive to invent, develop, and produce a new polymer in a new plant (total cost >$100 million). A new polymer blend, in contrast, will be less expensive to invent. Also, it will take less time to develop and will require low investment funding to produce or, if available, it could be produced in existing equipment. Blend composition can be optimized to meet specific end-use property requirements. The driving force behind development of these novel compositions is the economics, property attributes, ease of manufacture of the

Encyclopedia of Polymer Blends: Volume 2: Processing, First Edition. Edited by Avraam I. Isayev.
© 2011 Wiley-VCH Verlag GmbH & Co. KGaA. Published 2011 by Wiley-VCH Verlag GmbH & Co. KGaA.

Table 3.1 Some examples of compounding ingredients.

Additive	Function
Flame retardants	Improve performance in fire related situations
Stabilizers	Protect against hot air aging, exposure to UV, ozone, radiation, weathering
Colorants	Improve looks, enhance feel and show
Process aids	Better flow during fabrication
Foaming aids	Foaming to reduce part weight
Plasticizers	Increase flexibility, impact strength, reduction in modulus, glass transition temperature
Fillers	Increase rigidity, conductivity, improve flame resistance, reduce cost, and so on
Nanofillers	Emerging technology. Used for different end usage requirements
Crosslinkers	Better creep resistance, lower compression set, resistance to deformation

blends, and cost-to-benefit ratio. The scientific literature is full of novel blend compositions and their applications. There are tens of thousands of US patents associated with the blends of different polymers. More than 20 000 of them cover the blends of rubbers and plastics.

3.1.2 Classification of Polymer Blends

In general, one can have three types of blends: plastic/plastic, rubber/rubber, and plastic/rubber blend.

The current chapter will focus on one segment of the polymer blend sector, consisting of plastics and rubbers. These plastic/rubber blends offer several interesting possibilities and a wide variety of applications, starting from thermoset rubber replacement to toughened plastics and also from adhesives to soft touch overmolding compounds. Based upon the relative proportions of the components, they can vary from very soft elastic rubbery blends to very ductile impact resistant blends. Based upon their relative polarity, they can be homogeneous miscible blends or heterogeneous immiscible blends. Based upon relative proportions and viscosities of polymers used, the rubber phase or the plastic phase can be continuous or both the phases could be co continuous. These blends can also be crosslinked under static or dynamic conditions to produce interpenetrating networks [3] or to create continuous/dispersed phase morphology [4]. Appropriate additives could further modify their performance. Usually, additives are needed to optimize their performance in the targeted use environments and to improve adhesion, to resist property deterioration due to aging, and to reduce stress cracking in different environments. If desired, more than one rubber and more than one plastic can be used to form a blend with and/or without compatibilizers [5]. If we consider all of the above possibilities, then it is very apparent that a single pair of rubber and plastic could produce many blends, each with different end-use properties. This is what makes the polymer blend field very interesting.

A polymer blend is considered miscible if the free energy of mixing is zero or negative. If two polymers are miscible, then their blend properties, such as the glass transition temperature (T_g), will be the average of the two individual polymer component proportions. This may not be desirable for many applications because such a blend will lose its elasticity at low temperatures and the upper use temperature will be lower than that of the plastic used.

In reality, the best blend compositions are usually derived from the components that are partially miscible with each other. In general these blends are referred to as technologically compatible blends. These are the blends that provide useful compositions without the use of a compatibilizer. In blends, prepared from such technologically compatible pairs, the individual component properties such as the T_gs are retained. As a result, one gets the best of both the components, that is, the blend has the lower T_g of the rubber component and the upper use temperature of the plastic segment [2].

3.1.3
Types of Plastic/Rubber Blends

Plastic/rubber blends can be divided into four groups:

- for technologically compatible polymers:
  1) physical blends of plastic(s) and rubber(s),
  2) blends of plastic and, partially or highly crosslinked rubber(s), and
- for poorly compatible polymers:
  3) physical blends of plastic(s) and rubber(s) with compatibilizers,
  4) blends of plastic(s) and partially or highly crosslinked rubber(s) with compatibilizers.

When polymers are grossly incompatible, mixing of these polymers generates blends that have very poor mechanical properties and produce a rough surface [5]. Both drawbacks of such blends can be minimized by appropriate use of an additive known as a compatibilizer [5–9]. The compatibilizer can also be produced *in situ* during melt mixing process. This process will be considered later in this chapter.

Examples of common technologically compatible plastic/rubber blends are:

- polyolefin with styrenic block copolymer, EPDM (ethylene–propylene diene terpolymer rubber), EPR (ethylene–propylene rubber), NR (natural rubber), BR (butadiene rubber), SBR (styrene–butadiene rubber), or IIR (butyl rubber);
- poly(vinyl chloride) (PVC) with EVA (ethylene vinyl acetate), CPE (chlorinated polyethylene), ethylene vinyl acetate carbon monoxide terpolymer, acrylic rubber, acrylate rubber, polyurethane, or NBR;
- polyamides with NBR (nitrile rubber (acrylonitrile–butadiene copolymer)), HNBR (hydrogenated nitrile rubber), acrylate rubber or acrylic rubber;
- polyesters with NBR, HNBR, or acrylic rubber;
- polyphenylene ether with styrenic polymers.

Examples of plastic/rubber blends requiring compatibilizers are:

- polyolefin with NBR, acrylate and acrylic rubber, silicone rubber or urethane rubber;
- PVC with nonpolar rubbers such as EPDM, SBR, IIR, or BR;
- polyamide with EPDM and other nonpolar rubbers;
- polyester with EPDM and other nonpolar rubbers.

3.2 Methods of Blend Preparation

There are several ways in which polymer blends can be prepared. For example, polymer solutions of different polymers could be combined and co-precipitated to form a polymer blend. One can also combine polymer latex, emulsion, or suspension of different polymers from the polymer reactors and coagulate them to form a polymer blend [10]. One can also polymerize another monomer(s) in the polymer solution, emulsion, or suspension and create a blend, which can then be isolated by the usual polymer separation techniques. A more direct way with a great deal of flexibility would be to melt-mix the polymers to form the blends. Blend preparation by melt mixing avoids problems associated with time consuming removal of large amounts of water, solvent, and so on.

For the purpose of this discussion, the basic processes for the preparation of blends prepared by polymer melt-mixing will be considered. The procedures discussed here are applicable to most commercially produced plastic/rubber blends.

The goal here is to start with one or more plastics and rubbers and combine them together by a melt mixing process (irrespective of the type of mixing equipment) in such a way that the blend components are distributed evenly and well dispersed on a micro level, as shown by a conceptual drawing in Figure 3.1 [11]. In blends that are

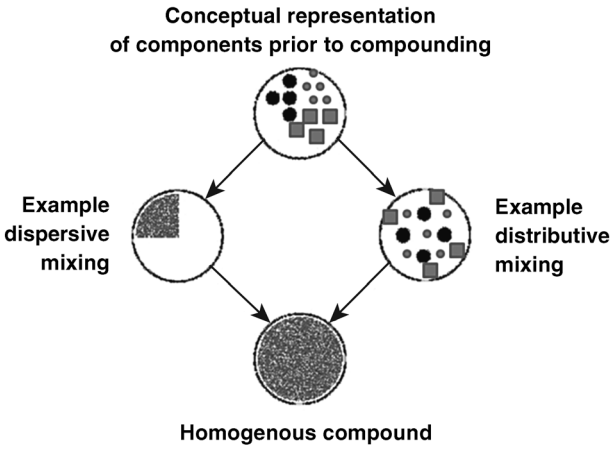

Figure 3.1 Mixing process.

technologically compatible there are enough polymer–polymer interactions to maintain phase individuality and yet produce commercially useful blends. Blending and melt mixing could be defined as follows:

- blending – the intimate intermingling of ingredients *without* phase change,
- melt mixing – the intimate intermingling of ingredients *with* a phase change.

The objectives of melt mixing are:

- melt/plasticate,
- mix: distribute/disperse on a micro level,
- devolatilize/remove gases.

3.3 Equipment for Blend Preparation by Melt Mixing of Polymers

One can use batch mixers, such as:

- a two roll mill,
- Banbury or internal mixers.

However, continuous mixers are widely used and more preferable. They have better control of product quality and consistency. Examples of continuous mixers are:

- single-screw extruder with a high shear mixing screw,
- reciprocating single-screw Buss co-kneader,
- intermeshing co-rotating or counter rotating twin-screw mixers.

3.3.1 Batch Mixers

3.3.1.1 Roll Mill

Figure 3.2 shows a roll mill. The process variables for a roll mill are:

1) nip gap,
2) roll rotation speed,
3) friction ratio (speed difference between the front and back roll),
4) roll temperature.

Most roll mills have only a fixed speed and a fixed friction ratio. Consequently, the actual process variables are the roll temperature and the nip gap. By nip gap adjustment one can increase the work input in the blend. The roll mill process capabilities (+) and limitations (−) can be summarized as follows:

+ residence time control;
+ melt temperature control;
+ dispersive mixing achieved by adjustable nip gap;
+ shear is only delivered in the nip area between the rolls;

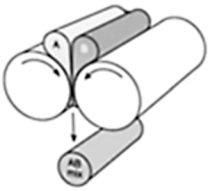

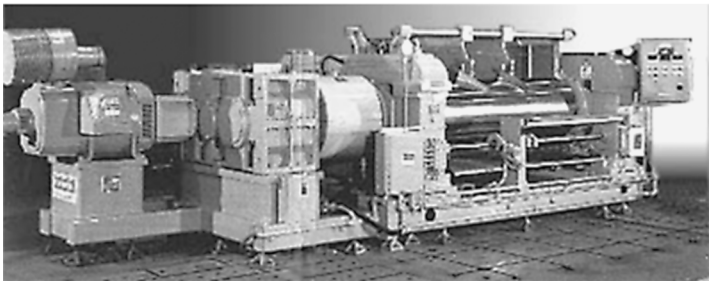

Figure 3.2 Two-roll mill. Kobelco Stewart Bolling Inc., 1600 Terex Road, Hudson, OH 44236.

- poor distributive mixing (distributive mixing is carried out only by operators cross-cutting);
- no pressure generation capability; however, the strips can be diced directly from the mill after cooling.

One can use a roll mill to prepare the plastic/rubber blends, using heated rolls, in the laboratory. However, for production this may be very cumbersome and, since the polymers are melt-mixed at high temperature in the atmosphere, handling of the molten polymer and degradation by heat could be an issue. Quality consistency could be another issue with this process.

3.3.1.2 **Banbury or Kneader Mixer**

Banbury and kneader mixers are available in various sizes and are used for melt mixing of the blends. Figure 3.3 gives a schematic view of a Banbury mixer [12]. The melt-mixed blend is then dropped on the roll mill and processed. The Banbury capacity is usually specified by chamber volume size. The size varies from less than a few hundred cubic centimeters to more than 800 liters. They are equipped with different types of mixing rotors (Kobelco Stewart Bolling, Inc., [12]). Some of them are shown in Figure 3.4. The main design variable here is the number of wings and the blade angle relative to rotation. Multiple liquid feeds are possible by adding feed ports at the back of the Banbury. Small batch mixers such as a Brabender, Figure 3.5, a Haake Rheomix (Thermo Electron Corporation, Newington NH 03801), or a small Banbury are used for product and process development work. Large units are used for production. From the Banbury mixer, the molten well-mixed blend is discharged at the bottom of the unit or on a side by tilting the chamber.

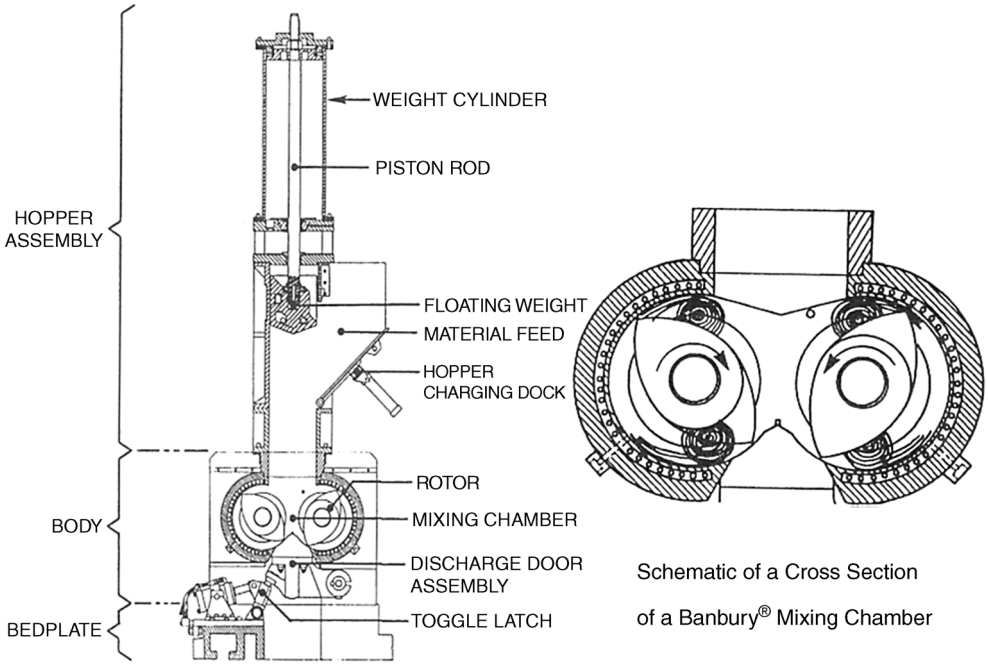

Figure 3.3 Schematic of a Banbury® mixer. Farrell Corporation, 25 Main Street, Ansonia, CT 06401.

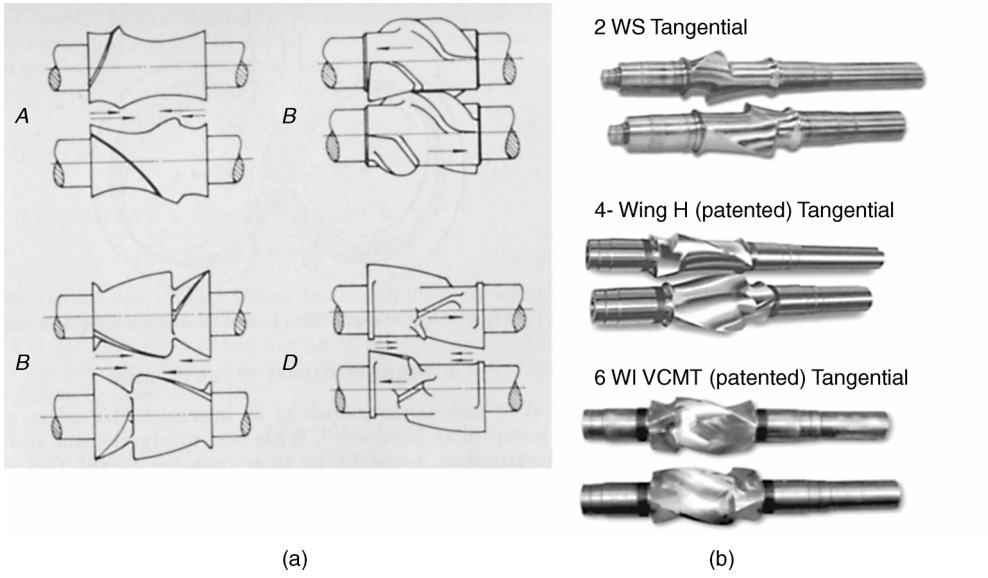

Figure 3.4 Examples of various rotor designs (a) and examples of Kobelco rotor designs (b).

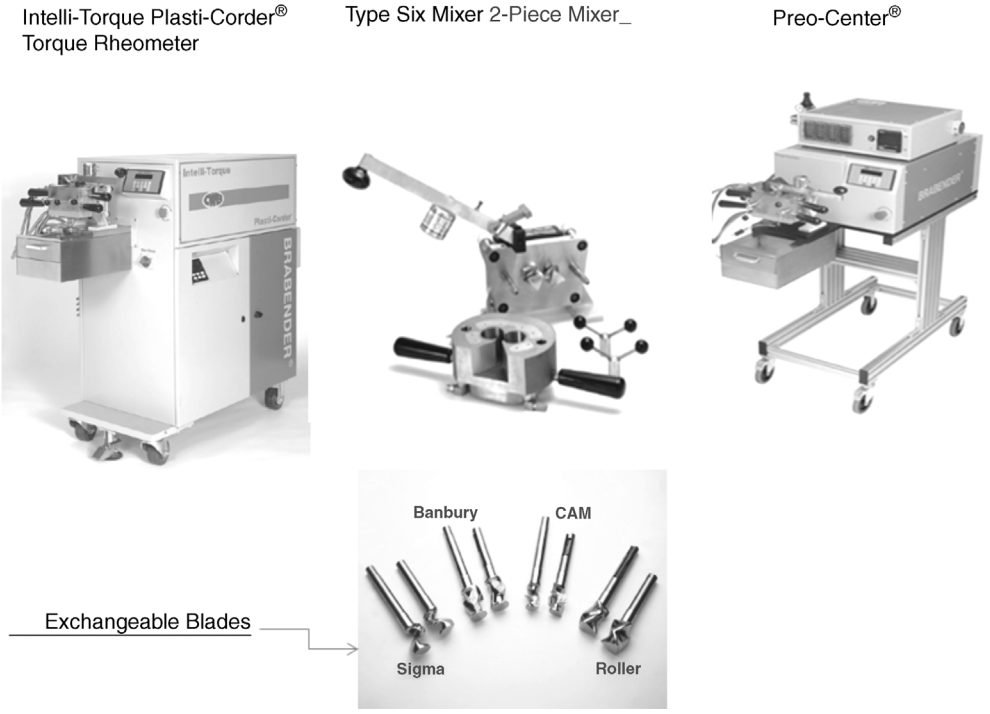

Figure 3.5 Laboratory process/product development equipment from C. W. Brabender. C.W. Brabender 50 Wesley Street, South Hackensack, N.J. 07606.

In batch process the mixing could be continued for:

- constant time,
- a time until a constant (same) temperature is reached,
- a constant energy input,
- equivalent heat history.

In a Banbury batch process, mixing with increased rotor speed, increased ram pressure, reduced cooling water temperature, and increased polymer viscosity has a positive effect if the mixing time is constant for each batch or the batch is removed each time from the Banbury when the same stock temperature is reached. If the batch is mixed for a constant energy input, then the rotor speed, ram pressure, water temperature, or polymer melt viscosity has very little or no effect on dispersion quality [12].

The Banbury process has the following attributes (+) and drawbacks (−):

+ Control on residence time – a batch can be removed from the Banbury when desired.
+ Batch temperature control – ability to limit overheating or under heating. There are several options available to control the batch temperature. They are:

cold water circulation, ram pressure, batch size, mixing speed, and/or mixing time in any combination.

+ Level of distributive and dispersive mixing could be controlled by adjusting mixing time, ram pressure, and mixing speed.
− Tacky materials tend to stick to rotors and mixing chamber walls. This is one of the drawbacks in this type of mixing. When this happens, one has to cool the Banbury walls and rotors. This is a time consuming process and slows down production. Occasionally, use of an appropriate lubricant eliminates this problem. Examples of common lubricants are fatty acids and their metal salts or amides, polyethylene waxes, and silicone compounds.

For an efficient operation, it is preferred to have units equipped with the following:

- variable rotor speed;
- high temperature stable rotor seals;
- heating and cooling for the body and rotors (electric/air, water; steam/water or oil/air) steam/water is a lot faster for heating and cooling, but upper temperature is limited by the steam pressure; if one of the components in the blend has a high melting point, then electric heating with water cooling is preferred;
- gravimetric or volumetric liquid injector to introduce plasticizer or extender oil during blend mixing;
- power integrator to monitor and control batch to batch consistency;
- torque indicator;
- temperature indicator;
- computer interface to monitor power, temperature, time, and torque during production.

Auxiliary equipment required:

- conveyer to transfer pre-weighed compounds from weigh station to the Banbury platform;
- heated vertical roll mill for processing the blend from the Banbury or other batch mixer such as a kneader;
- an extruder with an underwater pelletizer attachment or a strand die, water trough, and a dicer. One can also use a roll mill to form a sheet of the product from the mixer and dice it;
- bagging unit for finished product.

Figure 3.6 shows a batch mixer process flow diagram.

3.3.2 Continuous Mixers

3.3.2.1 Twin-Screw Mixer

The commercially available mixers start with a single screw shaft and can have as many as 12 shafts. For a continuous process, there are more choices in the production

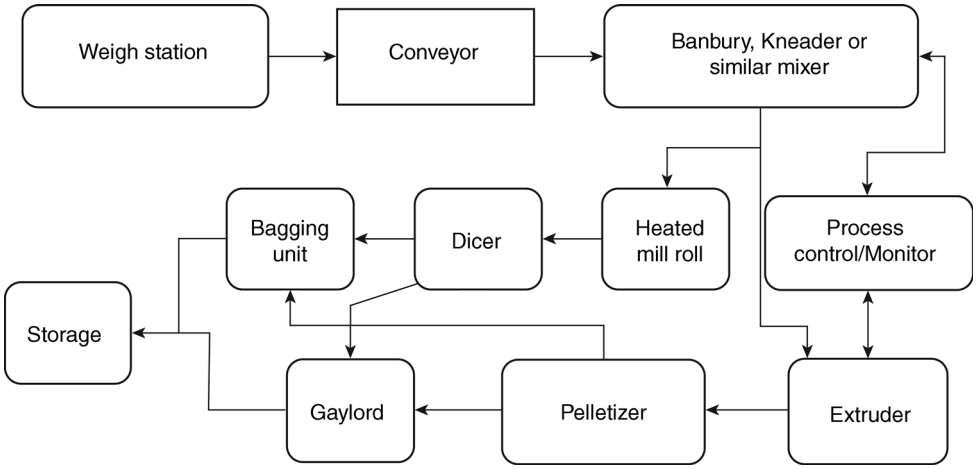

Figure 3.6 Batch mixer process flow diagram for production of elastomer-thermoplastic blends.

equipment and there are many suppliers of such units.[1)] Mixers with two screw shafts, such as that shown in Figure 3.7, are widely used for blend mixing. The size of these units is usually specified in millimeters, which refers to the screw diameter of the unit. The length is specified in terms of length/diameter (L/D). Twin-screw mixers are available in numerous different sizes, varying from a few to 300 + mm. The production rate of these units is from few hundred grams for micro twin-screw mixers to 20 000 + $\mathrm{kg\,h^{-1}}$ for larger units. Notably, these rates are for polymer pelletizing. In the case of blends, the rate would be lower, because the ability of the feed throat port would be limited in handling the low bulk density components in the blends.

Figure 3.8 shows different barrel configurations. Most barrels are solid core. Barrel openings for side feeder, liquid feeder, vacuum, and so on. Their locations have to be decided during initial set up. Of course, all barrels are individually configured; therefore, the barrel locations can be switched around as needed.

Some twin-screw mixers have fixed screw geometry. Most of them have shafts and different types of conveying and kneading element blocks to provide flexibility in screw geometry configuration (Figure 3.9). The relative functions of different types of elements and their efficiency toward a given operation are described in Table 3.2. As seen, even the width of the elements plays a very important role in the mixing processes.

The number of lobes on mixers varies from one to six. Figure 3.10 shows mixing elements having one to six lobes. The co-rotating twin-screw elements could have

1) For example: B & P Process Equipment Systems, Saginaw, MI, USA; Cincinnati Milacron Extrusion Systems, Batavia, OH, USA; Coperion, Ramsey, NJ, USA; Crown Machine Corp, Addison, IL, USA; Davis-Standard, Killion Specialty Systems, Pawcatuck, CT, USA; ENTEK Manufacturing Inc., Lebanon, OR, USA; Krauss-Maffei AG, Florence, KY, USA; Kobelco Stewart Bolling Inc., Hudson, OH, USA; Leistritz, Somerville, NJ, USA; National Feedscrew and Machining, Inc., Massillon, OH, USA; Twin Screw Extruders Incorporated, Charlotte, NC, USA.

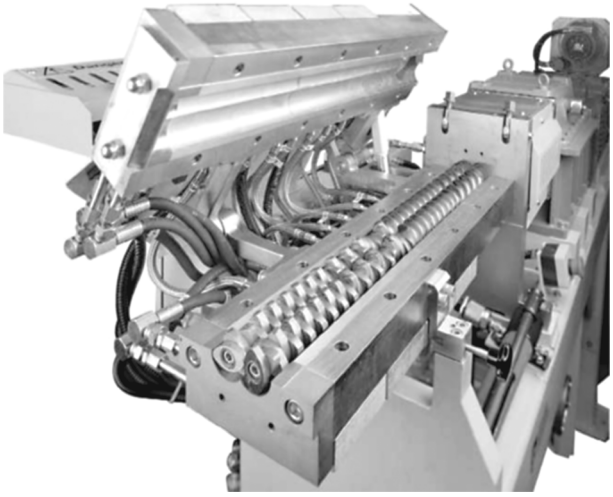

Figure 3.7 Fully intermeshing, co-rotating twin-screw extruder. BP Process Equipment Systems, Saginaw, MI, USA.

one, two, three, four, or six lobes. The counter rotating twin-screw elements have either one or two lobes. Two-lobe screw elements are used more widely.

The functions of different elements are [11, 13] as follows:

Conveying (flighted):

- move compound in the forward direction,
- control energy input.

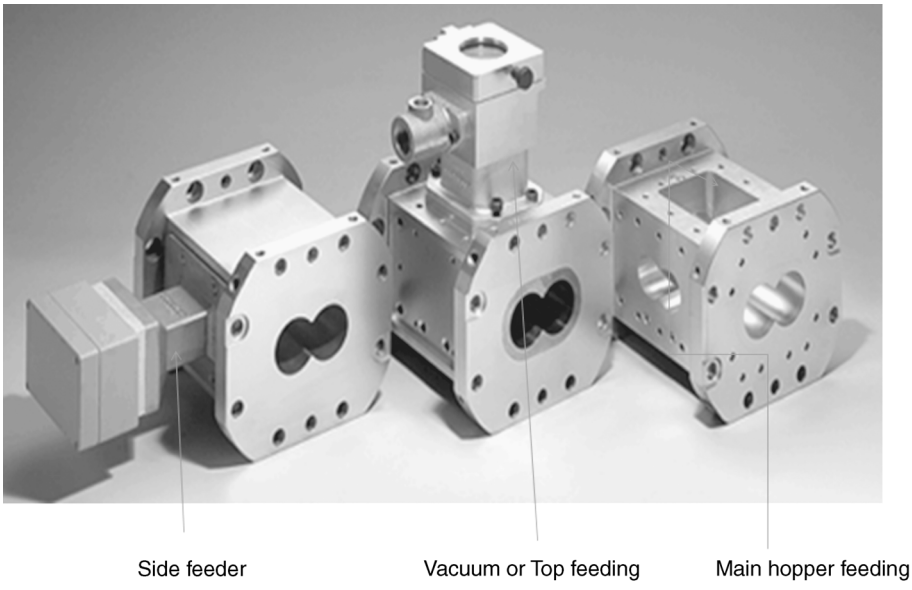

Figure 3.8 Barrel designs for different types of feeding options. Leistritz, Somerville, NJ, USA.

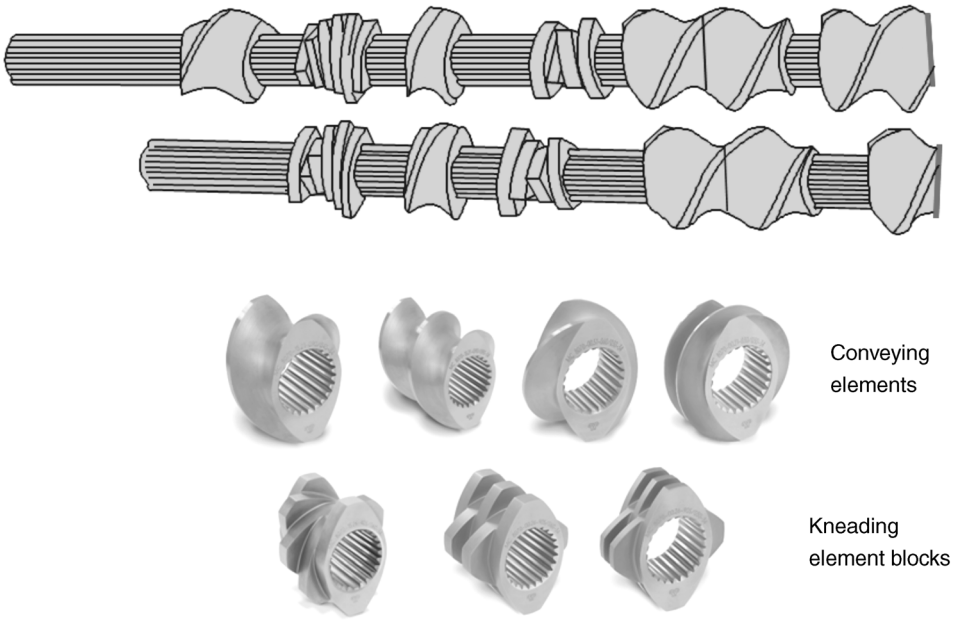

Figure 3.9 Examples of screw elements and a programmable screw design. Krupp Werner & Pfleiderer, Ramsey, NJ.

Mixing: neutral and different angles in forward and reverse direction:
- distribute (divide and recombine),
- disperse (lobal capture or shear),
- restrict,
- forward transport.

Zoning:
- restrict (facilitate vacuum seals).

Hybrid:
- more than one function.

Table 3.2 Effect of element type on mixing process during melt mixing.

	Forward N	Forward W	Reverse N	Reverse W	Neutral N	Neutral W
Conveying	G	P	NEG	NEG	0	0
Distributive	G	P	E	OK	E	OK
Dispersive	P	E	OK	E	G	E
Shear heating	L	H	AVG	VH	AVG	H
Pressure generation	AVG	VH	H	VVH	H	VH

N = narrow, G = good, P = poor, NEG = negative, 0 = none, E = excellent, OK = acceptable, L = low, H = high, AVG = average, VH = very high, VVH = very very high.

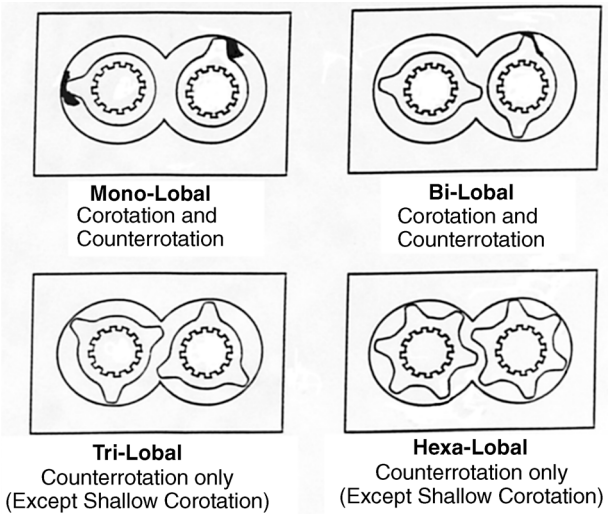

Figure 3.10 Screw elements with different number of lobes. Leistritz, Somerville, NJ, USA.

The screw elements simply slide on a slotted shaft. One has to carefully ensure that they are configured correctly so that they match and are at the correct angle and there is no gap between elements. When this is not done, the element, shaft, or the barrel could be damaged very quickly during the startup process. Twin-screw extruders with segmented screw elements provide more flexibility in custom tailoring the mixing screw configuration to achieve shearing, kneading, and pumping in different zones by selection of appropriate type of element combinations. The variable screw speed could be as high as 1200+ rpm for some of these units.

As the compound flows along the barrel length in a twin-screw mixer, regions of high and low pressure are created in the periphery for both co-rotating and counter-rotating twin-screw mixers. The material feeding ports should be located in the low pressure area for ease and efficiency of addition of the ingredients through these ports along the twin-screw mixer.

The kneading and conveying elements can be arranged in different configurations to perform different functions, such as conveying, mixing (distributive and dispersive) melting, pumping, and so on, as illustrated by an example of the screw design in Figure 3.11.

In general, the twin-screw mixer has the following attributes (+) and drawbacks (−):

+ programmable screw design with lots of flexibility,
+ multiple feeds at multiple locations (liquid and solids),
+ positive conveyance (independent of the frictional properties of the feed),
+ self-wiping operation (no polymer flow stagnation),
+ excellent heat transfer,
+ vacuum option allows compound degassing before pelletization,
+ good residence time control (within limits),
+ good melt temperature control,

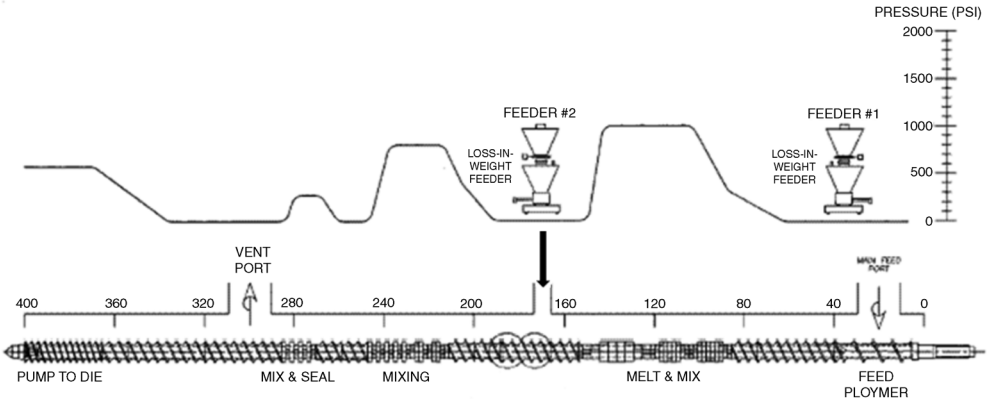

Figure 3.11 Controlling the mixing process by screw design in a twin-screw mixer. Leistritz, Somerville, NJ, USA.

+ excellent dispersive mixing (achieved by wide kneaders, shaped lobals, barriers, shear rings),
+ excellent distributive mixing (achieved by narrow kneaders, cut flights, gear mixers, low advance flighted elements),
– residence time is relatively short (1–2 min) and may be a drawback for compounds requiring longer processing time, particularly during reactive mixing,
– pressure generation capability is average but this can be improved by use of a melt gear pump,
– if the conveying and mixing elements are not placed properly compounds could be overheated and degraded,
– size of the rubber chunks that can be fed to the extruder is limited by the feed port opening; if chunks are larger, then the feed port will plug up.

Different process variables will have an effect on the quality of the final blend, for example, mixing rate will increase with the screw rpm. Increasing the feed rate will decrease the remastication, time in mixers, and process intensity. Increasing the number of lobal events and their intensity will increase process severity. Increasing the temperature will decrease the controlling modulus, E_c, in the equation below:

$$d\sigma/dt = E_c X \, d\varepsilon/dt \tag{3.1}$$

where

σ = shear stress,
ε = shear strain,
t = time,
E_c = controlling modulus.

For preparing blends, the mixer should be equipped with the following:

- main feed port,
- ports for liquid injection,

- ports for side feeder or a Cramer feeder,
- vacuum port,
- diverter port near end before the screen changer,
- strand die,
- preferably the barrels have both heating and cooling capability to control the temperature during the blend processing,
- computer interface to monitor, store, and display feeder consistency, power, torque, time, and barrel temperature (set and actual) during experiment.

In addition to the mixer, the following auxiliary equipment is desired for smooth operation:

- gravimetric solids feeders for pellets, crumb rubber, and powders;
- rubber grinder if rubber used is in a bale form or large crumbs;
- ribbon blenders or similar blenders to blend all the materials in the powder form for the powder feeder and to blend all the pelletized materials for the pellet feeder;
- gravimetric feeder with a Cramer feeder or side feeder attachment (if addition of solid materials is needed at other barrels);
- storage tanks for liquids;
- gravimetric liquid feeding pumps with variable speed controls;
- liquid injectors;
- melt gear pump to provide constant flow of the molten mass to the end processing equipment;
- automatic or manual screen changer;
- end processing equipment such as underwater pelletizer or belt conveyer and a dicer;
- bagging units for finished product.

Notably, the metering screws for feeding powder, rubber, and pellets would each have a different design, each optimized for trouble-free smooth delivery of the blend components.

Figure 3.12 shows the process flow layout for a twin-screw mixer.

3.3.2.2 **Buss Continuous Kneader**

The Buss continuous kneader (Buss America, Inc., Carol Stream, IL 60188) is another continuous mixer that has been used for blend preparation. It has split barrels for easy access of the interior section and a screw that oscillates and rotates to move the material. It has fixed pins along the barrel length. Its two stage arrangement enables one to optimize the processing section and pressurizing zones. The mixing screw flights and the stationary pins interact with each other during mixing. Figure 3.13 presents the Buss kneader and its working principle. Here also, one can use computer-aided design to change the screw configuration for optimum performance, as indicated in Figure 3.14. Different types of kneading elements, forward and backward conveying elements, and transition zone elements are available for custom tailored screw configuration. The blending occurs by splitting, folding, reorientation, and recombining of stock by each element and pin.

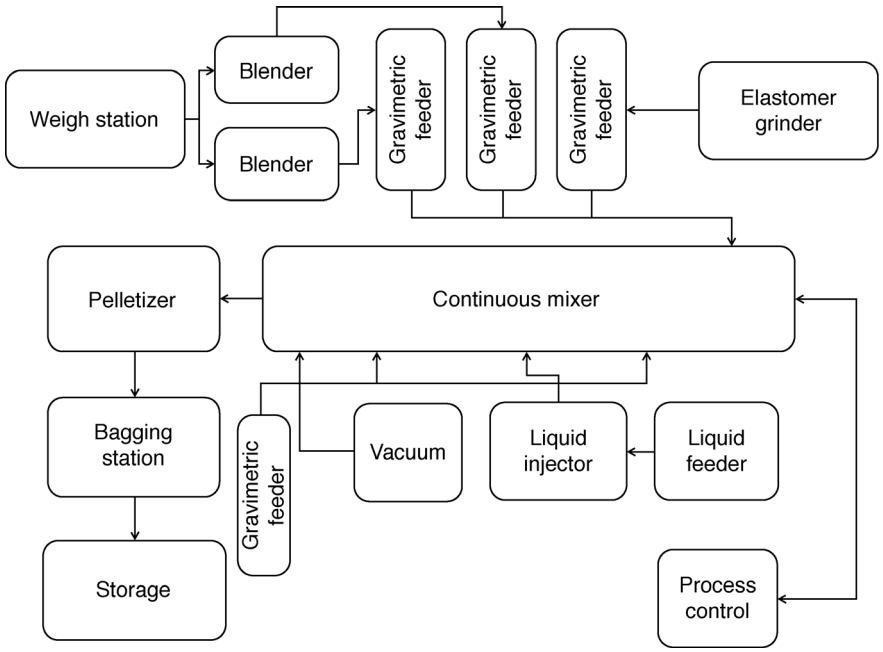

Figure 3.12 Process layout for production of elastomer-thermoplastic blends by a continuous process.

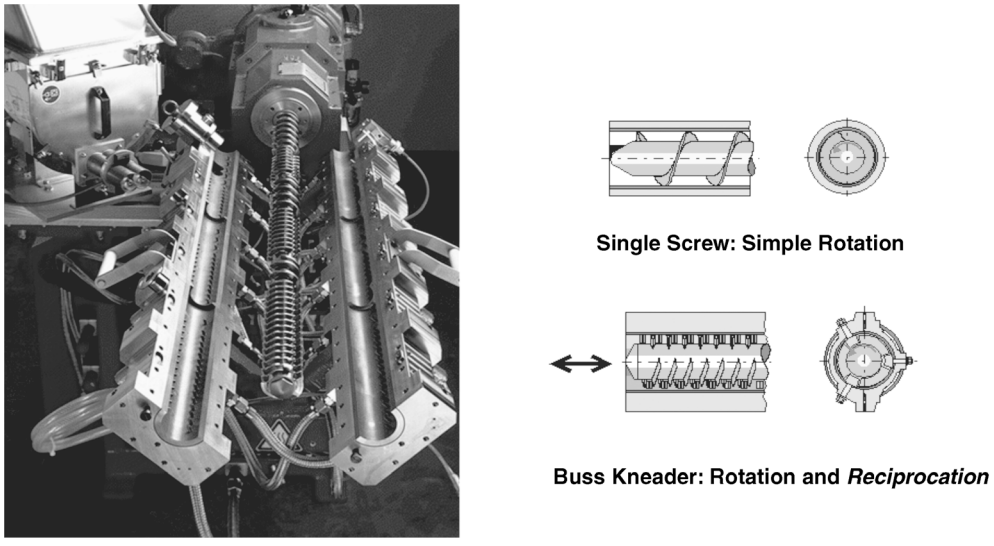

Figure 3.13 Buss continuous kneader. Buss America, Inc., Carol Stream, IL 60188.

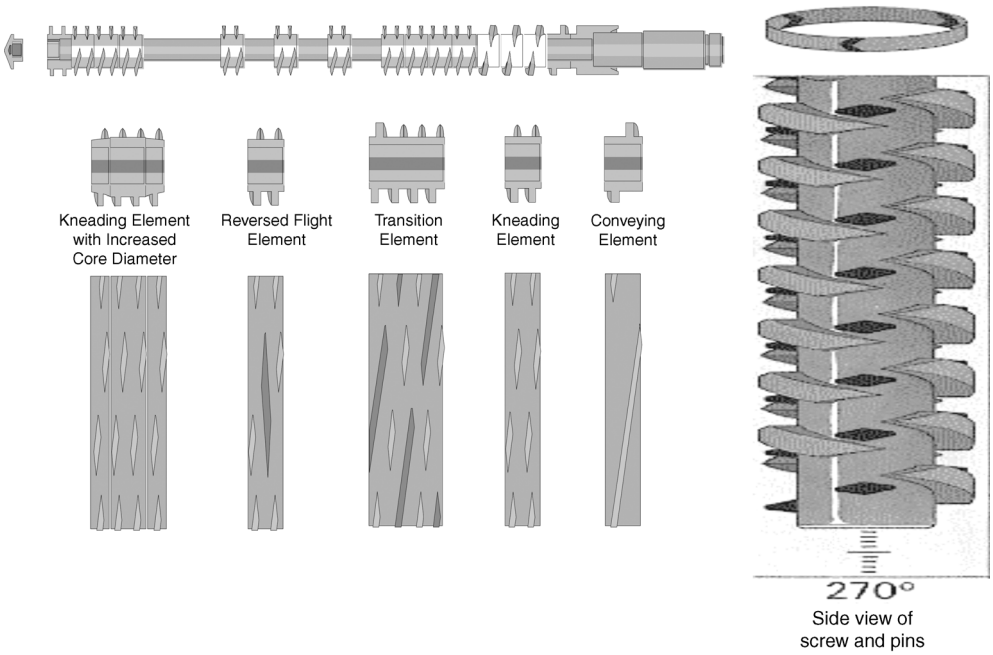

Figure 3.14 Programmable screw design.

The mixing action is a uniform and low shear process and as a result generation of heat is low during blend production. Because of its low shear and low heat generation, such machines are gaining in popularity in compounding of PVC and its blends.

The process flow layout for a Buss continuous kneader will be the same as that shown in Figure 3.12 for a twin-screw mixer.

3.4
Preparation of Physical Blends of Plastics and Rubbers

3.4.1
Laboratory Preparation of the Blends

Product development work is usually carried out in a pilot plant. Here one can use a small Banbury or a Brabender mixer for a batch process and a small twin-screw mixer or a co-kneader for development work on a continuous process.

Brabender-type units are preferred for product and process development work because they are easy to use, require only a small quantity of compounds, and provide very valuable information, which includes fusion rate and blend stability at mix temperature as well as reaction kinetics as a function of mixing speed, temperature, and rotor type. This information is very important in the production scale-up of

reactive blends. Brabender (C. W. Brabender) and Haake PolyLab mixers (Thermo Scientific) are equipped with a heating/cooling system, variable speed motor, and torque indicator/recorder. These mixers are now very sophisticated: computer controlled and have data acquisition capability (Figure 3.5).

Taking a polypropylene/EPDM blend as an example, the blend components were charged in the mixing chamber and the ram was closed. The mixing was carried out at 180 °C and a rotor speed of 80 rpm. Figure 3.15 shows the Brabender torque curve for the polypropylene/EPDM blend. As seen here, the torque starts at zero and increases slowly. Maximum torque occurs just before the onset of melting of polypropylene. As the melting progresses the torque decreases and levels off when PP (polypropylene) is melted. A few minutes after this the blend is removed from the Brabender and processed for evaluation. If the Banbury is equipped with a torque measurement, a similar process chart will be produced for the blend preparation. In a twin-screw mixer, since all processes are carried out simultaneously, one will get a composite torque at a reference point, unless the mixer is equipped to measure torque at different locations along the barrel. The composite torque will depend upon the relative viscosities of the blend components and process conditions such as the temperature profile, screw speed, screw configuration, and so on. If all the process conditions are equal then the torque could be used to measure the dispersion quality and blend consistency in conjunction with feed rate tracing from the computer log.

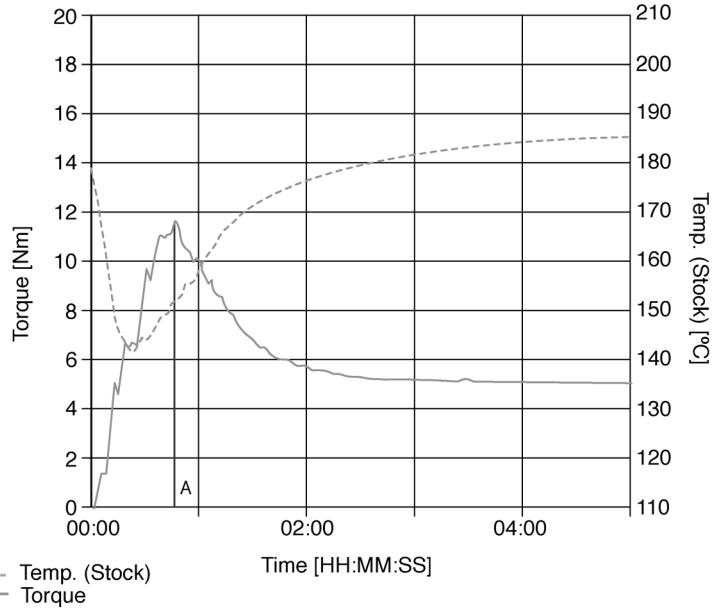

Figure 3.15 Brabender Plastograph recording during preparation of a thermoplastic-elastomer blend.

3.4.2
Production of Blends by a Batch Process

These are the easiest to prepare. Both the continuous process and batch process can be used to prepare these blends. Here, five main activities are needed to complete compounding:

1) uniform distribution of all components;
2) melting of all the polymer components;
3) dispersion or size reduction of the blend components;
4) incorporation of components to form a well mixed, uniform blend and create appropriate phase morphology;
5) conversion of finished compound into pellets for further processing.

The blends may contain one or more rubber(s) and one or more plastic(s) that are partially miscible or technologically compatible.

Batch size should be calculated to occupy 80–90% of the chamber volume of the Banbury for optimum mixing efficiency [10].

A generic batch process layout was shown in Figure 3.6. With few modifications, this process will be applicable to the production of most of the polymer blends by a batch process.

The steps involved in blend production by a batch process:

- weigh all the ingredients for a given batch size;
- combine them according to the physical form of the ingredients:
  – rubber as bales, crumbs, or pellets,
  – polymer pellets and other additive pellets,
  – powders, which includes fillers, stabilizers, lubricants, process aids, and so on;
- preheat the Banbury;
- start the Banbury at medium to high rotor speed;
- add rubber followed by powders and extender oil or plasticizer, if desired;
- lower the ram and mix for 1 min then lift the ram to prevent loss of powders during mixing;
- add polymer pellets and lower the ram, keep the ram lowered until the plastic is melted and continue the mixing for about 3–4 min after the plastic is melted;
- during this time, lift the ram and sweep down around the ram and wall to remove all the accumulated material from the blend, and mix it back with the molten blend; repeat this step as often as necessary so that all the unmixed material is transferred to the Banbury chamber and melt mixed with the molten polymer blend; repeat as often as needed.
- Add additional plasticizer or extender oil, if needed, during this time. When a liquid is added to the blend, the ram should be lowered and kept there until the liquid is mixed in thoroughly. If a liquid is added then mixing should be continued for about 2 min after the liquid is mixed in well with the polymer. This could be monitored by the torque. Initially, the torque will drop due to the lubricating effect

of the fluid. Then, it will increase and level off as the liquid is dispersed in the polymer blend. This is the indication of completion of the mixing process.

- Drop the batch on a heated roll mill, cut into a continuous strip and convey on an air-cooled belt to a dicer or feed to an extruder attached to an underwater pelletizer or a strand die, conveyer belt and a dicer. If rubber level is high, then the pellets may stick together. In such instances one can dust the pellets with a small amount of dusting agent. One can also use a two roll stuffer to feed the molten blend to the single-screw extruder.

Notably, during the mixing cycle, when the blend starts mixing, the torque will rise and reach a maximum when the plastic starts melting. The torque will then gradually decrease and level off. The mixing time is usually taken from the peak time when the plastic starts melting. After the plastic components are melted, it is very important to control the temperature at a point slightly (~20 to 30 °F[2)]) above the melting point of the plastic. This is to prevent degradation of the polymers used. This can be accomplished by turning off the steam and running hot or cold water through the chamber walls and rotors. If necessary, one can also reduce the rpm of the Banbury.

3.4.3
Production of Blends by a Continuous Process in a Twin-Screw Mixer

The process flow layout for the twin-screw mixer set up is presented in Figures 3.12 and 3.16. As noted above, the metering screws for feeding powder, rubber, and pellets would each have a different design, each optimized for trouble-free smooth delivery of the blend components. The rate is affected by the ability of the feed port to handle the bulky compounds. In reality, this is often the limiting factor in production of blend compounds that have fluffy fillers.

At least three separate gravimetric feeders are required: one for ground, crumb, or pellet rubber, one for materials in the pellet form, and one for the materials in the powder form. The feeders for pellets and powders may require different types of feeding screws. For feeding of additional solid materials at other barrel locations additional gravimetric feeders are required.

During the production run, the feeders could be loaded automatically or manually, as desired, from the material storage for individual components and from blenders for multicomponents.

The rubber, pellets, and powders are fed to the continuous mixer at the feed throat. The plasticizer, extender oil, or any other liquid components are fed downstream, usually at the third or fourth barrel. Other solid additives could also be added to the mixer using a top feeder or a side feeder at a barrel located further downstream. If the additives have a low melting point, adding them from the top with an auger-type of feeder is a better choice.

All the volatiles are removed through the vacuum port. If the melt viscosity of the blend is too high, then a melt gear pump may be used to reduce head pressure and

2) t_F (°F) = (9/5)[t (°C)] + 32.

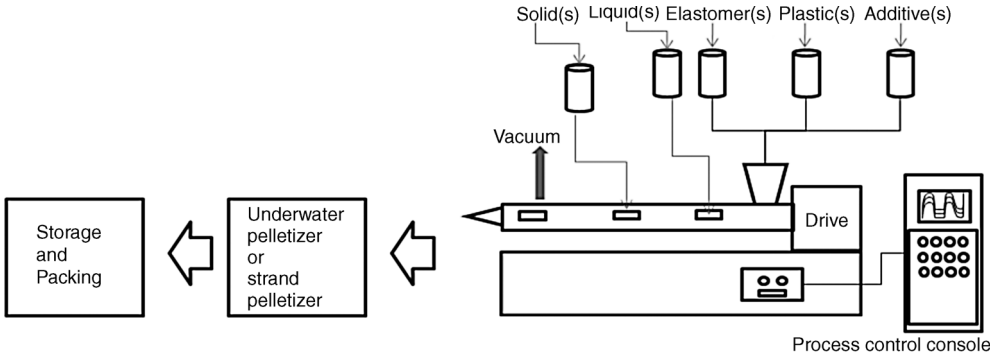

Figure 3.16 Process layout for production of rubber/plastic blends by a continuous process.

maintain constant flow of the material through the die. Finally, the molten blend will pass through metal screens with a fine mesh and a heated strand die. The strand could be diced after cooling by air on a conveyer belt or water bath. An underwater pelletizer attached to the die can also pelletize the compound.

The production process is usually automated such that all the feeders are synchronized with manual override.

The screw configuration, such as one shown in Figure 3.11, is selected so as to have the ability to convey, distribute, and disperse the material so that finished compound emerging from the mixer is well mixed on a micro-scale and is consistent.

The steps for the continuous production of a plastic/rubber blend in a twin-screw mixer are as follows:

1) If the rubber is in the bale form or large crumb form, it is ground in a rubber grinder. A partitioning agent, usually a small amount of the same filler that is used in the blend formulation, is added to prevent agglomeration of the ground rubber. It is then conveyed to the feeder or storage from where it is conveyed to the feeder as needed. If the rubber is in the small crumb form or pellet form, it is probably dusted and could be conveyed to the feeder directly from the storage. All components in the powder form (fillers, stabilizers, lubricants, process aids, etc.) are pre-weighed in the desired ratio and added to the ribbon blender or other similar mixer and mixed until dispersed uniformly. From here, the blend is conveyed to the feeder as needed. A uniform distribution of low level additives is very important in this process.
2) All components in the pellet form (polymer pellets and other additive pellets) are pre-weighed in the desired ratio and added to the ribbon blender or other similar mixer and mixed until dispersed uniformly. From here, the blend is conveyed to the feeder as needed.
3) Set the barrel temperatures to desired temperatures. The barrel #1 is usually not heated to prevent material from sticking in the feed zone.
4) Transfer the rubber, pellets, powders, liquids, and additives for side feeders to the feeders.

5) Start the extruder at a higher screw speed than normally used in steady state operation.
6) Start the main feeders to feed the blend components and wait until the molten polymer blend starts to come out of the diverter tube. Start liquid and additive feeders as needed.
7) After about 10 min, close the diverter valve and pass the molten polymer blend to the die and pelletizer.
8) Reduce the screw rpm to a level appropriate for steady state operation.
9) The pelletized blend is then conveyed to the storage or bagged using an automatic bagger.

Notably, in blending process attention must be paid to ensure uniform distribution of minor ingredients. In addition, when the rubber level is high, the blend is sticky and may require dusting.

As the rubber content is varied from low to high, the morphology of simple blends varies from dispersed rubber phase to co-continuous rubber phase to continuous rubber phase. In one set of experiments, EPDM and polypropylene were melt-mixed in different proportions. They were then removed from the mixer, cooled, and molded in a compression mold to form 10 cm × 10 cm sheets. Strips of these blends were then cold fractured in liquid nitrogen, stained by ruthenium tetroxide, and examined by scanning electron microscopy (SEM). Figure 3.17 shows the results of this work [4]. Here EPDM is a continuous phase and polypropylene is a disperse phase at high EPDM concentration. At low EPDM concentration, it is a dispersed

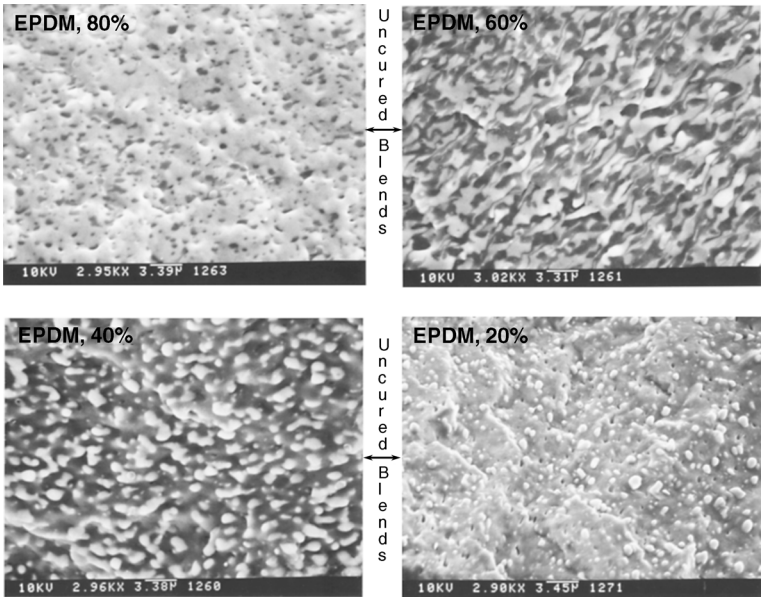

Figure 3.17 SEM micrographs showing the blend morphology for physical blends of EPDM and PP at different rubber to plastic ratios.

phase. Two co-continuous phases were observed for 50 : 50 plastic : rubber blend composition. It has been shown that the phase continuity depends upon the relative stresses and melt viscosity of the blend components according to the equation below [14]:

$$\sigma_A/\sigma_B = \eta_A/\eta_B \tag{3.2}$$

where

σ is the shear stress,
η is the viscosity,
A and B are polymer A and B, respectively.

For a given pair of a plastic and a rubber, the hardness and physical properties, such as the tensile strength, elongation at break, elasticity, and so on, will depend upon the relative proportions of the components. A higher level of plastic will produce blends with higher hardness and higher tensile properties but lower elasticity. Another variable in rubber selection is its composition. For example, in EPDM, as the ethylene level is increased the crystallinity will increase. Blends containing crystalline EPDM have higher tensile strength and elongation at break than those prepared from amorphous EPDM [15].

In nitrile rubber (NBR), the rubber polarity changes with the acrylonitrile (AN) content of the rubber. Since AN is polar and butadiene (BD) is nonpolar, the rubber polarity will increase with AN level. Therefore, the level of compatibility with other polymers will depend upon NBR composition. The glass transition temperature (T_g) also increases with increasing AN level.

Since the viscosity contributes to the phase morphology, the molecular weights of the blend components will also play an important role in blend preparation. Similarly in SBR and EVA, the relative monomer composition will affect the blend properties and compatibility.

Styrenic block copolymer blends with polyolefins are among the most widely used blends and they vary in hardness from low Shore A on the softer side to >60 D on the harder side and are used in a wide variety of applications. EPDM blends with polyolefin that are made by compounding or by direct reactor polymerization have also found several applications in the automotive industry. At low concentrations (~20% or less) EPDM and EPR have been used as an impact modifier for polyamides [16].

3.5
Crosslinking Agents and Crosslinking Processes

Rubbers have different functional groups for crosslinking them. The choice of crosslinking compound will depend upon the functional group. In general, crosslinking compounds possess two or more functional groups that will react with the reactive sites on a rubber molecule in a reasonable time with or without a cure activator, catalyst, or a co-agent. For example, EPR has active hydrogen and could only

be crosslinked by radical sources such as peroxides, radiation, and so on. In contrast, EPDM has active hydrogen as well as double bonds and therefore could be crosslinked by different types of sulfur curatives, dimethylol phenolic compounds, multifunctional silicon hydrides, and of course peroxide and radiation. Usually, a co-agent is used with peroxides to improve crosslinking efficiency of the peroxides. Of the different curatives available for EPDM, sulfur, peroxide, phenolic, and silicone hydride curative are used widely for the preparation of TPVs (thermoplastic vulcanizates).

The crosslinking of unsaturated rubbers by sulfur is a very complex process. It requires a zinc oxide/stearic acid activator, cure accelerators such as MBTS (benzothiazyl disulfide), MBS, TMTD (tetramethylthiuram disulfide), and so on, and sulfur, which usually exists as S_8. Scheme 3.1 shows a simplified mechanism for rubber crosslinking by sulfur [17].

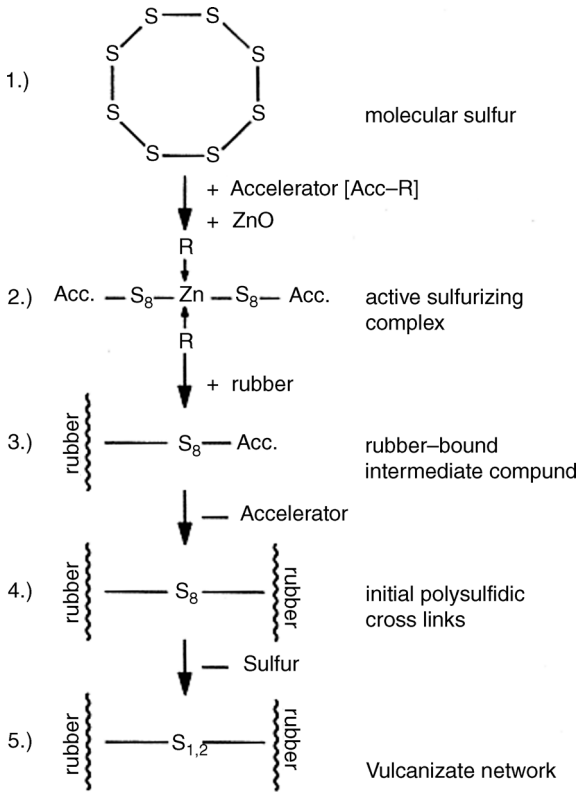

Scheme 3.1

Several peroxides are available, but only a few of them have a long enough half-life at the polypropylene melting temperature. The peroxide is decomposed by heat and generates radicals. The radicals add across the double bond and generate

polymeric macro-radicals. The radicals on different molecules then combine to form a crosslinked network. Also, the radicals abstract hydrogen from polymers having active hydrogen and thus form a radical on the polymer. These radicals then combine with other polymeric radicals to form a crosslink. In practice co-agents, usually di, tri, tetra or polyunsaturated monomers and prepolymers, are used with peroxides to improve their crosslinking efficiency.

Scheme 3.2 shows the unsaturated rubber crosslinking mechanism for peroxides.

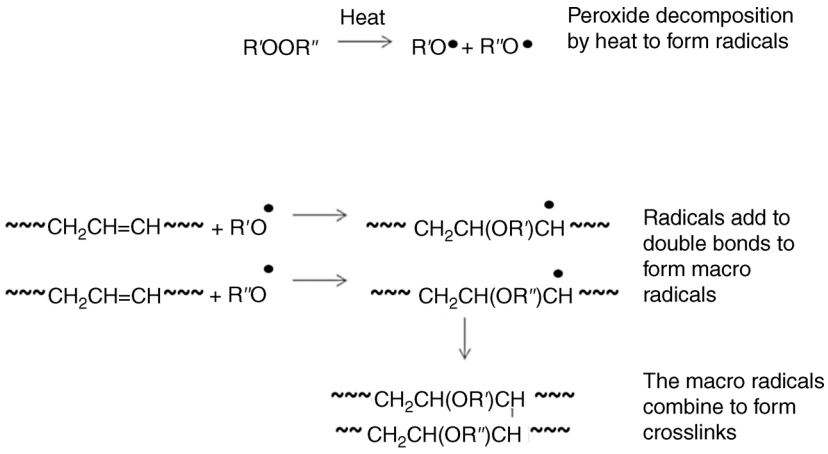

Crosslinking of unsaturated elastomer by a peroxide

Scheme 3.2

Examples of suitable peroxides for use in TPV preparation are dicumyl peroxide, di (*t*-butylperoxy)diisopropylbenzene, 2,5-dimethyl-2,5-di(*t*-butylperoxy)hexane, and 2,5-dimethyl-2,5-di(*t*-butylperoxy)hexene.

Examples of suitable co-agents are 1,2-polybutadiene, triallyl cyanurate, multifunctional acrylate and methacrylate monomers, and *N,N′-m*-phenylene-bis(maleimide).

The other widely used crosslinking system is Lewis acid catalyzed dimethylol phenolic resin. This system is used for batch and continuous twin-screw process. There are very few suppliers of phenolic resin. Phenolic resin has a bulky octyl group. This helps to improve its solubility in nonpolar rubbers such as EPDM. The −OH of terminal phenol groups and the methylol groups ($-CH_2OH$) participate in the crosslinking of unsaturated rubbers in the presence of a Lewis acid compound as shown below.

1) Figure 3.18 shows the structure of the dimethylol phenolic resin [18]. Dimethylol phenolic resins are linear polymers. They contain:

- reactive $-CH_2OH$ end-groups,
- polyfunctional aromatic hydroxyls,

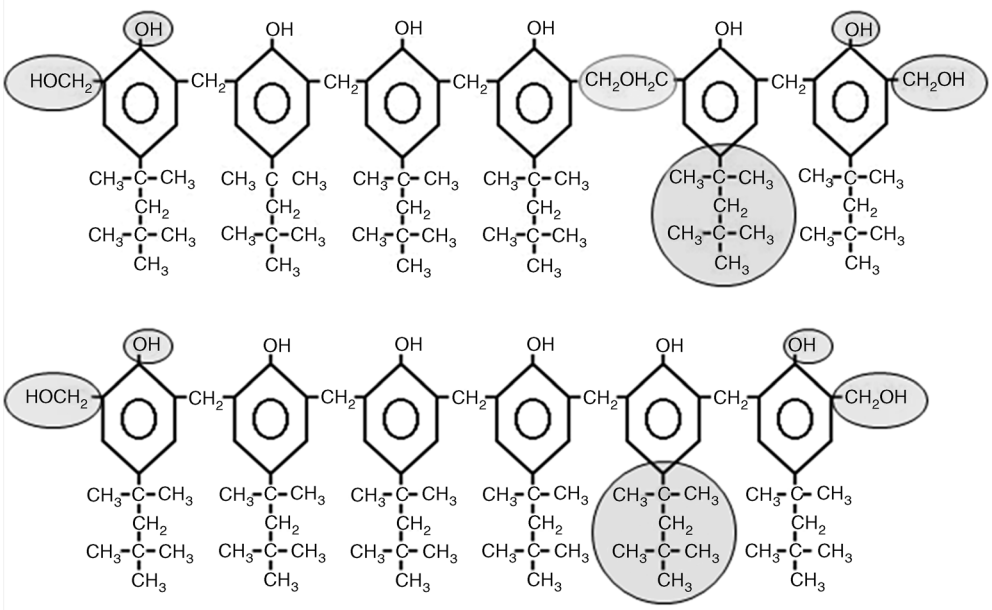

Figure 3.18 Structure of dimethylol resin.

- a high amount of olefinic character ($-C_8H_{17}$ octyl group on each benzene ring).

2) Crosslinking of an unsaturated rubber (EPDM) by Lewis acid catalyzed dimethylol phenolic resin occurs (Scheme 3.3).

Peroxide degrades some plastics, such as polypropylene (PP). Consequently, in peroxide crosslinked TPVs, polymers like PP degrade and polymers like polyethylene crosslink. In phenolic resin cured TPVs, thermoplastics like PP do not degrade but moisture is always an issue, because the stannous chloride or zinc chloride that are used as Lewis acid are hygroscopic.

The silicone hydride based crosslinking system overcomes both drawbacks. The plastic phase does not degrade and the catalyst used for the crosslinking system is not hygroscopic. Hydrosilation (or hydrosilylation) is the addition of an H-Si bond across a double bond. The crosslinking is catalyzed by platinum and other metal complexes as shown in Scheme 3.4 [19].

If the rubber has a carboxylic acid as a cure site, then one can use compounds with two or more functional groups that will react with the $-$COOH group. Examples of such compounds are polyhydroxy compounds such as ethylene glycol and pentaerythritol, diamines such as hexamethylenediamine and methylenebis(aniline), diisocyanates such as toluene diisocyanate, and so on. The crosslinking systems used for other rubber compounds will depend upon the cure site and are readily available from the rubber supplier.

Table 3.3 describes the attributes of different crosslinking systems for unsaturated polymers.

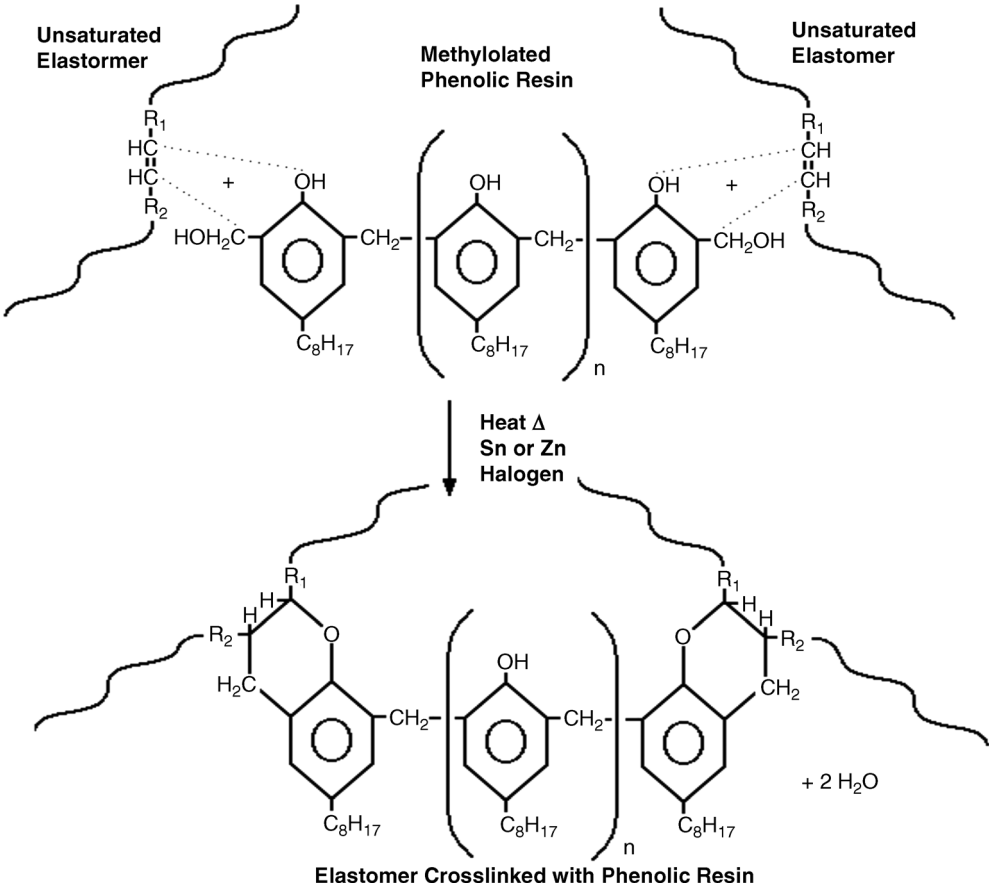

Scheme 3.3

For a thermoset process, the crosslinking agents are compounded with rubbers at a relatively low temperature. After forming a shaped object, they are crosslinked under pressure in an enclosed mold. When selecting a crosslinking system for crosslinking of the rubbers in molten blends with plastics at high temperature, attention should be paid to the thermal stability of the crosslinking agent. For a plastic/rubber blend, the crosslinking agents are added to the molten blend above the plastic melt temperature. Therefore, the crosslinking agent has to have good heat stability at this temperature and a long enough half-life to uniformly disperse through the blend and crosslink the rubber. The quality of the crosslinked blend will depend upon (i) the accuracy and consistency of the feeder delivering the crosslinking agent, (ii) distributive and dispersive distribution of the crosslinking compound in the molten blend, (iii) relative rate of curative mixing to rate of crosslinking reaction, and (iv) the half-life and stability of the crosslinking agent at the blend temperature.

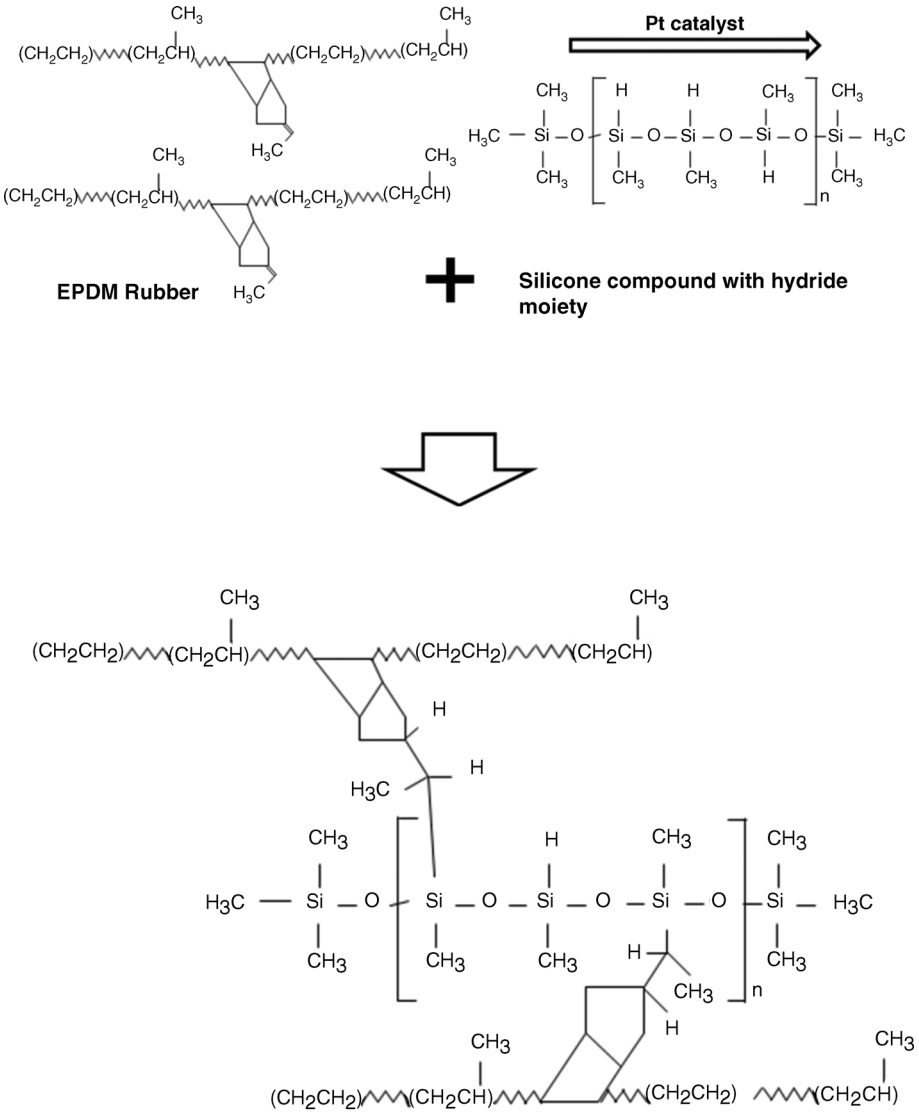
Pt catalyst
EPDM Rubber
Silicone compound with hydride moiety
Crosslinked EPDM Rubber

Scheme 3.4

Table 3.3 Attributes of different crosslinking systems for unsaturated polymers.

Crosslinking system	Attributes
Sulfur	Smell, high compression set, poor processing
Peroxide	Thermoplastic degradation (PP) or crosslinking (PE), low viscosity, good compression set natural color, moisture free
Radiation	Similar to peroxides
Urethane	Smell, slow cure rate, not popular
Phenolic	Very popular, colored, moisture sensitive, good physical properties, good compression set
Silane	Good compression set, natural color, moisture free
Hydrosilation	Good compression set, natural color, moisture free

3.6 Preparation of the Blends of Plastics and Crosslinked Rubbers

There are several ways to prepare such blends:

1) One can start with the plastic/rubber blend from one of the above processes and incorporate a crosslinking agent in the blend in such a way that crosslinking does not occur during this process. The blend is then converted into a desired shape and crosslinked under static conditions. The finished part may have a rubber as a continuous phase, co-continuous phase, or dispersed phase as determined by the relative viscosity and composition of the blend. This is a common procedure for rubber or rubber/rubber blends because they can be melt blended with the crosslinking agents at relatively low temperatures. In case of plastic/rubber blends, the mixing has to be done above the plastic melting point. Very few crosslinking systems have a long enough half-life to prevent premature crosslinking at such temperatures (sulfur/PVI, peroxide with inhibitor [20]). Moreover the rubbery blends with a higher proportion of rubber would be thermosets, and would not process as plastics. For compounds with a low rubber concentration, the rubber will be in a dispersed phase and if crosslinked under static conditions the crosslinked rubber would retain its shape before the onset of the crosslinking reaction.
2) Plastic-forming monomer(s) could be polymerized into a pre-crosslinked rubber latex, suspension, or emulsion. The rubber particles are usually very small. This process is practiced commercially, but is limited to very few blends. ABS (acrylonitrile butadiene styrene terpolymer) is produced by this process [21].
3) Rubber is compounded with appropriate additives and crosslinking agents and crosslinked under static conditions. The crosslinked rubber is then ground and mixed with a plastic. This is a very good method for preparing blends containing crosslinked rubber. Waste thermoset rubber is usually ground and melt blended with plastics to prepare blends. The properties of the plastic-crosslinked rubber blend prepared in this way seem to depend upon particle size [22]. The larger the

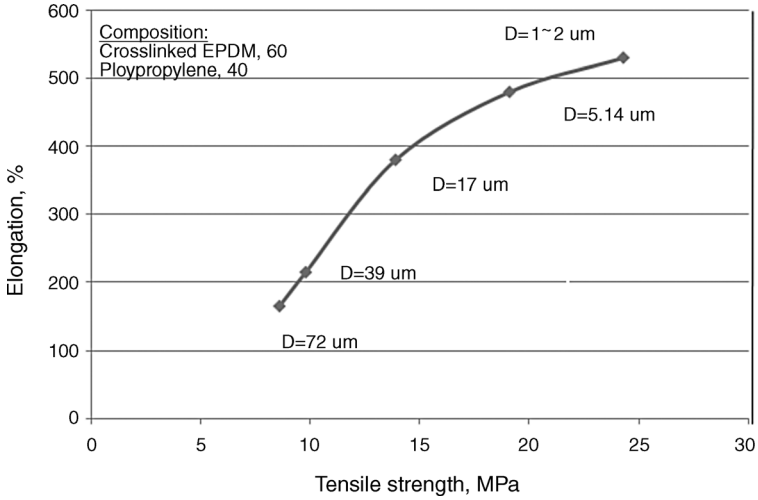

Figure 3.19 Effect of crosslinked rubber particle size on tensile properties.

rubber particles, the lower the tensile properties (Figure 3.19). Most of the ground rubber particles are large and therefore such blends do not have very good mechanical properties. However, these blends could be used in applications that do not require high-performance properties.

4) A preferred way to prepare plastic/crosslinked rubber blend is to add a crosslinking compound(s), during melt mixing of the blend, after the plastic has melted and formed a homogeneous blend with the rubber. Plastic-crosslinked rubber blends prepared in this way have very small crosslinked rubber particles and therefore very good mechanical properties. Moreover, once the crosslinked rubber particle is formed, morphology is stable and particles do not coalesce during subsequent processing steps. The process of crosslinking the rubber, while mixing the molten plastic/rubber blend, is known as dynamic vulcanization. The plastic/rubber blends prepared by this process are often called TPVs (thermoplastic vulcanizate) to distinguish them from physical blend based TPEs (thermoplastic elastomers) and block and graft copolymer based TPEs. Figure 3.20 shows a simplified process concept for crosslinked and non-crosslinked blends.

When the crosslinked rubber level in the blend is high, the blends are rubbery with good elastic recovery properties, have low compression set values at elevated temperatures, and are processable as plastics. At low crosslinked rubber levels (<25%), these blends are tough and have very good impact resistance. Dynamic vulcanization was first practiced by Gessler [23] around 1958, when he described the preparation of halogenated butyl rubber and polypropylene on a heated roll mill. Most of the blends in the examples had only a small amount of rubber (20 wt%) and the curative used was a metal oxide. The mixing time was about 20 min at 320 °F. It was shown that the dynamically vulcanized blends had better tensile properties than identical blends vulcanized at 320 °F under static conditions. Fischer [24] prepared

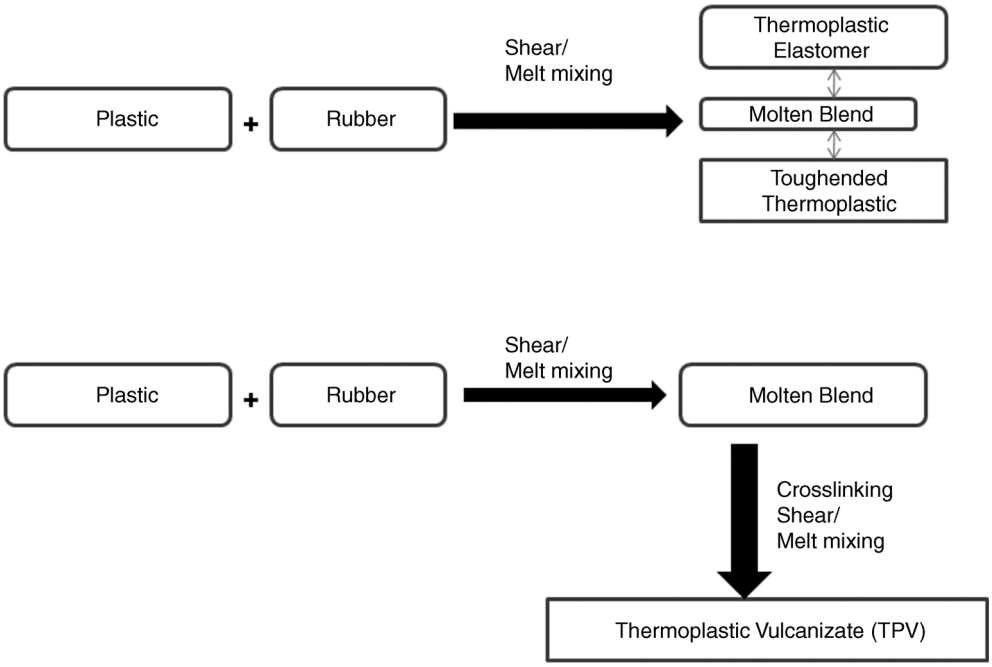

Figure 3.20 Process concept for making blends of plastics and rubbers.

partially crosslinked blends of EPDM and polyolefins (PP, PE (polyethylene)). In one set of compounds, the EPDM rubber was first partially crosslinked in an autoclave under static conditions or on a heated roll mill or a Banbury and then melt-mixed with either PP or PE in the Banbury. In another set of experiments, plastic and rubber was melt-mixed in the Banbury and then dynamically vulcanized by peroxide crosslinking agents. These compounds were commercialized as TPR (thermoplastic rubber) compounds.

Coran and Patel [25] extended the basic dynamic vulcanization technology to produce highly crosslinked TPV compounds and showed that these TPVs have superior rubber-like properties (good elastic recovery, low compression set at elevated temperatures) and very good physical properties and resistance to swelling in hot fluids. Coran and Patel investigated more than 100 different plastic–rubber pairs to correlate TPV properties with their individual blend component properties. Abdou-Sabet and Shen [26] were the first to introduce a commercial continuous TPV process. They showed that polyolefin/EPDM based TPVs prepared with a Lewis acid activated dimethylol phenol crosslinking system had excellent physical properties and fabricability and could be produced on a continuous twin-screw mixer. Based upon their calculations, if a twin-screw mixer, with three lobe kneading elements, operates at 400 rpm, the blend will be turned over about 1200 times per minute. The biggest advantage of the twin-screw mixer was in the preparation of softer blends with excellent fabricability. When they attempted to

prepare these compounds on a Banbury, the physical properties and draw down ratio were not as good as those obtained by the twin-screw continuous process.

In their process, the first third of the mixer was used to melt mix the blend. The curative was added towards the end of the one-third length of the extruder. The other two-thirds of the extruder was used to dynamically crosslink the EPDM/PP blend and perfect the morphology. The processes involved in the preparation of TPV are:

- distribution of different components,
- melting of the plastic phase,
- distribution and inter-dispersion of all the blend components,
- distribution and dispersion of the crosslinker in the blend,
- crosslinking of the rubber phase,
- breaking down of the crosslinked rubber phase into particulate matter under shearing force,
- phase inversion to create dispersed crosslinked phase morphology,
- degassing of the blend,
- pelletization of the blend for further processing.

In the batch process this is a stepwise process. Each of the above steps is completed before the next step. All of this is accomplished simultaneously in different zones along the length of the twin-screw mixer in a continuous process.

3.6.1 Preparation of Plastic and Crosslinked Rubber Blends (TPVs) by a Batch Process

3.6.1.1 Preparation of TPVs in a Brabender

The Brabender torque curve shown in Figure 3.21 [19] is used here for discussion. The blend components and cure activators, such as zinc oxide, stearic acid, and so on, are added to the preheated Brabender while mixing at a desired speed (usually, the rotor speed is 80–120 rpm) and temperature (usually corresponding to the plastic melting point). After about a minute or two, the plastic starts melting and the torque increases, goes through a maximum at time A (Figure 3.21), and then starts to decrease as the plastic continues to melt. Once the plastic is melted and the torque levels off at time X1, a crosslinking agent is added to the blend with continued mixing. Initially, the torque goes down slightly due to a lubricating effect of the liquid crosslinking agent (or solid melting and becoming liquid) but quickly starts to rise as the rubber starts to crosslink. The torque reaches its maximum at time X2 and then starts to decrease slowly as the perfection of phase morphology (breaking of crosslinked rubber particles by shearing forces) continues. Once this is over the torque starts to level off at time X3. At this point, if desired, additional compounds, such as a plasticizer, extender oil, stabilizer, and so on, could be added. Once they are mixed in well, as indicated by a leveled torque, mixing is usually continued for about a minute or two and the plastic vulcanizate (TPV) is removed from the Brabender. It is passed through a roll mill or pressed in a cold press between steel plates to form a sheet. This is then compression molded for testing.

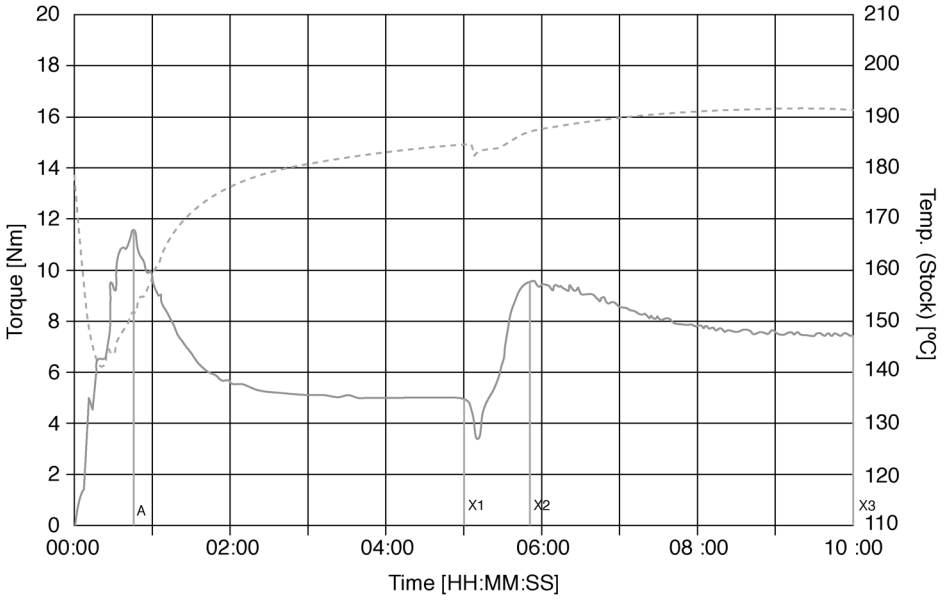

	Time HH:MM:SS 0–X	Time HH:MM:SS X–X	Torque Nm at X	Temp. °C at X	Energy kNm 0– X	Energy kNm X– X	Spec.Energy kNm/kg X– X
A	00:00:46	00:00:46	11.6	153	2.7	0.0	54.8
X1	00:05:00	00:04:14	5.0	185	15.3	12.5	250.3
X2	00:05:50	00:00:50	9.6	187	18.0	2.7	54.2
X3	00:10:00	00:04:50	7.4	191	34.9	17.0	339.6

Figure 3.21 Brabender Plastograph results for TPV preparation by dynamic vulcanization.

3.6.1.2 **Production of TPVs in a Banbury or Similar Batch Processing Equipment**

The process for the batch preparation of TPVs is very similar to the one described above. The process layout for a crosslinked rubber/plastic blend preparation is the same as that for non-crosslinked blends (Figure 3.6). The process steps involved in a plastic-crosslinked rubber blend production by a batch process are:

1) Weigh all the ingredients for a given batch size and combine them together (except crosslinking agents) according to the physical form of the ingredients:
   – rubber as bales, crumbs, or pellets;
   – polymer pellets and other additive pellets;
   – powders, which includes fillers, stabilizers, lubricants, process aids, and so on + activators such as ZnO + stearic acid;
   – curatives, depending upon the cure package, components could be weighed together or separately, for example, for a sulfur crosslinking system:
     a. cure activators: zinc oxide and stearic acid,
     b. accelerators: MBTS + TMTD or other accelerators,
     c. curative: sulfur.

2) Preheat the Banbury.
3) Start the Banbury at medium to high rotor speed.
4) Add rubber followed by powders, cure activators, and extender oil or plasticizer, if desired.
5) Lower the ram and mix for 1 min then lift the ram (this is to prevent a loss of powders during mixing).
6) Add polymer pellets and lower the ram; keep the ram lowered until the plastic is melted.
7) Continue the mixing for about 3–4 min after the plastic is melted.
8) During this time, lift the ram and sweep down around the ram and wall to remove all the accumulated material from the blend, and mix it back with the molten blend; repeat this step as often as necessary so that all the unmixed material is transferred to the Banbury chamber and melt mixed thoroughly with the molten polymer blend.
9) Add the curative package components (each group separately at about 30–60 s intervals) and lower the ram. The torque and the temperature will rise as the crosslinking level increases. The torque will level off and decrease slowly as phase inversion is completed and morphology is perfected. This usually takes about 2–3 min after crosslinking is completed (maximum torque point). During a dynamic vulcanization process, the ram should be lowered and kept there until crosslinking is completed as indicated by torque maximum.
10) At this point one can add plasticizer or extender oil, stabilizers, and so on. When a liquid is added to the blend, the ram should be lowered and kept there until the liquid is mixed in thoroughly. If a liquid is added then mixing should be continued for about 2 min after the liquid is mixed in well with the polymer. This could be monitored by the torque. Initially, the torque will drop due to the lubricating effect of the fluid. Then it will increase and level off as the liquid is dispersed in the polymer blend. This is the indication of completion of the mixing process.
11) The batch is then dropped onto a heated roll mill. From here it is cut into a continuous strip and (i) conveyed on an air-cooled belt to a dicer or (ii) fed to an extruder attached to an underwater pelletizer or a strand die, conveyer belt, and a dicer. If the rubber level is high, then the pellets may stick together. In such instances one can dust the pellets with a small amount of dusting agent.

Notably, after the plastic components are melted, it is very important to control the temperature at a temperature slightly above (~20–30 °F) the melting point of the plastic phase. This is to prevent degradation of the polymers used. Turning off the steam and running hot or cold water through the chamber walls and rotors can accomplish this. If necessary, one can also reduce the rpm of the Banbury. Also, when the blend starts mixing, the torque will rise and will reach a maximum when plastic starts melting. The torque will then gradually decrease and level off. The mixing time is usually taken from the peak time when the plastic starts melting. The batch drop time is usually ~5 min after maximum peak due to crosslinking is reached or 3 min after all the liquids are mixed well with the TPV and torque is leveled off.

3.6.1.3 Production of TPVs by a Continuous Process in a Twin-Screw Mixer

The preparation of TPVs involves chemical reactions and mixing of a crosslinking agent. When TPVs are prepared in a twin-screw mixer, one has to make sure that the crosslinking reaction is complete. The residence time in the twin-screw extruder depends upon several variables, such as:

- throughput rate,
- number of conveying elements,
- number of kneading blocks,
- backward conveying elements,
- backward kneading blocks,
- screw speed,
- higher screw speed – shorter residence time, lower torque, higher melt temperature, and better mixing.

The process lay out will be slightly different to that used for simple non-crosslinked blends. An additional feeder is required to feed a crosslinking agent to the molten blend along the mixer (Figure 3.22).

The rubber, pellets, and powders are fed to the continuous mixer at the feed throat. The plasticizer, extender oil, or any other liquid components are fed downstream, usually at the seventh or eighth barrel. Other solid additives could also be added to the mixer using a top feeder or a side feeder. If the additives have a low melting point, adding them from the top with an auger type of feeder is a better choice.

The crosslinking agents, in a liquid or a solid form, are added to the mixer at the third or fourth barrel. All the volatiles are removed through the vacuum port. If the melt viscosity of the blend is too high, then a melt gear pump may be used to reduce pressure and maintain constant flow of the material. Finally, the molten blend will pass through metal screens with a fine mesh and a heated strand die. The strand could be diced after cooling by air on a conveyer belt or water bath. An underwater pelletizer attached to the die can also pelletize the compound. The production process is usually automated such

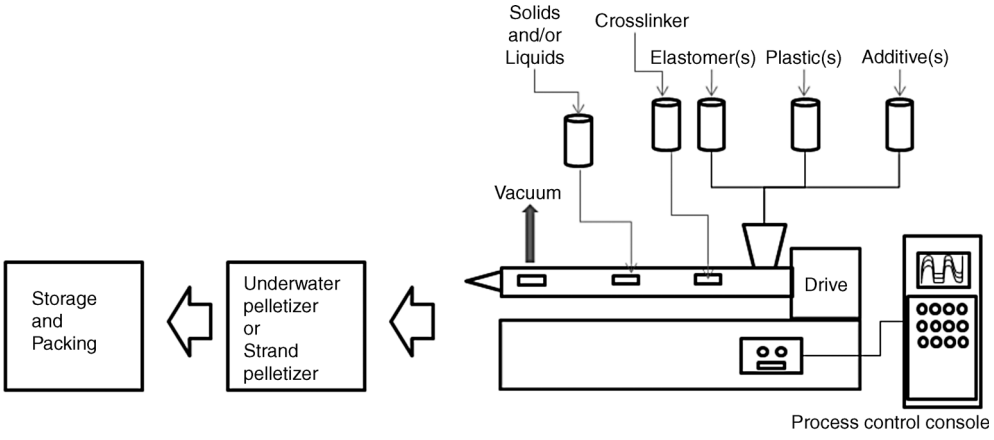

Figure 3.22 Process layout for production of TPVs by a continuous process.

that all the feeders are synchronized with manual override. The screw configuration is selected so as to have the ability to convey, distribute, and disperse the material so that finished compound emerging from the mixer is uniform and consistent.

The steps for the TPV preparation process in a continuous mixer are as follows:

1) If the rubber is in the bale form or large crumb form, it is ground in a rubber grinder. A partitioning agent, usually a small amount of the same filler that is used in the blend formulation, is added to prevent agglomeration of the ground rubber. It is then conveyed to the feeder or storage, from where it is conveyed to the feeder as needed. If the rubber is in either small crumb or pellet form, it is probably dusted and could be conveyed to the feeder directly from the storage. The ground rubber particle or the crumb size is limited to the twin-screw mixers' feed throat opening size and geometry. Larger or coagulated rubber particles will plug up the throat. Care should be taken to avoid this situation.
2) All components in the powder form are pre-weighed in the desired ratio and added to the ribbon blender or other similar mixer and mixed until dispersed uniformly. From here, the blend is conveyed to the feeder as needed. It is important to ensure uniform distribution of all the blend components for a consistent TPV.
3) All components in the pellet form are pre-weighed in the desired ratio and added to the ribbon blender or other similar mixer and mixed until dispersed uniformly. From here, the blend is conveyed to the feeder as needed.
4) The crosslinking agent is fed to the extruder with a separate feeder. It is not mixed with blend for feeder #1, #2, and #3. Set the desired barrel temperatures. (Barrel #1 is usually not heated to prevent material from sticking in the feed zone.)
5) Transfer the rubber, pellets, powders, liquids, additives, and crosslinker to appropriate feeders.
6) Start the extruder at a higher screw speed than normally used in the steady state operation.
7) Start the main feeders to feed the blend components and wait until the molten polymer blend starts to come out of the diverter tube.
8) Start the feeder for the crosslinking agent.
9) Start liquid and additive feeders as needed.
10) About 10 min after starting the crosslinker feeder, close the diverter valve and pass the molten polymer blend to the die and pelletizer.
11) Reduce the screw rpm to an appropriate level for steady state operation.
12) Usually after about an initial 5–10 min period, the pelletized blend is conveyed to the storage or bagged using an automatic bagger.

3.7
Blends of Plastics and Crosslinked Rubbers by Dynamic Vulcanization

When a rubber is crosslinked in the absence of a plastic, as the degree of crosslinking in the rubber increases the viscosity increases and eventually it becomes a thermoset that will not flow at all or melt at higher temperatures. In rubber/plastic blends, when

rubber is crosslinked, if the rubber phase is a continuous phase, then upon crosslinking under static conditions it will form a continuous network and will be a thermoset with the plastic acting as dispersed filler. Such a blend will not be melt processable. If both rubber and plastic are co-continuous phases before crosslinking, then under static crosslinking conditions the blend will form an interpenetrating network [27]. If, on the other hand, when rubber is a minor portion and a dispersed phase before crosslinking, then it will remain a dispersed phase after crosslinking and the crosslinked blend will be processable upon melting of the plastic phase. The particle size of the dispersed phase will depend upon the starting phase morphology before onset of the crosslinking reaction.

Now, in rubber/plastic blends, when crosslinking is carried out under dynamic conditions, while the blend is being melt mixed, as before the rubber viscosity will increase as the degree of crosslinking increases, but the plastic phase viscosity will remain essentially unchanged. Since this happens under continuous shear, the crosslinked rubber phase breaks down into small particles and disperses in the plastic matrix (dispersed or continuous at start). Thus, irrespective of initial plastic phase form, the plastic will always be a continuous phase in the end product, and, as a result, the plastic/crosslinked rubber blend will flow above the plastic melting point and process like a plastic. The particulate rubber morphology present in TPVs is shown by SEM micrographs in Figure 3.23 [4]. Even when rubber concentration is as high as 80 wt%, and the rubber forms a continuous phase before crosslinking, the rubber breaks down into small particles during the crosslinking process. As shown in Figure 3.17, the initial blend morphology for non-crosslinked rubber blends depended upon the relative proportions of the blend components. It varied from a continuous rubber phase for high rubber containing blend to co-continuous for a 50 : 50 blend to a dispersed rubber phase for a low rubber blend. When these blends were vulcanized

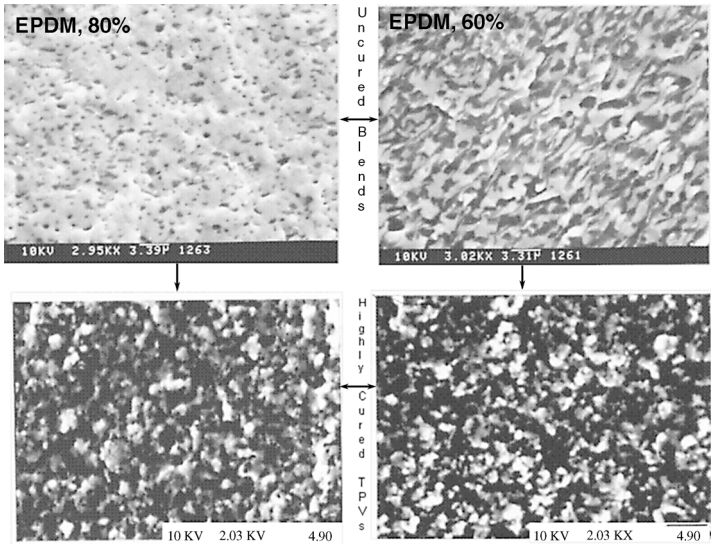

Figure 3.23 SEM micrographs showing the blend morphology at different elastomer (EPDM) concentrations for physical blends (upper) and highly crosslinked TPVs (lower).

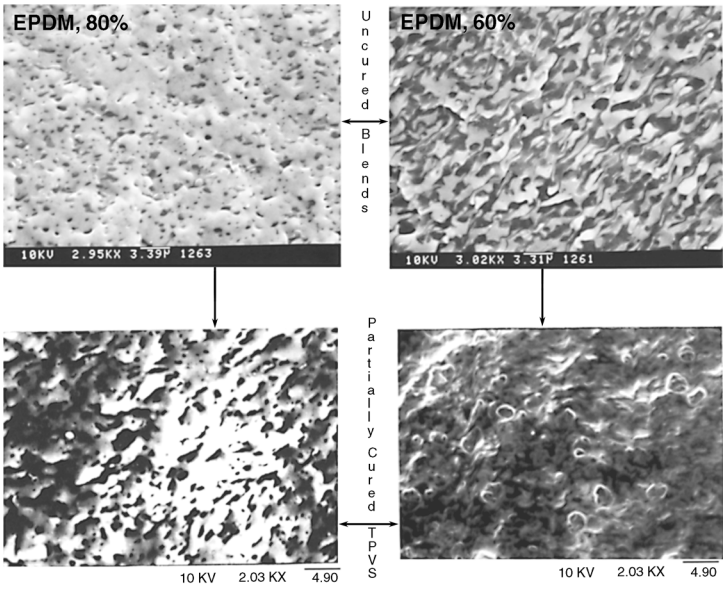

Figure 3.24 SEM micrographs showing the blend morphology at different rubber (EPDM) concentrations for physical blends (upper) and partially crosslinked TPVs (lower).

under dynamic conditions, phase inversion occurred during the vulcanization process and the crosslinked rubber turned into a dispersed phase.

Notably, however, if there is not enough plastic phase to fill all the voids among rubber particles then even though the plastic phase is a continuous phase it will not be a totally continuous phase and the resulting blend will have a very poor flow. From the known particle shape and size distribution, one can easily estimate the free volume in the rubber phase. The actual plastic concentration required to maintain plastic flow will be a few percentage points higher than this volume.

When the crosslinking level is low, the rubber viscosity may increase, but not be high enough for rubber to break down. In such cases the rubber remains a continuous phase and the morphology is not well defined (Figure 3.24) [4].

Table 3.4 gives the properties of EPDM/PP TPVs prepared with different cure systems. As shown, there is substantial improvement in tensile properties and tension set over uncured physical blends for all the crosslinked TPVs.

TPV technology has been practiced for the last 40 years. Nonetheless, new TPVs and their applications are still appearing at a fairly good pace.

3.8
Compatibilization and Compatibilized Blends

If the components are incompatible, then one can use an appropriate compatibilizer to enhance the morphology and properties of such blends. Figure 3.25 shows an idealized compatibilizer.

Table 3.4 Properties of EPDM/PP TPVs[a)] prepared by different crosslinking compounds.

Crosslinking system	None	Peroxide/ co-agent	Sulfur	Phenolic resin	Hydrosilation
Hardness (Shore D)	32	39	42	40	40
M100 (strength at 100% strain) (MPa)	4.8	8.1	8	7.5	—
Tensile strength (MPa)	4.9	16.0	24.3	23.6	17.2
Elongation (%)	190	450	490	430	410
Tension set (%)	66	—	16	15	22
Moisture pick up	No	No	No	Yes	No
Color of TPV	Natural	Natural	Yellowish light red	Yellowish	Natural
Melt stagnation	No	No	Yes	No	No
Fabricability	Good	Good	Good	Good	Good

a) Note: all compositions had 60% EPDM, 40% PP, and curatives as noted.

The compatibilizer is a block or a graft copolymer. One segment of this block/graft copolymer is miscible with one component of the blend, while the other segment is miscible with the other component of the blend. During the melt mixing process, the compatibilizer becomes located at the interface of these immiscible polymers and improves the adhesion between the two phases.

The compatibilizer can be prepared by polymerization of one monomer, followed by a second monomer. One can also polymerize monomers on a polymer backbone to form a graft copolymer. The formation of a graft or block copolymer can be made possible in the reactors or by chemical modifications of the polymers so that they will

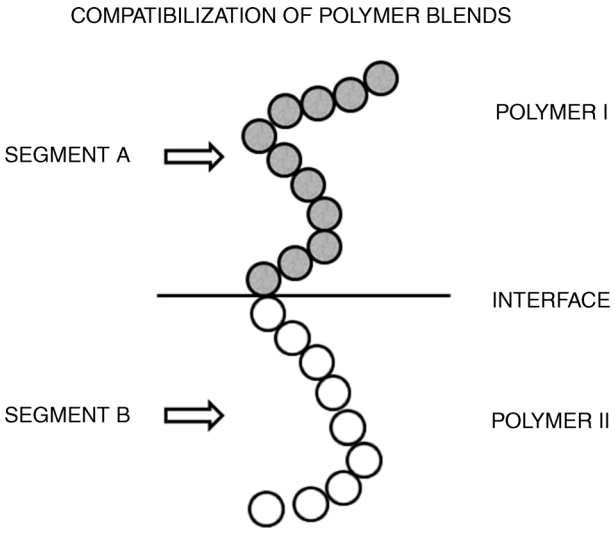

Figure 3.25 Idealized compatibilizing block copolymer.

react with each other directly or through other bifunctional bridging compounds. For a polyamide/EPDM blend, the compatibilizer will consist of a block or graft copolymer in which some of the segments are compatible with polyamide and the other segments are compatible with EPDM.

3.8.1 Preparation of a Compatibilizer

Compatibilizer preparations are needed for use with a polypropylene and NBR/HNBR blend, the components of which are grossly incompatible [7]. This could be a one-step process if one starts with commercially available maleic anhydride (MA) modified polypropylene and amine-terminated nitrile rubber. Then one can melt mix the above functionalized polymers in a batch or a continuous mixer and prepare the compatibilizer, as shown in step 2 below. One can also modify the polypropylene as described below in step 1, and use it to prepare the compatibilizer.

Polypropylene is melt mixed with an organic peroxide and maleic anhydride using a Brabender, Banbury, or twin-screw mixer to graft anhydride functionality on the polymer. The components could be blended together and fed to either a batch mixer or continuous mixer or the polymer is melted first and then the maleic anhydride and peroxide are added in that order. The unreacted maleic anhydride is removed before use.

Step 1: PP + MA → PP-MA (Scheme 3.5):

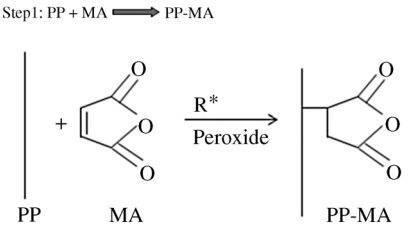

Scheme 3.5

Maleic anhydride modified polypropylene is then melt-mixed with secondary amine-terminated nitrile rubber (NHR-NBR, known as ATBN) to form a graft copolymer containing nitrile rubber (NBR) segments and polypropylene (PP) segments.

Step 2: PP-MA + NHR NBR → PP-NBR block copolymer (Scheme 3.6):

One can also prepare the block copolymer compatibilizer from two functionalized polymers that do not react with each other. In such instances two functionalized polymers are melt mixed with a bifunctional bridging compound that will react with both the groups (Scheme 3.7).

The PP segment of this compatibilizer will be compatible with PP or any other polymer that is compatible with polypropylene and the NBR segment will be

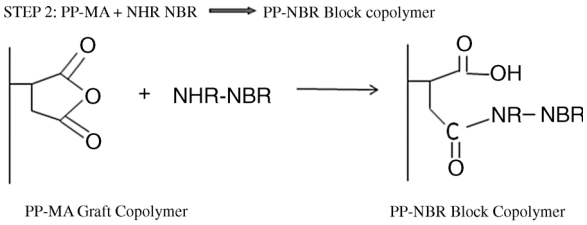

Scheme 3.6

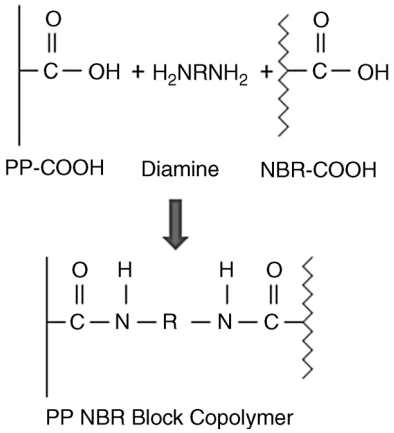

Scheme 3.7

compatible with NBR, HNBR, or any other polymer that is compatible with NBR. A similar process could be used to prepare compatibilizers from other polymer pairs or polymers with different functional groups.

The compatibilizer can be prepared first and melt blended with the polymer blend or it can be produced *in situ* during melt mixing of the blend. The compatibilizer composition will depend upon the polymer pair that is being compatibilized.

3.8.2 Production of Compatibilized Blends

The procedure for blend preparation with and without crosslinking the rubber phase is the same as that described above for the technologically compatible blends. Here the blends will contain a compatibilizer in addition to the other blend ingredients.

3.8.3 Compatibilized Blends

Only a small amount of compatibilizer is required to improve the blend properties. Compositions of NBR-PP were compatibilized with a block copolymer prepared from maleic anhydride (MA) modified PP (MPP) and secondary amine terminated liquid

Table 3.5 Effect of a compatibilizer (%) on tensile properties of NBR/PP TPVs.

	Recipe				
	1	**2**	**3**	**4**	**5**
Polypropylene	50	45	45	45	45
NBR	50	50	49.9	49.4	48.8
MA modified PP	0	5	5	5	5
ATBN (amine terminated liquid NBR)	0	0	0.1	0.6	1.2
SP-1045 phenolic resin	3.75	3.75	3.75	3.75	3.75
Stannous chloride	0.5	0.5	0.5	0.5	0.5
Tensile strength (MPa)	8.8	12	12.4	15.2	25.5
Elongation (%)	91	110	170	290	440

nitrile rubber (ATBN). As shown in Table 3.5, improvements in tensile properties of NBR/PP TPVs are realized even at a very low concentration of ATBN (0.1%). As the amount of ATBN is increased, there was a substantial (about threefold) increase in tensile properties (compare recipes #1 to # 5).

In another set of experiments, ethylene methacrylate acid terpolymer (Vamac®) was mixed with PP and MPP. The rubber was then crosslinked with the crosslinking agent also acting as a bridging compound to form a compatibilizer between the acid-terpolymer and MPP. Several experiments were carried out by varying the rubber to plastic ratio and the level of MPP. The results are shown in Figure 3.26 [6], where true

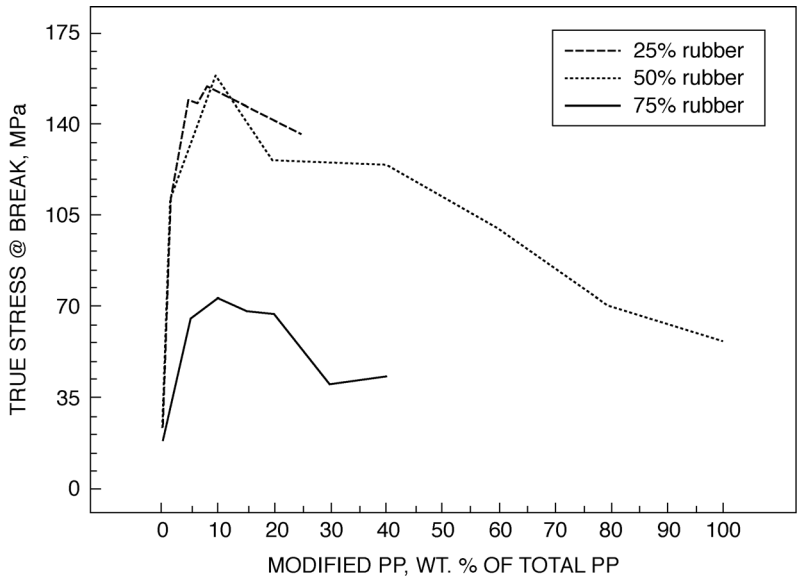

Figure 3.26 Effect of compatibilizer level on the true stress at break for acrylic rubber/PP TPVs.

stress at break (tensile strength × extension ratio) versus MPP is plotted. In all three sets of experiments, there was a marked increase in the tensile strength with increasing MPP, up to a maximum at ~10% MPP. The tensile strength then decreased at higher levels of MPP.

The compatibilization technique has been used successfully in preparing EPDM/polyamide and polyester blends, silicone rubber and polyamide blends, and blends of two dissimilar TPVs [25, 28–30].

3.9
Processing of Plastic/Rubber Blends

3.9.1
General

A thermoplastic elastomer (TPE) has elastic properties similar to conventional thermoset rubber, and also the processability and recyclability of a thermoplastic. Processing of a conventional thermoset rubber involves several steps, takes longer time to produce finished parts, and the scrap and defective parts generated along the way are not processable. A typical vulcanization time for a passenger tire is 10 min at 170 °C [31]. To make final products from thermoset rubbers takes long time. The rubber is difficult to process due to viscous and elastic properties in both the raw and the compounded state [32]. Figure 3.27 shows the schematic processing steps of both TPEs and typical thermoset rubber. Unlike the thermoset rubber, TPEs turn into a fluid upon heating and then solidify upon cooling, just like thermoplastics. This reversible process gives manufacturers the ability to produce various rubber-like TPE products in a short cycle time [33].

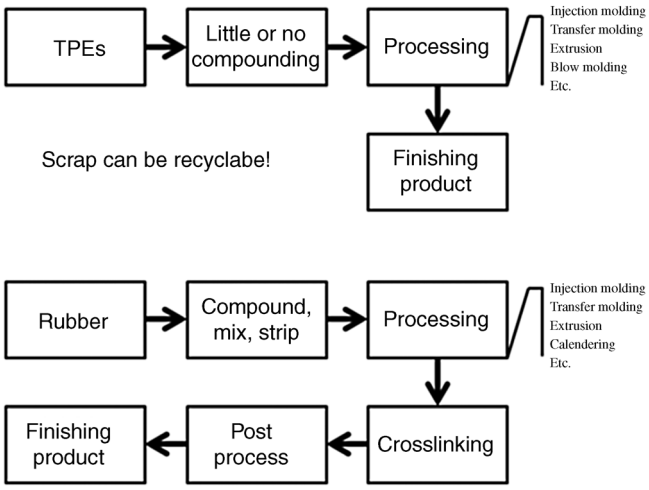

Figure 3.27 Processing steps for typical thermoset rubbers and TPEs.

The major benefits of TPEs are:

+ fast cycle times,
+ little or no compounding,
+ ease of processing,
+ ability to form complex parts,
+ consistent quality,
+ lower plant maintenance and low initial investment,
+ ability to add various additives, colorants, and so on during finishing operation (molding, extrusion),
+ adaptable to robotic operation,
+ ability to bond to other polymers and metals,
+ low inventory of materials,
+ cleaner process and plants,
+ recyclability of scrap,
+ economical,
+ custom tailored end-use properties and processing.

The disadvantages of TPEs/TPVs are:

– upper temperature is limited by the plastic melt temperature,
– limited creep resistance,
– often requires drying.

Rader and Richwine have [34] identified various processing methods and advantages of TPEs over thermoset rubber. Two of the most important advantages of TPEs are the economics and ability to produce complex parts.

Kear [35] estimated that the typical conventional thermoset process takes around 2–6 times longer and the total non-recyclable scrap is 10–50%. In contrast, the TPE scrap is usually 2–5% and is recyclable

The three major types of TPEs are block copolymers such as SEBS (styrene–ethylene–butylene–styrene block copolymer) (Kraton® by Kraton Polymer), polyether–-polyester (Hytrel® by DuPont), rubber/plastic blends (900 series Sumitomo Chemical), and dynamically vulcanized rubber/plastic alloys (Innoprene® by Kumho Polychem, Santoprene® by Exxon-Mobil, Sarlink® by DSM, Unipene® by Teknor Apex). Figure 3.28 shows the cost versus general performance comparison for different TPEs [31].

3.9.2 Injection Molding

Injection molding of TPEs is generally by melt processing methods used for thermoplastics. Owing to the recyclability of TPEs many injection molders adopt a hot runner system. This hot runner system generates a very small amount of scrap. The process has a relatively short cycle time and parts have better dimensional stability [36, 37]. Another special feature of TPE is over-molding to a hard thermoplastic substrate to add a "soft touch." Unlike bonding between hard thermoplastic and soft thermoset rubber, TPE over-molding eliminates the use of

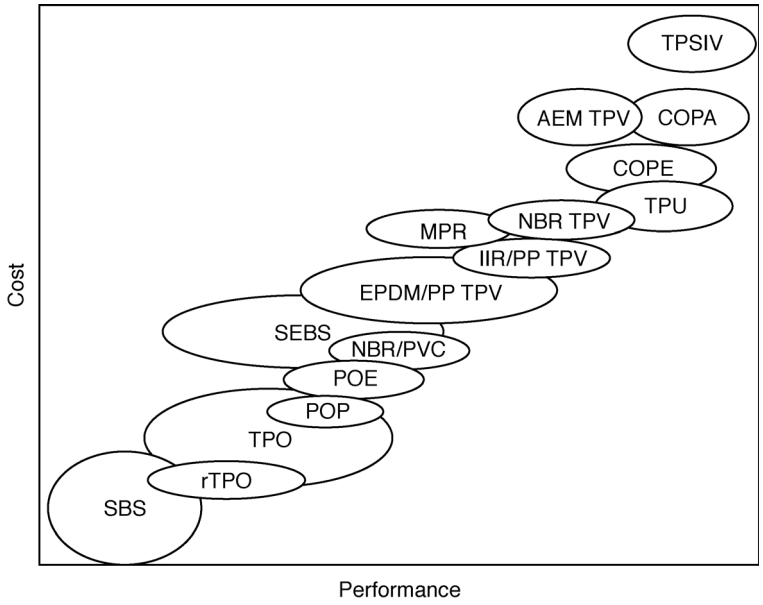

Figure 3.28 Cost versus general performance comparison for different TPEs.

chemical adhesive. For successful over-molding, proper gate size/location, flow length, and venting with mechanical interlocking (Figure 3.29) are the essential considerations.

The proper gate size/location can be determined by CAE (computer aided engineering) such as Moldflow®. The vents can be placed where the weld lines occur and the last area to be filled.

A standard injection molding machine equipped with typical reciprocating screw and barrel capacity of six or less shots can be utilized for over molding. A reciprocating screw generally delivers quick color change and provides smooth TPE

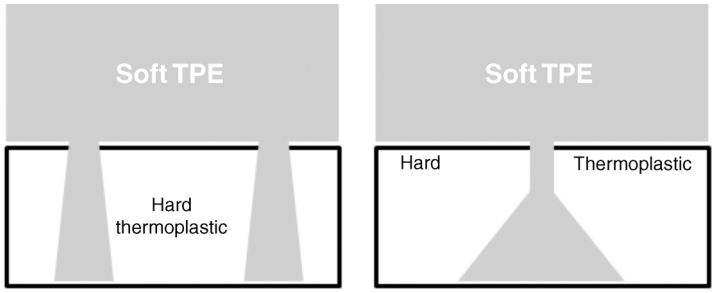

Depth: 0.0127 ~ 0.035 mm
- Land: 10 ~ 15 mm
- Land depth: 1.5 mm and over

Figure 3.29 Examples of mechanical interlocking.

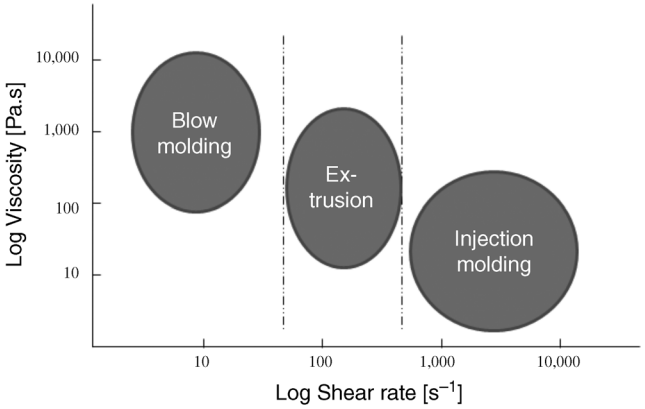

Figure 3.30 Typical process range of viscosity and shear rate ranges.

material processing. The general clamping force needed for a molding machine is 750 kg cm^{-2} of the projected area of parts. The typical shear rate range for TPE molding is around from 800 to 15 000 s^{-1} with a preferred viscosity range under 1000 Pa s. Figure 3.30 shows the viscosity requirement range for different processes. TPEs are shear responsive and the viscosity is reduced when they are processed at high shear rates, which is known as non-Newtonian behavior. This is particularly good for filling thin walled sections commonly encountered in TPE over-molding.

Understanding of melt flow is essential for success of a molding process. The viscosity of TPEs is much less sensitive to a change of barrel temperatures (Figure 3.31).

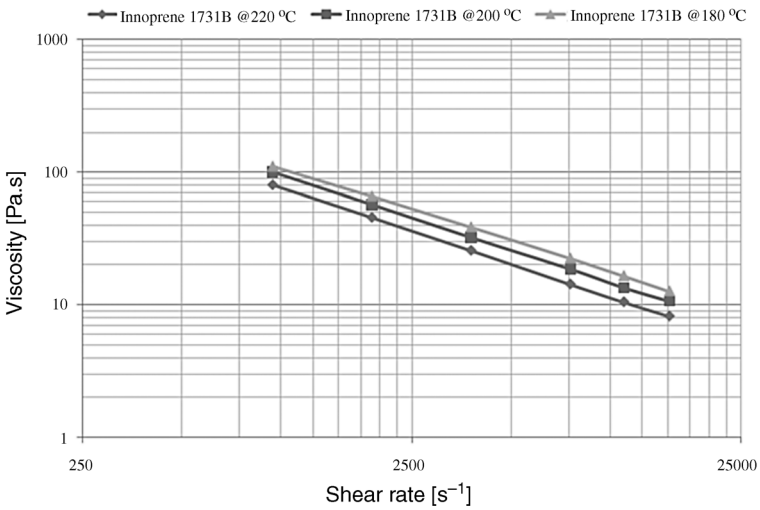

Figure 3.31 Flow curve of a typical TPE. Courtesy of Kumho Polychem.

Table 3.6 Typical start up conditions for various TPEs.

		SEBS	TPU (thermoplastic urethane)	COPE (polyether-polyester block copolymer)	TPO (thermo plastic olefin)/ TPV
Zone (°C)	Nozzle	200–220	190–210	220–250	210–230
	Front	180–200	170–190	210–240	200–220
	Center	170–190	160–180	190–220	190–210
	Rear	160–180	160–170	180–200	170–200
Injection time (s)		0.5–2	0.5–2	0.5–2	0.5–2
Pack/hold time (s)		1–15	1–15	1–15	1–15
Pack/hold pressure (%)		80% of fill pressure	80% of fill pressure	80% of fill pressure	80% of fill pressure
Mold temperature (°C)		45–55	25–70	25–55	10–50

This is the major difference between thermoplastics such as PP and Nylon, where flow of the material is more sensitive to conductive heat rather than shear rate or injection speed and pressure.

Tables 3.6 and 3.7 show, respectively, injection molding conditions and a trouble-shooting guide for various TPEs. However, one should contact the material supplier to obtain detailed information for the process.

3.9.3 Extrusion

Just like the injection molding machine, only thermoplastic processing equipment is recommended for TPE extrusion. In addition, TPE extrusion does not require a final vulcanization or crosslinking (curing) step. It only requires rapid cooling of extrudate to room temperature. There are some differences between thermoset rubber and thermoplastic extruders [38–43]. These are:

- feed section design due to the characteristics of material (strip or pellet),
- reduced L/D due to the high heat generation of thermoset rubber (24/1 or less for thermoset rubber),
- screw design due to shearing,
- heating and cooling due to high viscosity of thermoset rubber.

The recommended screw L/D for TPE is 30/1 with the compression ratio of 3 : 1. Mixing elements such as the Union Carbide mixing section invented by LeRoy [44] ensures good dispersion of color concentrates and improves melt uniformity. To distribute additives such as color concentrates, ultraviolet (UV) stabilizers in the TPEs, distributive mixing elements such as Pineapple, Dulmage, or Saxon mixing sections are recommended. Figure 3.32 shows dispersive and distributive mixing elements.

Table 3.7 Trouble shooting injection molding defects.

		Possible remedy	
Trouble	**Variables**	**Increase**	**Decrease**
Flash	Machine	3. Clamp pressure	1. Injection pressure 2.Melt temperature 4. Hold time 5. Back pressure 6. Injection speed 7. Mold temperature
	Mold	Check the size of vent	
Sink mark	Machine	1. Shot size 2. Injection pressure 4. Holding pressure 6. Injection speed 7. Back pressure 8. Screw speed	3. Mold temperature 5. Melt temperature
	Mold	Check the size of gate, sprue, and runner	
Short shot	Machine	1. Shot size 2. Injection pressure 3. Melt temperature 4. Mold temperature 7. Back pressure 8. Holding time	
	Mold	Check the size of vent, gate, sprue, and runner	
Shrinkage	Machine	1. Cooling time 5. Mold temperature	2. Melt temperature
	Mold	Check the temperature distribution of the cavity	
Part sticking	Machine	3. Cooling lime	1. Injection pressure 2. Holding pressure 4. Mold temperature 5. Holding time 6. Injection speed
	Mold	Check the size of vent, gate, sprue, and runner	
Warping	Machine	1. Cooling time 2. Holding time 3. Holding pressure	4. Injection pressure 5. Injection speed
	Mold	Check the size of gate	

Dispersive mixing can be achieved with mixing elements or with specially designed dual flighted barrier screws. The latter devices are used to help homogenize the melt. This is particularly important for thin film and profile extrusion. In these devices, one or more barrier flights are placed along the screw such that the material must flow over the barrier flights. In clearing the barrier the material is subjected to a high shear rate; the corresponding shear stress should be large enough to break down

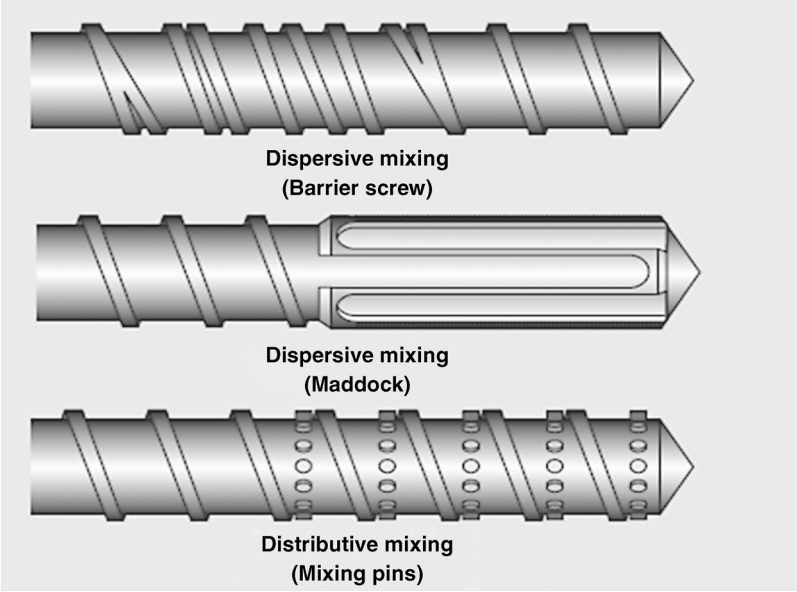

Figure 3.32 Dispersive and distributive mixing elements.

the particles in the polymer melt. A drawback of this mixing device is that it generates pressure, which can increase melt temperature. Dispersive mixing elements that have been used to process TPE with good results are Maddock, Maillefer, Egan sections, and blister rings.

Optimization of output for a given screw diameter is an important objective to deliver the largest amount of output at acceptable melt quality. As output goes up, residence time goes down and with it the time available for mixing the polymer melt. As a result, the mixing quality goes down when the output increases. However, the mixing quality can be improved by incorporating a mixing section as depicted in Figure 3.32. Output depends on several variables [45]:

- screw speed
- screw configuration
- pressure gradients
- temperature profile
- melt viscosity of TPE.

General recommendations for die design of TPEs are:

- flow balance of die to achieve constant linear exit velocity,
- enough land to avoid higher die swell due to elastic recovery,
- no decompression zones in the die,
- diverging channels angle should be less than 30°,
- minimum radius at sharp corners should be 0.2 mm.

3.10 Conclusions and Outlook

Plastic/rubber blends offer a way to combine the best of both worlds – the softness and elasticity of rubber and the processability of thermoplastic. As discussed in this chapter, there are several methods for the preparation of plastic/rubber blends. Physical melt mixing of the plastics and rubbers provides a simple, quick, and most economical way of producing such blends. One can also prepare multicomponent and specialty blends by this procedure. Both Banbury batch mixers and twin-screw mixers are used to produce these blends. Most physical blends are now prepared by this melt-mixing process.

These blends are used in many different applications in automotive, construction, wire and cable, and consumer goods. Styrenic block copolymer/polyolefin blends are the most popular and more than 60% of all blends produced contain styrenic block copolymers.

Most TPV work is done with twin-screw mixers. A batch process is rarely used for this purpose. In early 1970s dynamically vulcanized rubber/plastic blends (TPVs) were introduced onto the market under the trade name TPR®. They contain partially crosslinked rubber. In the late 1970s highly crosslinked rubber/plastic blends were introduced under the trade name Santoprene®. Highly crosslinked rubber based TPVs offer many advantages over physical blends and partially crosslinked blends, such as very low compression set and oil swell at elevated temperatures, good elastic recovery, and very good resistance to flex cracking. In initial TPVs, rubber was crosslinked with sulfur-based curatives. The properties were very good but the TPV had a typical sulfur smell. Then, very quickly the phenolic resin was used to replace sulfur [46]. Phenolic resin based TPVs have moisture issues and the TPVs have a light yellow color. In the 1990s hydrosilation-based curatives were used to complement phenolic curative [19]. The silicone-based TPVs have no color, odor, or moisture issues but are expensive, because the process uses an expensive catalyst such as a platinum complex or similar noble metal based complex.

Initially, there were only two to three major TPV producers. Now there are more than two dozen TPV producers and the list is growing. TPVs based on crosslinked EPDM/polypropylene have about 90% of the market share and it will stay that way in the near future. The product portfolio with other high-performance TPVs is also expanding. Dow-Corning has introduced plastic-crosslinked silicone rubber based TPVs under the trade name TPSIV® (Dow-Corning, Midland, MI, USA). Zion Chemical has developed polyamide-acrylate rubber based TPVs that are marketed under the trade name Zeotherm® (Zeon Chemicals, Louisville, KY, USA), and DuPont has introduced the ETPV product line (DuPont Engineering Polymers, Wilmington, DE, USA). Most of these TPVs are targeted for high temperature use in under-the-hood automotive applications. On the general purpose TPV side, Teknor Apex has introduced a TPV product line based on crosslinked styrenic block copolymer/polyolefin blends. In this particular product line both the soft rubber and hard styrenic blocks are crosslinked by a dynamic vulcanization process. It was shown that these TPVs retain a better compression set

when exposed to higher temperature over an extended time (Teknor Apex Company, Pawtucket, RI, USA).

TPVs can be processed by many different processing techniques used for thermoplastics, such as extrusion, injection molding, blow molding, slush molding and foaming. They are used in many industrial segments such as automotive, building and construction, medical and consumer goods.

Most curatives were developed for thermoset rubber goods. They have a very short half-life at higher temperatures. The stabilizers protect polymers but are also volatile at high temperatures. There is an opportunity and need for high-temperature stable curatives and stabilizers for the TPV industry. On the equipment side, newer mixing elements have been developed that improve mixing. Work on this side needs to continue to produce highly efficient mixing elements that generate a lower amount of heat. In addition, the equipment design should focus on higher quantity of heat removal from the mixer.

The first blend was invented in 1942. Ever since then numerous blends have been identified and used in many applications. With the development of dynamic vulcanization technology, plastic-rubber based TPVs have replaced thermoset rubber in many applications and generated many new applications on its own merits. The technology and usefulness of these TPV compounds will expand to an even higher level with the recent introduction of high-performance blends (Dow-Corning, Zeon Chemicals, DuPont Engineering Polymers, Teknor Apex Company). More blends and TPVs will be introduced in the future to meet the growing need for specialty polymers.

Abbreviations and Symbols

ABS	acrylnitrile butadiene styrene terpolymer
ATBN	amine terminated liquid nitrile rubber (amine group is a secondary amine)
BR	butadiene rubber
COPE	polyether-polyester block copolymer
CPE	chlorinated polyethylene
EPDM	ethylene – propylene diene terpolymer rubber
EPR	ethylene – propylene rubber
EVA	ethylene vinyl acetate
HNBR	hydrogenated nitrile rubber
IIR	butyl rubber
L/D	length over diameter
M100	strength at 100% strain
MA	maleic anhydride
MBS	N-(oxidiethylene)-2-benzothiazolyl sulfenamide
MBT	2-mercapto benzothiazole
MBTS	dibenzothiazyl disulfide
MPP	maleic anhydride modified polypropylene

NBR	nitrile rubber (acrylonitrile-butadiene copolymer)
NHR-NBR	secondary amine terminated nitrile rubber
NR	natural rubber
PE	polyethylene
PP	polypropylene
PVI	pre vulcanisation inhibitor
PVC	polyvinylchloride
R′OOR″	peroxide
R′O•, R″O•	radicals
SEBS	styrene ethylene butylene styrene block copolymer
SBR	styrene butadiene rubber
T_g	glass transition temperature
TMTD	tetramethylthiuram disulfide
TPE	thermoplastic elastomer
TPO	thermoplastic olefin
TPR	thermoplastic rubber
TPU	thermoplastic urethane
TPV	thermoplastic vulcanizate
UV	ultraviolet
ZnO	zinc oxide

References

1 Badum, E. (1942) US Patent 2297194.
2 Paul, D.R. (1985) Polymer blends. Phase behavior & property relationship; in *Multicomponent Polymeric Materials* (Eds D.R. Paul, L.H. Sperling), *Advances in Chemistry Series,* # 211, American Chemical Society, Washington D.C., pp. 3–19.
3 Sperling, L.H. (1985) Recent developments in interpenetrating polymer networks and related material; in *Multicomponent Polymeric Materials, Advances in Chemistry Series,* # 211, American Chemical Society, Washington D.C., pp. 21–56; 153–170.
4 Abdou-sabet, S. and Patel, R. (1990) paper presented at ACS, Rubber Division meeting, Washington D.C. (October 9–12, 1990).
5 Coran, A.Y. and Patel, R. (1981) US Patent 4299931;Coran, A.Y. and Patel, R. (1982) US Patent 04338413.
6 Patel, R. (1985) US Patent 04555546; Patel, R. (1987) US Patent 04654402.
7 Coran, A.Y. and Patel, R. (1983) *Rubber Chem. Technol.*, **56**, 1045.
8 Paul, D.R. (1978) *Polymer Blends,* vol. 2 (eds D.R. Paul and S. Newman) Academic Press, New York, p. 35.
9 Gaylord, N.G. (1975) *Adv. Chem. Ser.*, **142**, 76.
10 Corish, P.J. and Powell, D.W. (1974) *Rubber Chem. Technol.*, **47**, 481; Gessner, B.D. (1969) *Encyclopedia of Polymer Science and Technology,* vol. 10 (eds H.F. Mark and N.G. Gaylord), Interscience Publishers, New York.
11 (June 1998) Twin Screw Extrusion Work shop, American Leistritz Extruder Corporation, Somerville, NJ 08876.
12 Palmgren, H. (1975) *Rubber Chem. Technol.*, **48**, 1045.
13 Lim, S. and White, J.L. (1993) *Int. Polym. Process.*, **8**, 119.
14 White, J.L. and Min, K. (1987) Presented at the European Symposium on Polymer Blends, Strasbourg (France) May 25.
15 Kresge, E.N. (2004) in Polyolefin Based Thermoplastic Elastomers. *Thermoplastic Elastomers,* 3rd edn (eds G. Holden, H.R. Kricheldorf, and R.P. Quirk), Hanser Publication, Munich., pp. 93–117.

16 Epstein, B.N. (1979) US Patent 4172859; Epstein, B.N. (1979) US Patent 04174358.
17 Fedke, M. (1985) Reaktionen an Polymeren VEB DT Verlag für Grund stoffindustrie, Leipzig. P.R. Dluzeneski, (2001) *Rubber Chem. Technol.* 74, 451.
18 SI Group presentation Products for the rubber industry, SI Group Inc., Schenectady, NY, USA.
19 Medsker, R.E. and Patel, R. (1997) US Patent 05672660.
20 Keromnes, L., Defrancisci, A., Prebe, A. and Palys, H. (2005) Paper presented at ACS, Rubber Division Meeting, Pittsburgh, PA (Nov 1-3-2005)
21 Kruse, R.L. (1976) US Patent 4206293; Cincerl, D.L. (1976) US Patent 3957912.
22 Coran, A.Y. and Patel, R. (1979) *Rubber Chem. Technol.*, **53**, 141.
23 Gessler, A.M. (1962) US Patent 3037954.
24 Fischer, W.K. (1973) US Patent 3758643; Fischer, W.K. (1974) US Patent 3806558.
25 Coran, A.Y., Das, B., and Patel, R.P. (1978) US Patent 4130535;Coran, A.Y. and Patel, R.P. (2004) Thermoplastic elastomers based on dynamically vulcanized elastomer thermoplastic blends. *Thermoplastic Elastomers,* 3rd edn (eds G. Holden, H.R. Kricheldorf, and R.P. Quirk), Hanser Publication, Munich, pp. 143–181.
26 Abdou-Sabet, S. and Shen, K.-S. (1986) US Patent 4594390.
27 Sperling, L.H. (2004) Thermoplastic interpenetrating networks. *Thermoplastic Elastomers,* 3rd edn (eds G. Holden, H.R. Kricheldorf, and R.P. Quirk), Hanser Publication, Munich, pp. 431–441.
28 Datta, S. and Lohse, D.J. (1996) *Polymeric Compatibilizers,* Hanser Gardner Publication, Munich.
29 Dekkers, M.E.J. and Moffett, A.J. (1993) US Patent 05208287;Moffett, A.J. and Dekkers, M.E.J. (1993) US Patent 05272206.
30 Brewer, C.M., Chorvath, I., Fournier, F.M., Gross, C.S., Lee, M.K., Li, D., and Rabe, R.L. (2003) US Patent 06569955.
31 Kear, K.E. (2003) *Developments in Thermoplastic Elastomers,* Rapra Technology Limited, London.
32 Johnson, S.P. (2001) *Rubber Processing: An Introduction,* Hanser Publication, Munich.
33 White, J.L. and De, S.K. (2001) *Rubber Technologist's Handbook,* Rapra Techology Limited, London.
34 Radar, C.P. and Richwine, J.R. (1985) *Rubber Plastics News.*
35 Kear, K.E. (1995) Proceedings TPE TOPCON 1995, Society of Plastics Engineers.
36 Rosato, V.D. (1986) *Injection Molding Handbook,* Van Nostrand Reinhold, New York.
37 Lawrence, G.K. and Digiantonio, R.J. (1992) presented at Society of Plastic Engineers.
38 LeBras, J. (1957) *Rubber, Fundamentals of its Science and Technology,* Chemical Publication Co., New York.
39 Penn, W.S. (1968) *Synthetic Rubber Technology,* vol. **I**, Maclaren & Sons, Ltd., London.
40 Naunton, W.J.S. (1961) *The Applied Science of Rubber,* Edward Arnold, London.
41 Blow, M.C. (1971) *Rubber Technology and Manufacture,* Butterworth & Co., Ltd., London.
42 Eirich, R.F. (1978) *Science and Technology of Rubber,* Academic Press, New York.
43 Menges, M. and Lehnen, J.P. (1969) *Plastverarbeiter,* **20**, 31–39.
44 LeRoy, G. (1969) US Patent: 03486192.
45 Rauwendaal, C. (2001) *Polymer Extrusion,* Hanser Publication, Munich.
46 Abdou-Sabet, S. and Fath, M. (1982) US Patent 4311628.

4
Compounding and Processing of Rubber/Rubber Blends

Brendan Rodgers and Adel Halasa

4.1
Introduction

Blending of polymers and specifically elastomers is carried out principally for two reasons, first, improvement of the technical properties of the base elastomer and, second, improved compounded polymer processing behavior [1, 2]. Processing would include mixing, extrusion, and calendering of rubber compounds, which will also contain oils, carbon blacks, and other organic and inorganic chemicals. Technical properties such as mechanical and dynamic characteristics are impacted by the selection of elastomers in a blend, vulcanization system ingredient distribution in the blend, and filler distribution between elastomer phases. Filler distribution will be affected by the type of elastomers, molecular weight of each of the different polymers, mixing method, and polymer–filler interaction.

In this chapter the reasons for blending elastomers for compounds used in composite structures such as tires, hoses, and conveyor belts will be discussed along with secondary compounding topics with which the materials engineer should be familiar. The chapter will focus on several points:

1) basic principles of polymer science,
2) tire compounding,
3) elastomer blending and compounding,
4) secondary elastomer blend compound systems such as polymeric resins,
5) elastomer blends and tire performance.

Elastomers typically found in complex composite structures such as tires tend to be blends to obtain specific properties in order that the ultimate product may function according to the required mission profile. Several compounding references that the reader may find of value are provided in the References at the end of this chapter [1–5].

Encyclopedia of Polymer Blends: Volume 2: Processing, First Edition. Edited by Avraam I. Isayev.
© 2011 Wiley-VCH Verlag GmbH & Co. KGaA. Published 2011 by Wiley-VCH Verlag GmbH & Co. KGaA.

4.1.1 Fundamentals of Applied Polymer Chemistry

Before reviewing in detail the fundamental aspects of elastomer blends, it would be appropriate to first review the basic principles of polymer science. Polymers fall into three basic classes: plastics, fibers, and elastomers. Elastomers are generally unsaturated (though can be saturated as in the case of ethylene–propylene copolymers or polyisobutylene) and operate above their glass transition temperature (T_g). The International Institute of Synthetic Rubber Producers has prepared a list of abbreviations for all elastomers [3]. For example, BR denotes polybutadiene, IR is synthetic polyisoprene, and NBR is acrylonitrile–butadiene rubber (Table 4.1). There are also several definitions that merit discussion. The glass transition temperature (T_g) defines the temperature at which an elastomer undergoes a transition from a rubbery to a glassy state at the molecular level. This transition is due to a cessation of molecular motion as temperature drops. An increase in the T_g, also known as the second-order transition temperature, leads to an increase in compound hysteretic properties, and in tires to an improvement in tire traction

Table 4.1 International Institute of Synthetic Rubber Producers' abbreviations for selected elastomers [3].

Abbreviation	Elastomer
BR	Polybutadiene
BIIR	Brominated isobutylene-isoprene rubber (bromobutyl rubber)
BIMSM	Brominated isobutylene-*co-para*-methylstyrene rubber
CIIR	Chlorinated isobutylene-isoprene rubber (chlorobutyl rubber)
CPE	Chlorinated polyethylene
CR	Chloroprene rubber
CSM	Chlorosulfonyl polyethylene
EAM	Ethylene-vinyl acetate copolymer
EPDM	Terpolymer of ethylene, propylene, and a diene with a residual unsaturated portion in the chain
EPM	Ethylene propylene copolymer
GPR	General purpose rubber
HNBR	Hydrogenated acrylonitrile butadiene rubber
IIR	Isobutylene isoprene rubber
IR	Synthetic polyisoprene
NBR	Acrylonitrile butadiene rubber
SBR	Styrene butadiene rubber
E-SBR	Emulsion styrene butadiene rubber
S-SBR	Solution styrene butadiene rubber
X-NBR	Carboxylated acrylonitrile butadiene rubber
X-SBR	Carboxylated styrene butadiene rubber
Y-SBR	Block copolymer of styrene and butadiene

Sources: International Institute of Synthetic Rubber Producers, Synthetic Rubber Manual, 17th Edition, 2008; American Society for Testing and Materials. Standard Practice for Rubber and Rubber Lattices – Nomenclature, ASTM D1418.

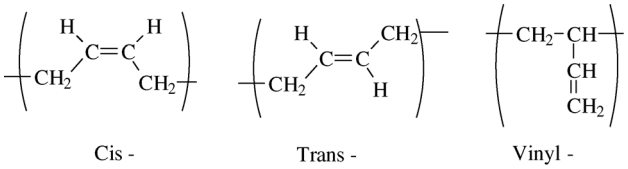

Figure 4.1 Possible configurations for butadiene in solution SBR and polybutadiene [1–3].

characteristics. A decrease in T_g leads to a drop in compound heat build-up and, typically, improved resistance to abrasion.

The microstructure of an elastomer similarly can affect the mechanical properties of the compounded elastomer. For solution SBR used in a tire tread compound, an increase in the vinyl butadiene (Figure 4.1) level will increase the T_g, improve tire wet traction performance, and result in a decrease in resistance to abrasion [4]. An increase in the cis-and trans-isomer of butadiene in SBR (styrene butadiene rubber), with a corresponding decrease in vinyl-butadiene isomer, will improve compound abrasion resistance. The amount of styrene in SBR will affect tire traction. Higher levels of styrene tend to give improvements in tire traction and tire/vehicle handling properties. The ratios of styrene, *cis*-butadiene, *trans*-butadiene, and vinyl-butadiene determine the ultimate T_g of the polymer. The higher the *cis*- or *trans*-butadiene level, the lower the T_g of either SBR or BR.

Tacticity describes the symmetry of the monomer orientation or stereochemistry of the monomer. In polybutadiene, atactic polymers have no steric order along the polymer. Isotactic polymers have the monomer pendent groups at the same relative position. Syndiotactic 1,2- polybutadiene has pendent groups alternating along the polymer chain. For illustrative purposes atactic, isotactic, and syndiotactic polypropylene are shown in Figure 4.2 [2, 4].

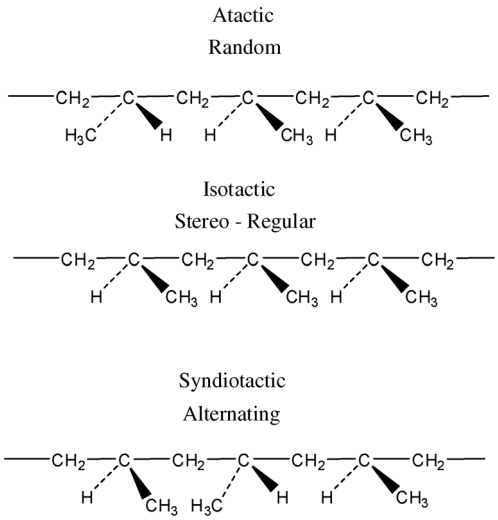

Figure 4.2 Polypropylene tacticity [2].

Table 4.2 Typical values of polybutadiene microstructure [5] (in absence of a modifier).

	Isomer level to ±1%		
Catalyst	**Cis- (%)**	**Trans- (%)**	**Vinyl- (%)**
Li	35	55	10
Ti	91–94	2–4	4
Co	96	2	2
Nd	98	1	1
Ni	96–98	0–1	2–4

The microstructure of polybutadiene can have a significant effect on the elastomer's performance. For example, lithium-catalyzed solution polymers, containing approximately 36% *cis*-butadiene, tend to process easily in tire manufacturing plants whereas high cis-polymers produced with titanium or nickel catalysts (cis-content >90%) tend to be more difficult to process in tire factories (Table 4.2). For example, gage control of extruded components may be more difficult though such compounded polymers have been reported to show better abrasion resistance when compared to the low cis-polymer [2].

The molecular weight of an elastomer or other polymeric material can be described by one of three basic terms. The number average molecular weight (M_n) is the weight near the peak of the weight distribution curve, or the most probable molecular weight, and is measured by freezing point depression or membrane osmometry. It is a measure of the number of defects in a polymer such as the degree of branching. Branching is of concern because it introduces extra chain ends for a given M_n, and therefore more network defects. This can lead to a shift in gum Mooney viscosity for a given M_n and therefore overall molecular weight must be lowered to maintain a given Mooney viscosity value. A consequence of lowering molecular weight can be loss in product mechanical properties such as tire tread wear, though in some instances tear strength may improve.

Weight average molecular weight (M_w) is measured by light scattering and correlates better with actual polymer molecular weight. Each molecule contributes to the M_w in proportion to its mass. The value of M_w tends to be influenced by the presence of high molecular weight species, much the same as M_n is impacted by the low molecular weight fraction of the polymer.

The Z-average molecular weight gives a measure of the upper limit of the polymer molecular weight distribution. The ratio M_w/M_n can be used as a measure of the breadth of the molecular weight distribution or polydispersity and is sometimes referred to as a polydispersity index (PDI).

Polymers are produced by one of two processes, addition or condensation polymerization. Addition polymerization occurs by one of three mechanisms, radical (e.g., low density branched polyethylene), cationic (e.g., butyl rubbers), or anionic (e.g., polystyrene). Condensation polymerization is used to produce Nylon 6,6 from adipic acid and hexamethylenediamine with the elimination of water. Industrially,

Table 4.3 Classification of emulsion elastomers by the International Institute of Synthetic Rubber Producers [3].

Series	Description
1000	Hot non-pigmented emulsion SBR Polymerized above 38 °C
1500	Cold non-pigmented emulsion SBR Polymerized below 10 °C
1600	Cold non-pigmented emulsion SBR Carbon black/oil masterbatch/14 phr oil max.
1700	Oil extended cold emulsion SBR
1800	Cold non-pigmented emulsion SBR Carbon black/oil masterbatch More than 14 phr oil
1900	Emulsion resin rubber masterbatches

Sources: International Institute of Synthetic Rubber Producers, Synthetic Rubber Manual, 17th Edition, 2008; American Society for Testing and Materials. Standard Practice for Rubber and Rubber Lattices – Nomenclature, ASTM D1418.

polymers are produced in bulk, solution, suspension, or emulsion processes. Elastomers are typically produced in a solution batch process, continuous solution process, or emulsion processes. Elastomers are then categorized according to a classification process defined by the International Institute of Synthetic Rubber Producers and the ASTM. Briefly, an emulsion polymerized SBR polymer such as IISRP SBR1500 has a bound styrene level of 23.5% and a bale Mooney viscosity of 50–55 Mooney units (MU). The oil extended version is classed as SBR 1712. Polymer/oil/carbon black masterbatches fall under either 1600 series or 1800 series classes (Table 4.3). Solution polymers similarly are classed as 1200 series for SBR and polybutadiene, and 2200 series for polyisoprene and copolymers of isoprene (Table 4.4) [3].

Table 4.4 Classification of solution elastomers by the International Institute of Synthetic Rubber Producers [3].

Category	Butadiene and copolymers	Isoprene and copolymers	Butadiene, isoprene, and styrene copolymers
Dry polymer	1200–1249	2200–2249	2250–2599
Oil extended	1250–1299	2250–2299	
Black masterbatch	1300–1349	2300–2349	
Oil–black masterbatch	1350–1399	2350–2399	
Latex	1400–1449	2400–2449	
Miscellaneous	1450–1499	2450–2499	

Sources: International Institute of Synthetic Rubber Producers, Synthetic Rubber Manual, 17th Edition, 2008; American Society for Testing and Materials. Standard Practice for Rubber and Rubber Lattices – Nomenclature, ASTM D1418.

Tires are the largest consumer of synthetic rubber. Automotive components and tires together account for nearly 70% of synthetic rubber consumption. Additional consumption is found in miscellaneous mechanical goods, plastic composites, and construction applications such as roofing, wire and cable covers, and adhesives. For SBR specifically, passenger tire production consumes approximately 50%, truck tires and tire retreading a further 20%, and the balance is in specialty tires, automotive and non-automotive components. Polybutadiene consumption is similar to SBR with tires accounting for nearly 75% of total polymer production.

A series of empirical guidelines have been developed that might be used in designing a polymer or blend of polymers to meet a set of tire performance targets [2, 4–6]. By preparing a series of blends of polybutadiene and SBR, a range of polymer T_g values can be obtained that vary from as low as $-100\,^{\circ}C$ to $-20\,^{\circ}C$. Evaluation of these blends has allowed the deduction of the following observations:

1) as T_g increases there is a near linear drop in abrasion resistance;
2) wet grip or traction improves, again nearly linearly with increase in compound T_g;
3) addition of styrene leads to an increase in traction performance and loss in abrasion resistance.

This information allowed the segmentation of the tan-delta curve of a tread compound run from $-100\,^{\circ}C$ to $+100\,^{\circ}C$, into zones that characterized the tread compound performance in a tire. The tan-delta value in the region of the compound T_g will define its abrasion characteristics. Ice, snow, and wet traction properties can be predicted by the tan-delta values in the region of $-20\,^{\circ}C$ to $0\,^{\circ}C$, while rolling resistance is determined by tan-delta values in the region of $+60\,^{\circ}C$ (Figure 4.3).

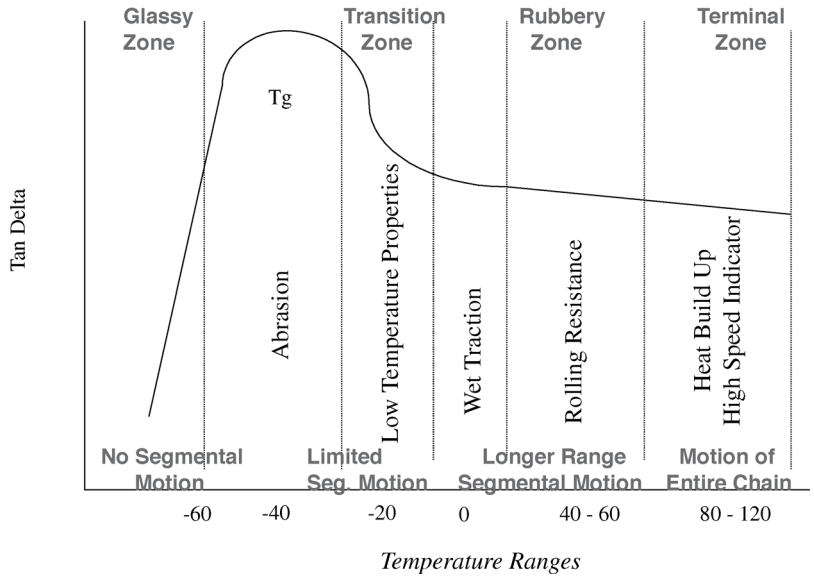

Figure 4.3 Tangent delta curve for tread compound property prediction [6].

Table 4.5 Effect of tread polymer vinyl-butadiene level on tire performance [8].

	Percent vinyl butadiene (%)	
	10	**50**
Glass transition temp. (°C)	−90	−60
Tire properties		
Wet traction	100	120
Rolling resistance	100	95
Tread wear	100	90

An example of how polymer microstructure and polymer T_g impact performance is when vinyl-butadiene is increased from 10 to 50% in polybutadiene (Table 4.5) [8]. The glass transition temperature increases from −90 to −60 °C, with a corresponding shift in the tan-delta curve. Traction performance has improved significantly, but tread wear and rolling resistance rating drop.

The concept of "integral rubber" or dual or multi-T_g polymers emerged from this fundamental work [6, 7].

4.1.2 Multiple T_g Elastomer Compositions

Rather than blending for example an SBR and a polybutadiene or polyisoprene, copolymers or terpolymers based on styrene and butadiene, butadiene and isoprene, styrene and isoprene, or styrene, butadiene, and isoprene can be prepared having a dual T_g. Using *n*-butyllithium catalyst and *N*′,*N*′,*N*′,*N*′-tetramethylethylenediamine (TMEDA) as a modifier, a range of polymer dual glass transition temperatures can be obtained (Table 4.6).

In addition to styrene, the TMEDA amount in the polymerization process will control the level of vinyl-butadiene and 3,4-isoprene and this can determine the upper T_g while the amount of *cis*-butadiene will control the lower T_g. This work led to the development of the styrene–isoprene–butadiene terpolymer, which proved to be

Table 4.6 Dual T_g IBR, SBR, and SIBR elastomers [7].

	Micro structure (%)			T_g (with TMEDA modifier)	
Polymer	**Styrene**	**Butadiene**	**Isoprene**	**Lower T_g (°C)**	**Upper T_g (°C)**
1		100		−98	−50
2		50	50	−80	−30
3		80	20	−85	−54
4	45	45	10	−75	−25
5	40	40	20	−78	−18
6	35	35	30	−78	−10

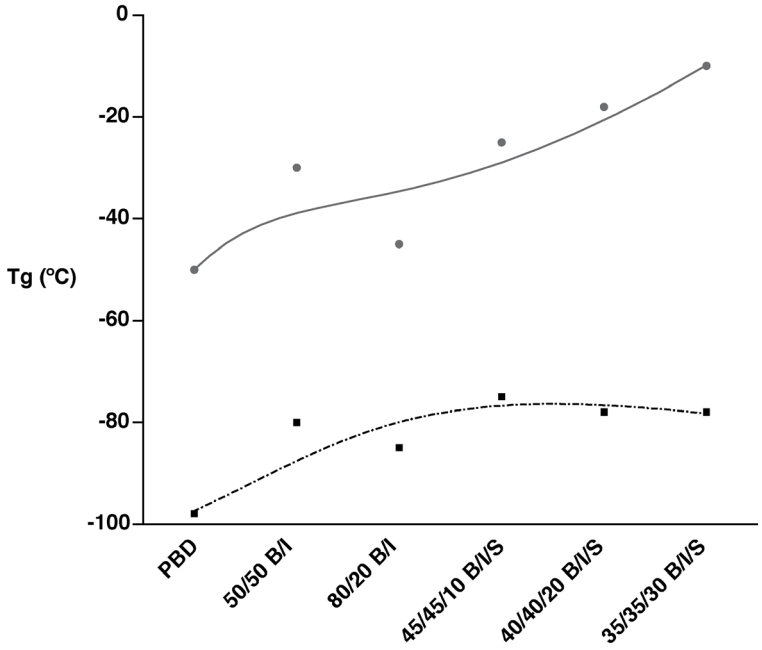

Figure 4.4 Empirical trends in T_g with variation in styrene, butadiene, and isoprene (vinyl-butadiene and isoprene allowing a second T_g) [7].

very effective in obtaining a balance of abrasion resistance, traction and vehicle handling qualities, and rolling resistance reduction. Trends can then be established illustrating how microstructure can be modified to achieve a specific combination of glass transition temperatures. This in turn allows specific tuning of the compounded rubber, for example, the tire tread compound, to meet a special set of traction or tire rolling resistance performance criteria (Figure 4.4).

4.2
Elastomers and Tire Compounding

The pneumatic tire consists of two basic areas: the tread area, which is responsible for ground contact, and the casing whose function is to support load and transmit power to the tread area. Each of these areas has several components with markedly different properties and which serve specific and unique functions, and all of which must interact together for designed performance. The role of the rubber compounds used in these basic components is threefold:

1) to provide the contact area between the vehicle and the road surface;
2) to provide the cohesive material that holds the tire together so it acts as an integral unit;
3) to provide protection for the strength-bearing components, that is, the textiles, steel beads, steel cords, and steel breakers in steel belted radial tires.

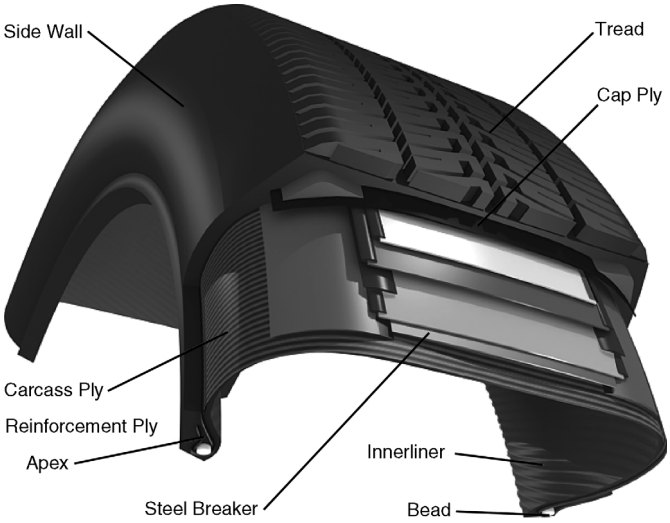

Figure 4.5 Tire construction.

4.2.1 Tire Component Parts

Desired properties in the components of a radial steel belted passenger car tire (Figure 4.5) are as follows [5, 9, 10]. The tread is designed and compounded for abrasion resistance, traction, low rolling resistance, and protection of the casing. It often is divided into two subcomponents to tune performance; the outer tread for surface contact and the undertread, which serves as a transition component and reduces tire rolling resistance through decreased hysteresis.

The steel belt, which provides strength and protection of the ply or plies, is encased in a compound that must possess adhesion to the steel and provide stress transfer from the very rigid steel to the many times more flexible tread, sidewall, and textile carcass components. The belt layup also provides a uniform tire tread footprint necessary for uniform wear. A wedge compound is formulated to reduce belt-edge shear stresses while tying the belt to the carcass and reducing hysteresis.

The casing ply and ply coat compound functions are basically the same as the steel belt compound. Normally, in the steel belted radial automobile tire the ply is a textile cord of polyester, nylon, or rayon fabrics, which are flexible. The steel belted radial truck tire normally uses a steel cord ply. Earthmover tires are of two basic constructions, that is, radial using steel and bias using textiles. The sidewall compound is compounded to protect the ply and must have resistance to weathering, ozone, abrasion, and tearing while providing flex fatigue resistance. The innerliner compound must provide good air-permeation resistance and resist aging caused by moisture or hot air aging.

The apex or bead filler compound are formulated for dynamic stiffness, enable stress distribution in the lower sidewall region, and provide good tire–vehicle

handling properties. The bead insulation compound must have good steel bead wire adhesion and also ply compound adhesion. The chafer or rim strip compound protects the plies from rim abrasion and helps seal the tire to the rim.

The elastomers and elastomer blends used in tire compounds, and particularly tread compounds, are thus equally important to the structural design parameters of the tire (Table 4.7). A properly designed tread compound will ensure the tire can meet its performance targets. Tread compounding materials fall into one of five general categories: polymers, fillers, protectants, vulcanization system, and various special purpose additives. Elastomers for tread compounds are typically natural rubber (NR), styrene-butadiene rubber (SBR), polybutadiene (BR), and in some instances isobutylene based polymers for winter and special performance tires.

Reinforcing fillers used are carbon black and non-black fillers such as silica, clay, and calcium carbonate although the latter two are used more in lower cost industrial applications and not in tires. Protectant systems consist of antioxidants, antiozonants, and waxes. The vulcanization system essentially ensures that the optimum mechanical properties of the polymer system are achieved. Finally, the tire compound can contain various miscellaneous materials such as processing aids and resins. The materials scientist when designing a tire compound formulation has a range of objectives and restrictions within which to operate. Product performance objectives define the initial selection of materials. These materials must not raise environmental concerns, be processable in tire production plants, and be cost effective for the end user [4].

Without migration of elastomer polymer ends across compound or component interfaces, adhesion of one component to another may be significantly weakened and inter-component separation might occur. Solubility parameters of materials are important in processing of compounds/components. A material used above its saturation point in a compound might bloom (migrate to the surface of the component), detrimentally affecting component tack and render it difficult to handle in final tire assembly or block other chemical's migration and weaken component interfaced adhesion.

4.2.2
Tire Elastomers

For the mechanical strength requirements of tires NR is better than SBR or BR, enabling better tread chipping, chunking, and cutting resistance, lower tire operating temperatures, and improved rolling resistance. Although more difficult to mix, it is very good in downstream processes such as extruding, and calendering, and for tire building. Natural rubber may show a faster wear condition in passenger and light truck over-the-road tires. It can enable improved ice traction performance and a lower brittle point in extreme low temperature service ($<-40\,^{\circ}C$). It is by far the preferred rubber for wire belt and textile ply/breaker coat compounds. Table 4.7 shows typical tread compound formulations and the relative amounts of elastomers used by tire line [11].

Table 4.7 Typical tread compound formulations and quantities of raw materials [11].

Compound	Economy line tire tread	High-performance tread	Low rolling resistance	Radial medium truck
Polymer	SBR 50–100 BR 0–50	VSBR 20–100 BR 0–20	NR 0–40 SSBR 60–100	NR 60–100 BR 0–40
Carbon black grades	N343, N399, N299	N121 N134, N343, N234	N351, N343, N299	N121, N220, N134
Loading	70–90	80–90	40–60	40–60
Oil includes oil in OE polymers	30–60	25–45	5–30	0–20
Antioxidants, antiozonants	1–4	1–3	1–3	1–4
Processing aids	2	2	2	2
Stearic acid	1–2	1–2	1–2	1–2
Zinc oxide	3–5	3–5	3–5	3–5
Sulfur	1–2	1–2	1–2	1–2
Accelerator types[a)]	CBS, MBTS	CBS, MBTS	CBS, MBTS, TBBS	TBBS, MBTS, DCBS
Accelerator loading	1–2	1–2	1–2	1–2

a) CBS, *N*-Cyclohexyl-2-benzothiazole sulfenamide

SBR is the primary elastomer for passenger car tire tread compounds, mainly due to better wear resistance and traction. It can also be the least expensive polymer when produced by the emulsion process. In the early 1980s, specialty solution SBRs (SSBRs) and vinyl SSBR (VSBR) were introduced. These rubbers, polymerized in a hydrocarbon solvent, typically hexane, with special catalyst systems, enabled improvements in tire rolling resistance and lower fuel consumption while maintaining high levels of wear resistance and traction. The specialty SSBRs accomplish this through control of the styrene–butadiene polymer backbone structure, coupling of polymers, and addition of reactive chemical units or coupling agents at the polymer ends. Not all of these changes are used in the same specialty polymer, but coupled polymers are in production and can significantly affect polymer molecular weights, compared to higher molecular weight, branched polymers, which may be difficult to produce and may not perform as well in tires. Many of the polymers are available in the oil/black masterbatch (premixed blends), as is the emulsion SBR. SBR, whether emulsion or solution, is still not as resilient as NR or BR, which limits applications in tires.

BR can be produced primarily by hydrocarbon solvent processes. It is the butadiene part of SBR that is controlled in specialty SSBRs. Originally polybutadiene was used in tires due its better abrasion resistance. It has high *cis*-butadiene content and high linearity structure and this also results in lower hysteresis and better fatigue resistance. BR is more difficult to process in the factory, particularly in milling operations. It does not possess the level of tack of NR, which makes tire building more difficult. BR is also lower in resistance to tearing.

Chlorobutyl rubber (CIIR) and bromobutyl rubber (BIIR) are used in tire innerliners and white sidewalls. These elastomers allow improvements in tire air retention due to lower air permeability as well as age resistance and flex fatigue resistance. The chlorine and bromine versions of isobutylene isoprene rubber (IIR) are both used to improve compatibility with the other commodity tire rubbers. It is a near-saturated polymer with few sites available for conventional sulfur curing. IIR shows high hysteresis at nominal tire operating temperatures and thus acts as a superior cushioning rubber. In the 1960s a tire using this rubber in the tread was produced by tire producers for improvement in vehicle handling performance. Vehicle–tire handling characteristics describe properties such as steering precision, aligning torque, cornering moment, stability, vibration, comfort, and noise generation. It is also the preferred rubber for tire curing press bladders.

Like halobutyl rubber (HIIR), ethylene propylene rubber (EPR) has a fully saturated backbone and has only unsaturation points available for vulcanization crosslinking in very small percentages of the pendent diene modifier (EPDM). It has good aging resistance and resistance to fatigue even when heavily loaded with fillers and is utilized in passenger tire white sidewalls.

Another example of how polymer blends are used is in truck tire sidewall, which must not only possess high strength but must also have excellent aging and fatigue resistance to survive multiple retreading, that is, vulcanizing a new tread to the worn original tire casing. The original casing (carcass) of a radial truck tire has been known to last for up to 750 000 miles while the original tread on this casing only delivers 70 000–350 000 miles.

In passenger car tires as many as four different polymers may be used for the tread compound, totaling 100 phr; for example, 25 phr emulsion SBR, 25 phr SSBR, 30 phr BR, and 20 phr NR. If solution SBR categories can be considered as each one falling with a 10 °C T_g range, there are at least nine groups of specialty SSBRs that are produced. SBR is available as oil and oil–carbon black masterbatches (oil and/or carbon black added to the rubber by the rubber producers), which may use a different SBR (usually higher molecular weight) than if it were produced without masterbatch. The Mooney viscosity of oil extended elastomers is sometimes called the bale Mooney, typically around 55 Mooney units (MU). The base Mooney is the original polymer Mooney viscosity, typically as high as 120 MU, before oil addition lowers it to give the final bale Mooney.

4.3 Blending Elastomers

Compounded elastomers have many unique characteristics not found in other materials, such as high elasticity, abrasion resistance, and dampening properties. A compound used in a tire tread for example consists of five major components: the polymer system, filler or reinforcement system, processing aids, antioxidants, and vulcanization system. Frequently, more than one polymer is employed in a

compound used in tire treads or sidewalls. There are some additional definitions that should be reviewed before discussing polymer blending. Compatibility of two elastomers is where the polymers are immiscible but when in combination provide properties or show characteristics that are more useful than the properties of the original polymers. Incompatible polymer blends typically show a dual T_g [1, 2].

Miscible blends are obtained when, at the molecular level, the two polymers are compatible. For example, blends of two highly polar polymers such as PVC and NBR are truly miscible elastomeric systems. Examples of elastomers that exhibit phase separation upon heating (lower critical solution temperature, LCST, behavior) include natural rubber and high vinyl solution SBR. This is important at high curing temperatures (180 °C) where rapid phase separation can occur before the onset of crosslinking. However, at curing temperatures, natural rubber and conventional emulsion SBR forms a single phase. Several terms can now be defined:

miscible	polymer blends shows a single T_g and single phase morphology;
semi-miscible	miscibility varies with temperature and concentration;
immiscible	polymers show two-phase morphology with a distinct domain size and shape;
compatible	polymers are not miscible at the molecular level.

It would now be appropriate to discuss polymer blending. A wide variety of compounds contain polymer blends. Blending can allow improved fatigue life, groove cracking resistance, hysteresis, and, many times, adhesion and abrasion resistance. Blending also improves extrusion, moldability, and calendering characteristics of a compound. For example, addition of natural rubber to a compound with a high synthetic polymer level will improve tire buildability as well as improving resistance to tearing of the compound.

Compounds containing blends include different polymer systems where the polymers can contain blocky segments, crystalline portions, isomers such as cis-, trans-, and vinyl-butadiene, or isotactic or atactic blocks.

Polymers can be grafted or can contain coupling agents. For two substances of different chemical composition to be miscible, the Gibbs free energy of mixing, ΔG, must be negative Eq. (4.1). The Gibbs free energy is a function of the enthalpy of mixing (ΔH), entropy of mixing (ΔS), and the absolute temperature (T), where:

$$\Delta G = \Delta H - T\Delta S \tag{4.1}$$

Miscible polymers tend to show hydrogen bonding or van der Waals forces between the chains. However, phase separation can occur should the temperature rise above the LCST. Polymers generally do not have an upper critical solution temperature (UCST), though lower molecular weight oligomers do. A final point to note is that truly miscible polymers will show a single T_g. Figure 4.6 illustrates the effect of temperature on phase mixing of SBR and polybutadiene. Two-phase heterogeneous systems are obtained both above the LCST and below the UCST. The critical solution temperatures also vary according to the polymer ratios present.

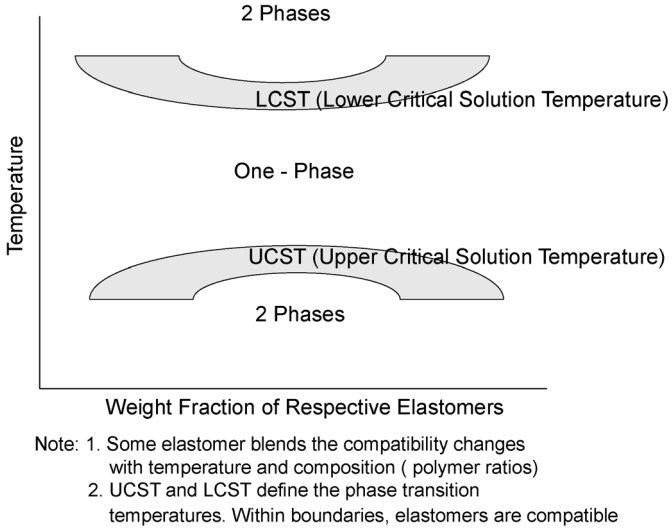

Figure 4.6 Theoretical illustration of a phase diagram for elastomer blends [2].

The phase morphology that two immiscible elastomers assume can take various forms, depending on viscosity or molecular weights, solubility, and polarity of the polymer chain. Examples might best be described as:

1) rubber particles within a plastic matrix,
2) plastic particles within a rubber matrix,
3) plastic networks in a rubber matrix,
4) rubber rods in a plastic matrix,
5) plastic rods in a rubber matrix,
6) plastic–rubber alternating sheets.

Many more alternatives could be developed with phase inversion between the polymer phases being dependent on polymer concentration, molecular weight, or mixing method.

Polybutadiene and natural rubber are blended in tire sidewalls to improve fatigue resistance, cut growth resistance, and improve abrasion resistance to minimize the effect of curb scuffing. Figure 4.7 shows atomic force micrographs (AFMs) of the model tire sidewall compound formulation given in Table 4.8. Many tire compounds are composed of two or more elastomer blends. Depending on the types of elastomers these blends may be:

1) miscible, showing a single T_g and one-phase morphology;
2) incompatible, showing two or more intermediate glass transition temperatures and two or more phase morphology.

Control of this phase morphology can become very important so as to prevent any deterioration in the tire tread wear performance, rolling resistance or traction and handling qualities, or loss in component to component adhesion.

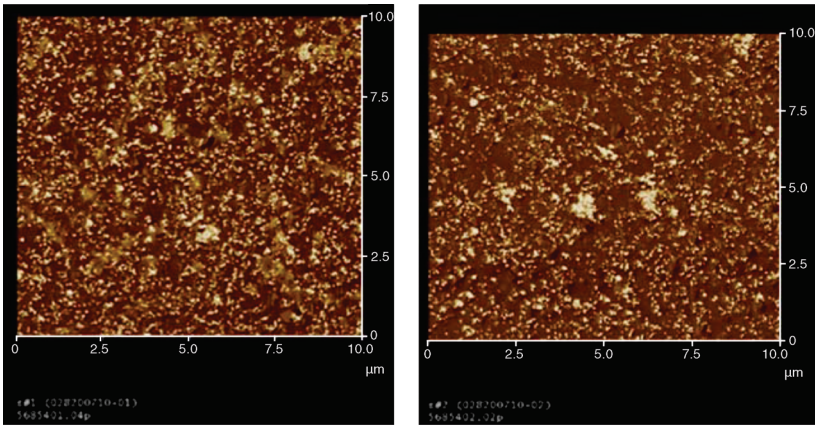

Figure 4.7 AFMs showing polymer phases for formulation 1 (a) and 2 (b); light spots are carbon black; continuous phase is polybutadiene; light brown is natural rubber.

Miscibility can be predicted from the Flory–Huggins theory, using interaction parameters, and in many instances is in close agreement with experimental data. Some empirical guidelines on elastomer miscibility can thus be proposed:

1) In general, the T_g of miscible blends is intermediate between the component polymers and may be a function of the weight percent or ratios of the constituent polymers. Miscible blends have one T_g, immiscible blends have two T_gs.

Table 4.8 Model tire sidewall compound; atomic force micrographs showing the polymer phases are given in Figure 4.7 [5, 8, 9].

Compound	Formulation 1	Formulation 2
Natural rubber (TSR20)	50.00	40.00
Polybutadiene IISRP1207	50.00	60.00
Carbon black (N330)	50.00	50.00
Wax	1.50	1.50
Antioxidant (TMQ)	1.00	1.00
Antiozonant (6PPD)	3.00	3.00
Phenolic tackifying resin	2.00	2.00
Zinc oxide	3.00	3.00
Stearic acid	2.00	2.00
Aromatic oil	10.00	10.00
Sulfur	2.00	2.00
Sulfenamide accelerator (TBBS)	1.00	1.00
Retarder (PVI)	0.15	0.15
Mooney viscosity[a)] (ML1 + 4), 100 °C, MU	52.0	81.9
Tensile strength (MPa)[b)]	18.4	12.1
Elongation (%)	448.4	375.7
300% Modulus (MPa)	10.2	8.9

a) Measured according to ASTM D1646.
b) Measured according to ASTM D412.

2) For SBR and BR blends, when the styrene level in SBR increases beyond 30% immiscible compositions are obtained.
3) The miscibility of polyisoprene and SBR increases with increase in 1,2-isoprene content.
4) 1,4-IR and 3,4-IR become immiscible when the 3,4-isoprene content exceeds 50%. Miscibility can be improved by lowering the molecular weight of the vinyl IR polymer.
5) For polyisoprene/polybutadiene blends:
   a) miscibility increases with BR 1,2-butadiene content;
   b) IR high vinyl BR blends can have a broad graduated T_g and can, thereby, sometimes be described as semi-miscible systems.

4.4 Solubility Parameters

4.4.1 Definition of Solubility Parameters

As an empirical guide, solubility parameters can be used to predict miscibility over an entire composition range when the solubility parameter of the two polymers does not exceed 0.7 $MPa^{1/2}$ for molecular weights greater than 10 000, 0.2 $MPa^{1/2}$ for molecular weights greater than 100 000, and 0.1 $MPa^{1/2}$ for molecular weights greater than 1 000 000.

As noted earlier, compatibility of two elastomers is defined as when the polymers are immiscible but if in combination provide properties or show characteristics that are more useful than the properties of the original polymers [2]. Incompatible polymers when blended will show a dual T_g. As discussed earlier, miscible blends are obtained when, at the molecular level, the two polymers are compatible. For example, blends of two highly polar polymers such as PVC and NBR are truly miscible. Polymer compatibility is governed by three parameters:

1) Thermodynamics: microdomain formation is achieved by surface energy reduction (i.e., use of processing aids) and vulcanization.
2) Viscosity: oil/filler levels in dissimilar elastomers can be adjusted in mixing.
3) Cure rate: NR/EPDM and NR/IIR or NR/HIIR systems where the respective polymers are significantly different.

Polymer compatibilization can therefore be achieved either by reduction of interfacial energy, improvement of dispersion during mixing, stabilization of the polymers to prevent phase separation after mixing, or improvement of interfacial or interdomain adhesion. This can be achieved as follows:

- use of grafted polymers to reduce interfacial energy,
- addition of a copolymer,
- crosslinking of blended polymers (dynamic vulcanization),
- polymer functionalization.

The solubility parameter (δ) for a material is related to the enthalpy of mixing. It is defined as the square root of the cohesive energy density, or attractive strength between molecules, that is:

$$\delta = (\Delta E/V)^{\frac{1}{2}} \tag{4.2}$$

where ΔE is the energy of vaporization and V is the molar volume of the polymer (in $MPa^{1/2}$). As an empirical guide, the solubility parameter difference between two polymers must be less than 1.0 to be compatible. There must also be no change in volume or reaction between the two elastomers. Solubility parameters can only be determined indirectly by methods such as solvency in a solvent such as hexane, toluene, dibutyl phthalate, or ethanol. Other measurement methods used have included swelling, refractive index, dipole moment measurements, and intrinsic viscosity. Table 4.9 shows the solubility parameters for a range of elastomers [12].

The solubility parameter of polybutadiene is in the range 16.2–17.6 $(MPa)^{1/2}$, depending on the microstructure. Nitrile elastomers range from 18.4 to 21.1 $(MPa)^{1/2}$ depending on the acrylonitrile content. Solution SBR solubility parameters range from 17.1 to 17.4 $(MPa)^{1/2}$ depending on the styrene level. These solubility parameters can be used to estimate the miscibility of the elastomers. For illustrative purposes, natural rubber with a solubility parameter of 16.6 $(MPa)^{1/2}$ when mixed with a NBR with a solubility parameter of 19.4 $(MPa)^{1/2}$ gives a solubility parameter differential of 2.8. As this is greater than 1.0, the two elastomers would be considered to be immiscible [2].

Table 4.9 Solubility parameters for selected elastomers [12] (in $MPa^{1/2}$).

Polymer	Solubility parameter
BR (range)	17.2 (16.2–17.6)
IR (range)	16.4 (16.2–16.82)
IIR (range)	16.06 (15.7–18.0)
NBR	
AN content	
16	19.4
20	18.4
30	20.26
40	21.1
NR (range)	16.6 (16.2–17.1)
S-SBR	
Styrene content	
10	17.13
15	17.19
25	17.29
30	17.35
40	17.4

Where the solubility parameter rule is in error is for natural rubber and polybutadiene. The differential in solubility parameters is around 0.6 but the two polymers are immiscible. Polybutadiene grade IISRP 1207 and an oil extended polymer such as IISRP 1712 have a differential of less than 0.1 and in this case the two elastomers are nearly fully miscible between the lower and upper critical solution temperatures. The blended elastomers mechanical properties then become a function of the filler type, distribution, vulcanization system, and any processing aids present.

Polymer blends in tire tread compounds have been reported to offer several performance advantages, which can be summarized as follows:

- Polybutadiene in natural rubber:
  - improve heat stability,
  - decrease tensile strength and 300% modulus,
  - improve resistance to fatigue,
  - increase resistance to abrasion, tread wear,
  - increase elasticity.
- Polybutadiene blended with SBR:
  - an increase in SBR level improves traction (due to the increase in T_g),
  - SBR increase improves tire–vehicle handling qualities, due to the increase in dynamic modulus (E'),
  - increase in percent BR improves wear performance,
  - blends of NR, SBR, BR can be optimized, depending on the tire design criteria, for factors such as aligning torque, steering precision, high-speed performance, and so on.

4.4.2 Estimation of Solubility Parameters

When solubility parameter data is needed quickly, experimental measurements may not be readily available. In such instances a broad approximation may be sufficient. This can be obtained through use of group contribution approaches. Two suggested methods are by use of coefficients prepared Small *et al.* (see Robeson [13]) and Coleman *et al.* [14]. The group contribution method for estimating solubility parameters is based on the expression shown in Eq. (4.3):

$$\delta_p = \varrho[\Sigma F_i/M] = \Sigma F_i/v \tag{4.3}$$

where

F_i is the molar attraction constant,
M is the molecular weight of the repeat unit,
v is molar volume.

A selection of the coefficients has been tabulated so as to provide a preliminary approach that the researcher might use to determine whether a more in-depth

Table 4.10 Group contribution values for estimating solubility parameter [13, 14] [δ_p, $(MPa)^{1/2}$].

	Small *et al.* (given in Reference [13])	Coleman *et al.* [14]
-CH_3	438	446
-CH_2-	272	270
-CH<	57	47
>C<	−190	−195
-CH=	227	231
>C=	39	37
Phenyl group	1504	1504
Phenylene	1346	1333
-O-	143	194
-CO-	563	536
-COO-	634	610
-COO- (acrylate)	634	610
-Cl	532	540
-CN	839	872
-CF_2-	307	—
-CF_3	560	—
-NH_2	—	563

experimental measurement is warranted (Table 4.10). Where errors or anomalies can enter into these estimations is when cyclization occurs and is not accounted for, which might result in a lower estimated value, or the monomer stereochemistry is not understood when the estimations are prepared.

4.5 Processing of Elastomer Blends

4.5.1 General Remarks

Generally, elastomers can be blended in one of five ways:

1) latex blending,
2) solution blending,
3) combined solution/latex blending,
4) mechanical blending,
5) mechano-chemical blending.

Latex blending gives a high quality dispersion of component materials, with the blend potentially having lower hysteretic properties and lower solvent swelling. Examples of where such blending is found would be in natural rubber SBR latex blends. Solution blending of elastomers is normally performed during the solution

polymerization process. At the same time, carbon black and oils can be added to produce carbon black masterbatches.

Solution blending of incompatible polymers is difficult due to phase separation. Furthermore, rapid solvent evaporation is required to minimize heterogeneity, which together restricts the applications of this technique. Combined solution and latex blending has an advantage in, for example, solutions of polymers mixed with aqueous suspensions. Carbon black migrates into the organic phase, thereby giving a highly homogeneous dispersion.

Mechanical mixing of polymers carried out on either an open mill or in a Banbury internal mixer has advantages in efficiency, productivity, and lower cost. However, natural rubber in many instances must first undergo an initial breakdown.

Mechano-chemical mixing of polymers can lead to interpolymerization, formation of block copolymers, and grafting of pendent groups. Bound rubber can also increase with loss in ease of processability.

Polymer blends can be characterized in several ways:

1) microscopic: characterize compatibility of polymers on the gross scale,
2) electron microscopy,
3) solubility measurements by swelling methods,
4) thermal and thermo-mechanical methods such as DSC,
5) dielectric relaxation,
6) infrared spectroscopy,
7) NMR,
8) X-ray analysis,
9) gel permeation chromatography,
10) refractive index,
11) viscosity,
12) light scattering,
13) rheological properties.

Several observations can thus be highlighted:

1) Phase micrographs can show discrete domains of polymers in blends. The dispersed zones range from 1.0 up to 30 μm in diameter, but more frequently 1.0–5.0 μm.
2) The area of a polymer domain approximates the proportion of the polymer volume in the blend.
3) The discrete zones are the secondary polymer dispersed in the continuous phase of the major polymer. Phase inversion can occur at the 50/50 blend ratio.
4) The midpoint is characterized by creation of an interpenetrating network.
5) Components of the lowest viscosity form the continuous phase (e.g., NR/CR blends where NR is the continuous phase up to a 25/75 blend ratio).
6) An increase in mix time and temperature will decrease the domain size.
7) IR/SBR and IR/PBD blends are heterogeneous. SBR/BR blends are homogeneous.

8) Ozone resistance improves as the fineness of the dispersion increases.
9) When polybutadiene has a high viscosity, blending is poor. There are large BR domains.
10) If the NR and BR polymers used have equivalent viscosities, then the blend will tend to be more homogeneous. This is also true of NR/SBR blends.
11) At high carbon black loadings in BR, the polymer is forced into the dispersed phase. The blend morphology is secondary to the impact of carbon black dispersion.

In summary, elastomer blends are essentially micro-heterogeneous systems. The continuous phase is either the polymer of highest concentration or the polymer of lowest viscosity. Phase inversion occurs at a ratio of typically 50/50 and zone sizes are in the order of 1–5 μm. Micro-crack growth termination is enhanced with smaller domains but poor dispersion of soluble compounding ingredients can have a detrimental effect on compound mechanical properties.

4.5.2
Natural Rubber/Bromobutyl Rubber Blends

Natural rubber is added to bromobutyl to improve calendering and improve green strength. For example, high compounded green strength is important in resisting tire ply cords pulling through a tire innerliner when the tire is being built and shaped. Although bromobutyl and natural rubber have different backbone structures, different degrees of functionality, and different vulcanization chemistry, they can be blended in various amounts to attain a desired combination of properties. This is due to the versatility of bromobutyl rubber vulcanization. Not only can bromobutyl rubber vulcanize independently from the natural rubber–sulfur cure system by merely crosslinking with zinc oxide, but it also uses sulfur efficiently in the presence of natural rubber to promote co-vulcanization.

The addition of bromobutyl rubber to a predominantly natural rubber compound reduces the permeability to gases and water vapor, increases the heat and flex crack resistance, and increases vibration damping. Blending natural rubber into bromobutyl rubber increases cured adhesion to general purpose rubber compounds as well as increasing building tack and green strength. In blends of two rubbers, the physical properties, in particular tensile strength, usually show a significant change compared to the properties of the separate rubber compounds. This infers either that one rubber disturbs the cured network of the other or that the two immiscible phases are curing separately. With bromobutyl/natural rubber blends, tensile strength values can change compared to the average of the two homopolymers, which implies crosslinking between the elastomer phases. A thiazole–sulfur vulcanization system generally exhibits the best balance of properties with blends containing 80% or more of bromobutyl. Below 70%, an alkylphenol disulfide cure system is suggested. Table 4.11 shows bromobutyl rubber and bromobutyl/natural rubber compound properties using the zinc oxide–sulfur–MBTS cure system.

Table 4.11 Model formulations for an automobile tire innerliner and summary of properties.[a].

Material		Units	Compound				
			1	2	3	4	5
EXXON™ Bromobutyl grade 2222		phr (1)	100.00	90.00	80.00	70.00	60.00
Natural rubber (technical specified rubber, TSR20)		phr	—	10.00	20.00	30.00	40.00
Carbon black N660		phr	60.00	60.00	60.00	60.00	60.00
Naphthenic oil		phr	8.00	8.00	8.00	8.00	8.00
Aromatic and aliphatic hydrocarbon resin blend		phr	7.0	7.00	7.00	7.00	7.00
Phenolic tackifying resin		phr	4.00	4.00	4.00	4.00	4.00
Magnesium oxide		phr	0.15	—	—	—	—
Stearic acid		phr	2.00	2.00	2.00	2.00	2.00
Zinc oxide		phr	1.00	1.00	1.00	1.00	1.00
Sulfur		phr	0.50	0.50	0.50	0.50	0.50
Mercaptobenzothiazyl disulfide (MBTS)		phr	1.50	1.50	1.50	1.50	1.50
Total (phr)			184.15	184.00	184.00	184.00	184.00
Typical properties	Test method						
Mooney viscosity ML 1 + 4	ASTM D1646	MU, 100 °C	53.4	50.6	46.4	43.6	42.5
Mooney scorch	ASTM D1646	@ 125 °C					
Time to 5pt rise		Minutes	29.5	22.0	19.2	16.9	16.8
Rheometer (MDR)	ASTM D5289	160 °C; 0.5° arc; 60 min					
Mh-Ml (delta torque)		dN m	3.7	3.3	3.8	4.4	5.1
Tc90 (time to 90% torque increase)		Minutes	12.6	7.6	8.4	8.8	9.5
Tensile strength	ASTM D412	MPa	9.9	9.8	9.7	10.6	11.6
Elongation at break		%	905	908	809	774	715
Modulus 300%		MPa	2.5	2.4	2.8	3.1	3.7
Tear strength (die B) peak load	ASTM D624	N	98.1	88.5	87.5	94.7	121.4
Tear strength (die B)		$kN\,m^{-1}$	51.2	46.1	45.7	49.6	62.0
Permeability coefficient	ExxonMobil method	cc mm $(m^2\text{-day-mmHg})^{-1}$ @ 60 °C	0.7	1.0	1.2	1.4	1.7

a) ExxonMobil chemical company data. See www.butylrubber.com for a more comprehensive list of properties.

Permeation of a gas or permeability through a membrane such as a tire innerliner consists of three distinct processes [15, 16]. First, the gas molecules must dissolve on one side of the membrane, then diffuse across the membrane or liner to the opposite side of lower gas concentration, the rate being dependent on the size of the diffusion gradient, and then evaporate or disperse in the adjacent tire component or other medium. The rate of diffusion of oxygen and nitrogen through a butyl, chlorobutyl, or bromobutyl rubber membrane is a function of several parameters. The size of oxygen and nitrogen molecules is 2.9 and 3.1 Å, respectively, with the smaller molecule expected to diffuse more rapidly. This is observed in practice. Van Amerongen [15, 16], in calculating the energy of activation of gas diffusion, also noted that diffusion coefficients can increase 1.2–3-fold with each 10 °C increase in temperature. The activation energy of diffusion was reported to be 50.6 and 49.8 kJ mol^{-1}, respectively, for nitrogen and oxygen with frequency constants, analogous to the Arrhenius constant, of 180 and 142. From thermodynamics this clearly suggests that oxygen diffuses more readily than nitrogen, as is observed. The permeability of gases through compounded bromobutyl or compounded bromobutyl natural rubber blends is defined as the amount of gas at standard temperature and pressure (STP) permeating through the compound sheet of area, *A*, thickness or gage, l, at a defined time interval, typically 1 day, with a pressure differential across the compound sheet. The permeability coefficient *(P)* can therefore be expressed in units of cc mm m^{-2} day^{-1} $mmHg^{-1}$, and is related to the diffusion coefficient *(D)* and the solubility constant *(S)* by the expression:

$$P = DS \tag{4.4}$$

Diffusion is dependent on the activation energy of diffusion and thus can be estimated through use of an Arrhenius expression:

$$D = D_o e^{-E_d/RT} \tag{4.5}$$

where E_d is the activation energy of diffusion. The value of E_d is related to the polymer and specific gas and will vary depending on the T_g. The solubility constant shows a similar relationship:

$$S = S_o e^{-\Delta H_s/RT} \tag{4.6}$$

where ΔH_s is the heat of sorption. Combining Eqs. (4.5) and (4.6) gives:

$$P = P_o e^{-E_p/RT} \tag{4.7}$$

where E_p can be referred to as the activation energy of permeation. The permeability coefficient for various compounded natural rubber and bromobutyl blends is shown in Table 4.11.

It is difficult to alter the scorch properties of bromobutyl/general-purpose rubber blends with classical retarders such as *N*-(cyclohexylthio)phthalimide. For instance, salicylic acid is a vulcanization retarder for general purpose rubbers (GPRs), but an accelerator for bromobutyl rubber. Alkaline retarders used with bromobutyl rubber are often accelerators for GPR. Therefore, the scorch time of blends is best set by

appropriately choosing the cure system and the compound viscosity (as it influences the heat history of the compound during processing). Magnesium oxide is frequently used at between 0.1 to 0.5 phr as a scorch inhibitor in compounds containing 100 phr content bromobutyl rubber or bromobutyl/natural rubber blends.

4.5.3
Bromobutyl/Butyl Rubber Blends

With bromobutyl/butyl rubber blends, elastomer structures are essentially the same, but the different reactive functionalities provide different vulcanization chemistry. Since bromobutyl rubber has greater cure reactivity, accelerators that will over-cure the bromobutyl rubber phase should be avoided. Briefly:

1) Low level blending of butyl rubber into bromobutyl rubber increases the scorch time and improves the heat resistance of the compound.
2) Blends with up to 20 phr of butyl rubber exhibit bromobutyl rubber-like adhesion.
3) Butyl rubber levels in excess of 20 phr sharply reduce adhesion to general purpose rubber compound substrates. Blending up to 30% butyl into bromobutyl rubber slows the cure rate and provides a small benefit in lower modulus increase and higher retained elongation after heat aging.

Because butyl has the same permeability coefficient as bromobutyl rubber, blending it into a bromobutyl rubber compound does not alter the compound permeability as, for example, natural rubber would.

4.5.4
Bromobutyl/Chlorobutyl Rubber Blends

In bromobutyl/chlorobutyl rubber blends, both elastomers have the polyisobutylene backbone and halogen reactive functionality. These polymers, being molecularly miscible, constitute an ideal system for co-vulcanization. Bromobutyl and chlorobutyl can be used interchangeably without significant effect on state of cure as measured by extension modulus, tensile strength, and cure rheometer torque development. Bromobutyl will increase the cure rate of a blend with chlorobutyl. However, where bromobutyl is the major part of the blends, chlorobutyl does not reduce scorch tendencies because the more reactive halogen unit can dominate.

4.5.5
Bromobutyl/Styrene Butadiene Rubber Blends

Like natural rubber, styrene butadiene rubber (SBR) can be blended in all proportions with bromobutyl rubber. However, SBR is less desirable for blending than natural rubber due to its low tack and green strength properties. In addition, heat, flex fatigue resistance, and weathering resistance are poorer with SBR blends than with natural rubber blends. Suggested cure systems are the same as those for bromobutyl/natural rubber blends.

4.5.6
Bromobutyl/GPR/EPDM Rubber Triblends

Ethylene propylene diene terpolymers (EPDM) can be used to improve the ozone resistance of bromobutyl/natural rubber binary polymer blends, eliminating the need for chemical antiozonants. Addition of 10 phr of EPDM (with a high ethylidene norbornene, ENB, content of 9%) to a 50/50 bromobutyl rubber/natural rubber blend results in a compound with good static and dynamic ozone resistance. EPDM with a 5.7% ENB level is another suggested grade of polymer.

Such blends have significant industrial significance as they are frequently used to prepare white sidewalls and white lettering on tires. In these blends, natural rubber contributes adhesion to adjacent components and lower energy loss, EPDM imparts static ozone resistance, and bromobutyl rubber provides flex and dynamic ozone resistance. EPDM rubbers with the highest degree of unsaturation are suggested for a high state of vulcanization in general-purpose rubber/bromobutyl blends. Bromobutyl rubber and EP or EPDM rubber can be blended in all proportions and can be co-vulcanized using either zinc oxide/sulfur cure systems or peroxide based cure systems.

4.5.7
Distribution of Compounding Ingredients: Insoluble Chemicals

When natural rubber and polybutadiene are blended carbon black normally locates preferentially in the polybutadiene phase [2]. This distribution can enable better compound performance such as tensile strength, tear strength, and hysteretic properties. Carbon black particles may migrate from the natural rubber masterbatch phase to the polybutadiene gum phase during mixing when the compound is at elevated temperatures and this transfer continues until phase saturation occurs. Under these conditions, the steric bulk of the carbon black aggregate, polymer viscosities, and mixing temperatures would be the principal factors affecting any particle distribution in the final compound. Table 4.12 shows the effect of carbon black polymer phase distribution on some compound mechanical properties.

The incorporation of carbon black into 50/50 elastomer preblends shows carbon black affinity decreases in the order BR, SBR, CR, NBR, EPDM, and butyl rubber. Poor carbon black dispersion causes an increase in hysteresis and a decrease in fatigue resistance. The effect of volume loading of a filler such as carbon black on the properties of the vulcanizate depends on whether the elastomer is strain-crystallizing or not.

The tensile strength of filled elastomers over the tensile strength of the gum rubber is much greater for SBR. A greater increase in tensile strength is attainable for non-crystallizable polymers. Filler distribution is also affected by filler type. Elaborating:

1) Reinforcing fillers such as carbon black and silica have a critical loading factor that is different for each polymer and filler type. For example, the optimum loading for SAF grade carbon blacks in natural rubber will be in the range 45–60 phr, whereas for highly dispersible silicas in solution SBR it will be in the range 75–85 phr.

Table 4.12 Natural rubber (50 phr)–polybutadiene (50 phr) casing compound with 40 phr GPF carbon black [1, 2].

	Compound		
	1	**2**	**3**
Natural rubber	100	50	50
Polybutadiene		50	50
Carbon black (N 660)	40	40	40
Carbon black location	NR phase	BR phase	MR phase
Tensile strength (MPa)[a)]	24.5	17.5	15.8
Elongation (%)	511	435	439
300% Modulus (MPa)	12.2	10.8	9.3
Tear strength (kN m^{-1})[b)]	18.7	14.8	11.3

a) Measured according to ASTM D412.
a) Measured according to ASTM D624.

2) Non-reinforcing fillers such as clay and calcium carbonate may be enhanced with surface treatments such as carboxylated polybutadiene, calcium stearate, or an organo-silane coupling agent.
3) With all types of fillers, distribution is important for wear resistance and tear strength.

As already noted, a higher distribution of carbon black in the polybutadiene phase will improve vulcanizate properties. As an empirical guideline, tire tread wear and compound tensile strength are improved while tear strength improves and then drops off as a higher percentage of carbon black is located in the polybutadiene phase (Figure 4.8). Similarly, as an empirical guideline, Figure 4.9 illustrates that hysteresis is also improved as the percentage of carbon black in the polybutadiene phase is increased.

These empirical trends suggest that an optimum distribution of 60% of the carbon black in the polybutadiene phase will give the best hysteretic characteristics in a compound.

As for natural rubber/SBR masterbatch blends, carbon black will migrate to the SBR gum phase. At equilibrium, the amount of carbon black in the natural rubber phase will depend on the particle size. For example, the amount of carbon black remaining in the natural rubber phase can drop from 41% for NSSO to only 27% when using N134. Other factors or empirical guidelines affecting the distribution of fillers include:

1) The surface polarity of carbon black influences its distribution in elastomer blends.
2) Silica will tend to accumulate in the natural rubber phase.
3) The filler phase distribution is influenced by the point of addition in the mix cycle.
4) The use of coupling agents will potentially bind a filler into one phase.
5) Bound rubber (NR/CB) tends to form more readily in the carbon black loaded natural rubber phase than in the polybutadiene phase.

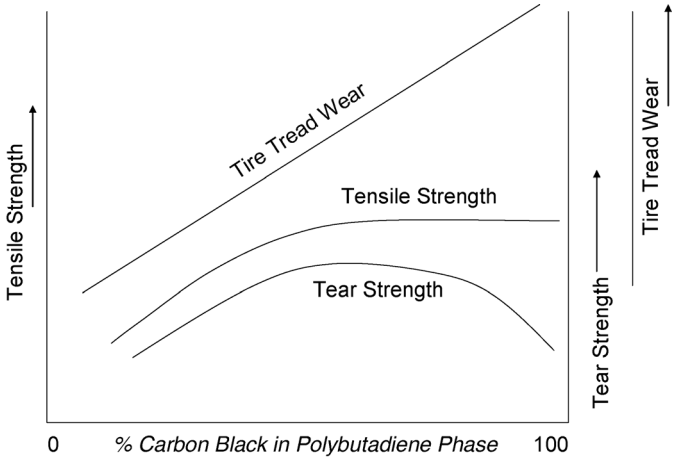

Figure 4.8 Carbon black dispersion and general trends in elastomer compound properties [1, 17].

The carbon black critical loading factor and the optimum loading level will be a function of the specific carbon black grade and specific grade of polymers in the rubber compound blend, and are therefore unique for each polymer and filler system.

4.5.8
Distribution of Compounding Ingredients: Soluble Chemicals

The distribution of soluble compounding ingredients, especially curatives, may significantly influence the performance of the vulcanized product. Diffusion of common vulcanizing ingredients, such as sulfur, tetramethylthiuram disulfide (TMTD), benzothiazole disulfide (MBTS), and diphenylguanidine (DPG) occurs

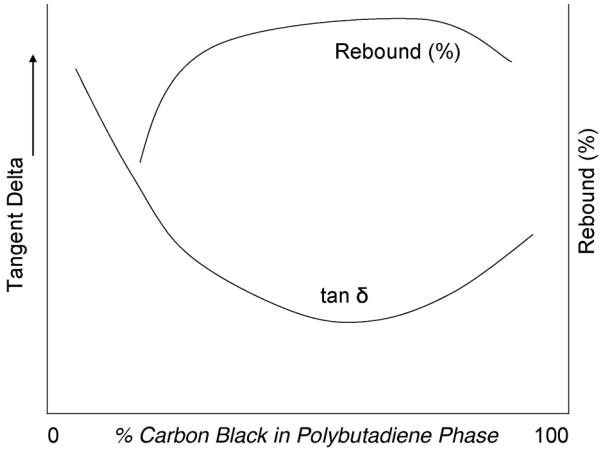

Figure 4.9 Carbon black dispersion and general trends in compound hysteresis [1, 17].

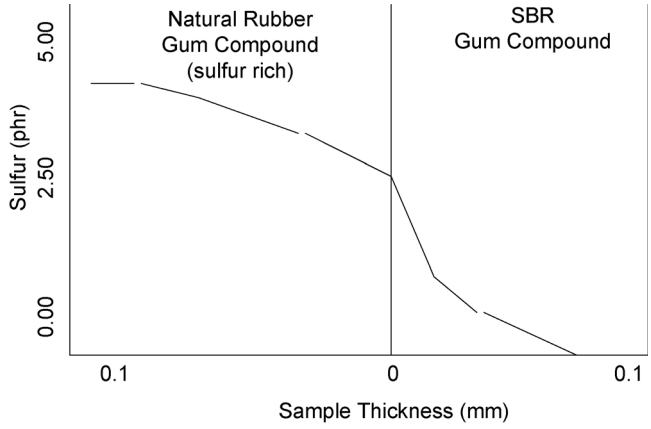

Figure 4.10 Illustration of the diffusion of sulfur from natural rubber to SBR at 150 °C [1, 2]. Adapted from Reference [1].

from compounded low unsaturated elastomers such as IIR and EPDM to high unsaturation elastomers such as NR and SBR.

The migration of curatives was observed to happen very quickly (e.g., 3 s at 150 °C). A diffusion gradient may be produced between the dissimilar elastomers well before any vulcanization occurs. The practical consequences of the solubility and diffusion differences in elastomer blends are curative imbalance between the component phases and associated over- and under-cure.

Methods to prevent this diffusion gradient include preparing a masterbatch of dithiocarbamate accelerators in the polymer (IIR, EPDM) and grafting accelerators onto the polymer (EPDM). One advantage of a cure system mismatch is improved ozone crack resistance. In any case, cure system location control is critical. Figure 4.10 shows the diffusion of sulfur from natural rubber to SBR. Two rubber samples are placed in contact with each other and heated. The sulfur concentration is then measured at increasing distances from the interface. In this case, considerable transfer occurs and significant concentrations build up in the SBR phase.

In contrast, the level of sulfur migration is much less from natural rubber to butyl rubber. The solubility of sulfur in butyl is much less than the solubility of sulfur in natural rubber (Figure 4.11). The diffusion of MBTS is similar to sulfur diffusion, but it occurs more slowly due to the large size of the MBTS molecule. MBTS is also less soluble than sulfur in each rubber type (Figure 4.12).

To summarize the distribution of soluble compound chemicals in polymer blends:

1) Sulfur diffuses from NR to SBR until equilibrium is reached.
2) Little diffusion of sulfur occurs from natural rubber to butyl due to the low solubility in butyl rubber.

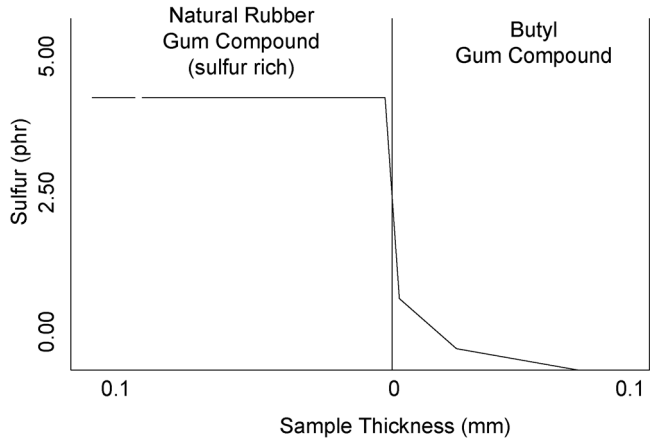

Figure 4.11 Simplified illustration of the diffusion of sulfur from natural rubber to butyl rubber at 150 °C [1, 2]. Adapted from Reference [1]..

3) The diffusion coefficient is lower for MBTS and *t*-butyl-2-benzothiazole sulfenamide (TBBS) due to:
   a) the larger steric bulk of its molecule compared to sulfur;
   b) the aromatic nature of MBTS and TBBS.
4) The cured properties imbalance may not be equal to that of homogenous polymers due to the level of curative imbalance between the phases.
5) Oil migration is also dependant on the polymer matrix.
6) Antioxidants and antiozonants diffuse to equilibrate themselves in the tire.

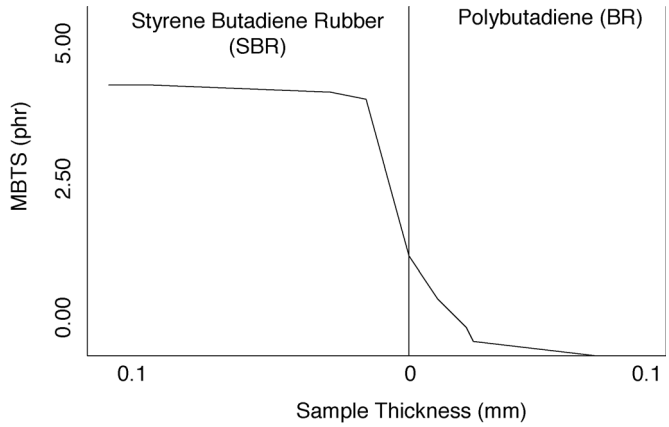

Figure 4.12 Illustration of the diffusion of MBTS from SBR to BR at 150 °C [1, 2]. Adapted from Reference [1].

7) 1,3-Dimethylbutyl-*N*′-phenyl-*p*-phenylenediamine (6PPD), which is an important antiozonant used extensively in tires, migrates preferentially during curing as follows:
   a) EPDM to SBR,
   b) SBR to NR,
   c) EPDM to NR.
8) The migration rate is the fastest for 6PPD but slower for mixed diaryl phenylenediamines, and slowest for polymerized dihydrotrimethyl-quinoline (TMQ).
9) In the category of processing aids, oil solubility parameters are in the range 15.0–16.5 $MPa^{1/2}$. Most processing aids have a T_g between −45 °C and −90 °C.

Where this has become of considerable importance is when using components in tires as reservoirs for migratory chemicals such as antiozonants and antioxidants. For example, the apex or shoulder wedge can be saturated with migratory antiozonants. As the protectants in the sidewall compound become depleted, then antiozonants from internal tire components can migrate into the sidewall, thereby offering extended protection from weathering, ozonolysis, and oxidation. This in turn contributes to an extension of the tire service life.

4.5.9
Effect of Blending on Compound Physical Properties

Most reported studies on elastomer blends focus on general purpose elastomers, with emphasis on processing and attainment of specific mechanical properties. It would therefore be appropriate to review these two factors. There are three methods by which a polymer blend may be mixed with carbon black:

1) mix the first polymer with carbon black, and then dilute it with the second polymer;
2) preblend the two polymers and then add carbon black;
3) mix a carbon black–polymer masterbatch for each of the two polymers and then blend the materials.

Uneven distribution of carbon black can be observed, particularly in the first two instances, with a potential loss in material mechanical properties. Furthermore, during processing and when the compound is in the uncured state, carbon black can migrate from the polymer with a low affinity for carbon black to one with a high affinity. This can be partially prevented by use of the concept of dynamic vulcanization where initial pre-vulcanization can lock carbon black into a particular phase. It would now be appropriate to describe the impact two specific polymer blends have on compounded material properties. Addition of polybutadiene to natural rubber can result in:

1) improvement in heat stability,
2) decrease in tensile strength,
3) decrease in 300% modulus,
4) increase in elasticity,

5) increase in abrasion resistance,
6) improvement in tread wear resistance,
7) improvement in fatigue resistance.

Polybutadiene/natural rubber blends tend to find application in truck tire tread compounds and sidewalls. Polybutadiene is also blended with SBR in treads. Here blend ratios tend to be optimized for factors such as wear resistance, traction requirements, rolling resistance, and damage resistance. Empirical guidelines for determining blend ratios are based on the work of Nordsiek and coworkers reviewed earlier [4]. Briefly:

1) an increase in SBR levels relative to polybutadiene allows improvement in traction due to the increase in compound T_g;
2) an increase in the SBR level improves handling, again due to the increase in T_g and increase in stiffness or storage modulus (E');
3) a drop in SBR level with increasing polybutadiene level improves wear performance;
4) blends of natural rubber, SBR, and polybutadiene can be optimized for high-performance tire treads, depending on requirements for factors such as aligning torque, steering precision, and high speed.

4.6
Secondary Polymer Blends Systems

Natural rubber or synthetic elastomers can be blended with a range of additional materials that can be defined as secondary polymer systems. This would include such materials as resin systems, high molecular weight green strength promoters, and polymeric antioxidant systems.

4.6.1
Resins Systems

Resins used in rubber compounding can be classified into one of three groups [18]:

1) **Tackifying resins**: , which remain predominantly unchanged during the vulcanization process.
2) **Reinforcing resins**: where the resin when mixed with a catalyst or hardening agent reacts with itself during vulcanization to form an interpenetrating network and does not participate in other crosslinking reactions to any significant degree.
3) **Curing resins**: where the resin reacts with the polymer, thereby crosslinking it.

There are exceptions in all three groups. For example, C_5 tackifying resins can have a significant level of unsaturation, which can crosslink at curing temperatures of 160 °C.

4.6.2
Tackifying Resins

Although there are many types of tackifying resins available, they can all be grouped into two major categories: natural resins or synthetic resins. Natural resins include pine gum and terpenes obtained from the tapping and distillation of pine tree stumps. Coumarone–indene resins are produced by acid-catalyzed polymerization of coumarone–indene fractions obtained from coal tar, which in turn are a by-product of coke manufacturing. Such resins, however, are in decline due to limited availability of raw material and the ease of obtaining hydrocarbon resins from petroleum feed stocks. Synthetic resins can in turn be classified in two broad categories: C_5 aliphatic resins (from C_4–C_6 petroleum feed streams) and C_9 aromatic resins (from C_8–C_{10} petroleum feed streams). The characteristics of tackifying resins influence not only how they will be used, but also the properties they impart when employed within a rubber compound. These resin characteristics include:

1) glass transition temperature,
2) viscosity,
3) molecular weight and molecular weight distribution,
4) solubility and compatibility,
5) residual unsaturation,
6) color,
7) acidity and basicity.

These properties will in turn control both the performance of the resin in a specific rubber formulation and the compound processing characteristics.

4.6.3
Reinforcing Resins

Reinforcing resins or novolacs form an interpenetrating network and can interact with other polymers. Hexamethylenetetramine–resorcinol systems do not start to react until temperatures exceed 120 °C. At vulcanization temperatures of 160 °C they can significantly increase the stiffness of rubber compounds though in dynamic service conditions such as in a tire tread compound the stiffness imparted by such novolac resins may be degraded.

Phenolic novolak resins and high styrene SBR resins are used for reinforcing and increasing the hardness and modulus of rubber compounds. Resorcinol novolak resins are used as a part of the adhesion system between rubber and brass plated steel cord or organic fibers. Both phenolic novolak and resorcinol novolak resins require the addition of a methylene donor such as hexamethoxymethylmelamine (HMMM) or hexamethylenetetramine (HMTA) to fully crosslink and become a thermoset. Phenol, alkyl phenols, and resorcinol can be reacted in bulk or in a polymeric formulation with methylene donors. Typical donors are 2-nitro-2methylpropanol (NMP), HMTA, and HMMM, used to produce a thermoset resin network in the

rubber compound. HMTA and HMMM are the preferred methylene donors used in rubber formulation.

Both of these curatives are added in the lower temperature, final mixing stage. HMTA must be isolated from the other rubber curatives during storage and batch preparation since its basicity can cause premature decomposition of the rubber cure accelerators and can accelerate the conversion of insoluble sulfur into the soluble form. The structure of HMTA and the reaction with resorcinol are illustrated in Scheme 4.1. Classical chemical studies indicate that as much as 75% of nitrogen remains chemically bonded to the rubber though some ammonia is released during the cure of the resin and the rubber, which can have detrimental effects on rubber composites reinforced with brass coated steel cords.

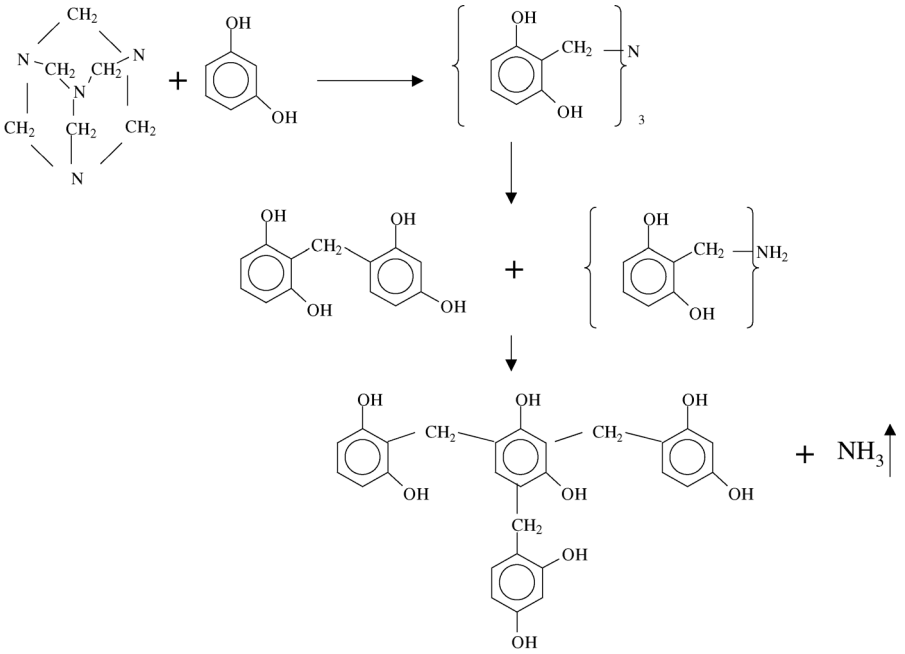

Scheme 4.1 HMTA and resorcinol IPN formation.

Scheme 4.2 shows the base structure of HMMM and the reaction with resorcinol. Although it is conceivable that a methylene group might be transferred from HMMM to the resorcinol, as is the case with HMTA, it is generally accepted that the entire melamine structure is joined to the resorcinol molecule through a methylene bridge. Formation of linear and branched structures occur through one of two paths: the addition of a second and third melamine methylene bridge to the same resorcinol or the reaction of additional resorcinol units onto the remaining site of the original melamine unit. Steric factors and chemical reactivities will determine the extent to which each pathway is followed in the formation of the branched resin structure [18].

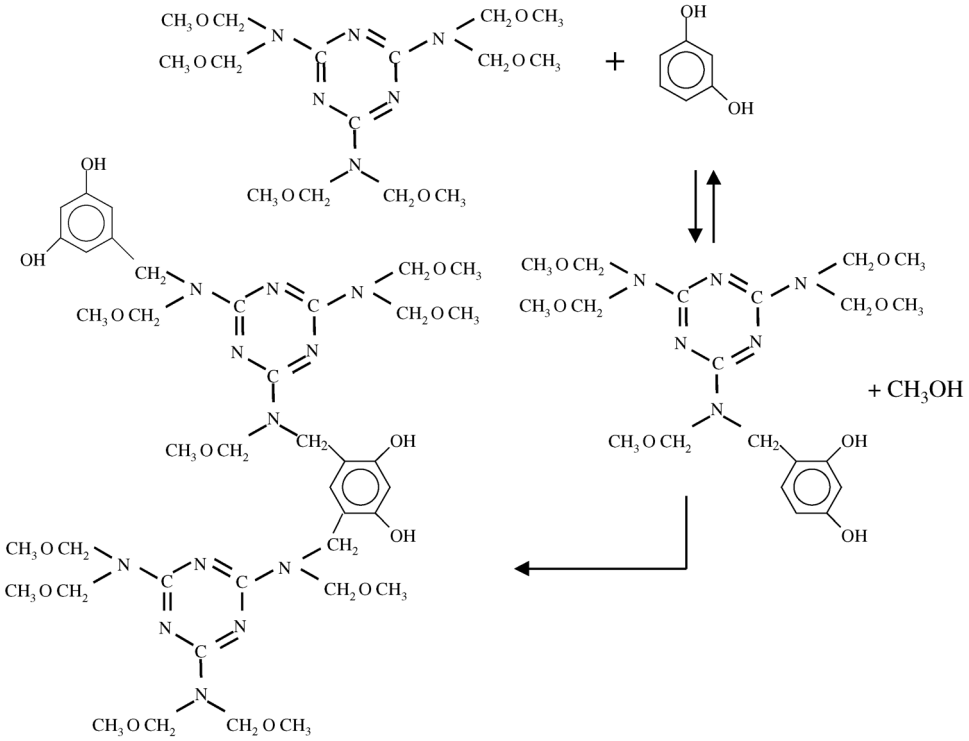

Scheme 4.2 HMMM and resorcinol IPN formation.

4.6.4
Curing Resins

A significant advance in improving the service life of tire curing bladders was the development of phenol formaldehyde based resol curing resins for vulcanization of butyl rubber. The resulting butyl rubber compound has a stable crosslink network and is not readily susceptible to reversion. Bladder compound curing temperatures of 190 °C are higher than typically seen for novolacs. However, if bladders have been over-cured they may be susceptible to tearing. Under-cured butyl bladder compounds may be result in wrinkles, which would then deform green tires at the start of the tire curing operation. Castor oil is typically used in bladder compounds to adjust viscosity as it is less volatile than paraffinic oils and can reduce the tendency for compound scorching.

Phenol formaldehyde curing resins are classified as resols. Unlike the linear novolak resins, resols are three-dimensional resin systems that form crosslinked networks that reinforce the resultant cured compound. A characteristic of these resins is the presence of an alkyl group in the *para*-position of phenol group. Resin curing of butyl rubber is a function of the reactivity of the phenol-methylol groups in the reactive phenol formaldehyde resin. Curing resins such as a heat-reactive octylphenol formaldehyde resin containing methylol groups can be used. For a faster cure, addition of a halogen donor such as polychloroprene or stannous chloride is required [18]. A more

reactive resin–cure system not requiring an activator is obtained when a portion of the methylol groups is replaced by bromine. An example of this resin is brominated octylphenol formaldehyde resin [18].

Two mechanisms have been proposed for resin curing of butyl rubber. One proposal involves an *ortho*-methylene-quinone intermediate that abstracts an allyl hydrogen from the isoprenoid group of the butyl polymer chain and would occur via the formation of a six-membered ring "ene" intermediate. This would be followed by formation of a second *ortho*-methylene-quinone intermediate with another isoprenoid group of an adjacent butyl polymer chain to form a monophenol crosslink (Scheme 4.3).

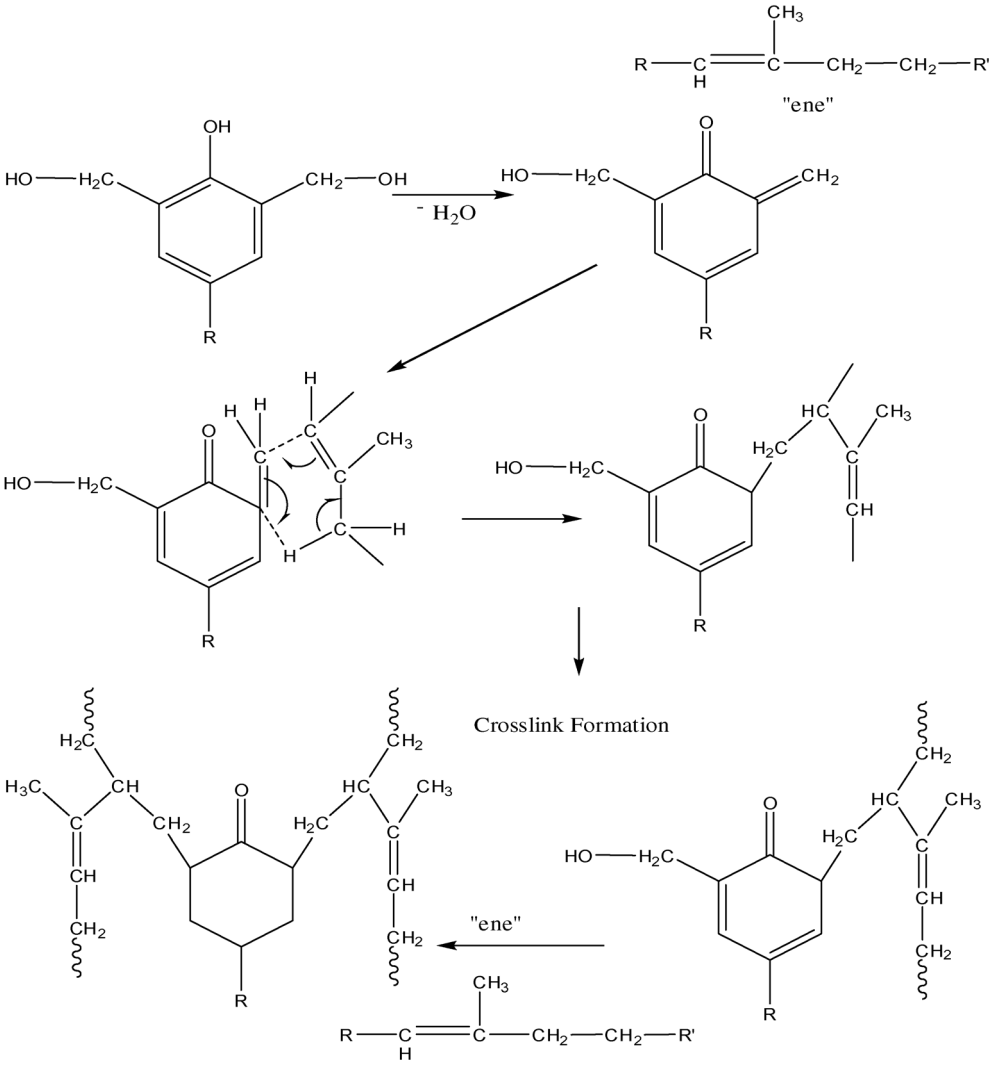

Scheme 4.3 Allyl hydrogen mechanism [18].

This mechanism is distinct from a Diels–Alder mechanism, which may also occur though, if so, in low yield. A chromanone mechanism has also been proposed and leaves no unsaturation upon crosslink formation. Though this has now become the most likely mechanism, the six-membered "ene" reaction mechanism may still play a role in crosslink formation but, again, at a low yield.

Scheme 4.4 illustrates schematically the reaction of a curing resin (heat reactive octylphenol formaldehyde) in the vulcanization of butyl rubber. Following the elimination of water in the reaction sequence, the exomethylene group and carbonyl oxygen react with an isoprenyl unit in butyl rubber to form a chroman ring. Chroman ring structures are very stable and are frequently found in natural product biosynthesis.

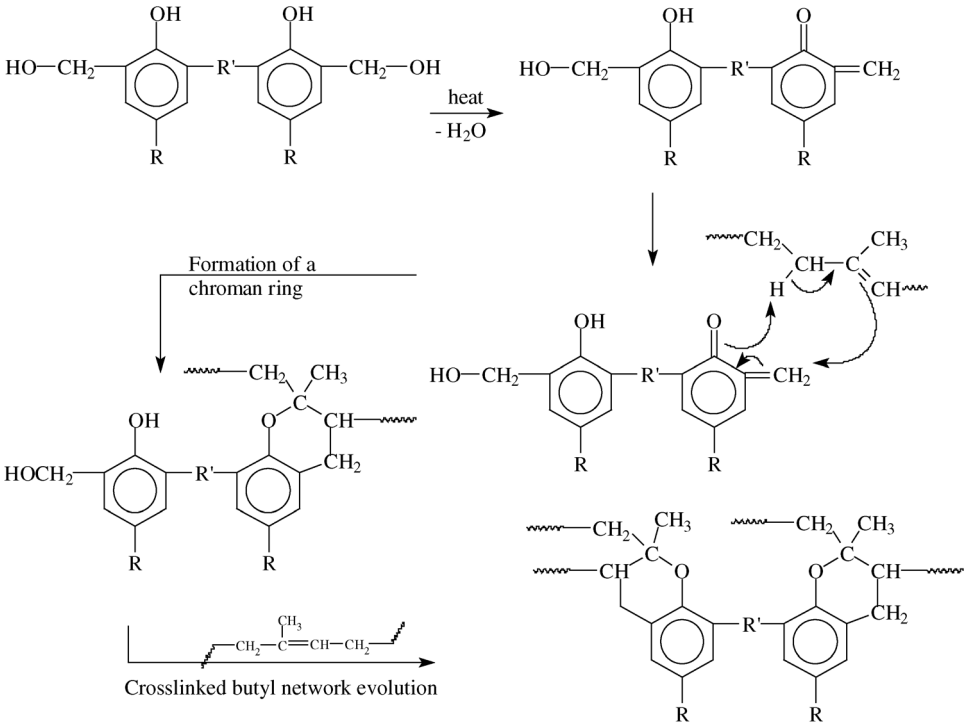

Scheme 4.4 Resin curing of butyl rubber [18].

4.6.5
Polymeric Green Strength Promoters

Several polymeric green strength promoters have been developed. The green strength promoter with commercial designation Vestenamer 8012 is a polyoctenamer manufactured by Huls [2]. The raw material for this polymer is cyclooctene. In a metathesis polymerization reaction cyclooctene is converted into a polyoctenamer. It was developed as a green strength promoter for tire sidewalls, apexes or bead fillers, and other

components where dimensional stability is important. It meets four requirements: serving as a green strength promoter, rapid crystallization rate, low viscosity, and unsaturation for participation in the vulcanization or crosslinking reaction.

Formation of a network of low molecular weight polymers will manifest itself through a loss in mechanical properties. Conversely, a network of unsaturated, cyclic, low molecular weight polymers will have the potential of improving the mechanical properties of the material in a composite structure such as a tire. This is due in part to their participation in vulcanization. The high macrocyclic ring structure of polyoctenamers improves heat stability at elevated temperatures, owing to the interpenetration of linear polymer chains and cyclic macromolecules.

4.7
Elastomer Blends and Tire Performance

Elastomer blends are used extensively throughout a tire. Sidewalls tend to be composed of natural rubber and polybutadiene. Sometimes SBR is also employed. Liners can contain butyl or halogenated butyl polymers. Natural rubber is often found in the liners of tube-type tires. Tread compounds can contain combinations of the general purpose elastomers, and additional specialty polymers such as the terpolymer styrene–isoprene–butadiene rubber (SIBR) or functionalized SSBR. Within one class of polymer such as polybutadiene, the microstructure can have a significant impact on performance. For example, polybutadiene can be polymerized by a range of metals such as lithium in solution polymerized systems, and nickel or titanium in Ziegler–Natta systems. Here, the *cis*-butadiene level can range from 43 to 98%. As an example of how this affects compounded properties, the fatigue life of a polybutadiene in a carbon black loaded compound can vary from 3 kilocycles to failure on the Monsanto fatigue-to-failure instrument to over 40 kilocycles to failure. Furthermore, an increase in the vinyl-butadiene level will tend to have a negative effect on resistance to fatigue. This in turn impacts tire performance. As a general rule, several guidelines can be outlined to predict abrasion resistance of a tread compound:

1) 100% polybutadiene gives the best tread wear performance or abrasion resistance.
2) SBR tends to give directionally better wear performance than natural rubber.
3) Blending natural rubber, or SBR, with polybutadiene gives an improvement in abrasion resistance or tread wear.
4) Similarly, the tread wear performance of natural rubber can be improved through addition of SBR.
5) A balanced set of tire tread material properties such as wear, traction, heat build-up, and damage resistance is achievable through effective blending of all three general purpose rubbers, natural rubber, SBR, and polybutadiene.
6) The properties of compounded blends will be affected by the vulcanization system and filler distribution.
7) Attainment of a single T_g is important in ensuring low hysteresis.

Table 4.13 Natural rubber (50 phr)–polybutadiene (25 phr) casing compound with 40 phr GPF carbon black. Adapted from Reference [1].

	Compound		
	1	**2**	**3**
Natural rubber	100	50	50
Polybutadiene		50	50
Carbon black (N660)	40	40	40
Carbon black (NR)	100	25	75
Percent location (BR)		75	25
Tensile strength (MPa)	23.1	19.1	17.4
Elongation (%)	509	451	444
300% Modulus (MPa)	11.5	10.7	10.1
Tear strength ($kN\,m^{-1}$)	26.5	19.7	18.4

Though the preparation of blends can enhance material performance properties, there are losses in other characteristics. Addition of polybutadiene to natural rubber compounds results in a drop in tensile strength, ultimate elongation, and tear strength. For example, on addition of 50 phr of polybutadiene to an all natural rubber compound, and having all of the carbon black in the polybutadiene phase, the tensile strength drops from 24.5 to 17.5 MPa. With all the carbon black in the natural rubber phase only, the tensile strength drops further to 15.8 MPa (Table 4.12) [1, 2].

Similar trends are observed in compounds with only 25 phr of polybutadiene added to the natural rubber compound (Table 4.13). The tensile strength drops from 23.1 to 17.4 MPa, with the location of the carbon black playing a critical role in generation of the compound mechanical properties. Several observations can be noted:

1) An increase in the amount of carbon black in the polybutadiene phase increases the compound tensile strength, tear strength, and resilience.
2) Adding all the carbon black to the natural rubber phase causes a drop in tensile strength of up to 25%.
3) Hardness increases with increasing carbon black content in the natural rubber phase.

In summary, several points can, briefly, be noted in the preparation of elastomer blends:

1) proper selection of polymers to be used in elastomer blends is critical;
2) the impact of microstructure, as determined by the polymer catalyst system, will influence the selection of polymers;
3) distribution of compound ingredients such as carbon black affects key mechanical properties such as tensile strength;
4) distribution of cure system components is affected by the selection of polymers in the blend;
5) high polybutadiene levels favor good tread wear performance, but there will be a trade-off in other properties, such as traction.

4.8
Tire Tread Compound Formulary

Tread compounds can be based on either a single polymer or a blend of polymers. Natural rubber, emulsion SBR, solution SBR, BR, and isobutylene-based elastomers are used in such blends. The following tables illustrate tread formulations designed for specific applications:

- Table 4.14: low rolling resistance passenger tire tread;
- Table 4.15: silica-based passenger tire tread;
- Table 4.16: high-performance passenger tire tread;

Table 4.14 Model low rolling resistance automobile tire tread compound [19].

	phr
Natural rubber (TSR 20)	50.00
SBR (IISRP 1500)	50.00
N299	45.00
Aromatic oil	9.00
Antioxidant	1.00
Antiozonant	2.00
Wax	1.00
Stearic acid	3.00
Zinc oxide	3.00
MBTS	0.80
Sulfur	1.60
DPG	0.40

Table 4.15 Model silica tread compound [19].

	phr
Solution SBR, 26% styrene	75.00
BR, 93% cis	25.00
Highly dispersible silica	80.00
Reinforcing agent, X50S	12.80
Aromatic oil, Sundex 8125	32.50
Antioxidant, 6PPD	2.00
Paraffin wax	1.50
Zinc oxide	2.50
Stearic acid	1.00
Sulfur	1.40
CBS	1.70
DPG	2.00

Table 4.16 High-performance tire tread compound.

Ingredient	phr
SBR 1712	110.00
BIIR 2255	20.00
N134	85.00
Aromatic oil	25.00
Antiozonant	2.00
Antioxidant	1.00
Stearic acid	2.00
Wax	2.00
Zinc oxide	3.00
Sulfur	2.50
N-Cyclohexyl-2-benzothiazole sulfenamide (CBS)	2.00
N-(Cyclohexylthio)phthalimide (PVI)	0.15

Table 4.17 Model winter tire tread compound.

Ingredient	phr
BIMSM	20.00
Polybutadiene	40.00
NR, (SMR 20)	40.00
Silica, HDS	75.00
Silane coupling agent	10.20
Processing oil	30.00
Stearic acid	1.00
Antiozonant, 6PPD	1.50
Antioxidant TMQ	1.00
Zinc oxide	2.00
Sulfur	1.00
DPG	2.00
TBBS	1.50

Table 4.18 Model CIIR winter tire tread compound.

Ingredient	phr
Natural rubber	30.00
SBR (IISRP 1500)	15.00
Polybutadiene	35.00
Chlorobutyl rubber	20.00
Carbon black (N339)	55.00
Butyl oleate	10.00
Stearic acid	2.00
Zinc oxide	5.00
TBBS	0.80
Sulfur	2.00

Table 4.19 Model truck tire tread compounds [4, 5].

	Rib tire tread pattern	Lug tire tread pattern
Ingredient	phr	phr
Natural rubber (TSR20)	100.00	50.00
Polybutadiene, low T_g BR (Budene 1207)		50.00
N220	50.00	60.00
Peptizer	0.25	0.25
Paraffin wax	1.00	1.00
Microcrystalline wax	2.00	2.00
Naphthenic oil	4.00	4.00
Antioxidant	1.00	1.00
Antiozonant	2.00	2.00
Stearic acid	1.00	1.00
Zinc oxide	4.00	4.00
Sulfur	1.00	1.00
TBBS	1.00	1.25
N-(Cyclohexylthio)phthalimide (PVI)	0.10	0.15

Table 4.20 Model earthmover tire tread compound [4, 5].

Component	phr
Natural rubber	100.00
N220 Black	45.00
Silica	15.00
Antioxidant	1.50
Antiozonant	1.50
Aromatic oil	3.00
Stearic acid	2.00
Zinc oxide	5.00
Poly(ethylene glycol)	0.30
Sulfur	1.90
TBBS	1.40

- Table 4.17: winter tire tread;
- Table 4.18: model CIIR winter tire tread compound;
- Table 4.19: Radial light and medium truck tire tread;
- Table 4.20: Earthmover tire tread.

4.9 Summary

This chapter has briefly discussed aspects of basic polymer science, tire compounding, and blending of elastomers. The impact of elastomer blends on tire performance and

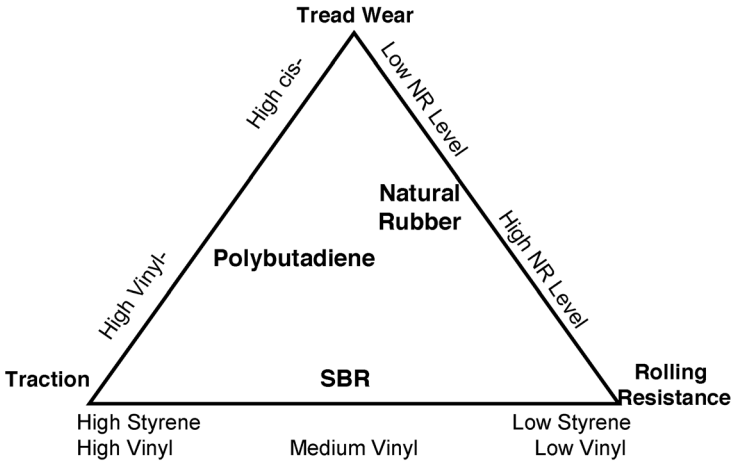

Figure 4.13 Performance triangle in elastomer selection for final product specification.

secondary polymer blend systems was also discussed. Phase morphology is influenced by the polymers used in a blend. Compounding of elastomers will have a significant effect on tire performance. Figure 4.13 illustrates the observations presented in this chapter in one diagram. For example, if rolling resistance and tread wear is preferred, then the polymers selected will tend to be low styrene, low vinyl SBR, natural rubber and high *cis*-polybutadiene. Conversely, if a high-performance tire tread compound is required, then there would be a predominant use of high styrene SBR with high vinyl polybutadiene depending on the degree of traction required.

The application of new, novel approaches to raw materials development and their use in elastomer blends could offer potential for the next breakthrough in polymer science. To conclude, a wide range of subjects in the field of elastomer blends offer opportunities for further research. These include:

1) block copolymers;
2) polyurethane and general purpose elastomer blends;
3) thermoplastic/elastomer blends;
4) application of novel monomers such as organosilanes and organometallic complexes such as those of zirconium, titanium, and cobalt.

References

1 Corish, P.J. (1994) Elastomer blends, in *Science and Technology of Rubber*, 2nd edn (eds J.E. Mark, B. Eurman, and F.R. Eirich), ch. 12, pp. 545–599, Academic Press, San Diego.

2 Rodgers, B. and Ryba, J. (1995) Principles of polymer blending. Paper V presented at the 147th Meeting of the Rubber Division, American Chemical Society. Philadelphia.

3 J. McGraw (ed.) (2008) *The Synthetic Rubber Manual*, 17th edn, International Institute of Synthetic Rubber Producers, Houston TX.

4 Rodgers, B. and Waddell, W. (2005) The science of rubber compounding, in *Science and Technology of Rubber*, 3rd edn (eds J.E. Mark, B. Eurman, and F.R. Eirich), ch. 9, pp. 401–454, Elsevier Press, San Diego.

5 Rodgers, B., Tracey, D., and Waddell, W. (2004) Tire applications of elastomers; treads. Paper H. Presented at a Meeting of the American Chemical Society Rubber Division, Grand Rapids MI.

6 Nordsiek, K.H. (1985) The 'Integral Rubber' concept – an approach to an ideal tire tread rubber. *Kaut. Gummi Kunstst.*, **38**, 178.

7 Halasa., A. (1997) Preparation and characterization of solution SIBR via anionic polymerization. *Rubber Chem. Technol.*, **70**, 295.

8 Day, G. and Futamura, S. (1987) A comparison of styrene and butadiene in tire tread polymers. *Kaut. Gummi Kunstst.*, **40**, 39; Day, G. and Futamura, S. (1986) A comparison of styrene and butadiene in tire tread polymers, Paper 22, Presented at a Meeting of the American Chemical Society, Rubber Division, 1986.

9 Waddell, W. and Rodgers, B. (2004) Tire applications of elastomers; casing. Paper I. Presented at a Meeting of the American Chemical Society Rubber Division, Grand Rapids MI.

10 Waddell, W. and Rodgers, B. (2004) Tire applications of elastomers; innerliner. Paper J. Presented at a Meeting of the American Chemical Society Rubber Division, Grand Rapids MI.

11 Rodgers, M.B. and Waddell, W. (2004) Rubber compounding, in *Encyclopedia of Polymer Science and Technology*, 3rd edn (ed. J. Kroschwitz) Vol. 11, pp 612–670, Wiley-Interscience.

12 Grulke, E.A. (1999) Solubility parameter values, in *Polymer Handbook*, 4th edn (eds J. Brandrup, E.H. Immergut, and E.A. Grulke.), pp. 675–714, John Wiley & Sons, Inc., New York.

13 Robeson, L.M. (2007) *Polymer Blends, A Comprehensive Review*, Hanser, Cincinnati.

14 Coleman, M.M., Serman, C.J., Bhagwagar, D.E., and Painter, P.C. (1990) A practical guide to polymer miscibility. *Polymer*, **31**, P1187.

15 Van Amerongen, G.J. (1955) The Effect of fillers on the permeability of rubber to gases. *Rubber Chem. Technol.*, **28**, P821–P832.

16 Van Amerongen, G.J. (1964) Diffusion in elastomers. *Rubber Chem. Technol.*, **37**, P1065–P1152.

17 Paul, D.R. and Newman, S. (1978) *Polymer Blends*, vol. **2**, Academic Press, New York.

18 Rodgers, B., Jacob, S., Curry, C., and Sharma, B.B. (2009) Butyl rubber curing bladder resin vulcanization systems: compositions and optimization. Paper 107. Presented at a Meeting of the American Chemical Society Rubber Division, Pittsburgh PA.

19 Waddell, W.H., Bhakuni, R.S., Barbin, W.W., and Sandstrom, P.H. (1990) Pneumatic tire compounding, in *Vanderbilt Rubber Handbook*, 13th edn (ed. R.O. Babitt), pp. 596–611, RT Vanderbilt, Norwalk CT.

5
Extrusion Technology for Manufacturing Polymer Blends

Kun Sup Hyun, Costas G. Gogos, and Myung-Ho Kim

5.1
Introduction

Extrusion technology for manufacturing polymer blends is commonly referred as polymer or plastics compounding and is manifested in Figure 5.1.

Mixtures of polymer(s), additives, fillers, and other ingredients are put through several elementary steps – solid feeding, melting, pumping, and sometimes reaction-involved melts and devolatilization in the processing equipment – to produce the molten polymer blends that are being pelletized in normal operations (Figure 5.2).

Figure 5.3 shows an SEM (scanning electron microscope) photograph of a compounded pellet. The same mixtures can go through the micro-structuring process during melting and mixing with or without reactions and can be made as "designer" pellets (Figure 5.4).

These micro-structured pellets are designed to provide particular characteristics; Tadmor and Gogos [1] called them "designer" pellets. These "designer" pellets are processed in extruders or in injection molding machines to form products with the possibility of further structuring or de-structuring [2].

The subject of polymer compounding has been treated in many books, notably in *Plastics Compounding – Equipment and Processing* edited by David Todd [3]. This book was published in 1998 as one of the Polymer Processing Institute Series Books and was intended to provide a pragmatic reference on compounding practice and equipment for industrial engineers in manufacturing as well as in research and development. All authors, including the editor, were practicing engineers from industry with extensive industrial experience. The book includes the following chapters:

- Introduction to compounding
- Single-screw compounding
- Counter-rotating intermeshing twin-screw extruders
- The Werner & Pfleiderer twin-screw co-rotating extruder system
- Co-rotating intermeshing twin-screw extruder: Berstorff's system
- APV (Baker Perkins) system

Encyclopedia of Polymer Blends: Volume 2: Processing, First Edition. Edited by Avraam I. Isayev.
© 2011 Wiley-VCH Verlag GmbH & Co. KGaA. Published 2011 by Wiley-VCH Verlag GmbH & Co. KGaA.

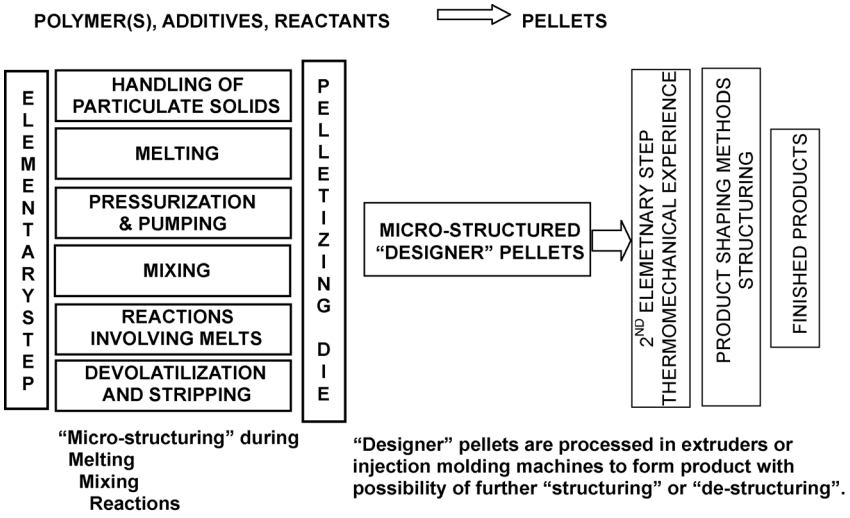

Figure 5.1 Conceptual breakdown of polymer compounding [1].

- Intermeshed TEX twin-screw extruder: JSW compounding system
- Welding Engineers' CRNI twin-screw extruders
- Farrel Continuous Mixer systems for plastics compounding
- The reciprocating single-screw extruder and its applicability to compounding.

A final chapter treats post-extruder processing. As there are no cross references between the various chapters, each chapter stands alone on its own merit.

In 2008, the book *Co-Rotating Twin-screw Extrusion – Fundamentals, Technology, and Applications* was published in English [4] (translated from the original German edition). This book is based on a seminar regularly held by the editor, Dr. Klemens Kohlgruber, and organized by the Association of German Engineers (VDI) on the subjects of fundamentals, technology, and applications of co-rotating twin-screw extruder.

These two books and others considered that an intermeshing co-rotating twin-screw extruder is the preferred choice among many pieces of equipment that have been used for manufacturing polymer compounds of various compositions. This chapter will highlight the key features of each type of equipment described in these two books and add current developments in the design of each equipment area that

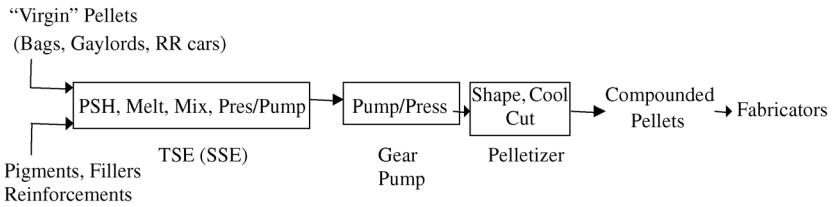

Figure 5.2 Flow sheet of polymer compounding process.

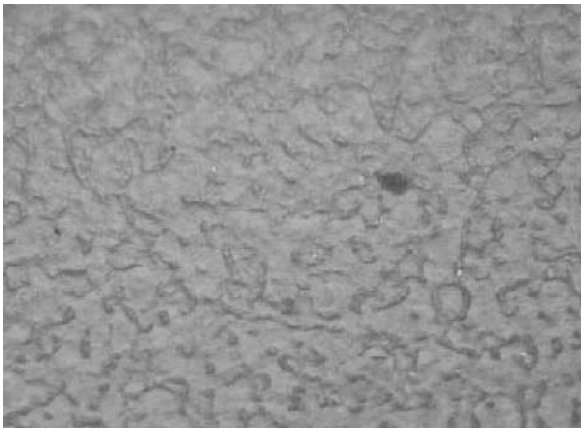

Figure 5.3 SEM photograph of a compounded designer pellet.

enhance the productivity of compounding operation. Since other chapters in this volume deal especially with various polymer blends, the uniqueness of certain equipment for various compounding operations will be discussed. Discussion of the equipment hierarchy in compounding manufacturing processing will follow the order of usage. The use of single-screw extrusion technology is still practiced with the advent of high-performance screws and mixing screws and specially designed dynamic mixers. Current advances in single-screw extrusion technology will be presented. Then, the melting process of single polymers and multicomponent polymer blend mixtures will be discussed.

The physical, chemical, and optical technologies used to monitor and assess the morphology and composition uniformity will be discussed with the relevant literature references and related patent references.

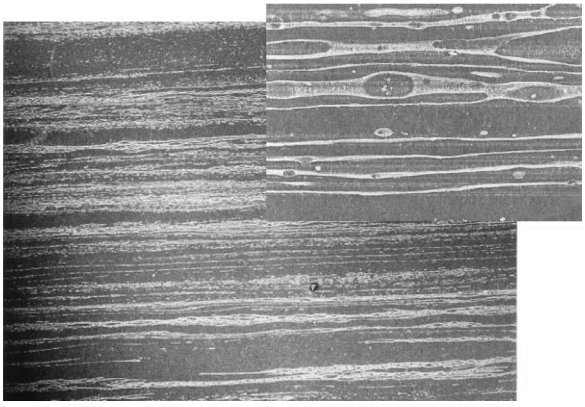

Figure 5.4 Product morphology obtained from a compounded "designer" pellet [2].

5.1.1
Hierarchy of Equipment in Manufacturing Polymer Blends

Kohlgruber classified extrusions according to the number of shafts (Figure 5.5).

The nomenclature for twin-screw extruders (TSEs) is not uniform – the nature of intermeshing can come after or before depending on whether it is are co-rotating or counter-rotating, as shown in Reference [3].

Typical equipment used in plastic compounding, in order of usage, is as follows:

1) **Intermeshing Co-rotating (or Co-rotating Intermeshing) Twin-Screw Extruder**: This is the most developed technology, which was produced by Bayer Company and licensed to Werner & Pfleiderer in 1953. After the original patent expired, many companies (Berstorff, Japan Steel Works, NFM, APV) also manufactured a TSE of this type [3].
2) **Single-Screw Extruder with a High-Performance Screw or Mixing Screw**: This extruder can be further classified based on the type of barrel that houses the screw, smooth barrel versus groove barrel (e.g., the newly developed Helibar® Transfer Mixer screw in the groove barrel).
3) **Intermeshing Counter-rotating (or Counter-rotating Intermeshing) Twin-screw Extruder**: This extruder is considered to be not effective in large-scale manufacturing.
4) **Tangential (Non-intermeshing) Counter-rotating Twin-Screw Extruder**: This extruder is used more for latex coagulation, recovery, devolatilization of polymer solutions, and for reactive extrusion.

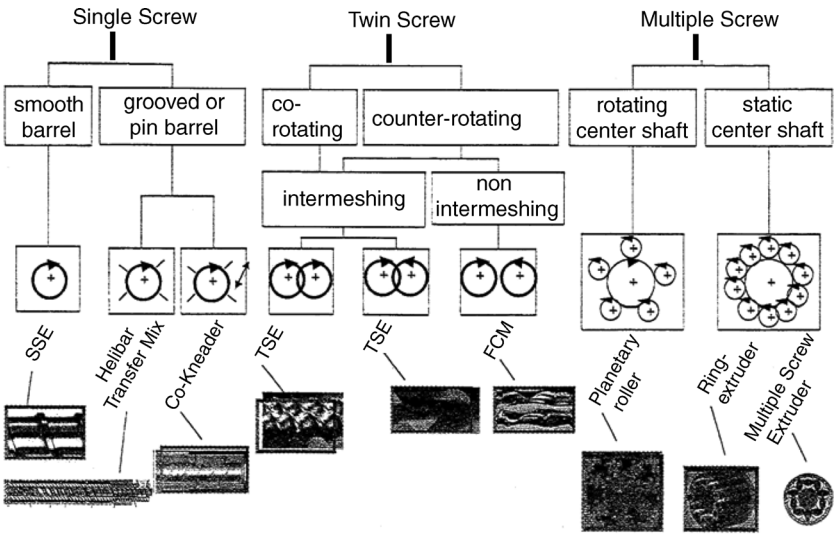

Figure 5.5 Classification of extrusions by the number of shafts [4].

5) **Others**:
–Co-Kneader (Ko-Kneader) having Reciprocating Screw and Pin Barrel
–Farrel Continuous Mixer
–List Continuous Mixer
–Ring Extruder.

All extruders commonly used equipment for compounding (items 1 and 2 above) perform many functions such as solid feeding of polymers and ingredients, melting (plastication), mixing (dispersion & homogenizing), and pumping (discharging) molten polymers through strand die, which go through a water bath and are pelletized in the pelletizer and packaged for shipping to fabricators. Solid particulates refer to pellets, powders, or granules. In many cases, degassing or devolatilization is required in the operation (Figure 5.6).

Polymeric materials are used for the fabrication of various molded or shaped articles. Plastication refers to the softening of a polymeric material to such an extent that it flows freely and assumes any shape. In the case of crystalline polymeric material, plastication is synonymous with melting. In contrast, for amorphous polymers, plastication occurs at or substantially above the glass transition temperature (T_g). For example, polystyrene will start to flow about 50–60 °C above T_g.

Polymeric materials include single polymer resins or a mixture or blend of polymer–polymer, polymer–filler, polymer–additives, or polymer–colorants. It has been stated that in the future the polymer blends having two or more polymer resins and others are needed to meet the material properties necessary for various

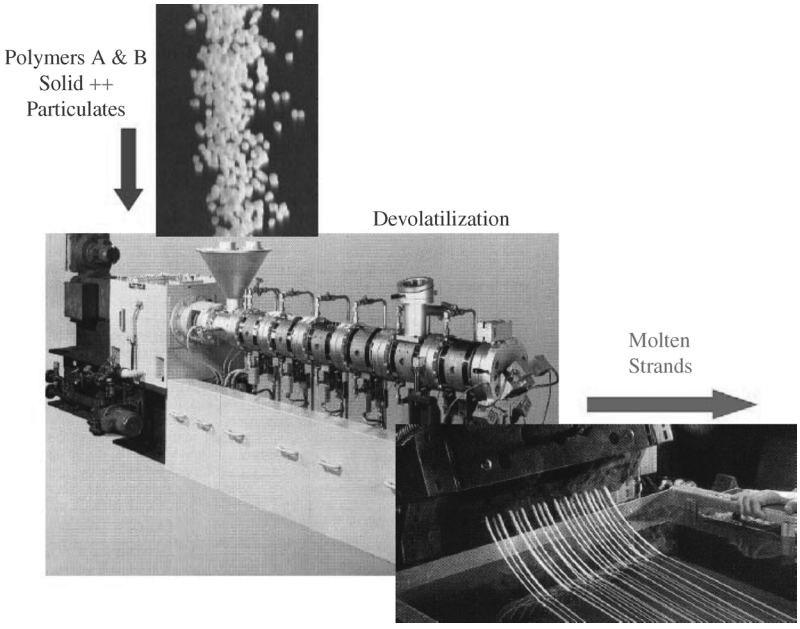

Figure 5.6 Simple view of compounding extrusion operation.

applications as building materials, medical devices, and packaging materials. Polymer blends can be prepared by compounding amorphous–amorphous, amorphous–crystalline, or crystalline–crystalline polymer components. When two polymers have different melting points, the melting mechanism can become complicated and will influence final morphology in the different equipment configurations.

5.1.2
Brief Historical Facts and Needs for Manufacturing of Polymer Blends

World War II, with the discovery of low-density polyethylene at ICI (which was a crucial component for the development of radar) and Nylon at DuPont, marks the beginning of the modern polymer industry, though, of course, PVC (poly(vinyl chloride)), PS (polystyrene), celluloid, and thermosets such as Bakelite preceded it, as did the rubber industry. Indeed most polymer processing machinery was derived from rubber and food processing machinery. The two decades following World War II were in many respects the "golden age" of the polymer industry with an avalanche of chemically new polymers flowing onto the marketplace, replacing conventional materials and finding new applications (Figure 5.7).

In fact over 95% of the resins manufactured today were invented in that period. More polymer blends have been developed since the year 2000.

5.2
Multiple-Screw Extruders

5.2.1
Twin-Screw Extrusion Technology

A multiple-screw extruder contains two or more screws, mainly two screws, each of which is similar in various basic respects to that used in a single-screw extruder

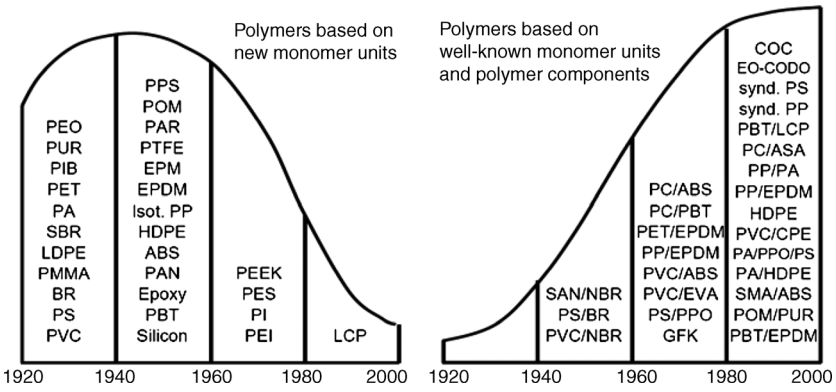

Figure 5.7 Chronology of discovery of polymers and their modification. Courtesy of Professor Hans G. Fritz of IKT [1].

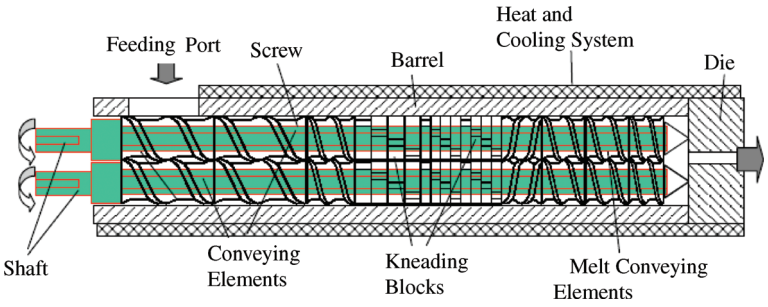

Figure 5.8 Schematics of a co-rotating intermeshing twin-screw extruder [5].

(Figure 5.8). Some of the discussion of performance of screw sections can be applied here. Such a screw is shaped generally in the form of an elongated cylinder, as in single-screw extruder, and has one or more flights helically disposed thereabout. A flight may have forward or reverse pitch, and the degree of pitch may be varied. When the screw is viewed in cross section (i.e., in a plane perpendicular to its central, longitudinal axis), the course of a particular flight, between one point of intersection with a line parallel to the screw axis and the next closest point of intersection of the flight with such a line, typically defines a 360° circle. The pointed or rounded tip of a flight that extends toward the perimeter of such a circular-shaped cross section defines a "lobe" above the root of the screw.

In the cross-sectional view of Figure 5.9, the lobes of a two-flighted screw are shown with two different sets of OD/ID. "A" is the center-to-center distance. The OD/ID ratio is defined by dividing the outer diameter (OD) by the inner diameter (ID) of each screw.

The space bounded by the root of the screw and the side walls of any two flights is a channel of the screw. The screw rotates on its longitudinal axis within a barrel or sleeve, which may be generally described as the bore of an annular cylinder.

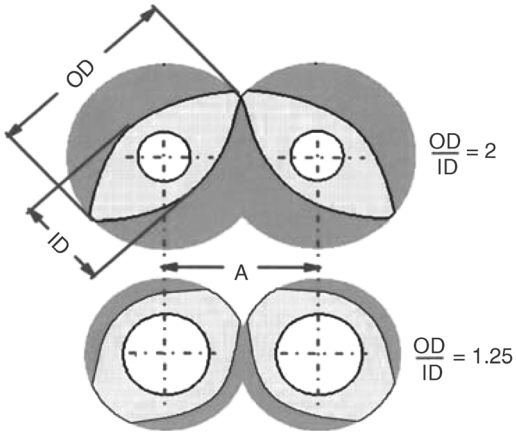

Figure 5.9 Schematic of two-lobe elements with two different OD/IDs.

The plasticating twin-screw typically has an initial, feed, section that begins the process of conveying solid polymeric material forward within the barrel of the extruder. Polymeric material may be flood fed into the extruder by means of a hopper that empties into the barrel, or may be metered into the barrel through a feed chute or a side feeder. The direction of travel of the polymeric material in the barrel as it is transported away from the feed port by the screw is considered the "downstream" direction. The feed section of the screw is typically followed, with or without other intervening sections, by a melting section in which partial or complete plastication of the polymeric material occurs. Plastication of the polymeric material occurs as a result of the combined effect of conductive heat produced, for example, by heater bands mounted on the outside of the extruder barrel and the physical deformation (plastic deformation energy, PDE), according to Gogos, Tadmor, and Kim and [6] and Kim [7], and viscous heating to which screw action subjects the polymeric material. The melting section of the screw is typically followed, again with or without other intervening sections, by a metering section. Its function is to pump the molten material, as extrudate, out through the downstream end of the extruder, which typically contains a die or some other form of restricted orifice. Aspects of a multi-screw extruder that have no direct analogy in a single-screw extruder pertain to the location, relative to each other, of the several screws within the barrel. Two screws in a multiple-screw extruder are said to be intermeshing if the flight of one screw is disposed within a channel of the other screw. In such configuration, the distance between the axes of each screw is less than the sum of the respective radii of the two screws, when each radius is measured from the axis to the top of the tallest or highest flight of the screw. To provide flexibility of design for a particular system, the screw elements in modular design are mounted in a keyed shaft. Figure 5.10 shows the assembly of conventional intermeshing screws for a twin-screw extruder.

When, on a pair of screws, a flight has a shape and size such that its fit into a channel in which it is intermeshed is so close that essentially allows no extrudable material passes through the space between the flight and channel, the screws are said to be conjugated. Otherwise, the screws are said to be non-conjugated, and the degree of intermeshing in the case of non-conjugation can be varied to an essentially unlimited extent. If the screws rotate in the same direction, that is, both clockwise or both counterclockwise, they are said to be co-rotating. If not, they are said to be counter-rotating (Figure 5.11).

When two counter-rotating screws are conjugated, there is little or no opportunity for polymeric material that is being extruded to remain in a channel of either screw in the region in which the screws intermesh. This is a result of the minimal clearance of the flight of one intermeshing screw within the channel of the other screw. Screws arrayed in such manner are said to "wipe" each other because polymeric material that is carried in the channel of either screw will be prevented from remaining in that

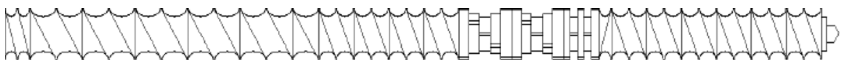

Figure 5.10 Assembly of conventional co-rotating intermeshing screw elements.

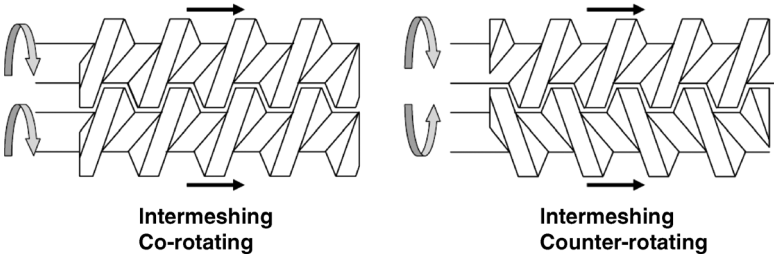

Figure 5.11 Counter-rotating versus co-rotating intermeshing conveying elements.

channel over a distance of more than one turn of the screw by the obstacle that the intermeshing flight of the other screw represents. In this configuration, most, if not essentially all, of the polymeric material resides in the portion of the channel on the top, bottom and outside (non-intermeshed side) of each screw, and the material consequently experiences significantly more movement in the downstream direction, parallel to the screw axis, than it does in a lateral direction, perpendicular to the axis. This arrangement results in efficient pumping of the polymeric material in the downstream direction, but does not achieve optimum intermixing of the whole body of polymeric material present in the extruder. This allows greater space for polymeric material to reside in the channels of both screws in the region of intermeshing. Intermixing of the polymeric materials is enhanced by the action of both flights in such a confined space; however, some efficiency of pumping is lost.

Co-rotating screws, even when conjugated, allow for extensive movement of polymeric material laterally from one screw to the other. Mixing is benefited by this movement around the "equivalent screw," and it is further enhanced when the screws are not conjugated. The shape of the flights on non-conjugated screws may be arranged to create the passage of polymeric material from one channel into two channels on another screw. Or, when screws are conjugated, or essentially conjugated, certain flights can be designed in a shape such that they wipe each other in the zone of intermeshing but do not wipe the wall of the barrel. For example, a multiple-screw, barrier-type extruder is disclosed in US Patent 4 300 839 in which one or more flights on each screw is reduced in height by an amount that is constant along the entire length of the screw, and which is sufficient to allow the passage of polymeric material between the two channels on either side of any such flight. This clearance between the wall and the top of the flight does not exist, however, for those flights in the zone of intermeshing. Designs such as these appear to provide thorough mixing, but considerations of pumping efficiency and residence time sometimes limit their usefulness. Other patents that aim to further increase performance will be discussed later.

Typical construction elements of screw on core shafts are shown in Figure 5.12a and corresponding barrel sections are shown in Figure 5.12b–g.

Figure 5.13 shows a schematic representation of the modular screw-element sequences, barrel sections, and overall assembly of an intermeshing co-rotating twin-screw extruder.

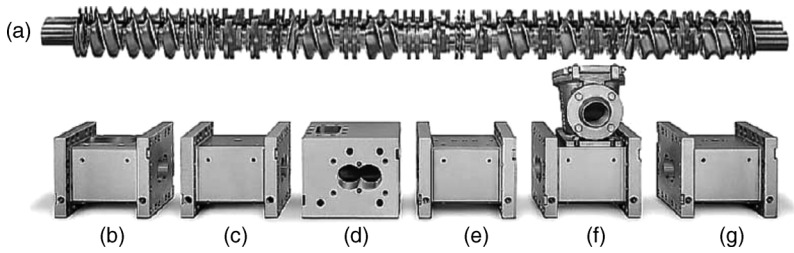

Figure 5.12 (a) Modular screw; typical 4 *L*/*D* C0-TSE barrel segments: (b) feed throat, (c) melting, (d) downstream feed section, (e) mixing, (f) devolatilization, and (g) pumping and limited pressurization. Courtesy of Coperion Werner & Pfleiderer.

Traditional designs of screw elements for improving mixing and achieving the desired morphology development in the twin-screw extruder have been covered in many books published to date. Since the last book dealing with twin-screw extrusion technology there has been progress in terms of optimization, energy saving, and environmentally green approach, which will be covered in this chapter.

In general, all twin-screw extruder manufacturers have developed their own specific equipment design to increase the extrusion rate by increasing the free volume of each element and increasing the ability to withstand a high torque requirement. Three major developments are described in the following sub-sections.

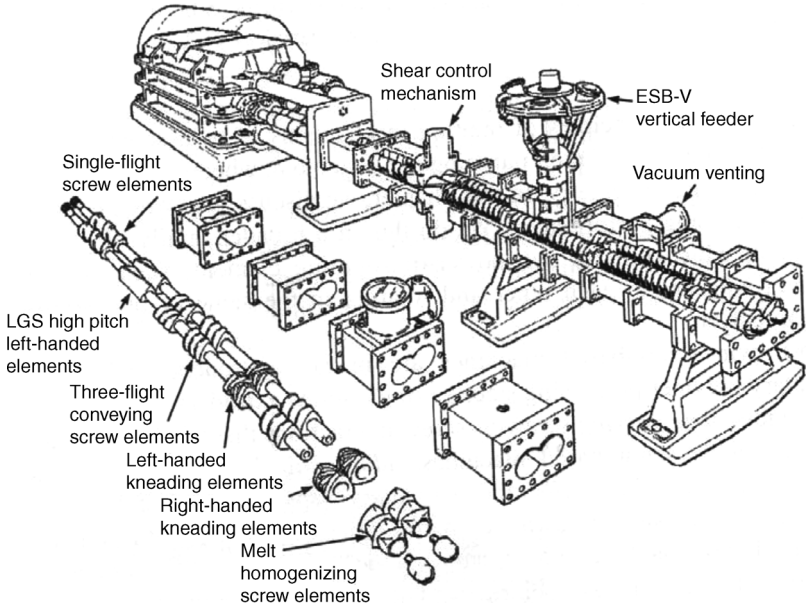

Figure 5.13 Schematic representation of the modular screw-element sequences and barrel sections of an intermeshing co-rotating TSE. Courtesy of Coperion Werner & Pfleiderer.

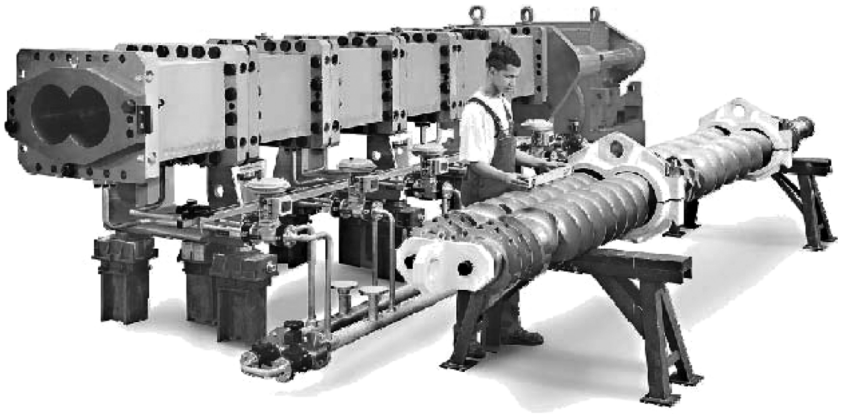

Figure 5.14 Photograph of the barrel assembly and assembled modular screws of a ZSK 320 MEGAcompounder. Courtesy of Coperion Werner & Pfleiderer.

5.2.1.1 Coperion Werner & Pfleiderer: ZSK MEGAcompounder [8]

The ZSK MEGAcompounder, having a modular design for screw elements and kneading blocks, is shown in Figure 5.14.

Figure 5.15 shows the modular technology of screw and kneading elements of a two-flight screw and indicates the flow patterns in each element.

Given the same size of machine, the co-rotating twin-screw extruders of the ZSK MEGAcompounder and ZSK MEGAcompounder PLUS series have an output capacity many times greater than that of their forerunners. With drive powers from 10 kW to 12 MW, the units can deliver rates between 5 kg h^{-1} and 75 t h^{-1}.

The decisive factors for the increase in output are the optimized screw geometry and the increase in available torque at the screw shafts:

$$\text{Specific torque } (M_d/a^3) = 13.6 \text{ Nm cm}^{-3}$$

where "a" is the center-to-center distance between the screws and the resulting possible increase in screw speed to 1200 rpm and over.

As shown in Figure 5.16, Coperion was able to combine this performance increase with other innovative measures in order to achieve high outputs in a great many different processes while at the same time maintaining, or even increasing, reliability in operation [8].

As free volume and torque values are inversely proportional to the flight depth, the optimum balanced ratio between free volume and torques can be found at the cross point of these two curves (Figure 5.17).

5.2.1.2 Effect of D_o/D_i and Screw Speed on Average Shear Rate

The effect of D_o/D_i and screw speed on average shear rate is shown graphically in Figure 5.18.

Higher screw speeds compensate for lower average shear rates of filled channels at the same total shear stress and temperature.

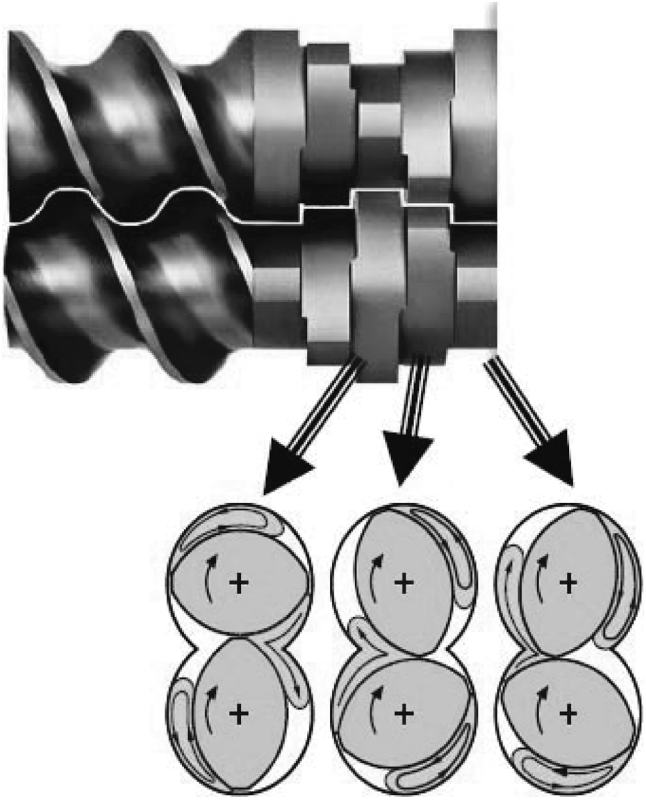

Figure 5.15 Modular technology ZSK screw and kneading elements, showing flow patterns in cross section of each kneading element (compression and decompression).

5.2.1.3 **Leistritz: HSEI (High Speed Energy Input) Twin-Screw Extruder [9]**

In 2004 a new HSEI twin-screw extruder series (Figure 5.19) was introduced by Leistritz. This HSEI TSE features screw elements with a 1.66/1 OD/ID ratio, made possible by a new asymmetrical screw shaft spline geometries. In Leistritz nomenclature, its HP series has a 1.55/1 OD/ID, and the MaXX series a 1.66/1 OD/ID ratio.

Screws are segmented and assembled on high torque splined shafts (Figure 5.20). Barrels are also modular and utilize liquid cooling. The motor inputs energy into the process via rotating screws that impart shear into the materials. Segmented screws/barrels, in combination with the controlled pumping and wiping characteristics of the screws, allows screw/barrel geometries to be matched to the process tasks. Solids conveying and melting occurs in the first part of the process section. Screw elements for mixing and devolatilization are then utilized as dictated by the process. Discharge elements finally build and stabilize pressure to the die or front-end device.

HSEI twin-screw extruders are starve fed with the output rate is determined by the feeder(s), which meter pellets, liquids, powders, and fibers into the process section. The extruder screw rpm is independent of the feed rate and is used to optimize compounding efficiencies. Because the pressure gradient is controlled, and zero for

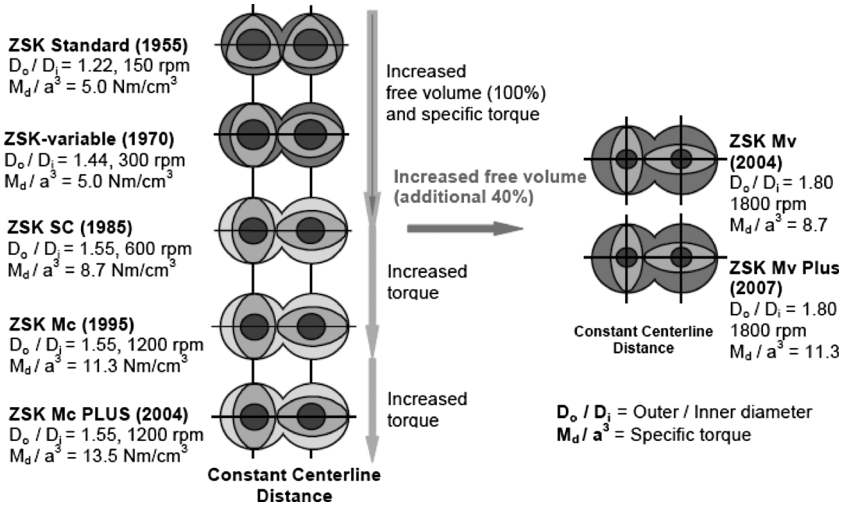

Figure 5.16 Evolution of torque and volume. Courtesy of Coperion, Werner & Pfleiderer.

much of the process, materials are easily introduced into downstream barrel sections (Figure 5.21).

The new HSEI twin-screw extruder features high free volume, an important design parameter that is directly related to the OD/ID ratio as discussed. The limiting factor for attainable torque in a HSEI twin-screw extruder has historically been the cross-sectional area of the screw shaft. Deeper screw flights result in more free volume, but with less torque, since a smaller diameter screw shaft is mandated. Based on the use of a symmetrical splined shaft a 1.55 OD/ID ratio was considered to give the best balance of torque and volume. Utilizing an asymmetrical splined shaft (patent pending), the MaXX series allow a smaller diameter shaft (1.66 OD/ID) to transmit power more efficiently so that a larger free volume is available without a decrease in torque. Now the torque limiting factor became the gearbox, which spawned a new generation of gearboxes that were introduced in 2007 that increased the torque capabilities of the MaXX series by an additional 30%.

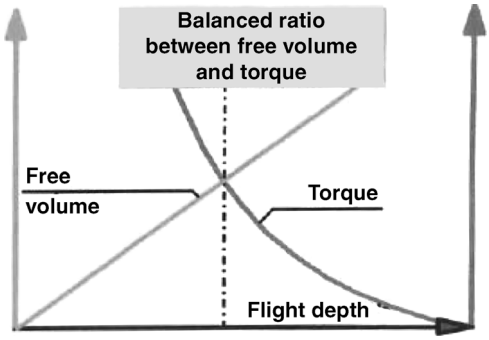

Figure 5.17 Screw free volume and permissible torque as a function of flight depth.

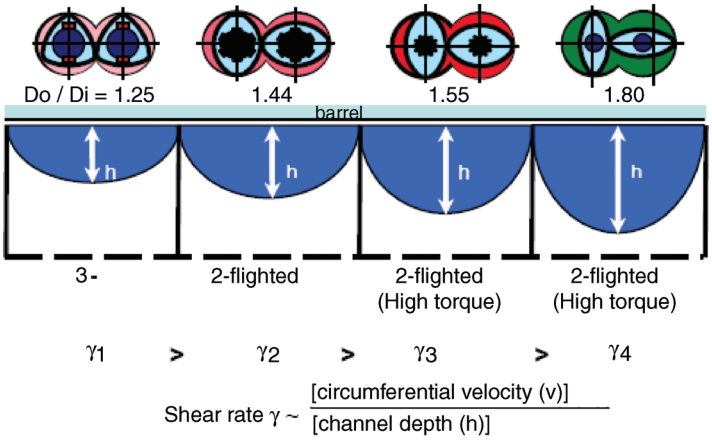

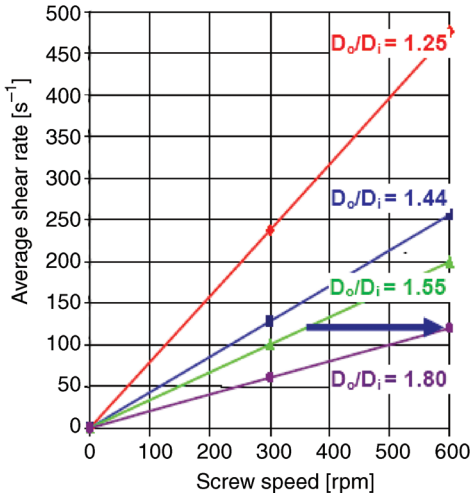

Figure 5.18 Effect of D_o/D_i and screw speed on average shear rate.

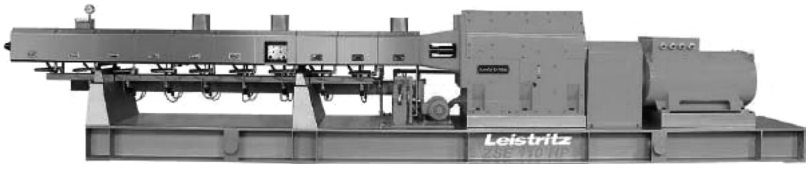

Figure 5.19 HSEI twin-screw extruder with provision for downstream feeding and venting. Courtesy of Charles Martin, Leistritz, Inc.

Figure 5.20 HSEI co-rotating intermeshing twin-screw extruder screw set.

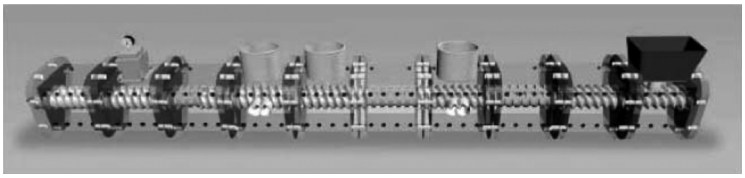

Figure 5.21 HSEI twin-screw extruder process section with multiple vents & downstream stuffing.

Impacts of Symmetrical versus Asymmetrical Splined Shafts The limiting factor for attainable torque in a HSEI twin-screw extruder is the cross-sectional area of the screw shaft. Deeper screw flights result in more free volume, but with less torque, since a smaller diameter screw shaft is mandated. Based on the use of a symmetrical, hammered splined shaft a 1.55 OD/ID ratio has been deemed to result in the best balance of torque and volume. With a smaller screw shaft, increased free volume has been possible, but at much lower torque levels.

The MaXX series utilizes an asymmetrical splined shaft (patent pending) that maintains the same or higher torque as standard HSEI twin-screw extruders with a smaller diameter shaft. The asymmetrical spline transmits power more efficiently into the screw elements (and process section), which allows for deeper flight depths and more free volume without a torque reduction. To restate, a symmetrical spline induces both tangential and radial force vectors. The resultant force is not optimized, as the radial force is not being applied in a beneficial direction (Figure 5.22). The asymmetrical shaft eliminates the radial force vector and isolates the tangential force vector. Therefore, equal or higher torque can be achieved by a smaller diameter shaft with a 30% increased free volume in the extruder process section. Figure 5.23 shows the end view of HP and MaXX screw elements geometries, illustrating the increased free volume of MaXX over HP.

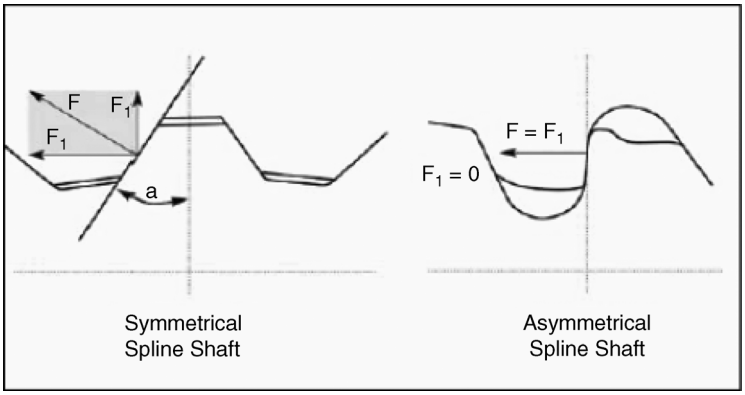

Figure 5.22 Comparison of one-tooth symmetrical and asymmetrical screw shaft spline geometries.

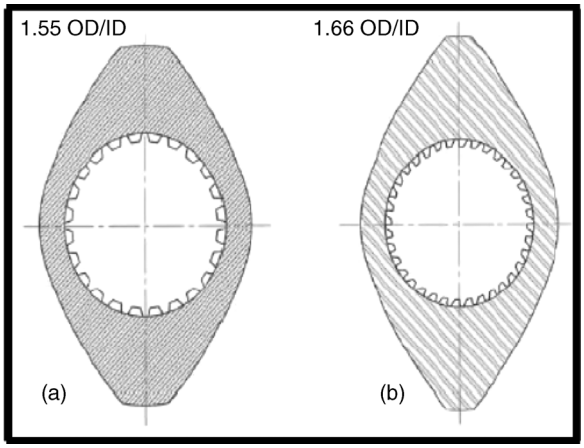

Figure 5.23 End view of (a) HP and (b) MaXX screw elements geometries.

5.2.1.4 **KraussMaffei Berstorff Twin-Screw Extrusion System [10]**

By integrating the extrusion operations of Krauss-Maffei and Berstorff in a single brand, KraussMaffei Berstorff have strengthened their position as a system supplier capable of offering single vendor solutions for all the main plastics and rubber extrusion processes. The Extrusion Technology Division supplies machinery and systems for compounding, for pipe, profile and sheet extrusion, physical foaming, and the production of technical rubbers and intermediates for tire production. They do not offer any specific system for polymer blend compounding operations, but a similar analogy can be used for compounding from the co-rotating intermeshing twin-screw systems. Figure 5.24 shows a modular assembly of screw and sectionized barrel (highlighting the kneading section and gear mixer section).

However, the company offers the ZE 25 System for pilot-plant development of any product, including polymer blends. KraussMaffei Berstorff compounding lines are designed to be tailored to customer's specific product and process requirements. They offer extensive process engineering know-how in all key processing and extrusion applications for plastics and other base materials.

All extruders in the new ZE Basic series are designed, as the name suggests, for basic processes. More than 80% of all the plasticizing, filling, and reinforcing applications can be covered by the ZE Basic series to produce the highest quality products. In other words, they are machines for processes that can be carried out

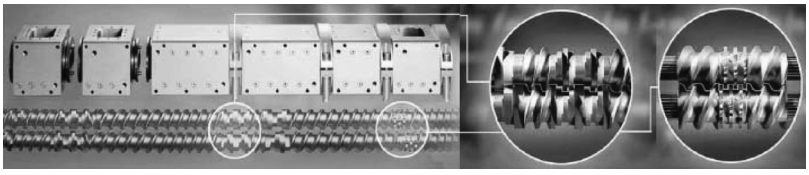

Figure 5.24 Modular assembly of screw and sectionized barrel (highlighting the kneading section and gear mixer section). Courtesy of KraussMaffei Berstorff [10].

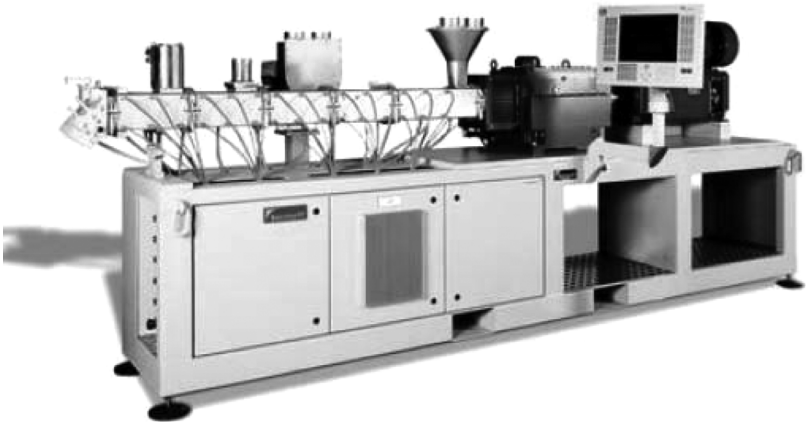

Figure 5.25 ZE Basic 25 mm TSE. Courtesy of KraussMaffei Berstorff.

without the need for too many types of barrel element and are thus more economical to purchase. This makes the ZE Basic the lowest-price, best-value twin-screw extruder made by KraussMaffei Berstorff (Figure 5.25).

5.2.1.5 Japan Steel Works TEX Twin-Screw Extrusion Systems [11]

In addition to a regular co-rotating intermeshing twin-screw extruder system, which is analogous to the above-mentioned twin-screw extruder systems, Japan Steel Works (www.jsw.co.jp) has patented a special modification for a TSE barrel and screw kneading section to enhance the polymer blend qualities, as presented in the following subsections.

JSW Special Kneading Cylinder "NIC" [11] NIC has been developed to increase significantly the compounding quality level as, recently, traditional compounding processes have been subject to simplification for the purpose of resource conservation or manufacturing cost reduction.

For over 40 years twin-screw extruders have been utilized in polymer compounding and various kinds of extruder screw design have been developed to suit the demands of each field. However, there is hardly any case of cylinder development to improve kneading performance.

Kneading is performed in the clearance between cylinder inside and the top of screw, in what is called "tip clearance." Compounding quality level can be increased by improving the structure of tip clearance. JSW has developed the special kneading cylinder "NIC" with a unique channel structure on the cylinder inside (Figure 5.26).

Applications are (i) polymer blending (e.g., ABS + AS, PP + EPR), (ii) powder filler compounding (e.g., talc, calcium carbonate, magnesium hydroxide, etc.), (iii) masterbatch compounding (e.g., carbon black, titanium oxide, etc.), and (iv) other compounding for which high-level micro-dispersion is required.

Expected advantages are (i) excellent kneading performance, (ii) energy saving, (iii) coloration performance, and (iv) higher compounding capacity.

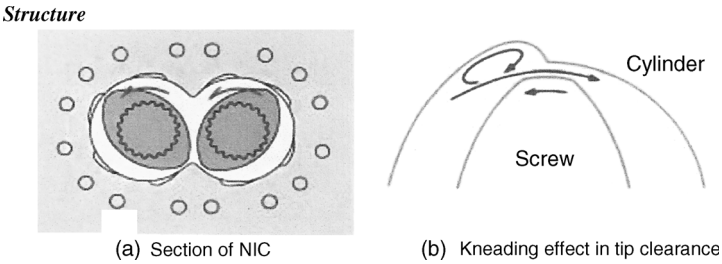

Figure 5.26 (a) Section of NIC; (b) kneading effect in tip clearance.

In detail, uniform kneading can be achieved with NIC installed in the optimum location because a larger amount of polymer passes through tip clearance, and kneading at low temperature is achieved because localized heating is prevented due to a lower shear rate in the NIC, which has a larger average tip clearance. Energy consumption can be reduced by 10–20% compared to standard types of cylinder and discharged polymer temperature is reduced because of lower energy consumption. Color change of any tone, for example, from black to white, can be achieved because of kneading in the high-viscosity area to prevent localized heating. The unique structure prevents polymer from accumulating and deteriorating in the channels. The unique channel structure of NIC helps to achieve higher processing rates than standard types of cylinder. Figure 5.27 compares NIC kneading performance for the blend ABS + 30%SAN running at 1200 kg h^{-1} per 600 rpm in TEX65. Figure 5.27a shows the distribution of SAN phase with a standard cylinder and Figure 5.27b shows the finer distribution of SAN phase with a special kneading cylinder (NIC).

Figure 5.28 shows the better Izod impact strength and flexural strength increase with NIC over a standard cylinder for bumper grade blend, and Figure 5.29 illustrates the better dispersion shown for NIC over the standard cylinder for a PE/CB blend.

In plastics compounding by twin-screw extruders, kneading discs or rotor elements are generally used for the mixing section of the screws depending on the material and the application.

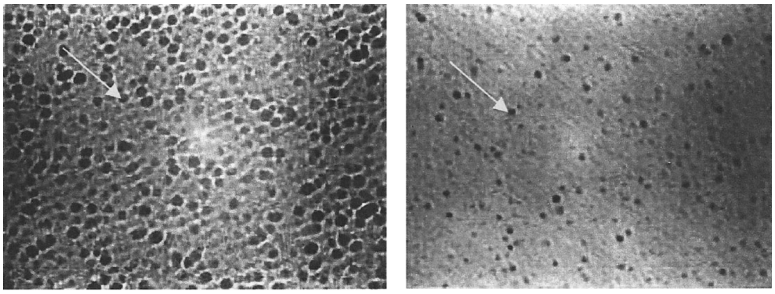

Figure 5.27 Dispersed phase (SAN) distribution of ABS + 30% SAN, 1200 kg h^{-1}–600 rpm (TEX65): (a) with a standard cylinder; (b) with a special kneading cylinder (NIC).

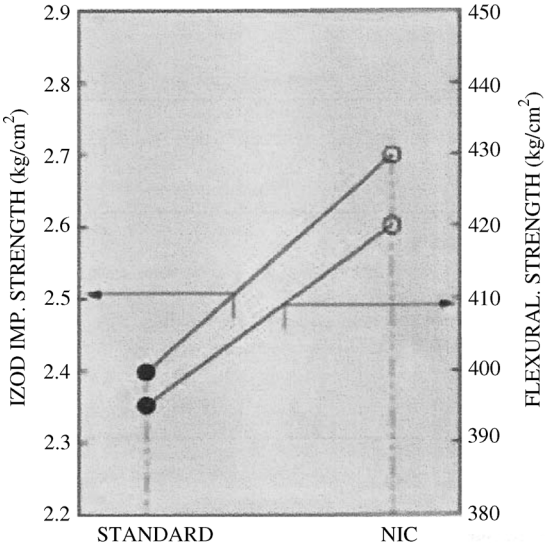

Figure 5.28 Bumper grade (PP + 24% EPR + 11% talc).

Features of "Twist Kneading Rotor (TKR)" [11] Another development by JSW in 2000 is the element called a Twisting Kneading Rotor (TKR), which was developed so as to combine the strong points of both kneading blocks and rotor elements, thereby enabling more energy-saving mixing than conventional kneading discs.

JSW achieved a mixing with less energy consumption at lower temperature with a TKR. A rotor element is divided into several discs and staggered at a relative angle;

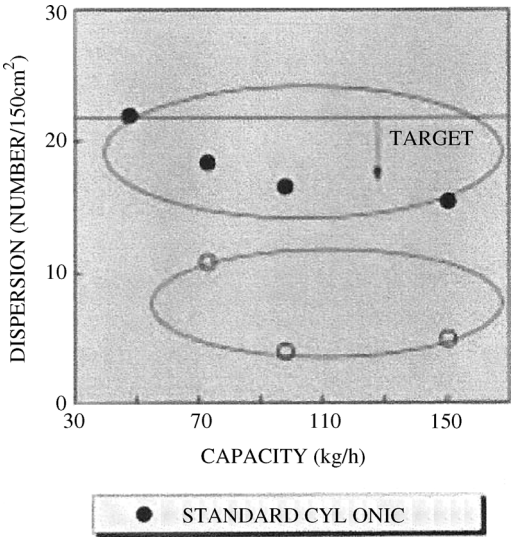

Figure 5.29 Dispersion of carbon black (PE + 40% carbon black).

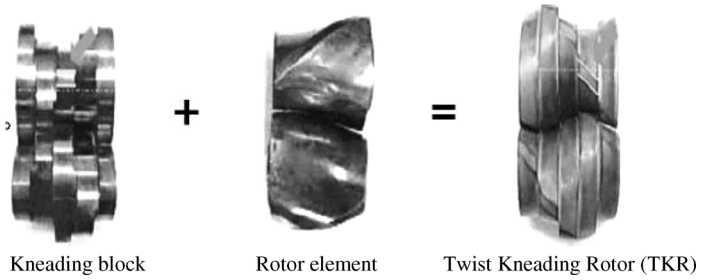

Figure 5.30 Development of TKR.

both forward and reverse flight combinations are available. Rotor disc tips provide adequate compression and shearing effect to the polymer. The mixing effect of a kneading block can be obtained with TKR as polymer passes through the gaps between staggered disc tips. Rotor tips provide a good milling effect to improve filler dispersion or to eliminate gels in the products. Discontinuous rotor tips will be advantageous to better dispersive mixing and higher processing rate. With the TKR, energy consumption and polymer temperature can be reduced by approx. 10% compared to a conventional kneading block. Furthermore, the combination of TKR and the "Special Kneading Cylinder (NIC)" can reduce energy consumption and polymer temperature by approximately 15%. Figure 5.30 graphically depicts the conception of the TKR.

5.2.1.6 **High Efficiency Twin-Screw Extruder [12]**

Two patents issued to The Dow Chemical Company on an improved design [12] are cited in Kohlgruber's monograph [4]. These two patents were issued in 1998 as WO 1998013189, EP 934151 and WO 19999025537, EP 1032492.

The High Efficiency Extruder is a co-rotating twin-screw extruder consisting of first and second intermeshing screws of more than one flight, modified to improve the quality of polymer blends. The first screw (A, Figure 5.31a) consists of first and second segments paired with first and second segments of the second screw (B), respectively. On the first segment of the first screw (A), the height of the first flight is less than the height of the second flight and on the second segment of the second screw, the height of the first flight is omitted half way around so it is far less than the height of the second flight and screws for use in a typical twin-screw extruder

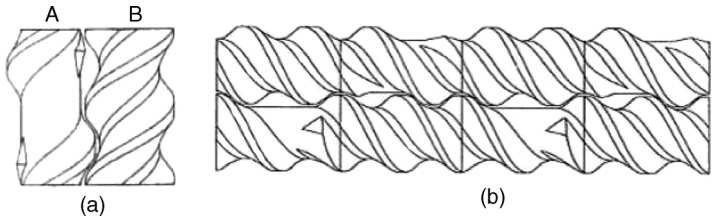

Figure 5.31 (a) Pair of basic units comprising the modified screw and the normal elements (vertical view); (b) four pairs of the first and second screw assembly.

(Figure 5.31a). It would therefore be beneficial to have a design for two intermeshing screws to be paired in a multiple-screw extruder to simultaneously obtain both a desirably high degree of intermixing, and a high rate of pumping, of extrudable material (Figure 5.31b).

It is consequently an object of this invention to provide a multiple-screw extruder in which even conjugated screws will furnish a desirably high level of compositional homogeneity and process stability.

5.2.1.7 **Intelligent Extruder for Polymer Compounding [13]**

A government funded project (period 1/8/1999–12/31/2002) has developed the Intelligent Extruder for Polymer Compounding [13], prepared by the Automation and Controls Laboratory, GE Global Research. The Final Technical Report was authored by Eker *et al*. for the US Department of Energy, Office of Industrial Technology. The project synopsis contains the following statement:

"Concepts developed in this program allow waste and energy reduction in polymer compounding operations for high value engineering materials. With advanced diagnostic and control software applied to existing extruder drive systems, benefits are obtained from a continuous quality audit synthesized by inferring material properties from readily measured machine variables. This allows rapid detection of out of spec material and corrective action in contrast to the infrequent quality checks that are performed today. We estimate that about 2% of first pass yield losses can conservatively be attributed to out of spec material produced this way, and caught after manufacture or when received at the customer. By increasing first pass yield by 2%, the 30 billion pound per year engineering plastics producers in North America would save some $391 MM dollars in material and energy costs, avoid land fill solids in excess of 600 MM lbs, save 624 000 Mwhr of electrical and equivalent steam energy, and remove 30 MM lbs of volatiles from the atmosphere. This also represents 600 MM lbs of found capacity, equivalent to 51 units running at a rate of 2000 lb/hr extruders operating two shifts, 5 days a week for a year. Commercialization of this technology will yield the benefits to the compounding industry."

US polymer resins and their compounds are produced at the rate of 90 billion lb yr^{-1}, one-third of which are engineering thermoplastics valued at more than $\$1\ lb^{-1}$ and used in applications from small electrical connectors to medical products, optics to computer cases, kitchen countertops, and automotive fenders and bumpers. Before reaching the injection molder manufacturer, nearly every pound of resin passes through a final "finishing" stage in a compounding line in which component materials are blended in a 1000 to 15 000 hp extruder to achieve critical properties such as melt flow behavior, color, mechanical strength, and fire resistance. Injection molders depend on the values of these properties for their equipment to produce quality parts. Variations in resin properties increase the initial setup time for injection molding and readjustments during a run, resulting in more scrapped parts due to incomplete or excessive mold flow or substandard properties such as

color. The outcome, for both molders and resin makers, is productivity loss, missed deliveries, additional landfill scrap, higher production costs, and dissatisfied customers.

Profile of Material State in Extruder Figure 5.32 shows what the internal material state transitions might look like; moving from the input to the output of the extruder barrel at the die head, recognizing that at any position the material flow and melt state is highly complex and three-dimensional. The design of the screw is a complex science and art that is not part of our investigation. For a given screw, base resin, and complementary components to create a desired alloy, there is a desired profile the process engineer seeks. The cartoon example shown illustrates typical complexities encountered, with dry ingredients added at two locations, an open devolatilization vent, and changes in the solid melt ratio along the barrel, but ultimately producing 100% melt at the die head with an appropriate melt temperature and pressure to assure well mixed strand formation. Heaters and/or cooling jackets are located along the barrel length to help maintain temperature conditions in the melt, but the bulk of the energy that melts and blends the material comes from the screw drive.

By improving the quality of material produced to meet molders expectations, the compounding industry and its customers benefit while energy and waste generated in recycle is reduced. Further work is needed to commercialize "intelligent extrusion technology" for manufacturing polymer blends.

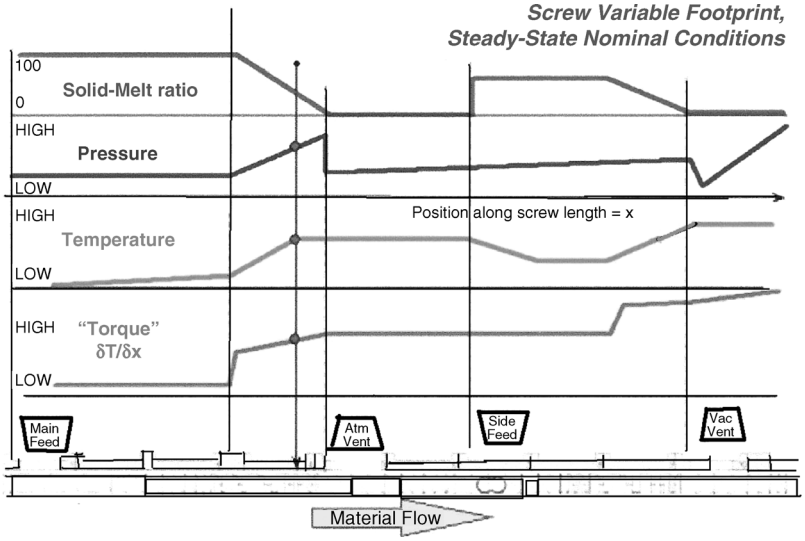

Figure 5.32 Cartoon of the material state in a twin-screw extruder.

5.2.2
Single-Screw Extrusion Technology

The single-screw extruder has been used at the end of the polymerization line to produce pellets that will be further converted into useful products. In addition, the separate extruder was used to melt powders and granules from suspension or emulsion polymerization to convert into pellets, since the pellet feed form provides better feeding in the extruder. The earlier single-screw extruders that were used for rubber processing were modified to process thermoplastic polymeric materials and screws were designed to include some mixing elements that were developed to enhance the mixing of additives, flow modifiers, and fillers.

Like most extruders, single-screw extruders must perform multiple functions. These functions include the conveying of the solid feedstock resins from the hopper into the first section of the barrel, melting, pressurization in the metering section, and mixing operations (Figure 5.33). This figure illustrates a potential use of a single-screw extruder with a special provision for compounding polymer blends, if one considers ABS virgin pellet is polymer A and color masterbatch as polymer B. To understand the performance in the device, it is important to first understand the operation of the sections. For single-stage, flood-fed processes, the metering section of the screw must control the specific rate of the process. The specific rate is defined as the mass rate divided by the rotation rate of the screw; that is, kg/(h rpm). If the metering section does not control the specific rate, then an operation upstream of the metering section is controlling and sections of the screw channel downstream of the rate controlling section will be operating partially filled. Partially filled channels can lead to inconsistent plasticating times, high cycle times (low production rates),

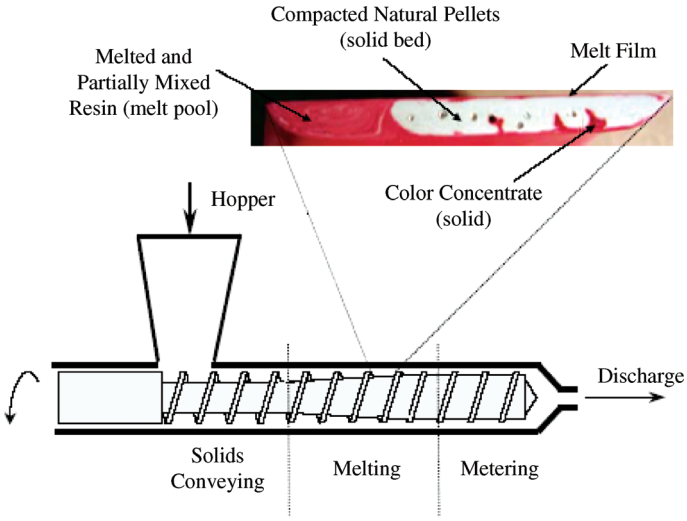

Figure 5.33 Schematic of the melting and mixing process that occurs during the plastication of natural ABS (white) resin with a red concentrate resin using a conventional, single-flighted screw.

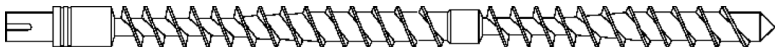

Figure 5.34 Schematic of a two-stage vented screw.

high discharge temperatures, high scrap rates, material degradation, poor mixing, and high labor costs per part [14, 15]. It is imperative that the machine is operating properly before other performance criteria are assessed. For two-stage extruders, the first stage metering section must control the rate. Otherwise flow of material out through the vent will occur (Figure 5.34).

For a flood-fed system, the solids conveying section of the screw must be able to provide resin at a rate fast enough and under pressure to keep the melting and metering sections full of resin.

The melting processes that occur in an extruder can be examined by performing a screw solidification experiment. The technique was pioneered by Maddock [17] in the late 1950s using an extruder. The technique consists of operating the extruder until a steady state is achieved, and then stopping screw rotation and simultaneously cooling the barrel, solidifying the molten polymer in the screw channels. Next, the screw with the solidified polymer is pushed out of the barrel and examined. Often a small amount of pigmented polymer is added to the feedstock resin at a ratio of about 100 : 1 to demarcate regions that were solid or molten prior to stopping the rotation of the screw. The regions in the screw that were molten will be tinted with the pigment while the solid regions will have the color of the main feedstock with small traces of pigmented particles. A cross-sectional view of the plastication process via a Maddock solidification experiment for an acrylonitrile butadiene styrene (ABS) resin is shown in the top insert of Figure 5.33. As shown, the natural (white) ABS pellet solids were compacted into a solid bed, and within the solid bed were smaller amounts of color concentrated solid pellets (red areas in the white bed). Plastication (or melting) occurs in a thin melt film between the solid bed and the barrel wall. The newly molten, highly viscous material is then conveyed by the motion of the rotating screw to the melt pool at the pushing side (left-hand side) of the channel. As indicated in Figure 5.33, the melt pool is mostly red with some small streaks of molten natural resin, indicating the high efficiency of the primary mixing process during melting. The term primary mixing is used here to designate the first major mixing that occurs between the different solid particles that enter the machine. For single-flighted, conventional screws, Benkreira *et al.* [16] provided evidence that most of the mixing occurs during the melting process, with only small levels of additional mixing occurring in the downstream channel. As will be shown below, if melting does not occur inside the extruder, significant defects will arise due to poor mixing. As melting progresses downstream, the width of the solid bed becomes smaller until all the resin is fully melted. For conventional single-flighted screws, the melting (or transition) section screw channel starts at the depth of the feed section and becomes shallower until it ends at the entry of the metering section. Recall that the metering channel depth is typically 1/2 to 1/6 the depth the feed channel. The melting process, however, is not limited to the transition section of the screw. In most cases, the melting process extends several diameters downstream of the transition section.

After substantial use of single-screw extruders with mixing elements for compounding, the need for effective devolatilization emerged. To handle this new requirement, multistage screw extruders were developed, making the extruder much longer.

While "improved single-screw extruders" have been used in many compounding operations, the twin-screw extruder was evolved and found to offer significant advantages over single-screw processing, particularly in the area of compounding. However, it has to bear the expense of high capital and operating cost.

As the market expanded globally and the capital cost per unit per volume decreased, many compounders invested in larger twin-screw extrusion systems, as discussed in Section 5.2.1 on twin-screw extrusion technology.

However, the demand for single-screw extruders with special high-performance screws or mixing screws of various designs remains strong. The following new developments are worth noting.

5.2.2.1 **High-Performance Screws [18]**

The industry trend is to operate single-screw extruders at increasingly higher rates. The achievement of higher production rates requires a combination of higher screw speeds and screws with deeper metering channels. As previously known, the operation of a conventional, single-flighted screw in a smooth barrel at relatively high speeds will cause some solids to discharge with the extrudate and thus create a poorly mixed extrudate for the subsequent forming operations (film, profile, sheeting, injection molding, etc.). Increasing the depth of the metering section will increase the specific rate of the process, but the melting capacity or the length of the transition zone for the screw is unchanged. Again solid particles are highly likely to be discharged with the extrudate. These limitations have been mitigated by the development of high-performance screws that have the ability to complete the melting process at higher rates, discharge at a lower melt temperature, and provide a higher quality extrudate. These devices all work by forcing the material to flow repetitively through regions with relatively small clearances. As the material passes through these clearances, large polymer solids will become trapped and forced to melt before passing through, and smaller polymer solids will be subjected to high elongational and shear stress fields that will aid in their melting. The lands for these clearances tend to be relatively short in the flow direction while the rest of the channels are relatively deep. The deeper main channels allow the devices to maintain high specific rates and low discharge temperatures, while the regions with the small clearances provide a level of mixing by completing the melting process. There are numerous devices currently on the market, several of which are discussed here in random order.

Some of the more widely used high-performance screws include the Energy Transfer (ET) screw [19], the Variable Barrier Energy Transfer (VBET) screw [20], the Double Wave™ screw [21], Stratablend® [22] and Stratablend® II [23] screws, and the Unimix™ [24] screw. Other devices can, however, act as a trap for solid materials from the melting section. These devices include Maddock-style mixers [25], spiral dams, and blisters. They will be briefly discussed in this section as many of them have been the subject of many articles on secondary mixing processes.

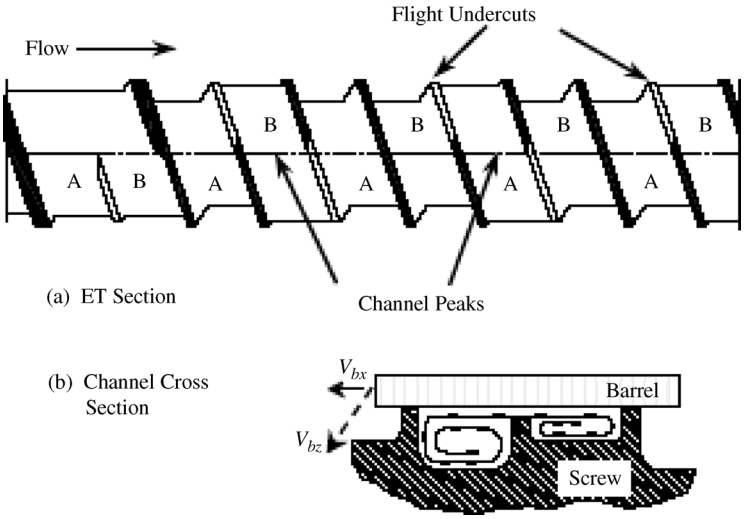

Figure 5.35 Schematic of an ET section: (a) the section is used in place of a metering section, and it has two channels labeled A and B; (b) cross-sectional view perpendicular to the flight tips, showing the two channels and a flight undercut between them – the arrows show the direction of the flows perpendicular to the flight. Courtesy of Jeff A. Myers of Robert Barr, Inc.

Higher rates and improved melting and thus mixing quality of the extrudate can be obtained using an ET screw. For this screw design, the metering section of a conventional, single-flighted screw is replaced with an ET section. Unlike a conventional metering channel, the ET section [19] consists of two channels (Figure 5.35a). One channel is positioned one-half turn downstream from the other, and both channels are of equal width. To create cross-channel mixing, the depths of both channels are periodic and out of phase. An undercut in the flight to the rear of a channel starts when that channel decreases in depth, permitting flow from the channel to the channel behind it. The undercut ends when the depth of the channel in front of that flight starts to increase. Most ET screws are designed with three regions where the channels become shallow, that is, peaks in the channel profile. The peak clearance and flight undercuts are the same for all three peaks. These peaks and flight undercuts create cross-channel mixing and disperse and melt the solid polymer fragments entering the section [20]. Some of the larger solids will remain as solids after passing through the first peak region, but will be reduced in size. The increased surface area of the smaller fragments will have a higher melting rate through heat conduction while being transported to the next peak region. Repetitive flow through the three peak regions produces extrudates with improved temperature homogenization, lower temperatures, lower levels of pressure and temperature fluctuations, and at increased rates as compared to conventional screws. As a comparison, conventional screws operating at high rates will sometimes permit solids to flow close to the screw tip or into the vented area of the second stage, producing extrudates with higher volatile levels, large temperature gradients, and with transfer line

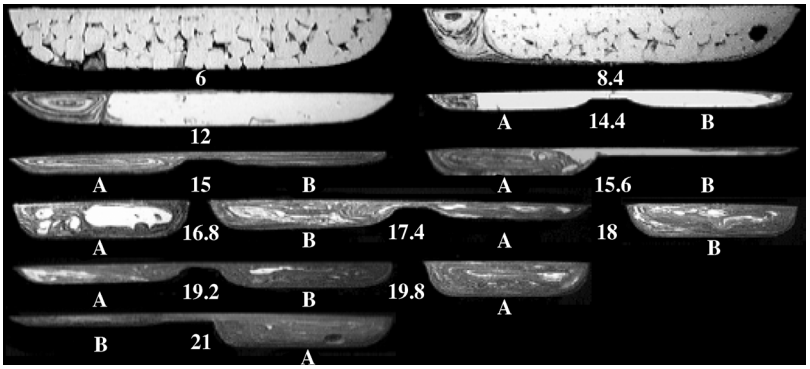

Figure 5.36 Cross-sectional views of an ET screw at a letdown ratio of 220 : 1 white pigmented ABS resin to a black color concentrate [26]. The A and B mixing channels are labeled. The views are for a screw speed of 66 rpm and a rate of 70 kg h^{-1} using a 63.5 mm diameter extruder.

pressures and temperatures that vary with time. Large geometry-induced pressure fluctuations with time were observed in the channels of an ET section, indicating complicated cross-channel flows [20]. These pressure fluctuations were considerably larger than those for a single-flighted metering section.

A solidification experiment has been performed using a 21 L/D, 63.5 mm diameter extruder with an ET screw [26]. Details of the channel dimensions were summarized previously [26], but changes in the channel geometries are obvious from the cross-sectional views shown by Figure 5.36.

This compares with the results obtained with a conventional screw shown in Figure 5.37.

Figure 5.38 shows the cross-sectional views of extrudate samples at a letdown ratio of 100 : 1 of a white pigmented ABS resin with a black color concentrate for an ET screw. The samples were produced at screw speeds ranging from 30 to 150 rpm. The

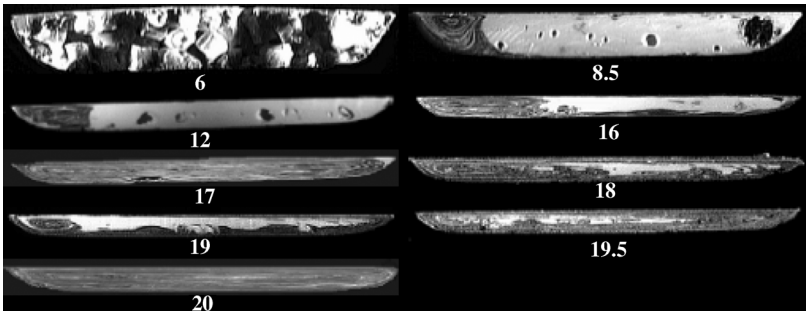

Figure 5.37 Cross-sectional slices for a conventional screw at a letdown ratio of 220 : 1. For each slice, the barrel surface is along the top, the screw root is along the bottom, and the pushing and trailing flights are along the left and right edges, respectively. Labels indicate the axial distances in screw diameters.

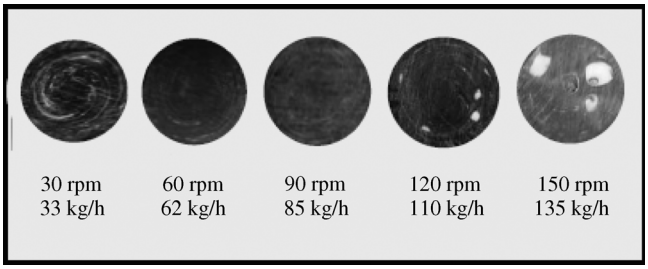

Figure 5.38 Cross-sectional views of extrudate samples at a letdown ratio of 100 : 1 of a white pigmented ABS resin with a black color concentrate for an ET screw.

large round white regions for the cross sections at screw speeds of 90 rpm and higher are solid particles discharged with the extrudate.

As previously stated, the mixing requirement presented here is extremely difficult and non-commercial due to the very high letdown ratio used and the use of TiO_2 in the main resin. For experiments where natural ABS resin (no added TiO_2) was used at a 100 : 1 letdown ratio with the black color concentrate, the very small white streaks were not visible. For commercial operations using letdown ratios of about 35–50 : 1 and translucent main resins, the white streaks in the extrudates would not be visible.

The VBET screw is an enhanced design based on the ET screw [28]. The original VBET design was a replacement design for blown film applications where a barrier section was followed by an ET section. For this application, the VBET section replaces the barrier and ET sections. In general, there are more peaks and undercuts for a VBET screw as compared to a standard ET screw. As previously discussed, ET screws have three peaks or channels with shallow regions, and all peak depths are identical. A VBET screw, however, will have five or more peaks, and the peaks become more restrictive as flow moves downstream.

A VBET screw was designed and built that was comparable to the ET screw presented previously. Details of the screw geometry were presented earlier [28]; here a sketch is shown in Figure 5.39. However, unlike the ET screw having the same diameter, the undercut clearance was gradually decreased from 2.3 mm at the entrance of the section to 1 mm at the discharge end of the screw for the five peaks. In contrast, the ET screw had three peaks and the undercut clearance was a constant 1.4 mm. The specific drag flow rate for ABS resin was calculated at 1.0 kg (h rpm)$^{-1}$ for the VBET screw, which was the same as the ET screw.

Like conventional and ET screws, the VBET screw was operated at a 100 : 1 letdown ratio of white pigmented ABS to a black color concentrate. The extruder was operated at screw speeds ranging from 30 to 150 rpm, and the extrudate samples were collected. Figure 5.40 shows cross-sectional views of the extrudate samples for the VBET screw. As before, the white spiral patterns indicate regions where little to no mixing occurred between the white and black resins. As previously discussed, these patterns would not be visible for a typical commercial application. At a screw speed of 30 rpm, very few white streaks were evident in the extrudate strand samples. When the screw speed was increased to 60 and 90 rpm, the extrudate changed little. As the screw speed was

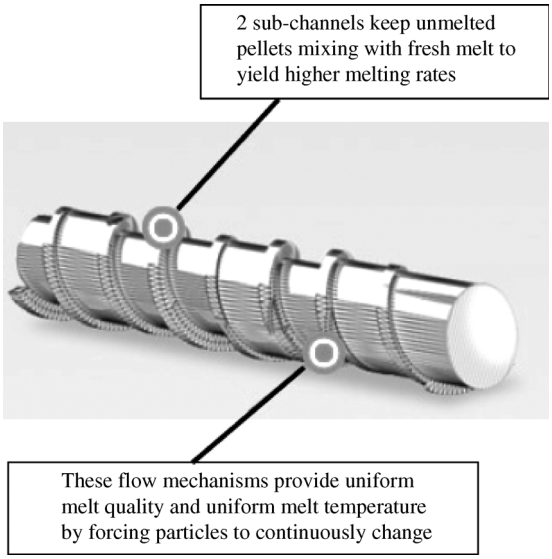

Figure 5.39 Schematic of a VBET screw showing two sub-channel designs.

further increased to 120 rpm, the spiral patterns became more obvious; however, there were no solid resin fragments in the extrudate samples. Some solid fragments, however, were evident in the extrudate for the ET screw at this speed (Figure 5.38). When the screw speed was increased to 150 rpm, a few solid resin fragments in the extrudate began to appear (Figure 5.40). The measured extrusion rate for the VBET screw is also shown in Figure 5.40. The specific rate was nearly constant at 1.0 kg $(\text{h rpm})^{-1}$ over the range of the screw speed. These results clearly indicate that the VBET screw has improved melting and mixing capacity, as there were fewer unmelted pellets in the extruder discharge at higher screw speeds and at higher specific rates than for the ET screw.

The Stratablend and Stratablend II screws are also high-performance designs that are capable of high rates while discharging high-quality mixed extrudates. The Stratablend screw is designed by positioning a Stratablend mixing section [22] in the metering section of a conventional screw. The device is constructed by placing

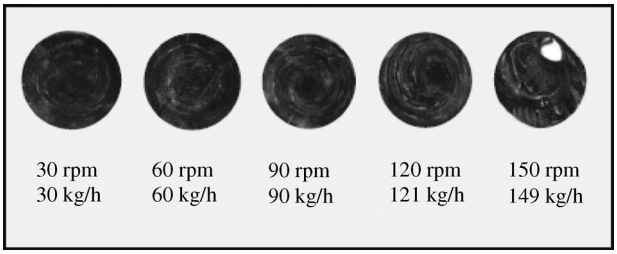

Figure 5.40 Extrudate samples as a function of screw speed for a 100 : 1 letdown ratio of white ABS (TiO_2) to black ABS resin using a VBET screw [28].

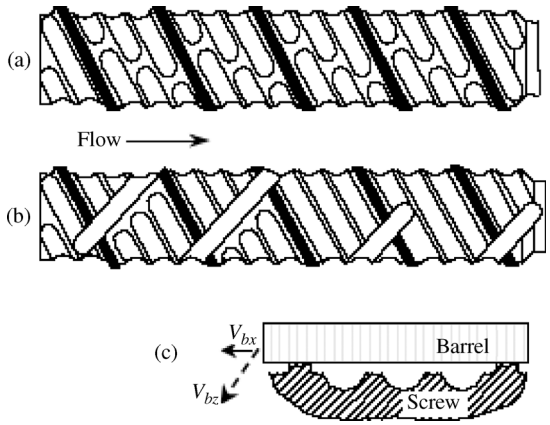

Figure 5.41 Schematics for Stratablend mixing sections: (a) Stratablend [22]; (b) Stratablend II [23]; and (c) cross-sectional view perpendicular to the flight tips, showing the three small channels or grooves and the flight undercuts between them. Courtesy of Timothy W. Womer of Xaloy, Inc.

three smaller advancing channels (or grooves) in the root of the main flight and parallel to the main flight (Figure 5.41). The base depth of the channel is generally very shallow relative to a standard metering section. The distance between the root of the small channels or grooves and the barrel wall is about the same depth as a standard metering channel for the same rate. The small channels are typically a half a screw turn in length.

Like the previously discussed high-performance screws, the Unimix [24] screw is designed by replacing all or part of the metering section with a Unimix mixing section. The Unimix section is designed with three channels positioned between the main flights, as shown by Figure 5.42, vary to a lesser extent, and these channels are

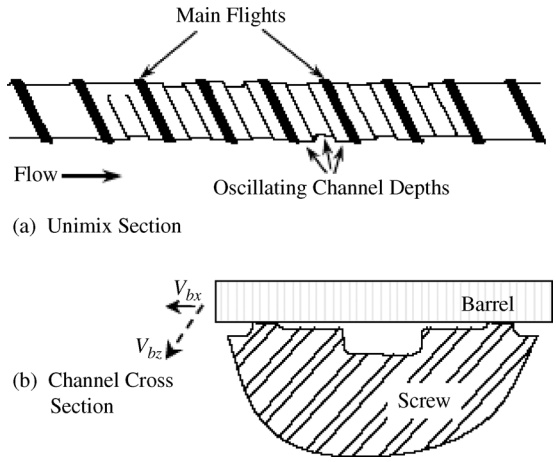

Figure 5.42 Schematic of a Unimix section: (a) the section is used in place of a metering section, and it has three channels with oscillating depths; (b) cross-sectional view perpendicular to the flight tips, showing channels at a local position. Courtesy of Lee Prettyman of Glycon.

shallower than the center channel. A typical Unimix screw is designed with at least three of these melting traps where the channel depths are the same and at a minimum.

The high-performance screws presented here and others (see Further Reading section) all have the objective of completing the melting process as early as possible in the extruder. As shown previously, complete melting is the first key to successful mixing in single-screw plasticating processes. High-performance screw sections are typically designed with multiple regions where the material must pass briefly through small channels, trapping and melting any solids present in the flow. Since the residence times in these small channels are very short, viscous dissipative heating of the resins is minimal, and thus temperature increases due to the devices are in general not significant. But since the main channels for these devices are typically deeper than a conventional metering section the specific rates are higher and the discharge temperatures are typically lower than those for conventional screw designs. The data presented here was based on single-stage screws. For two-stage, vented screws, the high-performance section is positioned in the first-stage meter and the second stage is of a conventional design. Placing the high-performance section in the first stage ensures that the material entering the vent region is completely molten, allowing for maximum volatile removal.

Many of the color mixing experiments cited here were designed under extremely difficult mixing conditions using well designed screws. The extruder used was relatively short at an L/D of only 21. Most commercial plasticators have an L/D that is comparable to this machine or slightly longer. A longer barrel length would allow improved melting and mixing capabilities. Moreover, the masterbatch color mixing experiments were performed by coloring a white pigmented (TiO_2) ABS resin instead of the commercial practice of coloring a natural resin. In several of the experiments in which incomplete mixing was observed for the white pigmented resin, the same experiment was performed using the natural resin. In all cases, the color streaks were not visible in the natural resin. Poorly designed high-performance screws can provide lower levels of mixing and the lower levels of performance.

5.2.2.2 **Secondary Mixing Processes and Devices**

Traditional mixing devices are commonly designed into screws downstream of the melting section for plasticating screws, or near liquid additive injection ports for melt-fed machines. For plasticating machines, these mixers are effective at trapping and melting solid fragments, homogenizing molten streams, and mitigating thermal gradients. As previously discussed, the first main mixing operation occurs during the melting process upstream of these mixers. Since these mixers were developed and are implemented as a secondary process they will be referred to here as secondary mixers. For liquid additive injection through the barrel wall and into molten polymer stream, the correct combination of distributive and dispersive mixing is required to produce an optimal extrudate. These mixers can be extremely important, especially for those processes operating at very high rates or for processes that demand a very high-quality extrudate.

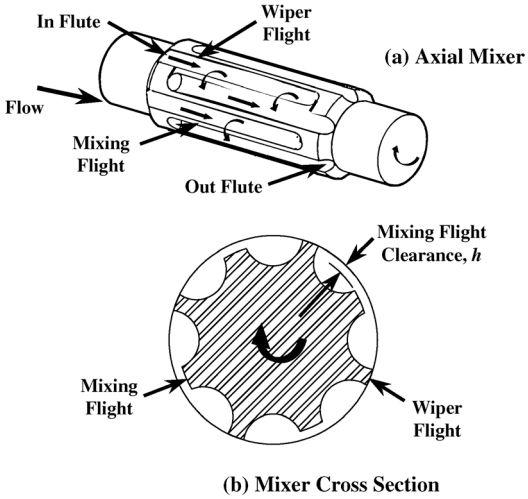

Figure 5.43 Schematic of Maddock-style mixers: (a) a mixer with the flutes aligned in the axial direction; (b) a cross-sectional view perpendicular to the screw axis, showing the clearance for the mixing flight. Courtesy of Jeff A. Myers of Robert Barr, Inc.

Maddock-style mixers [25] are very commonly used due to their low cost to manufacture, and their ability to disperse solid fragments, trap and melt polymer solids, and mitigate color and compositional gradients. Many styles are on the market under two basic types: (i) flutes parallel to the screw axis and (ii) flutes in a spiral pattern in the same direction as the flights. Figures 5.43 and 5.44 depict schematics for these devices. For small-diameter screws, the mixer is generally constructed with four in-flow flutes (or channels) and four out-flow flutes. Larger diameter screws will have more paired flutes due to the larger available area at the screw circumference.

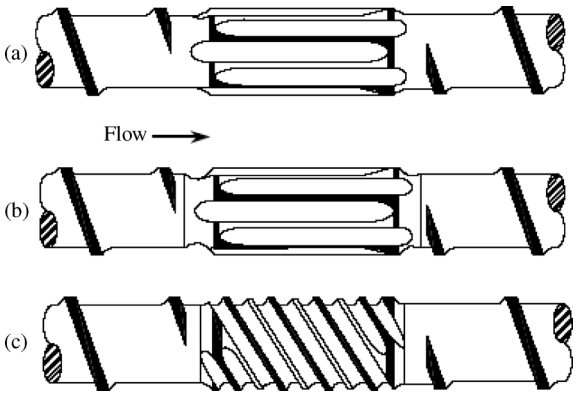

Figure 5.44 Schematic for Maddock-style mixers: (a) a mixer with the flutes aligned in the axial direction; (b) an axial mixer with pressure relief zones at the entry and exits; and (c) a mixer with spiral flutes. Courtesy of Jeff A. Myers of Robert Barr, Inc.

For a Maddock mixer with the flutes parallel to the axis of the screw, molten polymer flows into the in-flow flutes via a pressure gradient, and then either continues to flow downstream in the flute or is passed through a small clearance between the mixing flight and the barrel wall.

Spiral dams are dispersive mixers that are easily designed and constructed, and work well as a trap for solid polymer particles. The mixers are typically 2–5 diameters in length and are designed with a mixing flight starting at the pushing side of a flight channel and ending at the trailing side (Figure 5.45). They are generally positioned at the end of metering sections. Material enters the section on the trailing side, is forced to flow through a small clearance between the mixing flight tip of the secondary flight and the barrel wall, and is then flowed out of the device at the pushing side of the channel.

Distributive mixers work by dividing, reorienting, and re-combining the flow streams. For most devices, this process is performed multiple times. As previously stated, the flow channels on these devices are typically large, creating high mixing with very little pressure gradients and energy dissipation. These devices work well for streams that are completely molten, but they lack the ability to trap and melt solid polymer fragments. Pin mixers are commonly seen commercially due to their effectiveness at reorienting the flow, their low cost, and the ability to install them as a modification to an existing screw. Gear mixers have been used extensively to mix blowing agents into molten streams for foamed products applications. Gear-type mixers are distributive mixers that perform well for the addition of liquid additives to molten polymer streams. For this application the liquid additives are injected through a hole in the barrel wall and typically up-stream of the mixer and the polymer is fully molten. Applications include foam production where a blowing agent such as butane is added, or a devolatilization processes where a stripping agent such as water or

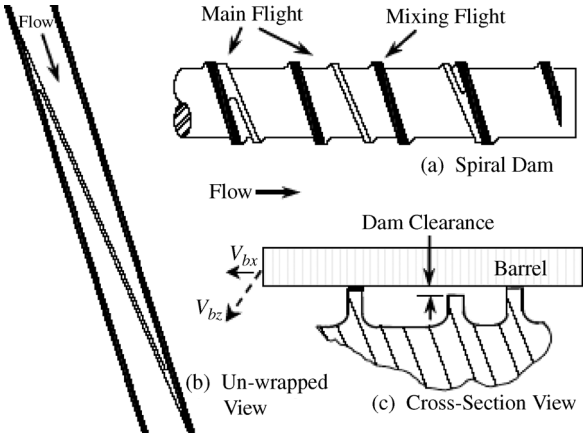

Figure 5.45 Schematic of a spiral dam: (a) side view; (b) un-wrapped view; and (c) a cross-sectional view perpendicular to the flight edge, showing the clearance between the dam and the barrel wall. Courtesy of Jeff A. Myers of Robert Barr, Inc.

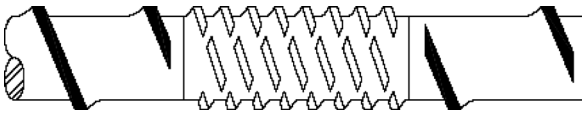

Figure 5.46 Schematic of a gear-type distributive mixer. Courtesy of Jeff A. Myers of Robert Barr, Inc.

nitrogen is added. For the devolatilization process, the stripping agent and volatile components are removed from the polymer using a downstream vent opening. Gear mixers are also used for the addition of liquid dyes or plasticizers. Many styles of gear mixers are available and they are typically designed using a multi-flighted channel design and slitting the flights to allow material to flow into the adjacent channel (Figure 5.46). In general, a well-designed gear mixer depends solely on a pressure gradient to flow material through the device.

The open channels of distributive mixers do not have the ability to trap and melt small solid polymer fragments from incomplete melting in upstream processes. Moreover, combination mixers that perform both dispersive and distribute mixing often only force a fraction of the resin to flow across a restrictive flight and thus some of the material can bypass without being subjected to a high shear stress. As previously indicated, devices that do not have the ability to trap and melt solid polymer particles can cause poorly mixed extrudates, especially at high screw speeds. Mixers that do not have the capacity to trap and melt solids should not be used if solid fragments are likely to occur in the melt stream.

In addition to the screws discussed above, there are other patented screws such as the Fusion™ Screw [29] which was designed for injection molding application but may be evaluated for compounding polymer blends. Figure 5.47 shows a schematic of the melting, homogenization, and chaotic mixing section of the Fusion screw.

5.2.2.3 Helibar® Transfer Mixing Screw in Groove Barrel

A new type of single-screw extruder with grooved barrel in the feeding and the melting section, called a "HELIBAR" screw, has been developed and successfully introduced in recent years at IKT at University of Stuttgart [30–32] and lately evaluated with several commodity polymers and found to provide a rate of 3–4 times higher than the same size conventional extruder with good quality extrudates (Figure 5.48). This system has wide use in blow molding applications and may need to be tested for polymer blend compounding.

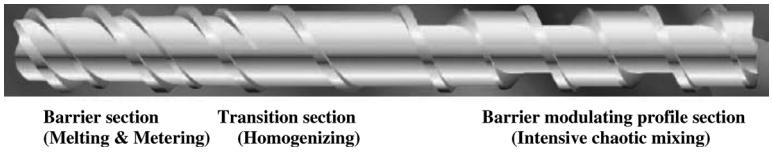

Figure 5.47 Schematic of the melting, homogenization, and chaotic mixing sections of the Fusion screw.

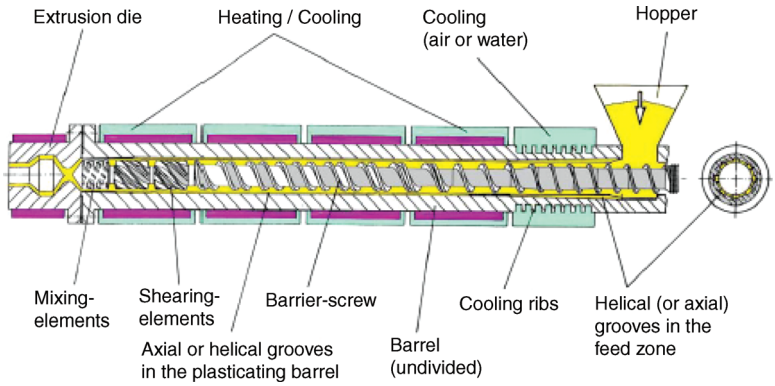

Figure 5.48 Basic design of the processing unit of a HELIBAR plasticating system.

5.2.2.4 **Dynamic Mixers**

Dynamic mixers are a class of secondary mixers where part of the mixing device is allowed to move relative to the barrel and screw surfaces, or has an active channel positioned in the barrel wall. In general, these mixers provide improved mixing over traditional secondary mixers, but they are more complicated and costly to produce, require higher maintenance levels, and they tend to have higher levels of wear. These devices are typically located at the tip of the screw and are developed for injection molding application but can be effective in compounding processes, like other secondary mixers; there are many of these mixers available on the market. The most common ones include the Cavity Transfer Mixer (CTM), Twente Mixing Ring (TMR), and the Barr Fluxion ring mixer. The CTM mixer [33, 34] is a device that is attached to the end of an existing extruder. It has both a barrel section and a screw section. Both sections have concave pockets bored into them, allowing the flowing material to be transferred between the rotor cavities on the screw and the stationary cavities on the barrel wall. The device combines a unique blend of elongational flows and dispersive mixing in the tight clearance regions, and flow reorientation in the cavities. The disadvantages of the device include cost and the need for a barrel extension. Additional mixing performance data for the device is given in Reference [28].

The Twente Mixing Ring (TMR) [35, 36] and the Barr Fluxion ring mixer [37, 38] are adaptations of the CTM design, allowing the addition of the mixer to the screw without requiring a barrel extension with inset cavities. Figures 5.49 and 5.50 show schematics for these mixers. Both devices are designed with a floating sleeve ring that is allowed to rotate freely from both the screw and barrel. For example, at a screw speed of 80 rpm, the speed of the sleeve rings was measured using high-speed data acquisition from pressure transducers at about 10–13 rpm [38]. The ring of the TMR is perforated with cylindrical holes (Figure 5.49). The material in the ring is temporarily suspended in the holes until it is allowed to transfer to the hemispherical cavities in the root of the screw. The floating mixing ring for the Fluxion mixer consists of a series of perpendicular holes that extend through the ring (Figure 5.50). Each series of holes is divided by a dam that prevents material from flowing directly into the adjacent channel. Material is only allowed to transfer to the adjacent channel

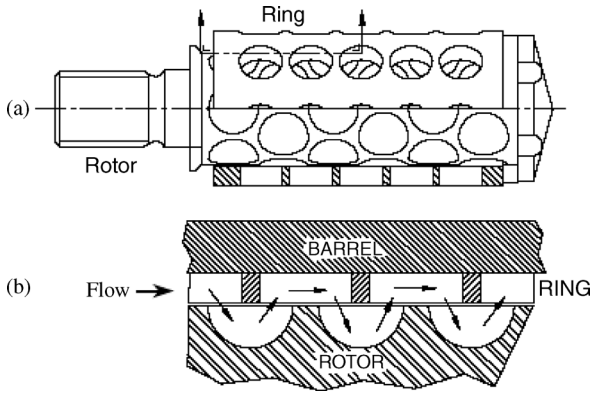

Figure 5.49 Schematic of a Twente Mixing Ring (TMR): (a) mixer with a cutaway section of the ring exposing the surface of the rotor; (b) flow path for the mixer.

by entering the grooves in the root of the screw. As expected, the performance of these mixers exceeds those of the typical secondary mixer, but because of the floating sleeve the potential for wear is high. Moreover, small amounts of foreign material that does not melt can get trapped in the holes of the sleeve, creating a restriction to flow and ultimately requiring a shutdown for cleaning.

The mixing performance for a TMR and a Barr Fluxion ring mixer was reported using a 63.5 mm diameter, 21 L/D extruder and a conventional screw with a removable tip [38]. The tip was 2.4 diameters in length and could be exchanged between a conventional flighted section, a TMR mixer, or a Fluxion mixer. The conventional flight tip had a channel depth of 3.56 mm. The experiments were performed with the same ABS resin as those for the studies presented previously. For these runs, the extruder was operated at a screw speed of 80 rpm with a 220 : 1 ratio of white ABS to a black color concentrate ABS resin. The extrudate samples, collected in the same manner as before, are shown in Figure 5.51. As shown by this figure,

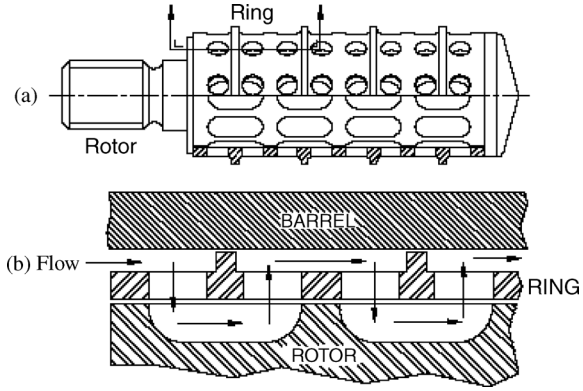

Figure 5.50 Schematic of a Barr Fluxion mixing ring: (a) mixer with a cutaway section of the ring exposing the surface of the rotor; (b) flow path for the mixer.

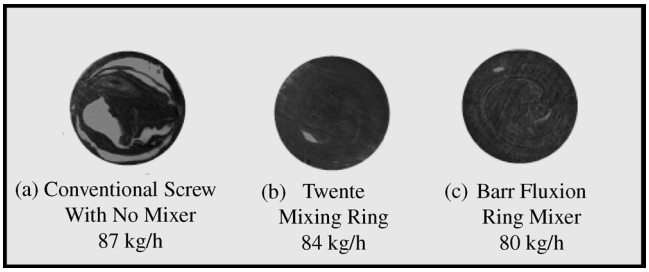

Figure 5.51 Cross-sectional views [32] of extrudate samples obtained using a conventional screw with segmented tip for the testing of different types of dynamic mixers: (a) conventional screw with no mixer; (b) Twente mixing ring; and (c) Barr Fluxion ring mixer. The extruder was operated at a screw speed of 80 rpm and a letdown ratio of 220: 1 of a white pigmented ABS resin to a black color concentrate.

considerable levels of solid polymer and unmixed material were discharged using the conventional flighted screw tip, that is, no mixer present. This result is consistent with the data shown by Figure 5.40 for a VBET screw with a slightly shallower metering channel depth. As indicated by Figure 5.51, similar mixing levels were obtained from the TMR and the Fluxion mixer. This level of mixing for the extrudate was extremely remarkable considering that the material entering the devices were essentially 60% unmixed (white pigmented ABS), and considering that the mixing criteria here exceeds the current demands of the commercial community. Other performance characteristics were previously presented in the literature [35, 36, 38].

5.3
Most Critical Step in the Production of Polymer Blends – Melting/Mixing

Many articles and research results have been reported for the melting mechanism of a single component polymer in single-screw or twin-screw extruders; however, few articles elucidate the melting of two or more polymers. To manufacture a polymer blend of two or more resins with unique properties one has to understand the melting and mixing of the components and morphology in the twin-screw extruder. To this end, two unique pieces of laboratory equipment were developed: (i) a 30-mm co-rotating twin-screw extruder in a clam-shell barrel (EPSIM II, Extrusion Process Simulator, Version II) and (ii) a 30-mm co-rotating twin-screw extruder in vertically opening modified clam-shell barrel (TSMEE, twin-screw mixing elements evaluator).

5.3.1
Extrusion Process Simulator Version II (EPSIM II)

EPSIM I [39] was a short twin-screw extruder mounted on a horizontal moving lathe. The barrel section was attached to the lathe. This unit was developed to

monitor the pressure development within the various (kneading or conveying) screw sections. Pressure and temperature transducers were mounted on the barrel so that barrel can be placed on the lathe to trace pressure at any points. The information obtained in the experiment was to aid the computer simulation development [40].

EPSIM II [41] is 30-mm diameter, 32 L/D twin-screw extruder with a specially constructed barrel mounted on the moving lathe. Screw elements and a centerline distance correspond to a Model ZSK-30 extruder by Werner & Pfleiderer Corp. The machine has a clam-shell barrel, rapid cooling capabilities, four heating zones, and seven ports for feeding, venting, or process measurements. The unit, powered by 11.2 kW motor, has pelletizing capabilities. A unique feature of EPSIM II is that the axial position of the barrel can be adjusted with respect to the screw. Consequently, the operation zones can be adjusted to simulate any length of the extruder. The first experimental results were reported on the melting behavior of virgin polymers, namely, PC and ABS. For PC, two feed forms were examined. Three different mechanisms were identified for first stage melting of polymers and were traced to differences in solid phase geometries and material properties, as processing parameters were held constant for all trials. A common observation was solid deformation and material accumulations in the intermeshing zone, indicating that this is a primary location of energy transfer to the polymer. This work was followed by a melting study of a polymer mixture of PC/ABS [42]. It was found that the melting of polymer blends is a non-additive (+) process. Blend components interact to complicate the direct application of knowledge from component melting mechanisms. Interactions arise in the form of solids exclusion from the high shear regions of the screw based on scaling considerations and modification of dynamic behavior because of physical interactions. Preferential melting of the higher T_g polymer took place when the lower T_g polymer was excluded from the region where high levels of frictional and viscous heat were generated. In PC flake/ABS case, PC flake excluded ABS pellets from the intermeshing zone of the extruder. The physical attraction of PC pellets to molten PC allowed PC pellets to have greater interaction than ABS in the high shear (intermeshing) region of the extruder after melting was started. It was also observed that barrel temperature profiles help to determine the axial position at which melting starts.

5.3.2
Twin-Screw Melt Mixing Evaluator (TSMEE)

In a Polymer Mixing Study at the Polymer Processing Institute, a similar unit to EPSIM I & II was developed to study the melting and mixing of polymer blends. PMS was a consortium of 40 member companies, including resin manufacturers, custom compounders, fabricators, and equipment manufacturers. The melting and mixing studies were carried out on various polymer systems (semi-crystalline–amorphous, amorphous–amorphous polymer blends). The study observed the melting behaviors of several virgin polymers and the blends of two polymers in different compositions. As reported in Reference [43], similar phenomena were observed in TSMEE as those

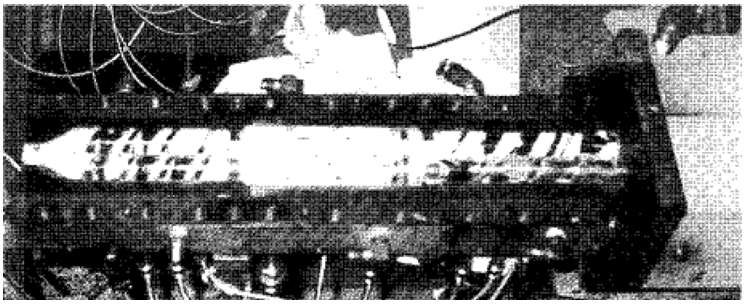

Figure 5.52 TSMEE with split barrel shown in the fully open position. Screw elements are ZSK elements from Werner & Pfleiderer. Thermocouples and pressure transducers that were used for on-line measurement of temperature and pressure are also shown. A more detailed description is shown in Reference [44].

by Busby *et al*. [41]. The TSMEE has the same screw geometry as a ZSK-30, but has a split barrel design and quick quench features. Figure 5.52 shows a photograph of the polymer carcass following quick quenching after the steady state run.

The study on the dispersive mixing of PC/SAN was reported by Lee, Ryu, and Kim [43] using TSMEE. They found that size reduction is mostly accomplished during the softening process and the mode of breakup follows in sequential formation of sheet, lace, and ligaments, which turn into droplets via Raleigh-type instability. They found the final domain sizes are less influenced by viscosity ratio but, instead, by the strong influence of elongational flow field in the kneading section. It was also indicated that the melting mechanism may have a strong influence on the dispersive mixing of the dispersed phase of the blend. A series of experiments in mixing utilizing TSMEE led to the concept of plastic energy dissipation (PED) in addition to viscous energy dissipation (VED). The first analysis for melting mechanisms of single-component polymers in TSMEE through visual and microscopic analysis has been reported [45].

Firstly, we should review most recent work of Kim, Gogos, and Tadmor [6] who introduced the importance of PED and follow-up work of Qian, Todd, and Gogos [47]. Figure 5.53 represents a rendition of the analyses of many experimental carcasses. Shown are the physical states of the pellets stream being melted, a schematic of the carcass "morphology," the screw conveying/kneading element sequence, and the melting mechanisms responsible for affecting melting of the pellets stream. The last row shows the melting mechanisms responsible for advancing melting of a PP powder feed.

5.3.3
Melting of Virgin Polymers

As mentioned above there are three sources of energy to melt polymer pellets or powders: (i) frictional energy dissipation (FED), (ii) PED, and (iii) VED . When the

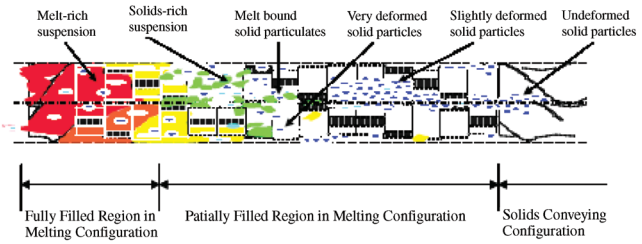

				"States" of the Stream Schematic Representation Co-TSE Screw Configuration
VED	PED VED (DMM)	PED	Conduction	Melting Mechanisms (Pellets)
VED	PED VED (DMM)	PED	Conduction	Melting Mechanisms (Powder)

Figure 5.53 Schematic representation of the evolution of melting of PP pellets in a 30-mm co-TSE [5].

sum of these energies equals the thermal energy required to melt a polymer, polymer will melt in case of crystalline polymers and start to flow in case of amorphous polymers.

5.3.3.1 Melting and Remelting

Most shaping operations consist of the flow and deformation of heat-softened or melted polymers; hence the preparation of the polymer for the shaping operation generally includes a "heating" or "melting" step. In either case we define the process of bringing polymers from the feed temperature to the desired processing temperature range, appreciably above T_g for amorphous polymers and above T_m for semi-crystalline polymers, as the "elementary step of melting." The thermal energy requirements for this process can be estimated from the specific enthalpy curves (Figure 5.54). The area under any given curve represents the thermal energy needed to heat/melt 1 kg of that polymer from room temperature to any higher temperature.

We note that semi-crystalline polymers, where the "break" points are indicative of T_m, require more energy because they must undergo the phase transition of fusion. As examples, about 700 kJ kg^{-1} are needed to heat HDPE (high density polyethylene) to 200 °C, while for the same processing temperature PS requires about 350 kJ kg^{-1}, that is, half the energy. Melting is a very important elementary step, in the sense that is consumes 70–80% of the total processing energy input. It is often a rate "bottleneck" to the processing and it must be carried out to completion in the "melting section" of the processing equipment. Additionally, during melting of blends of polymers, a major part of the *blend morphology* is established.

Below, we aim to elucidate the physical mechanisms of melting, to demonstrate some of the common mathematical tools used in solving melting problems, and to

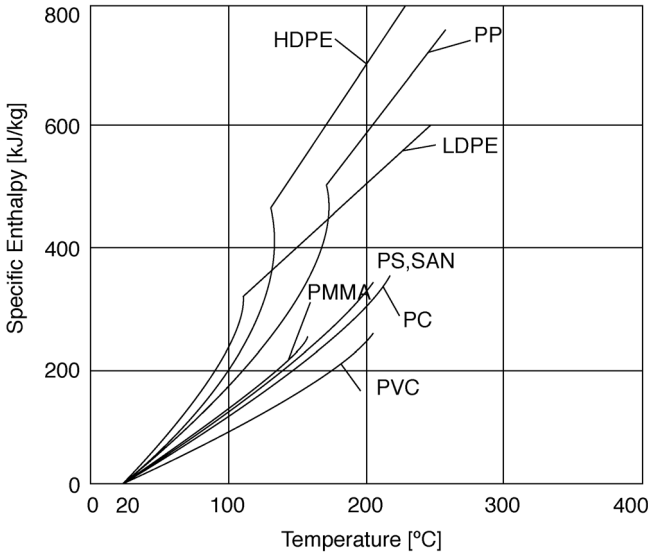

Figure 5.54 Specific enthalpy curves for some common polymers.

demonstrate how these mechanisms, in conjunction with inherent physical properties of polymers, lead to certain geometrical configurations of melting.

5.3.4
Classification and Discussion of Melting Mechanisms Important to Polymers

Every possible physical phenomenon that can bring about melting (heating) to any substance is included in the terms of the thermal energy balance:

$$\varrho \frac{DU}{Dt} = -\overline{\nabla} \cdot \bar{q} - P\left(\overline{\nabla} \cdot \bar{v}\right) - (\tau : \dot{\gamma}) + \dot{S} \tag{5.1}$$

Because polymers are "practically incompressible" in both the solid and liquid states, $\overline{\nabla} \cdot \bar{v} = 0$ and the energy balance becomes:

$$\varrho C_p \frac{DT}{Dt} = -\overline{\nabla} \cdot \bar{q} - (\tau : \dot{\gamma}) + \dot{S} \tag{5.2}$$

In the above equation the left-hand side represents the rate of increase of the enthalpy of a fluid element of an incompressible material moving downstream the processing equipment. The right-hand side terms "state" that there are only *three* physical phenomena through which the enthalpy for these materials can be increased: *conduction* heat fluxes at boundary surfaces, dissipation of mechanical energy during the flow of viscous liquids (VED, viscous energy dissipation), a heat *source* term defining *other sources* of thermal energy, due to, for example, chemical reactions, or dissipation of microwave energy. This equation, with $\dot{S} = 0$, coupled

with the equation of motion, has been very widely used to describe the temperature field of flowing non-reactive viscous fluids or melts. It has been used exclusively in fluid mechanics. To describe the heating of solids, the following form of this equation is used:

$$\varrho_s C_{ps} \frac{\partial T_s}{\partial t} = -\overline{\nabla} \cdot \bar{q} = \overline{\nabla} \cdot K_s \overline{\nabla T} \tag{5.3}$$

Let us now discuss, in *physical terms,* how important each of the above three mechanisms is to the melting of polymers and what are the limitations or advantages, due to the physical nature of polymers.

Heat conduction: the most common mode of raising the temperature of the solid and melting it. The rate controlling factors in conduction melting are the thermal conductivity, the attainable temperature gradients, and the available contact between the heat source and the melting solid, reflecting, respectively, material, operational, and configurational constraints. The low thermal conductivity of polymers, polymers are thermal insulators, and their temperature sensitivity makes them subject to thermal degradation at the attainable temperature gradients, thus, placing upper limits to the magnitude of heat fluxes that can be applied. Thermal degradation is characterized by two temperature-dependent parameters, the induction time for the onset and the rate of degradation (Figure 5.55).

The two graphs of indicate that:

$$m(t) = m_0 \quad t \leq \theta(T)$$
$$m(t) = m_0 \exp\left[Cte^{-\Delta E/RT}\right] \quad t > \theta(T)$$

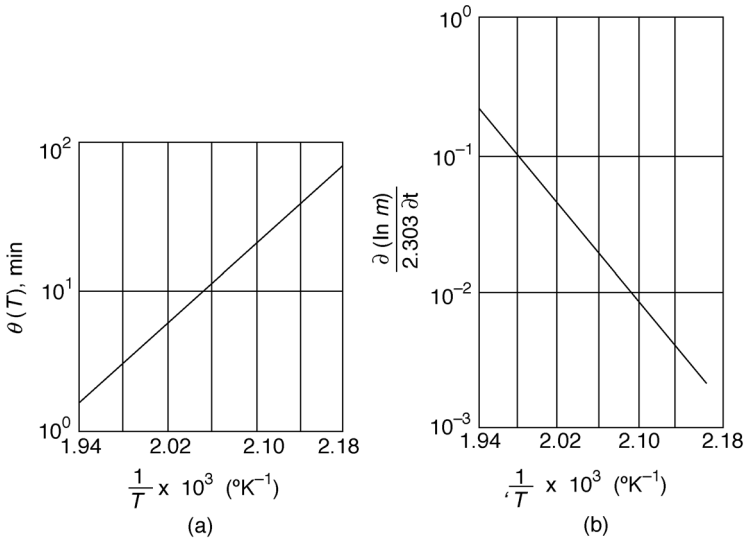

Figure 5.55 Thermal degradation of unplasticized PVC, Geon 101 EP-F24, as indicated by the time dependence of the consistency index m of the power law fluid model [1]. See text for details.

The induction time $\theta(T)$ is shown on Figure 5.55a and the function $m(t)$ for $t > \theta(T)$ on Figure 5.55b (cited in Tadmor and Gogos [1]).

To augment the limited ability of the conductive heating mechanism to heat polymer solids, other heating mechanisms have been tried, for example, through the use of dielectric or ultrasonic energies. These may be dissipated by polymer solids, creating volume-wide heat sources. The governing form of the energy balance becomes:

$$\varrho C_p \frac{\partial T}{\partial t} = -\bar{\nabla} \cdot \bar{q} + \dot{S} \tag{5.4}$$

Unfortunately, although feasible [1], these energy sources ($\dot{S}$) are limited in polymer processing practice as *primary* melting mechanisms.

In contrast, the potential exists for creating and using a huge energy source term if large and repeated deformations can be imposed on compacted polymer particulate beds: when individual polymer particles undergo large deformations, past their "elastic limit," part of such deformations are *plastic,* that is, irreversible; plastic deformations of viscoelastic polymer solids are very dissipative, since the stresses required are much higher than those needed for viscous flow. Thus, the heat source we have called plastic energy dissipation (PED) [5, 45], associated with irreversible polymer solid deformations of compacted particulates, is much higher than VED for the same polymer. Additionally, during deformation of compacted beds of polymer particulates, mechanical energy can be generated by inter-particle friction, giving rise to frictional energy dissipation (FED). Thus, for "active" compacted polymer particulates and assemblies undergoing plastic deformations there are two heat source terms that must be included:

$$\varrho_s C_{\varrho s} \frac{DT}{Dt} = -\bar{\nabla} \cdot \bar{q} + \text{PED} \ + \ \text{FED} \tag{5.5}$$

The PED and FED terms are not easy to describe mathematically, since they are not strictly speaking "homogeneous" sources, the reason being that particulate assemblies are not continua, but made up from discreet bodies. Nevertheless, *dominance* of co-TSEs in processing equipment is due to their capability of *very* rapid melting caused by repeated deformations imposed on compacted particulates by twin kneading elements. For extensive discussion, please refer to References [5, 45].

When molten polymer regions are formed because of PED and FED and if the deforming stresses persist, then both PED *and* VED will act simultaneously as heat sources, resulting in the powerful mechanism of dissipative mix-melting, which we will deal with again below.

Let us now turn to VED. Its magnitude is the local scalar product ($\tau : \dot{\gamma}$), which depends on the local melt viscosity and shear rate. As noted above, it is an appreciable heat source in flowing polymer melt streams. Since the melt viscosity is shear rate and temperature dependent, decreasing significantly with an increase in both, the dependence (sensitivity) parameters – the pseudo-plasticity index and the activation energy for flow – are important to the resulting *local heating*. Local overheating, because of VED, may be created for melt elements that are exposed continuously to

high stresses, as in the wall region of capillary flow. To obtain more spatially uniform temperatures, all melt elements must be exposed in an alternating fashion to high and low shear rates. This may be achieved by flows that promote laminar distributive mixing.

When polymer solids and melts *coexist* the melt will heat and may eventually melt the solid by conduction. If the melt in contact with the solid is at rest, then conduction melting *without* melt removal will take place. But, soon the rate of melting will become very slow, so much so that, in order to cause appreciable amounts of melting the melt temperature has to remain very high for long periods of time, leading to thermal degradation. If, on the other hand, the melt in contact with the solid is removed continuously from that region by intentionally applied flow, then conduction melting *with* forced melt removal will be the melting mechanism. Now the conduction melting rates achieved are much more rapid because (i) any surface portion of the solid that is melted is rapidly removed, exposing "fresh" solid layer to be melted, and (ii) the melt flowing under forced removal generates heat by VED. The combined effect is higher melt temperature gradients and higher rates of melting. The above two mechanisms involve solids that do not undergo large and repeated deformations, that is, "passive" solid beds. Finally, the maximum rate of melting is obtained when conduction melting with forced melt removal, VED, *and* deformation of the solid particulates take place simultaneously, giving rise to the dissipative mix-melting mentioned above.

In summary, the melting mechanisms that are effective in melting polymers at acceptable rates from the points of view of avoiding thermal degradation and achieving high processing rates are:

1) **Conduction melting with forced melt removal**: where both conduction and melt flow-induced VED achieve appreciable melting rates. This is the *primary* melting mechanism in *single rotor* polymer processing equipment. Such equipment, for example, single-screw extruders and injection molding machines, are primarily forming devices, with the large pumping capabilities needed for forming; single-screw extruders allow the compacted polymer particulates to remain *passive,* not participating in the melting process.
2) **Plastic energy dissipation and frictional energy dissipation**: in that order of importance, where compacted polymer particulates are "relentlessly" deformed by *twin rotor devices,* thus rapidly raising their temperature and creating regions of melts.
3) **Dissipative mix-melting**: becomes the operative melting mechanism *after* PED and FED have created a "solids rich" melt suspension. In this early two-phase stage, PED may still be dominant. Very soon after, as "melt-rich suspensions are created, VED becomes the dominant mechanism, capable of rapidly elimination all solids regions. Again *only* twin-screw co- and counter-rotating devices can cause the solid particulate assemblies to deform rapidly and repeatedly and become participants to the melting process. This is the reason why such devices are used when uniform and very rapid melting is required, as in the "mega" rates

post-reactor polymer "finishing" operations, as described in Section 5.2.1 on twin-screw extrusion technology.

For a further elaboration of many melting mechanisms, the reader should refer to Reference [1].

When physical blended multiple polymer pellets are going through the melting steps, the mechanism can be very complicated. Therefore, many analytical methods are employed to improve the effectiveness of equipment to produce blends having consistent morphology and uniform compositions. The unique laboratory equipment was used to characterize the screw elements and their arrangement on the capability of providing cost-effective polymer blends.

5.3.5
Characterization of Mixing Elements

For example, the performance of several mixing elements were evaluated and compared at the Polymer Processing Institute by using the TSMEE (twin-screw mixing elements evaluator) [34].

TSMEE is a specially designed 12 : 1 L/D TSE with a clam-shell barrel for quick opening to study polymer blend carcass or visually observe the mixing process with liquid–liquid mixtures.

Figure 5.56 shows mixing enhancers used in the experiments.

Experiments were carried out to measure the relationship between the rates and the pressure drop over the length of mixing element, thus assessing how much is due to drag flow and how much is due to pressure flow generated by the mixing elements. Figure 5.57 shows the screw arrangements employed. The conclusions are:

1) ZMEs (forward slotted, single start reversing lead screws) are essentially pressure neutral – the tilted slots do as much forwarding as the helix does reversing.
2) TMEs are also close to pressure neutral, with a minor forwarding or retaining action due to the direction of the slots.
3) SMEs (reverse slots in the twin start feed screws) are positive conveying. Because of the pressure gradient that a full section develops, there is more back-mixing through the slots (pressure driven) than with the ZMEs or TMEs. This behavior suggests that SMEs would be the elements of choice in melt sections of the extruder to dampen out feed irregularities – especially for high rpms and short residence times of the super compounders.

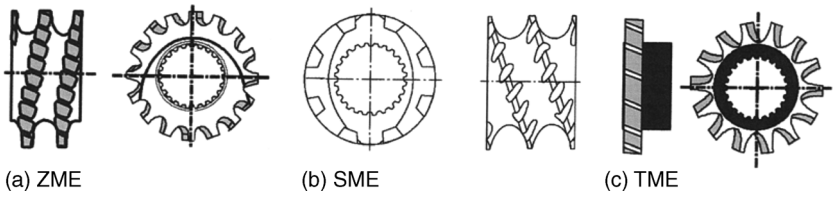

Figure 5.56 Mixing enhancers: (a) ZME, (b) SME, and (c) TME [46].

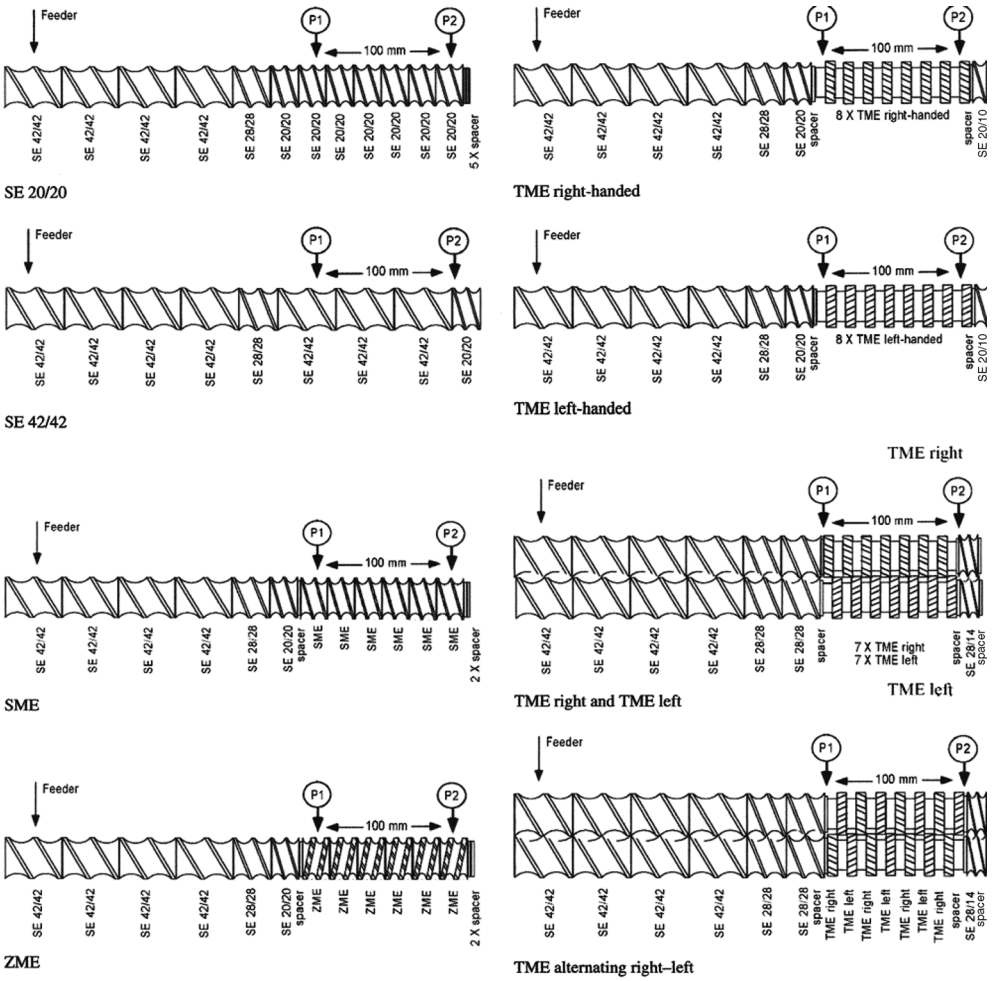

Figure 5.57 Schematics of screw configurations with different mixing enhancers.

4) The major mixing effect of slotted mixing elements is distributive, with only short range axial back-mixing, but probably improved radial mixing.
5) The spread of residence times during transit out of the bulk of the fluid through an extruder can frequently be characterized by a single parameter, the Péclet number, analogous to plug flow with varying amounts of axial eddy diffusion across the plug flow front. This is not the actual mechanism, but the mathematical model does allow assigning numbers for comparison of the relative effects of screw rpm, feed rate, and screw configuration.
6) Some portion of the flow (5–10%) may evidence a long RTD tail, probably due to zero velocity at the metal walls. The amount and duration of the tail will be affected by the wetting properties of the melt, clearances, and screw configuration.

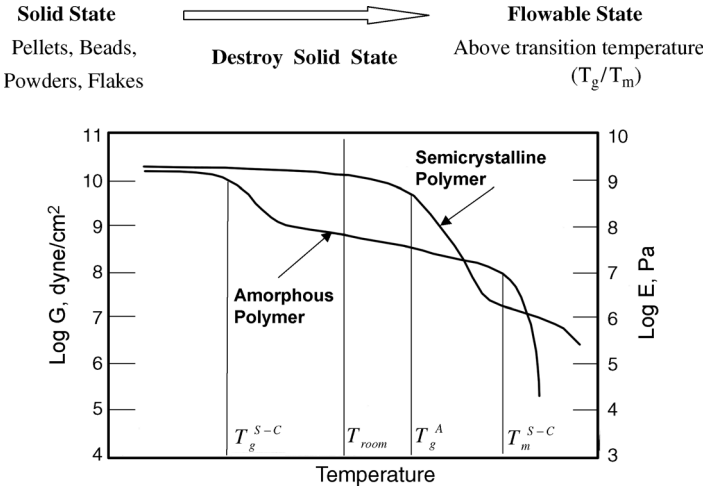

Figure 5.58 Modulus of elasticity as a function of temperature for amorphous and semi-crystalline polymers.

5.3.6
Melting of Solid Mixtures of Polymer Blend Components

The melting modes in the twin-screw extruders will depend on the plasticating temperature of each component. When a high temperature melting polymer (HTMP) is blended with a low temperature melting polymer (LTMP), as soon as the LTMP melts, the melts start to lubricate the pellets/particulates of the HTMP and further delays the melting of HTMP particles. Therefore, a polymer blend of components with closely matching melting points will have a narrower range of melting than a blend of components that have widely separated melting points.

Figure 5.58 shows the modulus of elasticity as a function of temperature for amorphous and semi-crystalline polymers. Polymer feed temperatures are at or near room temperature (T_{room}). For common amorphous plastics the glass transition temperature (T_g) is higher than room temperature, $T_{room} < T_g$, while for semi-crystalline polymers T_g is lower than room temperature and the melting point is higher than room temperature, $T_g < T_{room} < T_m$. As shown above, PED, through large solid state irreversible deformations, makes the solid an "active participant" of the melting process, rapidly destroying the solid and creating a molten state. The modulus of an amorphous polymer is higher and less temperature dependent in the temperature region above room temperature, $T > T_{room}$. Consequentially, the magnitude of amorphous PED is larger and less temperature dependent when compared to semi-crystalline PED. Thus, when physical blends of amorphous and semi-crystalline polymers are fed into the twin-screw extruder, very complicated process can take place during the melting process.

The Polymer Mixing Study carried out in Polymer Processing Institute selected typical semi-crystalline polymers and amorphous polymer. Figure 5.59 shows the energy required to reach the transition temperature for the polymers selected.

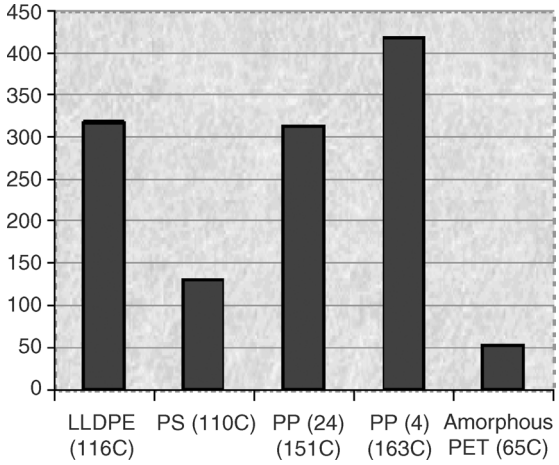

Figure 5.59 Energy required (kJ kg^{-1}) to reach the transition temperature of each polymer. (Number in parenthesis in the legend is T_m or T_g.)

The Twin Screw Melting Evaluation Extruder (TSMEE) was used, which facilitates opening of the barrel to monitor the carcass of the polymer mixtures along the extruder after the extruder was stopped and the content quickly frozen and dissected to assess the degree of mixing. Differently colored pellets were used for macroscopic observations and detailed morphology was analyzed by microscopy.

5.3.6.1 Melting Behavior of Single Components and the Blend

The carcass experiments for melting were conducted in the TSMEE. After the process became steady, normally after 30 min of running under set conditions, the extruder was "dead-stopped." All barrel sections were then quenched with circulating cold water to preserve the melting and mixing state inside the extruder. Images of the quickly frozen carcass, revealing the evolution of melting along the screw axis, were captured with a digital camera.

To determine visually the melting/mixing state from the solidified carcass, some of the feed pellets used were pre-compounded into colored pellets that contain a very small amount of pigment. We assume that the presence of this small amount of pigment does not affect the melting characteristics of the polymer. Basically, two types of melting screw configurations were examined. The first consisted of 45° staggering angle forward kneading blocks, each kneading block containing five kneading paddles with a total length of 28 mm, followed by a half-lead reverse screw element 10-mm long. The other melting screw design was just four neutral kneading blocks (each with five kneading paddles and the same total length of 28 mm) without any reverse elements. The objective of carcass experiments was to examine whether the higher PED amorphous PS would also melt faster than the lower PED semi-crystalline PE in PS/PE blends, the same phenomena observed as the melting of each individual component in twin-screw extruders. The studies were started with PS/LDPE blend, PP/PS blend, and then PS/LLDPE blend were more extensively analyzed as presented

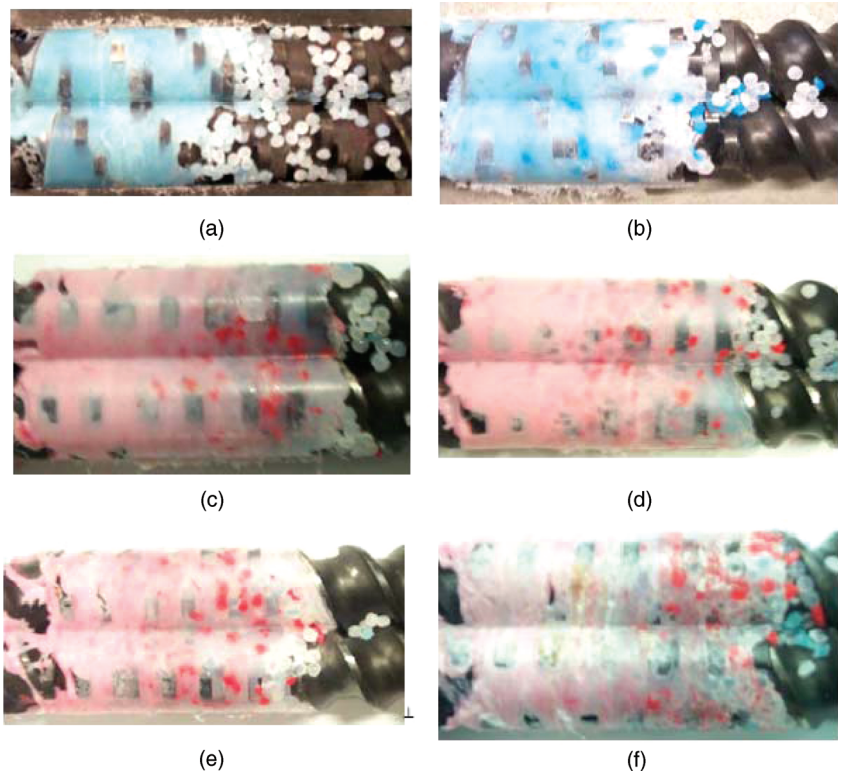

Figure 5.60 Melting carcasses of LLDPE/PS blends in a co-TSE TSMEE: (a) LLDPE, 4KB45/5/28 + 20/10(R), 200 rpm, 16 kg h^{-1}, 200 °C; bulk melting commenced only in the consolidated section. (b) LLDPE/PS blend (90/10 wt), 3KB45/5/28 + 20/10(R), 100 rpm, 12 kg h^{-1}, 200 °C; 10% of LLDPE pellets colored light blue. (c) LLDPE/PS blend (90/10), 4KB90/5/28, 100 rpm, 8 kg h^{-1}, 200 °C/200 °C/200 °C; 10% of LLDPE pellets colored light blue, PS pellets colored red. (d) LLDPE/PS blend (90/10), 4KB90/5/28, 100 rpm, 24 kg h^{-1}, 200 °C/200 °C/200 °C; 10% of LLDPE pellets colored light blue; PS pellets colored red. (e) LLDPE/PS blend (90/10), 4KB90/5/28, 100 rpm, 8 kg h^{-1}, 100 °C/130 °C/123 °C; 10% of LLDPE pellets colored light blue; PS pellets colored red. (f) LLDPE/PS blend (50/50), 4KB90/5/28, 100 rpm, 8 kg h^{-1}, 100 °C/129 °C/119 °C; 10% of LLDPE pellets colored in light blue; 10% of PS pellets colored red.

below. Single-component LLDPE was melted using a melting screw design with 45° staggering angle forward kneading blocks followed by a reverse screw element. Figure 5.60a shows typical results. All three barrel-sections were set at 200 °C. The screw speed was 200 rpm, and the flow rate 16 kg h^{-1}. From the carcass image, it was found that melting commenced at the fully consolidated region. Without consolidation, the forward kneading blocks behaved somewhat like conveying screw elements (Figure 5.60a). Although a few pellets may be caught and get deformed, most pellet feed was conveyed with little change in the partially filled section. Melting was very effective once polymer particulates were consolidated due to the barrier (reverse) screw

element downstream, and a very short melting length (1–2 L/D) was observed. Compared with the melting of single-component amorphous PS, semi-crystalline PE has a much longer melting length [45, 46]. Mixing or blending morphology evolves concurrently with the melting process. Figure 5.60b shows the typical melting carcass of a two-component polymer blend (LLDPE/PS: 90/10 wt%). The blend consisted of 80% of "virgin" LLDPE, 10% of the colored LLDPE in light blue, and 10% of PS, all in pellet form. Again, all three barrels were set at 200 °C. The feeding rate was 12 kg h^{-1} and the screws were running at 100 rpm. The total melting length for the blends was comparable to that of a single-component LLDPE. More unmelted PS "escapees" (detected as more transparent spots in the melting carcass while it was held against the light) were observed than LLDPE "escapees" (seen from the light blue spots in the carcass) just before the reverse screw element. Amorphous PS, while it melts much faster as a single-component polymer, did *not* show the same high rate of melting as a participant in polymer blend melting with softer LLDPE, which can be readily explained by the PED behavior of the blend. As a single component, amorphous PS with a higher level of PED exhibited a shorter melting length in twin-screw extruders than the relatively softer semi-crystalline LLDPE [45, 46]. The melting behavior of their blends, however, is more complicated. The tougher PS, which has a much shorter melting length when melted alone, took much longer to become melted as a blend component with the softer LLDPE. The same blend melting behavior was observed in a melting screw configuration consisting of all neutral kneading blocks (Figure 5.60c–e), for the same LLDPE/PS blends of weight ratio of 90/10. The only process variable difference between the samples shown in Figure 5.60c and d was the flow rate, which was much higher in the latter. Figure 5.60c and e differs in that the latter had much lower barrel temperature. Figure 5.60f also shows low barrel temperature melting, but with a blend of LLDPE and PS in a 50/50 weight ratio. In all of the above carcass melting experiments of LLDPE/PS blends under various conditions and compositions, the softer LLDPE part always melted *faster* than the harder PS component. This can also be explained by their different PED behaviors when compressed together in series. Though PS has a higher PED, and thus melts faster as an individual component than LLDPE, the blend PED behavior showed that most (~95%) of the plastic energy was dissipated inside the softer LLDPE part. The much larger TSE-generated PED of LLDPE than PS in their blends, though LLDPE is the softer component, resulted in a faster heating/melting of LLDPE melting behavior in twin-screw extruders. After the soft LLDPE was melted and formed a continuous phase, the melting of remaining PS pellets and LLDPE "escapees" is via heat conduction from the surrounding melt, which is heated mainly by viscous energy dissipation (VED). A physically sound melting model should be able to account for the initial heating/melting of polymer or polymer blends due to their respective PED behaviors and subsequent melting of "escapees" due to heat transfer and VED of the melt. Although not specifically studied, it is possible that in high melt viscosity blends the "escapees," remaining as solid particulates, may undergo deformation and thus generate PED. As this type of melting study is difficult to carry out, the researchers chose monitoring by physical, chemical, and mechanical means to assess the degree of mixing by characterizing the final product.

5.4
Monitoring of Morphology and Compositions of Polymer Blends

In 1987, Van Oene reported that twin-screw extrusion showed better performance than other blending methods in a study of the phase behavior and mechanical properties of a series of polyarylate/polycarbonate blends [48]. The polymers are known to transesterify, the extent of which depends upon the thermal and shear history, and so affect phase behavior and properties. In this study, single-screw extrusion, twin-screw extrusion, and solution casting were employed for blend preparation. Two transition temperatures, corresponding to a polycarbonate-rich phase and to a polyarylate-rich phase, were seen in blends that were solution cast or compounded in a single-screw extruder at 285 °C. But after injection molding a single T_g was observed. When annealed at 180 °C for several hours the molded blend was found to phase separate. Blends that were compounded in a twin-screw extruder exhibited a single T_g and could not be phase separated. The flexural and tensile properties of blends that were prepared in a twin-screw extruder show a small positive synergism. But the impact properties were substantially below the rule of mixtures values, probably as the result of advanced exchange reaction and thermal degradation. Over the last 20 years, many researchers have reported studies on polymers blends prepared with the twin-screw extruder. In doing so, they have employed physical, chemical and mechanical ways to monitor the development of polymer blends and morphology development.

The influence of extrusion parameters on the morphology of non-reactive blends has been investigated by means of online light-scattering measurements. A light-scattering device was especially designed to be mounted on a twin-screw extruder at different locations along the barrel. The obtained light-scattering patterns were interpreted with respect to the variation of the processing parameters. Preliminary results show that there is little effect of the rotational speed, position along the screw, and feed throughput on the morphology, but a quite noticeable effect of the blend composition. These results were confirmed by SEM micrographs [49]. Out of more than 200 references over the past 20 years, we have selected the most relevant papers published over the period 2000–2009, which are included as References [50–79].

5.5
Future Development in Polymer Blends Compounding

5.5.1
Mass Customization

Creating compatibilized polymer blends allows polymer compounders to supply potential product fabricators with a very broad spectrum of required properties. Over the last 50 or so years, progress in successful blends formation has rested on experimental studies. This has been achieved, primarily, by the international

polymer resin manufacturing community, as well as academic researchers worldwide. Despite the technological and scientific progress we have discussed in preceding sections, there remains a large unfulfilled potential in polymer blends manufacturing, one which we call the potential of "mass customization" [80]. What is mass customization? It is a future technology through which it becomes technologically and commercially possible for individual processors to obtain the custom-made "designer" pellets that they need to use to fabricate specific products with specific properties (long and short term). But, then, what scientific, technological, and commercial advances have to be developed to achieve mass customization? First and foremost a scientific and computational breakthrough has to be attained: the development of a massive computational "knowledge base" for the prediction of resulting stable blend morphologies, given the relevant properties of the polymer components, the compatibilizer(s), or reactive compatibilizer(s), as well as processing variables and protocols, and finally screw element configurations and machine geometric variables. This sounds like a very difficult undertaking. Indeed it is, and, with the present available knowledge, not currently attainable. The reasons are: first, computational fluid dynamics (CFD) simulations for the melting and mixing of two or more polymers in the presence of compatibilizers has not even been tried yet. Thus, it is impossible to predict from first principles the development and final blend morphologies of blend systems. This is only achievable experimentally [81]. There are two reasons for this: first, the two-phase flow of two partially miscible, compatibilized polymers melts with evolving interfacial morphology cannot be handled computationally. At least, it has not been handled yet. The reason for this inability is the evolving and breaking interfacial surface morphology. Second, while melting in a TSE may be taking place in filled kneading element channels [82], mixing normally requires partially filled TSE element regions. This means that there exists a melt–air interface that is unknown. To carry out a CFD simulation even of this goal, a single polymer melt, the shape of this unknown surface has to be known or specified. Consequently, at best, if we specify the evolving interface shape, the simulation will be approximate, a simple guess. Incidentally, as mentioned above, if we want to simulate the two-phase flow of compatibilized melts then we have to, in filled channels, specify the melt-to-melt evolving interfacial morphology, to "mesh" the domain of each polymer phase. And this is impossible, because we would specify what we want to obtain computationally. Having mentioned these enormous difficulties, rapid advances in rheologically sound CFD [83–87] and the exponential growth of computing power bode well for achieving this goal. Second, heralded technological and developmental advances are being made in the area of instrumentation and control for process analysis [88]. This, of course, involves in-line, real time process probing and data analysis. As mentioned above, advances are being made in this area. With the maturing of the above two areas, we can envision the emergence of "scientific compounders," holders of banks of CFD programs that make up the knowledge base for predicting blends morphology and blend properties. These scientific compounders will then be able to provide customers with appropriate blends having specific product properties and blend morphologies. Hence the term "mass

customizations": Blends will be customized and compounded scientifically for the individual needs of the masses (i.e., each and everyone) of polymer products fabricators. This capability will revolutionize the "mind set" in the plastics industry. Large resin manufacturers and specialty additives producers will provide polymers of different grades and chemistry to the scientific compounders who will then be able to produce and give an unlimited choice of blends with specific properties, as needed by individual product fabricators. We hope to see more "designer" pellets like Hyperier products [2].

5.5.2 Single-, Twin-, or Multiple-Screw Extruders

The selection of single-screw or twin-screw technology will depend on the desired products and economics of manufacturing costs, which will be based on capital investment and maintenance and the product yield and capacity. The multi-screw extruder needs to be proven for large-scale production in terms of cost effectiveness, maintenance, and multifunctional equipment maintenance. Since most technologies are now at the mature stage, with more process control under high power computer systems, prolonging the life of equipment will be critical. In this respect, the material selection in terms of wear and corrosion will be an important factor for future development. Equipment manufacturers, aware of long-term sustainability, have devoted a lot of effort to the efficiency and reliability of compounding equipment and its operations.

References

1 Tadmor, Z. and Gogos, C.G. (2007) *Principles of Polymer Processing*, 2nd edn, John Wiley & Sons, Inc., Hoboken.

2 Kim, M.H. *et al.* (Nov. 2006) Nanocomposite blend composition having super barrier property, US Patent 7,138,452; Kim, M.H. *et al.* (May 2008) Nanocomposite composition having super barrier property and article using the same, US Patent 7,368,496.

3 Todd, D.B. (ed.) (1998) *Plastics Compounding – Equipment and Processing*, Hanser, Munich.

4 Kohlgruber, K. (ed.) (2008) *Co-Rotating Twin-Screw Extruders – Fundamentals, Technology, and Applications*, Hanser, Munich.

5 Zhu, L.(May 2004) 3-D numerical simulation of reactive extrusion and its application to polymerization of ε-caprolactone in co-rotating twin screw extruders. PhD dissertation, New Jersey Institute of Technology, Newark, NJ 07102.

6 Gogos, C.G., Tadmor, Z. and Kim, M.H. (1998) *Adv. Polym. Technol.*, **17** (4), 285.

7 Kim, M.-H. (1999) Melting phenomena and mechanism in polymer processing equipment. PhD dissertation, Stevens Institute of Technology, Castle Point on Hudson, Hoboken, NJ, 07030.

8 Coperion Werner & Pfleiderer (2009) ZSK twin screw extruder (and personal communication with Dr. Paul Andersen), CTO, Coperion Werner & Pfleiderer, Ramsey, NJ 2009. Brochure available at http://www.coperion.com/en/compounding-extrusion/machines-systems/zsk-series/ (accessed 21 February 2011).

9 Martin, C. (2009) Twin screw extrusion advances for compounding,

devolatilization, and direct extrusion. Presented at Plastics Extrusion Asia Conference, Bangkok, Thailand, March 17–18, 2009.
10 KraussMaffei Berstorff (2011) Extrusion technology, KraussMaffei Berstorff GmbH, An der Breiten Wiese 3–5, 30625 Hannover, Germany. Available at http://www.krauss-maffei.com/en/News/Downloads/Brochures/Brochures-Extrusion-Technology__1129/ (accessed 21 February 2011).
11 Oda, N., Yoshida, M., Mizuguchi, H., and Sumioda, K. (1996) US Patent 5,516,205, The Japan Steel Works; The Japan Steel Works (September 19, 2000) JSW Plastic Processing Technology News Letter, No. 0002ERRCRR; The Japan Steel Works (November 17, 2000) JSW Plastic Processing Technology News Letter, No. 0008ERRCRR.
12 Dow Chemical Patents: Herring, R., Kirk, R.O., Busby, F., and Jones, K.S. (2000) US Patent 6,022,133; Busby, F., Herring, R., Kirk, R.O., and Jones, K.S. (2000) US Patent 6,062,719; Herring, R., Kirk, R.O., Busby, F., and Jones, K.S. (1999) EP934151; Hyun Kun S [United States]; Kirk Richard O [United States]; Herring Ray A [United States]; Busby Forest [United States]http://www.europatentbox.com/patent/EP1032492A1/abstract/2226758.html (2000) EP1032492 (A1).
13 was prepared by A. Eker, M. Giammattia, P. Houpt (principal investigator), A. Kumar, O. Montero, M. Shah, N. Silvi, and T. Cribbs (GEIS) (2002) Intelligent Extruder for Polymer Compounding, Final Technical Report, Automation and Controls Laboratory, GE Global Research, Contract DE-FC02-99-CH10972 for US Department of Energy, Office of Industrial Technology 100. Available at http://www.bcsmain.com/mlists/files/metalcasting/documents/reports/intelligent_extruder.pdf (accessed 21 February 2011).
14 Spalding, M.A., Powers, J.R., Wagner, P.A., and Hyun, K.S. (2000) *SPE-ANTEC Tech. Papers*, **46**, 254.
15 Hyun, K.S., and Spalding, M.A. (1996) *Adv. Polym. Technol.*, **15**, 29.
16 Benkreira, H., Shales, R.W., and Edwards, M.F. (1992) *Int. Polym. Process.*, **7**, 126.
17 Maddock, B.H. (1959) *SPE J.*, **15**, 383.
18 Spalding, M.A., and Hyun, K.S. (2009) The plasticating system for injection molding machines, in *Injection Molding –Technology and Fundamentals* (eds M. Kamal, I. Isayev, and S.J. Liu), Hanser, Germany. 133–169
19 Chung, C.I. and Barr, R.A. (1983) US Patent 4,405,239.
20 Barr, R.A. (2003) US Patent 6,599,004.
21 Kruder, G.A. (1979) US Patent 4,173,417.
22 Frankland Jr., J.D. (1987) US Patent 4,639,143.
23 Womer, T.W. and Lepore, B.L. (2002) US Patent 6,488,399.
24 Myers, J.A. (1994) US Patent 5,432,125.
25 Maddock, B.H. (1967) *SPE J.*, **23**, 23.
26 Somers, S.A., Spalding, M.A., Dooley, J., and Hyun, K.S. (2002) *SPE-ANTEC Tech. Papers*, **48**, 307.
27 Plumley, T.A., Spalding, M.A., Dooley, J., and Hyun, K.S. (1994) *SPE-ANTEC Tech. Papers*, **40**, 332.
28 Hogan, T.A., Spalding, M.A., Kim, E.K., Barr, R.A., and Myers, J.A. (2003) *SPE-ANTEC Tech. Papers*, **49**, 92.
29 Womer, T.W., Buck, E.J., and HudakJr., B.J. (2004) US Patent 6672753.
30 Gruenschloss, E. (2002) *Int. Polym. Process.*, **17** (4), 291.
31 Gruenschloss, E. (2007) *SPE-ANTEC Tech, Papers*, **53**, 405.
32 Chung, C., Choi, M., Yoon, D., Gunning, L., and Gruenschloss, E. (2009) *SPE-ANTEC Tech. Papers*, **55**, 1192.
33 Gale, G.M. and Hindmarch, R.S. (1982) *Eur. Rubber J.*, **164**, 7/8, 29.
34 Wang, C. and Manus-Zloczower, I. (1994) *Polym. Eng. Sci.*, **34**, 1224.
35 Esseghir, M., Gogos, C.G., Yu, D.W., Todd, D.B., and David, B. (1998) *Adv. Polym. Technol.*, **17**, 1.
36 Ingen-Housz, A.J. and Norden, S.A. (1995) *Int. Polym. Process.*, **10**, 120.
37 Barr, R.A. (1999) US Patent 5,988,866.
38 Myers, J.A., Barr, R.A., Spalding, M.A., and Hughes, K.R. (1999) *SPE-ANTEC Tech. Papers*, **45**, 157.
39 McCullough, T.W. and Hilton, B.T. (1993) *SPE-ANTEC Tech. Papers*, **39**, 3372.

40 Busby, F., McCullough, T., Hughes, K.R., and Kirk, R.O. (1996) *SPE ANTEC Tech. Papers*, **42**, 3571.

41 Busby, F., McCullough, T., Hughes, K.R., and Kirk, R.O. (1997) *SPE ANTEC Tech. Papers*, **43**, 3683.

42 Gogos, C.G., Esseghir, M., Yu, D.W., Todd, D.B. and Curry, J. (1994) *SPE ANTEC Tech. Papers*, **40**, 270.

43 Lee, S.C., Ryu, S.H., and Kim, H. (1998) *Korean J. Rheol.*, **10** (3), 152.

44 Esseghir, M, Yu, D.W., and Gogos, C.G. (1997) *SPE-ANTEC Tech. Papers*, **43**, 452.

45 Qian, B. and Gogos, C.G. (2000) *Adv. Polym. Technol.*, **19** (4), 287.

46 Cogos, C.G. and Qian, B. (2002) *Adv. Polym. Technol.*, **21** (4), 287.

47 Qian, B., Todd, D.B., and Gogos, C.G. (2003) *Adv. Polym. Technol.*, **22** (2), 85.

48 Golovoy, A., Cheung, M.F., and Van Oene, H. (1987) *Polym. Eng. Sci.*, **27** (21), 1642.

49 Serra, S.C., Schlatter, G., Bouquey, M., Muller, R., and Terrisse, J. (2002) *Can. J. Chem. Eng.*, **80** (6), 1036.

50 Wang, W., Manas-Zloczower, I., and Kaufman, M. (2003) *AIChE J.*, **49** (7), 1637.

51 Mighri, F. and Huneault, M.A. (2002) *Can. J. Chem. Eng.*, **80** (6), 1028.

52 Covas, J.A., Carneiro, O.S., Maia, J.O., Filipe, S.A., and Machado, A.V. (2002) *Can. J. Chem. Eng.*, **80** (6), 1065.

53 Chowdhury, R., Banerji, M.S., and Shivakumar, K. (2002) *J. App. Polym. Sci.*, **83** (10), 2148.

54 Tasdemr, M. and Yildirim, H. (2002) *J. Appl. Polym. Sci.*, **83** (14), 2967.

55 Lin, X.D. and Cheung, W.L. (2003) *J. Appl. Polym. Sci.*, **88** (14), 3100.

56 Kim, J.K., Lee, S.H., and Hwang, S.H. (2002) *J. Appl. Polym. Sci.*, **85** (11), 2276.

57 Araújo, J.R., Vallim, M.R., Spinacé, M.A., De, S., and Paoli, M.A. (2002) *J. Appl. Polym. Sci.*, **86** (6), 1473.

58 Nam, J.D., Kim, J., Lee, S., Lee, Y., and Park, C. (2003) *J. Appl. Polym. Sci.*, **87** (4), 861.

59 Lin, X.D. and Cheung, W.L. (2009) *J. Appl. Polym. Sci.*, **89** (7), 1743.

60 Liu, G., Chen, Y., and Huilin, L. (2004) *J. Appl. Polym. Sci.*, **94** (3), 977.

61 Yquel, V., Machado, A.V., Covas, J.A., and Flat, J.J. (2008) *J. Appl. Polym. Sci.*, **114** (3), 1768.

62 Pinheiro, L.A., Bitencourt, C.S., Pessan, L.A., and Canevarolo, S.V. (2006) *Macromol. Symp.*, **245–246** (1), 347.

63 Machado, A.V., Yquel, V., Covas, J.A., Flat, J.J., Ghamri, N., and Wollny, A. (2006) *Macromol. Symp.*, **239** (1), 86.

64 Mélo, T.J.A. and Canevarolo, S.V. (2005) *Polym. Eng. Sci.*, **45** (1), 11.

65 Treece, M.A., Zhang, W., Moffitt, R.D., and Oberhauser, J.P. (2007) *Polym. Eng. Sci.*, **47** (6), 898.

66 Yin, B., Zhao, Y., Yu, R.Z., An, H.N., and Yang, M.B. (2007) *Polym. Eng. Sci.*, **47** (1), 14.

67 Potente, H., Bastian, M., Bergemann, K., Senge, M., Scheel, G., and Winkelmann, T. (2007) *Polym. Eng. Sci.*, **47** (2), 222.

68 Pinheiro, L.A., Hu, G.H., Pessan, L.A., and Canevarolo, S.V. (2008) *Polym. Eng. Sci.*, **48** (4), 806.

69 Shon, K., Bumm, S.H., and White, J.L. (2008) *Polym. Eng. Sci.*, **48** (4), 756.

70 Shin, B.Y., Narayan, R., Lee, S.I., and Lee, T.J. (2008) *Polym. Eng. Sci.*, **48** (11), 2126.

71 Pötschke, P. and Paul, D.R. (2003) *Macromol. Symp.*, **198** (1), 69.

72 Haba, Y., Balazs, Y.L., Carmiel, O., Katz, I., Narkis, M., Shanshan, A.S., and Ye, D.L. (2008) *Polym. Adv. Technol.*, **19** (8), 1069.

73 Yue, Q., Ren, J., Pan, B., Wang, H., Jian, L., Zhang, J., and Yang, S. (2006) *Polym. Comp.*, **27** (6), 608.

74 Wang, H., Zeng, Z., Elkovitch, M., Lee, L.J., and Koelling, K.W. (2001) *Polym. Eng. Sci.*, **41** (11), 2036.

75 Ratnagiri, R., Scott, C.E., and Shih, C.K. (2001) *Polym. Eng. Sci.*, **41** (6), 1019.

76 Pesneau, I., Kadi, A.A., Bousmina, M., Cassagnau, P., and Michel, A. (2002) *Polym. Eng. Sci.*, **42** (10), 1990.

77 Sun, Z., Jen, C.-K., Shih, C.-K., and Denelsbeck, D.A. (2003) *Polym. Eng. Sci*, **43** (1), 102.

78 Tchomakov, K.P., Favis, B.D., Huneault, M.A., Champagne, M.F., and Tofan, F. (2004) *Polym. Eng. Sci.*, **44** (4), 749.

79 Gemeinhardt, G.C., Moore, A.A., and Moore, R.B. (2004) *Polym. Eng. Sci.*, **44** (9), 1721.

80 Gogos, C.G., Todd, D.B., and Qian, B., Personal communication (2002) *SPE ANTEC Tech., Papers*, **42** (8).

81 Qian, B., Todd, D.B., and Gogos, C.G. (2003) *Adv. Polym. Technol.*, **22** (2), 85.
82 Tadmor, Z. and Gogos, C.G. (2007) *Principles of Polymer Processing,* 2nd edn, ch. 11, John Wiley & Sons, Inc., Hoboken.
83 Todd, D.B. (1993) *Int. Polym. Proc.*, **8**, 113.
84 Bravo, B.L., Hrymak, A.N., and Wright, J.D. (2000) *Polym. Eng. Sci.*, **40**, 525.
85 Jaffer, S.A., Bravo, B.L., Wood, P.E., Hrymak, A.N., and Wright, J.D. (2000) *Polym. Eng. Sci.*, **40**, 892.
86 Funatsu, K., Kihara, S.I., Miyazaki, M., Kaisuki, S., and Kajiwara, T. (2002) *Polym. Eng. Sci.*, **42**, 707.
87 Gotsis, A.D., Ji, Z., and Kalyon, D.M. (1990) *SPE ANTEC Tech., Papers,* **36**, 139.
88 Wang, Y., White, J.L., and Szydlowski, W. (1989) *Int. Polym. Process.*, **4**, 262.
89 Wetzel, M.D., Shih, C.K., Denelsbek, D.A., and Latimer, S.L. (2005) *SPE ANTEC Tech., Papers,* **51**, 354.

Further Reading

Chung, C.I. (2000) *Extrusion of Polymers: Theory and Practice,* Hanser, Munich.
Tadmor, Z. and Klein, I. (1970) *Engineering Principles of Plasticating Extrusion,* Van Nostrand Reinhold Co., New York.
Vlachopoulos, J. and Wagner, J.R.(technical eds) (2001) *The SPE Guide on Extrusion Technology and Troubleshooting,* SPE Division Series, Society of Plastics Engineers, Brookfield, CT.
White, J.L. and Potente, H. (vol. eds) (2003) *Screw Extrusion,* PPP Series (series ed. K.S. Hyun), Hanser, Munich.

6
Manufacturing of Polymer Blends Using Polymeric and Low Molecular Weight Reactive Compatibilizers

Eung Kyu Kim and James L. White

6.1
Introduction

During the past 50 years there has been a great increase in the development and production of blends of different polymers because many of them have performed well in new applications. The application areas of the various polymeric material blends systems are limitless and blending of the polymers has also been recognized as a faster and less expensive method of developing a new material than synthesizing a new polymer with a new chemical structure.

Reactive blending has been a very attractive blending compatibilization strategy for immiscible polymer blend systems with a wisely selected chemistry since the 1970s. The properties and performance of polymer blends depend on the blend morphology. The morphology of a polymer blend is mainly determined by (i) polymer components, (ii) interfacial reaction, and (iii) mixing process. For a commercial polymer blend manufacturing process, possible maximum production rate, and process controls to minimize energy consumption during a manufacturing process are also required for lowering product cost (Figure 6.1). The major equipment for manufacturing various kinds of polymer blends is a screw extruder. Understanding of a screw extrusion process design and operation is critical. An intermeshing co-rotating twin-screw extruder is the major continuous processing machine among various screw extruders and is the main subject of discussion in this chapter.

Section 6.2 briefly describes reactive blending and compatibilization. We then discuss the mixing and morphology development during polymer melt blending process in Section 6.3. In Sections 6.4 and 6.5 we turn to intermeshing co-rotating twin-screw extrusion technology, including the modeling of a modular intermeshing co-rotating twin-screw extrusion process, and extrusion process design for reactive polymer blending.

Encyclopedia of Polymer Blends: Volume 2: Processing, First Edition. Edited by Avraam I. Isayev.
© 2011 Wiley-VCH Verlag GmbH & Co. KGaA. Published 2011 by Wiley-VCH Verlag GmbH & Co. KGaA.

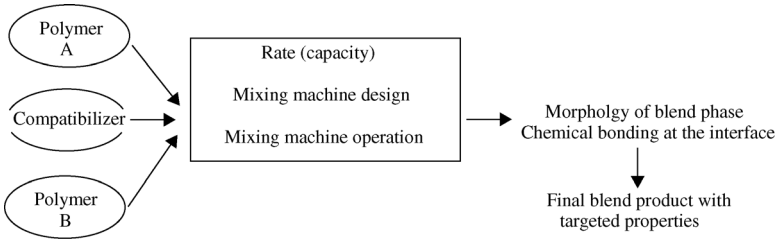

Figure 6.1 Schematic of a reactive polymer blending process.

6.2 Reactive Blending and Compatibilization

The practice of blending polymers is as old as the polymer industry itself, with early examples involving natural rubber. Over the last 50 years two additional directions have evolved in the polymer industry. First is the development of significant new polymerization processes to manufacture both homopolymers and copolymers based on the monomers used much earlier. Meanwhile, during approximately the same period, a separate development has flourished, namely, polymer blending. While most monomers cannot be easily copolymerized to achieve target properties that are required for a specific application of interest, it was gradually recognized that their polymers could be melt blended economically to produce a range of new materials, using the diverse and improving processing technologies [1–4].

Most polymers are immiscible with each other. When two or more immiscible polymers are melt blended the components of the blend form different phases, which are separated from each other in the final product due to the high surface tension between the immiscible polymer components in the interfacial region. The overall performance of immiscible blends depends on the properties of the individual components, but also depends significantly on the morphology of the blends and the interfacial properties between the blend phases. Compatibilization is a process or technique that allows control of both the morphology and interfaces of phase separated blends [2, 5–10]. The compatibilization of an immiscible polymer blend relies on a reduction of interfacial tension. Normally, a blend that has been compatibilized can still be phase separated, but with a finer, stabilized dispersion of minor phase in the matrix. Improvements in the properties of compatibilized blends such as physical, mechanical, or other properties are often observed due to a better adhesion between different phases. Cleverly designed diblock and triblock copolymers, which had no chemical functionality, were developed that aided in improving the performance of blends [11–17]. However, a complexity of their design and difficulty of use led to innovations starting in the 1970s that use selective chemistry to enhance performance by controlling and stabilizing preferred morphologies and influencing interfacial adhesion. Some of the first applications and developments related to polyamide blends, but now reactive blending and compatibilization extends to essentially all polymeric material classes. The basic principles

are the same for non-reactive compatibilization and reactive compatibilization, while chemical reactions are involved in reactive blending process. This makes reactive compatibilization very attractive and cost-effective because it offers the possibility of generating compatibilizers during melt blending directly at the interfaces between the base polymer components. Since the copolymer is formed directly at the interfaces, there is no problem getting it to the interfaces where it is most needed. Thus, reactive compatibilization is also known as *in situ* compatibilization or reactive blending [4].

There are mainly two *in situ* compatibilization methods of immiscible polymer blends. First is the compatibilization of polymer blends through copolymer formation by addition of low molecular weight reactive compounds such as bis(2-oxazolines), various organic peroxide and coagent systems, and others. The second is the compatibilization of polymer blends through copolymer formation by addition of functional polymers as a compatibilizer such as maleic anhydride grafted polymer. Graft or block copolymers acting as compatibilizers for polymer blends can be formed *in situ* through covalent or ionic bonding during the melt blending of suitable functionalized polymers. In this kind of reactive compatibilization, generally, one phase contains reactive groups inherent in the polymer, while the other has no inherent functionality. Reactive groups can be incorporated into the second phase by adding to it a functionalized polymer that is miscible. In some cases, both phases may have to be functionalized. The *in situ* formed copolymer compatibilizer is located preferentially at the interface where they it most needed, reducing the size of the dispersed phase.

Reactive polymers undergo various chemical reactions during melt blending, including (i) addition and substitution reactions such as amidation, imidation, esterification, concerted addition, and so on; (ii) interchange reactions such as transesterification, ester interchange, amide interchange, amide–ester exchange, aminolysis, and acidolysis, and so on; (iii) ring opening reactions involving heterocyclic groups; (iv) ionic bonding involving pyridine, tertiary amine, acids, ionomers; and (v) others.

Applications of these reactive polymers to the compatibilization of various polymer blends are made to improve the impact strength, tensile strength, permeability, heat resistance, crystallization, morphology, and other properties of polymers and recycled plastics.

Excellent reviews for reactive blending and reactive compatibilization have been given by Baker *et al.* [4].

6.3
Mixing Mechanism and Morphology Development

The properties and performances of polymer blends depend on the blend morphology. The morphology development of a polymer blend is closely related to mixing provided by processing equipment. Mixing is a process that enhances composition uniformity. Mixing can mainly be classified into two different mixing mechanisms. The achievement of compositional homogeneity in a mixing process is said to occur through distributive mixing. The second concern is to produce as fine a dispersion of

the ingredients as possible. The reduction in disperse phase size during the mixing is described as dispersive mixing.

In describing the mixing process we need to specify first whether the materials being mixed are of the same phase such as all solids or all liquids (e.g., molten thermoplastics) or whether they are combinations of particulates, that is, solids and liquids. Among the various mixing operations, those involving polymeric liquids and solid-polymer–liquid systems are perhaps most important in polymer processing. Further, we need to distinguish whether the substances being mixed are fully miscible, partially miscible, or totally immiscible. In most cases we are concerned with systems that can be considered totally immiscible. We will first discuss the mixing mechanism, both distributive and the dispersive mixing, and then morphology development of a liquid–liquid system (e.g., melt blending), which is closely related to mixing mechanism, including material properties such as interfacial tension and viscosity ratio.

6.3.1 Distributive Mixing

The pioneering thoughtful investigation of mixing in polymer blend systems was described in a 1951 article by R.S. Spencer and R.M. Wiley [18] of the Dow Chemical Company. They hypothesized that distributive mixing could be represented by the generation of interfacial area during flow. This is equivalent to the study of mixing of very viscous immiscible liquids without interfacial tension and no difference in viscosity. To represent mixing in this simple situation, Spencer and Wiley [18] developed, in 1950, a global kinematics. Spencer and Wiley [18] limited themselves to shear flow, but subsequently Mohr [19, 20] and Erwin [21–24] extended this to elongational flows [21, 22] as well as to interrupted shear flows [23, 24]. This allowed improved understanding of mixing effects in various geometries. Subsequently, Ottino and his coworkers [25–27] developed a broader formalism of interfacial area generated in flow.

Deformation and flow can be represented in terms of second-order quantities such as deformation and rate of deformation tensor [28]. These may be defined in terms of the variation of length of a differential line element $\mathbf{dx}$ of the material as it is transformed by deformation and displacement into $\mathbf{dX}$. We may express this deformation and its rate of change through:

$$(ds)^2 = \boldsymbol{C} \cdot \mathbf{dX} \cdot \mathbf{dx} \tag{6.1}$$

$$\frac{\mathrm{d}}{\mathrm{d}t}(ds)^2 = 2\mathbf{d} \cdot \mathbf{dx} \cdot \mathbf{dx} \tag{6.2}$$

The quantities $\boldsymbol{C}$ and $\mathbf{d}$ are the second-order tensors that are an array of nine $C_{ij}(i,j = 1,2,3)$ and d_{ij} terms; $\boldsymbol{C}$ is known as the Green deformation tensor and $\mathbf{d}$ is the rate of deformation tensor. It is always possible to find a "principal axis" coordinate system where $\boldsymbol{C}$ and $\mathbf{d}$ have "diagonal" forms, that is, where C_{ij} and d_{ij} are zero when i is not equal to j. In this principal axis coordinate system, all deformations are representable as multi-axial elongational and may be expressed through extension ratios λ_{I}, λ_{II}, and λ_{III} corresponding to these principal axes.

Consider an element of area oriented relative to a 1, 2, 3 axes that may be considered laboratory axes. The element of area is subject to elongation ratios λ_I, λ_{II}, and λ_{III}. Normal to the surfaces make angles $\alpha_1, \alpha_2, \alpha_3$ with respect to these axes. This relative increase of area A/A_0 is, after Mohr [19] and Erwin [21]:

$$\frac{A}{A_0} = \left[\frac{\cos^2\alpha_1}{\lambda_1^2} + \frac{\cos^2\alpha_2}{\lambda_2^2} + \frac{\cos^2\alpha_3}{\lambda_3^2}\right]^{1/2} \tag{6.3}$$

and by the Pythagorean theorem:

$$\cos^2\alpha_1 + \cos^2\alpha_2 + \cos^2\alpha_3 = 1 \tag{6.4}$$

Equation (6.4) may be substituted to eliminate one of the angles. Thus:

$$\frac{A}{A_0} = \left[\frac{1}{\lambda_3^2} + \left(\frac{1}{\lambda_1^2} - \frac{1}{\lambda_3^2}\right)\cos^2\alpha_1 + \left(\frac{1}{\lambda_2^2} - \frac{1}{\lambda_3^2}\right)\cos^2\alpha_2\right]^{\frac{1}{2}} \tag{6.5}$$

Usually, only incompressible deformations need be considered so that:

$$\lambda_1\lambda_2\lambda_3 = 1 \tag{6.6}$$

Thus, λ_3 might also be eliminated to give:

$$\frac{A}{A_0} = \left[\lambda_1^2\lambda_2^2 + \left(\frac{1}{\lambda_1^2} - \lambda_1^2\lambda_2^2\right)\cos^2\alpha_1 + \left(\frac{1}{\lambda_2^2} - \lambda_1^2\lambda_2^2\right)\cos^2\alpha_2\right]^{\frac{1}{2}} \tag{6.7}$$

For uniaxial deformation where:

$$\lambda_2 = \lambda_3 = \frac{1}{\sqrt{\lambda_1}} \tag{6.8}$$

Equations (6.5) and (6.7) become:

$$\frac{A}{A_0} = \left[\lambda_1 + \left(\frac{1}{\lambda_1^2} - \lambda_1\right)\cos^2\alpha_1\right]^{\frac{1}{2}} \tag{6.9}$$

If the interface is aligned with the maximum principal extension ratio, $\cos\alpha_1 = 0$:

$$\frac{A}{A_0} = \lambda_1^{\frac{1}{2}} \tag{6.10}$$

For a constant uniaxial elongation rate flow with $\cos\alpha_1 = 0$; we have for the rate of deformation tensor $\mathbf{d}$ of Eq. (6.2):

$$\mathbf{d} = \begin{vmatrix} E & 0 & 0 \\ 0 & -\frac{E}{2} & 0 \\ 0 & 0 & -\frac{E}{2} \end{vmatrix} = \frac{1}{\lambda_1}\begin{vmatrix} \frac{d\lambda_1}{dt} & 0 & 0 \\ 0 & -\frac{1}{2}\frac{d\lambda_1}{dt} & 0 \\ 0 & 0 & -\frac{1}{2}\frac{d\lambda_1}{dt} \end{vmatrix} \tag{6.11}$$

where

$$\frac{1}{\lambda_1}\frac{d\lambda_1}{dt} = E \tag{6.12}$$

Thus:

$$\lambda_1 = \lambda_1(0)e^{Et} \tag{6.13}$$

and:

$$A = A_0 e^{Et/2} \tag{6.14}$$

That is, the interfacial area increases exponentially with time. This is attributed to Erwin [22]. Equation (6.14) forms the basis of the view that uniaxial elongational flow is important to achieve good mixing.

For a simple shear flow, the principal extension ratios λ_I, λ_{II}, and λ_{III} may be shown to be [28]:

$$\lambda_I = \left[1 + \frac{s^2}{2} + \frac{s}{2}\left(4 + s^2\right)^{\frac{1}{2}}\right]^{\frac{1}{2}} \tag{6.15a}$$

$$\lambda_{II} = \left[1 + \frac{s^2}{2} - \frac{s}{2}\left(4 + s^2\right)^{\frac{1}{2}}\right]^{\frac{1}{2}} \tag{6.15b}$$

$$\lambda_{III} = 1 \tag{6.15c}$$

This leads, as noted by Erwin [22], to an increase of area A/A_0 of:

$$\frac{A}{A_0} = \left\{1 + \left[\frac{s^2}{2} - \frac{s}{2}\left(4 + s^2\right)^{1/2}\right]\cos^2\alpha_1 + \left[\frac{s^2}{2} + \frac{s}{2}\left(4 + s^2\right)^{\frac{1}{2}}\right]\cos^2\alpha_2\right\}^{\frac{1}{2}} \tag{6.16}$$

For a very large value of shear, s:

$$\frac{A}{A_0} = s\cos\alpha_2 \tag{6.17}$$

The deformation rate tensor has the form:

$$\mathbf{d} = \tfrac{1}{2}\begin{vmatrix} 0 & \dot{\gamma} & 0 \\ \dot{\gamma} & 0 & 0 \\ 0 & 0 & 0 \end{vmatrix} = \tfrac{1}{2}\begin{vmatrix} 0 & \dfrac{ds}{dt} & 0 \\ \dfrac{ds}{dt} & 0 & 0 \\ 0 & 0 & 0 \end{vmatrix} \tag{6.18}$$

If the shear rate $\dot{\gamma}$ is constant:

$$\frac{A}{A_0} = \dot{\gamma}t\cos\alpha_2 \tag{6.19}$$

That is, the interfacial area increases linearly with time. If we consider instead a number of elements that are initially randomly oriented, we obtain:

$$\frac{A}{A_0} = \frac{1}{2}s = \frac{1}{2}\dot{\gamma}t \tag{6.20}$$

Mohr *et al.* [20] have introduced the concept of a striation thickness (r) for shear flows, which was based on Spencer and Wiley's work [18]. The value of r is calculated by using the following equation when the melt viscosity difference between two components exists in the shear flow field:

$$r = \left(\frac{l_d}{\dot{\gamma}t_R\phi_d}\right)\left(\frac{\eta_d}{\eta_m}\right) = \left(\frac{l_d}{\gamma\phi_d}\right)\left(\frac{\eta_d}{\eta_m}\right) \tag{6.21}$$

A smaller r results in better distributive mixing in the laminar flow field. The shear rate and residence time in shear flow between parallel plates where one plate is moving can be written as:

$$\dot{\gamma} = \frac{\pi DN}{H} \tag{6.22}$$

$$t_R = \frac{V_f}{\hat{Q}} \tag{6.23}$$

where

l_d is the length of a cube of a lower concentration component,
ϕ_d is the volume fraction of a dispersed component,
η_m is the melt shear viscosity of a matrix component,
η_d is the melt shear viscosity of a dispersed component,
$\dot{\gamma}$ is the shear rate,
t_R is the residence time,
γ is the shear strain,
D is the diameter,
N is the screw rotational speed,
H is the screw channel depth,
V_f is the free volume in the screw channel,
$\hat{Q}$ is the volumetric flow rate.

From Eqs. (6.20) through (6.23) we can easily recognize that a larger shear strain γ contributes to better mixing. To improve distributive mixing, we generally design for higher shear rate, which means higher screw speed and/or shallower channel depth. As the diameter of a screw extruder increases, viscous dissipation heating increases and heat transfer decreases. Typically, the production-scale extruder operates at a slower screw speed and the mixing capability becomes poorer. The throughput also affects mixing significantly, Eq. (6.23). The distributive mixing is further enhanced by forcing the laminar flow field through reorientations.

6.3.2 Dispersive Mixing

In the case of dispersive mixing, larger shear stresses and extensional forces in a flow field should be imposed if the break-up of agglomerates and droplets of each polymeric component are required [29–35]. Dispersive mixing during a blending process has a close relationship with morphology development of polymer blends. There are many similarities in morphology development of reactive and non-reactive blends. Much of our knowledge concerning reactive blending has been obtained through comparison with or extension from knowledge of non-reactive blending. We first discuss two main material properties, interfacial tension between the matrix polymer and dispersed polymer and viscosity ratio, which affect significantly the morphology development of the polymer blends.

6.3.2.1 Interfacial Tension

The concept of a tension over the surface of liquids, that is, the surface tension, has a long history. The characteristics of surface tension were carefully discussed by the English scientist Thomas Young [36] 200 years ago. J.W. Strutt (Lord Rayleigh) [37] in the latter part of the 1800s showed the role of the surface tension in breaking liquid filaments into droplets. In 1878, J.C. Maxwell [38] wrote an extensive review on surface tension.

The interfacial tension (κ) between liquids was also considered in the nineteenth century. Young was concerned with the interfacial tension between liquids, but the first extensive investigations were by G. Quincke [39]. Maxwell [38] also discussed the interfacial tension. During the 1930s, G.I. Taylor [40, 41] studied the flow of liquid emulsions and the breakup of droplets during flow. S. Tomotika [42] generalized Strutt's (Lord Rayleigh's) theory to the breakup of liquid filaments immersed in a second liquid by the interfacial tension. An article published in 1938 by Andreas *et al.* [43] presented a detailed method of interfacial tension measurement using a pendant drop technique.

The magnitude of the interfacial tension between two liquids would seem to measure their level of incompatibility with each other. When the interfacial tension between two liquids is zero, they dissolve in each other. As the interfacial tension increases, the two liquids are increasingly incompatible and immiscible with each other, in a thermodynamic sense.

The first measurements of the interfacial tension for polymer melts were made in the 1960s [44]. By the end of the decade, notably through the efforts of S. Wu [45–47] of DuPont and R.J. Roe [48] of Bell Laboratories, measurement techniques, notably the pendant drop technique of Andreas *et al.* [43], became well established. Although efforts continued into the early 1970s [49–51], the area did not develop significantly further, in some part apparently because polymer blend science had not developed sufficiently. Certain results were well established at this time, however. The interfacial tension between two homopolymer melts was found to be largely determined by the differences in polarity of the structural units. The interfacial tensions were largely insensitive to molecular weight and to temperature. There are small negative

Table 6.1 Methods of measurement of interfacial tension with polymer melts [62].

Technique	Investigators
Pendant drop	Andreas *et al.* [43], Chappelear [44], Wu [45,46,51], Roe [48], Anastasiadis *et al.* [53], Escudie *et al.* [54], Chen and White [60], Yoon and White [61]
Thread breakup	Chappelear [44], Elmendorp [52], Elemans *et al.* [57], Yoon and White [61]
Rotating drop	Patterson *et al.* [49], Wu [51]
Shape evolution of fibers (imbedded fiber retraction)	Carriere *et al.* [55], Carriere and Cohen [58], Sammler *et al.* [59]

temperature coefficients. Interest in the interfacial tension has revived since the mid-1980s [52–61]. This is in part associated with growing interest in understanding phase morphology during polymer melt blending.

A wide range of experimental techniques has been proposed through the years to measure the interfacial tension. Most popular has been the pendent drop technique but there has been increasing interest in techniques based upon breaking molten polymer threads. Methods of measurement of interfacial tension are summarized in Table 6.1 and values of the interfacial tension for different polymer-melt pairs are summarized in Table 6.2. The larger the polarity difference is, the larger the interfacial tension. Thus the greatest interfacial tension in Table 6.2 is for polyethylene and polyamide 6.

It was found in the earlier years of the present century that low molecular weight compounds such as organic acids, esters, and soaps collected at the interface between

Table 6.2 Values of interfacial tension between polymer-melt pairs.

Polymer-melt pair	Melt temperature (°C)	Interfacial tension (dyne cm^{-1})	Reference
Polyethylene–polypropylene	—	1.2	[52]
Polyethylene–polystyrene	180	4.1	[45]
Polyethylene–polystyrene	290	4.0–5.0	[61]
Polyethylene–polystyrene	—	4.9	[52]
Polyethylene–polysulfone	290	6.5–7.0	[61]
Polyethylene–poly(phenylene sulfide)	290	7.2–7.9	[61]
Polyethylene–poly(methyl methacrylate)	180	9.0	[45]
Polyethylene–poly(ethylene terephthalate)	290	9.2–9.4	[61]
Polyethylene–polycarbonate	290	12.5–13.0	[56]
Polyethylene–polyamide-6	290	12.8–13.2	[45]
Polyethylene–polyamide	—	10.6	[52]
Polypropylene–polystyrene	220	5.8	[54]
	250	3.7	[54]
Polystyrene–poly(methyl methacrylate)	180	1.2	[45]

water and organic liquids. These compounds, which have hydrophilic and lyophilic sections, were determined to have lowered interfacial tensions [63–65]. It has been found in recent years that block and graft copolymers collect at the interfaces in immiscible polymer blends, reducing the interfacial tension between polymer phases. This was first clearly shown for two bulk polymer systems by Patterson *et al.* [49] of DuPont in 1971. In our laboratories, we found that introducing a styrene hydrogenated butadiene (ethylene butane) triblock copolymer into a polyethylene/polystyrene blend reduced the interfacial tension from about 5.0 to 1.1 dyne cm^{-1} [60]. Other examples are cited in the same article [60].

6.3.2.2 **Shear Viscosity of Polymer Blends**

The shear viscosity in polymer melts and solutions has been investigated for more than a half century. The blending process of polymers is generally performed in the molten state, particularly in shear flow. It is thus necessary to understand the flow (or better rheological) characteristics of polymer melts [66–70]. In both reactive and non-reactive blends, the shear viscosity of each polymer, and thus viscosity ratio, and bulk viscosity of polymer blend system needs to be understood.

The effects of shear viscosity of individual polymers in a blend system and viscosity ratio of the blend on the morphology development of the polymer blend will be discussed next (Section 6.3.3).

To understand and model the flow during the blending process, the bulk shear viscosity of a polymer blend must be understood. The rheology of multiphase systems has been investigated by many researchers [2, 71–73]. Figure 6.2 shows the schematics of both solid particle-filled liquid (curve a) and polymer blends

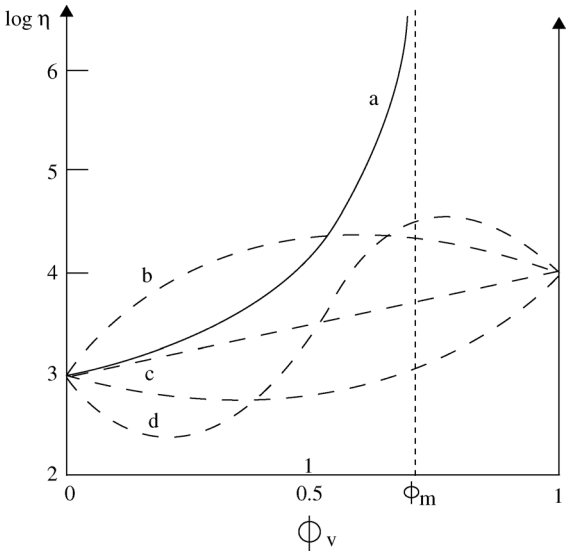

Figure 6.2 Concentration dependence of shear viscosity for (a) a solid particle-filled liquid and (b)–(d) polymer blends.

(curves b–d). At constant stress, the viscosity of a particulate-filled melt versus concentration (curve a in Figure 6.2) shows a monotonic increase with an asymptote at $\phi_v = \phi_m$. In contrast, this dependence for blends may show either a positive (over 60% of blends) or negative (about 30%) deviation from the log additive rule (curves b and c in Figure 6.2). For about 10% of the blends the η versus ϕ_v dependence passes through a local minimum and maximum (curve d in Figure 6.2). Blends with concentrations corresponding to these extrema are of special interest because they are easier to process and may show more interesting properties.

The bulk shear viscosity of the polymer blend at a given composition must be measured to understand the non-isothermal, non-Newtonian flow behavior of a polymer melt to control mixing and reaction at the interface during a melt blending process to manufacture polymer blends with desired properties.

6.3.3
Morphology Development

Morphology development is the path of morphological change that the material undergoes during its transformation from large into small domain size. An optimized commercial operation will achieve this transformation efficiently with a minimal amount of energy input and concomitant polymer degradation; it will achieve it reliably and robustly with minimum sensitivity to process or material variations; it will consistently produce a stable target morphology, which provides for the desired material properties and performance. An interfacial chemical reaction or an addition of the third component, that is, compatibilizer, greatly aids the realization of these goals. In reactive blending, morphology development and generation of interfacial area between the reactive polymers is critical for obtaining a sufficient extent of reaction. Mixing by diffusion is extremely slow in high molecular weight polymer systems and is not nearly fast enough for commercial blending operations. The reaction chemistries themselves are typically very fast and irreversible. Thus, the overall reaction kinetics are controlled primarily by the kinetics of interfacial area generation.

6.3.3.1 Initial Breakup of Polymer Melt Phases

Most researchers on blending of polymers have emphasized the later stages of the blending process and not the early stages, which usually follow the melting of both phases, when the major relative reductions of phase dimensions occur (see, for example, Lim and White [74]). The progress of phase morphology development clearly depends on the material volume ratio, interfacial tension, and viscosity ratio as well as the nature of the flow during processing. The maximum shear stress, accompanied with frictional and extensional forces, in a reactive blending process is usually generated at the melting zone of a screw extruder. In this melting region, each component is ground and dispersed as a result of undergoing strong dispersive mixing effects. Under dissipative melting each polymeric component changes into very small particles as droplets within a very short time, typically 0.1–10 s.

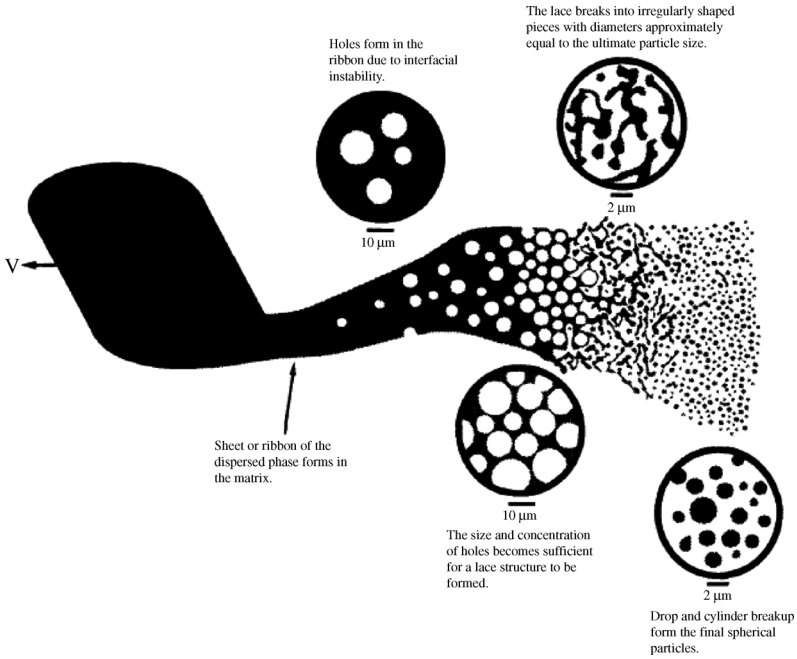

Figure 6.3 Morphology development model proposed by Scott and Macosko [75].

The first article that treats the initial stages of phase morphology evolution during blending of polymers was published by Scott and Macosko [75] in 1991. They report on the evolution of the morphology of a blend of polystyrene and an amorphous polyamide in a Haake Rheomix 600 laboratory mixer over short times. This morphology first develops in the form of a dispersed phase of sheets and ribbon. These dispersed structures are produced from the melting of the pellets as they are worked against the chamber wall by the rotation of the internal mixer rotor. The dispersed sheets develop holes with continued mixing, with the sheets evolving into a lace structure. Subsequently, the lace breaks up into ligaments that then break up into small spheres. Figure 6.3 shows a generalized structure development model for an immiscible polymer alloy [75]. The domain size of about 10 μm level is quickly attained from polymer pellets of 2–5 mm only at the final stage of melting.

In studies published the following year, Sundararaj *et al.* [76] followed the early stages of morphology development in a polyethylene/polystyrene blend in a modular co-rotating twin-screw extruder. Again the formation of sheets of the dispersed phase was first observed, followed by the formation of holes in the sheets and the breakup of the sheets into ligaments. The ligaments then break up into small particles. Lindt and Ghosh [77] have reported the evolution of phase morphology of polystyrene with poly (ethylene-*co*-vinyl acetate) and a poly(butadiene-*co*-styrene) star block copolymer in a single-screw extruder. They also observed an evolution to ligaments to small particles in their investigations.

6.3.3.2 **Breakup of Liquid Filaments in a Liquid Matrix**

In 1935–36, S. Tomotika [42, 78] published such an analysis based on liquid filament of viscosity η' immersed in a second liquid of viscosity η. He showed that viscous threads are unstable to disturbances with wavelengths greater than the circumference of the filament and form droplets of definite size. The instability is associated with the interfacial tension (Section 6.3.2.1) and viscosity differences between the two phases. The wavelength of the maximum growth rate and the rate of growth of the disturbance both depend upon the viscosity ratio as well as the interfacial tension as shown in Figure 6.4. Generally, low-viscosity liquid filaments in very highly viscous matrices are very unstable. In contrast, highly viscous filaments surrounded by low-viscosity matrices have very low disturbance growth rates. Obviously, as the viscosity ratio η'/η becomes very large, Tomotika's analysis goes asymptotically to the theory of Rayleigh's 1892 article [79]. The critical wavelength (λ) of a disturbance that determines the drop size becomes very large when either the viscosity of the matrix greatly exceeds that of the filament (i.e., $\eta'/\eta \to 0$) or the viscosity of the filament to that of the matrix (i.e., $\eta'/\eta \to \infty$). When the viscosity ratio η'/η is between 0.1 and 1.0:

$$\lambda \approx 5.5(2R) \tag{6.24}$$

and when the ratio is 10:

$$\lambda \approx 7.7(2R) \tag{6.25}$$

This suggests droplets of diameter d in the case of Eq. (6.24):

$$\tfrac{1}{6}\pi d^3 = \pi R^2 \lambda = \pi R^2 (5.5R) \tag{6.26}$$

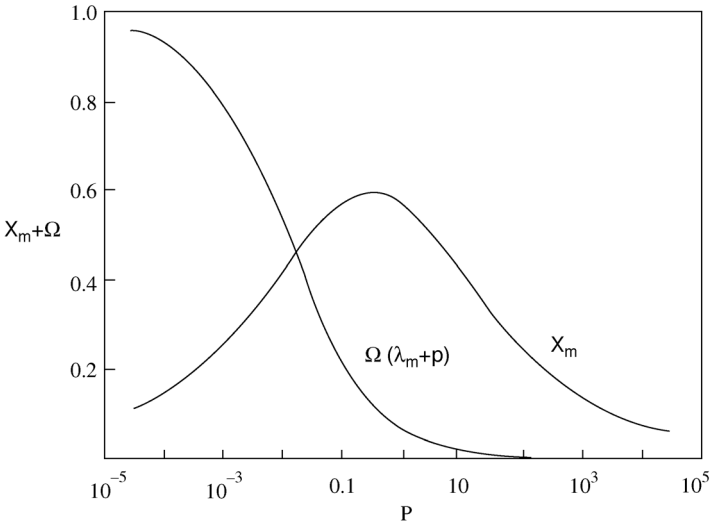

Figure 6.4 Tomotika's prediction of growth of disturbances and critical wavelength versus viscosity ratio. X_m is the dominant wavenumber and Ω_m is the corresponding growth function. From Elmendorp [52].

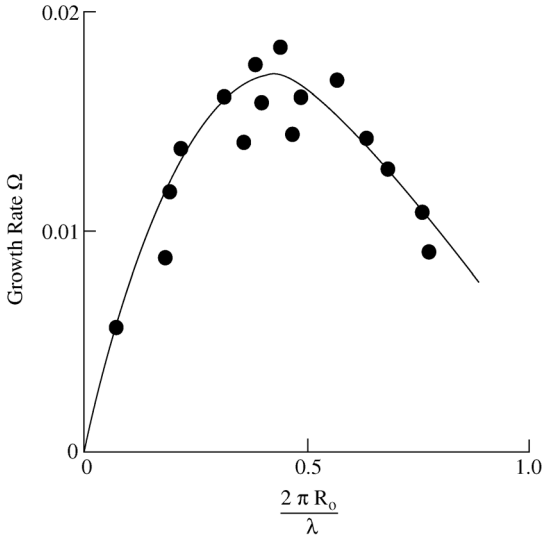

Figure 6.5 Elmendorp's [52] comparison of breakup of Newtonian liquid filaments with Tomotika's theory.

There have been various experimental observations of the breakup of liquid filaments in liquid matrices, including Taylor [41], Rumscheidt and Mason [80], Karam and Bellinger [81], and, notably, Elmendorp [52]. Tomotika [42] reported agreement of Taylor's experiments with his result. Elmendorp [52] noted his results to be in good agreement with the theory of Tomotika [42] and compared his observed critical wavelengths to Tomotika's predictions. This is shown in Figure 6.5.

The first serious investigations of the breakup of drops of polymer solutions were by Chin and Han [82], who were concerned with the influence of viscoelasticity. Subsequent studies of the breakup of droplets of polymer solutions in liquid fluid matrix were by Elmendorp [52]. Some discrepancies with Tomotika's theory were found and filaments seem generally more stable. Elmendorp also considered experiments with molten polymer filaments in a polymer matrix. Specifically, he looked at the systems (polyethylene)/(polystyrene), (polyethylene)/(polypropylene), and (polyethylene)/(polyamide-6). The filaments exhibited breakup characteristics in agreement with Tomotika's theory (Figure 6.6).

6.3.3.3 **Deformation of Droplets**

We now come to the final stages of morphology development (for disperse systems). Deformation and breakup of liquid droplets in a liquid matrix was first studied in series of articles by G.I. Taylor [40, 41] in 1932. Taylor first modeled the viscosity of emulsions and in a second article studied the deformation and breakup of liquid droplets. The basis of the work of Taylor is again the concept of the interfacial tension between immiscible liquid phases (Section 6.3.2.1). Taylor [41] subsequently described experiments with "parallel-band" (for shear flow) and "four roller" apparatus for extensional flow using individual droplets based upon combinations of

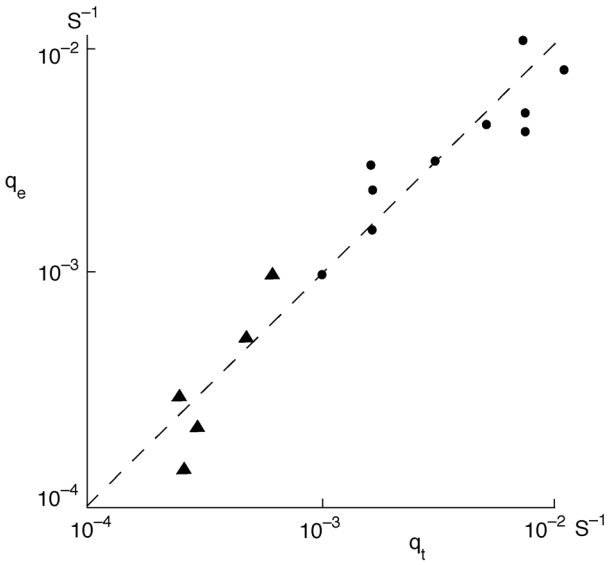

Figure 6.6 Comparison of Elmendorp's [52] results on disturbance growth rate in molten thermoplastics with Tomotika's predictions.

liquids with different viscosity ratios. For a drop of initial radius a, the deformation of the drop was characterized by the ratio:

$$\frac{L-\bar{B}}{L+\bar{B}} = \frac{L/\bar{B}-1}{L/\bar{B}+1} \tag{6.27}$$

where L is the length of the drop and $\bar{B}$ its breadth. Taylor's measurements were contrasted with a theory [41] of deformation of droplets in an emulsion. Taylor balances viscous stresses on deformation droplets with interfacial tension forces. For the elongational flow that was carried out in a four-roller apparatus:

$$v_1 = Ex_1 \quad v_2 = 0 \quad v_3 = -Ex_3 \tag{6.28a}$$

where E is the elongation rate. Taylor predicts that:

$$\frac{L-\bar{B}}{L+\bar{B}} = \frac{2aE}{\kappa}\left(\frac{19\eta'+16\eta}{16\eta'+16\eta}\right) \approx \frac{2aE}{\kappa}\left(\frac{19p+16}{16p+16}\right) \tag{6.28b}$$

where p is the viscosity ratio η'/η. Here κ is the interfacial tension and η' the viscosity of the droplet. For the shear flow (carried out with a parallel-band apparatus):

$$v_2 = \dot{\gamma}x_2 \quad v_2 = 0 \quad v_3 = 0 \tag{6.29a}$$

$$\frac{L-\bar{B}}{L+\bar{B}} = \frac{\eta a\dot{\gamma}}{\kappa}\left(\frac{19\eta'+16\eta}{16\eta'+16\eta}\right) \approx \frac{\eta a\dot{\gamma}}{\kappa} \tag{6.29b}$$

One may interpret this dimensionless group $\eta a\dot{\gamma}/\kappa$ (or $\eta aE/\kappa$) as the ratio of viscous forces tending to deform (and break up) droplets to the interfacial tension forces tending to hold them together. It is most appropriately called a Taylor number.

Taylor describes experiments with η'/η having values of 0.0003, 0.5, 0.9, and 20. He observed that, in the parallel-band apparatus that produced a shearing flow, when (η'/η) is 0.0003 (i.e., a very low viscosity drop is placed in a high-viscosity matrix) the drop is elongated indefinitely in flow. However, $(L-\bar{B})/(L+\bar{B})$ increases less rapidly than $\eta a\dot{\gamma}/\kappa$, unlike the expectation from Eq. (6.28b). In the four-roller elongational flow apparatus, the deformation of the drop $(L-\bar{B})/(L+\bar{B})$ was a unique function of $\eta aE/\kappa$ and obeyed Eq. (6.28b) at low stretch rates. At higher stretch rates $(L-\bar{B})/(L+\bar{B})$ increases less rapidly. The results were quantitatively similar to the shear flow behavior.

When η'/η was 0.5, the drop in the parallel-band apparatus elongated into a threadlike form. The deformation of the droplet was related to $\dot{\gamma}$ at low shear rates through Eq. (6.29b). When $(L-\bar{B})/(L+\bar{B})$ reached 0.8, the drop burst. This was at a value of $\eta a\dot{\gamma}/\kappa$ of 1.5.

For the case of η'/η of 0.9, the drop again elongated into a filament in both apparatuses and broke. In the shear flow apparatus, the drop drew out more rapidly than expected by Eq. (6.29b) except at the lowest shear rates. The drop burst at a value of $\eta a\dot{\gamma}/\kappa$ of 0.5.

For the case of η'/η of 20, the droplet began to rotate as it was a rigid ellipsoid in a shear flow. In the elongational flow four-roller device, the same droplet in the same fluid moves, stretched and burst rapidly when $\eta a\dot{\gamma}/\kappa$ was 0.14.

Taylor suggested that the mechanism of droplet breakup was the occurrence of the flow-induced disruptive pressure being greater than the interfacial tension.

The deformation of droplets in flow has been considered in subsequent articles by Bartok and Mason [83], Rumscheidt and Mason [80, 84], Torza *et al.* [85], Karam and Bellinger [81], Kumar and Saradhy [86], Flumerfelt [87], and Elmendorp and Maalke [52, 88]. The observations of Mason and his coworkers, using a four-roller and shear flow devices, generally confirm those of Taylor at low droplet deformation and, as remarked by Rumscheidt and Mason [80], agree with Taylor's Eq. (6.27) better than with Taylor's data. They observe in the four-roller apparatus that when η'/η was less than 0.2 the droplet could be extended until its diameter reached 10–50 μm, when it would break up into droplets. Initial drops were elongated (or extended) to form the elongated threads and the diameters of the threads (not the diameter of spherical shape droplet) were 10∼50 micron range and then break up to the droplets with retraction of the diameter to 20∼80 micron. When drops were elongated the diameter of the drop could be (thinner portion not elongated portion) smaller than the droplets with sperical shape. The results of Karam and Bellinger [81], using a Couette shear flow device, also support Taylor's Eq. (6.28b). In shear flow experiments, researchers, beginning with Taylor, found the drops were sigmoidal with pointed ends. They tended to draw down, with very small drops breaking off the ends, which might be called "tip streaming." For drops with viscosity ratios around unity, the drops would draw out into a thread and break up into droplets, the details varying with

deformation rate. When η'/η was very high, the droplet drew out in the four-roller device and burst. Only small finite deformations were achieved in shear flow. This observation has led to the conclusion that elongational flow is important in mixing of dispersed systems.

Karam and Bellinger [81] and later Grace [89] developed correlations for the shear rate of droplets at burst ($\dot{\gamma}_b$) using a Couette apparatus. They expressed their formulation using Taylor's Eq. (6.29a), thus including interfacial tension, viscosity ratio, and drop size. This is presented in the form of a correlation of:

$$\frac{\eta a \dot{\gamma}_b}{\kappa}\left(\frac{19p+16}{16p-16}\right) = f(p) \tag{6.30}$$

The two correlations are shown in Figure 6.7 (the reader should note that both sets of authors use the symbol μ rather than η for viscosity). The value of $\dot{\gamma}$ at fixed a has its minimum in the range of η'/η of 0.1 to 1.0. At larger and smaller η'/η, the value of the left-hand dimensionless group of Eq. (6.30) becomes much larger, especially when η'/η becomes much larger than unity. In the latter case it is often not possible to

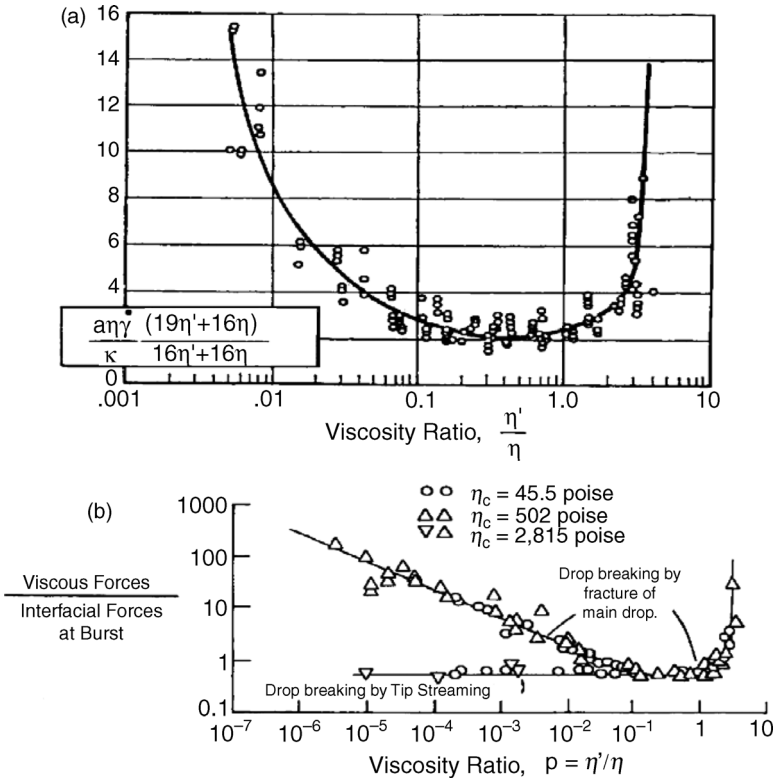

Figure 6.7 (a) Karam and Bellinger's [81] correlation of: $\frac{\eta a \dot{\gamma}_b}{\varkappa}\frac{(19\eta'+16\eta)}{(16\eta'+16\eta)}$ versus $\left(\frac{\eta'}{\eta}\right)$; (b) Grace's [89] correlation of: $\frac{\eta a \dot{\gamma}_b}{\varkappa}\frac{(19\eta'+16\eta)}{(16\eta'+16\eta)}$ versus $\left(\frac{\eta'}{\eta}\right)$.

achieve droplet breakage in shear flow. However, it is possible in elongational flow, as shown by Grace.

Karam and Bellinger [81] suggest that the formulation of Taylor allows the determination of a minimum drop size from Eq. (6.28a), arguing that this is equivalent to a balance of disrupting viscous forces and interfacial tension forces. This leads to:

$$a = \frac{\kappa}{\eta\dot{\gamma}}\left(\frac{16p+16}{19p-16}\right) \approx \frac{\kappa}{\eta\dot{\gamma}} \tag{6.31}$$

which indicates that the final droplet size is proportional to the interfacial tension and inversely proportional to shear viscosity of the medium, its shear rate, and shear stress. Using mixtures of silicone fluids with polyglycols and corn syrup in a Couette flow apparatus, they found that Eq. (6.31) is valid within a factor of three.

6.3.3.4 Observations on Mechanically Mixed Polymer Blends

Certain observations on polymer blends, prepared by mechanical mixing in the melt, are well known. In blend ratios of 70/30 and more by volume, the minor phase is dispersed in the major phase. In the range 40/60 to 60/40, there are usually co-continuous phases. However, material variables such as the interfacial tension and viscosity ratio strongly influence the morphology of the blend [90–94].

Danesi and Porter [90], studying (polypropylene/ethylene propylene rubber) blends, found that finer dispersions were obtained when the minor phase had an equal or lower viscosity than the major phase. If the minor phase had a higher viscosity, coarser blends were obtained.

Min *et al.* [91] found in a study of blends of polyethylene/polyamide-6 that the interfacial tension seemed to have a greater effect than the viscosity ratio on phase morphology. They found that the lower the interfacial tension, the finer is the morphology achieved. They suggest the role of $\kappa/\eta a\dot{\gamma}$ (or its inverse) as a correlation parameter. (Compare Eq. (6.28–6.30).)

This conclusion seems to be confirmed by various studies on the addition of "compatibilizing agents," which reduce the interfacial tension and make phase morphologies finer [92, 93]. Wu [93] – based on a study of the system (polyamide-6,6)/(ethylene propylene copolymer) and [poly(ethylene terephthalate)]/(ethylene propylene copolymer), prepared in a modular co-rotating twin-screw extruder – suggests that final morphology may be correlated by using:

$$\frac{a\eta\dot{\gamma}}{\kappa} = F\left(\frac{\eta'}{\eta}\right) \tag{6.32}$$

where F is a function of the viscosity ratio (η'/η). Wu's correlation is shown in Figure 6.8. This plot resembles the "burst shear rate" correlations of Karam and Bellinger [81] and Grace [89]. Isolated droplets are smaller when interfacial tension is low, the shear rate is high, and the viscosity ratio is close to unity. Wu proposed the specific equations:

$$\eta' < \eta \quad \frac{a\eta\dot{\gamma}}{\kappa} = 4\left(\frac{\eta'}{\eta}\right)^{0.84} \tag{6.33a}$$

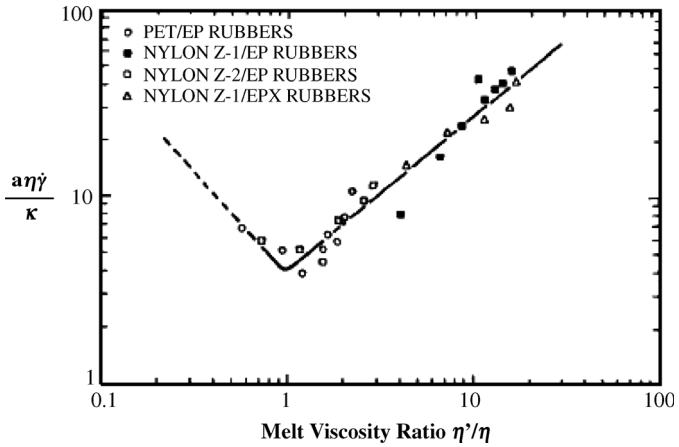

Figure 6.8 Wu's correlation of blend phase morphology using $\kappa/a\eta\dot{\gamma}$ and η'/η.

$$\eta' > \eta \quad \frac{a\eta\dot{\gamma}}{\kappa} = \frac{4}{(\eta'/\eta)^{0.84}} \tag{6.33b}$$

The correlation of Wu [93] is in the spirit of Karam and Bellinger's Eq. (6.30). They become essentially the same for η'/η of unity.

Generally, it is easier to obtain a fine domain size under conditions where the two melt viscosities are close. Furthermore, the domain size reduction easily occurs when the interfacial tension (κ) between each polymer particle is low, even if there exists a considerable melt viscosity difference. This means that both the addition of a compatibilizer and interfacial copolymerization reactions result in lower surface tension and, consequently, the domain size reduction is effectively accelerated. To develop and stabilize the optimum morphology of a polymer alloy, it is very important to utilize a particular interfacial reaction or a pre-designed compatibilizer to improve the surface tension or interaction between the domain and matrix polymeric components, as well as to select the optimum operational conditions for mixing.

6.3.3.5 **Coalescence**

Following the mixing process, the disperse phases often recombine or coalesce. This is a well-known phenomenon with a low-viscosity liquid such as combinations of oil in water or in salad dressings. There is a long history of investigations of coalescence in polymer melt blends, especially under quasi-quiescent conditions [60, 92, 94–97]. The rate of coalescence of dispersed phases is increased by large interfacial tensions, small droplet size, anisotropic droplet shape, and quiescent low deformation rate conditions. Coalescence is retarded by introducing compatibilizing agents to a lower interfacial tension [60, 92, 96], and by isotropic droplet shape [97].

Coalescence has also been argued to occur during the mixing process and thus to affect the final morphology. Indeed, dispersed phase size is always found to increase with concentration. There seems no logical explanation for this other than coalescence.

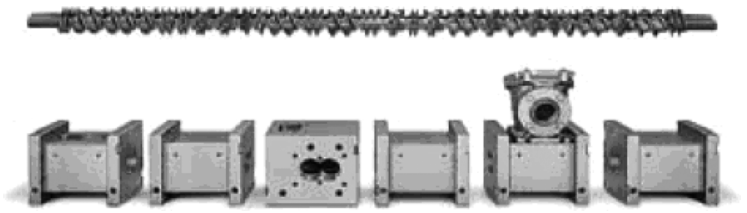

Figure 6.9 Photograph of extruder, modular screw, and barrel sections of a Werner & Pfleiderer ZSK. Courtesy of Coperion Werner & Pfleiderer.

6.4
Intermeshing Co-rotating Twin-Screw Extruder

Screw extruders represent the major processing machine of the thermoplastic industry, and play an important role in many related industries. A wide range of commercial screw extruders is used for manufacturing various kinds of both non-reactive blends and reactive blends. Among various twin-screw machines, intermeshing co-rotating twin-screw extruders with modular design have been a major continuous screw extruder for manufacturing polymer blends and they have various practical advantages (Figure 6.9).

Co-rotating twin-screw extruders have a long history dating back to the nineteenth century. The origin of co-rotating twin-screw extrusion technology appears to be in the 1860s. The book by White and Kim [98] describes the technology origins and developments of intermeshing (self-wiping) co-rotating twin-screw extruders as well as other types of continuous twin-screw extruder and mixers (see also Section 5.2.1).

6.4.1
Geometry and Flow Mechanisms

Intermeshing co-rotating twin-screw extruders generally have self-wiping profiles for both their screw and kneading disc elements, as may be seen in the Werner & Pfleiderer screw and kneading disc assemblies of Figure 6.10. Knowledge of this shape is explicit in an early patent of Wunsche [99], who modeled the characteristic of self-wiping shapes in his patent. In a 1971 article, Martelli [100], who then marketed LMP equipment in the United States, discussed this problem, though rather incompletely, giving credit to Colombo for the solution. Erdmenger [98] has reviewed the I.G. Farbenindustrie-Bayer AG development and credits this to efforts of A. Geberg in the 1940s. However, the first publication beyond Wunsche [99] describing and solving this problem was by Booy [101] in 1978.

Consider Figure 6.11: it identifies the cross-sections of two intermeshing co-rotating screw shafts, each of which has maximum screw radius R_S and a centerline distance C_L. We may define the important characteristic quantity:

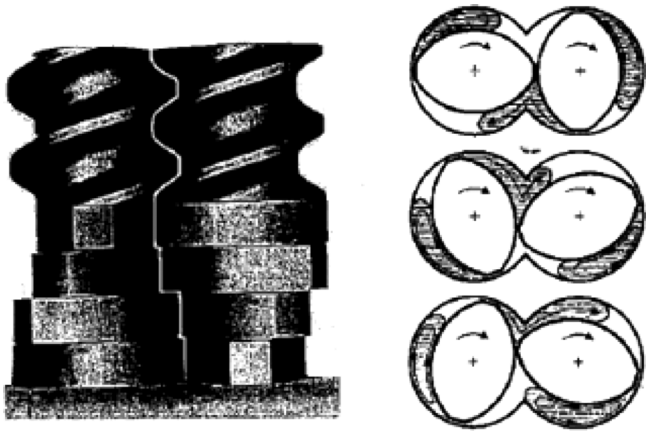

Figure 6.10 Self-wiping Werner & Pfleiderer screw and kneading disc assembly. Courtesy of Werner & Pfleiderer.

$$\varrho_c = \frac{C_L}{R_S} \tag{6.34}$$

The radius of the root of the screw is R_B. Thus:

$$R_S + R_B = C_L \tag{6.35}$$

and the maximum channel depth H_{max} is:

$$\begin{aligned} H_{max} &= R_S - R_B = R_S - (C_L - R_S) \\ &= 2R_S - C_L = R_S[2 - \varrho_c] \end{aligned} \tag{6.36}$$

We may define an angle θ that describes the angle swept out by the screw as it rotates. It is necessary to know the form that $H(\theta)$ must have as the screw rotates.

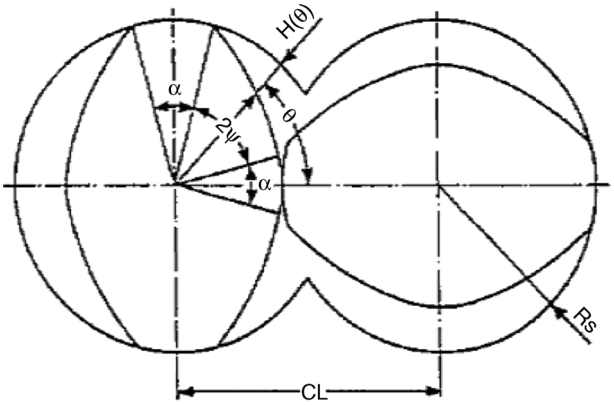

Figure 6.11 Geometry of intermeshing self-wiping co-rotating twin-screw extruder.

Generally a cross-section with N_T tips corresponds to a screw with N_T equivalent independent thread starts. Each tip makes an angle α in the circumference. Thus, we may divide the circumference of a screw shaft between an angle α describing the tips and the angle ψ describing the remainder of the circumference so that:

$$N_T(2\alpha + \psi) = 2\pi \tag{6.37}$$

With $N_T = 1$, the cross-section resembles a cam; with $N_T = 2$, the cross-section resembles an ellipse; with $N_T = 3$, it resembles a triangle. The values of $H(\theta)$ describe the cross-section of the screw and are related to R_S, C_L, and ϱ_c.

In Figure 6.11, the axes of the two screw cross-sections are perpendicular to each other and the point of contact is along the line connecting the axes. When the screws rotate an angle ψ given by:

$$\psi = \cos^{-1}\left(\frac{C_L/2}{R_S}\right) = \cos^{-1}\frac{\varrho_c}{2} \tag{6.38}$$

the point of contact of the two screws is intermediate between the screw axes. When the screws rotate at a second angle (ψ) they will be in a position of reversed configuration. Booy suggests that Eq. (6.37) may be replaced with:

$$N_T(2\alpha + 4\psi) = 2\pi \tag{6.39}$$

Clearly α depends upon ϱ_c through:

$$\begin{aligned}\alpha &= \frac{\pi}{N_T} - 2\cos^{-1}\frac{\varrho_c}{2} \\ &= \frac{\pi}{N_T} - 2\cos^{-1}\left(\frac{C_L}{2R_S}\right)\end{aligned} \tag{6.40ab}$$

and:

$$C_L = 2R_S\cos\left[\frac{\pi}{2N} - \frac{\alpha}{2}\right] \tag{6.40c}$$

The value of $H(\theta)$ around the circumference has been determined by Wunsche [99] and Booy [101]. At $\theta = 0$ we have the situation of Eq. (6.36):

$$H(0) = 2R_S - C_L = R_S[2 - \varrho_c] \tag{6.41a}$$

At angle θ, we have:

$$H(\theta) = R_S(1 + \cos\theta) - \sqrt{C_L^2 - R_S^2\sin^2\theta} \tag{6.41b}$$

or:

$$H(\theta) = R_S\left[1 + \cos\theta - \sqrt{\varrho_c^2 - \sin^2\theta}\right] \tag{6.41c}$$

Taking into consideration the width of the tips and the clearance, Denson and Hwang [102] essentially rewrote this as:

$$H(\theta) = 2R_S - C_L \text{ for } 0 < \theta < \frac{\alpha}{2}$$

$$H(\theta) = R_S\left[1+\cos\left(\theta-\frac{\alpha}{2}\right)\right] - \sqrt{C_L^2 - R_S^2\sin^2\left(\theta-\frac{\alpha}{2}\right)} \text{ for } \frac{\alpha}{2} < \theta < \frac{\pi}{N_T} - \frac{\alpha}{2}$$

$$H(\theta) = 0 \text{ for } \frac{\pi}{N_T} - \frac{\alpha}{2} < \theta < \frac{\pi}{N_T} \tag{6.42}$$

6.4.1.1 Right-Handed Screw Elements

The primary element of modular co-rotating twin screw elements are right-handed screw elements. Right-handed screw elements are also called forward pumping elements. The role of right-handed modular co-rotating screw elements is to direct and pump material toward the die. Screws have a well-known geometry that may be readily specified. The axial distance of one full turn of a screw is called the "screw lead" or pitch (S). The axial distance between successive flights is designated B and e is the perpendicular width of the flights.

Consider a helical axis ξ_1 that runs along the deepest channel depth of the screw channel; ξ_2 is a coordinate axis normal to the screw axis and passing through ξ_1; ξ_3 is an axis normal to the plane of ξ_1 and ξ_2. The helix angle ϕ is the angle described by both the ξ_1 direction and the screw flight. The helix angle ϕ depends upon radius because the pitch is by definition radius independent. The pitch is related to the helix angle through the expression:

$$S = 2\pi r \tan\phi(r) \tag{6.43}$$

The distance between the screw flight parallel to the screw axis is $B(\xi_2)$.

Screws can be single or multiple flighted, that is, have one or multiple thread starts (Figure 6.12). The pitch of a single flighted screw is:

$$S = B + \frac{e}{\cos\phi} \tag{6.44a}$$

where e is the flight width. The pitch of screws with double, triple, and m thread leads or m flighted screws are, on the other hand, respectively:

$$S = 2\left(B + \frac{e}{\cos\phi}\right) \tag{6.44b}$$

$$S = 3\left(B + \frac{e}{\cos\phi}\right) \tag{6.44c}$$

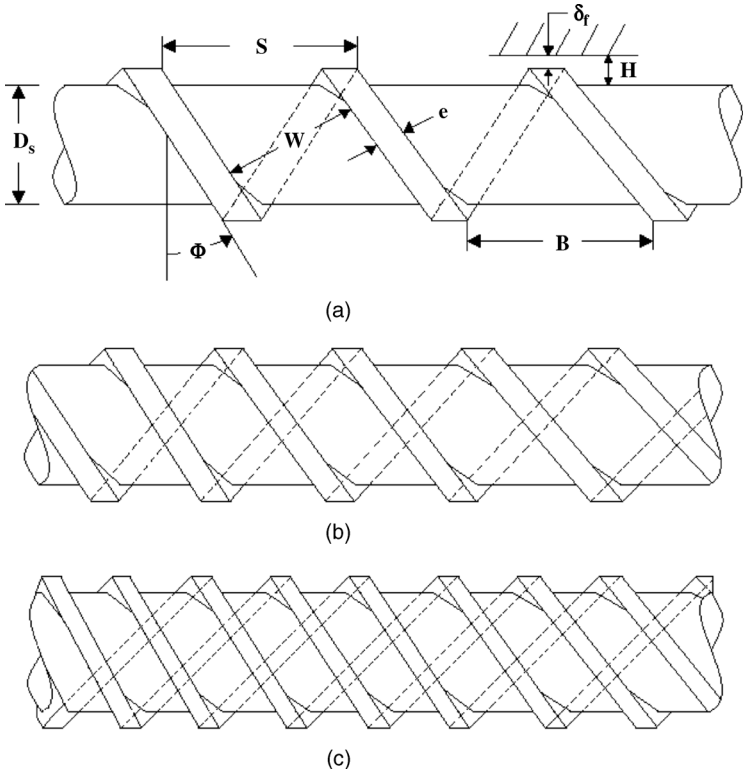

Figure 6.12 (a) Single-, (b) double-, and (c) triple-flighted screws (not self-wiping).

$$S = m\left(B + \frac{e}{\cos\phi}\right) \tag{6.44d}$$

The cross-sections of single-flighted screws are cam shaped, whereas those of double-flighted screws have roughly a double-tipped elliptical shape (Figure 6.13). Triple-flighted screws have three tips.

Many screw profiles have been proposed through the years. The simplest screw profile is one with constant thickness flights and a constant channel depth (H). Such a cross-section, however, does not allow self-wiping screws. The screw profiles must be such as to satisfy Eq. (6.42).

The earliest studies of flow in an intermeshing co-rotating twin-screw extruder are those of Erdmenger [103–105]. Erdmenger used a tracer technique to show that flow in an intermeshing co-rotating twin screw machine was essentially a drag flow in a figure-of-eight shape as the fluid moves along the channel in the twin-screw machine (Figure 6.14). In a self-wiping co-rotating twin screw machine with double-flighted screws, it was found that there are three parallel fluid streams moving through the screw channels. Left-handed screw elements can only provide forward flow through negative pressure gradients and are thus always filled.

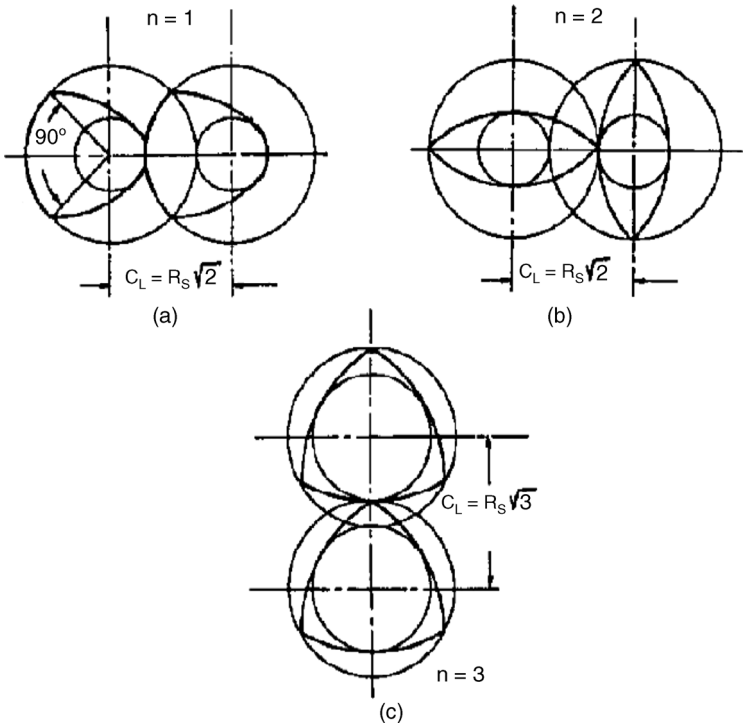

Figure 6.13 (a) single-flighted screws; (b) double-flighted screws; (c) triple-flighted screws.

Table 6.3 summarizes the effects of screw geometry on pumping capability, degree of fill, mean residence time, and pressure build-up capability of the screw elements. Different types of screw elements should be used to design an optimum screw configuration for an application of interest.

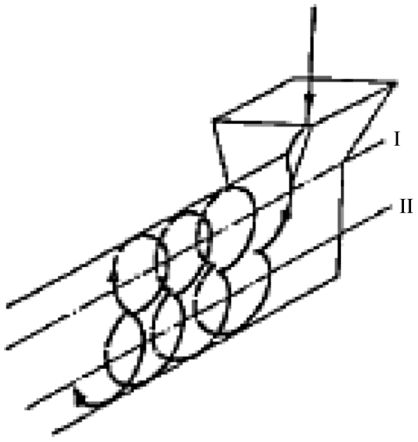

Figure 6.14 Flow in screw regions of an intermeshing co-rotating twin-screw extruder. Erdmenger [105].

Table 6.3 Effects of screw element geometries on flow behavior.

Number of flight starts	Pumping capability	Degree of fill	Residence time	Pressure build-up
Single	High	Low	Short	Low
Double	Medium	Medium	Medium	Medium
Triple	Low	High	High	High
Pitch				
High pitch	High	Low	Short	Low
Low pitch	Low	High	High	High

6.4.1.2 Left-Handed Screw Elements

It is well known that screws may have a mirror image. This is equivalent to a screw having a negative pitch. It is possible to produce such a left-hand element in all the variations of design developed for screws (Figure 6.15). This includes the number of threads starts and axial diameter profile.

Left-handed screw elements are used to generate backpressure and therefore create a fully filled section. Left-handed screw elements are inserted behind melting or mixing sections where the polymer melt is fully filled and mixing takes place.

6.4.1.3 Kneading Disc Blocks

Kneading disc blocks are first found in a 1931 patent application of Nelson [106] and were subsequently redeveloped from a broader viewpoint by Erdmenger [107] in 1949. Kneading disc blocks consist of a series of staggered self-wiping "short shafts" of constant axial shape. These may be staggered relative to each other at any angle, for example, 30°, 45°, 90°, and so on. As these short shafts are generally less than 10 mm thick, they are referred to as discs. Nelson [106] suggested double-tipped discs, whereas Erdmenger [108–111] described single-tipped, double-tipped discs, and triple-tipped discs. Figures 6.16 and 6.17 show the kneading disc blocks of Erdmenger. The tips of discs resemble screw flights and kneading disc blocks resemble screws with zigzag interrupted flights. Not surprisingly, kneading disc blocks possess some screw-like connection, it is possible to devise left-handed as opposed to right-handed kneading discs. Neutral kneading discs are also used.

The purpose of kneading disc blocks is to induce both dispersive and distributive mixing. A basic study of flow and mixing by kneading discs was given by Werner [112, 113]. Motions of materials in the kneading disc block area have been described by Szydlowski *et al.* [114, 115]. Materials do not flow uniformly through kneading disc

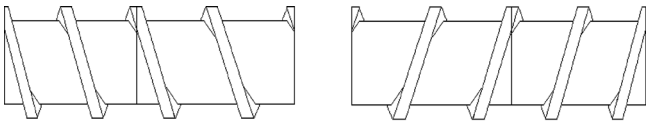

Figure 6.15 (a) Forward pumping (right-handed) and (b) backward pumping (left-handed) screws.

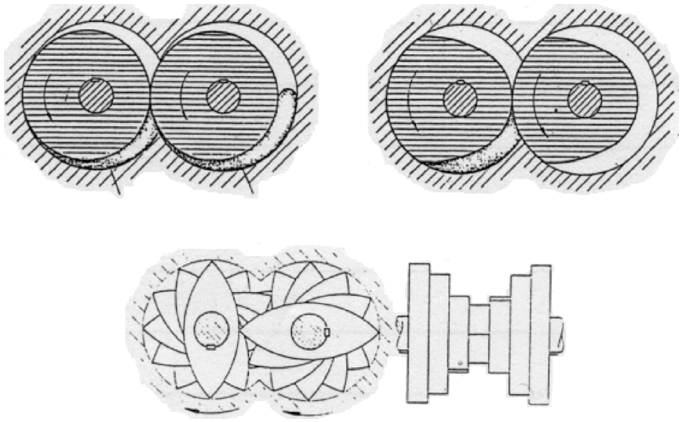

Figure 6.16 Erdmenger's single- and double-tipped kneading disc block machine [107].

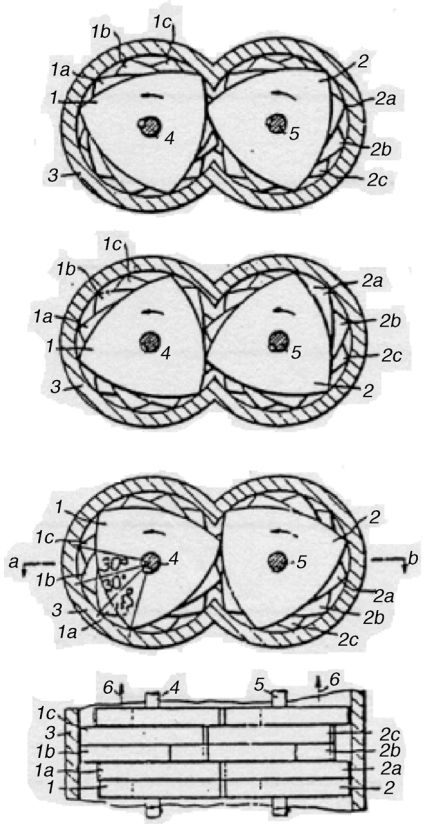

Figure 6.17 Erdmenger's triple-tipped kneading disc block machine [111].

blocks. If a material flows over the disc tips it encounters high stresses and dispersive mixing occurs. If, on the other hand, material flows through the openings between the discs rather than along the "pseudo helix," distributive mixing occurs.

Erdmenger [105] gave the first discussions of flow in the kneading disc regions of a modular twin-screw extruder. This work was supplemented by later studies of Werner [112, 113] and by Szydlowski and his coworkers [114]. The kneading disc section has an approximate screw-like character. Right-handed kneading disc blocks usually provide a weak forward drag flow. They also provide stagnation regions where material can be captured and then pushed over the kneading disc tips. If the kneading disc block is fully filled and pressurized, the gaps between the rejoining kneading discs provide regions where backward leakage flows may occur. Szydlowski and White [115] provide an argument that there is, in addition, in this geometry a peristaltic pumping phenomenon in fully filled regions due to local variations in volume that occur during each screw rotation. Left-handed kneading disc blocks act in a similar manner to left-handed screws, providing back pressure. Generally, melting and mixing occurs in kneading disc blocks.

6.4.1.4 **Special Distributive Mixing Elements**

There is a long history of intermeshing co-rotating twin screw extrusion by using mixing elements other than kneading disc blocks. Often much better distributive mixing is desired, especially for materials of greatly varying viscosity levels. We briefly summarize these in this section. In a 1950 patent application Kraffe de Laubarede [116] suggested self-wiping discs containing slots as shown in Figure 6.18. These were machined into the shape of screw sections.

In a 1964 patent application, Robert Colombo [117] of LMP described a mixing section consisting of a left-handed screw element with a helical groove cut in it (Figure 6.19). This should have distributive mixing capability.

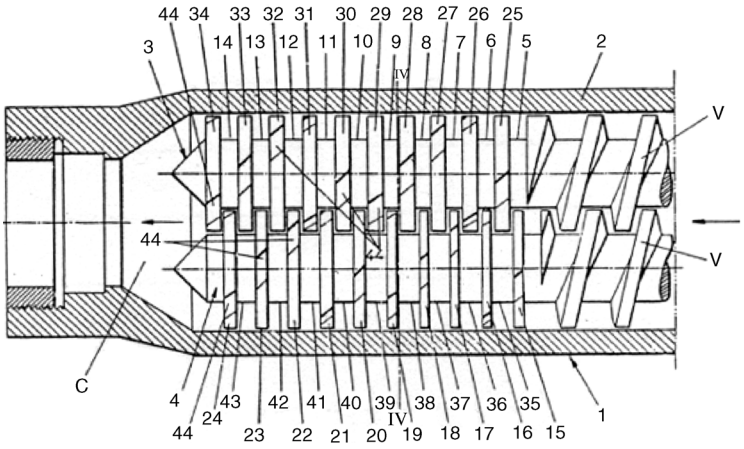

Figure 6.18 Kraffe de Laubarede's mixing screw element containing slots in a disc [116].

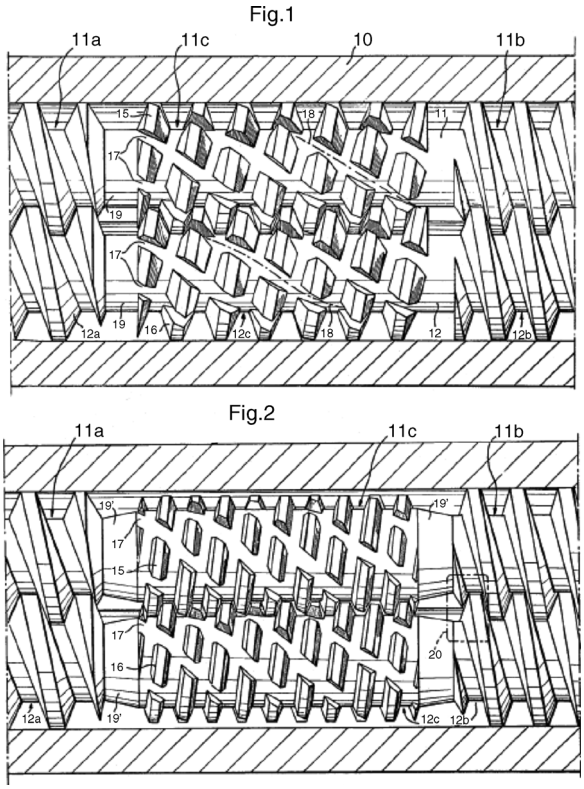

Figure 6.19 Colombo's mixing element [117].

Another special mixing section was described by Loomans [118] of Baker Perkins in a 1967 patent application. This is shown in Figure 6.20. These are essentially double-zipped kneading disc blocks with a 90° staggering angle.

In a 1980 patent application, Rathjen and Ullrich [119, 120] of Bayer AG proposed self-wiping co-rotating twin screw elements with grooves in the screw flights (Figure 6.21). This was to help with fluid streams with crystallizing components.

Gear-like elements were introduced by Berstorff in the late 1980s for improved distributive mixing (Figure 6.22).

In 1991, Burbank *et al.* [121] of Werner & Pfleiderer described Turbine Mixing Elements (TMEs) (Figure 6.23a). These elements are argued to be most effective in distributing low-viscosity or difficult to mix liquids in polymer melts.

Grillo *et al.* [122] of Werner & Pfleiderer described, in 1992, a "Zahn Misch element" (ZME) that consists of toothed elements (Figure 6.23b). This was used to provide milder mixing than kneading discs which tend to break glass fibers.

Polygonal elements for melting and mixing have been introduced by Leistritz and Farrel. The former company uses elements in both co-rotating and counter-rotating machines. Canedo and Valsamis [123] have discussed Farrel designs (Figure 6.24).

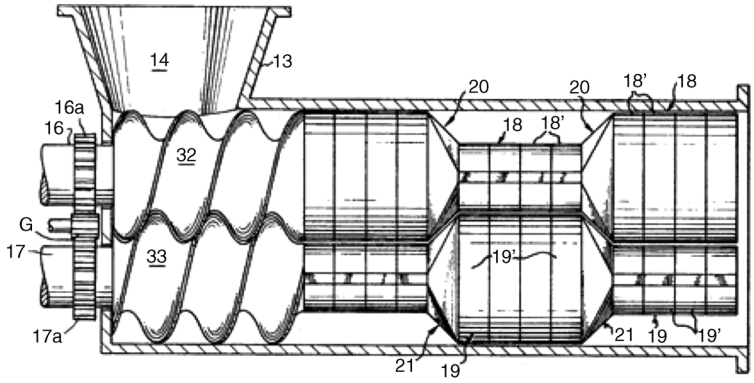

Figure 6.20 Loomans' intermeshing continuous mixing and kneading apparatus [118].

6.4.2
Residence Time Distributions

There is a long history of investigations of residence times in twin-screw extruders [124–136]. The first studies of residence time distribution in intermeshing co-rotating twin-screw extruders were reported in 1966 by Herrmann [124] of Werner & Pfleiderer. Table 6.4 summarizes the many different techniques have been used to measure the residence time distribution in intermeshing co-rotating twin-screw extruders.

The residence time distribution of a screw extruder is basically sharp (Figure 6.25) [125]. Depending on extruder type and screw design, the distribution can be controlled depending on the longitudinal mixing.

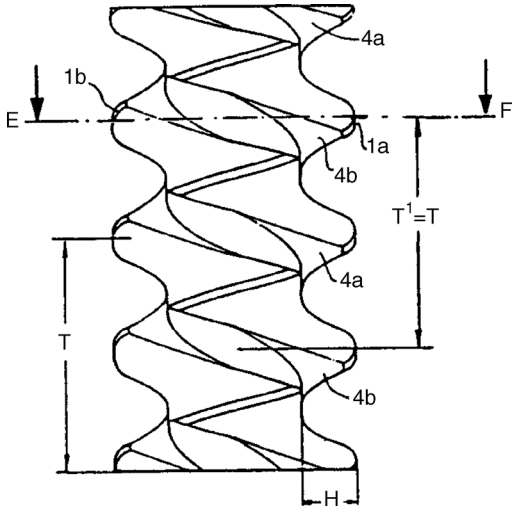

Figure 6.21 Rathjen and Ullrich modified screw elements for crystallization [119, 120].

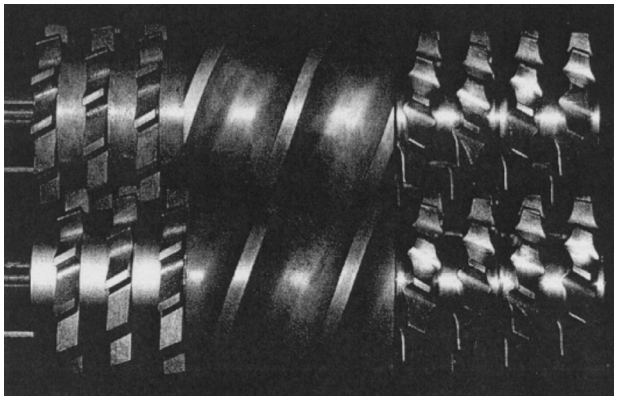

Figure 6.22 Typical arrangement of Berstorff gear mixing elements assembled on a ZE 90A twin-screw extruder: parallel gear rings (left-hand side); gear cut on a helix (right-hand side). Courtesy of Berstorff.

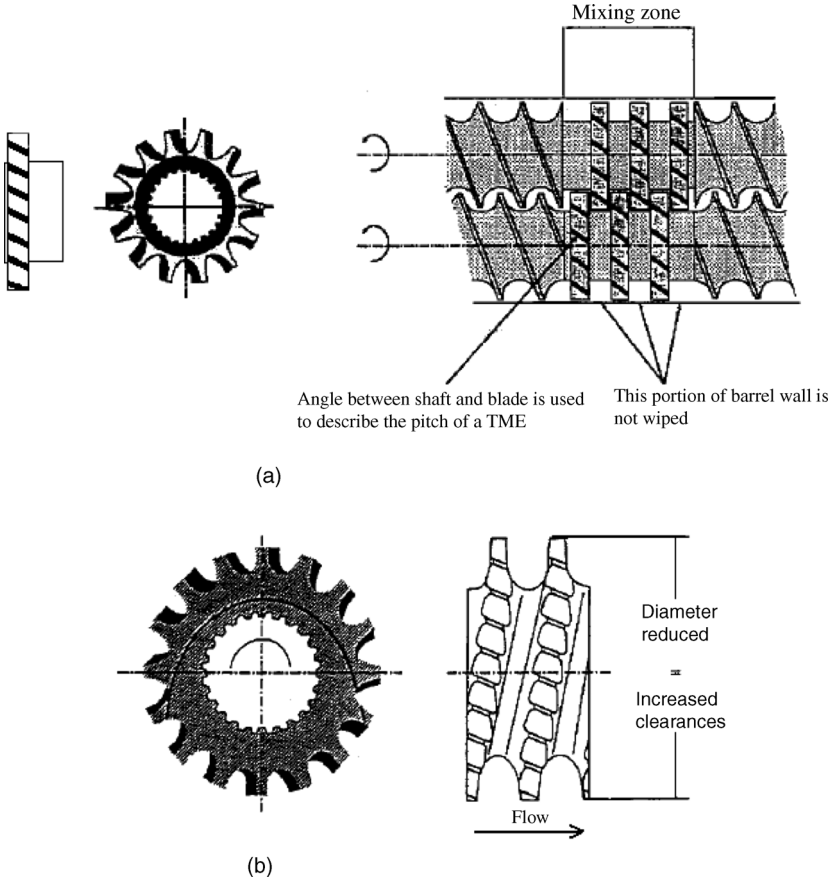

Figure 6.23 Werner & Pfleiderer special mixing elements: (a) Turbine Mixing Elements (TMEs); (b) Zahn Misch Elements (ZME). Courtesy of Werner & Pfleiderer.

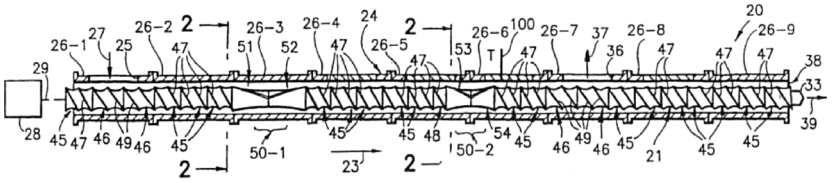

FIG. 1

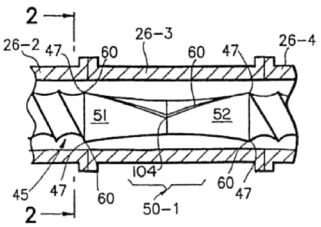

FIG. 1A

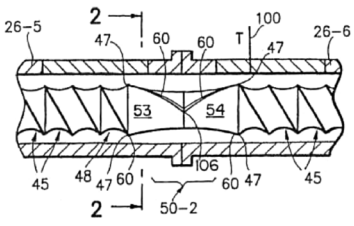

FIG. 1B

Figure 6.24 Farrel rotor-type modular mixing element from US patent application [123].

The average residence time is directly calculated from the available holdup volume divided by the volumetric flow rate (see Eq. (6.23)).

Residence times are usually found for any screw configuration and feed rate to be in the range 1–5 min. The residence time generally decreases with increasing feed rate and screw speed. This reflects decreasing degrees of modular screw fill. It is also found that increasing feed rate reduces residence times. Owing to the improvement of mechanical design, machining, and metallurgical technology, twin-screw extruders have moved in the direction of deeper screw channels and lengths up to 65 length-to-diameter ratio (L/D), particularly in the case of an intermeshing co-rotating twin-screw extruder.

Residence time distribution measurements have been presented by Sakai [127], who contrasted the behavior of the various types of twin-screw extruders (Figure 6.26). Sakai found that intermeshing co-rotating twin screw machines produce a narrower distribution of residence time than a single-screw extruder. He argues that this is

Table 6.4 Summary of residence time distribution measurements in intermeshing co-rotating twin-screw extruders.

Technique	Investigators
Tracer	Herrmann [124], Todd and Irving [125], Potente and Ansahl [130], Kim and White [133], Kye and White [134], Shon *et al.* [136]
Radioactive decay of $^{56}MnO_2$	Todd [126], Hornsby [129]
Ultraviolet absorbing group	Cassagnau *et al.* [131]
Fluorescence	Bur and Gallant [132]

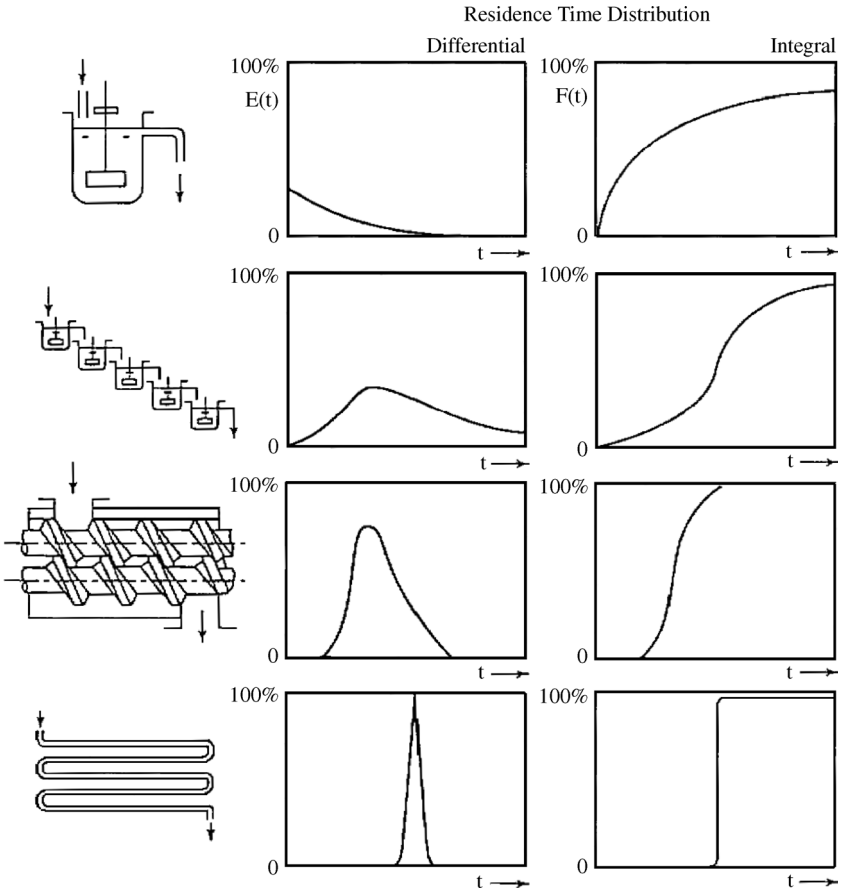

Figure 6.25 Comparison of residence time distribution curves for various reactors [125].

associated with the self-wiping character of the screws, which prevents the retention of stagnant layers on the screw surface. The intermeshing counter-rotating machine is also found to have a narrower residence time distribution, which Saki associates with the C-chamber mechanism. Residence time and residence time distribution breadth in modular machines increase with the introduction of left-handed elements and kneading disc blocks into the screw configuration. This again reflects increasing screw fill.

6.4.3
Morphology Development for Reactive Blends

Published investigations of phase morphology development in polymer melt blends in twin-screw extruders began with the work of Plochocki *et al.* [137] in 1988. Since 1992, several different research groups have described investigations [76, 138–147].

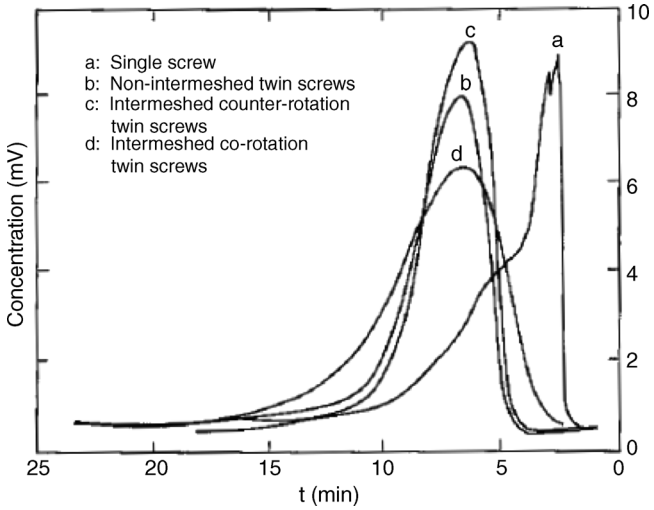

Figure 6.26 Residence time distributions of Sakai [127].

It has been found that when one phase is predominant the disperse phase in a polymer blend system evolves from a pellet usually to a lacelike sheet and then filaments and ultimately to droplets [76, 147]. The evolution from pellet to droplet occurs rapidly as soon as both phases melt. Lee and White [146, 147] find in studies of various polymer blends that if there is a large viscosity difference between the two phases and the low viscosity polymers melt first, the latter will wet the screw and barrel and lubricate the motions of the pellets of the other phase. This delays the position of melting late in the extruder, thus reducing mixing time and producing coarse blends.

Lim and White [74, 139–141] explored the influence of screw configuration on the development of phase morphology in blending using the polyethylene/polyamide-6 system. The presence of kneading disc blocks early in the extruder results in early melting of both phases and the reduction in disperse phase size to a very fine level. If no kneading disc blocks are involved, melting is delayed until the very end of the twin-screw extruder and a coarse morphology is developed. Increasing the number of kneading disc blocks decreases the phase size of the disperse phase.

Lim and White [74] studied the influence of a compatibilizing agent (SEBS-g-MA, maleic anhydride grafted styrene–ethylene-*co*-butadiene–styrene triblock copolymer) on the phase morphology of a polyethylene/polyamide-6 (75/25 by weight) blend in a laboratory-scale self-wiping co-rotating twin-screw extruder with diameter of 30.7 mm. The polyethylene pellets melted in the first kneading disc block close to the hopper. The polyamide-6 melted completely only at a position of 360 mm from the hopper. Thus, the polyethylene, which melted prior to the polyamide-6, acted as a transporting agent for the unmelted polyamide-6 pellets. A very interesting finding was that the addition of a compatibilizing agent not only decreased the ultimate polyamide-6 domains but also increased the rate of morphology development.

The larger the amount of compatibilizing agent added, the greater the magnitude of reduction in the ultimate polyamide-6 domain size and increase in the rate of morphology development (Figure 6.27).

There is much less literature concerning the morphology development of reactive blending than there is concerning that of unreactive blending. However, all the results essentially demonstrate that the domain size of dispersed phase is smaller and the rate of morphology development is faster when a compatibilizer is added [148, 149].

6.4.4
Process Simulation of Intermeshing Co-rotating Twin-Screw Extruders

Intermeshing co-rotating twin-screw extruders play an important role in polymer processing technology and are widely used in blending, compounding, devolatilization, and reactive extrusion. Modern intermeshing co-rotating twin-screw extruders are designed in a modular manner. This makes it possible for the user to change the screw as well as the barrel configurations. This kind of design can greatly expand the flexibility of the twin-screw extruder for different applications. Unfortunately, however, most users have not been able to do so due to lack of knowledge of what screw configurations should be used for certain applications. Those who did do experiments with different screw configurations, have generally done so by intuition and trial and error. Much time and effort may have been wasted on this kind of work. This situation has prevented the users from employing their expensive intermeshing co-rotating twin-screw extruders more efficiently. Commercially available non-isothermal, non-Newtonian flow simulation packages for intermeshing co-rotating twin-screw extruders have been developed by various research groups [150]. They may be used to suggest optimized screw configuration and working conditions. They may also be used to evaluate the extrusion process or be used for predicting disastrous situations such as vent flushing. White and Kim discussed very detailed flow modeling for screw elements, kneading disc blocks, and non-isothermal energy balance as well as melting [150].

With intermeshing co-rotating twin screw extrusion simulation program packages the user can perform a non-isothermal simulation and obtain axial fill factor, pressure, temperature, melting, average residence time, power consumption, torque and specific energy consumption profiles. In Figure 6.28a–e we show, for one set of conditions, the fill factor, pressure, cup mixing temperature, mean residence time, power consumption, and torque profiles along the axis of a modular co-rotating twin-screw extruder calculated by Akro Co Twin Screw™ software (Table 6.5).

More ambiguously stated similar developments are given by Potente and his coworkers [151, 152] in 1996 and 1999 and by Canedo [153] in 1999. A better and more readable presentation of such a development was given by Vergnes *et al.* [154, 155] in 1996–1998. They propose and describe forward fluid mechanical and energy balances (Table 6.5).

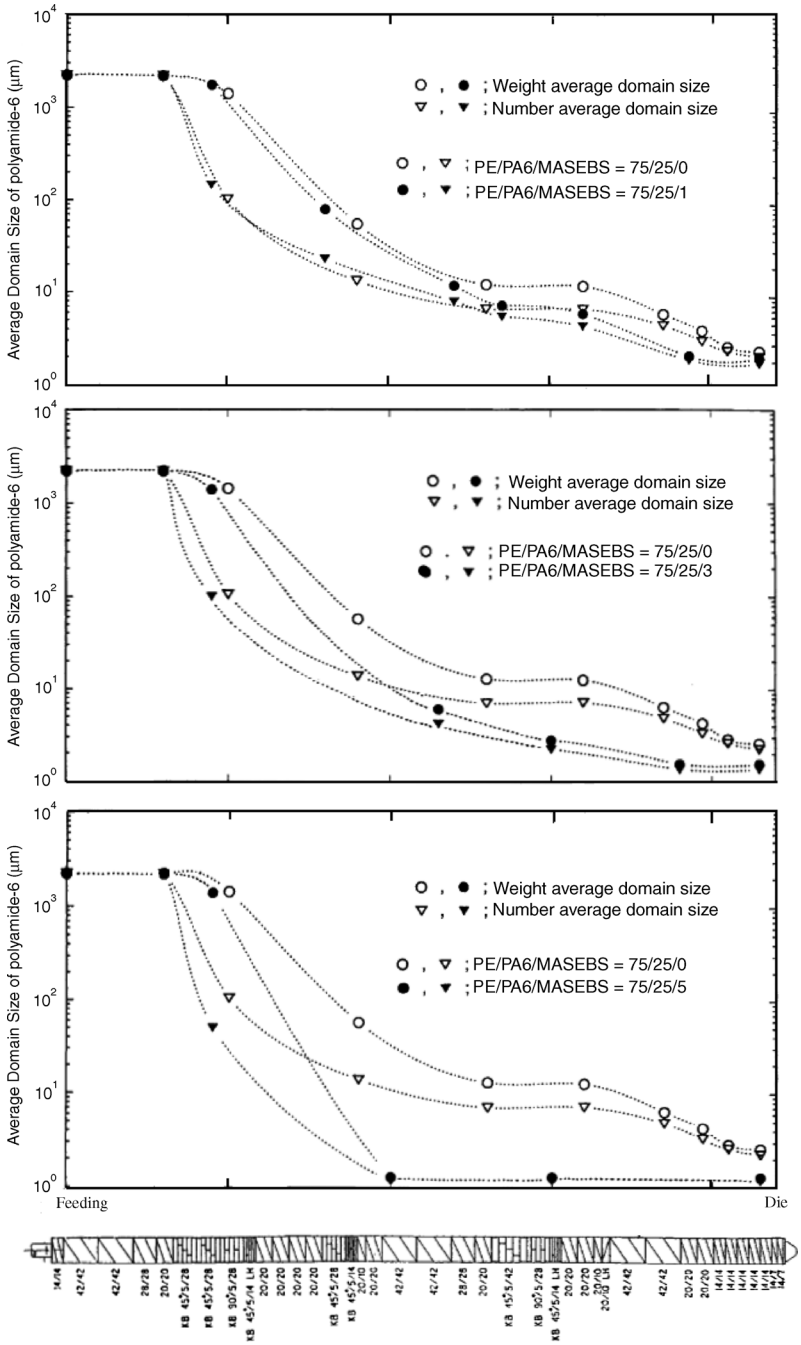

Figure 6.27 Morphology development of polyethylene/polyamide-6/SEBS-g-MA reactive blends system in an intermeshing co-rotating twin-screw extruder [74].

(a)

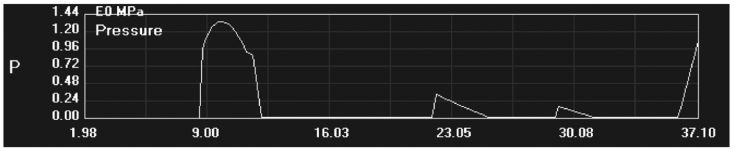

(b)

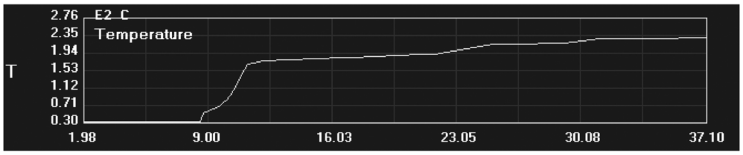

(c)

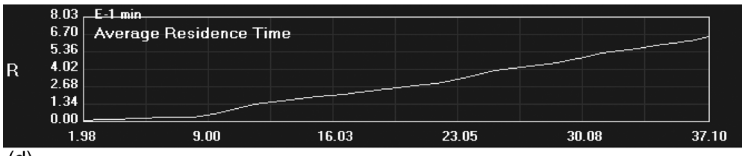

(d)

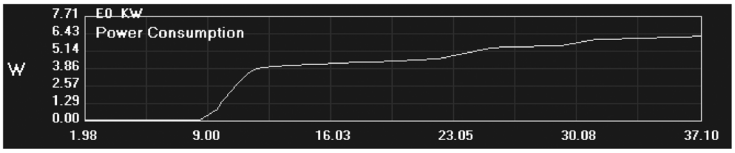

(e)

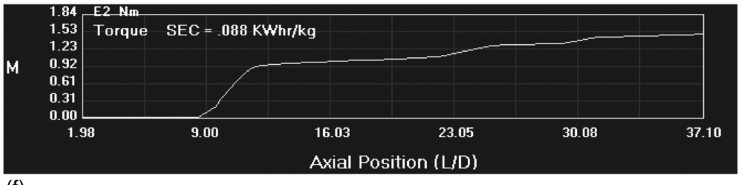

(f)

Figure 6.28 Simulation of (a) fill factor, (b) pressure, (c) cup mixing temperature, (d) mean residence time, (e) power consumption, and (f) torque profiles in a 40-mm diameter co-rotating twin-screw extruder for a polypropylene at 300 lb h^{-1} and 300 rpm.

Table 6.5 Global software for modular co-rotating twin screw.

Software name	Features	References
Akro Co Twin Screw		
Version 1 (1989)	Isothermal, non-Newtonian melt flow	Wang *et al.* [158]
Version 2 (1993)	Non-isothermal, non-Newtonian melt flow	Chen and White [159]
Version 3 (1997)	Non-isothermal, non-Newtonian melt flow with melting	Bawiskar and White [157]
Version 4 (2003)	Add reactive extrusion and devolatilization to Version 3	White *et al.* [156]
Sigma (1996–1999)	Non-isothermal	Potente *et al.* [151]
	Non-Newtonian melt flow with melting	Potente *et al.* [152]
Ludovic (1996–1998)	Non-isothermal, non-Newtonian melt flow	Vergnes *et al.* [154, 155]
TXS (1999)	Non-isothermal, non-Newtonian melt flow with melting, oversimplified screw characteristic curve calculations	Canedo [153]

It is possible to include additional features in this type of software. In a 2006 paper, White *et al.* [156] describe software that allows the user to do all the calculations described by Bawiskar and White [157] and also to model reactive extrusion and devolatilization.

To run a simulation of an intermeshing co-rotating twin-screw extrusion process, the working conditions such as throughput, screw speed and optionally die pressure, and material properties have to be specified. Table 6.6 gives material parameters for various polymers.

Shi and Utracki [160] in a 1992 article were the first to try to model phase morphology development in a twin-screw extruder. They focused on the breakup of filaments by a capillary mechanism into droplets using the analysis of Tomotika [42] (compare Section 6.3.3.2). A more sophisticated development of this model, considering the detailed flows in the kneading disc blocks, was published by Huneault *et al.* [144, 161] of the same group in 1995–96. Delamare and Vergnes [154] have sought to improve the model by attempting to include coalescence.

However, notably, none of these models follow the process beginning with the original pellet that then melts and evolves from a pellet to a sheet to a lace and only then to a filament. The models described in the preceding paragraph [144, 154, 160, 161] are further limited to rather dilute systems. More work is required in modeling of morphology development of polymer blends.

6.5 Manufacturing Process Design for Polymer Blending Process

We have reviewed mixing mechanism, morphology development, and intermeshing co-rotating twin screw extrusion technology in the previous sections. For a given

Table 6.6 Summary of material parameters for various polymers.

Material parameter	Low density polyethylene (LDPE)	High density polyethylene (HDPE)	Poly(ethylene terephthalate) (PET)	Polypropylene (PP)	Polycarbonate (PC)	Acrylonitrile–butadiene–styrene (ABS)	Polystyrene (PS)	Polyamide 6 (PA6)	Poly(methyl methacrylate) (PMMA)	Poly(vinyl chloride) (PVC)
Melt section										
Density of input stream ($g\,cc^{-1}$)	0.75–0.8	0.75–0.82	0.9–1.0	0.7–0.8	1.0–1.2	0.8–1.02	0.95–1.05	0.84–0.98	0.95–1.1	1.30–1.35
Power law consistency ($kPa\,s^n$)	20.5–27.5	22.5–58.6	3.5–8.0	0.4–0.6	1.7–3.0	27.0–53.8	5.0–13.8	1.5–20.7	65.7–189.6	3.5–30.6
Power law index	0.3–0.4	0.35–0.45	0.6	0.35	0.7	0.25–0.37	0.22–0.3	0.43–0.7	0.14–0.25	0.4–0.3
Viscosity temp dependency ($°C^{-1}$)	0.01	0.01	0.03	0.02	0.05	0.008–0.009	0.002–0.04	0.003–0.005	0.007–0.011	0.017–0.039
Reference temp (°C)	110–120	135	210–230	160–170	300–280	210	280	250	180	200
Heat capacity ($kJ\,kg^{-1}\,K^{-1}$)	1.55–1.75	1.55–1.76	1.13–1.55	1.63–1.76	1.17–1.4	1.3–1.6	1.2–1.4	1.47–2.15	1.3–1.6	0.9–1.1
Solid/melting sections										
Bulk density of solids ($g\,cc^{-1}$)	0.52–0.59	0.52–0.60	0.8–1.0	0.5–0.6	0.7–0.9	0.4–0.6	0.5–0.6	0.65–0.75	0.5–0.6	0.8–1.0
Heat capacity of solid ($kJ\,kg^{-1}\,K^{-1}$)	1.55–1.75	1.55–1.76	1.13–1.55	1.63–1.76	1.17–1.4	1.3–1.6	1.2–1.4	1.47–2.15	1.3–1.6	0.9–1.1
Thermal conductivity of solids ($W\,m^{-1}\,K^{-1}$)	0.25–0.35	0.3–0.4	0.25–0.35	0.13–0.2	0.18–0.23	0.18–0.33	0.1–0.13	0.2–0.3	0.16–0.25	0.12–0.29
Density of solid–melting region ($g\,cc^{-1}$)	0.52–0.59	0.52–0.60	0.8–1.0	0.5–0.6	0.7–0.9	0.4–0.6	0.5–0.6	0.65–0.75	0.5–0.6	0.8–1.0
Heat capacity of solid–melting region ($kJ\,kg^{-1}\,K^{-1}$)	2.05–2.24	2.05–2.25	1.95–2.43	2.4–2.6	1.17–1.4	1.3–1.6	1.2–1.4	2.38–3.49	1.3–1.6	0.9–1.1
Melting temp (°C)	110–120	120–130	275	160–175	200–210	170–180	160–170	225–250	165–170	130–140
Heat of fusion ($J\,g^{-1}$)	80–100	138–245	137	234	0	0	0	190–260	0	0

polymer blend system with a comparibilizer, which means that the material components in the formulation are fixed, design of a screw configuration and optimization of extrusion blending process operation conditions are critical to manufacture a polymer blend product with target properties for a specific application. As previously discussed, the final properties and performance of the polymer blend are directly related to the morphology development of the polymer blend.

Commercial polymer blending operation generally begins with the components in pellet or powder form with mean particle sizes ranging from 3 to 0.1 mm. Target morphologies for the final product often require domain sizes in the range 0.1–10 μm to achieve superior performance characteristics. To achieve the target morphology of the blend system of interest through the mixing process of each component, the components in solid form must melt first. The manufacturing of polymer blends with targeted properties and performances in a screw extruder is a complex process involving various steps:

- pre-treatment of components in blend formulation,
- feeding (feeding solid or/and liquid materials, and sequence of feeding),
- melting,
- mixing (dispersive and distributive),
- interfacial reaction,
- devolatilization of residuals,
- product formation (pellet or other product forms).

In addition to the morphology development during the melt blending extrusion process, the commercial manufacturing process of polymer blends should be designed such that the economics of polymer blend manufacturing is acceptable from a market standpoint. Process control becomes important in applying the right amount of energy in the right place for the right amount of time to affect the blending process to produce a uniform product with an economical use of energy.

There are two distinguished melting mechanisms in screw-type processing machine though each continuous processing machine shows different melting mechanisms. The maximum shear stress, accompanied with frictional and extensional forces, in a reactive blending process is usually generated at the melting zone of an intermeshing co-rotating twin-screw extruder. In this melting region, each component is ground and dispersed as a result of undergoing strong dispersive mixing effects. Under dissipative melting each polymeric component changes into very small particles as droplets within a very short time, typically 0.1–10 s.

Screw configuration design in the melting zone is a very important factor for achieving the complete melting of solid polymers and must be optimized to prevent excessive mechanical energy input from the motor. Too aggressive design in the melting zone will enhance the complete melting of polymer blend in shorter melting zone length, but will increase the melt temperature significantly due to the higher specific energy consumption in the melting zone with the aggressive design. The mechanical energy from the drive motor is transferred to the polymer melt via the rotation of screw and is converted into the thermal energy. Maintaining the melt temperature below the critical temperature where side reactions such as thermal

degradation, crosslinking, or any undesired reaction is required for certain applications. In this case, the design of the melting zone is important not only to control the mechanical energy input from the motor but also to prevent excessive heat generation during the melting process.

The domain size of the dispersed phase in a polymer blend reduces significantly after the melting zone; a downstream mixing zone(s) will also be required to complete the interfacial reaction and morphology development. As discussed in Section 6.4.1, various screw, kneading disc block, and special distributive mixing elements are commercially available for various applications of intermeshing co-rotating twin-screw extruders. The modeling and simulation of extrusion process along with baseline experimental data will help processing engineers to find the optimum screw configuration design.

Alternatively, the specific energy input to the polymer blend melt from the drive motor of an intermeshing co-rotating twin-screw extruder can be estimated by Eqs. (6.45) and (6.46). The specific energy is defined here as the amount of energy required to increase the temperature of the polymer from 25 °C up to the processing temperature. The amount of energy supplied to the extruder can be expressed as a specific mechanical energy input (SEI), which is estimated from the power input calculation:

$$P_{\mathrm{m}} = P_{\max} \times \frac{N}{N_{\max}} \times \frac{Amp}{Amp_{\max}} = P_{\max} \times \frac{N}{N_{\max}} \times \text{Torque}\,\% \tag{6.45}$$

where

P_{m} represents the power input to the melt from a drive motor of an extruder via the rotation of screws in kW,
$P_{\max}$ is the rated maximum motor power for the extruder (kW),
$N_{\max}$ is the rated extruder maximum screw speed for the extruder,
$Amp_{\max}$ is the rated maximum amperage for the extruder,
N is the actual operating screw rotational speed,
Amp is actual the operating amperage.

The SEI can be estimated using Eq. (6.46):

$$\mathrm{SEI}\ (\mathrm{Jg}^{-1}) = \frac{P_{\mathrm{m}}\ (\mathrm{kW}) \times 3600\ (\mathrm{sh}^{-1}) \times 0.9}{Q\ (\mathrm{kgh}^{-1})} \tag{6.46}$$

where Q is represents the mass per unit time of the polymer mixture fed into the devolatilizing extruder and P_{m} is as defined in Eq. (6.45). In Eq. (6.46), the 0.9 factor represents an estimate of the fraction of the power P_m that is transmitted to the screw (s), and reflects, for example, power losses within the motor and in the gearbox. From Eqs. (6.45) and (6.46), we can recognize that the SEI for a given polymer blend system can be controlled via a drive motor size, maximum screw speed and drive torque available, screw speed, rate, and screw configuration design. At the same operating conditions, such as the same rate and screw speed, the screw configuration with more

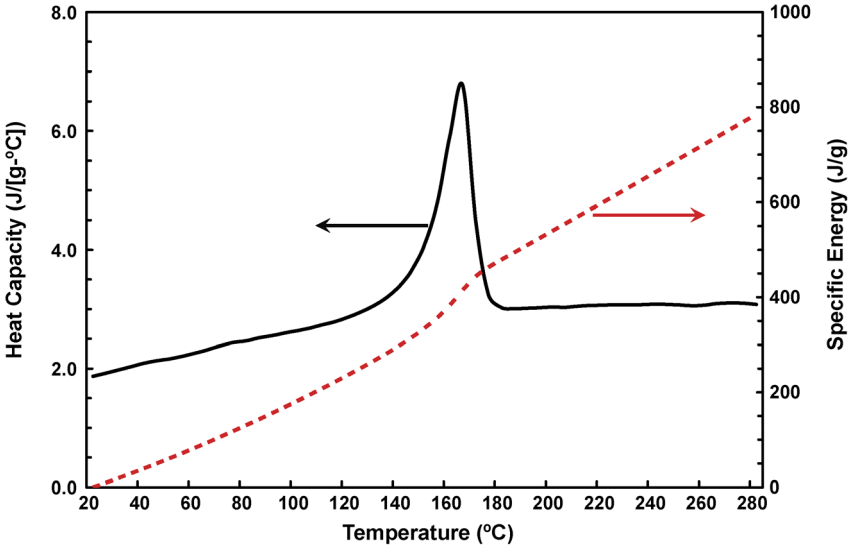

Figure 6.29 Heat capacity and specific energy for polypropylene (PP).

kneading disc block elements will require more SEI. The selection of the element module in both melting and mixing zones is very important to control the SEI, residence time distribution, and hence morphology development. If the liquid injection or downstream addition of solid material as well as devolatilization of the residuals during the reactive blending process are desired, the design of screw configuration and barrel configuration become even more important.

Once the SEI is estimated, then the increase in the blend melt temperature by the specific energy input during the blending extrusion process can be estimated using heat capacity data. The heat capacity data for a given polymer system is integrated with respect to temperature to calculate the specific energy (or specific enthalpy) in $J\,g^{-1}$ as shown in Figure 6.29:

$$\hat{E}\left(J\,g^{-1}\right) = \int_{25}^{T} C_p dT \tag{6.47}$$

For example, if an intermeshing co-rotating twin-screw extruder extrudes polypropylene resin at a specific energy of $600\,J\,g^{-1}$, and the measured discharge temperature of the polypropylene melt is 260 °C, then about $120\,J\,g^{-1}$ must have been transferred out through the barrel wall as an energy flux.

Once the reactive blending process of polymers using an intermeshing co-rotating twin-screw extruder is appropriately designed and optimized, the reactive blending process has to be scaled up to commercial production. The problem of scale-up in single-screw extruder has long attracted serious attention [162–174]. The problem of scale-up in intermeshing co-rotating twin-screw extruder has also discussed by

various investigators [175, 176]. Equation (6.48) is typically used to scale up an intermeshing co-rotating twin-screw extruder:

$$\frac{Q_1}{Q_2} = \left(\frac{D_1}{D_2}\right)^{\alpha} \tag{6.48}$$

where

Q_1 is the feed rate used for a laboratory-scale or pilot plant-scale intermeshing co-rotating twin-screw extruder ($kg\,h^{-1}$),
Q_2 is the target production rate ($kg\,h^{-1}$),
D_1 is the screw diameter of a laboratory-scale or pilot plant-scale intermeshing co-rotating twin-screw extruder (mm),
D_2 is the screw diameter of a production-scale intermeshing co-rotating twin-screw extruder,
α is the scale-up factor.

Typically, a scale-up factor of 2.7–3.0 is used for general compounding without any solvent involved, and a scale-up factor of 2.3–2.7 is used for special compounding and reactive extrusion, while a scale-up factor of 2.0–2.3 is used for dewatering and devolatilization extrusion processes with a large amount of solvent.

Todd's 1998 book *Plastic Compounding: Equipment and Processing* [176] is a good technological treatment from machinery manufacturers and is recommended to the reader.

6.6 Concluding Remarks

The development of a new polymer blend material is closely related to the control of the morphology development and reaction at interface (compatibilization method). The presence of an interfacial reaction during blending of two polymers allows the effective achievement of desirable performance characteristics. This is realized primarily through control and stabilization of the morphology. The reaction also has a strong influence on the evolution of blend morphology development even in the very early stages of domain deformation at the onset of melting. As the size scale of the domains is reduced and the extent of reaction increases during the melting and melt flow stages, effects of the interfacial reaction become even more important. The reaction affects several separate parameters that influence the size of the dispersed phase domains, including the formation of a copolymer at the interface, which reduces the interfacial tension, and changes in the rheological properties of the blend and reduction in the rate of particle–particle coalescence due to the presence of the copolymer. Today, controlling the morphology and interface of polymer blends is achieved more and more by reactive compatibilization using reactive polymers. The formation of the copolymer at the interface, where it is needed most directly during the melt blending, leads to a significant reduction in particle size and significant

reinforcement of the interfacial toughness without having to synthesize the copolymer separately. It is possible to vary the particle size over two orders of magnitude by only changing the amount of the copolymer formed in the blends while maintaining the same processing conditions.

The modular co-rotating twin-screw extruder is the most widely used of all twin-screw extruders. There is probably no application for twin-screw extruders to which it has not been applied. Applications include all aspects of compounding and blending of thermoplastics with particulates, oils, and other polymers. The machine is also widely used for removal of liquids, that is, devolatilization and for reactive extrusion. The modular co-rotating twin-screw extruder has also been used for both polymerization and for grafting reactions.

The general direction of modular co-rotating twin-screw extruder is to increase productivity. This has been accomplished in recent years by (i) deepening screw channels and (ii) increasing screw speeds and machine torque capacity. There are a few advantages of reactive extrusion in twin-screw extruders. They include high levels of local mixing, which can be produced by suitable modular screw designs and choices of elements (especially mixing elements), as well as possible special designs of feed ports. There are, however, disadvantages. Reaction times need to be small because of the low residence times of twin-screw extruders. Heat transfer is poor, especially as screw diameters increase.

Formation of the morphology and the interface of the polymer blends in an intermeshing co-rotating twin-screw extruder is an extremely complex process involving many steps. These steps are related to selection of polymer blend system for optimum materials' thermal, physical, rheological, and thermodynamic properties as well as the interfacial chemistry, the machine type and size, and the processing conditions. In early studies about the morphology of polymer blends, it is assumed that the base polymer components are already molten and that one polymer phase is dispersed in the other and the final dispersed phase particle size is not achieved yet. It is now known that melting/plastification not only has a significant bearing on the morphology development but also on the ultimate scale of dispersion of reactive blends. Moreover, the steps involved in the morphology development occur simultaneously. Thus, both the design of reactive blending extrusion process, including the optimum screw and barrel configuration designs, and control operating conditions such as rate, screw speed, and operation temperature are extremely important during reactive melt blending to manufacture the blend products with targeted properties.

Abbreviations

ABS	Acrylonitrile butadiene styrene
LDPE	Low density polyethylene
HDPE	High density polyethylene
PA6	Polyamide 6
PC	Polycarbonate

PET	Polyethylene terephthalate
PMMA	Polymethylmethacrylate
PP	Polypropylene
PS	Polystyrene
PVC	Polyvinylechloride
SEBS-g-MA	Maleic anhydride grafted styrene-ethylene-co-butadiene-styrene tri-block copolymer
SEI	Specific energy input
TME	Turbine mixing element
ZME	Zahn Misch element

Symbols

A	area
A_0	initial area
Amp	amperage
Amp_{max}	maximum amperage of an extruder
a	initial radius of a drop
B	axial distance between successive flights
$\bar{B}$	breadth of drop
$\mathbf{C}$	Green deformation tensor
C_L	centerline distance
C_p	heat capacity
C_{ij}	arrays of the Green deformation tensor
D	diameter
d	droplet diameter
$\mathbf{d}$	rate of deformation tensor
d_{ij}	arrays of the rate of deformation tensor
ds	deformation
$\mathrm{d}s/\mathrm{d}t$	deformation rate of change
$\boldsymbol{dx}$	differential line element
$\boldsymbol{dX}$	differential line element after deformation and displacement
E	elongation rate
$\hat{E}$	specific energy
e	perpendicular width of the flights
f	fill factor
H	screw channel depth
H_{max}	maximum screw channel depth
L	length
l_d	length of a cube of a lower concentration component
M	torque
N	screw rotational speed
N_{max}	maximum screw rotational speed of an extruder
N_T	number of tips

P	pressure
P_m	power input to the melt
P_{max}	maximum motor power of an extruder
p	viscosity ratio ($=\eta'/\eta$)
$\hat{Q}$	volumetric flow rate
Q	throughput rate
q_e	experimental growth rate
q_t	predicted growth rate
R	radius
R_B	radius of screw root
R_0	initial thread radius
R_s	screw radius
r	striation thickness
S	pitch
s	shear
T	temperature
t	time
t_R	mean residence time
V_f	free volume in the screw channel
v_i	flow velocity in principal directions
W	screw channel width
X_m	wave number
x_i	principal directions.

Greek Symbols

α	angle made by each screw tip in the circumference
α_i	angles with respect to principal axes
γ	shear strain
$\dot{\gamma}$	shear rate
$\dot{\gamma}_b$	shear rate at drop burst
δ_f	clearance between screw tip and barrel inner surface
η	melt shear viscosity
η'	shear viscosity of liquid filament
η_d	melt shear viscosity of a dispersed component
η_m	melt shear viscosity of a matrix component
θ	angle swept out by the screw as it rotates
κ	interfacial tension
λ	wavelength of disturbance
λ_i	principal axes
ξ_i	helical axes
ϱ_c	ratio of centerline distance and screw radius
ϕ	helix angle
ϕ_d	volume fraction of a dispersed component

ϕ_m volume fraction of a matrix component
ϕ_v volume fraction
ψ angle made by screw channel in the circumference
Ω growth rate

References

1 White, J.L. and Min, K. (1988) *Makromol. Chem., Macromol. Symp.*, **16**, 19.
2 Utracki, L.A. (1989) *Polymer Alloys and Blends*, Hanser, Munich.
3 Utracki, L.A. (1998) *Commercial Polymer Blends*, Chapman & Hall, London.
4 Baker, W., Scott, C., and Hu, G.H. (eds) (2001) *Reactive Polymer Blending*, Hanser, Munich.
5 Paul D.R. and Newman, S. (eds) (1978) *Polymer Blends*, Academic Press, New York.
6 Olabishi, O., Robeson L.M., and Show, M.T. (1979) Polymer-Polymer Miscibility, Academic Press, New York.
7 Folkes, M.J. (1993) *Polymer Blends* and Alloys, Blackie, London.
8 Solc, K. (1982) *Polymer Compatibility and Incompatibility: Principles and Practices*, Harwood Academic, New York.
9 Fayt, R., Jerôme, R., and Teyssié, Ph. (1981) *J. Polym. Sci., Polym. Lett. Ed.*, **19**, 79;Fayt, R., Jerôme, R., and Teyssié, Ph. (1986) *J. Polym. Sci., Polym. Lett. Ed.*, **24**, 25;Fayt, R., Jerôme, R., and Teyssié, Ph. (1986) *Makromol. Chem.*, **187**, 837;Fayt, R., Jerôme, R., and Teyssié, Ph. (1982) *J. Polym. Sci., Polym. Phys. Ed.*, **20**, 2209; Fayt, R., Jerôme, R., and Teyssié, Ph. (1989) *J. Polym. Sci., Polym. Phys. Ed.*, **27**, 775;Fayt, R., Jerôme, R., and Teyssié, Ph. (1987) *Polym. Eng. Sci.*, **27**, 328;Fayt, R., Jerôme, R., and Teyssié, Ph. (1990) *Polym. Eng. Sci.*, **30**, 937.
10 Fayt, R. and Teyssié, Ph. (1986) *Macromol*, **19**, 2077;Fayt, R. and Teyssié, Ph. (1989) *J., Polym., Sci.,, Polym., Lett. Ed.*, **27**, 481.
11 Heikens, D., Hoen, N., Barentsen, W., Piet, P., and Ladan, H. (1978) *J. Polym. Sci. Polym. Symp.*, **62**, 309.
12 Bywater, S. (1984) *Polym. Eng. Sci.*, **24**, 104.
13 Barlow, J.W. and Paul, D.R. (1984) *Polym. Eng. Sci.*, **24**, 525.
14 Jerome, R., Fayt, R., and Teyssié, Ph. (1987) *Polym. Eng. Sci.*, **27**, 328.
15 Paul, D.R. (1987) Compatibilization of polymer blends by styrene/hydrogenated butadiene block copolymers, in *Thermoplastic Elastomers: a Comprehensive Review* (eds N.R. Legge, G. Holden, and H.E. Schroeder), Hanser, Munich, Chapter 12, Section 6.
16 Teyssié, Ph., Fayt, R., and Jerome, R. (1988) *Makromol. Chem. Macromol. Symp.*, **16**, 41.
17 Fayt, R., Jerome, R., and Teyssié, Ph. (1989) *ACS Symp. Ser.*, **395**, 38.
18 Spencer, R.S. and Wiley, R.M. (1951) *J. Colloid Sci.*, **6**, 133.
19 Mohr, W.D. (1959) Mixing and Dispersing, in *Processing of Thermoplastic Materials* (ed. E.C. Bernhardt), Reinhold, New York, chapter 3, pp. 117–152.
20 Mohr, W.D., Saxton, R.L., and Jepson, C.H. (1957) *Ind. Eng. Chem.*, **49**, 1855.
21 Erwin, L. (1978) *Polym. Eng. Sci.*, **18**, 738.
22 Erwin, L. (1978) *Polym. Eng. Sci.*, **18**, 1044.
23 Erwin, L. (1978) *Polym. Eng. Sci.*, **18**, 572.
24 Ng, K.Y. and Erwin, L. (1981) *Polym. Eng. Sci.*, **21**, 212.
25 Ottino, J.M., Ranz, W.E., and Macosko, C.W. (1981) *AIChE J.*, **27**, 565.
26 Ottino, J.M. (1983) *AIChE J.*, **29**, 159.
27 Ottino, J.M. and Chella, R. (1983) *Polym. Eng. Sci.*, **23**, 357.
28 Truesdell, C. and Toupin, R.A. (1960) The classical field theories, in *Handbuch der Physik*, vol. **III**, pt. 1, Springer Verlag, Berlin, pp. 226–793.
29 Bergen, J.T. (1959) Mixing and Dispersing Processes, in *Processing of Thermoplastic Materials* (ed. E.C. Bernhardt), Reinhold, New York, chapter 7, pp. 405–446.

30 Bolen, W.R. and Colwell, R.E. (1958) *SPE J.*, **14**, 24;Bolen, W.R. and Colwell, R.E. (1958) *SPE ANTEC Tech. Papers*, **4**, 1004.

31 Manas-Zloczower, I., Nir, A., and Tadmore, Z. (1982) *Rubber Chem. Technol.*, **55**, 1250.

32 Manas-Zloczower, I. and Feke, D.L. (1989) *Int. Polym. Process.*, **4**, 3.

33 Rwei, S.P., Manas-Zloczower, I., and Feke, D.L. (1990) *Polym. Eng. Sci.*, **30**, 701.

34 Rwei, S.P., Manas-Zloczower, I., and Feke, D.L. (1991) *Polym. Eng. Sci.*, **31**, 558.

35 Rwei, S.P., Manas-Zloczower, I., and Feke, D.L. (1992) *Polym. Eng. Sci.*, **32**, 130.

36 Young, T. (1805) *Philos. Trans. R. Soc.*, **5**, 65.

37 Strutt, J.W.(Lord Rayleigh) (1894), *Theory of Sound*, 2nd edn, MacMillan, London.

38 Maxwell, J.C. (1878) Surface Tension, Encyclopedia Britannica.

39 Quincke, G. (1876) *Ann. Phys. Chem. (Poggendorfl)*, **19**, 1;Quincke, G. (1871) *Philos. Mag*, **41**, 245.

40 Taylor, G.I. (1932) *Proc. R. Soc. London, Ser. A*, **138**, 41.

41 Taylor, G.I. (1934) *Proc. R. Soc. London, Ser. A*, **146**, 501.

42 Tomotika, S. (1935) *Proc. R. Soc. London, Ser. A*, **150**, 322.

43 Andreas, J.M., Hauser, E.A., and Tucker, W.B. (1938) *J. Phys. Chem.*, **42**, 1001.

44 Chappelear, D.C. (1964) *ACS Polym. Prepr.*, **5**, 363.

45 Wu, S. (1969) *J. Colloid Interface Sci.*, **31**, 153.

46 Wu, S. (1970) *J. Phys. Chem.*, **74**, 632.

47 Wu, S. (1971) *J. Polym. Sci.*, **34**, 19.

48 Roe, R.J. (1969) *J. Colloid Interface Sci.*, **31**, 228.

49 Patterson, H.T., Hu, K., and Grindstaff, T.H. (1971) *J. Polym. Sci.*, **C34**, 31.

50 Gaines, G.L. (1972) *Polym. Eng. Sci.*, **12**, 1.

51 Wu, S. (1974) *J. Macromol. Sci. Rev. Macromol. Chem.*, **C10**, 1.

52 Elmendorp, J.J. (1986) *Polym. Eng. Sci.*, **26**, 418.

53 Anastasiadis, S.H., Chen, J.K., Koberstein, J.T., Sohn, J.F., and Emerson, J.A. (1986) *Polym. Eng. Sci.*, **26**, 1410.

54 Escudie, E., Gracia, A., and Lachaisw, J. (1986) *J. Mater. Chem. Phys.*, **14**, 239.

55 Carriere, C.J., Cohen, A., and Arends, C.B. (1989) *J. Rheol.*, **33**, 681.

56 Cohen, A. and Carriere, C.J. (1989) *Rheol. Acta*, **28**, 223.

57 Elemans, P.H.M., Janssen, J.M.H., and Meijer, H.E.H. (1990) *J. Rheol.*, **34**, 1311.

58 Carriere, C.J. and Cohen, A. (1991) *J. Rheol.*, **35**, 205.

59 Sammler, R.L., Dion, R.P., Carriere, C.J., and Cohen, A. (1992) *Rheol. Acta*, **31**, 554.

60 Chen, C.C. and White, J.L. (1991) *SPE ANTEC Tech Papers*, **37**, 968;Chen, C.C. and White, J.L. (1993) *Polym. Eng. Sci.*, **33**, 923.

61 Yoon, P.J. and White, J.L. (1994) *J. Appl. Polym. Sci.*, **51**, 1515.

62 White, J.L. (2001) Mechanisms of Mixing and Dispersion, in *Polymer Mixing: Technology and Engineering* (eds J.L. White, A.Y. Coran, and A. Moet), Hanser, Munich, pp. 1–23.

63 Pickering, S.U. (1917) *J. Chem. Soc.*, **111**, 86.

64 Harkins, W.D., Davies, E.C.H., and Clarke, G.L. (1917) *J. Am. Chem. Soc.*, **39**, 541.

65 Langmuir, I. (1917) *J. Am. Chem. Soc.*, **39**, 1848.

66 White, J.L. (1990) *Principles of Polymer Engineering Rheology*, John Wiley & Sons, Inc., New York.

67 Middleman, S. (1967) *The Flow of High Polymers*, John Wiley & Sons, Inc., New York.

68 Vinogradov, G.V. and Malkin, A.Y. (1980) *Rheology of Polymers*, Mir, Moscow.

69 Dealy, J.M. and Wissbrun, K.F. (1990) *Melt Rheology and Its Role in Plastics Processing: Theory and Applications*, Van Nostrand Reinhold, New York.

70 Macosko, C.W. (ed.) (1994) *Rheology: Principles, Measurements, and Applications*, VCH, New York.

71 Han, C.D. (1981) *Multiphase Flow in Polymer Processing*, Academic Press, New York.

72 Collyer, A.A. and Clegg, D.W. (eds) (1988) *Rheological Measurements*, Elsevier Applied Science, London.

73 Utracki, L.A. (ed.) (1991) *Two-Phase Polymer Systems*, Hanser, Munich.

74 Lim, S. and White, J.L. (1993) *Int. Polym. Process.*, **8**, 119.

75 Scott, C.E. and Macosko, C.W. (1991) *Polym. Bull.*, **26**, 341.
76 Sundararaj, U., Macosko, C.W., Rolando, R.J., and Chan, H.T. (1992) *Polym. Eng. Sci.*, **32**, 1814.
77 Lindt, J.T. and Ghosh, A.K. (1992) *Polym. Eng. Sci.*, **32**, 1802.
78 Tomotika, S. (1936) *Proc. R. London Soc., Ser. A*, **153**, 302.
79 Strutt, J.W. (1892) (Lord Rayleigh), *Philos. Mag.*, **34**, 145.
80 Rumscheidt, F.D. and Mason, S.G. (1961) *J. Colloid Sci.*, **16**, 238.
81 Karam, H.J. and Bellinger, J.C. (1968) *IEC Fund*, **7**, 576.
82 Chin, H.B. and Han, C.D. (1980) *J. Rheol.*, **24**, 1.
83 Bartok, W. and Mason, S.G. (1957) *J. Colloid Sci.*, **12**, 243.
84 Rumscheidt, F.D. and Mason, S.G. (1961) *J. Colloid Sci.*, **16**, 210.
85 Torza, S., Cox, R.G., and Mason, S.G. (1972) *J. Colloid Interface Sci.*, **38**, 395.
86 Kumar, R. and Saradhy, V. (1972) *IEC Fundam.*, **11**, 307.
87 Flumerfelt, R.D. (1972) *IEC Fundam.*, **11**, 312.
88 Elmendorp, J.J. and Maalke, R.J. (1985) *Polym. Eng. Sci.*, **25**, 1041.
89 Grace, H.P. (1982) *Chem. Eng. Commun.*, **14**, 225.
90 Danesi, S. and Porter, R.S. (1978) *Polymer*, **19**, 448.
91 Min, K., White, J.L., and Feller, J.F. (1984) *Polym. Eng. Sci.*, **24**, 1327.
92 Chen, C.C., Fontan, E., Min, K., and White, J.L. (1988) *Polym. Eng. Sci.*, **28**, 69.
93 Wu, S. (1987) *Polym. Eng. Sci.*, **27**, 335.
94 Nelson, C.J., Avgeropoulos, C.N., Weissert, F.C., and Bohm, G.G.A. (1977) *Angew. Makromol. Chem.*, **60/61**, 49.
95 Liang, B.R., White, J.L., Spruiell, J.E., and Goswami, B.C. (1993) *J. Appl. Polym. Sci.*, **28**, 2011.
96 Endo, S., Min, K., White, J.L., and Kyu, T. (1986) *Polym. Eng. Sci.*, **26**, 45.
97 Ghiam, F. and White, J.L. (1991) *Polym. Eng. Sci.*, **31**, 76.
98 White, J.L. and Kim, E.K. (2010) *Twin Screw Extrusion: Technology and Principles*, 2nd edn, Hanser, Munich.
99 Wunsche, A. (1901) German Patent, 131,392.
100 Martelli, F. (1971) *Soc. Plast. Eng. J.*, **27**, 67.
101 Booy, M.L. (1978) *Polym. Eng. Sci.*, **18**, 973.
102 Denson, C.D. and Hwang, B.K. (1980) *Polym. Eng. Sci.*, **20**, 965.
103 Erdmenger, R. (1978) *Schneckenmaschinen fur die Hochviskos – Verfahrenstechnik*, Bayer AG, Leverkusen.
104 Erdmenger, R. (1962) *Chem. Ing. Tech.*, **34**, 751.
105 Erdmenger, R. (1964) *Chem. Ing. Tech.*, **35**, 175.
106 Nelson, W.K. (1932) US Patent (filed June 4, 1931) 1,868,671.
107 Erdmenger, R. (1951) German Patent (filed September 29, 1949) 813,154.
108 Erdmenger, R. (1954) US Patent (filed September 20, 1950) 2,670,188.
109 Riess, K. and Erdmenger, R. (1951) *VDI Zeit.*, **93**, 633.
110 Telle, O. and Erdmenger, R. (1956) German Patent (filed July 22, 1953) 945,686.
111 Erdmenger, R. (1956) German Patent (filed July 28, 1953) 940,109;Erdmenger, R. (1957) US Patent (filed July 27, 1954) 2,814,472.
112 Werner, H. (1976) Das Betriebsverhalten der zweiwelligen Knetscheibenpresse vom Typ ZSK bei der Verarbeitung von hochviskosen Flüssigkeiten, Dr. Ing Dissertation, University of Munich.
113 Werner, H. and Else, K. (1979) *SPE ANTEC Tech. Papers*, **25**, 181.
114 Szydlowski, W., Brzoskowski, R., and White, J.L. (1987) *Int. Polym. Process.*, **1**, 207.
115 Szydlowski, W. and White, J.L. (1988) *Int. Polym. Process.*, **2**, 148.
116 Kraffe de Laubarede, L. (1953) US Patent (filed July 10, 1950), 2,631,016.
117 Colombo, R. (1966) US Patent (filed January 15, 1964) 3,252,182.
118 Loomans, B.A. (1969) US Patent (filed January 12, 1967) 3,423,074.
119 Ullrich, M. and Rathjen, C. (1982) European Patent Application 0.049,835 A2.
120 Ullrich, M. and Rathjen, C. (1986) *Chem. Ing. Tech.*, **58**, 590.

121 Burbank, F., Baruer, F., and Andersen, P. (1991) *SPE ANTEC Tech. Papers*, **37**, 149.

122 Grillo, J., Andersen, P., and Papazoglou, E. (1992) *SPE ANTEC Tech. Papers*, **38**, 20.

123 Valsamis, L.N., Canedo, E.L., Pereira, J.M., and Poscich, D.U. (1996) U.S. Patent (filed June 3, 1994) 5,487,602.

124 Herrmann, H. (1966) *Chem. Ing. Tech.*, **38**, 25.

125 Todd, D.B. and Irving, H.F. (1969) *Chem. Eng. Prog.*, **65** (9), 85.

126 Todd, D.B. (1975) *Polym. Eng. Sci.*, **15**, 437.

127 Sakai, T. (1978) *Gosé Jushi*, **24**, 7.

128 Herrmann, H. and Eise, K. (1981) *SPE ANTEC Tech. Papers*, **39**, 614.

129 Hornsby, P.R. (1983) Plastic Compounding, (Sept/Oct) 65.

130 Potente, H. and Ansahl, J. (1990) *Kunststoffe*, **86**, 926.

131 Cassagnau, P., Mijangos, C., and Michel, A. (1991) *Polym. Eng. Sci.*, **31**, 772.

132 Bur, A.J. and Gallant, F.M. (1991) *Polym. Eng. Sci.*, **31**, 1365.

133 Kim, P.J. and White, J.L. (1994) *Int. Polym. Process.*, **9**, 108.

134 Kye, H. and White, J.L. (1994) *J. Appl. Polym. Sci.*, **52**, 1249.

135 Fie, X., Tomayko, D., Bigio, D.I., and Batch, G. (1997) *SPE ANTEC Tech. Papers*, **43**, 89.

136 Shon, K., Chang, D., and White, J.L. (1999) *Int. Polym. Process.*, **19**, 44.

137 Plochocki, A.P., Oacci, S.S., and Mack, M.H. (1988) *Kunststoffe*, **78**, 254.

138 Bordereau, V., Shi, Z.H., Utracki, L.A., Sammut, P., and Carrega, M. (1992) *Polym. Eng. Sci.*, **32**, 1869.

139 Lim, S. and White, J.L. (1992) *SPE ANTEC Tech. Papers*, **38**, 2682.

140 Setua, D.K., Lim, S., and White, J.L. (1992) *SPE ANTEC Tech. Papers*, **38**, 2686.

141 Lim, S. and White, J.L. (1994) *Polym. Eng. Sci.*, **34**, 221.

142 Gogos, C., Essegnir, M., Yu, D.W., Todd, D.B., and Curry, J.E. (1994) *SPE ANTEC Tech. Papers*, **40**, 270.

143 Vainio, T.P., Harkin, A., and Seppala, J.V. (1995) *Polym. Eng. Sci.*, **35**, 225.

144 Huneault, M.A., Champagne, M.F., and Luciani, A. (1996) *Polym. Eng. Sci.*, **36**, 1694.

145 Cho, J.W. and White, J.L. (1996) *Int. Polym. Process.*, **11**, 21.

146 Lee, S.H. and White, J.L. (1996) *SPE ANTEC Tech. Papers*, **42**, 316.

147 Lee, S.H. and White, J.L. (1997) *Int. Polym. Process.*, **12**, 316;Lee, S.H. and White, J.L. (1998) *Int. Polym. Process.*, **13**, 247.

148 Scott, C.E. and Lazo, N.D.B. (2001) Morphological and Rheological Aspects of Reactive Polymer Blending in *Reactive Polymer Blending* (eds W. Baker, C. Scott, and G.H. Hu), ch. 5, Hanser, Munich, pp. 113–141.

149 Hu, G.H. (2001) Reactive Blending in Screw Extruder in *Reactive Polymer Blending* (eds W. Baker, C. Scott, and G.H. Hu), ch. 6, Hanser, Munich, pp. 142–179.

150 White, J.L. and Kim, E.K. (2010) Flow Mechanisms and Modeling of Intermeshing Co-Rotating Twin Screw Extruders in *Twin Screw Extrusion: Technology and Principles*, 2nd edn, ch. 5, Hanser, Munich, 93–122.

151 Potente, H., Melisch, U., and Flecke, J. (1996) *SPE ANTEC Tech. Papers*, **42**, 334.

152 Potente, H., Bastian, M., and Flecke, J. (1999) *Adv. Polym. Technol.*, **18**, 147.

153 Canedo, E.L. (1999) *SPE ANTEC Tech. Papers*, **45**, 310.

154 Delamare, L. and Vergnes, B. (1996) *Polym. Eng. Sci.*, **36**, 1685.

155 Vergnes, B., Dellavalle, G., and Delamare, L. (1998) *Polym. Eng. Sci.*, **38**, 1781.

156 White, J.L., Keum, J.M., Jung, H., Ban, K., and Bumm, S.H. (2006) *Polym. Plastics Technol. Eng.*, **45**, 539.

157 Bawiskar, S. and White, J.L. (1997) *Int. Polym. Process.*, **12**, 331.

158 Wang, Y., White, J.L., and Szydlowski, W. (1989) *Int. Polym. Process.*, **4**, 262.

159 White, J.L. and Chen, Z. (1994) *Polym. Eng. Sci.*, **34**, 229.

160 Shi, Z.H. and Utracki, L.A. (1992) *Polym. Eng. Sci.*, **32**, 1834.

161 Huneault, M.A., Shi, Z.H., and Utracki, L.A. (1995) *Polym. Eng. Sci.*, **35**, 115.

162 Carley, J.F., Mallouk, R.M., and McKelvey, J.M. (1953) *Ind. Eng. Chem.*, **45**, 974.

163 Carley, J.F. and McKelvey, J.M. (1953) *Ind. Eng. Chem.*, **45**, 989.

164 Carley, J.F. and Strub, R.A. (1953) *Ind. Eng. Chem.*, **45**, 970.
165 Mohr, W.D. and Mallouk, R.S. (1959) *Ind. Eng. Chem.*, **51**, 765.
166 Maddock, B.H. (1959) *SPE J.*, **15** (November), 983.
167 McKelvey, J.M. (1962) *Polymer Processing*, John Wiley & Sons, Inc., New York.
168 Maddock, B.H. (1974) *Polym. Eng. Sci.*, **14**, 853.
169 Fenner, R.T. (1975) *Polymer*, **16**, 298.
170 Pearson, J.R.A. (1976) *Plastics Rubber Process.*, 113.
171 Schenkel, G. (1972) *Ind. Anzeiger*, **94**, 113; Schenkel, G. (1973) *Kunststofftechnik*, **12**, 171, 203;Schenkel, G. (1978) *Kunststoffe*, **68**, 155.
172 Potente, H. and Fischer, P. (1977) *Kunststoffe*, **67**, 242.
173 Potente, H. (1978) *Rheol. Acta*, **17**, 406.
174 Potente, H. (1981) *Auslegen von Schneckenmaschinen Baureihen*, Hanser, Munich.
175 Davis, W.M. (1992) Heat Transfer in Extruder Reactors, in *Reactive, Extrusion: Principles and Practice* (ed. M. Xanthos), ch. 7, Hanser, Munich, pp. 257–282.
176 Todd, D.B. (ed.) (1998) *Plastics Compounding: Equipment and Processing*, Hanser, Munich.

7
Polymer Blend Compatibilization by Copolymers and Functional Polymers

Jose A. Covas, Luiz Antonio Pessan, Ana V. Machado, and Nelson M. Larocca

7.1
Introduction

7.1.1
Polymer Blends and the Need for Compatibilization

Blending polymers has become an essential and efficient procedure to develop new higher performance polymeric materials having a valuable combination of properties, under relatively short times and with low development and production costs [1–6]. In fact, polymer blending can create materials with targeted properties and competitive prices, allows for fine tuning of the properties via adjustments of composition, and provides an interesting route for plastics waste recycling. The market for polymer blend based materials has increased continuously and significantly during recent decades, especially for automotive, electrical and electronic, packaging, building and construction, and household applications. Polymer blending is usually performed in standard polymer processing equipment, such as twin-screw extruders. Thus, not only the financial risks inherent to the development of new materials are limited, but well-known scale-up, automation, and control techniques are readily available.

Since polymer blends result from the physical combination of at least two polymers, they are usually classified as either miscible or immiscible. As for other mixtures, polymer/polymer miscibility is governed by the laws of thermodynamics [3, 4]. To guarantee thermodynamic miscibility, the free energy of mixing (ΔG_m) should be negative. Since the monomer units in the polymer chains are covalently bonded to each other, the number of ways that they can be arranged in a mixture is limited. Thus, the entropy of mixing (ΔS_m) is very small for polymer mixtures and approaches zero for very high molecular weight polymers. Consequently, thermodynamics predicts that polymer/polymer miscibility has to result from the exothermic heat of mixing ($\Delta H_m < 0$). The latter occurs when the interactions between

Encyclopedia of Polymer Blends: Volume 2: Processing, First Edition. Edited by Avraam I. Isayev.
© 2011 Wiley-VCH Verlag GmbH & Co. KGaA. Published 2011 by Wiley-VCH Verlag GmbH & Co. KGaA.

neighboring segments of structurally different polymers are energetically more favorable than the intermolecular interactions between segment pairs. Examples of interactions yielding exothermic heats of mixing include hydrogen bonds and dipole–dipole and anionic interactions. However, most of the interesting polymer pairs are immiscible and actually possess poor physical and mechanical properties – thus compatibilization is necessary.

7.1.2 Compatibilization Routes

The central challenge of the compatibilization of immiscible polymer blends is to generate materials having a stable optimum morphology, that is, to maximize performance under service conditions [7–11]. Interface characteristics such thickness, strength, and interfacial tension strongly determine the bulk properties; poor chemical or physical interaction between two polymers usually implies a high interfacial energy and a low interfacial thickness. Compatibilization is a process of modifying the interfacial properties of immiscible polymer blends, resulting in the reduction of the interfacial tension and in the formation and stabilization of the desired morphology. Thus, compatibilization converts polymer blends into alloys that have the desired set of performance characteristics. In practice, it entails the incorporation of "interfacial agents," "emulsifiers," "adhesion promoters," or, more frequently, "compatibilizers." Usually, the chains of a compatibilizer have a blocky structure, with one constitutive block being miscible with one blend component and a second block being miscible with the other blend component. As a result, a fine and stabilized morphology can be created; the interfacial thickness increases and the interface is strengthened due to the interpenetration of the two types of chains across the interface.

Blend compatibilization can be promoted via several routes [5–11], including (i) *ex situ*, that is, adding a pre-synthesized copolymer to the components, (ii) *in situ*, that is, creating a copolymer during blend preparation, (iii) stabilizing the dispersed phase via dynamic vulcanization, or crosslinking, (iv) introducing specific interactions, (v) incorporating ionomers, and (vi) adding a small quantity of a co-solvent – a third component, miscible with both phases. Owing to the large amount of research work and practical applications of each of these routes, this chapter will focus on the compatibilization *ex situ,* by the addition of a pre-synthesized copolymer and *in situ,* by creating a copolymer during blend preparation. Machado *et al.* [11] have compared the efficiency of these two strategies for the compatibilization of polyamide/polyolefin blends. As shown in Figure 7.1, *ex situ* compatibilization yields the blend with the largest particle size and particle size distribution. Even though both blends exhibit dramatic changes in morphology from $L/D = 8$ to $L/D = 9$ (screw length/diameter ratio, L/D), morphology development of the *in situ* blend along the extruder is particularly fast, changes being only perceived up to $L/D = 9$. For the other compatibilization route, the initial developments in the first kneading block are also similarly quick, but a regular evolution along the barrel seems to be noticeable.

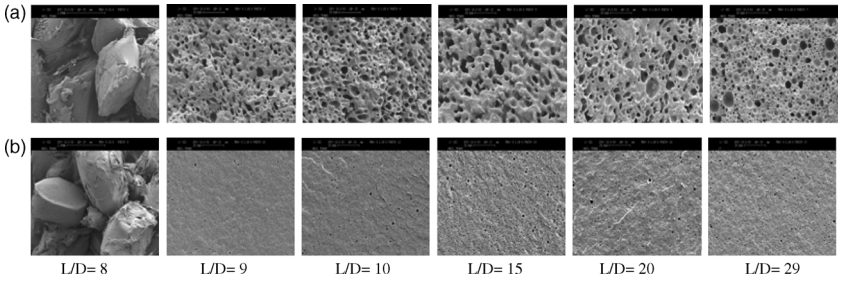

Figure 7.1 Scanning electron microscopy (SEM) micrographs of a polyamide/polyolefin compatibilized blend along the extruder: (a) *ex situ* and (b) *in situ* [11].

7.1.3
Reactive Extrusion/Processing

The use of extruders as continuous chemical reactors is nowadays commonly known as reactive extrusion (REX) and has proven to be a key technology in the polymer industry [12–14]. As explained above, the growing demands of specialty grades of plastic materials induced an increasing scientific and industrial interest in melt blending and also in the chemical modification of polymers. REX combines two operations traditionally separated, that is, chemical reactions (e.g., for the synthesis or modification of macromolecules, or the *in situ* compatibilization of polymer blends) and melt processing. Twin-screw extruders are often used, as they comply with the main requirements of REX. Xanthos [12] identified six types of reactions that can be performed by REX: bulk polymerization, grafting, interchain copolymer formation, coupling/crosslinking, controlled degradation, and functionalization (functional group modification).

Currently, REX is an important post-reactor technology to functionalize nonpolar polymers, or to adjust the functionality of polar polymers to specific applications and properties. In the field of polymer blends, functionalized polymers are currently employed to improve the compatibility and adhesion between immiscible polymers by a process called reactive blending.

7.2
Compatibilization by Copolymers

Ex situ compatibilization, or compatibilization by the addition of a pre-synthesized copolymer, provides an opportunity to easily control the molecular architecture of the additive to be used. Theoretically, block copolymers should seek the interfaces during melt mixing, to decrease unfavorable interactions [15, 16]. Therefore, block or graft copolymers whose segments are chemically identical to, or have affinity with, the polymer components are often used as emulsifiers to reduce the interfacial tension, promote the dispersion of one phase into the other, and stabilize the resulting blend [17]. Hence, the polymeric compatibilizer to be added to a blend

should have: (i) maximum miscibility with the individual polymeric components, (ii) the molecular weight of each block slightly higher than the molecular entanglement, and (iii) a concentration just above the critical micelle concentration [1].

Initially, the addition of a third polymeric component to a polymer blend was the most common compatibilization method. It was assumed that the compatibilizer would migrate to the interface, broadening the segmental concentration profile. However, it remains to be demonstrated that most of the copolymer added actually proceeds to the interface. Also, there is evidence that the addition of a block or graft copolymer reduces the interfacial tension and alters the molecular structure at the interface, but rarely increases the interphase thickness. Moreover, the actual preparation of the copolymer requires specific chemical routes and reaction conditions.

The influence of a block copolymer on the droplet breakup and coalescence in model immiscible PEP/PPO polymer blends was investigated by Ramic *et al.* [18], who found that the addition of 0.1 wt% or 1.0 wt% of PEO-b-PPO-b-PEO [poly (ethylene oxide)–poly(propylene oxide) copolymer] triblock copolymers facilitated breakup and inhibited coalescence. The steady-state droplet size resulting from breakup was reduced only slightly by the addition of 0.1 wt% copolymer, but more substantially by addition of 1 wt%. However, the kinetics of coalescence were suppressed effectively even when 0.1 wt% of copolymer was added. In these systems, the copolymer seems to reduce the efficiency of both droplet collision and film drainage and/or rupture.

Several researchers [19–24] carried out extensive studies on the use of emulsification curves to evaluate the efficiency of copolymers as compatibilizers. The evolution of the dispersed phase size with copolymer concentration was monitored. After an initial important decrease in the size of the dispersed phase domains with the addition of the copolymer, a leveling-off at higher copolymer concentrations was observed. The shape of the emulsification curve depended both on molecular weight and copolymer molecular architecture and on processing conditions. Similar work was performed by Zhang *et al.* [25], who studied the compatibilization efficiency of graft copolymers and the effect of the feeding mode on the compatibilization efficiency of polystyrene (PS) and polyamide 6 (PA-6) blends, using the emulsification curve approach. The feeding mode had a major effect on the size of the dispersed phase domains at short mixing times, its effect decreasing, or becoming negligible, at long mixing times. The molecular structure of the polystyrene–polyamide-6 graft copolymer (PS-g-PA-6) also had a profound effect on its compatibilization efficiency. The longer the PA-6 grafts (from 1.7 to 5.1 kg mol^{-1}) the higher the compatibilization efficiency. When the PA-6 grafts were short (1.6–1.7 kg mol^{-1}), their number had little effect on compatibility. As for the feeding mode, various studies showed that it can play an important role, but this appears to be blend specific [26–31].

Creton *et al.* [32] used a series of block copolymers with different molecular weights to compatibilize blends of PS and poly(2-vinylpyridine) (PVP). Only those copolymers whose PVP block polymerization degree was above 200 were found to be effective in preventing failure at the interface. This critical value corresponded roughly to the molecular weight between entanglements (M_e), suggesting therefore

that at least one average "entanglement" between the PVP block and the PVP homopolymer is necessary to have good stress transfer at the interface.

The effect of the molecular weight of block copolymers on the co-continuous morphology of 50/50 (w/w) PS/HDPE blends (HDPE, high density polyethylene) was investigated by Gallowaya *et al.* [33] using symmetric polystyrene–polyethylene block copolymers (PS-b-PE) (PE, polyethylene) with molecular weights varying from 6 to 200 kg mol^{-1}. An intermediate molecular weight PS-b-PE (40 kg mol^{-1}) showed remarkable results in reducing the phase size and in stabilizing the blend morphology during annealing. Mixing small amounts of 6, 100, or 200 kg mol^{-1} PS-b-PE in the blend did not significantly reduce the phase size, but did decrease the coarsening rate during annealing. The effect of 6 kg mol^{-1} PS-b-PE as morphology stabilizer was inferior to that of 100 and 200 kg mol^{-1}. The authors concluded that the existence of an optimal molecular weight block copolymer is due to a balance between the ability of the block copolymer to reach the interface and its relative stabilization effect at the interface.

A-B-A type block copolymers, consisting of styrene end-blocks and butylene, isoprene, or ethylene/butylene mid-blocks, are thermoplastic elastomers exhibiting physical properties typical for rubbers, but with melt processability similar to that of conventional thermoplastics. Besides their success as impact modifiers for several thermoplastics, these materials have been shown to act as compatibilizers for different polymer blends – especially for those of polystyrene or polyesters with polyolefins – where they bridge the blended polymers through physical or chemical interactions. For this purpose, the versatility of SEBS block copolymers can be significantly improved by grafting functional groups, such as maleic anhydride or epoxy groups, to the mid-block that can react, for example, with the end groups of polyamides or polyesters [34–37]. Among others, Sun *et al.* [38] investigated the compatibility effect of three different styrene–ethylene/butylene–styrene (SEBS) triblock copolymers on the toughness of blends of poly(ethylene terephthalate) (PET) and polypropylene (PP). The compatibilizers involved an unfunctionalized SEBS and two functionalized grades containing either maleic anhydride (MA) (SEBS-g-MA), or glycidyl methacrylate (GMA) (SEBS-g-GMA) grafted to the mid-block. An effect on morphology and impact strength was noticed on adding only 5 wt% of a SEBS copolymer, but this was much more pronounced when using the functionalized copolymers. High toughness combined with rather high stiffness was achieved with SEBS-g-GMA for the PET-rich composition. The addition of the functionalized SEBS copolymers resulted in a finer dispersion of the minor phase and clearly improved the interfacial adhesion. Anastasiadis *et al.* [39] studied the compatibilizing effect of block copolymer addition on the interfacial tension between two immiscible homopolymers as a function of additive concentration for the ternary system polystyrene/l,2-polybutadiene/poly(styrene-*block*-l,2-butadiene). With the addition of small amounts of copolymer, a sharp decrease in interfacial tension was observed, followed by a plateau as the copolymer concentration was increased above the apparent critical micelle concentration.

The effect of molecular weight of atactic polystyrene-*b*-poly(ethylene-*co*-butylene)-*b*-atactic polystyrene triblock copolymers on the morphology, impact strength, and

rheological behavior of syndiotactic polystyrene (sPS)/ethylene–propylene rubber (EPR) blends was investigated by Hong and Jo [40]. They observed that the size of the dispersed EPR phase in sPS/EPR/SEBS blends decreases and the particle size distribution becomes narrower with increasing amounts of SEBS in the blends. It was also discovered that the low molecular weight SEBS was more effective in increasing the impact strength than the high molecular weight SEBS. A possible explanation was that the blocks in the low molecular weight SEBS penetrate into the corresponding phase more easily than those with high molecular weight. A comparative study on the compatibility efficiency of styrene–butadiene–styrene (SBS) versus SEBS copolymer on polypropylene/polystyrene (PP/PS, 90/10) blends was carried out by Macaúbas and Demarquette [41]. The morphological, viscosity and interfacial tension results showed that SEBS was a better compatibilizer than SBS.

Various reports [19–25, 32–41] on the effects of the copolymer molecular weight and molecular architecture on its compatibilization efficiency for polymer blends rank in the order: tapered diblock > conventional diblock > triblock and smaller molecular weight > higher molecular weight.

7.3
In Situ Compatibilization or Reactive Blending

In situ compatibilization is based on a specific chemical reaction between two functional polymeric components during blending, and thus is also known as reactive blending [5, 17]. Scheme 7.1 exemplifies reactions that take place at the interface between reactive functional polymers. Because the chemical reaction takes place within the interphase, the copolymer is produced *in situ*, where it is necessary, with segments from the two homopolymers. The process needs: (i) sufficient

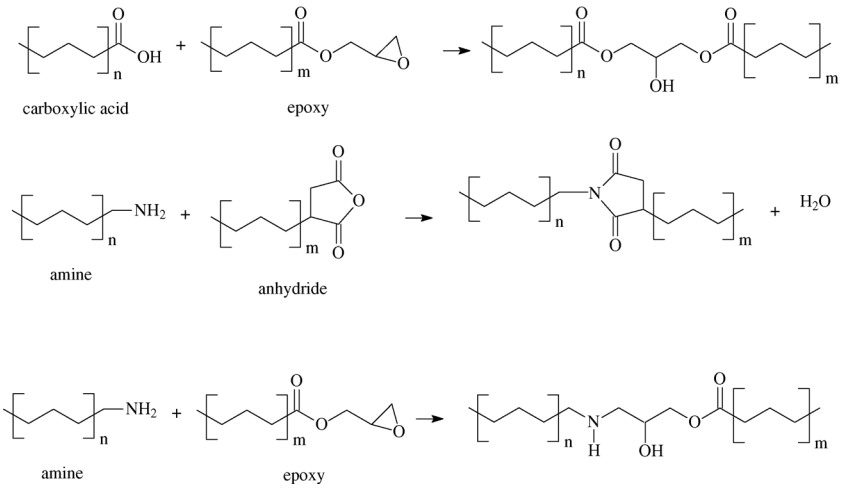

Scheme 7.1 Reactive groups and related copolymer formation.

dispersive and distributive mixing to guarantee the required interface regeneration, (ii) the existence of functional groups suitable to react across the interphase, (iii) a sufficiently high reaction rate to make it possible to produce enough copolymer during the residence time in the processing unit, (iv) copolymer stability, and (v) morphology stability. As the copolymer is formed at the interface, this method generates particularly thick interphases, which thus have good morphology stability.

7.3.1
Kinetics of Melt Coupling Reactions at Interfaces

Fredrickson and Milner [42] and O'Shaughnessy *et al.* [43–48] developed theoretical approaches to the mechanism of interfacial reactions between reactive polymers. Accordingly, the kinetics of copolymer formation at the interface follows basically two time regimes (see also Figure 7.2):

1) In the early reaction stages, the density of functional chains in the interface can be considered to be the same as that of functional chains in the bulk. If the reactivity of the reactive groups is relatively weak, the reaction is rate-controlled and is predicted to follow a second-order reaction rate with respect to the density of copolymers formed at interface (Σ):

$$\frac{d\Sigma}{dt} = k(t) C_a C_b \tag{7.1}$$

where k is the reaction rate constant and C_a and C_b are the concentrations of the reactive groups at the interface. This second-order rate leads to a linear time dependence of Σ. If the reactivity of the reactive groups is high, the reaction would change to first-order diffusion-controlled kinetics and the time dependence of Σ would no longer be linear.

2) During the subsequent reaction time, the interfacial coverage of the copolymers formed reactively becomes so high that the diffusion of more reactive chains towards the interface is hindered by the dense copolymer brush. In other words, an energy barrier develops delaying the diffusion of further precursor homopolymers towards the interface. This energy appears from the entropy loss due to the location of the homopolymer chains end at the interface and to the stretching of the copolymer blocks in the brush formed at the interface. As a result, the reaction becomes diffusion-controlled and a time dependence of the form $\Sigma \sim t^{1/2}$ is predicted.

Figure 7.2 illustrates the coupling of reactive end-functionalized chains in an interface of finite thickness. While in the early reaction stages the density of the block copolymers formed at the interface is small and the reaction is rate-controlled, at a later reaction stage the interface becomes crammed with block copolymers; for that reason, the chain are stretched and the length of the copolymer chains segments becomes larger than the unperturbed gyration radius (R_g). Owing to the dense copolymer brush at the interface, the diffusion of further reactive specimens towards

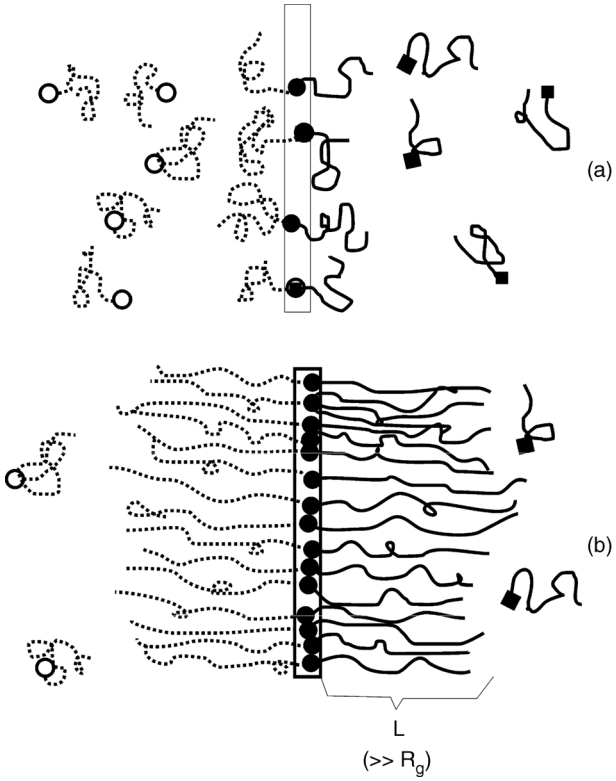

Figure 7.2 Schematic of the coupling of reactive end-functionalized chains in an interface of finite thickness: (a) initially, the density of block copolymers formed at the interface is small and the reaction is rate-controlled; (b) later, the interface becomes full of block copolymers, hence the chains are stretched and the length of the copolymer chains segments becomes larger than the unperturbed gyration radius (R_g). Adapted from Reference [46].

that same interface decreases significantly, causing a large reduction of the reaction rate, which becomes diffusion-controlled.

Several studies confirmed that the coupling reactions in the first time regime are indeed reaction-controlled for the most common reactive pairs, epoxy/carboxylic acid [49, 50] and anhydride/aliphatic amine [51, 52]. For polymers functionalized with these reactive pairs, it was found that chain ends can get to the interface well before the occurrence of reactions [50, 51], that is, the characteristic reaction time is larger than the characteristic diffusion time. The magnitude of the reaction activation energy is also an indicator that the reaction kinetics are reaction controlled. For example, Oyama and Inoue [52] estimated a value of 120 kJ mol^{-1} for reactions between the pair amine/anhydride. This high value is characteristic of a chemical process, in contrast with physical diffusion, which is expected to have a low activation energy ($<$30 kJ mol^{-1}).

The reaction rate constant, k, is governed mainly by temperature and reactivity of the complementary functional groups in the polymers. The k values of various pairs of the latter were determined by Orr *et al.* [53]. Again for the epoxy/carboxylic acid and anhydride/aliphatic amine pairs, values around 2.1 and 1400 $kg\,mol^{-1}\cdot min^{-1}$, respectively, at 180 °C, were reported for precursor chains with a molecular weight of about 25 $kg\,mol^{-1}$. For the reactive pair amine/epoxy, the authors found a k of about 0.2 $kg\,mol^{-1}\cdot min^{-1}$. Noticeably, despite of the large k for the reactive pair amine/anhydride, the reaction between polymeric precursors containing these reactive groups was shown to be rate controlled at common processing temperatures [50–52, 54]. The reactions with carboxylic acid and amine are particularly important, as several commercial polymers have at chains ends these functional groups; for example, polyesters are end-functionalized with carboxylic acid groups and polyamides are end-functionalized with amine groups. Consequently, the potential reactive precursors for the reactive compatibilization of blends containing polyesters and polyamides are polymers functionalized with epoxy and anhydride groups, respectively.

7.3.2
Effect of Interfacial Reactions on the Interface Morphology

Various studies relating to the morphology of static reactive interfaces demonstrated that these can become highly irregular after the reaction between the reactive precursors [55–58]. A few researchers [59–63] measured the interfaces irregularity as a function of the reaction time and compared them with the Σ values determined experimentally. A continuous increase in interface roughness with increasing Σ was observed, but that increase becomes sharp as Σ reaches a critical value. Using self-consistent mean-field theory, SCMFT, methods (described by Shull [64]), the interfacial tension was calculated from Σ values. It was found that this sharp increase takes place when Σ reaches the value corresponding to the absence of the interfacial tension [59]. Molecular dynamics simulations also predict the emergence of irregularities when the interfacial tension fades away [65]. Since the interfacial tension is given by $\gamma = dE/dA$, where dE is the variation of free energy and dA is the variation of the interfacial area, if γ vanishes there is no longer a free-energy penalty associated with the creation of a new interfacial area. Consequently, large curvatures may arise at the interface, due to thermal fluctuations. As more reactive chains migrate to the freshly created interfacial area, more interfacial copolymer is formed and this area is progressively covered. In turn, this gradual covering keeps the interfacial tension small; the interface curvature can further develop, eventually creating a very rough interface, a process known as interface roughening.

If the roughness grows to a sufficiently great extent, large droplet-like protuberances of one phase are formed. These are known as pinch-offs and can eventually become completely encapsulated by the interface crowded with copolymers. In this case, micro-emulsions can form inside one of the phases. These micro-emulsions have a dimension around 100 nm and consist of a homopolymer surrounded by the interfacial copolymers. Figure 7.3 illustrates the formation of a pinch-off in an interface and the consequent formation of micro-emulsions. Evidence of the

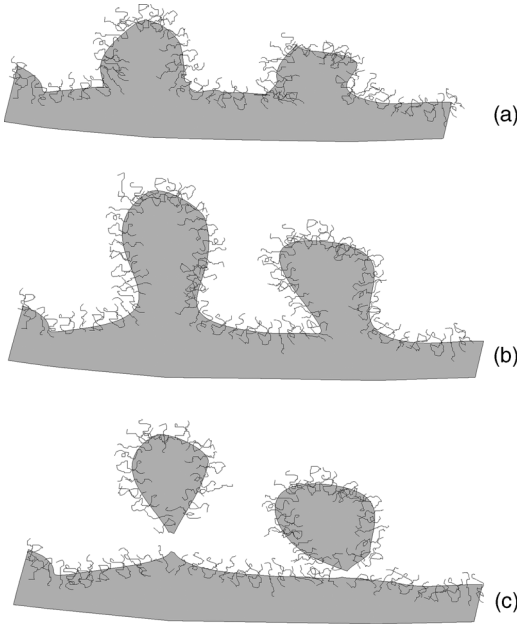

Figure 7.3 Evolution of the interfacial morphology due to crowding of the interface by interfacial copolymers and consequent decrease of the interfacial tension: (a) interfacial roughening; (b) formation of pinch-offs; and (c) formation of micro-emulsions on the continuous phase.

formation of pinch-offs and micro-emulsions was observed by Kim *et al.* [57] in the interface of PS-*end*-carboxylic/PMMA-*ran*-epoxy (PMMA, poly(methyl methacrylate)), as the interfacial reaction progressed for more than 6 h at 180 °C. In this work, it was noted that the pinch-offs grow only towards the PMMA phase, and that the micro-emulsions are likewise formed in this phase. This takes place because the micro-emulsions are more stable if their graft chains have the branched portions situated outside the micro-emulsion curvature, as in this case the steric hindrance of the branched chains is minimized. In addition to the micro-emulsions, smaller particles (most probably micelles) are also formed. Micelles contain only copolymers and their size is approximately equal to the radius of gyration of the copolymer (about 20 nm). Evidences of interfacial pinch-offs were also observed by Zhang *et al.* [60] and Lyu *et al.* [58] for reactive static interfaces of PS-end-NH_2/PMMA-end-anhydride after 1 h of reaction. However, in these experiments insufficient time was given to the eventual development of micro-emulsions and micelles.

7.3.3
Effect of the Interfacial Copolymer Structure

Jeon *et al.* [66] investigated the effect of the interfacial copolymer precursor structure on the reaction rate constant (k). The authors used PMMA chains end-functionalized and mid-functionalized with phthalic anhydride. Both were reacted with PS chains

end-functionalized with amine groups, that is, block and graft copolymers were formed at the interface. Under static (no-flow) conditions, the k value for the reactions of the end-functionalized chains is more than ten times higher than that for mid-functionalized chains, that is, it is faster to form block than graft copolymers at reactive interfaces. This was attributed to a higher segregation of chain ends to the interface as compared with the bulk, due to polymer dynamics [67]. Under flow conditions, the k ratio between end- and mid-functionalized chains decreases from 10 to 2.6–3.2. Probably, the shear flow induced convection reduces the concentration of the chains ends at the interface in comparison with the concentration of the chains ends at equilibrium. The effect of flow will be discussed later in more detail. The higher reaction rate constant for end-functionalized chains, as compared with the mid-functionalized ones, was confirmed by Jeon *et al.* [68], who studied 70/30 PA-6,6/PS blends (PA6,6 = polyamide 6,6) containing as reactive precursors PS chains end-functionalized with anhydride groups and random functionalized with the same groups, that is, SMA (styrene–maleic anhydride) copolymers. By comparing blends with the same concentration of functionalized PS, it was observed that those containing end-functionalized PS chains presented faster conversion.

Another important feature concerning the formation of graft copolymers on the interface is the grafting efficiency. Jeon *et al.* [66] reported that even though the SMA has on average 6.4 anhydride groups per chain, only nearly two PA-6,6 chains were grafted per SMA chain. This is due to the effect of the steric hindrance in the SMA chains already grafted by a PA-6,6 chain, in addition to the restricted interfacial volume at the interface. As described above, the interfacial reaction can only occur in the interface, which is a few nanometers thick. Since it is unlikely that the SMA copolymer extends fully along the interface, there are actually few anhydride groups per SMA chain available for the reaction. This low grafting efficiency at interfaces of polymer chains with random reactive groups has also been reported for reactive blends of PS-carboxylic/PMMA-epoxy [59, 69] and PBT/PS-epoxy (PBT, poly(butylene terephthalate)) [70].

7.3.4
Effect of the Reactive Precursor Molecular Weight

Several studies demonstrated that the reaction rate at the interface depends on the reactive precursor molecular weight (functional polymer), being higher for lower molecular weights [55, 71, 72]. This effect cannot be associated with the diffusion of the low molecular weight chains, since several studies evidenced that the interfacial reaction is controlled by the collision efficiency of the reactive groups and not by diffusion. Instead, Yin *et al.* [55] proposed that the dependence of the reactivity on the molecular weight could be related to the interfacial thickness, as shown by Helfand and Tagami [73] and Broseta *et al.* [74]. As described before, the reaction rate at the interface usually decreases dramatically as the critical concentration of interfacial copolymers is formed. Thus, the reaction at the interface can be suppressed before the interfacial tension vanishes and, therefore, extensive roughening may not occur. Owing to this effect of rate decrease, the interfacial roughness is likely to be larger for

low molecular weight reactive precursors, since low molecular weight reactive chains are more able to diffuse through the copolymer barrier, to reach the interface and to continue the reactions. Furthermore, self-consistent mean field theory [73, 74] predicts that the critical value of Σ that minimizes the interfacial tension decreases with the molecular weight of the interfacial copolymer. In fact, it has been shown that the roughening at the interface is larger for low molecular weight reactive chains [55].

7.3.5 Effect of the Flow

In industry, reactive polymer blends are generally prepared in conventional compounding machines, such as continuous extruders, or batch-type internal mixers, which promote complex melt flow patterns. The flow can influence significantly the reaction kinetics. Several studies have shown that the reactive blends prepared under flow have reaction rate constants more than 1000 times higher than those of reactive blends prepared in static bilayer films [56, 72, 75]. This effect of flow on the reaction rate is not yet well understood, but Jeon *et al.* [66] speculated that it can be due to convection, which can increase the collision probability between the reactive groups of the polymers at interface. These authors also conjectured that the increase of the reaction rate due to flow can be overestimated, as the initial stages of morphology development of immiscible polymer blends in mixers is very complex and therefore the interfacial area at this stage could be much larger than that found in the final stage of the completely developed blend.

Flow also induces the formation of micro-emulsions, as it can detach the pinch-offs from the interface. As shown by Kim *et al.* [76] for a bilayer of reactive PS-end-carboxylic and PMMA-ran-epoxy, micro-emulsions could be observed in a shear flow under a shear rate of $100\,s^{-1}$ after less than 50 min, while for static conditions they would form after 15 h [57]. In the case of melt blends prepared in internal mixers, micro-emulsions could be detected after less than 5 min of mixing, thus demonstrating again the importance of flow [68].

Apart from pinch-offs detachment, flow may also speed up the pull-out of copolymers from the interface and their subsequent dispersion as micelles in the continuous blend phase. This pull-out mechanism depends on the frictional shear force exerted on the interfacial copolymer chains, which is determined by the thermodynamical interaction of the interfacial copolymer chain with the blend chains at each phase and by the molecular weight and structure of the copolymer chains [77]. The experimental studies of Inoue *et al.* [77–79] corroborate the frictional theory and show that the pull-out tendency depends on the structure of the interfacial copolymer, on its molecular weight, and on the intensity of shear stress during flow:

1) It is easier to pull-out a linear block copolymer formed at the interface than a graft copolymer with a branch structure located at the dispersed phase. However, graft copolymers whose branch structure is located at the continuous phase (where the external shear forces are acting) have a higher tendency to be pulled out. The number of grafted chains of the continuous phase attached to the backbone

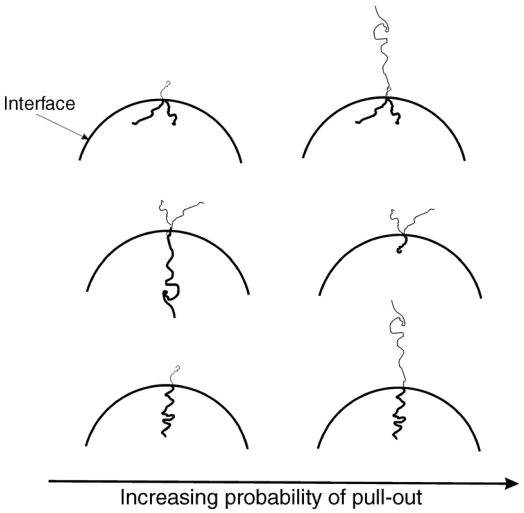

Figure 7.4 Pull-out tendency of block and graft copolymers at the interface, for varying molecular weight of the segments. Adapted from Reference [77].

of the reactive copolymer should also be considered. If there are many chains grafted, the thermodynamic interaction of the graft copolymer with the continuous phase becomes higher and, therefore, there will be a considerable tendency for the migration of the graft chains to the continuous phase, forming micelles. These can be avoided by increasing the molecular weight of the reactive precursor copolymer and/or reducing the copolymer functionality [68]. Figure 7.4 illustrates the effect of the interfacial copolymer structure.

2) The pull-out tendency also depends on the molecular weight of the copolymers. This tendency increases as the molecular weight of the copolymer segment miscible in the continuous blend phase increases and the molecular weight of the segment miscible in the dispersed phase decreases. It is very likely that pull-out occurs for a copolymer having a segment miscible in the dispersed phase with a molecular weight close or below its critical entanglement molecular weight (M_c). For example, if the segment miscible in the dispersed phase is PMMA, then pull-out is expected if the molecular weight of this segment is below 10 000 g mol^{-1}, which is the M_c of PMMA [80].
3) Since the frictional shear force increases with shear stress, pull-out is more likely to occur at high shear rates ($\dot{\gamma}$) and high matrix viscosity, $\eta(\tau = \dot{\gamma}\eta)$.

Inoue *et al.* [77–79] showed that micelles can be formed at the matrix even when the interfacial copolymer is a symmetric block copolymer. This is not predicted by the theory of block copolymers at interfaces [81], which asserts that only very asymmetric block copolymers are unstable and tend to depart from the interface, forming micelles in the phase where the longer block of the copolymer is miscible. In fact, this theory does not account for the effect of the shear stress, which has an important role on the stability of the interfacial copolymers at interfaces, as seen above.

The formation of micro-emulsions and/or micelles in blends with reactive interfacial copolymers should be avoided, because if the copolymers leave the interface (by interfacial roughening or by pull-out), the interfacial coverage of the dispersed phase decreases and, therefore, its interfacial tension and coalescence increases, leading to a blend with a coarser morphology. This effect was clearly demonstrated by Jeon *et al.* [68] for PA-6,6/PS blends with PA-6,6 as the continuous phase. The authors used end-functionalized PS with anhydride groups with two molecular weights (10 000 g mol^{-1} (PS10) and 37 000 g mol^{-1} (PS40)) as reactive interfacial precursors. Blends containing 2 wt% of reactive precursors PS10 presented tiny 50 nm particles dispersed in the PA-6,6 phase, which could not be detected in the blends with PS40. These particles are micro-emulsions of block copolymers that were removed from the interface by interfacial roughening and/or a pull-out mechanism. As discussed above, interfacial roughening and pull-out mechanisms are both more likely to occur for low molecular weight reactive precursors, such as PS10. As the copolymers in the micro-emulsion/micelles are removed from the PS/PA-6,6 interface, the interfacial coverage of copolymers in the surface of PS particles becomes lower in the blend with PS10 than in the blend with PS40 and as a result the average PS particle size is larger in the former than in the latter.

7.3.6
Role of the Reaction Rate on the Dispersed Phase Morphology

Morphology control is an important constraint to create polymer blends with enhanced properties [5]. During blending, the size of the dispersed phase changes from millimeters to micro and/or nano dimensions. Morphology development is influenced by the composition, the viscosity of the components and their viscosity ratio, and the processing conditions (operating conditions, type of geometry of the mixing equipment) [82].

There has been much speculation regarding the mechanisms of particle size reduction and the effect of the interfacial reaction on morphology development. Karger-Kocsis and Vergnes [83] reported no significant changes in morphology between 5 and 40 min of mixing PP/rubber blends. Favis and Chalifoux [84] prepared PP/PC blends (PC, polycarbonate) in a batch mixer and concluded that the most significant changes in morphology occurred during the first 2 min of mixing, when melting and softening of the materials would also occur. Scott and Macosko [85, 86] showed that at short mixing times the two phases are sheared into ribbon or sheet structures, which will subsequently breakup due to shear and interfacial tension. Sundararaj *et al.* [87–89] provided evidence that the most significant morphology development of a PS/PP blend in a twin-screw extruder occurred in the first two disks of the first kneading section. They also detected sheet structures and demonstrated that, after the initial breakup, the particle size was not reduced significantly. Moreover, they observed a phase inversion mechanism when the minor component melted or softened at a lower temperature than the major component. Cartier and Hu [90] studied the preparation of PP/PA-6 blends in a twin-screw extruder and

concluded that the morphology develops very rapidly, but even faster in the case of *in situ* compatibilized blends with PP grafted with maleic anhydride (PP-g-MA). In this case, the size of the dispersed phase undergoes an abrupt reduction from a few millimeters to sub-micrometer levels during the transition from solid pellets to a viscoelastic fluid, with the final morphology being attained as soon as that transition is completed. In systems containing rubber and polyamide/polyesters, the rubber phase is dispersed from millimeter to micrometer level within a few seconds [91]. This means a decrease of the diffusion distance of the polycondensate chains to the rubber interface by a factor of 10^3 and an increase of the interface by a factor of 10^9, that is, the rate of interfacial reactions is dramatically enhanced. In the case of PA-6/EPM-g-MA blends (EPM-g-MA, ethylene and propylene monomer grafted with maleic anhydride) the reaction is so fast that as interfaces are created upon melting they become immediately covered with PA-6 chains, causing a quick reduction of the interfacial tension and preventing coalescence, which induces a further refinement of the dispersed phase.

To study the morphology progression of PA-6/EPM-g-MA blends, Machado *et al.* [92, 93] developed a technique to rapidly collect samples from fully filled sections of a twin-screw extruder. It was shown that at the beginning of the melting zone, even though the material was mostly solid, the non-reacted MA content decreased to less than half of its original value. One screw turn later, a fully melted conventional polymer blend morphology was present, with relatively good distributive and dispersive mixing levels, having caused a further important reduction in MA (Figure 7.5). Before the end of the extruder, a stable and controlled morphology had been achieved.

The stability of PA-6/EPM-g-MA compatibilized blends was evaluated by measuring the average particle size of the dispersed phase after processing by injection molding and capillary rheometry. No changes could be detected, that is, the blend morphology was stable [11].

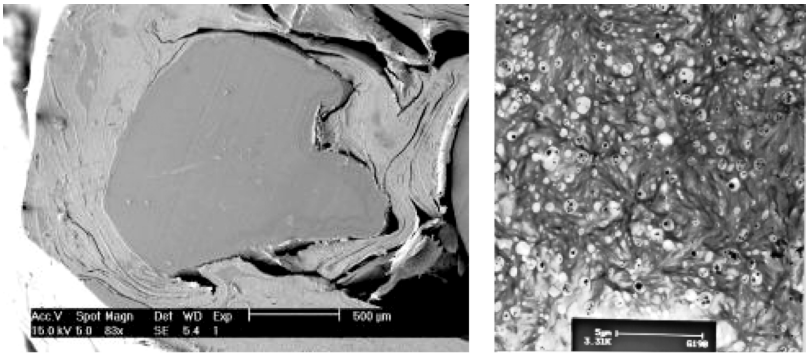

L/D = 12 L/D = 13

Figure 7.5 Morphological evolution along the extruder (*L*/*D*, screw length to diameter ratio) of a PA-6/EPM-g-MA blend.

When a blend is prepared by melt mixing under high shear rates, the interfacial area increases due to the progressive break-up of the dispersed phase caused by the shear stress. When these particles run into each other coalescence may occur, which increases their size [94–96]. Various studies have suggested that the main function of interfacial copolymers is actually to suppress this coalescence, thus yielding a reduction in the size of the dispersed phase, and that this suppression takes place if the interfacial area coverage reaches a minimum value, Σ_{min}, [88, 94–98]. It has been shown that Σ_{min} is lower than the maximum interface coverage, Σ_o, and that its value depends on the thermodynamic interactions between the polymers. For instance, for the PS/PMMA system, Σ_o is 0.171 or 0.131 chains nm^{-2} for interfacial copolymers with a molecular weight of 38 000 or 84 000 g mol^{-1}, respectively [72], but the Σ_{min} value that suppresses dynamic coalescence is about 0.02 chains nm^{-2}. This means that only about 20% interfacial coverage is necessary to stabilize the morphology. Conversely, for the PS/PE system, Σ_o is 0.25 chains nm^{-2} for a molecular weight of 40 000 g mol^{-1}, while Σ_{min} is around 0.2 chains nm^{-2}, that is, in this case it is necessary to cover 80% of the interface to suppress coalescence [98].

Owing to the dynamics of the breakup/coalescence process, the formation of interfacial copolymers should be fast enough to promote at least an interfacial coverage of Σ_{min} in any interface created by break-up before coalescence develops, otherwise the average particle size increases. To achieve a very fine dispersed phase, it is necessary to ensure a very high reaction rate, since the interfacial area is large and, for that reason, a high concentration of interfacial copolymers should be formed. As a result, there is a correlation between the size of the dispersed phase and the reaction rate, which means that the desired blend morphology can be achieved by adjusting the parameters that influence the reaction rate, such as the concentration of reactive groups, the molecular weight of the reactive chains, the type of reactive groups, and so on.

Figure 7.6a illustrates how the average size of the dispersed phase of a reactive blend changes with the growing concentration, *C*, of reactive groups. Clearly, the

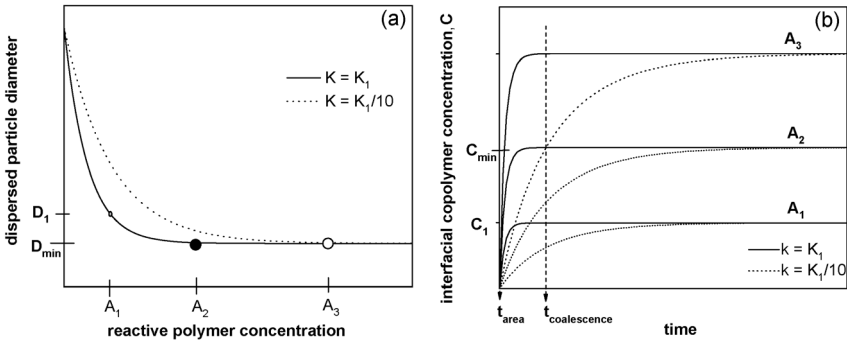

Figure 7.6 Average size of the dispersed phase as a function of the concentration of reactive groups (a); concentration of interfacial copolymer (b).

particle size decreases exponentially and levels off at a given concentration. This behavior has been described extensively in the literature [49, 99, 100] and can be explained by the change with time of the concentration of copolymer formed at the interface. To simulate the kinetics of this reaction, it is assumed that the concentration, A, of the reactive groups at the interface is low, which means that the reactions at the interface end before the formation of a densely packed brush of copolymers. The resulting equation follows second-order reaction kinetics and the concentration of interfacial copolymer follows a correlation of the type $C \propto -\exp(-t)$.

Figure 7.6b shows this second-order kinetics for various concentrations of A reactive groups (or concentrations of the polymer containing these groups). This figure also identifies the concentration of interfacial copolymer C_{min} that should be formed at the interface to completely suppress coalescence, that is, the coverage Σ_{min} in a blend with a dispersed phase particle size of D_{min}. The stabilization of this morphology can only take place if C_{min} is attained at the interface before coalescence begins, that is, before time $t_{coalescence}$; this occurs when the concentration of A is A_2, as seen in Figure 7.6b. If A is below A_2 (say A_1), the concentration of copolymer formed between t_{area} and $t_{coalescence}$ is C_1, which is lower than C_{min}. As the copolymer concentration is now insufficient to form a Σ_{min} coverage on the particles with D_{min}, coalescence takes place and D will increase (decreasing the interfacial area) up to D_1, when the coverage reaches Σ_{min} for concentration C_1. Conversely, if $A > A_2$ (e.g., A_3), the copolymer concentration formed between t_{area} and $t_{coalescence}$ is C_3, higher than C_{min}. Now, the copolymer concentration induces a coverage larger than Σ_{min} on the particles with D_{min}, but this does not promote a further reduction in particle size below D_{min}, because the minimum size of the dispersed particles is governed only by the breakup process, which is hardly affected by the interfacial coverage. Therefore, for a concentration $A > A_2$, a leveling off is observed in Figure 7.6a.

Figure 7.6b also demonstrates the effect of decreasing the reaction rate (by reducing the reaction rate constant, k) on the relation between particle diameter and the concentration A of reactive group. At constant A, decreasing k from k_1 to $k_1/10$ (dashed lines) slows down the rate of copolymer formation, causing a reduction of the concentration of copolymer at the interface until the initiation of coalescence, $t_{coalescence}$. Therefore, at concentration A_2, the amount of copolymer formed until $t_{coalescence}$ is lower than C_{min} and, as a result, coalescence occurs. For the slower reaction, the formation of C_{min} before the beginning of coalescence only occurs when A increases from A_2 to A_3. As a consequence, the beginning of the plateau is also shifted from A_2 to A_3, meaning that a slower reaction requires more reactive polymer to suppress coalescence. Notably, in addition to k, the other parameters discussed above that influence the rate of copolymer formation can promote similar results in terms of morphology.

In summary, the concentration of interfacial copolymers that suppresses coalescence is increased by:

- Enhancing the reaction rate constant, k. This can be accomplished increasing the temperature and/or altering the reactive groups pairs, for instance, changing the pair carboxylic/epoxy for amine/anhydride.

- Reducing the molecular weight of the reactive polymer. However, the molecular weight should not be too small, to avoid the formation of micro-emulsions and micelles, as discussed above.
- Utilizing polymers with end-functionalized reactive groups, instead of polymers with reactive groups distributed along the chains. This means the formation of block copolymers at the interfaces instead of grafted ones.
- Boosting the thermodynamic interactions between the two phases and, consequently, the interfacial width.

7.3.7
Examples of Applications of Reactive Blending in Polyester and Polyamide Blends

This section presents and discusses a few examples of reactive blending during the preparation of polyester and polyamide blends, by reaction of epoxy/carboxylic acid (polyesters blends) and anhydride/amine (polyamide blends) groups.

7.3.7.1 Polybutadiene Terephthalate Blends

PBT/ABS blends boast a potentially attractive combination of good mechanical properties and processability: while PBT provides stiffness and good melt processability, the rubber from ABS offers impact resistance and the SAN (styrene–acrylonitrilecopolymer) from ABS (acrylonitrile–butadiene–styrene copolymer) confers increased Heat Deflection Temperature (HDT) [99]. However, these blends have a relatively high brittle–ductile transition temperature, BDTT, limiting their use at low temperatures. The high BDTT is normally attributed to the existence of coarse ABS particles dispersed in the PBT matrix. Some authors have suggested that BDTT depends not only on particle size but also on interparticle distance, with a coarse morphology causing a larger interparticle distance [100–107]. Furthermore, there is evidence that the morphology of melt compounded PBT/ABS blends is unstable when they are injection molded [99].

The incorporation of reactive species in these blends can decrease the size of the ABS particles and thus reduce the BDTT. An efficient reactive precursor is the copolymer MGE (methyl methacrylate–glycidyl methacrylate–ethyl acrylate copolymer), which is a copolymer of methyl methacrylate (MMA)–glycidyl methacrylate (GMA)–ethyl acrylate (EA). The MGE copolymer is miscible with the SAN phase of ABS [108], its synthesis is relatively simple [108], and only small quantities (about 5 wt %) are necessary for blend compatibilization. Since SAN is the continuous phase in ABS, in a PBT/ABS blend most of the MGE dissolved in SAN is in contact with the PBT phase. Owing to this SAN/PBT interface, during melt processing the epoxy groups of glycidyl methacrylate will react with the carboxylic groups of the PBT chains that are located at this interface, forming a graft copolymer of PBT-g-MGE. PBT chains can also have hydroxyl groups at the chains ends that may also react with the epoxy groups of MGE. However, the reaction epoxy-hydroxyl is less probable to occur than the epoxy-carboxyl one, since it has been shown that the reaction rate of the former is slower than that of the latter [109, 110]. Figure 7.7 shows the effect of the

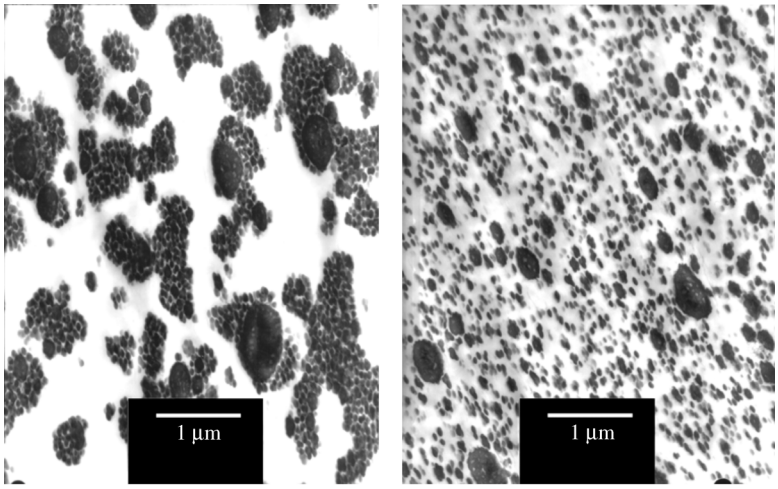

Figure 7.7 Dispersion of ABS particles in PBT/ABS blends containing 30 wt% ABS: (a) without compatibilizer MGE and (b) with 5 wt% MGE (Ambrósio, J.D., Lanea, N.M., Pessan, L.A., and Hage, E.: unpublished results).

incorporation of MGE on the phase-dispersed morphology of a PBT/ABS blend. The effect of MGE on the morphology and other properties of PBT/ABS blends has been studied extensively [111–114].

MGE was used by Mantovani *et al.* [115] in PBT/ABS blends containing 40 wt% ABS. The BDTT was −10 and −50 °C for the blends without and with compatibilizer (5 wt%), respectively. This drop was associated with the better dispersion of the ABS particles obtained with the incorporation of MGE. However, a decrease of the impact strength at room temperature relative to the physical blend was reported. Hale *et al.* [111], who obtained similar results, speculated that this decrease is due to the crosslinking that takes place in addition to the reactions that form the graft copolymers at the interface. The occurrence of crosslinking reactions between PBT and polymers functionalized with epoxy groups has also been described by Martin *et al.* [116]. Crosslinking reactions can occur due to the bifunctionality of PBT. Since its chains can have carboxylic groups at both chain ends, the PBT molecules can act as a crosslinking agent between the chains containing epoxy groups. It is also possible that the chains with epoxy groups act as crosslinks. This can occur if the epoxy group opens and creates alcohol functionalities, which can react with other epoxy groups present in other chains. Hale *et al.* [111] have also found evidence that acid residues of polymerization found in ABS can act as catalysts of these reactions.

MGE copolymers are also efficient reactive precursors to compatibilize PBT/AES blends. Since AES (acrylonitrile–ethylene–styrene copolymer) is itself a two-phase blend, consisting of EPDM grafted to SAN, it is likely that MGE can promote coalescence suppression in PBT/AES through a mechanism similar to that found in PBT/ABS/MGE blends. In fact, Figure 7.8 shows that the incorporation of MGE leads

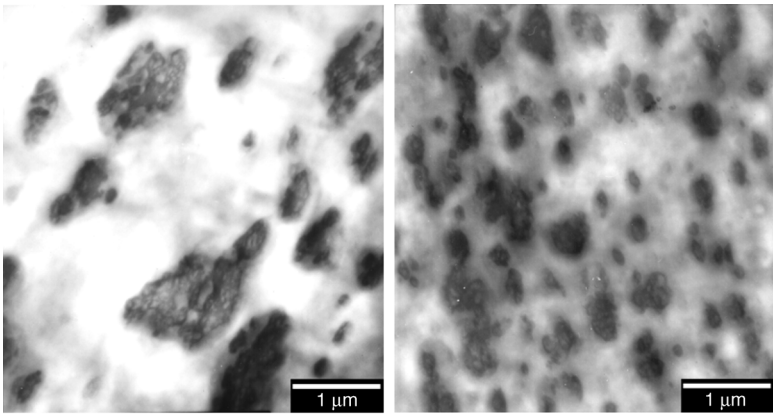

Figure 7.8 Effect of MGE on the dispersed phase morphology of a PBT/AES blend containing 30 wt% AES without compatibilizer (a) and with 5 wt% of MGE (MGE contains 10 wt% GMA) compatibilizer (b) (Larocca, N.M., Hage, E., and Pessan, L.A.: unpublished results).

to a better dispersion of AES particles in PBT/AES blends. PBT/AES blends containing 30 wt% of AES, with and without MGE copolymers, were studied by Larocca *et al.* [117, 118]. Evidence that *in situ* reactions took place upon MGE incorporation includes the large increase in blend viscosity and the refinement of the blend morphology. As the epoxy concentration in the blend increases, the AES particles size reduces. This decrease levels off when the concentration of GMA in the blend reaches 0.5 wt%. The decrease in particle size of AES seems to be correlated with the DBTT of the blends, as it decreases exponentially up to the GMA concentration of 0.5 wt% and then also levels off. In the case of a PBT/SAN model blend containing 5 wt% of MGE, the dependence of the SAN particles size on the GMA concentration in MGE also follows an exponential decrease and the particle diameter also levels off for the GMA concentration of 0.5 wt%. The analogous performance of both DBTT and dispersed particle size clearly indicates that MGE reduces the DBTT through reduction of the dispersed phase particle size.

Larocca *et al.* [118] also studied the influence of the molecular weight of MGE containing 10 wt% GMA on the morphology and DBTT of PBT/AES/MGE blends. As the molecular weight of MGE decreases from 380 000 to 120 000 g mol^{-1}, the DBTT decreases from −5 to −17 °C and the morphology becomes finer. However, a further decrease in molecular weight leads to higher DBTTs. As discussed previously, low molecular weight reactive polymers promote a faster reaction rate and the formation of more copolymer at the interface, thus hindering coalescence more efficiently and, consequently, causing a decrease in AES particles size and a concomitant decrease in DBTT. However, in the case of a too low MGE molecular weight, pull-out of the low molecular weight interfacial copolymer and/or interfacial roughening could occur [55, 77–79], generating a decrease of the copolymer interfacial coverage and a consequent increase of the coalescence of AES particles.

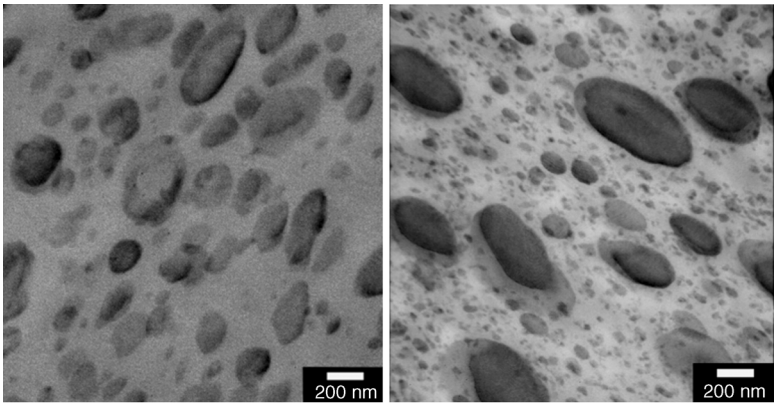

(a) (b)

Figure 7.9 Effect of MGE molecular weight on the morphology of PBT/SAN blends containing 20 wt% SAN with high molecular weight MGE (a) and low molecular weight MGE (b) (Larocca, N.M., Hage, E., and Pessan, L.A.: unpublished results).

In fact, it has been observed that low molecular weight MGE copolymers really lead to the formation of micelles and/or micro-emulsions in the PBT/SAN/MGE blend (Figure 7.9). Figure 7.9b shows the presence of tiny micro-emulsions, in addition to the presence of larger SAN particles. Both blends contain 5 wt% of MGE, which, in turn, contains 10 wt% of GMA. PBT/SAN/MGE is a suitable model blend for the study of interfacial reactions in the more complex PBT/ABS/MGE blend, since in both cases the interfacial reactions take place in the PBT/SAN interface.

Another reactive copolymer containing epoxy groups, with possible commercial attractiveness, is polystyrene–glycidyl methacrylate (PS-GMA). Its synthesis is also simple and it can compatibilize blends of PBT with polymers containing styrene moieties, such as SBS. PS-GMA is miscible with polystyrene, at least when it has low molecular weight and low GMA concentration [119]. Studied PBT/SBS/PS-GMA blends where some SBS and PS-GMA characteristics were varied. They observed that most blends did not show signs of a decrease of DBTT with increasing PS-GMA content; neither was there a morphology refinement of the SBS dispersed phase. This was explained by the microphase separation of the SBS copolymer at the processing temperatures (about 240 °C). As the microphase develops, the SBS morphology becomes lamellar, with alternating lamellas of PS and PB. This reduces the interfacial PBT/PS area, deterring the formation of the interfacial copolymers that would stabilize the SBS particles against coalescence. Nevertheless, a DBTT decrease was observed when a SBS with high polystyrene content (38 wt%) and long polystyrene blocks (about 20 000 g mol^{-1}) and a PS-GMA with moderate GMA content (4 wt%) and high molecular weight (about 35 000 g mol^{-1}) were used. These characteristics favored a higher PBT/PS interface, as well as the miscibility of the PS-GMA and PS phases, enabling graft copolymer formation at the interface.

7.3.7.2 Polyamide-6 Blends

Polyamide-6 is a widely used engineering thermoplastic also suitable to be used in reactive blends due to the amine and carboxylic functional groups present in its chains ends. Likewise, compatibilized PBT/ABS and compatibilized PA-6/ABS blends have attracted great interest, due to their very attractive combination of properties [120–123]. Araújo *et al.* [124–128] studied the effect of two compatibilizers, MGE and copolymers of methyl methacrylate–maleic anhydride (MMA-MA), on the morphology and properties of PA-6/ABS blends. These copolymers were selected because the epoxy groups of MGE can react with the carboxyl and amine groups of polyamide, whereas the maleic anhydride (MA) groups of MMA-MA can react only with the amine groups of polyamide. Moreover, MGE and MMA-MA are miscible with the SAN phase of ABS, hence it is expected that interfacial reactions take place at the interface of PA-6/SAN, forming grafted copolymers of PA-6–g–MGE or PA-6-g–MMA-MA. While PA-6/ABS blends containing 50 wt% ABS possess a notched Izod impact strength around 70 J m^{-1} (until 90 °C), the incorporation of only 5 wt% of MMA-MA containing 3 wt% of maleic anhydride created a super-tough blend, with an impact strength on the order of 800 J m^{-1}, holding until a temperature of −10 °C. However, when using MGE instead of MMA-MA, no super-tough blends at any temperature were generated, even when adding 5 wt% of MGE containing 10 wt% of GMA. The significant improvement in impact strength of the PA-6/ABS blends containing MMA-MA can be accounted by the morphological changes caused by the incorporation of this compatibilizer. PA-6/ABS blends have a coarse dispersion of ABS in the PA matrix that causes their low impact strength. However, blends containing 5 wt% of MMA-MA show a refinement of the ABS dispersion. This decrease of particle size is due to the formation of graft copolymers at the PA-6/SAN interface. The larger coalescence suppression efficiency of the reactive compatibilizer containing anhydride groups, as compared with the reactive compatibilizer containing epoxy groups, is coherent with the very high reaction rate of the pair cyclic anhydride/amine versus the slower reaction rate of the pairs epoxy/amine and epoxy/carboxylic acid [53].

To better understand the interfacial reactions of the PA-6/ABS/MMA-MA system, studies using the simpler amorphous PA/SAN/MMA-MA model blend were conducted by Becker *et al.* [129–131]. For blends containing 5 wt% of MMA-MA, these authors found a minimum in the SAN particle size at 1 wt% of MA in the compatibilizer. At higher MA content in the MMA-MA, an increase of the SAN particles size was observed. It was speculated that the graft copolymers formed from the MMA-MA compatibilizer with higher MA content are more easily pulled-out from the polyamide/SAN amorphous interface, which would significantly diminish the interfacial coverage of the SAN particles and make them more susceptible to coalescence. This conjecture is corroborated by the increased blends viscosity, as well as by the presence of micelles of graft copolymers on the matrix of these blends.

The reactive compatibilization of PA-6/polyolefins blends using polyolefins containing MA was studied by Machado *et al.* [11, 92, 132, 133]. It was shown that the MA content of the modified polyolefins decreases strongly upon melting of the PA pellets and melt flow through the first set of staggering kneading blocks, that is, the grafting

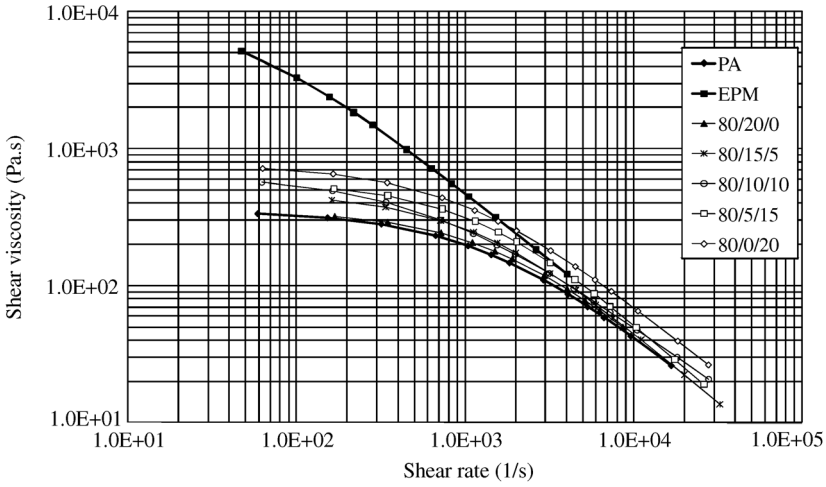

Figure 7.10 Shear flow curves of the original polymers (PA and EPM) and of their extruded blends. Adapted from Reference [134].

reaction is very fast. Simultaneously, the morphology changed dramatically in this zone of the extruder, from mm to (sub)μm level. It was also observed that the final morphology depends on the amount of the copolymer formed at the interface and on the processing conditions used.

The rheological behavior of PA-6/EPM/EPM-g-MA (80/20/0 to 80/0/20 w/w/w) blends was also investigated [134]. The flow curves depicted in Figure 7.10 show that at high shear rates the viscosity of all materials, except the compatibilized blend (80/0/20), is very similar. For the non-compatible PA-6/EPM blend the viscosity curve is similar to that of the PA-6 reference. The increase in viscosity with increasing EPM-g-MA content was attributed to an increase of the interfacial adhesion as a result of *in situ* compatibilizer formation. Moreover, the viscosity of the blends increases with increasing MA content in the rubber phase, that is, with the amount of copolymer formed at the interface. The shape of the curves indicates that the rheology of the blends is mainly governed by the matrix, but the shift between the curves also suggests that other parameters also play a role.

7.4
Application to Manufacturing of Polymer Blends

7.4.1
Equipment

7.4.1.1 Introduction

Successful reactive extrusion, that is, the combination of melt extrusion and chemical reactions in a single operation to continuously polymerize monomers and/or modify

polymers, requires not only that the reactions to take place inside the extruder be compatible with the general characteristics of these machines, but also that the extruders selected have certain constructional and functional features. Despite its obvious advantages and practical success, especially in the last 15–20 years, reactive extrusion is a complex technology, which requires simultaneously mastering plasticating extrusion and controlling a chemical reaction under very specific conditions. For the purposes of reactive extrusion, chemical reactions should [12, 14, 135–138]:

- have low activation energy and be rapid; for example, in the case of polymer blending, the polymers should have either a high concentration of reactive groups or these should be highly reactive, to ensure a high conversion into copolymers;
- involve reagents that are stable at the usual compounding temperatures;
- yield reaction sub-products that can be easily removed;
- not be affected by the instabilities that are inherent to the extrusion process.

Modern reactive extrusion operations can be multifaceted and involve a series of individual steps, such as feeding the components (either together or sequentially), melting them (but liquid ingredients may also be utilized), melt mixing the composition (distributive and dispersive homogenization), devolatilizing, and die forming for subsequent pelletization. Therefore, an extruder is adequate to be used as a chemical reactor if it:

- guarantees efficient control and adjustment of output, temperature, and residence time;
- creates a thermally homogeneous environment, provides efficient interfacial generation, and good mixing;
- is able to work with materials that may present a wide range of characteristics (gas, solid, powder, fluids (namely with high viscosity levels);
- allows the sequential addition of the reaction ingredients (monomer, polymer, water, solvent, reactant, etc.);
- provides the efficient removal of sub-products or of low molecular weight by-products via devolatilization;
- allows working in an inert atmosphere;
- can be easily attached to downstream pelletization equipment.

Single-screw extruders began to be used as chemical reactors for polymerization purposes in the 1950s, to ensure continuous production, avoid the use of solvents and bring about energy savings (e.g., through elimination of solvent heating and cooling) [139]. During the following two decades these machines were also applied for polymer chain breaking and grafting of monomers to polyolefins. However, and despite the progressive improvements in pressure generation and distributive mixing efficiency, single-screw extruders offer limited sequential addition capabilities, which confines their application to relatively simple operations, such as modification of polyolefins with peroxide, or silane grafting [140].

Counter-rotating and co-rotating twin-screw extruders, or combinations of various types of equipments [136, 141], have been progressively recognized as more suitable to the specificities of some chemical reactions. Counter-rotating intermeshing self-

wiping twin-screw extruders fulfill most of the requirements listed above, but they can only operate at low screw speeds (typically below 50 rpm, to minimize the pressure developing in the mechanical calender gap, in the screws intermeshing zone, which pushes them against the barrel wall, generating wear). Consequently, shear rate levels are moderate and so is the dispersion efficiency. Copolymerization of styrene–*n*-butyl methacrylate, polymerization of ε-caprolactam, grafting of maleic anhydride onto polyethylene, polymerization of urethanes, and radical polymerization of methacrylates are examples of reactions performed using this machine [142]. Non-intermeshing counter-rotating extruders are utilized for polycondensation reactions, as they provide excellent distributive mixing even at low shear rates, but they have limited pressure generation capacity and dispersive mixing efficiency.

Co-rotating intermeshing twin-screw extruders are currently the most widely used for reactive extrusion. The output of commercial machines can range from a few kilograms to around 100 tonnes per hour. In general, they possess the following features:

- modular construction, whereby the geometries of both the screws and barrel can be adapted to the specific needs of each application, in terms of the feeding sequence of the components, of the melting location, of the mixing type and intensity (the total deformation resulting from local flow fields and flow time), of the average residence time, or of the devolatilization location and level;
- independent control over output and screw speed, enabling operation in starve fed mode (i.e., the screws work partially filled over a significant portion of their length), which facilitates the introduction or the removal of ingredients and by-products, respectively, decreases the total mechanical power consumption and helps to control melt temperature (by allowing for thermal relaxation to take place after viscous dissipation during flow in mixing zones);
- the screws can rotate at high screw speeds (up to $>$1500 rpm), thus promoting high dispersion levels whilst guaranteeing high production rates;
- they generate the pressure required for melt flow through a pelletizing die or, via the insertion of a gear pump between extruder and die, for the direct extrusion of a final product (e.g., reactive spinning of elastomeric polyolefin fibers [143]).

Nevertheless, only a limited number of the chemical reactions performed in batch reactors can be transposed to reactive extrusion, due to the following shortcomings of extruders:

- Residence times in extruders are very short (frequently, less than 1 min); hence very fast kinetics, high conversion, and selectivity are necessary.
- Since extruders have limited cooling capacity, exothermal reactions, or highly viscous media (inducing significant viscous dissipation) must be avoided, as they can induce side reactions (e.g., thermal degradation), the severity of this problem increasing with the size of the extruder, as heat transfer becomes progressively less efficient.
- Owing to the complexity of the thermo-mechanical environment inside of an extruder, and the difficulty in monitoring the evolution of the physicochemical

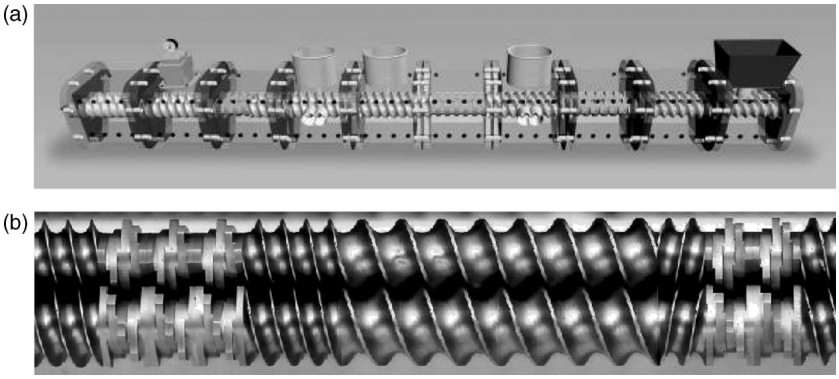

Figure 7.11 Intermeshing co-rotating twin-screw extruder: (a) extruder set-up, with multiple vents, devolatilization, and side feedings [144]; (b) section of a typical screw profile (www.coperion.com).

phenomena along the screw axis, it is difficult to scale-up a laboratorial production to industrial application. This explains the current scientific and technological interest in process modeling and optimization.

7.4.1.2 Main Operational Features of Co-rotating Twin-Screw Extruders

As shown in Figure 7.11, an intermeshing co-rotating twin-screw extruder consists of two parallel screws – interpenetrating mechanically as much as possible – rotating at the same speed inside a hollow heated barrel. Each screw is generally built by assembling a certain number of individual elements along a shaft, while the barrel results from coupling together unit modules in such a way that the assemblage may contain various apertures in the downstream direction for feeding and/or devolatilization purposes. Thus, quite distinct extruders can be created by the proper selection of screw and barrel elements. Figure 7.11 also shows that the screw profile can be quite complex, encompassing conventional conveying sections separated by mixing zones that induce different levels and types of mixing, depending on their geometry and length. Figure 7.12 presents some of the most common types of commercial screw elements. Conveying/screw type elements give rise to conveying sections that drag the material downstream and induce some distributive mixing. A kneading element contains several disks staggered with a positive, neutral, or negative angle (the disk thickness and staggering angle may also vary); one or several adjacent elements of this type create a kneading block in the screw. As the staggering angle changes from positive to neutral and negative, the conveying capacity decreases, becomes nil, or negative, and the levels of distributive and dispersive mixing increase. At the right-end side of Figure 7.11b one may identify a conveying element with a negative helix, which is often used to create an effect similar to that of a negative kneading block. These last two types of elements are generally known as "restrictive," in terms of their flow conveying capacity. Table 7.1 summarizes the conveying and mixing characteristics of the most widespread types of screw elements.

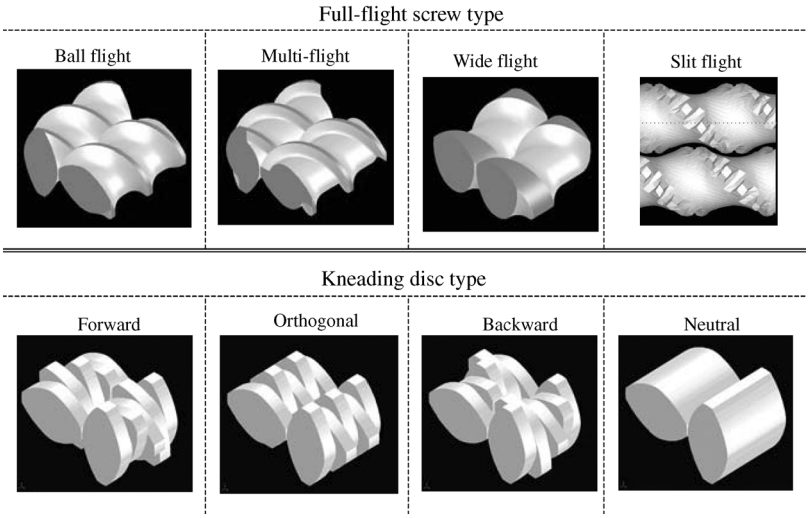

Figure 7.12 Representative individual screw elements used in twin-screw extruders [137].

As noted above, these machines operate in starve fed mode, that is, the output is determined by the feeding rate of volumetric or gravimetric raw material feeders, not by the screw speed. When the material enters the extruder, it follows a figure-of-eight flow pattern along the channels of the partially-filled conveying elements (Figure 7.13). The figure also demonstrates that instead of having a continuous channel from hopper to die, as in the case of the single-screw extruder, here the

Table 7.1 Main characteristics of conveying elements and kneading blocks of twin-screw extruders[a)] ((a) and (b) should not be directly compared) [44].

		Mixing			
		Conveying	**Distributive**	**Dispersive**	**Local residence time**
(a) Conveying elements (helix angle)	Low	+	+	0	+ + +
	Medium	+ +	+	0	+ +
	High	+ + +	+	0	+
	Negative	−	+ + +	+ +	+ + + +
(b) Kneading blocks (staggering angle)	Positive (low)	+ +	+	0	+
	Positive (medium)	+	+ +	+	+ +
	Orthogonal	0	+ + +	+ + +	+ + +
	Negative	−	+ + + +	+ + +	+ + + +

a) + + + + very high; + + + high; + + medium; + low; 0 nil; − negative.

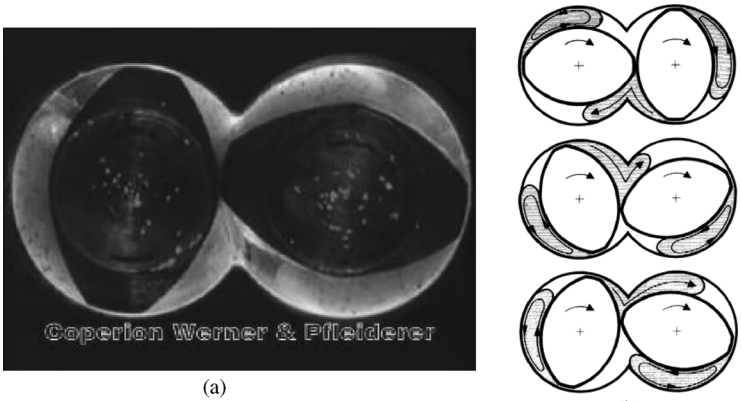

(a) (b)

Figure 7.13 (a) Cross-section of a twin-screw extruder; (b) figure-of-eight flow pattern. (a) Courtesy of Coperion Werner & Pfleiderer; (b) adapted from Reference [145].

rotation of the screws originates three independent flow channels (for a double-start screw), whose volume expands and reduces upon rotation, thus inherently bringing on some distributive mixing.

Once the flow reaches a restrictive zone, it must generate the pressure required to overcome the resistance created by the latter and continue its progression towards the die. Consequently, the material accumulates directly upstream of that restriction, filling up a few screw turns and spending longer local residence times before traversing it. The higher the restriction (defined by its geometry and length), the higher the pressure to be generated, and the higher the number of screw turns upstream working fully filled. Accordingly, restrictive elements generate locally more efficient heat transfer, create a complex 3D flow (particularly in the apex region) – this is important for mixing purposes – and induce significant shear and extensional stresses, which may promote important viscous dissipation. Figure 7.14 presents a series of sequential pictures describing the progress along two kneading blocks having different staggering geometries of a liquid tracer injected into a highly viscous Newtonian silicone oil (1000 Pa·s) [145, 146]. In the case of the kneading block with disks staggered at 90° (Figure 7.14a) there is hardly any flow accumulation upstream (although this also depends on the relative magnitude of output and screw speed) and the repetitive flow division and merging along the block is evident. When a more restrictive geometry is used (in this case, a kneading block staggered at $-30°$, followed by a left-handed element, Figure 7.14b), several screw turns upstream work fully filled. In due course, the material progresses downstream along the channels created by the staggered disks. In both situations, the rotation of the disks also subjects the flow to a kneading effect (hence their designation). Generally, when the material supplied to the extruder attains the first screw restrictive section it melts rapidly, due to the combined contribution of local frictional forces, repetitive material compression, and heat transfer [147, 148]. Melting in a twin-screw extruder is much more rapid than in a single screw machine, although a clear understanding of the

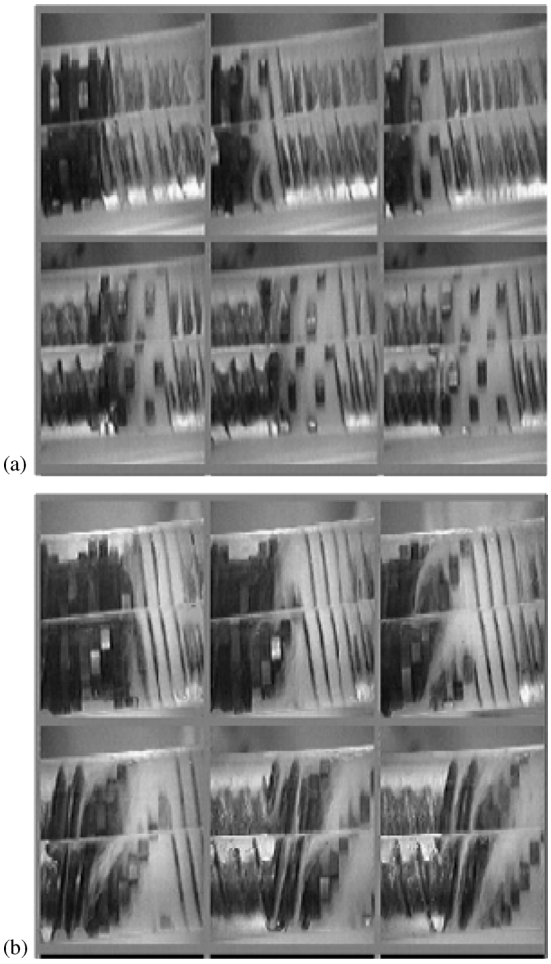

Figure 7.14 Flow visualization for a highly viscous silicone oil along the mixing zone of a twin-screw extruder: (a) orthogonal kneading block (90°); (b) kneading block with negative staggering (−30 °C), plus left-handed element [146].

underlying mechanisms is still lacking (see, for example, References [149–155]). In any case, melting is controlled by screw design, operational parameters, and thermophysical properties of the material.

7.4.2
Evolution Along the Extruder

Generally, reactive extrusion deals with high melt-viscosity systems and diffusion-based reactions. Moreover, chemical reactions also frequently entail a morphology development (e.g., reactive blending, dynamic vulcanization) that progresses along the screw at a rate that depends on local temperatures, residence time, stress levels, and

velocity fields – these being mostly determined by the screw geometry and operating conditions. Nonetheless, the reactions are also controlled by specific parameters. For example, monitoring the grafting of maleic anhydride (MA) onto polyolefins with different ethene/propene ratios along the extruder axis showed that the MA-graft content followed the same profile as the peroxide decomposition profile, with the chemical reactions occurring along the extruder until the peroxide was fully converted [156].

Mixing is always very important in reactive extrusion, as the machine should efficiently generate the necessary contact areas between the ingredients. For instance, reactive functionalized polymers can then form *in situ* block or graft copolymers at the interface of the blend components. Kneading blocks can be designed to generate the extensive melt deformation and reorientation that are mandatory for distributive mixing (as determined by the flow field complexity, average shear rate, and time), while dispersion is governed by the intensity and type of the stresses induced (a strong extensional component is particularly effective for dispersion). As for the morphology development, it is now generally accepted that in the case of polymer blends it involves the formation of sheets or ribbons of the minor component due to the magnitude of the local stresses, which subsequently become unstable and give rise to the formation of a two-dimensional network. When this becomes also unstable, particles or droplets are finally formed [157–160]. In reactive compatibilization, the graft or block copolymers formed at the interface induce a large reduction both in the interfacial tension and in the dispersed phase coalescence due to steric stabilization [161, 162].

In any case, the evolution of the morphology (with time or, equivalently, along the screw length) is far from gradual, sudden changes in particle size or in chemical conversion having been reported. This is especially true for fast reactive systems, where melting is also determinant, as reactions start to occur once this step is initiated. The rheological modification of PP via peroxide induced controlled degradation is a good, but not unique, example of a fast rate reaction. It was demonstrated [163] that PP degradation occurs by chain scission and depends on the level of stresses imposed by the screw elements, on temperature, and on the concentration of the hydrogen-abstracting agent. The reaction was found to be extremely rapid, that is, most of it took place in the first kneading block, upon melting, when the peroxide decomposed and abstracted one hydrogen from the PP chain, facilitating the β-scission mechanism. Similarly, during the dynamic vulcanization of PE/EPDM blends using a resol–$SnCl_2$ system, it was observed that crosslinking of the EPDM phase took place mostly in the first kneading zone, reaching a plateau thereafter [164]. As for PA-6/EPM-g-MA blends, it was reported that although the material remained mostly solid immediately upstream of the first screw restrictive zone, the unreacted MA content had already decreased to less than half of its original value. One L/D (screw length to diameter ratio) later, a fully melted conventional polymer blend morphology was present, with relatively good distributive and dispersive mixing levels, a further important reduction in MA having been measured [133, 165]. This means that the rubber phase was dispersed from a millimeter to a micrometer scale within a few seconds/screw lengths.

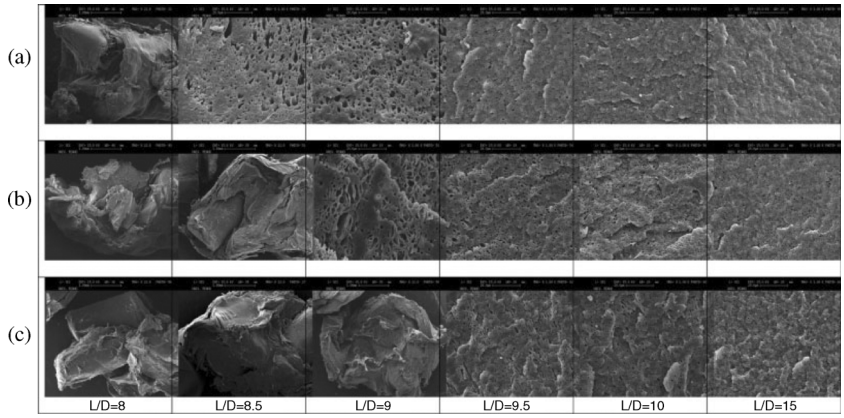

Figure 7.15 PA/PE blend morphology along the extruder for different screw speeds: 300 (a), 200 (b), and 100 rpm (c).

Recently [166], it has been suggested that melting (in terms of onset location and rate) may be the decisive parameter that influences chemical conversion and morphology evolution of fast reactive compatibilization systems. As seen in Figure 7.15 for a PA/PE system, melting in the co-rotating twin-screw extruder is very fast. In the three experiments, performed at different screw speeds, within 0.5 L/D there is a quick transition from a basically solid material to a more or less homogeneous melt. Although at 300 rpm a stable morphology seems to have been achieved around $L/D = 9.5$, at 100 rpm this apparently happens only at $L/D = 15$. As soon as one of the polymer components melts (in this case, PE), it surrounds, even if only partially, the other polymer pellets' surface. The interface thus generated allows straight away for high conversion ratios to be quickly attained. However, at this stage, this can only have a minor impact on the morphological development, as the magnitude of the material deformation does not generate new orders of magnitude of interfacial area, which in turn averts new major gains in chemical conversion. Thus, processing conditions inducing slow melting will also hold back chemical conversion. Considerable gains in interfacial area require full melting of the surviving solids. As this occurs, a dispersed phase is quickly created, and the formation of the copolymer (i.e., a further increase in chemical conversion) helps to swiftly stabilize the size and shape of the suspended particles, which evolve rapidly from large, elongated particles to sub-micrometer regular units. This sequence of events is schematized in Figure 7.16, which illustrates also the effect of the screw speed.

7.4.3 Modeling and Optimization

Since reactive extrusion is an industrially relevant but complex technology, it seems important to develop theoretical approaches that can accurately predict the best

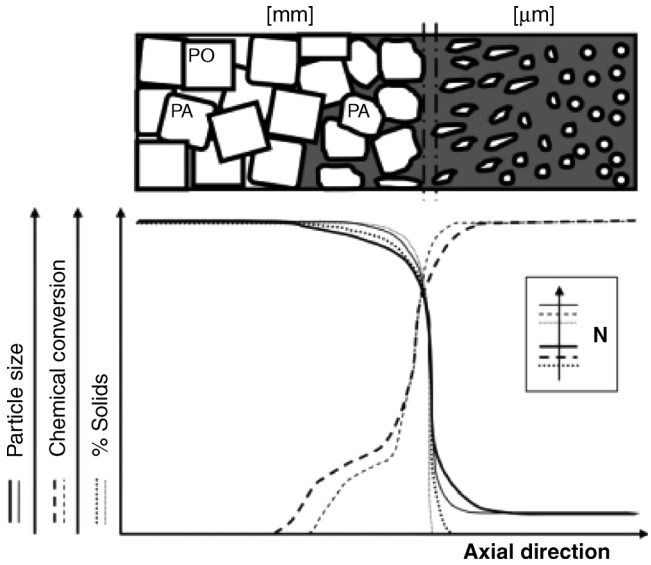

Figure 7.16 Schematic evolution of the physicochemical processes along the extruder during reactive polymer blending [166].

conditions for carrying out successfully a practical reactive extrusion operation as well as to control the process. Two approaches have been adopted, one based on chemical engineering models, the other on continuum mechanics [137, 167]. The first considers the twin-screw extruder as a series of ideal chemical reactors (generally, continuous stirred-tank and/or plug-flow reactors) connected through direct flows and eventual leakage backflows. Mass balances for each reactor provide an approximation to the flow conditions. Similarly, energy balances and kinetic equations permit one to estimate the reactive process. Usually, these methods oversimplify the flow conditions and the parameters used need to be adjusted to each specific situation considered, which limits their predictive capacity and makes them useless for scale-up problems; however, because computations are quick, they can be useful for process control.

The second technique is based on continuum mechanics and requires three models that have to be inter-coupled:

1) The heat transfer and flow inside the extruder are calculated by solving the classical continuum mechanics equations (mass, momentum and energy balances), according to the local geometry and boundary conditions.
2) The rate of the chemical reaction can be expressed by a series of kinetic equations of the type:

$$-\frac{\mathrm{d}c_j}{\mathrm{d}t} = r(c_j, c_i, T) \tag{7.2}$$

where c is concentration and subscript j refers to the reacting species in question and i to other reactants; the kinetic constants depend on local values of time, temperature, mixing conditions, concentration of reagents, and so on.

3) The variations of the physical and rheological properties of the material with the reaction are described by constitutive equations. In particular, changes in viscosity with reaction extent can encompass several orders of magnitude, so it is important to establish adequate rheokinetic relationships.

The reaction kinetics depend on the local values of temperature and residence time; in turn, their evolution changes the viscosity of the material, which affects the flow characteristics. To handle this interdependence, Vergnes and Berzin [167] developed a procedure that consists in performing an initial simulation of the flow in the extruder, to estimate the residence times, temperatures, and reaction extents. The local viscosity changes can then be calculated using the respective constitutive equation. Next, a second simulation is performed, coupling at each location the flow conditions, the reaction development, and the viscosity changes. This technique has predictive capacity but, because it is computationally demanding, cannot be used for control purposes. The two approaches have been adopted in the literature (see examples in References [14, 168, 169]).

Modeling the flow in twin-screw extruders is difficult because of the starve-fed conditions and of the intricacy of the channel geometry (that also changes significantly in the down-channel direction), which create a complex 3D strongly non-isothermal flow pattern. Generally, there are two types of programs (Cassagnau *et al.* [14] recently reviewed these efforts):

1) Global process analyses from hopper to die, which compute the average pressure, temperature, residence time, shear rate, shear stress, and degree of fill axial profiles for a given throughput and screw speed, together with total power consumption, or specific energy consumption. Often, these programs are based on simplified 1D or 2D flow descriptions. Several of them are available commercially [170], the underlying models and algorithms being also accessible in the literature (see, for example, References [171, 172]). As an example, Figure 7.17 illustrates the evolution of melt temperature and pressure along the axis of a twin-screw extruder, as predicted by the Ludovic© software. As shown in the figure and explained above, screw channels become fully filled upstream of, and during flow along, restrictive elements, simultaneously with the development of an important viscous dissipation. In a few programs, the calculations have been extended to reactive systems, yielding the reaction extent profile along the screw.
2) 3D flow simulations are applied for detailed local flow descriptions, producing accurate information on velocity, temperature, and stress fields, as well as flow trajectories, thus enabling one, for instance, to characterize local mixing conditions. Since the computational efforts involved are generally considerable, recent efforts resort to parallel computing and may be based on simplified fictitious domain methods coupled to a "level-set" approach to represent the rotating screws (e.g. in Reference [175], commercialized as XimeX® software).

Figure 7.18 depicts the particle distribution in a twin-screw element after a certain flow time, after having been initially inserted in the gap between the screws. A quantitative estimation of distributive mixing could be applied to this data.

Another theoretical approach worth mentioning is the attempt to develop tools that can optimize automatically the processing conditions and/or the screw

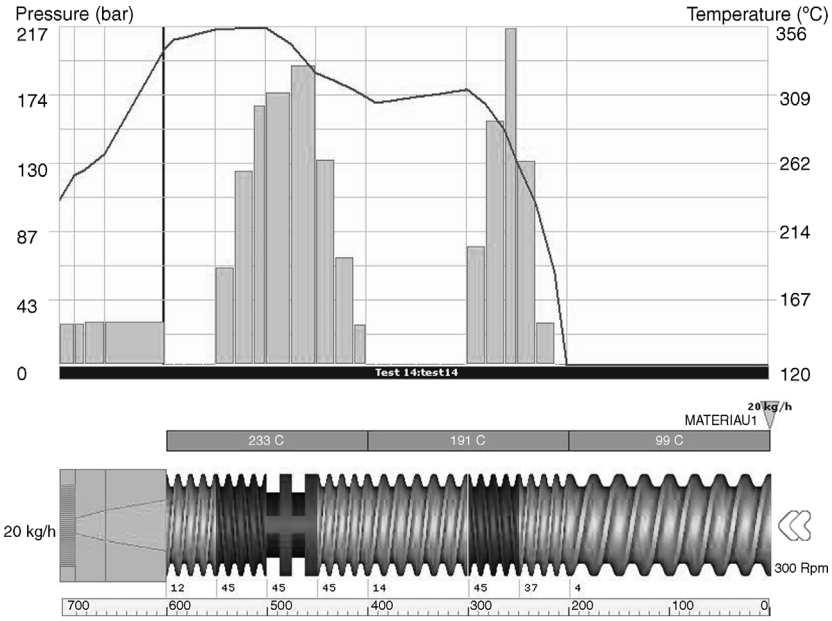

Figure 7.17 Temperature and pressure evolution along the screw profile, as predicted by Ludovic© V5.2 (http://www.scconsultants.com).

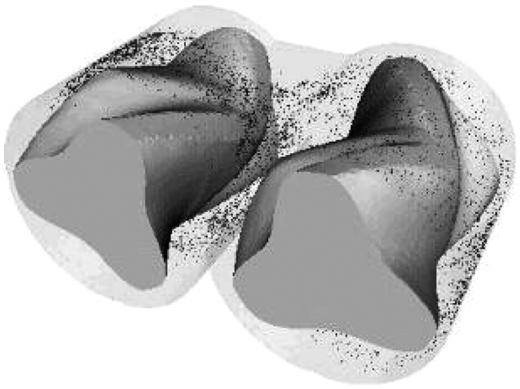

Figure 7.18 Particle distribution in a twin-screw element after a certain flow time, as predicted by XimeX® (http://www.scconsultants.com).

geometry of a co-rotating twin-screw extruder. In the second case, the problem consists in selecting the most adequate location along the screw axis of an available number of screw elements, to maximize a process performance. Multi-objective evolutionary algorithms have been successfully used for this purpose and extension of the method to reactive extrusion has also been attempted [173].

A relevant example of optimization concerns the polymerization of ε-caprolactone, which was modeled by Poulesquen *et al.* [174]. Monomer $[M_0]$ and activator $[I_0]$ are mixed at the entry of the extruder and polymerization (coordination–insertion mechanism) develops progressively. The objective is to reach full conversion at maximum output at the die exit, a major difficulty being the huge change in viscosity of the reactive system (from 10^{-3} to 10^{3} Pa s). Gaspar-Cunha *et al.* [173] applied an optimization algorithm to automatically establish the relative positions of ten screw elements (see dashed areas of the screws represented in Figure 7.19) that maximize output and minimize the melt temperature at the die exit (elements 1 and 2 on one end, and 13 and 14 on the opposite end, were kept unmoved during the optimization). Chemical conversion ratio was used as a restriction, that is, the solutions were taken as valid only if the conversion ratio at the screw end was higher than 99.9%. Since the reaction rate is controlled by the ratio between the initial monomer and initiator concentrations ($[M_0]/[I_0]$), independent runs were carried out using values of 400, 800, and 1000. The optimal screw configurations that maximize output depend on the $[M_0]/[I_0]$ ratio. As this increases, the restrictive elements are located more downstream (and the set barrel temperature increases – not shown), resulting in the efficient axial conversion profiles plotted in the figure.

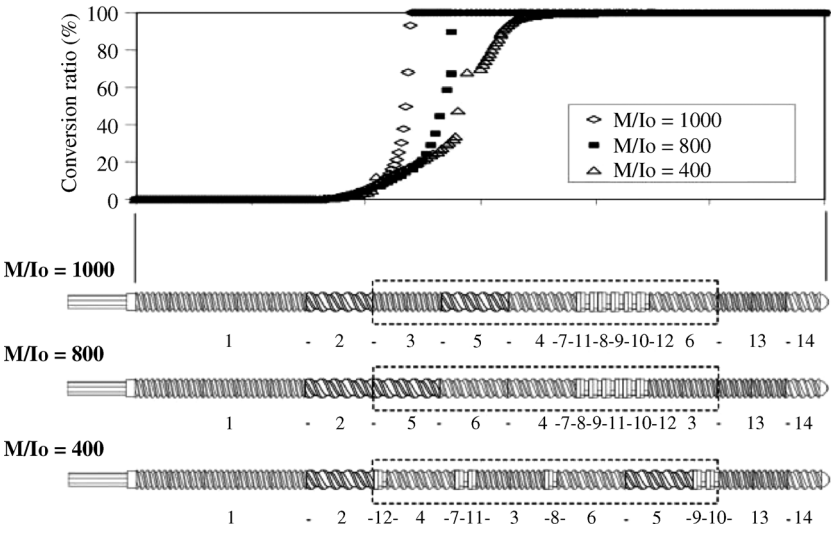

Figure 7.19 Best screw configurations for ε-caprolactone polymerization [173].

7.5 Conclusions

Throughout this chapter it was shown that compatibilization is a viable and cost-effective way of controlling the morphology and morphology stability of immiscible polymer blends, thus converting these systems into successful materials for engineering applications.

The chapter concentrated on two major compatibilization routes, both using copolymers. In *ex situ* compatibilization, a pre-synthesized block or graft copolymer, whose segments are chemically identical to or have affinity with the blend components, are added to the system. The various types of copolymers, their molecular weight, and architecture can be used to control the final morphology. In the case of *in situ* compatibilization, the copolymer is formed at the interface, as a result of the reaction between the functional groups of the blend components. The location and functionality of the reactive groups, the precursors' molecular weight, and the flow characteristics determine the architecture of the copolymers produced as well as the interfacial characteristics. These were illustrated by examples of blends of PBT and PA-6.

Twin-screw extruders can be successfully used for industrial reactive blending. The evolution of chemical conversion and morphology development along the screw of the high reactive systems that are usually converted in these machines is far from gradual. It was shown that melting is a major step for compatibilization, as significant interface regeneration and temperature rise are ensured. Modeling and optimization of reactive blending may contribute to a further increase of the present efficiency levels of this operation.

Abbreviations

Polymers and Monomers

ABS	Acrylonitrile, butadiene and styrene copolymer
AES	Acrylonitrile, ethylene and styrene copolymer
EA	Ethyl acrylate
EPM-g-MA	Ethylene and propylene monomer grafted with maleic anhydride
EPR	Ethylene and propylene rubber
GMA	Glycidyl methacrylate
HDPE	High density polyethylene
MGE	Methyl methacrylate, glycidyl methacrylate and ethyl acrylate copolymer
MMA	Methyl methacrylate
MMA-MA	Methyl methacrylate and maleic anhydride copolymer
PA-6	Polyamide 6
PA-6,6	Polyamide 6,6

PBT	Polybuthylene terephthalate
PC	Polycarbonate
PE	Polyethylene
PEO-b-PPO-b-PEO	Polyethylene oxide and polypropylene oxide copolymer
PET	Polyethylene terephthalate
PMMA	Polymethyl methacrylate
PP	Polypropylene
PP-g-MA	Polypropylene grafted with maleic anhydride
PS	Polystyrene
PS-b-PE	Polystyrene and polyethylene copolymer
PS-GMA	Polystyrene and glycidyl methacrylate copolymer
PS-g-PA-6	Polystyrene and polyamide 6 copolymer
PVP	Poly(2-vinylpyridine)
SAN	Styrene and acrylonitrile copolymer
SBS	Styrene, butadiene and styrene copolymer
SEBS	Styrene, ethylene, butylenes and styrene copolymer
SEBS-g-GMA	Styrene, ethylene, butylenes and styrene copolymer grafted with glycidyl methacrylate
SEBS-g-MA	Styrene, ethylene, butylenes and styrene copolymer grafted with maleic anhydride
SMA	Styrene maleic anhydride
sPS	Syndiotactic polystyrene

Others

M_c	critical entanglement molecular weight
M_e	molecular weight between entanglements
REX	Reactive extrusion
SEM	Scanning electron microscopy
TEM	Transmission electron microscopy

References

1 Utracki, L.A. (1989) *Polymer Alloys and Blends,* Hanser Publishers, New York.

2 Paul, D.R., Barlow, J.W., and Keskkula, H. (1988) *Polymer Blends,* in *Encyclopedia of Polymer Science and Engineering,* vol. 12, 2nd edn (eds H.F. Mark, N.M. Bikales, C.G. Overberger, and G. Menges), Wiley-Interscience, New York, p. 399.

3 Paul, D.R. and Newman, S. (1979) *Polymer Blends,* Academic Press, New York.

4 Utracki, L.A. (1994) *Encyclopaedic Dictionary of Commercial Polymer Blends,* ChemTec Publishing, Toronto.

5 Datta, S. and Lohse, D. (1996) *Polymeric Compatibilizers,* Hanser Publishers, New York.

6 Koning, C., Duin, M., Pagnoulle, C., and Jerome, R. (1998) *Prog. Polym. Sci.*, **23**, 707.

7 Gaylord, N. (1989) *J. Macromol. Sci.*, **26**, 1211.

8 Xanthos, M. and Dagli, S. (1991) *Polym. Eng. Sci.*, **31**, 929.

9 Triacca, V.J., Ziaee, S., Barlow, J.W., Keskkula, H., and Paul, D.R. (1991) *Polymer,* **32**, 1401.

10 Dali, S.S., Xanthos, M., and Biesenberger, J.A. (1994) *Polym. Eng. Sci.*, **43**, 1720.

11 Machado, A.V., Yquel, V., Covas, J.A., Flat, J.-J., Ghamri, N., and Wollny, A. (2006) *Macromol. Symp.*, **233**, 86.

12 Xanthos, M. (1992) *Reactive Extrusion: Principles and Practice*, Hanser Publishers, New York.

13 Lambla, M. (1993) Reactive processing of thermoplastic polymers, in *Comprehensive Polymer Science* (eds G. Allen and J.C. Bewington), 1st supplement, Pergamon Press, New York.

14 Cassagnau, P., Bounor-Legare, V., and Fenouillot, F. (2007) *Int. Polym. Proc.*, **3** (XXII), 218–258.

15 Leibler, L. (1982) *Macromolecules*, **15**, 1283.

16 Noolandi, J. and Hong, M. (1982) *Macromolecules*, **15**, 482.

17 Baker, W., Scott, C., and Hu, G.H. (2001) *Reactive Polymer Blending*, Hanser Publisher, Munich.

18 Ramic, A.J., Stehlin, J.C., Hudson, S.D., Jamieson, A.M., and Manas-Zloczower, I. (2000) *Macromolecules*, **33**, 371–374.

19 Matos, M., Favis, B.D., and Lomellini, P. (1995) *Polymer*, **36**, 3899.

20 Chio, W.M., Park, O.O., and Lim, J.G. (2004) *J. Appl. Polym. Sci.*, **91**, 3618.

21 Hong, B.K. and Jo, W.H. (2000) *Polymer*, **42**, 1062.

22 Cigana, P., Favis, B.D., and Jerome, R. (1996) *J. Polym. Sci. Part B, Polym. Phys.*, **34**, 1691.

23 Cigana, P. and Favis, B.D. (1998) *Polymer*, **39**, 3373.

24 Harrats, C., Fayt, R., and Jérôme, R. (2002) *Polymer*, **43**, 863.

25 Zhang, C., Feng, L., Gu, X., Hoppe, S., and Hu, G.-H. (2007) *Polymer*, **48**, 5940–5949.

26 Cimmino, S., Coppola, F., D'Orazio, L., Greco, R., Maglio, G., and Malinconico, M. (1986) *Polymer*, **27**, 1874.

27 Chen, C. and White, J.L. (1993) *Polym. Eng. Sci.*, **33**, 923.

28 Carte, T.L. and Moet, A. (1993) *J. Appl. Polym. Sci.*, **48**, 611.

29 Kalfoglou, N.K., Skafidas, D.S., Kallitsis, J.K., Lambert, J.C., and Van der Stappen, L. (1995) *Polymer*, **36**, 4453.

30 La Mantia, F.P., Vinci, M., and Pilati, F. (1994) *Polym. Recycl.*, **1**, 33.

31 Heino, M., Kirjava, J., Hietaoja, P., and Seppala, J. (1994) *J. Appl. Polym. Sci.*, **54**, 1613.

32 Creton, C., Kramer, E.J., and Hadziioannou, G. (1991) *Macromolecules*, **24**, 1846.

33 Gallowaya, J., Jeon, H., Bellc, J., and Macosko, C. (2005) *Polymer*, **46**, 183.

34 Willis, J.M. and Favis, B.D. (1988) *Polym. Eng. Sci.*, **28**, 1416.

35 Lee, J.D. and Yang, S.M. (1995) *Polym. Eng. Sci.*, **35**, 1821.

36 Fayt, R., Jerome, R., and Teyssie., Ph. (1989) *J. Polym. Sci. Part B, Polym. Phys.*, **27**, 775.

37 Hu, G.H., Sun, Y.J., and Lambla, M. (1996) *Polym. Eng. Sci.*, **36**, 676.

38 Sun, Y.J., Hu, G.H., Lambla, M., and Kotlar, H.K. (1996) *Polymer*, **25**, 4119.

39 Anastasiadis, S., Gancarz, I., and Koberstein, J. (1989) *Macromolecules*, **22**, 1449.

40 Hong, B.K. and Jo, W.H. (2000) *Polymer*, **41**, 2069.

41 Macaúbas, P.H.P. and Demarquette, N.R. (2001) *Polymer*, **42**, 2543.

42 Fredrickson, G.H. and Milner, S.T. (1996) *Macromolecules*, **29**, 7386.

43 O'Shaughnessy, B. and Sawhney, U. (1996) *Phys. Rev. Lett.*, **76**, 3444.

44 O'Shaughnessy, B. and Sawhney, U. (1996) *Macromolecules*, **29**, 7230.

45 O'Shaughnessy, B. and Vavylonis, D. (1999) *Europhys. Lett.*, **45**, 638.

46 O'Shaughnessy, B. and Vavylonis, D. (1999) *Macromolecules*, **32**, 1785.

47 O'Shaughnessy, B. and Vavylonis, D. (2000) *Phys. Rev. Lett.*, **84**, 3193.

48 O'Shaughnessy, B. and Vavylonis, D. (2000) *Eur. Phys. J. E*, **1**, 159.

49 Jeon, H.K. and Kim, J.K. (2000) *Macromolecules*, **33**, 8200.

50 Guégan, P., Macosko, C.W., Ishizone, T., Hirao, A., and Nakahama, S. (1994) *Macromolecules*, **27**, 4993.

51 Schulze, J.S., Cernohous, J.J., Hirao, A., Lodge, T.P., and Macosko, C.W. (2000) *Macromolecules*, **33**, 1191.

52 Oyama, H.T. and Inoue, T. (2001) *Macromolecules*, **34**, 3331.

53 Orr, C.A., Cernohous, J.J., Guegan, P., Hirao, A., Jeon, H.K., and Macosko, C.W. (2001) *Polymer*, **42**, 8171.

54 Oyama, H.T., Ougizawa, T., Inoue, T., Weber, M., and Tamaru, K. (2001) *Macromolecules*, **34**, 7017.

55 Yin, Z., Koulic, C., Pagnoulle, C., and Jérôme, R. (2003) *Langmuir*, **19**, 453.

56 Jones, T.D., Schulze, J.S., Macosko, C.W., and Lodge, T.P. (2003) *Macromolecules*, **36**, 7212.

57 Kim, H.Y., Jeong, U., and Kim, J.K. (2003) *Macromolecules*, **36**, 1594.

58 Lyu, S., Cernohous, J.J., Bates, F.S., and Macosko, C.W. (1999) *Macromolecules*, **32**, 106.

59 Kim, B.J., Kang, H., Char, K., Katsov, K., Fredrickson, G.H., and Kramer, E.J. (2005) *Macromolecules*, **38**, 6106.

60 Zhang, J., Lodge, T.P., and Macosko, C.W. (2005) *Macromolecules*, **38**, 6586.

61 Jiao, J., Kramer, E.J., de Vos, S., Möller, M., and Koning, C. (1999) *Polymer*, **40**, 3585.

62 Jiao, J., Kramer, E.J., de Vos, S., Möller, M., and Koning, C. (1999) *Macromolecules*, **32**, 6261.

63 Kim, J.K., Jeong, W., Son, J., and Jeon, H.K. (2000) *Macromolecules*, **33**, 9161.

64 Shull, K.R. (1991) *J. Chem. Phys.*, **94**, 5723.

65 Yeung, C. and Herrmann, K.A. (2003) *Macromolecules*, **36**, 229–237.

66 Jeon, H.K., Macosko, C.W., Moon, B., Hoye, T.R., and Yin, Z. (2004) *Macromolecules*, **37**, 2563.

67 Zhao, W., Zhao, X., Rafailovich, M.H., Sololov, J., Compost, R.J., Smith, S.D., Satkowski, M., Russell, T.P., Dozier, W.D., and Mansfield, T. (1993) *Macromolecules*, **26**, 561.

68 Jeon, H.K., Feist, B.J., Koh, S.B., Chang, K., Macosko, C.W., and Dion, R.P. (2004) *Polymer*, **45**, 197.

69 Jeon, H.K., Hyun, T.O., and Kim, J.K. (2001) *Polymer*, **42**, 3259.

70 Jeon, H.K. and Kim, J.K. (1998) *Macromolecules*, **31**, 9273.

71 Yin, Z., Koulic, C., Pagnoulle, C., and Jérôme, R. (2001) *Macromolecules*, **34**, 5132.

72 Yin, Z., Koulic, C., Jeon, H.K., Pagnoulle, C., Macosko, C.W., and Jérôme, R. (2002) *Macromolecules*, **35**, 8917.

73 Helfand, E. and Tagami, Y. (1971) *J. Polym. Sci.*, **9**, 741.

74 Broseta, D., Fredrickson, G.H., Helfand, E., and Leibler, L. (1990) *Macromolecules*, **23**, 132.

75 Moon, B., Hoye, T.R., and Macosko, C.W. (2002) *Polymer*, **43**, 5501.

76 Kim, H.Y., Lee, D.H., and Kim, J.K. (2006) *Polymer*, **47**, 5108.

77 Charoensirisomboon, P., Inoue, T., and Weber, M. (2000) *Polymer*, **41**, 6907.

78 Charoensirisomboon, P., Chiba, T., Solomko, S.I., Inoue, T., and Weber, M. (1999) *Polymer*, **40**, 6803.

79 Pan, L., Chiba, T., and Inoue, T. (2001) *Polymer*, **42**, 8825.

80 Fetters, L.J., Lohse, D.L., Richter, D., Witten, T.A., and Zirkel, A. (1994) *Macromolecules*, **27**, 4649.

81 Leibler, L. (1988) *Makromol Chem. Macromol Symp*, **16**, 1.

82 Elemans, P.H.M. and Meijer, H.E.M. (1988) *Polym. Eng. Sci.*, **28**, 2751.

83 Karger-Kocsis, J. and Vergnes, B. (1996) *Polym. Eng. Sci.*, **36**, 1685.

84 Favis, B.D. and Chalifoux, J.P. (1988) *Polymer*, **29**, 1761.

85 Scott, C.E. and Macosko, C.W. (1991) *Polym. Bull.*, **26**, 341.

86 Scott, C.E. and Macosko, C.W. (1994) *Polymer*, **35**, 5422.

87 Sundararaj, U., Dori, Y., and Macosko, C.W. (1995) *Polymer*, **36**, 1995.

88 Sundararaj, U. and Macosko, C.W. (1995) *Macromolecules*, **28**, 2647.

89 Sundararaj, U. and. Macosko, C.W. (1996) *Polym. Eng. Sci.*, **36**, 1769.

90 Cartier, H. and Hu, G.H. (1999) *J. Polym. Eng. Sci.*, **39**, 996.

91 Duin, M., Gurp, M., Leemans, L., Walet, M., Aussems, M., Martin, P., Legras, R., Machado, A.V., and Covas, J.A. (2003) *Macromol. Symp.*, **198**, 135–145.

92 Machado, A.V., Covas, J.A., and van Duin, M. (1999) *J. Appl. Polym. Sci.*, **71**, 135–141.
93 Duin, M., Machado, A.V., and Covas, J.A. (2001) *Macromol. Symp.*, **170**, 29.
94 Minale, M., Mewis, J., and Moldenaers, P. (1998) *AIChE J.*, **44**, 943.
95 Lyu, S.P., Bates, F.S., and Macosko, C.W. (2002) *AIChE J.*, **48**, 7.
96 Milner, S.T. and Xi, H.W. (1996) *J. Rheol.*, **40**, 663.
97 Macosko, C.W., Guégan, P., Nakayama, A.K.K.A., Marechal, P., and Inoue, T. (1996) *Macromolecules*, **29**, 5590.
98 Lyu, S., Jones, T.D., Bates, F.S., and Macosko, C.W. (2002) *Macromolecules*, **35**, 7845.
99 Hage, E., Hale, W., Keskkula, H., and Paul, D.R. (1997) *Polymer*, **38**, 3237.
100 Corte, L. and Leibler, L. (2007) *Macromolecules*, **40**, 5606.
101 Borggreve, R.J.M., Gaymans, R.J., Schuijer, J., and Ingen Housz, J.F. (1987) *Polymer*, **28**, 1489.
102 Wu, S.H. (1988) *J. Appl. Polym. Sci.*, **35**, 549. Proceeding 8th International Conference on Deformation, Yield and Fracture of Polymers, Churchill College, Cambridge, 8-11 April 1991, Plastic and Rubber Institute, London, 78.
103 Bartczak, Z., Argon, A.S., Cohen, R.E., and Weinberg, M. (1999) *Polymer*, **40**, 2331.
104 Loyens, W. and Groenickx, G. (2002) *Polymer*, **43**, 5679.
105 Wu, S. (1985) *Polymer*, **26**, 1855.
106 Jiang, W., Liang, H., and Jiang, B. (1998) *Polymer*, **39**, 4437.
107 Jiang, W., Liu, C., Wang, Z., An, L., Liang, H., Jiang, B., Wang, X., and Zhang, H. (1998) *Polymer*, **39**, 3285.
108 Gan, P.P. and Paul, D.R. (1994) *Polymer*, **35**, 3513.
109 Sun, Y.J., Hu, G.H., Lambla, M., and Kotlar, H.K. (1996) *Polymer*, **37**, 4119.
110 Angew, H.M. (1992) *Makromol. Chem.*, **196**, 89.
111 Hale, W., Keskkula, H., and Paul, D.R. (1999) *Polymer*, **40**, 3665.
112 Hale, W., Pessan, L.A., Keskkula, H., and Paul, D.R. (1999) *Polymer*, **40**, 4237.
113 Ito, E.N., Pessan, L.A., Covas, J.A., and Hage, E. (2003) *Int. Polym. Process.*, **18**, 376.
114 Ambrósio, J.D., Larocca, N.M., Pessan, L.A., and Hage, E. (2010) *Polym. Eng. Sci.*, **50**, 2382.
115 Mantovani, G.L., Canto, L.B., Hage, E., and Pessan, L.A. (2001) *Macromol. Symp.*, **176**, 167.
116 Martin, P., Devaux, J., Legras, R., van Gurp, M., and van Duin, M. (2001) *Polymer*, **42**, 2463.
117 Larocca, N.M., Hage, E. and Pessan, L.A. (2004) *Polymer*, **45**, 5265.
118 Larocca, N.M., Hage, E., and Pessan, L.A. (2005) *J. Polym. Sci. Part B: Polym. Phys.*, **43**, 1244.
119 Canto, L.B., Torriani, I.L., Plivelic, T.S., Hage, E. and Pessan, L.A. (2007) *Polym. Int.*, **56**, 308.
120 Kitayama, N., Keskkula, H., and Paul, D.R. (2000) *Polymer*, **41**, 8053.
121 Kudva, R.A., Keskkula, R.A., and Paul, D.R. (2000) *Polymer*, **41**, 225.
122 Kudva, R.A., Keskkula, H., and Paul, D.R. (2000) *Polymer*, **41**, 239.
123 Kudva, R.A., Keskkula, H., and Paul, D.R. (1998) *Polymer*, **39**, 2447.
124 Araújo, E.M., Hage, E., and Carvalho, A.J.F. (2003) *J. Appl. Polym. Sci.*, **87**, 842.
125 Araújo, E.M., Hage, E., and Carvalho, A.J.F. (2003) *J. Appl. Polym. Sci.*, **90**, 3512.
126 Araújo, E.M., Hage, E., and Carvalho, A.J.F. (2003) *J. Mater. Sci.*, **38**, 3515.
127 Araújo, E.M., Hage, E., and Carvalho, A.J.F. (2003) *J. Appl. Polym. Sci.*, **90**, 2643.
128 Araújo, E.M., Hage, E., and Carvalho, A.J.F. (2004) *J. Mater. Sci.*, **39**, 1173.
129 Becker, D., Porcel, F., Hage, E., and Pessan, L.A. (2008) *Polym. Bull.*, **61**, 353.
130 Becker, D., Hage, E., and Pessan, L.A. (2010) *J. Appl. Polym. Sci.*, **115**, 2540.
131 Becker, D., Hage, E., and Pessan, L.A. (2007) *J. Appl. Polym. Sci.*, **106**, 3248.
132 Machado, A.V., Covas, J.A., and Duin, M. (2002) *Polym. Eng. Sci.*, **42**, 2032.
133 Machado, A.V., Covas, J.A., and Duin, M. (2001) *J. Appl. Polym. Sci.*, **80**, 1535.

134 Covas, J.A., Machado, A.V., and Duin, M. (2000) *Adv. Polym. Technol.*, **19**, 260.

135 Michaeli, W., Grefenstein, A., and Berghaus, U. (1995) *Polym. Eng. Sci.*, **35**, 1485.

136 Tzoganakis, C. (1989) *Adv. Polym. Technol.*, **9**, 321.

137 Sakai, T. (2008) Twin-screw extruders used for reactive design processing: design and application. Plastic Extrusion Asia 17–18 March 2008, Bangkok, Thailand.

138 Machado, A.V., Covas, J.A., Bounor-Legare, V., and Cassagnau, P. (2009) Reactive polymer processing and design of stable micro and nano structures, in *Advances in Polymer Processing: Macro- to Nano-Scales* (eds S. Thomas and Y. Weimin) Woodhead Publishing Ltd., UK, pp. 579–621.

139 Janseen, L.P.B.M. (1988) *Polym. Eng. Sci.*, **38**, 2010.

140 Isac, S.K. and George, K.E. (2001) *J. Appl. Polym. Sci.*, **81**, 2545.

141 Mack, W.A. and Herter, R. (1976) *Chem., Eng. Progr.*, **72**, 64.

142 Van Der Goot, A.J., Hettema, R., and Jansen, L.P.B.M. (1997) *Polym. Eng. Sci.*, **37**, 511.

143 Beyreuther, R., Tandler, B., Hoffmann, M., and Vogel, R. (2001) *J. Mater. Sci.*, **36**, 3103.

144 Martin, C. (2008) Twin screw extrusion – advances for compounding, devolatilization, and direct extrusion. Plastic Extrusion Asia 17–18 March 2008, Bangkok, Thailand.

145 Tang, H., Wrobel, L.C., and Fan, Z. (2003) *Model. Simul. Mater. Sci. Eng.*, **11**, 771.

146 Carneiro, O.S., Caldeira, G., and Covas, J.A. (1999) *J. Mater. Process. Technol.*, **309**, 92.

147 Gogos, C.C., Tadmor, Z., and Kim, M.H. (1998) *Adv. Polym. Technol.*, **17**, 285.

148 Zhu, L. and Narh, K.A. (2006) *Simulation*, **82**, 543–548.

149 Bawiskar, S. and White, J.L. (1998) *Polym. Eng. Sci.*, **38**, 727–740.

150 Kim, D.S., Lee, B.K., Kim, H.S., Lee, J.W., and Gogos, C.G. (2001) *Korea-Australia Rheol. J.*, **13**, 89–95.

151 Vergnes, B., Souveton, G., Delacour, M.L., and Ainser, A. (2001) *Int. Polym. Proc.*, **16**, 351.

152 Liu, T., Wong, A.C.-Y., and Zhu, F. (2001) *Int. Polym. Proc.*, **16**, 113.

153 Yichong, G. and Fuhua, Z. (2003) *Polym. Eng. Sci.*, **43**, 306.

154 Chen, H., Sundararaj, U., Nandakumar, K., and Wetzel, M.D. (2004) *Ind. Eng. Chem. Res.*, **43**, 6822.

155 Garge, S.C., Wetzel, M.D., and Ogunnaike, B.A. (2007) *Polym. Eng. Sci.*, **47**, 1040.

156 Machado, A.V., Van Duin, M., and Covas, J.A. (2000) *J. Polym. Sci. Part A: Polym. Chem.*, **38**, 3919.

157 Sundararaj, U., Macosko, C.W., Rolando, R.J., and Chan, H.T. (1992) *Polym. Eng. Sci.*, **32**, 1814.

158 Scott, C.E. and Macosko, C.W. (1995) *Polymer*, **36**, 461.

159 Majumdar, B., Paul, D.R., and Oshinski, A.J. (1997) *Polymer*, **38**, 1787.

160 Lee, J.K. and Han, C.D. (2000) *Polymer*, **41**, 1799.

161 Cho, K. and Li, F. (1991) *Macromolecules*, **24**, 2752.

162 Creton, C., Hooker, J., and Shull, K.R. (2001) *Langmuir*, **17**, 4948.

163 Machado, A.V., Maia, J.M., Canevarolo, S.V., and Covas, J.A. (2004) *J. Appl. Polym. Sci.*, **91**, 2711–2720.

164 Machado, A.V., van Duin, M., and Covas, J.A. (2006) *Mater. Sci. Forum*, **514–516**, 838.

165 Machado, A.V., Covas, J.A., and Duin, M. (1999) *J. Polym. Sci. Part A: Polym. Chem.*, **37**, 1311.

166 Yquel, V., Machado, A.V., Covas, J.A., and Flat, J.J. (2009) *J. Appl. Polym. Sci.*, **114**, 1768.

167 Vergnes, B. and Berzin, F. (2006) *C.R. Chim.*, **9**, 1409.

168 Jia, Y., Zhang, G., Wu, L., Sun, S., Zhao, G., and An, L. (2007) *Polym. Eng. Sci*, **47**, 667–674.

169 Anon (2005) *Plastics Additives Compound.*, March/April, 34.

170 Vergnes, B., Della Valle, G., and Delamare, L. (1998) *Polym. Eng. Sci.*, **38**, 121.

171 White, J.L., Keum, J., Jung, H.L., Ban, K., and Bumm, S. (2006) *Polym. Plast. Technol. Eng.*, **45**, 539.

172 Valette, R., Vergnes, B., and Coupez, T. (2008) *Int. J. Mat. Form.*, **1**, 1131.

173 Gaspar-Cunha, A., Covas, J.A., and Vergnes, B. (2005) *Polym. Eng. Sci.*, **45**, 1159.

174 Poulesquen, A., Vergnes, B., Cassagnau, P., Gimenez, J., and Michel, A. (2001) *Int. Polym. Process.*, **16**, 31.

8
Chemical and Engineering Aspects of Morphology Development and Processing of Multiphase Polymer Blend Nanocomposites

I. Sedat Gunes and Sadhan C. Jana

8.1
Introduction: The Promise and Challenge of Polymer Blending

Polymer mixing and blending has been one of the major research fields of polymer engineering and science [1]. The growing economic importance of polymers and their blends in the post-World War II era served as the major impetus for industrial and academic research efforts although the origin of polymer blending dates back to the early nineteenth century, as discussed by White [2]. Mausser [3] suggested that residents of ancient Mesoamerica regularly performed rubber processing – possibly also blending – as rubber balls were produced and used in social and religious rituals as early as 600 AD. Recent research revealed that the history of rubber processing in Mesoamerica is much older, starting as early as 1600 BC [4]. However, "modern" polymer blending emerged mostly due to commercial interests, as a relatively inexpensive means to produce "new" materials with improved properties from existing polymers [5]. Even today, only around two dozen commercially viable polymers are found in the market although the number of different blend combinations using these existing polymers may reach a very large number. Of these, only a handful of polymer blends have fulfilled the expectations of desired properties improvement.

Several factors are found responsible for why numerous blend systems are not successful. First, the component polymers are usually not miscible with each other due to thermodynamic constraints, for example, lack of solubility and finite interfacial tension. Second, immiscible polymer blend preparation is often affected by kinetic constraints, for example, slower rate of deformation of the dispersed polymer and faster rate of coalescence of the droplets. In turn, these rates are directly influenced by the type of flow field, for example, shear versus extensional, strain history, chemical reactions, for example, grafting reactions at polymer–polymer interfaces or polymerization-induced phase separation, and polymer properties, such as viscosity and interfacial tension. Accordingly, the multidisciplinary efforts to analyze, understand, and design polymer blends with improved properties extend from synthesis and characterization to processing and manufacturing. Such efforts

Encyclopedia of Polymer Blends: Volume 2: Processing, First Edition. Edited by Avraam I. Isayev.
© 2011 Wiley-VCH Verlag GmbH & Co. KGaA. Published 2011 by Wiley-VCH Verlag GmbH & Co. KGaA.

in turn created a plethora of data [6, 7]. More recently, research on polymer blends has been extended to include the effects of inorganic fillers on the dynamics of morphology development and the final properties [8].

Inorganic fillers have been observed to make two positive contributions to the final properties of polymer blends. The first is the "usual" improvement in mechanical and thermal properties originating from the presence of stiff inorganic fillers in an organic matrix. Note that the "usual" effects in this case can be rationalized using continuum mechanics or relatively simple rule of mixtures [9]. The second, and purportedly more crucial, impact originates from the ability of fillers to change the morphology of polymer blends. This can give birth to an unprecedented number of possibilities in positively tailoring the properties of polymers. Thus, this section reviews the physical mechanisms responsible for morphology development in filled polymer blends and presents an engineering perspective on processing and compounding of these materials using the arguments from rheology, thermodynamics, and the nature of physical interactions in composites.

In the following, we first discuss the behavior of conventional fillers, such as carbon fibers, carbon black, and talc, in polymer blends and their effects on morphology and engineering properties. We specifically aimed to identify the interplay between the filler–matrix interactions and the fundamental morphological features, such that the filler particles can be identified preferentially in one of the phases or at the interfaces and the effects of such selective localization on blend morphology. In subsequent sections, we focus on polymer blends filled with nanofillers, such as layered silicate clay and graphene, carbon nanotubes, and nano-silica. In this context, we also aim to illustrate the parallels between the blends filled with micron-sized fillers and nano-sized fillers. An analysis of the potential origins of the reported deviations is then presented. Finally, we present a detailed discussion on processing of polymer blend nanocomposites, especially their rheological and mechanical properties.

8.2
Inorganic Particles in Small Molecule Liquid Emulsion: A Model System for Filled Polymer Blends?

There are fundamental similarities between small molecule immiscible liquid–liquid dispersions, for example, emulsions, and immiscible polymer blends. It is obvious to the reader that the basic laws of equilibrium thermodynamics applies to all physical systems, whether composed of small molecules or long-chain polymers. The thermodynamic considerations can be relatively easily visualized in terms of a simple principle such as "like dissolves like" (Figure 8.1).

Inorganic particles can be selectively wetted by the liquid phase if the particles and the liquid undergo favorable energetic interactions, such as polar–polar interactions, hydrogen bonding, or acid–base interactions. Thermodynamic equilibrium and the highest attainable entropy are easily reached in the cases of suspensions in liquids of low molecular weight due to very low liquid viscosity and fast molecular diffusion.

Figure 8.1 Appearance of carbon nanofiber (CNF) and oxidized carbon nanofiber (ox-CNF) dispersions in methylene-iso-butyrate (MIB). MIB is a low-viscosity liquid at room temperature and the dispersions were prepared by shaking by hand. The ox-CNF/MIB dispersion was stable at room temperature for at least a couple of weeks without any visible phase separation. The CNF/MIB dispersion immediately phase separated upon ceasing hand shaking. Note that MIB is a highly polar liquid. CNF is almost completely nonpolar, whereby ox-CNF is considerably polar.

However, as we discuss later in this chapter, the equilibrium thermodynamic considerations can address only a part of the issues encountered in polymer–polymer, polymer–filler, and polymer–polymer–filler blends. In these cases, high viscosity of polymers limits attaining the thermodynamic equilibrium. Hence, kinetic factors, such as mixing rate, strain type, and strain history, become dominant, although the information from thermodynamics is still useful. Here, we only discuss certain aspects of filled emulsions. A more detailed description of all relevant phenomena is beyond the scope of this chapter. Interested readers are referred to fundamental studies reported elsewhere [10].

The practical industrial knowledge on stabilization effects of inorganic particles on emulsions has been apparently known since the nineteenth century [11]. Scientific analyses in this field followed up to the early twentieth century [12, 13]. A few words are in order to elaborate the intended meaning of the term "stabilization." In small molecule liquid emulsions, the inorganic particles may locate themselves at the interfaces of the immiscible phases, if the affinity for any of the phases is not strong.

Often, the entire interface may be completely covered by the particles [14]. Hence, the physical presence of the particles at the interfaces effectively prevents coalescence of the individual droplets and the overall morphology of the dispersed droplets is preserved or "stabilized" without macroscopic phase separation. A direct comparison between the emulsions of small molecular liquids and polymer blends is difficult. First, as we discuss later, most filler particles in immiscible polymer blends do not locate themselves at the interfaces. Second, it is rare that the droplet–matrix interface in polymer blends is completely covered by the inorganic particles. Third, obtaining conclusive evidence of "stabilization" of polymer blends by inorganic particles is difficult. Unlike small molecular liquid emulsions, polymer blends do not undergo large scale, straight-forward phase separation apparent to the naked eye in the presence or in the absence of inorganic particles. This can be attributed to slow molecular diffusion and high viscosity of the medium. Studies on filled polymer blends also suggested that the fillers indeed do not exert much impact on the phase separation behavior and the critical solution temperatures [15]. As we discuss later, most observations on filler impacts on morphology of polymer blends have been limited to the formation of smaller droplets in the presence of inorganic particles, the origin of which might be, at least partially, different than that of filler impacts in small molecular liquid emulsions.

Before moving further, let us first present a brief review of polymer blends filled with micron-sized particles to gain more insight into filled polymer blends. Indeed, the majority of the fundamental issues, such as selective filler dispersion, filler exclusion due to high viscosity, and changes in droplet size and shape in the presence of inorganic particles, had been first identified in blend composites filled with micron-size particles.

8.3
Chemical Aspects of Morphology Development and Processing of Multiphase Polymer Blend Nanocomposites

8.3.1
Conventional Fillers in Polymer Blends

Micron-sized fillers, such as glass fibers, carbon fibers, carbon black, talc, and micron-sized silica particles have been considered as conventional fillers. Polymer composites filled with conventional fillers have been widely investigated by both academic and industrial researchers. A wide spectrum of archival reports is available on how these fillers impact the properties. As expected, various fundamental issues of interest to nanocomposites research, such as the state of filler dispersion, filler–matrix interactions, and processing methods, have already been widely analyzed and documented in the context of conventional composites, especially those of carbon black and silica-filled rubber compounds [16]. It is worth mentioning that carbon black (CB) could not be considered as a nanofiller. There appears to be a general tendency in contemporary literature to designate CB as a nanofiller – apparently derived from

the perception that the primary particles are on the order of 10 nm. However, the primary CB particles form aggregates due to covalent bonding and the aggregate sizes often approach a few micrometers [17].

In view of the long history of research efforts on filled rubbers, it is not surprising that the initial works on filled polymer blends appeared in publications authored by rubber compounders and carbon black vendors [17, 18]. For instance, Walters and Keyte [17] observed that the compound ingredients, such as CB and zinc oxide, were not homogenously dispersed in rubber blends. Hess *et al.* [18] also reported a series of fundamental observations. First, they observed that filler particles tend to remain in the lower viscosity phase, in the absence of significant filler–matrix interactions. However, in the presence of strong polar–polar interactions between the filler particles and one of the phases, the particles were found to be selectively dispersed in the more polar phase and the viscosity became less important. More recently, Portal *et al.* [19] also presented similar observations about selective localization of CB particles in the natural rubber (NR) phase in NR/polybutadiene blends.

Similar to CB-filled rubber blends, CB-filled immiscible thermoplastic polymer blends have also received significant attention due to their commercial importance in applications requiring electrically conductive compounds [20]. In these blends, carbon black was found to be located either in one of the phases or at the interfaces between the phases [21]. In the former case, CB has the potential to exert a strong influence on the morphology of the phase in which it is dispersed. For example, distinct droplet morphology of the dispersed phase may change to a co-continuous morphology in the presence of CB. This, in turn, can drastically change the electrical conductivity of the blends; an insulator with dispersed droplet morphology may now offer conductive pathways by double electrical percolation [21]. In the case where CB remains at the interfaces, the electrical percolation occurs at much lower filler concentration [22]. A similar behavior has also been documented in filled semi-crystalline polymers in which the conductive particles are expelled from the crystalline regions and their effective local concentration increases substantially (Figure 8.2).

Following the initial observations on filled rubber and thermoplastic blends, an array of studies focused on the chemical and engineering aspects of filled polymer blends. Most notably, Lipatov and coworkers [23, 24] presented several reports on phase behavior and engineering properties in filled blends. They offered extensive mechanistic explanations on observed "stabilization" effects using the arguments derived from polymer absorption on filler surfaces [25] and changes in calculated thermodynamic interaction parameters [26]. Counter arguments and experimental evidence of the absence of compatibilization effects using thermal and dynamic mechanical data were also presented [27].

The focus on visual evidence of morphological forms of filled polymer blends emerged in the literature in conjunction with studies on electron microscopy. Breuer *et al.* [28] used a series of SEM images to study morphology development in CB-filled linear low density polyethylene (LLDPE)/high impact polystyrene (HIPS) blends. These authors made the following observations. First, CB particles were observed to be localized in LLDPE droplets. Second, the presence of CB particles reduced the size

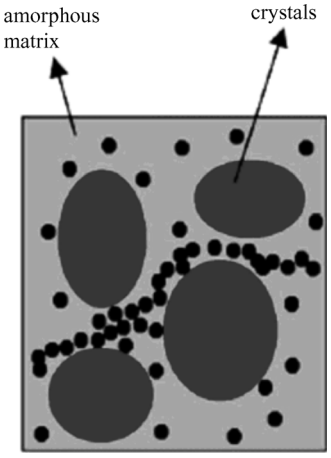

Figure 8.2 Schematic illustration of the non-uniform dispersion of conductive fillers (depicted as small, black spheres) in semi-crystalline polymers, which, in turn, facilitates easier formation of conductive filler networks. Reprinted with permission from Reference [22]. © 2009, Elsevier Science Ltd.

of LLDPE droplets and remarkably changed the droplet shapes from nearly spherical domains to elongated domains of aspect ratio of at least 5.0 [28]. In this context, it should also be mentioned that CB particles exerted no apparent improvement in miscibility as distinct LLDPE droplets were observed both in the absence and in the presence of CB particles. In addition, the SEM images presented by Breuer *et al.* [28] were generated from freeze fractured surfaces and did not show any evidence of interfacial interactions, such as diffused interfaces, between the droplets and the matrix. These observations suggested that CB particles changed the morphology of droplets without exerting any significant impact on the extent of interfacial interactions between the two phases. As we discuss later, similar observations have been reported for various other polymer blends filled with micron- or nano-sized fillers. For instance, Zoldan *et al.* [29], Srivastava *et al.* [30], and Xu *et al.* [31] reported similar observations on selective localization of CB particles in polyamide 6 (PA6) droplets dispersed in a continuous polypropylene (PP) matrix. It was observed that the presence of CB particles resulted in smaller PA6 droplets. Dharaiya and Jana [32] observed that CB particles initially located inside PP-phase migrated to continuous PA6-phase after PP droplets were generated. In this case also, PP droplets were found to be much smaller in diameter than without CB. Other observations were reported for an array of CB filled blends [33–35].

The dominant effect of the viscosity of the phases on filler dispersion in polymer blends was illustrated by Feng *et al.* [36] in blends of PP and ultrahigh molecular weight PE (UHMWPE). It was observed that CB particles were localized on the interface and were unable to penetrate to the UHMWPE phase due to its high viscosity. Feng *et al.* [37] further analyzed the effects of viscosity on filler localization by systematically changing the viscosity of the poly(methyl methacrylate) (PMMA)

phase and by keeping constant the viscosity of the PP-phase in CB filled PMMA/PP blend. They observed that CB was selectively localized in the PMMA phase if a low viscosity PMMA grade was used. CB particles were gradually expelled from the PMMA droplets as higher viscosity PMMA grades were used in blend. The CB particles were completely excluded from the PMMA droplets when the highest viscosity PMMA grade was used.

The role of filler particles on blend morphology development cannot be reduced to those of "compatibilizers," as is evident from the work of Zhang *et al.* [38]. These authors prepared PP and HDPE blends filled with 1.5 phr carbon fiber (CF) and obtained elongated droplets. The average length and average diameter of CF particles were respectively 10 and 0.2 μm (Figure 8.3). It was observed that CF particles were selectively localized in HDPE phase and not at the interfaces as is expected if they acted as compatibilizers. Similarly, Ersoy and Nugay [39–41] observed selective localization of talc particles in PA6-phase in PP/PA6/talc blends and found that the presence of talc particles helped reduce the size of PA6 droplets.

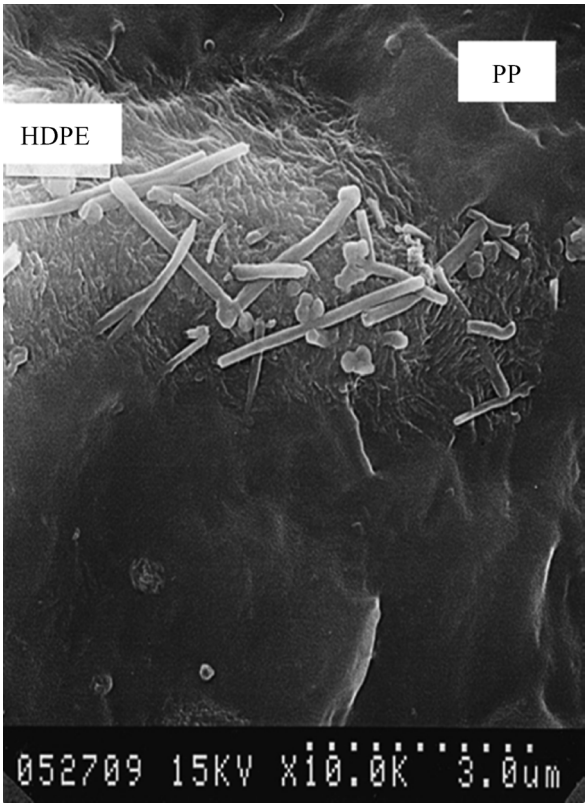

Figure 8.3 Selective localization of carbon fibers (CFs) in HDPE phase in HDPE/PP blends. Note the elongated shape of the HDPE droplet in the presence of CF. Reprinted with permission from Reference [38]. © 1998, Elsevier Science Ltd.

We can now summarize the major morphological observations on immiscible polymer blends filled with micron-size inorganic particles. Filler particles are selectively localized in the phase if they have higher affinity for it, given the viscosity of the phase is not high enough to prevent filler penetration. In scarce examples, the filler particles are found located at the interfaces; most common are cases where particles are located inside the droplets. Two common effects of filler particles on droplet morphology are observed – droplets are smaller and assume elongated forms. The filler particles do not change the immiscible nature of the blends. The observations presented above on polymer blends filled with micron-sized particles will now be contrasted with those filled with nano-size fillers. It is expected that most observations will be similar, although the extent of the impact of nanofillers is expected to be more significant as nanofillers provide a much larger number of particles and hence much larger surface area per unit mass of the filler.

8.3.2
Nanofillers in Polymer Blends

Research efforts on filled polymer blends have been more focused on nanoparticle-filled systems [42, 43]. One usual observation is the same as those with microscopic fillers – polar nanofillers localize in more polar phases [44–53]. In cases where both phases are polar or nonpolar, the filler particles have been observed to be expelled from both phases in the blend [54–56]. Selective localization of nano-sized particles has been an interesting topic of research. We discuss some of the results here. Gahleitner *et al.* [57] observed a preferential localization of clay particles in PA6 droplets in PA6/PP blends. Recall that clay, especially montmorillonite, is highly polar in both its pristine and various organically modified forms [58–62]. Similarly, Wang *et al.* [63] reported selective localization of clay particles in maleic anhydride grafted ethylene–propylene–diene (EPDM-MA) rubber droplets in poly(trimethylene terephthalate)/EPDM-MA blends. Selective localization of fillers other than clay particles has also been reported. For instance, Ou and Li [64] observed that toluene diisocyanate modified titania particles selectively localized in PA6 droplets in PP/PA6/titania blends.

Changes in the morphology of blends in the presence of nano-sized fillers have also been widely reported. Gelfer *et al.* [65] studied PS/PMMA/nanoclay blends and reported significant impact of clay on the dispersed phase size. They observed that clay particles were selectively located in the PMMA phase and reduced the domain sizes of PS and PMMA. The authors also recognized that the presence of clay did not improve the compatibility at molecular level [65]. Wang *et al.* [66] and Sinha Ray *et al.* [67] observed smaller domains in PS/PP blends in the presence of clay and suggested "compatibilization" effects induced by intercalated chains of PS and PP that shared the same clay galleries. Khatua *et al.* [68] showed that the clay particles in PA6/(ethylene–propylene–rubber) (EPR) blends were in a PA6 matrix phase. These authors attributed the size reduction of dispersed EPR-phase to subdued coalescence by the physical presence of the clay particles in PA6-phase, although no direct evidence of reduced coalescence rate was presented. These authors and several other

research groups [69–89] also did not address how smaller droplets were formed during the droplet breakup process in the presence of clay. Chow *et al.* [90] reported that clay particles were located inside the PA6-phase in PA6/PP blends and observed that the presence of clay did not improve the poor interfacial bonding between the phases; only the presence of additional compatibilizer – maleic anhydride grafted PP (PP-MA) – improved the interfacial bonding between PA6 and PP. Similarly, the presence of clay did not improve the impact strength [91] while the presence of a known "compatibilizer" did [92]. Mehrabzadeh and Kamal [93] also compared the effects of clay particles on morphology with those of a compatibilizer – maleated high density polyethylene (HDPE-MA) – in PA6/HDPE blends. They observed that clay particles were located in PA6 droplets and significantly reduced the size of dispersed PA6 droplets, although the individual droplets could be seen on the fractured surfaces. In the presence of HDPE-MA, on the other hand, the individual droplets were practically impossible to recognize and the morphology of the fractured surfaces approached that of a single phase. Similar comparison between the effects of clay and compatibilizer were also presented by Chow *et al.* [94], Filippone *et al.* [95], and Shim *et al.* [96]. Karim and coworkers [97–99] investigated the thermodynamic properties of filled immiscible blends. They determined that the presence of fillers mostly did not change the thermodynamic properties of the blends, such as the cloud points and phase diagrams [97, 98], however, delayed the kinetics of phase separation [97].

A few words are now in order about the effects of fillers on liquid crystalline polymer (LCP)/polymer blends. It has been known that fibrillation of LCP droplets could be induced during high shear melt processing of immiscible blends, especially during injection molding and fiber spinning [100–102]. In these blends, stiff LCP droplets act similarly to high aspect ratio, reinforcing fibrous fillers and, hence, these materials have been widely known as the self-reinforced polymer blends [103, 104]. In the context of LCP/polymer blends, certain continuum equations derived by Taylor [105, 106] could be used as a first approximation to describe the deformation and break-up of liquid droplets in a liquid matrix. The limitations of these continuum equations, such as the omission of the effects of viscoelasticity and high deformation rates, have also been widely known and discussed in Reference [107]. Taylor [105, 106] analyzed the relative effects of hydrodynamic and interfacial stresses and presented a dimensionless number, called the capillary number (*Ca*), to explain various deformation and breakup regimes:

$$Ca = \text{hydrodynamic stress}/\text{interfacial stress} = (\mu\dot{\gamma})/(\sigma/R) \tag{8.1}$$

where

μ is the viscosity of the matrix,
$\dot{\gamma}$ is the rate of shear,
σ is the interfacial tension,
R is the radius of the droplets.

Taylor observed that the extent of droplet deformation is a linear function of *Ca* at low rates of deformation. Later, Taylor's approach was extended to large

deformations [108–111] by considering a critical capillary number (Ca_c) which is the value of the capillary number beyond which the droplet cannot form a stable deformed shape and spontaneously breaks up into smaller droplets [107]. The value of Ca_c is strongly dictated by the flow field and the ratio of viscosities of the matrix and the droplet [108]. If the value of Ca is significantly higher than Ca_c – usually a factor of 4 or higher – the droplet affinely deforms under the effect of the imposed flow field [107].

More recent reports [112, 113] established that the presence of nano-sized inorganic fillers, such as clay and silica, improved the extent of fibrillation of LCP droplets in LCP/polymer blends. Wu *et al.* [113] analyzed the effects of silica in pristine polycarbonate (PC) and LCP/PC blends. They found that the presence of silica reduced the shear viscosity of LCP/PC blends by increasing the viscosity of pristine PC and in turn caused more LCP fibrillation. A similar viscosity reduction on clay filled LCP/polymer blends was also presented by Zhang *et al.* [112]. In view of the expression of Ca in Eq. (8.1), one may argue that either an increase in matrix-phase viscosity or a reduction in interfacial tension can result in better fibrillation. Note that the increase in matrix viscosity in the presence of small amounts of spherical silica particles, especially at higher shear rates, is relatively negligible [113]. However, the presence of a small amount (1 wt%) of silica particles induced a 50% reduction in shear viscosity of LCP/PC blends. Hence, the experimental data did not suggest the presence of a strong correlation between the increase in matrix viscosity in the presence of silica particles and the higher extent of fibrillation observed.

An insightful analysis was performed by Sinha Ray *et al.* [114] using clay filled PMMA/PC blends. These authors observed that the presence of clay in PMMA matrix induced considerably smaller dispersed PC droplets. They also invoked the physical significance of Ca and identified that a possible reduction in interfacial tension or possible increase in matrix viscosity in the presence of clay particles gave rise to smaller droplets. However, the shear viscosity data did not support the argument of increased matrix viscosity as the origin of reduced droplets size [114].

Dharaiya and Jana [115] examined the widely adopted hypothesis of compatibilization in the presence of nanofillers. These authors proposed that smaller droplets must first originate from the breakup process. They determined, using the thread break-up method, that interfacial tension between PP and PA6 reduced in the presence of organically modified clay particles, even though the particles were not located at the interfaces. This caused substantial reduction of the droplet size. They analyzed clay filled PP/PA6 blends using different mixing sequences in which clay particles were first mixed with either of the phases. Dharaiya and Jana [115] observed that clay particles, initially located inside PP-phase, eventually migrated to PA6-phase. An array of other studies also presented evidence for the reduction in interfacial tension in immiscible polymer blends in the presence of filler particles [116–120]. A reduction in surface tension of single-phase polymers in the presence of fillers has also been documented [121–123]. Note that reduced interfacial

tension directly translates to the formation of smaller droplets [124]. Evidently, this also implies that filler particles affect the continuum – the matrix or the droplets – in which they are embedded and change the chemical composition of it, independent from the presence of the other polymeric phase. Hence, one may argue that filler particles only indirectly reduce the interfacial tension between the phases, by reducing the surface tension difference.

The above presented reasoning inevitably gives birth to a further question on the origin of interfacial tension reduction induced by the fillers. In this context, one may ask: How do the inorganic fillers reduce the surface tension of organic polymers, if they are not located at the interfaces? In our opinion, the accumulated knowledge on the effects of fillers on the properties of polymers could be a useful guide in this discussion.

It has been well documented that the presence of fillers impacts the surrounding polymer chains and changes their properties [125]. One of the oldest and widely analyzed examples is the formation of bound rubber which is present in the vicinity of carbon black filled rubbers [125, 126]. It was presented using theory and experiments that the mobility and free volume of rubber chains reduce remarkably due to constraining effects imposed by the rigid carbon black surfaces [127–129]. Similar observations have also been documented in the context of barrier properties and, especially, solubility properties of filled polymers [130]. These also form a strong argument against the applicability of continuum diffusion models to the experimental data obtained for filled polymers [130]. Relatively recent reports presented conclusive evidence that the fillers affect not only the mobility and free volume but also influence the conformation and spatial arrangement of polymers, as discussed next. Evidently, the individual polymer chains in filled polymers cannot easily conform. Even the theoretical studies do not always agree with each other on the behavior of individual polymer chains on filler surfaces [131]. However, a collective behavior of several polymers could be analyzed relatively easily, if they act similarly as a group. In this context, the studies on polymer nucleation and crystallization in filled polymers could be useful, since formation of crystals could be determined relatively easily by various experimental methods.

Lopez and Wilkes [132] and Desio and Rebenfeld [133] showed that nucleation and crystallization of chains in filled polymers are significantly affected by the surface chemistry and the resulting filler–matrix interactions between the polymer chains and filler surfaces. The findings clearly indicated that the presence of fillers and noncovalent interactions between polymer chains and filler surface changed the conformations of chains, which facilitated nucleation. Further analysis performed by Gunes *et al.* [134–136] suggested that the impact of the presence of fillers on polymer nucleation and crystallization in the presence of fillers was universal. The filler effects were observed to be much stronger on slowly crystallizing polymers due to the already limited nucleation rates of the pristine matrix polymer. A further analysis by Gunes *et al.* [136] using fluorescence emission spectroscopy revealed the direct and strong relationship between the extent of filler–matrix interactions and the level of crystallinity (Figure 8.4). Their data suggest that there is a strong positive correlation

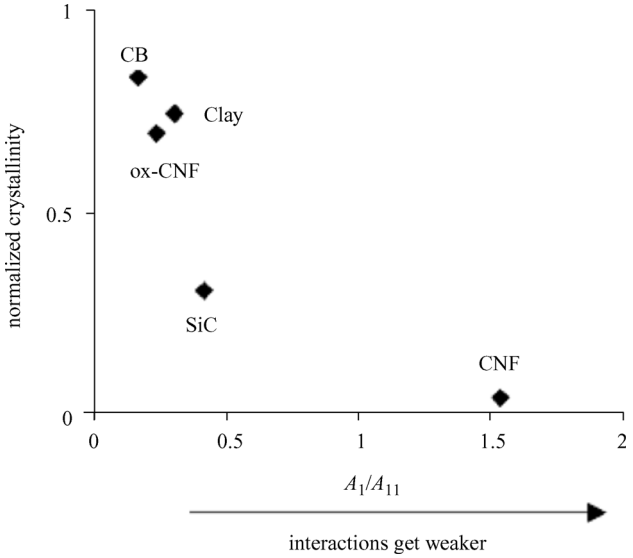

Figure 8.4 Relationship between soft segment crystallinity and the extent of non-covalent filler–matrix interactions in shape memory polyurethane (SMPU) composites filled with organoclay, carbon nanofiber (CNF), oxidized carbon nanofiber (ox-CNF), silicon carbide (SiC), and carbon black (CB). The ratio A_I/A_{II}, determined from fluorescence emission spectroscopy experiments, is a measure of the extent of filler–matrix interactions in the composites – a lower value indicates stronger non-covalent interactions. All composites contained 1 wt% filler particles. A direct correlation between the soft segment crystallinity and the extent of filler–matrix interactions is evident. Reprinted with permission from Reference [136]. © 2010, The Royal Society of Chemistry.

between the non-covalent interactions and segmental adsorption on filler surfaces. The data presented by Gunes *et al.* [136] also suggested that more polar functional groups were selectively located in the closer proximity – around 3 Å or less – of polar filler surfaces.

In view of the above findings on filler–matrix interactions and in view of the previously presented discussion on filled polymer blends, one may suggest the following hypothesis for the origin of reduced surface tension of polymer droplets in the presence of filler particles. It can be anticipated that the conformations of polymer chains, both on the surface and in the inside of a droplet, are changed due to filler–matrix interactions. In addition, in view of the recent findings by Gunes *et al.* [136], one may consider that more polar groups on polymer chains are more closely located to the filler surfaces, which inevitably pushes away the nonpolar groups or chain segments further away from the filler surfaces. Thus, the surface composition of a droplet in which a filler particle is located can be made of less polar groups due to the relatively higher concentration of the polar groups inside of the droplet which is closer to the filler surface. The above hypothesis on the origin of reduced surface tension in the presence of fillers is yet to be proved.

8.4
Engineering Aspects of Morphology Development and Processing of Multiphase Polymer Blend Nanocomposites

We now turn to engineering aspects of morphology development and processing of filled polymer blends. The engineering and kinetic arguments in polymer blends are more dominant than the thermodynamic considerations. First, achieving thermodynamic equilibrium in polymer blends is difficult. This somewhat limits the applicability of the insights gained from equilibrium thermodynamics. Second, the diffusion of small molecular liquids is orders of magnitude faster than that of polymers. In various cases, the fast diffusion alone creates a satisfactory state of mixing in small molecular emulsions even in the absence of any flow field [137]. Third, and more crucial from an engineering perspective, turbulent flow could be remarkably easily induced in small molecular liquids, which in turn facilitates better state of mixing. Hence, the flow of polymers is exclusively laminar, which requires our attention from mixing and processing perspectives.

8.4.1
Miscibility, Homogeneity, and Interfaces of Polymer Blends

Polymeric liquids, similar to other low molecular weight liquids, can be classified as miscible, immiscible, or partially miscible. Miscible polymeric liquids can mix molecularly through diffusion and produce homogeneous mass at molecular scales, but cannot mix readily enough, for example, on time scales of a few seconds to few minutes typical of polymer processing applications, due to high values of viscosity and low values of molecular diffusion coefficient. Consequently, mechanical stirring is needed to reduce the scale of inhomogeneity to a certain level such that molecular diffusion is able to produce homogeneous mixtures on the time scale of interests.

Immiscible polymers cannot produce molecularly homogeneous mixtures due to finite and often high values of interfacial tension. Consequently, a mixed state in an immiscible polymer system may consist of polymer domains with sharp or diffuse interfaces depending upon how the local properties, such as concentration, viscosity, and density, vary on both sides of the interfaces [138]. A sharp interface results if the properties are discontinuous and there is no mass transport across the interface. In contrast, a diffused interface is obtained when the properties vary gradually and continuously across the interface. A material parameter, the interfacial tension, σ, characterizes immiscible polymer systems and is defined as:

$$\sigma = \left.\frac{\partial G}{\partial A}\right|_{T,P,c}$$

where

G is Gibbs free-energy of the system,
A is the interfacial area between the polymers,

T is the temperature,
P is the pressure,
c denotes composition of the system.

The morphology of immiscible polymer systems is largely dictated by the value of interfacial tension, composition, and the values of viscosity of the component polymers.

Two types of polymer morphology may result in the blending of immiscible polymers – co-continuous or dispersed-continuous. Some dispersed-continuous type systems may appear homogeneous due to dispersed domain size of the order of a few nanometers, although locally the immiscible nature is maintained with well-defined interfaces. The scale of dispersed domains, customarily encountered in the range of a few nanometers to hundreds of micrometers, is a direct result of the relative importance of the shear and interfacial forces. Smaller size dispersed domains result when large values of shear forces are applied by mechanical stirring. Therefore, the success of dispersion process in polymeric systems is often judged in terms of the characteristic domain size and the uniformity of distribution of the dispersed phase in the continuous material.

A third class of liquid polymeric systems, classified as partially miscible, exhibits very small degree of molecular mixing at and around the interfaces, and also leads to formation of diffused interfaces. In this case, both polymers have finite, non-zero concentration at the interfaces, which changes continuously from the bulk of one phase to the bulk of the other.

In the rest of this section, discussion and elaboration of concepts are presented based on the existence of sharp interfaces. Note also that the following discussion assumes that the considerations presented for unfilled polymer blends also apply to filled polymer blends. This assumption is based on the continuum approximation, which in turn is based on the approximation that the presence of fillers, when used in small quantities, does not significantly change the flow field. The continuum approximation is considered to be valid in view of the relatively small impact of fillers on the flow field, especially at low loading levels and at relatively higher shear rates that are common in processing flows [139].

8.4.2 Definition of Mixing and Intermaterial Area Generation

In view of the immiscibility of polymer components and negligible molecular diffusion, mixing can be defined as a unit operation by which *intermaterial* areas are created [140]. The term intermaterial area is included in the definition of mixing as it represents the interfacial area for immiscible polymer systems or for polymer/filler systems, while for miscible polymers it represents the area where polymer components are brought together. In the latter case, the microstructure retains its lamellar nature till the end of mixing period, as breakup and coalescence of domains do not take place [141]. This definition is also useful in solid–liquid mixing, such as encountered in the mixing of fillers and pigments with polymers. In this case, the

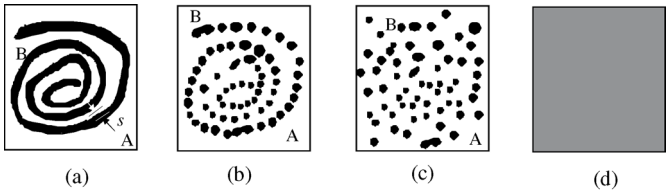

Figure 8.5 Intermaterial area generation by mixing: (a) top view of lamellar structure formed by miscible polymer B in polymer A; (b) droplets of immiscible polymer B dispersed in polymer A; (c) solid filler B dispersed in polymer B; (d) miscible polymer B or soluble pigment B homogeneously mixed with polymer B.

intermaterial area is generated as large solid agglomerates break down into smaller ones with mixing. At an intermaterial surface, continuity of velocity and stresses is maintained.

Figure 8.5 presents schematically the applicability of this definition to different systems frequently encountered in polymer processing.

For miscible polymer systems with low values of diffusion coefficient, the polymers form lamellar structures with crisp material surfaces, that is, sheets of one polymer intimately intertwined in the other in a nested three-dimensional structure. The lamellar structures appear as alternating striations on a cross-sectional plane as in Figure 8.5a, with a characteristic striation thickness, s, which follows a distribution, defined as the striation thickness distribution [141]. A usual definition of striation thickness s is:

$$s = \frac{\lambda_A + \lambda_B}{2} \tag{8.2}$$

where λ_A and λ_B are local lamella thickness of polymers A and B, respectively.

Figure 8.5b represents a common morphological form encountered in the blending of immiscible polymers. Intermaterial area is created in this case by breakup of large domains of polymer B into smaller domains during mixing. Particulate fillers are also dispersed in polymer with the creation of intermaterial area through breakup of large size agglomerates, as in Figure 8.5c, although the breakup processes are different in these two cases. Oftentimes soluble pigments are mixed with polymers to produce esthetic appeal in some products. In such a case, the intermaterial area generation proceeds initially as in Figure 8.5a. Finally, a homogeneous mixture is produced (Figure 8.5d) through rapid molecular diffusion.

The speed and the extent of intermaterial area generation for a given system depend upon the nature of mixing flows and the rheological and interfacial properties of the components. An intermaterial surface can be active, that is, with finite values of interfacial tension as in Figure 8.5b and c, or passive, that is, without interfacial tension as in Figure 8.5a and d, and in this context mixing in polymer processing can be classified in two categories, as distributive and dispersive mixing.

Intermaterial area generation in materials with passive interfaces is termed distributive mixing. Mixing of miscible liquids or soluble pigments as in Figure 8.5a and d is distributive mixing. On the other hand, mixing with intermaterial

Table 8.1 Distinguishing features of distributive and dispersive mixing.

Distributive mixing	Dispersive mixing
1. Repeated stretching and folding generate intermaterial areas	1. Breakup of large size domains into smaller ones generates intermaterial areas. Mixing of immiscible polymers up to the point of breakup is distributive mixing, but breakup of domains occurs by dispersive mixing
2. Polymer components and pigments to be mixed are thermodynamically miscible	2. Polymer components and solid particulate fillers are thermodynamically immiscible
3. No interfacial tension between the components	3. Finite interfacial tension present
4. Molecular diffusivity may be high or low	4. Molecular diffusivity is negligibly small
5. Exceptions include mixing of immiscible polymers up to the point of breakup. In this case, finite interfacial tension exists	

generation of passive interfaces that lead to breakup of domains is termed dispersive mixing. Mixing of immiscible liquids (Figure 8.5b) and liquid polymer with solid fillers (Figure 8.5c) fall into this category.

Table 8.1 lists the major differences between these classes of mixing.

One major difference between these two classes of mixing is the continuity of domains. In distributive mixing, the dispersed component does not go through breakup or coalescence; intermaterial area generation occurs through repeated stretching and folding of the components. Notably, all the domains of each component remain connected in distributive mixing. Dispersive mixing is always associated with breakup of agglomerates and dispersed domains.

In this context, an early stage of mixing of immiscible polymer systems can be described distributive, if the minor component does not go through breakup and, on the contrary, produces lamellar structures with well-defined striation thickness distribution. At later stages of mixing of immiscible polymers, however, the lamellar structures become unstable and holes are developed in thin layers, which undergo stretching and produce fibrillar morphology in the interim [142–151]. The fibrils produce droplets through a well-known capillary breakup process [152, 153]. Figure 8.6 illustrates the pathway of morphology development in the blending of immiscible polymers.

If the interfacial tension between the polymers is high, the lamellar structures may not form at all. In this case, the domains deform directly in the form of threads, which in turn undergo breakup by capillary instability [154–162].

8.4.3
Mixing Flow and Kinematics of Mixing

Mechanical stirring of polymeric liquids in a mixing device generates mixing flows. Mixing flows, in turn, cause deformation of the components and create intermaterial

areas through repeated stretching and folding of the interfaces and breakup of domains. Therefore, the quality of mixing produced depends on the kinematics of mixing flow, which in turn depends on the geometry of the mixer and the design of stirring elements, apart from the rheological properties and the value of interfacial tension of polymeric components.

Mixing flows create intermaterial areas through continuous deformation of the components, which has been known since the time of Osborne Reynolds [163]. The motion of extruder screws, screw elements, kneaders, and rotors produces mixing flows in polymer processing operations. A part of the mechanical energy, consumed in the motion, is used to produce deformation of the polymeric components. Another part provides kinetic energy and pressure so that the mixture can be extruded through the dies or molds. The rest is converted into thermal energy by viscous dissipation and raises the temperature.

The length scales of polymer domains reduce with time, as intermaterial areas between the polymer phases are created. Striation thickness of lamellae (Figure 8.6a) and effective diameter of dispersed polymer domains (Figure 8.6b) represent characteristic length scales. Reduction of length scales not only generates finer morphology but also causes a sharp increase of concentration gradients at the polymer–polymer interface and inside polymer domains to expedite molecular diffusion [164] and chemical reactions [165, 166].

Deformation of a polymer phase can be studied with the aid of flow kinematics. The motion of a polymeric fluid element can be expressed in terms of the local velocity field $\boldsymbol{u}$ as:

$$\frac{\mathrm{d}\boldsymbol{x}}{\mathrm{d}t} = \boldsymbol{u}(\boldsymbol{x}, t); \nabla \cdot \boldsymbol{u} = 0 \tag{8.3}$$

$$\mathrm{IC} : \boldsymbol{x} = \boldsymbol{X} \,\mathrm{at}\, t = 0 \tag{8.4}$$

where $\boldsymbol{x}$ is the present location of the fluid element and IC = initial condition). The local velocity field $\boldsymbol{u}$ is obtained from the solution of momentum balance equations for the mixer and satisfies the equation of continuity.

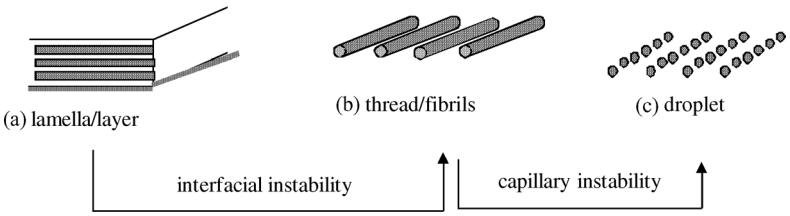

Figure 8.6 Route map of morphology development in the blending of immiscible polymer systems: (a) lamellar structures produced by self-similar mixing process; (b) breakup of lamellar structures into fibrils by interfacial instability; (c) breakup of fibrils into droplets through capillary instability.

8.4.3.1 Intermaterial Area Generation in Miscible Fluids

For miscible polymers of the same viscosity, Eq. (8.3) can be used with the initial condition (8.4) to track deformation of the composition interface and to monitor the intermaterial area as follows:

$$d\boldsymbol{a} = (\det \boldsymbol{F})(\boldsymbol{F}^{-1})^{T} \cdot d\boldsymbol{A} \tag{8.5}$$

$$d\boldsymbol{x} = \boldsymbol{F} \cdot d\boldsymbol{X} \tag{8.6}$$

Equation (8.5) describes how a small intermaterial area $d\boldsymbol{A}$ with its center at $\boldsymbol{X}$ and initial orientation $\boldsymbol{N}$ ($=d\boldsymbol{A}/|d\boldsymbol{A}|$) changes by the application of mixing flow as in Eq. (8.3) to $d\boldsymbol{a}$ with current orientation $\boldsymbol{n}$ ($=d\boldsymbol{a}/|d\boldsymbol{a}|$) and center at $\boldsymbol{x}$ (Figure 8.7).

Note that both $\boldsymbol{N}$ and $\boldsymbol{n}$ are unit tangent vectors to the area elements $d\boldsymbol{A}$ and $d\boldsymbol{a}$, respectively. In Eqs. (8.5) and (8.6), $\boldsymbol{F}$ denotes the deformation gradient tensor to be calculated from the fluid element trajectories through integration of Eq. (8.3). The ratio of intermaterial areas, also called area stretch, η can be defined as:

$$\eta = \frac{|d\boldsymbol{a}|}{|d\boldsymbol{A}|} \tag{8.7}$$

An evolution equation for the magnitude of the intermaterial area $d\boldsymbol{a}$ and its orientation $\boldsymbol{n}$ can be presented as follows [167]:

$$\frac{d}{dt}(\ln \eta) = \nabla \cdot \boldsymbol{u} - \boldsymbol{D} : \boldsymbol{nn} \tag{8.8}$$

$$\boldsymbol{n} = (\det \boldsymbol{F})(F^{-1}) \cdot \frac{\boldsymbol{N}}{\eta} \tag{8.9}$$

$$\boldsymbol{D} = \frac{\left(\nabla \boldsymbol{u} + \nabla^{T} \boldsymbol{u}\right)}{2} \tag{8.10}$$

In Eq. (8.8), $\boldsymbol{D}$ is the stretching tensor defined in Eq. (8.10).

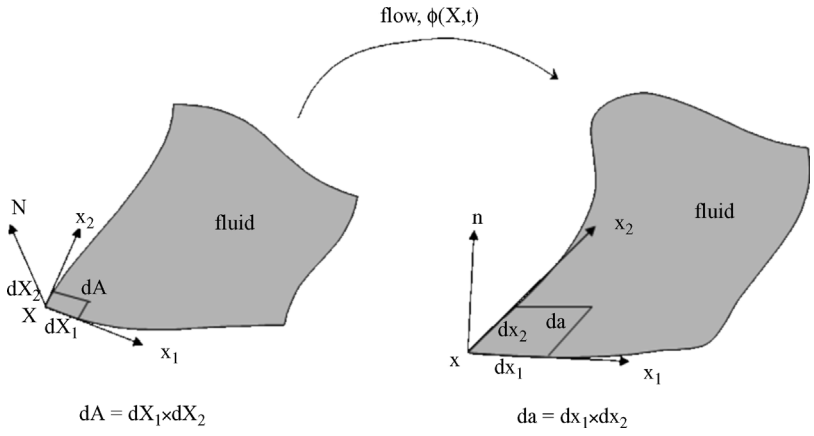

Figure 8.7 Intermaterial-area creation due to deformation.

In the following, the intermaterial area growth in several simple flow cases is discussed. Of these, simple shear and pressure driven flows are prevalent in screw extrusion and injection molding. Elongational flows are present in many mixing devices.

Case 8.1: Simple Shear Flow

In this case, the velocity field can be expressed as:

$$u_1 = \dot{\gamma} x_2; u_2 = 0; u_3 = 0 \tag{8.11}$$

and the following simple expression is obtained for the intermaterial area growth function, η:

$$\eta = \sqrt{1 + \dot{\gamma} t N_2 (\dot{\gamma} t N_2 - 2N_1)} \tag{8.12}$$

where N_1 and N_2 are the components of unit tangent vector $\boldsymbol{N}$. For large values of strain, that is, $\dot{\gamma} t \gg 1$:

$$\eta_{\max} = \dot{\gamma} t N_2 \tag{8.13}$$

Equation (8.12) is obtained from Eqs. (8.8–8.10) using an eigenvalue approach [167]. The same expression can also be obtained using simple geometrical arguments of deformation of line vectors [168–173]. As is evident from Eq. (8.13), the largest value of η is obtained for a given value of strain when $N_2 = 1$, that is, the initial area element is oriented perpendicular to the flow direction. In addition, the intermaterial area grows linearly with time. It is also evident from Eq. (8.12) that intermaterial area does not increase at all if the differential area element is oriented along the flow direction, that is, $N_1 = 1$, $N_2 = 0$. These observations highlight the importance of occasional reorientation of fluid elements in producing rapid growth of intermaterial areas, which forms the basis of many mixing element designs [174–178] as well as some new mixing flows, such as chaotic mixing flows as will be discussed later.

Case 8.2: Pressure Flow through a Circular Tube

The velocity field is expressed as:

$$u_1 = U\left(1 - \frac{r^2}{R^2}\right); u_2 = 0; u_3 = 0, \tag{8.14}$$

where

U is the maximum velocity in the tube,
r is the radial location,
R is the radius of the tube.

The intermaterial area increases as follows:

$$\eta = \sqrt{1 + \dot{\gamma} t N_1 (\dot{\gamma} t N_1 - 2N_2)}. \tag{8.15}$$

The value of shear rate $\dot{\gamma}$ (>0) changes with radial location r as follows:

$$\dot{\gamma} = 2U\frac{r}{R^2} \tag{8.16}$$

In this case, for large value of strain, the intermaterial area increases as:

$$\eta_{\max} \approx \dot{\gamma}t \tag{8.17}$$

that is, the maximum increase in intermaterial area occurs for surfaces aligned perpendicular to the flow direction. Once again, the intermaterial area increases linearly with time.

Case 8.3: Uniaxial Extensional Flow

Let us consider intermaterial area growth of a rectangular fluid element oriented in a uniaxial extensional flow (Eq. (8.18)) with an initial orientation vector ***N***, as in Figure 8.8:

$$\begin{aligned} u_1 &= \dot{\varepsilon}x_1 \\ u_2 &= -\frac{\dot{\varepsilon}}{2}x_2 \\ u_3 &= -\frac{\dot{\varepsilon}}{2}x_3 \end{aligned} \tag{8.18}$$

In Eq. (8.18), $\dot{\varepsilon}$ is the rate of extension and u_1, u_2, and u_3 are the velocities along directions x_1, x_2, and x_3, respectively. The ratio of intermaterial areas increases as follows:

$$\eta = \left[N_1^2\exp(2\dot{\varepsilon}t) + N_2^2\exp(-\dot{\varepsilon}t) + N_3^2\exp(-\dot{\varepsilon}t)\right]^{\frac{1}{4}} \tag{8.19}$$

The fastest growth in intermaterial area occurs when the rectangular element is oriented along the direction of flow:

$$\eta_{\max} = \exp\left(\frac{\dot{\varepsilon}}{2}t\right) \tag{8.20}$$

Comparison of Eqs. (8.17) and (8.20) reveals that the intermaterial area grows linearly with time in shear flows, while it grows exponentially with time in extensional flows. In view of this, many mixing devices have been built to include extensional flow components [179, 180]. However, such efforts are fraught with two limitations. First, it is difficult to sustain uniform extensional flow in a mixing device. Second, a very

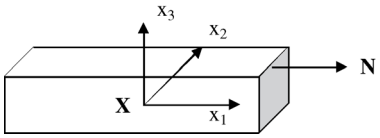

Figure 8.8 Intermaterial-area creation due to deformation in uniaxial flow.

high rate of extension also causes higher rates of shear heating, which may lead to material degradation.

For reactive systems, such exponential thinning of fluid elements may cause a sharp increase in concentration gradient and, along with increased intermaterial area, lead to a rapid increase of chemical reaction rates. The width (W) of the fluid element changes as:

$$\frac{W}{W_0} = \left[N_1^2 \exp(2\dot{\varepsilon}t) + N_2^2 \exp(-\dot{\varepsilon}t) + N_3^2 \exp(-\dot{\varepsilon}t)\right]^{-\frac{1}{4}} \tag{8.21}$$

where W_0 is the width of the original fluid element. At any instant of time, the rate of reactions (R) between two functional groups A and B, assuming instantaneous reactions at the interface, can be written as:

$$R = \frac{\eta}{W} A_0 D_{AB} C_{A,0} \frac{d\varrho}{d\xi} \tag{8.22}$$

where

D_{AB} is the molecular diffusion coefficient,
ϱ is the dimensionless concentration of reactant A,
ξ is the dimensionless thickness of the fluid element containing A,
A_0 is the initial intermaterial area,
$C_{A,0}$ is the initial concentration of reactant A in the fluid element.

The rate goes up as the ratio η/W increases exponentially with the progress of mixing. An estimate of time for appreciable reactions between A and B can be obtained from the time of diffusion (t_d) of component A from the centerline to the interface:

$$t_d \sim \frac{W^2}{4D_{AB}} \tag{8.23}$$

However, purely uniaxial extension can rarely be achieved in typical mixing devices, as fluid elements go through a series of deformation steps amid shear and extensional flow fields in the mixing equipment. As the intermaterial area increases linearly with time in the zones of shear (Eq. (8.17)) and exponentially with time in the zones of extensional flows (Eq. (8.20)), the overall effect is much less than the best case scenario of purely extensional flow, presented above. Moreover, only a small fraction of materials can experience purely extensional flows.

Case 8.4: Planar Elongational Flow

The flow field for a planar elongational flow is given as:

$$\begin{aligned} u_1 &= \dot{\varepsilon} x_1 \\ u_2 &= -\dot{\varepsilon} x_2 \\ u_3 &= 0 \end{aligned} \tag{8.24}$$

The intermaterial area increases as:

$$\eta = \left[N_1^2 \exp(2\dot{\varepsilon}t) + N_2^2 \exp(-2\dot{\varepsilon}t) + N_3^2\right]^{\frac{1}{2}} \tag{8.25}$$

The maximum rate of increase of intermaterial area is given as:

$$\eta_{\max} = \exp(\dot{\varepsilon}t) \tag{8.26}$$

Case 8.5: Rotational Flow

For purely rotational flow:

$$\begin{aligned} u_1 &= \dot{\gamma} x_2 \\ u_2 &= -\dot{\gamma} x_1 \\ u_3 &= 0 \end{aligned} \tag{8.27}$$

where $\dot{\gamma}$ is the shear rate. In this case the fluid elements follow closed streamlines and the intermaterial area ratio, η, oscillates around a mean value of 1 with a frequency of $2\dot{\gamma}$.

Case 8.6: Chaotic Flow

Chaotic flows are produced by time-periodic and space-periodic reorientation of the fluid elements in simple shear flows [181–191]. The three-dimensional flow of viscous liquids through the channels of single screw extruders also produces chaotic fluid element trajectories due to periodic obstructions residing in the screw channel [192–195]. Chaotic mixing was recently found efficient in processing of nanocomposites filled with fibrous fillers, such as carbon nanofibers [196, 197]. It was determined that chaotic trajectories facilitated an improved state of filler dispersion due to high mixing efficiency, whereas the filler aspect ratio was more preserved due to low shear rate in the chaotic mixer [198]. However, the low shear rate used in most chaotic mixers also limits the usefulness of such mixers in promoting clay exfoliation as high shear forces are required for delamination of clay tactoids [199].

In chaotic mixing, rapid generation of intermaterial areas in both distributive and dispersive mixing is obtained. This is illustrated in association with simple shear flow as in Eq. (8.11), and also in Figure 8.9.

A fluid element of original length L_0 is aligned initially perpendicular to the shear direction. If shearing of the material element is continued for long time, the interfacial area grows linearly with time as in a simple shear flow, given in Eqs. (8.12) and (8.13). In chaotic flow, the material element is reoriented periodically. To imitate this, the shear flow is turned off after a time-period T, the elongated fluid element is reoriented to along the x_2-direction, and the flow is turned on for another time-period T. If this sequence is repeated n-times, the intermaterial area ratio of the fluid element increases as follows:

$$\eta = \left(1 + \dot{\gamma}^2 T^2\right)^{\frac{n}{2}} \tag{8.28}$$

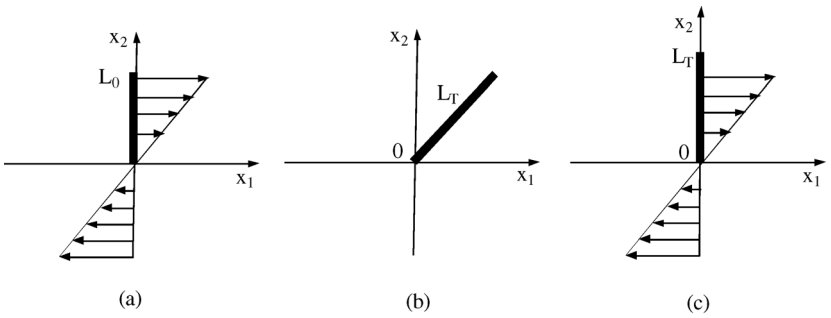

Figure 8.9 Chaotic flow by time-periodic reorientation of fluid elements: (a) shear flow applied for time-period T on element of length L_0; (b) shear flow stopped; (c) extended fluid element of length L_T reoriented and shear flow applied for another time-period T.

which assumes an exponential behavior if n is very large. For comparison, the intermaterial area grows only to:

$$\eta = \left(1 + \dot{\gamma}^2 n^2 T^2\right)^{\frac{1}{2}} \tag{8.29}$$

if the shear flow is continued for a total time of nT unit. The expression in Eq. (8.28) presents an upper bound of area stretch that can be obtained from the application of shear flow with periodic reorientation, as no realistic mixing device can produce such vertical reorientation in such a precise manner.

In real chaotic mixing devices, reorientation occurs randomly and a small fraction of fluid elements assume reorientation perpendicular to the flow direction. One such example is presented in Figure 8.10, where chaotic mixing is produced by time-periodic rotation of two circular rotors.

The alternating motion of left and right rotors produces crossing of streamline portraits, thus giving opportunities for fluid element reorientation. The more transverse the crossing is the better is the reorientation abilities. The fluid element AB, oriented along a streamline produced by the motion of left-hand rotor, reorients to a form AC due to the motion of the right-hand rotor. If this sequence of motion is repeated, the fluid element length and intermaterial area increases exponentially fast.

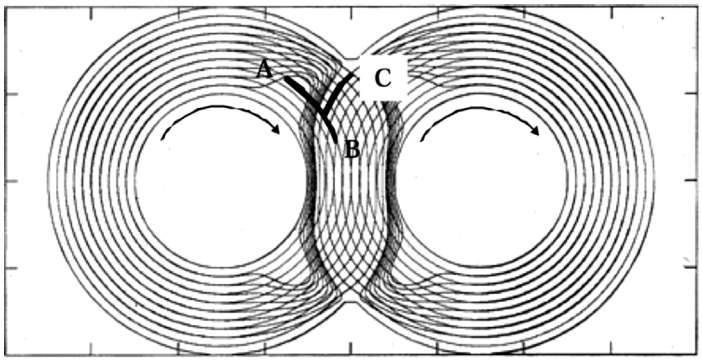

Figure 8.10 Fluid element reorientation in a chaotic mixing device [204–206].

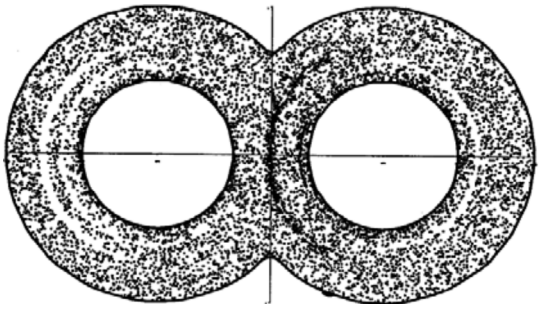

Figure 8.11 Spreading of fluid elements as seen in this Poincaré map due to periodic reorientation in a chaotic mixing device [204, 206].

In addition, neighboring fluid elements diverge and spread around in the mixing device, thus producing uniform mixtures, as shown in Figure 8.11, in the form of a computed Poincaré map.

Chaotic mixing flows have recently been used for rapid development of morphology of immiscible polymers. Three morphological forms have been identified – lamella, fibrils, and droplets (Figure 8.12) [200–205].

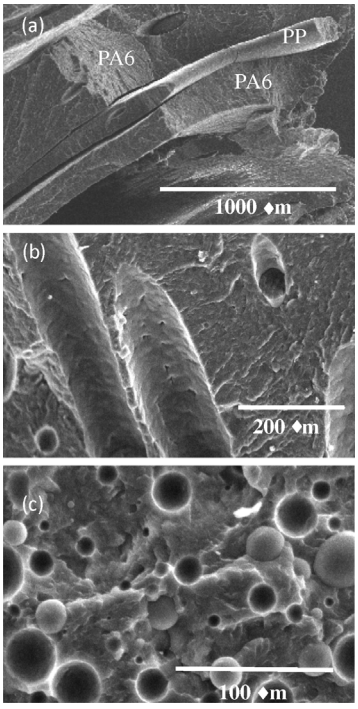

Figure 8.12 Evolution of polypropylene (PP) morphology in blending with polyamide 6 (PA6) at various times of mixing in chaotic mixing: (a) at short time, mostly lamellar; (b) mostly fibrillar at intermediate stage of mixing; and (c) mostly droplets at later stages of mixing [204–206].

The application of chaotic flows leads to much smaller droplets than allowed by the equilibrium between the shear and interfacial forces [204–206] and than those obtained in some commercial mixers. The smaller size of droplets can be directly traced back to their precursor thinner fibrils as the droplets originate from the fibrils by capillary instability and breakup. The exponential stretching encountered in chaotic mixers subdues the growth of interfacial instabilities in both lamellas and fibrils and consequently smaller diameter fibrils are produced. In some cases, fibrils with an aspect ratio as high as 1000 are produced [204]. In addition, the chaotic mixing conditions have been shown to slow down the rate of coalescence of droplets [207]. Another study utilized the rapid intermaterial area generation in chaotic flows to promote chemical reactions in the synthesis of thermoplastic polyurethanes [140].

8.4.3.2 Relevance of Intermaterial Area Generation to Dispersive Mixing

Dispersive mixing of two immiscible polymers or particulate fillers in a polymer benefits greatly from intermaterial area generation. The increased intermaterial area promotes wetting and homogenization of fillers by polymers and also leads to rapid deformation and breakup of minor component polymers. The interfacial reactions can still occur, but the reaction products – the molecules of the new polymer – stay at the interface and compatibilize the domains.

8.4.4 Demixing of Filler Particles and Droplets Induced by Non-uniform Shear Flows Encountered During Usual Processing Operations

Non-uniform shear fields are inherent to usual polymer processing operations, such as extrusion and injection molding [208]. During the shear flow in a circular pipe, which is common in both injection molding and extrusion, the shear stress is highest at the wall and lowest at the center of the pipe. The non-uniform flow fields induce migration of filler particles and liquid droplets dispersed in the polymer matrix during processing [209] which in turn creates non-isotropic and heterogeneous mixing of the components. The migration of the particles and droplets and the resulting morphologies are usually undesirable due to associated reductions in final engineering properties, such as loss of electrical conductivity [210]. In some instances, however, the migration of particles is deliberately induced and it has been common engineering practice in processing of some immiscible blends, such as rubber toughened glassy plastics [211]. In the following, we briefly review some relevant experimental reports and theoretical treatments of the subject.

The migration phenomenon under shear forces was first reported in conjunction with the rubber-toughened plastics, such as HIPS [212]. Dispersed rubber particles in a glassy matrix significantly improve the impact strength [213]; however, they could negatively impact appearance-related optical properties, most notably gloss [214], by increasing the extent of light scattering from the molded or extruded sample. Giuffria *et al.* [212] observed that extruding HIPS sheets under high shear rates improved their

surface gloss. Using electron and optical microscopes, they determined that high shear processing induced migration of rubber particles from the surface to the center of the produced sheet, which in turn reduced the extent of light scattering and improved gloss due to a reduced number of particles located in close to the surface. In this context, high shear flow conditions usually impact negatively other appearance-related optical properties of polymers, such as transparency and haze by increasing the birefringence in processed parts [215, 216]. Kato [217] extended the analysis of rubber particle migration and determined that peeling and delamination in thin walled acrylonitrile–butadiene–styrene (ABS) parts originated from the formation of surface and subsurface layers which had reduced concentration of rubber particles (Figure 8.13).

Similar to migration of polymer droplets in immiscible blends, filler particles have also been observed to migrate under non-uniform flow conditions, which in turn creates concentration gradients in processed parts [218]. The most dramatic impact of filler migration has been observed on electrical properties of filled polymers, especially if the electrically conductive filler concentration, that is, carbon black (CB) content, is at around the percolation threshold. In this case, even an incremental reduction in local filler content converts the conductive compound into an insulator. Numerical analyses and predictions of filler migration under shear were presented by Jana [209]. Later experimental studies [210] verified the validity of the numerical simulation results, which indicated the formation of a particle-depleted skin layer of about 20 μm during injection molding of CB filled PP and PS.

8.5 Conclusions

The following conclusions can be drawn from the discussion presented in this chapter:

1) There are similarities and differences between the filled immiscible polymer blends and filled immiscible liquid emulsions. The difficulty in reaching thermodynamic equilibrium and the lack of turbulent mixing and the lack of significant molecular diffusion are among the most notable differences between them.
2) The selective localization behavior of micron-sized and nano-sized inorganic fillers in polymer blends appears to be similar. The filler particles choose to be located in the phase for which they have a higher affinity. The selective localization of both micron-sized and nano-sized particles changes the morphology and induces formation of smaller droplets.
3) A survey of published data in the literature strongly suggests that filler particles do not act as "compatibilizers" between the phases. There is strong experimental evidence in the literature that indicates that smaller droplets in the presence of

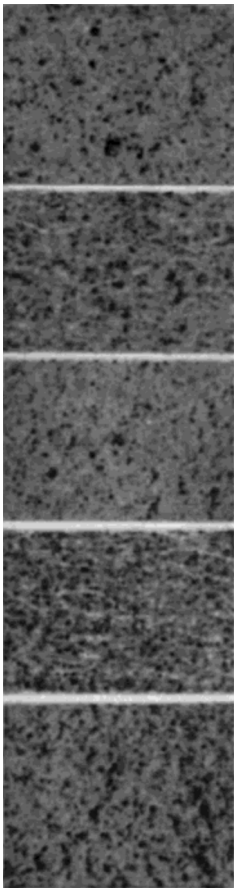

Figure 8.13 Optical micrographs of the cross-sectional surfaces of acrylonitrile–butadiene–styrene (ABS) part processed under high shear conditions (from top to bottom). Magnification ratio is 550 and the rubber particles appear as black droplets. The sections were cut along the flow direction. Note the rubber particle depleted surface layers on the very top and bottom layers. Reprinted with permission from Reference [217]. © 1968, Elsevier Science Ltd.

fillers originate from reduced interfacial tension, which in turn impacts droplet deformation and breakup.

4) In view of the experimental findings on filler–matrix interactions and their effects on conformations of polymer chains, it is suggested that non-covalent filler–matrix interactions and the resulting increases of the exposure of less polar groups and chains segments at the interfaces reduce the polarity of the droplets, which in turn reduces the interfacial tension.
5) Mixing conditions, such as mixing protocol and type of flow field, significantly affect the morphology development and the state of the final mixture. Chaotic

mixing is the most efficient mixing method, producing the features of extensional flow using repeated combinations of shear flows. This in turn creates the highest extent of stretching and folding of liquids droplets, which results in rapid intermaterial area generation.

6) Non-uniform flow fields that are commonly encountered during polymer processing, such as extrusion and injection molding, induce migration of filler particles and dispersed liquid droplets during processing, which creates concentration gradients of fillers and dispersed droplets in the finished parts.

Symbols

Variables

A	interfacial area
A_0	initial intermaterial area
c	composition of the system
Ca	capillary number
Ca_c	critical capillary number
$C_{A,0}$	initial concentration of reactant A in the fluid element
D_{AB}	binary molecular diffusion coefficient
G	Gibbs free energy
P	pressure
r	radial location
R	radius
t	time
t_d	time of diffusion
T	temperature
u_1, u_2, and u_3	velocities along the respective directions x_1, x_2, and x_3
U	maximum velocity in the tube
W_0	width of the original fluid element
W	current width of the fluid element

Vectors and Matrices

$d\boldsymbol{a}$	current area elements
$d\boldsymbol{A}$	initial area element
$\boldsymbol{D}$	stretching tensor
$\boldsymbol{F}$	deformation gradient tensor
$\boldsymbol{n}$	unit tangent vector (current orientation)
$\boldsymbol{N}$	unit tangent vector (initial orientation)
$\boldsymbol{u}$	local velocity field
$\boldsymbol{x}$	current location of the fluid element
$\boldsymbol{X}$	initial location of the fluid element

Greek Symbols

$\dot{\gamma}$	shear rate
$\dot{\varepsilon}$	rate of extension
η	ratio of intermaterial areas, also called area stretch
λ	local lamella thickness
μ	shear viscosity
ξ	dimensionless thickness of the fluid element containing A
ϱ	dimensionless concentration of reactant A
σ	interfacial tension

References

1 Manson, J.A. (1976) *Polymer Blends and Composites,* Plenum Press, New York.
2 White, J.L. (1995) *Rubber Processing: Technology, Materials, Principles,* Hanser Gardner Publishers, Cincinnati.
3 Mausser, R.F. (1987) Latex and foam rubber, in *Rubber Technology* (ed. M. Morton), ch. 19, Kluwer Academic Publishers, Norwell, pp. 518–560.
4 Hosler, D., Burkett, S.L., and Tarkanian, M.J. (1999) Prehistoric polymers: rubber processing in ancient Mesoamerica. *Science,* **284**, 1988.
5 Robeson, L.M. (2007) *Polymer Blends: A Comprehensive Review,* Hanser Gardner Publishers, Cincinnati.
6 Paul, D.R. and Newman, S. (1978) *Polymer Blends. Volume 2,* Academic Press, New York.
7 Perilla, J.P. and Jana, S.C. (2004) A time-scale approach for analysis of coalescence in processing flows. *Polym. Eng. Sci.*, **44**, 2254.
8 Utracki, L.A. (1990) *Polymer Alloys and Blends,* Hanser Gardner Publishers, Cincinnati.
9 Hull, D. (1981) *An Introduction to Composite Materials,* Cambridge University Press, New York.
10 Ross, S. and Morrison, I.D. (1988) *Colloidal Systems and Interfaces,* Wiley-Interscience, New York.
11 Bancroft, W.D. (1912) The theory of emulsification, II. *J. Phys. Chem.*, **16**, 345.
12 Ramsden, W. (1903) Separation of solids in the surface-layers of solutions and suspensions. *Proc. R. Soc. London,* **72**, 156.
13 Binks, B.P. and Horozov, T.S. (2006) *Colloidal Particles at Liquid Interfaces,* Cambridge University Press, Cambridge.
14 Aveyard, R., Binks, B.P., and Clint, J.H. (2003) Emulsions stabilized solely by colloidal particles. *Adv. Colloid Interface Sci.*, **100–102**, 503.
15 Yurekli, K., Karim, A., Amis, E.J., and Krishnamoorti, R. (2004) Phase behavior of PS-PVME nanocomposites. *Macromolecules,* **37**, 507.
16 Mark, J.E. and Erman, B. (2005) *Science and Technology of Rubber,* Academic Press, New York.
17 Walters, M.H. and Keyte, D.N. (1965) Heterogeneous structure in blends of rubber polymers. *Rubber Chem. Technol.*, **38**, 62.
18 Hess, W.M., Scott, C.E., and Callan, J.E. (1967) Carbon black distribution in elastomer blends. *Rubber Chem. Technol.*, **40**, 371.
19 Portal, J., Carrot, C., Majeste, J.C., Cocard, S., Pelissier, V., and Anselme-Bertrand, I. (2009) Quantification of the distribution of carbon black in natural rubber/polybutadiene blends by differential scanning calorimetry. *Polym. Eng. Sci.*, **49**, 1544.
20 Norman, R.H. (1970) *Conductive Rubbers and Plastics: Their Production, Application, and Test Methods,* Elsevier, Amsterdam.

21 Huang, J.C. (2002) Carbon black filled conducting polymers and polymer blends. *Adv. Polym. Technol.*, **21**, 299.

22 Gunes, I.S., Jimenez, G.A., and Jana, S.C. (2009) Carbonaceous fillers for shape memory actuation of polyurethane composites by resistive heating. *Carbon*, **47**, 981.

23 Lipatov, Yu.S. (1995) *Polymer Reinforcement*, ChemTec Publishing, Toronto.

24 Nesterov, A.E., Lipatov, Yu.S., Horichko, V.V., and Gritsenko, O.T. (1992) Filler effects on the compatibility and phase separation kinetics of poly (vinyl acetate)-poly(methyl methacrylate) mixtures. *Polymer*, **33**, 619.

25 Lipatov, Yu.S. (1974) *Adsorption of Polymers*, John Wiley & Sons, Inc., New York.

26 Gritsenko, O.T. and Nesterov, A.E. (1991) Segmental adsorption energy and phase behavior of filled polymer blends. *Eur. Polym. J.*, **27**, 455.

27 Kalfoglou, N.K. (1986) Effect of fillers on the compatibility of polymer blends. *J. Appl. Polym. Sci.*, **32**, 5247.

28 Breuer, O., Tchoudakov, R., Narkis, M., and Siegmann, A. (1997) Segregated structures in carbon black-containing immiscible polymer blends: HIPS/LLDPE systems. *J. Appl. Polym. Sci.*, **64**, 1097.

29 Zoldan, J., Siegmann, A., and Narkis, M. (2006) Anisotropy in the electrical behavior of immiscible polypropylene/nylon/carbon black blends processed slightly below the melting temperature of the nylon. *Polym. Eng. Sci.*, **46**, 1250.

30 Srivastava, S., Tchoudakov, R., and Narkis, M. (2000) A preliminary investigation of conductive immiscible polymer blends as sensor materials. *Polym. Eng. Sci.*, **40**, 1522.

31 Xu, Z., Zhao, C., Gu, A., Fang, Z., and Tong, L. (2008) Effect of morphology on the electric conductivity of binary polymer blends filled with carbon black. *J. Appl. Polym. Sci.*, **106**, 2008.

32 Dharaiya, D.P., Jana, S.C., and Lyuksyutov, S.F. (2006) Production of electrically conductive networks in immiscible polymer blends by chaotic mixing. *Polym. Eng. Sci.*, **46**, 19.

33 Breuer, O., Tchoudakov, R., Narkis, M., and Siegmann, A. (1999) The interrelation between morphology, resistivity, and flow properties of carbon black-containing HIPS/EVA blends. *J. Appl. Polym. Sci.*, **73**, 1655.

34 Feng, J. and Chan, C.M. (1998) Carbon black-filled immiscible blends of poly (vinylidene fluoride) and high density polyethylene: electrical properties and morphology. *Polym. Eng. Sci.*, **38**, 1649.

35 Feng, J. and Chan, C.M. (1999) Carbon black-filled immiscible blends of poly (vinylidene fluoride) and high density polyethylene: the relationship between morphology and positive and negative temperature coefficient effects. *Polym. Eng. Sci.*, **39**, 1207.

36 Feng, J. and Chan, C.-M. (2000) Double positive temperature coefficient effects of carbon black-filled polymer blends containing two semicrystalline polymers. *Polymer*, **41**, 4559.

37 Feng, J., Chan, C.M., and Li, J.X. (2003) A method to control the dispersion of carbon black in an immiscible polymer blend. *Polym. Eng. Sci.*, **43**, 1058.

38 Zhang, C., Yi, X.S., Yui, H., Asai, S., and Sumita, M. (1998) Selective localization and double percolation of short carbon fiber filled polymer blends: high-density polyethylene/isotactic polypropylene. *Mater. Lett.*, **36**, 186.

39 Ersoy, O.G. and Nugay, N. (2003) Effect of inorganic filler phase on mechanical and morphological properties of binary immiscible polymer blends. *Polym. Bull.*, **49**, 465.

40 Ersoy, O.G. and Nugay, N. (2004) A new approach to increase weld line strength of incompatible polymer blend composites: selective filler addition. *Polymer*, **45**, 1243.

41 Ersoy, O.G. and Nugay, N. (2007) Combined effect of the nature of the filler and the compatibilizer on the weld line properties of filled blends. *Compos. Part A*, **38**, 162.

42 Sinha Ray, S. and Okamoto, M. (2003) Polymer/layered silicate nanocomposites: a review from

preparation to processing. *Prog. Polym. Sci.*, **28**, 1539.
43 Gunes, I.S. and Jana, S.C. (2008) Shape memory polymers and their nanocomposites: a review of science and technology of new multifunctional materials. *J. Nanosci. Nanotechnol.*, **8**, 1616.
44 Ahn, Y.C. and Paul, D.R. (2006) Rubber toughening of nylon 6 nanocomposites. *Polymer*, **47**, 2830.
45 Zhang, L., Wan, C., and Zhang, Y. (2009) Investigation on morphology and mechanical properties of polyamide 6/maleated ethylene-propylene-diene rubber/organoclay composites. *Polym. Eng. Sci.*, **49**, 209.
46 Kontopoulou, M., Liu, Y., Austin, J.R., and Parent, J.S. (2007) The dynamics of montmorillonite clay dispersion and morphology development in immiscible ethyleneepropylene rubber/polypropylene blends. *Polymer*, **48**, 4520.
47 Ophir, A., Zonder, L., and Rios, P.F. (2009) Thermodynamic characterization of hybrid polymer blend systems. *Polym. Eng. Sci.*, **49**, 1168.
48 Ozkoc, G., Bayram, G., and Tiesnitsch, J. (2008) Microcompounding of organoclay–ABS/PA6 blend-based nanocomposites. *Polym. Compos.*, **29**, 345.
49 Ozkoc, G., Bayram, G., and Quaedflieg, M. (2008) Effects of microcompounding process parameters on the properties of ABS/polyamide-6 blends based nanocomposites. *J. Appl. Polym. Sci.*, **107**, 3058.
50 Ashab, L., Jafari, S.H., Baghaei, B., Khonakdar, H.A., Potschke, P., and Bohmec, F. (2008) Structural analysis of multicomponent nanoclay-containing polymer blends through simple model systems. *Polymer*, **49**, 2119.
51 Xu, Z., Zhao, C., Gu, A., and Fang, Z. (2007) Electric conductivity of PS/PA6/carbon black composites. *J. Appl. Polym. Sci.*, **103**, 1042.
52 Le, H.H., Ilisch, S., Heidenreich, D., Wutzler, A., and Radusch, H.J. (2010) Kinetics of the phase selective localization of silica in rubber blends. *Polym. Compos.*, **31**, 1701.
53 Ali, Z., Le, H.H., Ilisch, S., and Radusch, H.J. (2009) Morphology development in nanoclay filled rubber compounds and rubber blends detected by online measured electrical conductance. *J. Mater. Sci.*, **44**, 6427.
54 Baudouin, A.C., Devaux, J., and Bailly, C. (2010) Localization of carbon nanotubes at the interface in blends of polyamide and ethylene–acrylate copolymer. *Polymer*, **51**, 1341.
55 Fang, Z., Harrats, C., Moussaif, N., and Groeninckx, G. (2007) Location of a nanoclay at the interface in an immiscible poly(e-caprolactone)/poly(ethylene oxide) blend and its effect on the compatibility of the components. *J. Appl. Polym. Sci.*, **106**, 3125.
56 Lee, M.H., Dan, C.H., Kim, J.H., Cha, J., Kim, S., Hwang, Y., and Lee, C.H. (2006) Effect of clay on the morphology and properties of PMMA/poly(styrene-co-acrylonitrile)/clay nanocomposites prepared by melt mixing. *Polymer*, **47**, 4359.
57 Gahleitner, M., Kretzschmar, B., Van Vliet, G., Devaux, J., Pospiech, D., Bernreitner, K., and Ingolic, E. (2006) Rheology/morphology interactions in polypropylene/polyamide-6 nanocomposites. *Rheol. Acta*, **45**, 322.
58 Dharaiya, D. and Jana, S.C. (2005) Thermal decomposition of alkyl ammonium ions and its effects on surface polarity of organically treated nanoclay. *Polymer*, **46**, 10139.
59 Pattanayak, A. and Jana, S.C. (2005) Thermoplastic polyurethane nanocomposites of reactive silicate clays: effects of soft segments on properties. *Polymer*, **46**, 5183.
60 Pattanayak, A. and Jana, S.C. (2005) Synthesis of thermoplastic polyurethane nanocomposites of reactive nanoclay by bulk polymerization methods. *Polymer*, **46**, 3275.
61 Pattanayak, A. and Jana, S.C. (2005) Properties of bulk-polymerized thermoplastic polyurethane nanocomposites. *Polymer*, **46**, 3394.
62 Cao, F. and Jana, S.C. (2007) Nanoclay-tethered shape memory polyurethane nanocomposites. *Polymer*, **48**, 3790.

63 Wang, K., Chen, Y., and Zhang, Y. (2008) Effects of organoclay platelets on morphology and mechanical properties in PTT/EPDM-g-MA/organoclay ternary nanocomposites. *Polymer,* **49**, 3301.

64 Ou, B. and Li, D. (2009) The effect of functionalized-TiO_2 on the mechanical properties of PP/PA6/functionalized-TiO_2 nanocomposites prepared by reactive compatibilization technology. *J. Compos. Mater.,* **43**, 1361.

65 Gelfer, M.Y., Song, H.H., Liu, L., Hsiao, B.S., Chu, B., Rafailovich, M., Si, M., and Zaitsev, V. (2003) Effects of organoclays on morphology and thermal and rheological properties of polystyrene and poly(methyl methacrylate) blends. *J. Polym. Sci. B,* **41**, 44.

66 Wang, Y., Zhang, Q., and Fu, Q. (2003) Compatibilization of immiscible poly (propylene)/polystyrene blends using clay. *Macromol. Rapid Commun.,* **24**, 231.

67 Sinha Ray, S., Pouliot, S., Bousmina, M., and Utracki, L.A. (2004) Role of organically modified layered silicate as an active interfacial modifier in immiscible polystyrene/polypropylene blends. *Polymer,* **45**, 8403.

68 Khatua, B.B., Lee, D.J., Kim, H.Y., and Kim, J.K. (2004) Effect of organoclay platelets on morphology of nylon-6 and poly(ethylene-ran-propylene) rubber blends. *Macromolecules,* **37**, 2454.

69 Mehrabzadeh, M. and Kamal, M.R. (2004) Melt processing of PA-66/Clay, HDPE/Clay and HDPE/PA-66/clay nanocomposites. *Polym. Eng. Sci.,* **44**, 1152.

70 Yoo, Y., Cui, L., Yoon, P.J., and Paul, D.R. (2010) Morphology and mechanical properties of rubber toughened amorphous polyamide/MMT nanocomposites. *Macromolecules,* **43**, 615.

71 Chen, G.X., Kim, H.S., Kim, E.S., and Yoon, J.S. (2005) Compatibilization-like effect of reactive organoclay on the poly(L-lactide)/poly(butylene succinate) blends. *Polymer,* **46**, 11829.

72 Li, Y. and Shimizu, H. (2004) Novel morphologies of poly(phenylene oxide) (PPO)/polyamide 6 (PA6) blend nanocomposites. *Polymer,* **45**, 7381.

73 Lee, H.S., Fasulo, P.D., Rodgers, W.R., and Paul, D.R. (2005) TPO based nanocomposites. Part 1. Morphology and mechanical properties. *Polymer,* **46**, 11673.

74 Li, W., Karger-Kocsis, J., and Thomann, R. (2009) Compatibilization effect of TiO_2 nanoparticles on the phase structure of PET/PP/TiO_2 nanocomposites. *J. Polym. Sci. B,* **47**, 1616.

75 Filippone, G., Dintcheva, N.Tz., La Mantia, F.P., and Acierno, D. (2010) Selective localization of organoclay and effects on the morphology and mechanical properties of LDPE/PA11 blends with distributed and co-continuous morphology. *J. Polym. Sci. B,* **48**, 600.

76 Fang, Z., Xu, Y., and Tong, L. (2007) Effect of clay on the morphology of binary blends of polyamide 6 with high density polyethylene and HDPE-graft-acrylic acid. *Polym. Eng. Sci.,* **47**, 551.

77 Kelnar, I., Khunova, V., Kotek, J., and Kapralkova, L. (2007) Effect of clay treatment on structure and mechanical behavior of elastomer-containing polyamide 6 nanocomposite. *Polymer,* **48**, 5332.

78 Moghbelli, E., Sue, H.J., and Jain, S. (2010) Stabilization and control of phase morphology of PA/SAN blends via incorporation of exfoliated clay. *Polymer,* **51** (18), 4231.

79 Goodarzi, V., Jafari, S.H., Khonakdar, H.A., Monemian, S.A., Hassler, R., and Jehnicehn, D. (2009) Nonisothermal crystallization kinetics and determination of surface-folding free energy of PP/EVA/OMMT nanocomposites. *J. Polym. Sci. Part B: Polym. Phys.,* **47**, 674.

80 Martins, C.G., Larocca, N.M., Paul, D.R., and Pessan, L.A. (2009) Nanocomposites formed from polypropylene/EVA blends. *Polymer,* **50**, 1743.

81 Zhang, L., Wan, C., and Zhang, Y. (2009) Investigation on the multiwalled carbon nanotubes reinforced polyamide 6/ Polypropylene composites. *Polym. Eng. Sci.,* **49**, 1909.

82 Khare, R.A., Bhattacharyya, A.R., Kulkarni, A.R., Saroop, M., and Biswas, A. (2008) Influence of multiwall carbon nanotubes on morphology and electrical conductivity of PP/ABS blends. *J. Polym. Sci. Part. B: Polym. Phys.*, **46**, 2286.

83 Hom, S., Bhattacharyya, A.R., Khare, R.A., Kulkarni, A.R., Saroop, M., and Biswas, A. (2009) Blends of polypropylene and ethylene octene comonomer with conducting fillers: influence of state of dispersion of conducting fillers on electrical conductivity. *Polym. Eng. Sci.*, **49**, 1502.

84 Martin, Z., Jimenez, I., Angeles-Gomez, M., Ade, H., and Kilcoyne, D.A. (2010) Interfacial interactions in PP/MMT/SEBS nanocomposites. *Macromolecules*, **43**, 448.

85 Wu, D., Wu, L., Zhang, M., Zhou, W., and Zhang, Y. (2008) Morphology evolution of nanocomposites based on poly (phenylene sulfide)/poly(butylene terephthalate) blend. *J. Polym. Sci. Part B: Polym. Phys.*, **46**, 1265.

86 Lee, S.H., Kontopoulou, M., and Park, C.B. (2010) Effect of nanosilica on the co-continuous morphology of polypropylene/polyolefin elastomer blends. *Polymer*, **51**, 1147.

87 Mishra, J.K., Chang, Y.W., and Choi, N.S. (2007) Preparation and characterization of rubber-toughened poly(trimethylene terephthalate)/organoclay nanocomposite. *Polym. Eng. Sci.*, **47**, 863.

88 Kelarakis, A., Giannelis, E.P., and Yoon, K. (2007) Structure–properties relationships in clay nanocomposites based on PVDF/(ethylene–vinyl acetate) copolymer blends. *Polymer*, **48**, 7567.

89 Austin, J.R. and Kontopoulou, M. (2006) Effect of organoclay content on the rheology, morphology, and physical properties of polyolefin elastomers and their blends with polypropylene. *Polym. Eng. Sci.*, **46**, 1491.

90 Chow, W.S., Mohd Ishak, Z.A., and Karger-Kocsis, J. (2005) Atomic force microscopy study on blend morphology and clay dispersion in polyamide 6/polypropylene/organoclay systems. *J. Polym. Sci. Part B: Polym. Phys.*, **43**, 1198.

91 Filippi, S., Dintcheva, N.Tz., Scaffaro, R., La Mantia, F.P., Polacco, G., and Magagnini, P. (2009) *Polym. Eng. Sci.*, **49**, 1187. Effects of organoclay on morphology and properties of nanocomposites based on LDPE/PA-6 blends without and with SEBS-g-MA compatibilizer.

92 Dharaiya, D., Jana, S.C., and Shafi, A. (2003) A study on the use of phenoxy resins as compatibilizers of polyamide 6 (PA6) and polybutylene terephthalate (PBT). *Polym. Eng. Sci.*, **43**, 580.

93 Mehrabzadeh, M. and Kamal, M.R. (2002) Polymer-clay nanocomposites based on blends of polyamide-6 and polyethylene. *Can. J. Chem. Eng.*, **80**, 1083.

94 Chow, W.S., Mohd Ishak, Z.A., Karger-Kocsis, J., Apostolov, A.A., and Ishiaku, U.S. (2003) Compatibilizing effect of maleated polypropylene on the mechanical properties and morphology of injection molded polyamide 6/polypropylene/organoclay nanocomposites. *Polymer*, **44**, 7427.

95 Filippone, G., Dintcheva, N.Tz., Acierno, D., and La Mantia, F.P. (2008) The role of organoclay in promoting co-continuous morphology in high-density poly(ethylene)/poly(amide) 6 blends. *Polymer*, **49**, 1312.

96 Shim, H.H., Joo, J.H., Jung, S.H., and Yoon, J.S. (2007) Effect of silane-grafted polypropylene on the morphology of polypropylene and nylon 6/clay composites. *J. Polym. Sci. Part B: Polym. Phys.*, **45**, 607.

97 Yurekli, K., Karim, A., Amis, E.J., and Krishnamoorti, R. (2003) Influence of layered silicates on the phase-separated morphology of PS-PVME blends. *Macromolecules*, **36**, 7256.

98 Karim, A., Liu, D.W., Douglas, J.F., Nakatani, A.I., and Amis, E.J. (2000) Modification of the phase stability of polymer blends by fillers. *Polymer*, **41**, 8455.

99 Karim, A., Yurekli, K., Meredith, C., Amis, E., and Krishnamoorti, R. (2002) *Polym. Eng. Sci.*, **42**, 1836.

100 Isayev, A.I., Kyu, T., and Cheng, S.Z.D. (eds) (1996) *Liquid Crystalline Polymer Systems: Technological Advances. ACS Symposium Series*, vol. 632, American Chemical Society, Washington D.C.

101 Mehta, A. and Isayev, A.I. (1991) The dynamic properties, temperature transitions and thermal stability of PEEK-thermotropic liquid crystalline polymer blends. *Polym. Eng. Sci.*, **31**, 963.

102 Mehta, A. and Isayev, A.I. (1991) Rheology, morphology and mechanical characteristics of PEEK-LCP blends. *Polym. Eng. Sci.*, **31**, 971.

103 Akhtar, S. and Isayev, A.I. (1993) Self-reinforced composites of two thermotropic liquid crystalline polymers. *Polym. Eng. Sci.*, **33**, 32.

104 Viswanathan, R. and Isayev, A.I. (1995) Blends of a PPO-PS alloy with a liquid crystalline polymer. *J. Appl. Polym. Sci.*, **55**, 1117.

105 Taylor, G.I. (1932) The viscosity of a fluid containing small drops of another fluid. *Proc. R. Soc. London, Ser. A*, **138**, 41.

106 Taylor, G.I. (1934) The formation of emulsions in definable fields of flow. *Proc. R. Soc. London, Ser. A*, **146**, 501.

107 Han, C.D. (1981) *Multiphase Flow in Polymer Processing*, Academic Press, New York.

108 Utracki, L.A. and Shi, Z.H. (1992) Development of polymer blend morphology during compounding in a twin-screw extruder. Part I: droplet dispersion and coalescence – a review. *Polym. Eng. Sci.*, **32**, 1824.

109 Shi, Z.H. and Utracki, L.A. (1992) Development of polymer blend morphology during compounding in a twin-screw extruder. Part II: theoretical derivations. *Polym. Eng. Sci.*, **32**, 1834.

110 Bordereau, V., Carrega, M., Shi, Z.H., Utracki, L.A., and Sammut, P. (1992) Development of polymer blend morphology during compounding in a twin-screw extruder. Part III: experimental procedure and preliminary results. *Polym. Eng. Sci.*, **32**, 1846.

111 Huneault, M.A., Shi, Z.H., and Utracki, L.A. (1995) Development of polymer blend morphology during compounding in a twin-screw extruder. Part IV: a new computational model with coalescence. *Polym. Eng. Sci.*, **35**, 115.

112 Zhang, B., Ding, Y., Chen, P., Liu, C., Zhang, J., He, J., and Hu, G.H. (2005) Fibrillation of thermotropic liquid crystalline polymer enhanced by nano-clay in nylon-6 matrix. *Polymer*, **46**, 5385.

113 Wu, L.C., Chen, P., Chen, J., Zhang, J., and He, J.S. (2007) Noticeable viscosity reduction of polycarbonate melts caused jointly by nano-silica filling and TLCP fibrillation. *Polym. Eng. Sci.*, **47**, 757.

114 Sinha Ray, S., Bousmina, M., and Maazouz, A. (2006) Morphology and properties of organoclay modified polycarbonate/poly(methyl methacrylate) blend. *Polym. Eng. Sci.*, **46**, 1121.

115 Dharaiya, D.P. and Jana, S.C. (2005) Nanoclay-induced morphology development in chaotic mixing of immiscible polymers. *J. Polym. Sci. B*, **43**, 3638.

116 Elias, L., Fenouillot, F., Majeste, J.C., and Cassagnau, Ph. (2007) Morphology and rheology of immiscible polymer blends filled with silica nanoparticles. *Polymer*, **48**, 6029.

117 Hong, J.S., Kim, Y.K., Ahn, K.H., Lee, S.J., and Kim, C. (2007) Interfacial tension reduction in PBT/PE/clay nanocomposite. *Rheol. Acta*, **46**, 469.

118 Hong, J.S., Namkung, H., Ahn, K.H., Lee, S.J., and Kim, C. (2006) The role of organically modified layered silicate in the breakup and coalescence of droplets in PBT/PE blends. *Polymer*, **47**, 3967.

119 Nushtaeva, A.V. and Kruglyakov, P.M. (2004) Investigation of model emulsion films stabilized by solid particles: thickness of films, their stability, and interfacial tension. *Colloid J.*, **66**, 456.

120 Elias, L., Fenouillot, F., Majeste, J.C., Alcouffe, P., and Cassagnau, P. (2008) Immiscible polymer blends stabilized with nano-silica particles: rheology and effective interfacial tension. *Polymer*, **49**, 4378.

121 Lin, H.C., Kuo, S.W., Huang, C.F., and Chang, F.C. (2006) Thermal and surface properties of phenolic nanocomposites containing

octaphenol polyhedral oligomeric silsesquioxane. *Macromol. Rapid Commun.*, **27**, 537.

122 Misra, R., Fu, B.X., and Morgan, S.E. (2007) Surface energetics, dispersion, and nanotribomechanical behavior of POSS/PP hybrid nanocomposites. *J. Polym. Sci. Part B: Polym. Phys.*, **45**, 2441.

123 Song, M., Xia, H.S., Yao, K.J., and Hourston, D.J. (2005) A study on phase morphology and surface properties of polyurethane/organoclay nanocomposite. *Eur. Polym. J.*, **41**, 259.

124 Wu, S. (1987) Formation of dispersed phase in incompatible polymer blends: interfacial and rheological effects. *Polym. Eng. Sci.*, **27**, 335.

125 Kraus, G. (1965) Interactions of elastomers and reinforcing fillers. *Rubber Chem. Technol.*, **38**, 1070.

126 Le, H.H., Kolesov, I., Ali, Z., Uthardt, M., Osazuwa, O., Ilisch, S., and Radusch, H.J. (2010) Effect of filler dispersion degree on the Joule heating stimulated recovery behaviour of nanocomposites. *J. Mater. Sci.*, **45**, 5851.

127 Blow, C.M. (1973) Polymer/particulate filler interaction – the bound rubber phenomena. *Polymer*, **14**, 309.

128 Boonstra, B.B. (1979) Role of particulate fillers in elastomer reinforcement: a review. *Polymer*, **20**, 691.

129 Hamed, G.R. (1989) On the role of bound rubber in carbon black reinforcement. *Rubber Chem. Technol.*, **62**, 143.

130 Gunes, I.S. and Jana, S.C. (2010) Barrier properties of polyurethane nanocomposites and their relationship to shape memory properties, in *Barrier Properties of Polymer Clay Nanocomposites* (ed. V. Mittal) Nova Science Publishers, New York, 41–72.

131 Erguney, F.M. and Mattice, W.L. (2008) Response of matrix chains to nanoscale filler particles. *Polymer*, **49**, 2621.

132 Lopez, L.C. and Wilkes, G.L. (1991) Some aspects of carbon fiber type and its surface treatment on the nucleation behavior of poly(p-phenylene sulfide) based composites. *J. Thermoplast. Compos Mater*, **4**, 58.

133 Desio, G.P. and Rebenfeld, L. (1992) Crystallization of fiber reinforced poly (phenylene sulfide) composites. I. Experimental studies of crystallization rates and morphology. *J. Appl. Polym. Sci.*, **44**, 1989.

134 Gunes, I.S., Cao, F., and Jana, S.C. (2008) Evaluation of nanoparticulate fillers for development of shape memory polyurethane nanocomposites. *Polymer*, **49**, 2223.

135 Gunes, I.S., Cao, F., and Jana, S.C. (2008) Effect of thermal expansion on shape memory behavior of polyurethane and its nanocomposites. *J. Polym. Sci. Part B: Polym. Phys.*, **46**, 1437.

136 Gunes, I.S., Perez-Bolivar, C., Cao, F., Jimenez, G.A., Anzenbacher, P. Jr., and Jana, S.C. (2010) Analysis of non-covalent interactions between the nanoparticulate fillers and the matrix polymer as applied to shape memory performance. *J. Mater. Chem.*, **20**, 3467.

137 Ottino, J.M. (1989) *The Kinematics of Mixing: Stretching, Chaos, and Transport*, Cambridge University Press, New York.

138 van der Waals, J.D. (1979) The thermodynamic theory of capillarity under the hypothesis of a continuous density variation. *J. Stat. Phys.*, **20**, 197.

139 Jung, C., Jana, S.C., and Gunes, I.S. (2007) Analysis of polymerization in chaotic mixers using time scales of mixing and chemical reactions. *Ind. Eng. Chem. Res.*, **46**, 2413.

140 Ottino, J.M., Ranz, W.E., and Macosko, C.W. (1981) A framework for description of mechanical mixing of fluids. *AIChE J.*, **27**, 565.

141 Ottino, J.M., Ranz, W.E., and Macosko, C.W. (1979) A lamellar model for analysis of liquid-liquid mixing. *Chem. Eng. Sci.*, **34**, 877.

142 Vanoene, H. (1972) Models of dispersion of viscoelastic fluids in flow. *J. Colloid Interface Sci.*, **40**, 448.

143 Ghosh, A.K., Ranganathan, S., Lindt, J.T., and Lorex, S. (1991) Blend morphology development in a single screw extruder. *Proc. SPE ANTEC*, 232.

144 Scott, C.E. and Macosko, C.W. (1991) Model experiments concerning morphology development during the

initial stages of polymer blending. *Polym. Bull.*, **26**, 341.

145 Sundararaj, U., Macosko, C.W., Rolando, R.J., and Chan, H.T. (1992) Morphology development in polymer blends. *Polym. Eng. Sci.*, **32**, 1814.

146 Lindt, J.T. and Ghosh, A.K. (1992) Fluid mechanics of formation of polymer blends. Part I. Formation of lamellar structure. *Polym. Eng. Sci.*, **32**, 1802.

147 Scott, C.E. and Macosko, C.W. (1995) Morphology development during the initial stages of polymer-polymer blending. *Polymer*, **36**, 461.

148 Sundararaj, U., Dori, Y., and Macosko, C.W. (1995) Sheet formation in immiscible polymer blends: model experiments on initial blend morphology. *Polymer*, **36**, 1957.

149 Lyngaae-Jorgensen, J. (1996) Experimental methods for *in situ* studies of morphology development during flow: The case of instability of thin films studied by light scattering. *J. Macromol. Sci. Phys.*, **B35**, 357.

150 Zumbrunnen, D.A., Miles, K.C., and Liu, Y.H. (1996) Auto-processing of very fine-scale composite materials by chaotic mixing of melts. *Compos. Part A*, **27**, 37.

151 Sau, M. and Jana, SC. (2004) A study on the effects of chaotic mixer design and operating conditions on morphology development in immiscible polymer systems. *Polym. Eng. Sci.*, **44**, 407 [Errata: (2004), *Polym. Eng. Sci.* **44**, 1403].

152 Tomotika, S. (1935) On the instability of a cylindrical thread of viscous liquid surrounded by another viscous liquid. *Proc. R. Soc. London, Ser. A*, **150**, 322.

153 Grace, H.P. (1971) Dispersion phenomena in high viscosity immiscible fluid systems and application of static mixers as dispersion devices in such system. Proceedings 3rd. Eng. Found. Conf. Mixing, Andover;the same article was republished in: Grace, H.P. (1982) *Chem. Eng. Commun.*, **14**, 225.

154 Elmendrop, J.J. (1986) A study on polymer blending microrheology. *Polym. Eng. Sci.*, **26**, 418.

155 de Bruijn, R.A. (1993) Tipstreaming of drops in simple shear flows. *Chem. Eng. Sci.*, **48** (2), 277.

156 Elemans, P.H.M., Bos, H.L., Janssen, J.M.H., and Meijer, H.E.H. (1993) Transient phenomena in dispersive mixing. *Chem. Eng. Sci.*, **48**, 267.

157 Rallison, J.M. (1984) The deformation of small viscous drops and bubbles in shear flows. *Annu. Rev. Fluid Mech.*, **16**, 45.

158 Khakhar, D.V. and Ottino, J.M. (1987) Breakup of liquid thread in linear flows. *Int. J. Multiphase Flow*, **13**, 71.

159 Stone, H.A. and Leal, L.G. (1989) Relaxation and breakup of an initially extended drop in an otherwise quiescent fluid. *J. Fluid Mech.*, **198**, 399.

160 Stone, H.A. (1994) Dynamics of drop deformation and breakup in viscous fluids. *Annu. Rev. Fluid Mech.*, **26**, 65.

161 Tjahjadi, M. and Ottino, J.M. (1991) Stretching and breakup of droplets in chaotic flows. *J. Fluid Mech.*, **232**, 191.

162 Janssen, J.M.H. and Meijer, H.E.H. (1993) Drop breakup mechanisms: stepwise equilibrium versus transient dispersion. *J. Rheol.*, **37**, 597.

163 Reynolds, O. (1894) Study of fluid motion by means of colored bands. *Nature*, **50**, 161.

164 Raynal, F. and Gence, J.-N. (1997) Energy savings in chaotic laminar mixing. *Int. J. Heat Mass Transfer*, **40**, 3267.

165 Ottino, J.M. (1994) Mixing and chemical reactions: a tutorial. *Chem. Eng. Sci.*, **49**, 4005.

166 Muzzio, F.J. and Liu, M. (1996) Chemical reactions in chaotic flows. *Chem. Eng. J.*, **64**, 117.

167 Chella, R. and Ottino, J.M. (1985) Stretching in some classes of fluid motions and asymptotic mixing efficiencies as a measure of flow classification. *Arch. Rat. Mech. Anal.*, **90**, 15.

168 Spencer, R.S. and Wiley, R.M. (1951) The mixing of very viscous liquids. *J. Colloid Sci.*, **6**, 133.

169 Mohr, W.D., Saxton, R.L., and Jepson, C.H. (1957) Mixing in laminar flow systems. *Ind. Eng. Chem.*, **49**, 1855.

170 Erwin, L. (1978) An upper bound on the performance of plane strain mixers. *Polym. Eng. Sci.*, **18**, 738.

171 Erwin, L. (1978) Theory of laminar mixing. *Polym. Eng. Sci.*, **18**, 1044.

172 Erwin, L. (1978) Theory of mixing sections in single screw extruders. *Polym. Eng. Sci.*, **18**, 572.

173 Bigio, D.I., Boyd, J.D., Erwin, L., and Gailus, D.W. (1985) Mixing studies in the single screw extruder. *Polym. Eng. Sci.*, **25**, 305.

174 Shearer, C.J. (1973) Mixing of highly viscous liquids: flow geometries for streamline subdivision and redistribution. *Chem. Eng. Sci.*, **28**, 1091.

175 Ng, K.Y. and Erwin, L. (1981) Experiments in extensive mixing in laminar flow. I. Simple illustrations. *Polym. Eng. Sci.*, **21**, 212.

176 Bigg, D.M. (1975) On mixing in polymer flow systems. *Polym. Eng. Sci.*, **15**, 684.

177 Erwin, L. and Mokhtarian, F. (1983) Analysis of mixing in modified single screw extruders. *Polym. Eng. Sci.*, **23**, 49.

178 Pinto, G. and Tadmor, Z. (1970) Mixing and residence time distribution in melt screw extruders. *Polym. Eng. Sci.*, **10**, 279.

179 Utracki, L.A. and Luciani, A. (2000) Mixing in extensional flow field. *Appl. Rheol.*, **10**, 10.

180 Bourry, D., Godbille, F., Khayat, R.E., Luciani, A., Picot, J., and Utracki, L.A. (1999) Extensional flow of polymeric dispersions. *Polym. Eng. Sci.*, **39**, 1072.

181 Aref, H. (1984) Stirring by chaotic advection. *J. Fluid Mech.*, **143**, 1.

182 Chaiken, J., Chevray, R., Tabor, M., and Tan, Q.M. (1986) Experimental study of Lagrangian turbulence in Stokes flow. *Proc. R. Soc. London, Ser. A*, **408**, 165.

183 Chen, W.-L., Rising, H., and Ottino, J.M. (1986) Laminar mixing and chaotic mixing in several cavity flows. *J. Fluid Mech.*, **170**, 355.

184 Khakhar, D.V. and Ottino, J.M. (1986) Fluid mixing (stretching) by time periodic sequences of weak flows. *Phys. Fluids*, **29**, 350.

185 Kusch, H.A. and Ottino, J.M. (1992) Experiments on mixing in continuous flows. *J. Fluid Mech.*, **236**, 319.

186 Leong, C.W. and Ottino, J.M. (1989) Experiments on mixing due to chaotic advection in a cavity. *J. Fluid Mech.*, **209**, 463.

187 Jana, S.C., Tjahjadi, M., and Ottino, J.M. (1994) Chaotic mixing of viscous fluids by periodic changes in geometry: the baffled cavity flow. *AIChE J.*, **40**, 1769.

188 Ottino, J.M., Muzzio, F.J., Tjahjadi, M., Franjione, J.G., Jana, S.C., and Kusch, H.A. (1992) Chaos, symmetry, and self-similarity: exploiting order and disorder in mixing processes. *Science*, **257**, 754.

189 Liu, M., Muzzio, F.J., and Peskin, R.L. (1994) Quantification of mixing in aperiodic chaotic flows. *Chaos, Solitons, Fractals*, **4**, 869.

190 Alvarez-Hernández, M.M., Shinbrot, T., Zalc, J., and Muzzio, F.J. (2002) Practical chaotic mixing. *Chem. Eng. Sci.*, **57**, 3749.

191 Arratia, P.E., Shinbrot, T., Alvarez, M.M., Muzzio, F.J., and Arratia, P.E. (2005) Mixing of non-Newtonian fluids in steadily forced systems. *Phys. Rev. Lett.*, **94**, 1.

192 Tjahjadi, M. and Foster, R.W. (1996) Single screw extruder capable of generating chaotic mixing. US Patent 5,551,777.

193 Jana, S.C., Scott, E., and Sundararaj, U.T. (2000) Single extruder screw for blending of miscible and immiscible polymeric materials, US Patent No. 6,132,076.

194 Kim, S.J. and Kwon, T.H. (1996) Enhancement of mixing performance of single-screw extrusion processes via chaotic flows. Part I. Basic concepts and experimental study. *Adv. Polym. Technol.*, **15**, 41.

195 Kim, S.J. and Kwon, T.H. (1996) Enhancement of mixing performance of single-screw extrusion processes via chaotic flows. Part II. Basic concepts and experimental study. *Adv. Polym. Technol.*, **15**, 55.

196 Jimenez, G. and Jana, S.C. (2009) Composites of carbon nanofibers and thermoplastic polyurethanes with shape memory properties prepared by chaotic mixing. *Polym. Eng. Sci.*, **49**, 2020.

197 Jimenez, G. and Jana, S.C. (2007) Polymer composites of oxidized carbon nanofibers prepared by chaotic mixing. *Carbon*, **45**, 2079.

198 Jimenez, G. and Jana, S.C. (2007) Electrically conductive polymer nanocomposites of polymethylmethacrylate and carbon nanofibers prepared by chaotic mixing. *Compos. Part A: Appl. Sci. Manuf.*, **38**, 983.

199 Jung, C. (2005) Synthesis of thermoplastic polyurethanes and polyurethane nanocomposites under chaotic mixing conditions. Ph.D. Thesis, University of Akron, Akron, OH.

200 Liu, Y.H. and Zumbrunnen, D.A. (1996) Emergence of fibrillar composites due to chaotic mixing of molten polymers. *Polym. Compos.*, **17**, 187.

201 Zumbrunnen, D.A. and Inamdar, S. (2001) Novel sub-micron highly multi-layered polymer films formed by continuous flow chaotic mixing. *Chem. Eng. Sci.*, **56**, 3893.

202 Zumbrunnen, D.A. and Chhibber, C. (2002) Morphology development in polymer blends produced by chaotic mixing at various compositions. *Polymer*, **43**, 3267.

203 Sau, M. (2003) Morphology development in chaotic mixing of polymers. PhD Thesis, University of Akron, Akron, OH.

204 Jana, S.C. and Sau, M. (2004) Effects of viscosity ratio and composition on development of morphology in chaotic mixing of polymers. *Polymer*, **45**, 1665.

205 Sau, M. and Jana, S.C. (2004) Effect of waveforms on morphology development in chaotic mixing of polymers. *AIChE J.*, **50**, 2346.

206 Zumbrunnen, D.A., Inamdar, S., Kwon, O., and Verma, P. (2002) Chaotic advection as a means to develop nanoscale structures in viscous melts. *Nano Lett.*, **2**, 1143.

207 Perilla, J. and Jana, S.C. (2005) Coalescence of immiscible polymer blends in chaotic mixers. *AIChE J.*, **51**, 2675.

208 Isayev, A.I. (1991) *Modeling of Polymer Processing – Recent Developments*, Hanser Publishers, Munich.

209 Jana, S.C. (2003) Loss of surface and volume electrical conductivities in polymer compounds due to shear induced migration of conductive particles. *Polym. Eng. Sci.*, **43**, 570.

210 Hong, C.M., Kim, J., and Jana, S.C. (2004) Shear induced migration of conductive fillers in injection molding. *Polym. Eng. Sci.*, **44**, 2101.

211 Bucknall, C.B. (1977) *Toughened Plastics*, Elsevier, Amsterdam.

212 Giuffria, R., Carhart, R.O., and Davis, D.A. (1963) High gloss of extruded high impact polystyrene sheet. A microscopical study of sheet morphology. *J. Appl. Polym. Sci.*, **7**, 1731.

213 Grancio, M.R. (1972) Cold rolled ABS. Part 1: the effect of rubber particle size on the tensile properties of ABS before and after cold rolling. *Polym. Eng. Sci.*, **12**, 213.

214 Grancio, M.R., Bibeau, A.A., and Claver, G.C. (1972) Cold rolled ABS. Part 2: rubber morphology and tensile properties of hot stretched and cold rolled ABS. *Polym. Eng. Sci.*, **12**, 450.

215 Gunes, I.S. and Ersoy, O.G. (2006) Effects of injection molding processing parameters on appearance related optical properties of polycarbonate. *J. Polym. Eng.*, **26**, 743.

216 Gunes, I.S. and Ersoy, O.G. (2007) Effects of injection molding processing parameters on appearance related optical properties of styrene-acrylonitrile copolymer and comparison with the case of polycarbonate. *J. Polym. Eng.*, **27**, 233.

217 Kato, K. (1968) Molding anisotropy in ABS polymers as revealed by electron microscopy. *Polymer*, **9**, 225.

218 Jana, S.C., Kapoor, B., and Acrivos, A. (1994) Apparent wall slip velocity coefficients in concentrated suspensions of noncolloidal particles. *J. Rheol.*, **39**, 1123.

Index

a

abrasion resistance 165, 168, 180
additives 109f., 129
– accelerator 131f.
– adhesion promoters 316
– non-additive (+) process 244
– plasticizer 110, 127
agents
– co- 133
– compatibilizer 20, 27, 33, 47, 111f., 147ff.
– coupling 188
– crosslinking 131ff.
– interfacial 20, 316
aggregation 34, 37, 361
– breakup 270
– fractal-type 44
Ajji and Choplin theory 80
atomic force microscopy (AFM) 54, 176

b

binodal 53f., 80
blending
– continuous 10
– mechanical 181f.
– mechano-chemical 181f.
– reactive 264f., 320f., 332ff.
– solution 181f.
– third-order rule 49
Bondi's tables 51
breaking thread method 19
breakup
– dispersed phase 330
– domain 372
– droplets 42, 58, 61, 63f., 270, 276, 318
– initial 273f.
– liquid filaments 275f.
– sheets 275
Brownian dynamics 57
Bumper grade 225

c

capillarity number 40f., 365f.
– critical 61, 366
capillary
– breakup process 372
– instability 373
– viscometer 70, 329
carbon black (CB) 167, 182, 187ff.
– dspersion 189, 225, 362
– particles 360ff.
carbon nanofiber (CNF) 359f.
Carreau–Yasuda equation 37
channel
– depth 283
– downstream 230, 255
– geometry 233
– up-stream 239f.
Choi and Schowalter model 42, 63
clam-shell barrel 243f., 251
clearance 234, 239
– tip flight 8
– variable 10
cluster
– continuous 32
– dynamic 38
– non-coalescing 80
– SEBS (styrene–ethylene/butene–styrene) 74
coagulation
– shear 42, 54
– threshold energy 42
coalescence 19, 42f., 44, 63, 281f., 318
– third model 64
cohesive energy density (CED) 48
compatibilization 146ff.

Encyclopedia of Polymer Blends: Volume 2: Processing, First Edition. Edited by Avraam I. Isayev.
© 2011 Wiley-VCH Verlag GmbH & Co. KGaA. Published 2011 by Wiley-VCH Verlag GmbH & Co. KGaA.

– copolymers 315ff.
– efficiency 318, 320
– *ex situ* 316f.
– functional polymers 315ff.
– *in situ* 265, 316f., 320ff.
– non-reactive 265
– reactive 32, 264ff.
– routes 316f.
compatibilizer, *see* agent
compounding
– capacity 223f.
– ingredients 109f., 189ff.
– plastic/rubber blends 163ff.
– process 208f.
computational fluid dynamics (CFD) 258
copolymer
– block 20, 34, 44f., 54, 147f., 152, 265, 272, 318ff.
– graft 19f., 147f., 178, 265, 272, 317ff.
– interchain 317
– melt flow 45
– pre-synthesized 316
Couette flow apparatus 279f.
creep compliance 71
critical micelle concentration (CMC) 32, 319
crosslinking 65, 83, 110f., 316
– agents 131ff.
– efficiency 133
– processes 131ff.
– systems 147
crystallization 54, 292, 367
cure
– rate 178
– /resin system 197
– systems 186f., 201

d

Deborah number (*De*) 54
deformation
– incompressible 267
– rates 21, 27, 267f.
– tensor 266, 374
– uniaxial 267
– vulcanizing ingredients 189ff.
degassing, *see* devolatilization
degradation
– rate 248
– thermal 248, 250
devolatilization 211, 216, 240, 340
diffusion
– coefficient 191, 369, 371, 377
– -controlled 322, 343
– mixing 273
– molecular 360, 369, 371, 377
– physical 322
dispersion
– carbon black 225
– filler 226, 360ff.
– flow-induced 64
– micro- 223
– sheets 274
disturbance growth rate 277
Doi–Ohta theory 55, 58f., 61f.
domain
– breakup 372
– micro- 178
– size 274
droplet
– coalescence 19, 42f., 44, 63f., 81, 281
– deformability 41f., 44, 66, 276ff.
– density 43
– diameter 32f., 41, 61, 64f.
– –drop drainage 77
– elasticity 61
– fibrillation 81
– pendant technique 270f.
– radius 43
– rotation 44
dynamic vulcanization, *see* vulcanization

e

Einstein relation 34
elasticity
– molecular theories 28
– molten polymer 70
elastomer 164ff.
– blending 174ff.
– crosslinking 133ff.
– emulsion 167
– microstructure 165
– multi-T_g 169f.
– phase diagram 176
– solubility parameters 178ff.
– solution 167
– unsaturated 133ff.
elongation, *see* flow
emulsification 316, 318
emulsions 27, 34
– bio- 44
– diluted 41, 43
– dynamic moduli 69
– ionic 47
– micro- 324, 326, 328
– non-ionic 47
– PVC 37
– small molecule liquid 358ff.
– water/oil (W/O) 44, 77
energy

– frictional dissipation (FDE) 249f.
– heat conduction (HCE) 245
– plastic deformation (PDE) 214, 245f., 249f.
– thermal 246
– viscous dissipation (VDE) 245ff.
entanglement 27, 50, 318f.
enthalpy
– of mixing 31, 175, 315
– specific 246f., 304
entropy
– configurational 31
– of mixing 18, 175, 315
exothermic 315f.
extrudate
– diameter 28
– swell 28, 38
extruders
– Baker Perkins (APV) system 207
– Banbury 4f., 7, 14f., 114ff.
– Barr Fluxion ring mixer 241ff.
– batch 2f., 113, 116ff.
– Brabender 126, 140f.
– Buss Kokneter 11, 16f., 123f.
– Cavity Transfer Mixer (CTM) 241
– co-kneader 114, 121, 211
– continuous 10f., 117ff.
– conveying elements 119, 121, 143, 245
– Farrel Continuous Mixer systems for plastic compounding 15f., 211, 294
– gear-type distributive 239f., 293
– Haake polyLab 126
– high efficiency twin-srew 226f.
– high speed energy input (HSEI) 218ff.
– hybrid 120
– intelligent 227f.
– intermeshing co-rotating twin-srew 13f., 118f., 128f., 207f., 282ff.
– Knetwolf 11, 13, 16
– KraussMaffei Berstorff twin-srew system 222f.
– Japan Steel Works (JSW) TEX twin srew system 210
– List Continuous Mixer 211
– Maddock-style 238f.
– modular co-rotating twin-srew 13f., 207, 290
– modular intermeshing counter-rotating twin-srew 16f., 121f., 207, 210ff.
– multiple srew 212, 214, 259
– non-intermeshing (tangential) counter-rotating twin-srew 11, 15, 210
– Post–Cooke intermeshing internal 9
– reciprocating single-srew 208
– scale-up 304f.
– self-wiping co-rotating twin-screw 12f., 283f.
– single-srew 2, 10f., 207f., 229ff.
– Tenner GG 16
– Thiele counter flight 16
– transparent glassy 7
– Twente Mixing Ring (TMR) 211, 241ff.
– variable clearance intermeshing internal 10
– Welding Engineere' CRNI twin-srew 208
– Werner Pfleiderer ZKS modular co-rotating twin-srew 13f., 216ff.
extrusion
– die 21f.
– process simulator version II /EPSIM II), *see* process simulation
– reactive (REX) 300, 305, 317, 337ff.
– TPEs 155ff.
Eyring theory of rate 30

f
fibers
– glass 14, 17, 360
– mini- 21f.
fill factors 15, 299
filler
– clay 76f., 365f.
– conventional 360ff.
– dispersion 226, 360ff.
– exclusion 360
– nano- 360, 364ff.
– non-reinforced 188
– penetration 364
– -phase distribution 188
– polymer– 188
– polymer blend 358ff.
– /oil levels 178
– solid particle 272f.
flow
– chaotic 378ff.
– dilatant 28
– dynamic shearing 28f., 38, 68f.
– elongational 28f., 72f., 268, 277, 279, 375
– field characteristics 29
– Newtonian behavior 28, 40
– non-isothermal 273, 297
– non-Newtonian behavior 28, 38, 43f., 273, 297
– planar elongational 377f.
– plug 28, 38
– pressure 375
– rate 269
– repetitive 232
– rotational 378

– segregation 44, 78
– shear 375
– steady state shearing 28f., 38, 40, 53
– turbulent 369
– uniaxial extensional 376f.
– visualization 6, 342f.
fluid
– miscible 374
– model 248
– non-reactive viscous 247
– viscoelastic 329
Fourier-transform rheological method 60
free volume theory 27
friction ratio 113

g
Gambacher and Meissner model 56
general equation of non-equilibrium reversible–irreversible coupling (GENERIC) 59, 63
Gibbs free energy of mixing 30, 369
glass fibers, *see* fibers
glass transition temperature 51, 131, 175ff.
– AN level 131
– elastomer 164, 175ff.
– PS 53, 211
– PVME 53
green strength promoters 197f.
Grmela's Poisson bracket formalism 63
gutta-percha 18

h
heat
– conduction energy (HCE), *see* energy
– fluxes 247f.
heating
– /cooling system 126
– local 249
– viscous dissipation 269
Helfand model 67
Helmholtz free energy 59
Hencky
– deformation rate 72
– strain 28, 72f., 75
Hildebrand dependence 48
Huggins–Flory binary interaction parameter 31, 48

i
injection molding 22, 329
– defects 156
– TPEs 152ff.
interaction
– anionic 316
– dipole–dipole 316
– dispersive-type 30
– drop–drop 43, 68, 77
– enthalpic 77
– filler–matrix 358, 367f.
– hydrodynamic 34
– hydrogen bond 316
– inter-domain 38
– interface 41
– intermolecular 316
– interparticle 28, 44
– non-covalent 368
– parameter 30
– polar–polar 358
– polymer–filler 163
– polymer–polymer 113, 330
interface 18f.
– droplet–matrix 360
– energy 32, 65, 178
– folding 373
– polymer–polymer 373
– roughening 323ff.
– stretching 373f.
– thinning 64
– unstable 19
interfacial
– adhesion 264
– agents 20
– area 266, 268, 330
– bonding 365
– co-polymer 323ff.
– instability 373
– reactions 322f.
– tension 19f., 270ff.
– tension coefficient 31, 33, 40, 43, 46, 56, 58, 64
– thickness 316
intermaterial area generation 370ff.
interphase
– effects 40
– thickness 32, 69

k
Kerner model 63
kinetic
– constants 347
– energy 373
– equations 346
kinetics
– melt coupling reactions 321ff.
– phase separation 53
– reaction 331, 347
– semi-phenomenological equation 57
kneading

– elements 121, 125, 143, 245
– cylinder 223f.
– disc blocks 288f., 316, 342
Krieger–Dougherty relation 35ff.

l
latex 37, 181
liquid
– injection 117, 122, 124
– low-viscosity 281
– matrix 275
lower critical solution temperature (LCST) 51ff.

m
macromolecule
– bead-spring 57
– cyclic 198
– mobility 49
macroparticles, *see* particles
manufacturing
– application 327
– operational features 340
– process design 301ff.
mass customization 257f.
masterbatch (MB) method 81, 188, 237
McAllister equation 30
Mclaurin series 33
melt
– coupling reactions 321ff.
– flow of block copolymer 45
– mixing 109, 111, 113ff.
– removal 250
– spinning 21
– spun blends 21
– temperature 113, 250, 252
melting
– conduction 250
– mechanisms 247ff.
– /mixing state 243f., 254
– natural ABS 229f.
– rates 250
– re- 246
– section 231
– virgin polymers 245f.
Mertsch and Wolf equation 51
microphase separation temperature (MST) 45
mill roll 2f., 113f.
mixer, *see* extruder
mixing
– chamber volumes 6
– cross-channel 232
– de- 381f.
– dispersive 112f., 117, 120, 156f., 237, 266, 270ff.
– dissipative melt 250
– distributive 112, 114, 117, 120, 157, 237, 239, 266ff.
– elements 251f., 290f.
– flows 372ff.
– longitudinal 292
– mechanical 280f.
– mechanism 265
– solid–liquid 370
modeling, *see* process simulation
molar attraction constant 180
molecular dynamics (MD) 75
molecular weight
– average 166
– distribution (MWD) 30f., 50, 56, 73
– elastomer 166
– high 166, 315
– low 166, 198, 263, 325f., 358
– MGE 335
– reactive precursor 263, 325f.
– ultrahigh PE(UHMWPE) 362
monodispersed 35, 43
morphology
– co-continuous 110, 370
– development 344f.
– dispersed-continuous 110, 370
– dispersed phase 328ff.
– flow imposed 65f.
– immiscible blends 60f.
– initial stages of phase 274
– interface 323f.
– reactive blends 295ff.
– stabilization 18f., 330f.
multiphase systems 27f.

n
nanoparticles, *see* particles
network
– interpenetrating 110
– vulcanizate 132
neutron magnetic resonance (NMR) 48, 182
NIC, *see* kneading cylinder
nucleation and growth (NG) 53, 367

o
oil–carbon black masterbatches 167
oil/filler levels 178
Oldroyd's model 43, 47
optical microscope 54
organoclays 80ff.

Ostwald ripening 63f.
ozone resistance 183, 187

p
packing volume fraction 36f.
Palierne model 56, 63, 75, 79
parallel-band apparatus 277f.
particle
– clay 364f.
– distribution 348
– inorganic 358f.
– macro- 27
– nano- 27, 76ff.
– SiO_2 78ff.
– size 316, 329ff.
pellets 127, 129f., 155
– compounded designer 207, 209
– microstructured 208f.
– virgin 229
percolation threshold 32
permeability 185f.
peroxide 132ff.
phase
– continuous 20, 110, 370
– diagram 176
– dispersed 20, 28, 31, 110, 328ff.
– inversion 32, 176
– inversion coefficient 67
phase morphology
– elastomers 176
– processing operations 21ff.
phase
– segregation 60
– separation 53f.
– size 22
– stabilization 18f., 330f.
phenomenological parameter 62
pinch-offs 323f., 326
plastic deformation energy (PDE), *see* energy
plastication, *see* melting
plateau modulus 50, 52
Poisson bivector 59
polarity 110, 131, 188
polydispersity 31, 35f.
– index (PDI) 166
– miscible blends 49
– molecular weights 73
– parameters 38
polymer
– acrylonitrile–butadiene rubber (NBR), *see* rubber
– acrylonitrile–butadiene–styrene (ABS) 230, 233f., 242f., 332f.
– alloys and blends (PAB) 27f.
– amorphous 211f., 246, 253
– crystalline 211f., 246
– defects 166
– ethylene–propylene diene terpolymer (EPDM), *see* rubber
– ethylene–propylene rubber (EPR), *see* rubber
– functionalization 178, 315ff.
– glycidyl methacrylate (GMA) 319, 332, 334f.
– high-density polyethylene (HDPE) 60, 246, 319, 363
– high-impact polystyrene (HIPS) 18f., 361, 381
– high-temperature melting (HTMP) 253
– homo- 72, 77
– linear low density polyethylene (LLDPE) 33, 49, 74, 254f., 361f
– liquid crystalline (LCP) 70, 365f
– low-temperature melting (LTMP) 253
– maleic anhydrite (MA) 51, 71, 319
– methyl methacrylate (MMA) 332, 336
– MGE 332ff.
– molten 38, 70
– multi-T_g 169
– polyamide (PA) 21, 317, 328f.
– polybutadiene (PB) 55, 179ff.
– polybutadiene terephthalate (PBT) 332ff.
– polycarbonate (PC) 48, 70, 73, 244
– polycaprolactam (a-PCL) 48
– poly(dimethyl butadiene) (PDMB) 18
– poly(dimethyl siloxane) (PDMS) 56, 59, 64f.
– poly(ethyl ethylene) (PEE) 56
– polyethylene (PE) 21f., 73, 75
– polyethylene terephthalate (a-PET) 48, 70
– polyisoprene (PI) 18, 55
– poly(methyl methacrylate) (PMMA) 46f., 71, 75, 327, 330f.
– poly(*n*-butyl methacrylate) (PnBMA) 48
– polyolefin resins 73, 316f.
– polyoxymethylene (POM) 60
– polypropylene (PP) 73, 126, 130
– polystyrene (PS) 18, 21f., 48, 51ff.
– poly(styrene-*co*-acrylonitrile) (SAN) 48, 51, 71, 76, 332
– poly(vinyl chloride) (PVC) 18, 33, 37, 48, 125
– poly(vinylidene fluoride) (PVDF) 47
– poly(vinyl methyl ether) (PVME) 48, 51, 53
– styrene–butadiene–styrene (SBS) 54, 320
– styrene–maleic anhydrite (SMA) 51, 71
– styrene–butadiene rubber (SBR), *see* rubber
– styrene–ethylene–butylene–styrene (SEBS) 319f.
– styrene–isoprene–butadiene rubber (SIBR), *see* rubber

– unsaturated 133ff.
polymer blend
– acrylonitride copolymer–poly(vinyl chloride) 18
– amorphous PVC/PMMA 48
– bromobutyl/butyl rubber 186
– bromobutyl/chlorobutyl rubber 186
– bromobutyl/GPR/EPDM rubber 187
– bromobutyl/styrene butadiene rubber 186
– compatibilized 147ff.
– dynamic moduli 55, 58, 69, 80
– elastomer–thermoplastic 118, 124, 126
– HDPE/POM 60
– heterogeneous 110
– homogeneous 110, 112
– homologous (HPB) 31
– immiscible 18, 28, 60, 110, 175f., 264, 266, 318
– LLDPE/PVC 33
– miscible 18, 28, 110, 175f., 266, 315
– multiphase nanocomposites 257ff.
– natural rubber/bromobutyl rubber 183ff.
– NBR/PP 149f.
– negatively deviating (NDB) 66, 68
– PA-6/EPR/EPR-MA 76
– PA/polyolefin 316f.
– performance 27, 168
– PE/PS 21f.
– PE/PA 21
– PEE/PDMS/PEE–PDMS 56
– PEP/PPO 318
– physical 125
– PI/PB 55f.
– PID/PDMF 62, 64
– plastic/crosslinked rubber 137ff.
– plastic/rubber 109ff.
– PMMA/PS 71, 75
– PNBD 68
– polyamide-6 336f.
– polybutadiene terephthalate (PBT) 332ff.
– polyethylene 33, 49
– positively deviating (PDB) 27, 66, 68
– PP/EPDM 126, 130, 140, 146f.
– PPE/PS 52
– PP/PC 328
– PS/EDR 320
– PS/LLDPE 58
– PS/PVME 53, 55
– PVDF/polyimide 47
– reactive 32, 264ff.
– SAN/SMA 71
– secondary systems 193ff.
– semi-miscible 175, 266
– solid–polymer–liquid system 266
– stabilization 360f.
– synthetic 18
polymeric
– liquids 266
– macro-radicals 133
– matrix 27, 31f.
– nanocomposites (PNCs) 76ff.
polymerization 147, 338
– addition 166, 265
– co- 281
– condensation 166
– degree 45, 77
– interchange 182, 265
– ionic bonding 265
– rate 321f., 328ff.
– ring opening 265
– substitution 265
preparation
– compatibilizer 148
– elastomer 201
– plastic/rubber blends 112ff.
– TPVs 140f.
pressure profiles 15, 229, 233
process simulation
– chemical engineering models 346
– continuum mechanics 346
– extrusion process simulator version II /EPSIM II) 243ff.
– flow modeling 347f.
– intermeshing co-rotating twin-screw exruders 297ff.
– physico-chemical 346
– TSMEE (twin-screw melt mixing evaluator) 244f., 251, 253f.
processing
– elastomer blends 181ff.
– flow diagram 117f.
– plastic/rubber blends 151ff.
pseudoplastic 28, 38, 43
pull-out 327f.
Pythagorean theorem 267

r

radius of gyration 54
Rayleigh theory 273, 275
reaction, *see* polymerization
reinforced 27, 38, 188, 193ff.
relaxation
– dynamics 76
– Gross' frequency 49
– Lee and Park term 58
– Marangoni 44
– Rouse 54
– time 38, 41, 50

reptation model 31, 49
resins
– curing 193, 196f., 199
– reinforcing 193ff.
– tackifying 193f.
residence time 113, 116, 269, 339
– distributions 292ff.
resistance
– abrasion 165, 168, 180, 200
– rolling 168ff.
– ozone 183, 187
– wear 188
rheology
– emulsion 39
– equations of state 57ff.
– micro- 41, 61, 68
– models for immiscible blends 31ff.
– models for miscible blends 28f., 47ff.
– organoclays 81ff.
– suspension 35
– thermo- 70
rheometer
– Meissner elongational (RME) 74, 83
– test cavity 28
rheopexy 38
rotor
– doubled-flighted 8
– four-flighted non-intermeshing 9, 16f.
– Kobelco 115
– seals 117
– speed 116f.
– twist kneading (TKR) 225f.
rubber
– acrylonitrile–butadiene rubber (NBR) 18, 164
– bound 188
– bromobutyl (BIIR) 174, 183ff.
– butadiene (BR) 18, 111, 172f., 187
– butyl 186
– chlorobutyl (CIIR) 174, 186f.
– crosslinked unsaturated 133ff.
– ethylene–propylene (EPR) 73, 76, 111, 131, 168, 174, 320, 364
– ethylene–propylene diene terpolymer rubber (EPDM) 73, 111, 126, 130ff.
– general purpose rubber (GPRs) 185, 187
– halobutyl (HIIR) 174
– heat stability 180, 192
– integral 169
– isobutylene isopropene (IIR) 174
– natural 18, 111, 172f., 175, 180, 183ff.
– nitrile (NR) 109, 131
– /plastic blend production 127ff.
– polarity 131
– styrene–butadiene (SBR) 18, 111, 167f., 172f., 186f.
– styrene–isoprene–butadiene rubber (SIBR) 199
– synthetic 18, 164
– tensile properties 138, 150, 180, 192, 201
– thermoset 110, 151
– wear resistance 188

S

scanning electron microscopy (SEM) 46
– CB-filled blend 361f.
– compounded pellet 207, 209
– crosslinked TPVs 145f.
– hydrophillic SiO_2 nanoparticles 79
– PA/polyolefin blend 317
– physical PP/EPDM blend 130
screw
– design 122, 125, 155
– Double Wave 231
– elements 120f., 157, 214f., 340f.
– energy transfer (ET) 231ff.
– four-flighted 7, 215, 219f., 285ff.
– fusion 240
– HELIBAR 240
– high-performance 231ff.
– left-handed elements 288
– length/diameter (L/D) 118, 155, 242, 316, 329
– modular 216ff.
– outer diameter/inner diameter (OD/ID) 213, 217ff.
– right-handed elements 285ff.
– single-flighted 229, 285ff.
– speed 157, 217, 220, 269, 342
– Stratablend 231, 235
– symmetrical/asymmetrical splinded shafts 221f.
– two-flighted 7, 16f., 213, 215, 219f., 285ff.
– Unimix 231, 236f.
– variable barrier energy transfer (VBET) 231, 234f., 243
segregation
– flow-induced 44, 78
– phase 60, 78
self-consistent mean-field theory (SCMFT) 323, 326
shear
– de-mixing (SID) 54
– flow field 269
– frictional force 327
– mixing (SIM) 54
– rate 154, 217, 220, 268f., 365
– strain 122, 269

– stress 6, 20f., 122, 131
shielding effects 34f.
Simha and Somcynsky (S–S) statistical thermodynamic theory 48
Simha equation 35f.
simulation, *see* process simulation
single pass (SP) method 81
size exclusion chromatography (SEC) 31
skin–score structures 66
small angle laser light scattering (SALLS) 54
small angle neutron scattering (SANS) 45, 48
small angle X-ray scattering (SAXS) 45, 48, 182
softening 328
solidification 60, 230, 233
solubility parameters, *see* elastomers
solution 28
– blending 181
– critical solution temperature 360
specific energy input (SEI) 303f.
spinodal (SD) 52ff.
strain
– compatibilization 54
– hardening (SH) 73f., 76
– Hencky 41, 72
stress 28, 65
– growth 62, 72
– hardening 75
– interfacial 365
– hydrodynamic 365
– -sensitive 3D structure 83
stress–strain theory 47
striation thickness 269, 371ff.
surface
– forces apparatus (SFA) 65
– tension 367
suspension 27, 34f.
– dilute 34
– flocculated 37
– hard-sphere 35f., 39
– nano- 83

t

tangent delta curve 168
Taylor
– theory 41, 277ff.
– number 64, 278
thermodynamic 27
– equilibrium 359, 369
– interaction parameter 361
– rheology 52ff.
thermoplastic 33, 65
– elastomers (TPEs) 138f., 151ff.
– molten 277
– rubber (TPR) 139
– toughend 139
– vulcanizates (TPVs) 132f., 138ff.
thixotropy 38, 43
Thomas empirical equation 35f.
Tikhonov's regularization method 46
tip
– clearance 223f.
– mixing flight 238f.
– spinning 42
– streaming 278
tire
– component parts 171f., 193
– compounding 170ff.
– construction 171
– elastomers 172ff.
– innerliner 184f.
– performance 199f., 205
– pneumatic 18
– rolling resistance 168ff.
– tread compound formulary 201ff.
Tokita model 64
Tomotika theory 276f.
transition
– section 230
– temperature 51
transmission electron microscopy (TEM) 46, 79
t–*T* superposition principle 54f., 70
turbidity 54, 81
TSMEE (twin-srew melt mixing evaluator), *see* process simulation (TSMEE)
two-dimensional cell model 47

u

upper critical solution temperature (UCST) 51, 54, 175f.
UV-stability 47, 155

v

viscoelastic
– drop 61ff.
– emulsion 43f.
– fluid 329
– linear 73
– melt 72
– nonlinear 72
viscometer, *see* capillary
viscoplastic 39
viscosity
– concentration dependence 66f., 272
– dynamic 69f.
– elongational 37
– high melt- 343

– intrinsic 40
– matrix 64, 366
– melt 19f., 116
– Mooney units 166f., 174, 184
– plastisols 37
– ratio 61, 279
– shear 38f., 272f., 366
– steady-state 69
– suspension 34f.
– zero-shear 50ff.
– zero-shear solution 30
– zero-shear suspension 34ff.
viscous dissipation energy (VDE), *see* energy
vulcanization
– co- 186
– dynamic 144f., 316
– TPV preparation 140f.
– plastics/crosslinked rubbers preparation 144ff.

x
X-ray photoelectron spectroscopy (XPS) 54

z
Ziegler–Natta systems 199
zoning 120